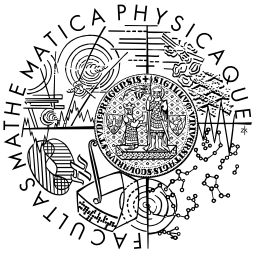

FACULTY
OF MATHEMATICS
AND PHYSICS
Charles University

DOCTORAL THESIS

Tomáš Nosek

Study of Neutrino Oscillations at the NOvA Experiment

Institute of Particle and Nuclear Physics

Supervisor of the doctoral thesis:	RNDr. Karel Soustružník, Ph.D.
Study programme:	Physics
Study branch:	Particle and Nuclear Physics

Prague 2021

I declare that I carried out this doctoral thesis independently, and only with the cited sources, literature and other professional sources.

I understand that my work relates to the rights and obligations under the Act No. 121/2000 Sb., the Copyright Act, as amended, in particular the fact that the Charles University has the right to conclude a license agreement on the use of this work as a school work pursuant to Section 60 subsection 1 of the Copyright Act.

In ..... date ..... signature of the author

Title: Study of Neutrino Oscillations at the NOvA Experiment

Author: Tomáš Nosek

Institute: Institute of Particle and Nuclear Physics

Supervisor: RNDr. Karel Soustružník, Ph.D., Institute of Particle and Nuclear Physics

Abstract: NOvA is a two detector long-baseline neutrino oscillation experiment using Fermilab's 700 kW NuMI neutrino beam. It studies the disappearance of muon (anti)neutrinos and the appearance of electron (anti)neutrinos in the beam over a distance of 810 km between the detectors. This thesis presents the latest 2020 update of the NOvA neutrino oscillation analysis within the standard model of three neutrinos mixing. With about +50% new data in NuMI neutrino mode (+22% of the total available data) and numerous analysis upgrades compared to the previously reported results, the experiment has made over 4σ-significant observation of electron antineutrino appearance in muon antineutrino beam and constrained the oscillation parameters $|\Delta m^2_{32}|, \sin^2\theta_{23}$ and δ_{CP}. The text closely depicts the analysis and all its novelties and changes. A detailed inspection is dedicated to the systematic uncertainties and their estimation and validation. Although statistical uncertainties currently dominate in these measurements, understanding the major sources of systematic uncertainties and their correlations is vital for both the interpretation and precision of the results and for further improvements of the analysis.

Keywords: neutrino, neutrino masses, neutrino oscillations, NOvA

To the Cat.

I would like to thank my supervisor Karel Soustružník for the support and opportunity to collaborate with the NOvA experiment. By the same token, I thank all my NOvA colleagues, especially those I have often worked with: Liudmila Kolupaeva, Nitish Nayak, Shiqi Yu, Gavin Davies, Louise Suter, Alex Himmel, Michael Baird, Christopher Backhouse, and Jeremy Wolcott.

Whenever and wherever, I appreciate all the moments spent with my friends from the Czech NOvA Group, notably Peter Filip, Filip Jediný, and Jaroslav Zálešák, for their diverse perspectives on the questions of particle physics, the life, the universe, and everything.

A very special thanks goes to Dalibor Nosek for his professional criticism, advice, technical suggestions, and help, not only within this thesis.

Contents

Introduction

Neutrinos are likely the second most abundant of all known particles. There are at least three different neutrino types or "flavors" as identified in the charged current weak interactions: electron, muon, and tau (e, μ, τ). It is a well-established experimental fact that neutrino flavor is not conserved in space-time propagation, and the neutrino flavors "oscillate". A possible explanation requires neutrino (lepton) mixing and their non-vanishing mass. With the paramount evidence of neutrinos being massive, neutrino oscillation experiments are the foremost witnesses of the physics beyond the Standard Model, at the frontier of the human perception of the universe.

Neutrinos have been studied intensively for several decades. The simplest mixing model of three neutrino mass states in three interaction (flavor) states described by three mixing angles $(\theta_{12}, \theta_{23}, \theta_{13})$, a complex phase, and two differences of squared neutrino masses seems to be very well understood. However, there are still many questions whose answers are of utmost importance to finally provide a satisfactory theory of elementary particles.

- Are neutrinos their own antiparticles? Are they Majorana or Dirac particles?
- Are there lepton number violating processes? At what energy scale?
- What is the nature of neutrino masses? Do they fit into the Standard Model framework?
- What are the absolute values of neutrino masses? Why are they so tiny compared to other elementary particles?
- How many massive neutrinos are there? Is there the same number of massive and active flavor neutrino states?
- What is the ordering of the neutrino mass spectrum? Is it "normal" with smaller differences between lighter neutrinos or "inverted" with smaller differences between heavier ones?
- Is the CP symmetry violated in the weak leptonic interactions? If so, how much?
- Is the mixing model of three massive neutrinos a good effective description of physical reality? Are there any light sterile neutrinos?
- What are the precise values of the neutrino mixing parameters?
- Is the mixing angle θ_{23} maximal, *i.e.*, $\theta_{23} = 45°$? If so, why is there such $2-3$ symmetry? Is it important?

Neutrino oscillation experiments are capable of investigating the second half of the above listed enquiries. The NOvA experiment is one of them and recently in operation. With its two detectors, it has been (for more than five years) looking for the disappearance of muon neutrinos and the appearance of electron neutrinos of ∼GeV energies in (as of yet) the most powerful muon neutrino beam over an 810 km distance (long-baseline).

This thesis intends to depict the NOvA neutrino oscillation analysis within the minimal model of three massive neutrinos in the latest state of the art (Jun 2020).

The text is organized into five subsequent chapters.

Chapter 1 reviews the neutrino oscillations *status quo*. It introduces neutrinos within the Standard Model of particle physics, and it presents the model of three massive neutrinos and the neutrino oscillation phenomenon. It strives to state all the relevant necessities for understanding the importance of the neutrino oscillation experiments, especially the accelerator long-baseline experiments (NOvA).

Chapter 2 is an informative overview of the NOvA experiment, its dispositions, instrumentation, operation, and capabilities.

Chapter 3 unveils the NOvA neutrino oscillation analysis within the three neutrinos model. It briefly describes the analysis strategy, the updates compared to the previous analyses, and the standard techniques for simulation, detectors calibration, events reconstruction, and selection. The NOvA specific features of particle identification and prediction generation exploiting the NOvA's two detectors design are detailed.

Chapter 4 lists all the considered systematic uncertainties and their treatment. It surveys their primary sources, the studies performed, their motivations, implementation, validations, and it estimates the uncertainties on the analysis predictions.

Chapter 5 shows the selected data observed, and it reports the estimates of the neutrino oscillation parameters and corresponding confidence regions of the applied statistical inference. The results are discussed within the three neutrinos model and w.r.t. the systematic uncertainties. They are compared to other neutrino oscillation experiments.

The system of natural units ("Planck units") is used throughout the text, $c = \hbar = k_{\mathrm{B}} = 1$, and the CPT theorem is assumed to be valid unless stated otherwise.

Please note that in accordance with the current tendency in the field of neutrino oscillation physics, this text adopts the term "normal/inverted ordering" instead of anachronistic "hierarchy" (in collision with the concept of the "hierarchy problem" of theoretical physics). However, as the latter is still to be seen in many references and graphics including the NOvA plots, it is often written alongside in parentheses.

Author's note

I had several inputs into the presented analysis. Firstly, I participated in an extensive collaboration-wide validation campaign to check the improved MC and data production pertinence (2019, new reconstruction methods and simulation models) to the NOvA neutrino oscillation analysis and its previous rounds. Secondly, together with A. Mislivec, we upgraded the NOvA software for generating extrapolated Far Detector predictions, and we assembled all the nominal and systematically shifted Far Detector predictions as described in Sections 3.10 to 3.13. Thirdly, I was responsible for incorporating the considered systematic uncertainties into the analysis – Chapter 4. I evaluated and implemented several of them, provided a comprehensive framework for their validation – Section 5.3 and Appendix C, and calculated the uncertainties on the estimated neutrino oscillation parameters – Subsection 5.3.2.

The results have been presented on many occasions since Jun 2020, notedly at Neutrino 2020[1] and ICHEP 2020[2] (online) conferences.

I also directly contributed to the previously published analyses in Ref. [1, 2] with many individual studies, collaboration duties, and service tasks.

[1] The XXIX International Conference on Neutrino Physics and Astrophysics, https://conferences.fnal.gov/nu2020/ (as of Mar 2021)

[2] 40^{th} International Conference on High Energy Physics, https://ichep2020.org (as of Mar 2021)

1. Neutrinos and neutrino oscillation phenomena

The first chapter presents the broader theoretical context of neutrinos as genuine objects of particle physics and reveals the immediate phenomenological milieu of neutrino oscillations. Section 1.1 compiles the general perception of neutrinos within the Standard Model, the concept of neutrino mass, and its consequences. Section 1.2 introduces the basic paradigm of three massive neutrinos mixing, its viability, and the classic formulation of the neutrino oscillations. The first two sections 1.1 and 1.2 are based on information available in great books of neutrino physics in Refs. [3, 4, 5, 6] and texts in Refs. [7, 8, 9, 10, 11, 12, 13]. Section 1.3 reviews the experimental foundations of neutrino flavor transitions and the key results, which are later summarized in Section 1.4. The last Section 1.5 declares the applicable neutrino oscillation (transition) probability formulae for the accelerator long-baseline experiments.

1.1 Standard Model and neutrinos

Neutrinos belong to the set of currently considered "elementary particles", *i.e.* fundamental physical objects with unrecognized substructure or intrinsic constituents. Elementary particles and their interactions, except for the gravitational interaction, are well described in the framework of quantum field theory by the Standard Model (SM) of particle physics (*e.g.*, see Ref. [14]). The key principle of the SM is its gauge invariance (*i.e.* local internal symmetry [15, Part III]) based on the local symmetry group $SU(3)_C \otimes SU(2)_L \otimes U(1)_Y$, where C, L, Y denote color, left-handed chirality (isospin), and weak hypercharge, respectively. The SM interactions are mediated by twelve vector gauge bosons that correspond to the generators of the symmetry group. Whereas to its fundamental representations, the subjects to the SM interactions, elementary fermions, are assigned.

Eight massless color gluons (eight generators of $\mathrm{SU}(3)_C$) mediate strong interactions formulated in quantum chromodynamics, QCD. Two massive charged $W^{\pm}$, one massive neutral Z, and one massless neutral γ (photon) mediate electroweak interactions. With a non-trivial mixing of the neutral bosons (Z, γ) characterized by the Weinberg angle θ_{W}, they correspond to three generators of $\mathrm{SU}(2)_L$ and one generator of $\mathrm{U}(1)_Y$. Together with the so-called "Higgs mechanism" and quark mixing, this formulation is known as the electroweak theory (EWT) or Glashow-Weinberg-Salam model (GWS) [16, 17]. Electroweak interactions can be further categorized w.r.t. the individual mediators. In analogy to quantum electrodynamics (QED), interactions with γ are electromagnetic, and particles coupled to γ carry an electric charge (or simply charge). Finally, there are weak charged current (CC) interactions with $W^{\pm}$ (an exchange of an electric charge, a charged combination of interacting fermions) and weak neutral current (NC) interactions with Z.[1] They are expressed as chiral gauge interactions acting on left-handed components of related fermionic fields grouped into "flavor" doublets to describe the observed (maximal) parity, P, violation in the weak processes (β-decay). The formulation of CC and NC interactions (the weak part of the EWT or the SM) is sometimes referred to as quantum flavordynamics (QFD).

Elementary fermions of spin 1/2 are divided into quarks (subjects to all SM interactions, strong + electroweak) and leptons (subjects to electroweak interactions only). They occur in three generations of identical properties differentiated only by unequal masses. The ex-

[1] NC sometimes refers to interactions mediated by both Z (weak NC) and γ (electromagnetic NC) as they are both electrically neutral (no exchange of electric charge). This text uses the convention from Ref. [18] and distinguishes between NC and electromagnetic (QED) interactions, for neutrinos do not have an electric charge, and they do not couple to γ and do not participate in electromagnetic interactions.

istence of these three generations is a mere experimental fact with no explicit dynamical, cosmological, ontological, or other theoretical cause. However, fourth and further fermionic generations are mostly considered unlikely.[2]

The last SM ingredient is the Higgs mechanism [19, 20] of the particle masses "generation". The property of "mass" manifests as particle coupling with a scalar (Higgs) field, which has a symmetric potential and non-zero vacuum expectation value (non-invariant ground state). Such "spontaneously broken (hidden) symmetry" of $SU(2)_L \otimes U(1)_Y$ instinctively justifies the masses of the vector bosons, and it materializes as a scalar boson in the spectrum of elementary particles (at least one as in the SM). Fermion masses come from supplementary Yukawa couplings with the field. See Ref. [18, Chapter 6] for further information.

Each massive and charged elementary particle of the SM has an antiparticle partner with opposite additive quantum numbers (such as charge) and identical dynamical quantum numbers (such as spin). The corresponding operator, charge conjugation C, transforms one into another. In this sense, all neutral bosons are their own antiparticles, and the term "antiparticle" does not have a clear interpretation for them. Since neutrinos are also neutral, it might be they are, in contrast to other fermions, their own antiparticles too. That would allow total lepton number violating processes (*e.g.* neutrinoless double β-decay, see Ref. [4, Chapter 8]), and this type of neutrinos are described as Majorana particles in theory. Still, no such processes have been observed yet.

The complete set of the SM elementary particles, their properties, interactions, and relations are illustrated by Fig. 1.1. By the topic of this thesis and this section, the following text focuses on the neutrinos and their features only, *i.e.* lepton mixing, neutrino oscillations, and neutrino masses. For more details on QCD, QED, Higgs physics, quark physics, and mixing, please refer to Refs. [14, 18, 21].

1.1.1 Neutrino interactions

The SM interactions of neutrino fields ν (ν_L, ν_R are the left- and right-handed chiral components)[3] are described by the leptonic CC (via $W^{\pm}$) interaction part of the SM Lagrangian between neutrinos and corresponding charged leptons l [18]

$$\mathcal{L}^{(\mathrm{CC})}_{\mathrm{int,lep}} = -\frac{g}{2\sqrt{2}} \sum_{\alpha} \bar{\nu}_{\alpha} \gamma^{\lambda} (1-\gamma_5) l_{\alpha} W^{+}_{\lambda} + \mathrm{h.c.} = -\frac{g}{\sqrt{2}} \sum_{\alpha} \bar{\nu}_{\alpha L} \gamma^{\lambda} l_{\alpha L} W^{+}_{\lambda} + \mathrm{h.c.} \tag{1.1}$$

and by the neutrino NC (via Z) interaction part [18]

$$\mathcal{L}^{(\mathrm{NC})}_{\mathrm{int},\nu} = -\frac{g}{4\cos\theta_{\mathrm{W}}} \sum_{\alpha} \bar{\nu}_{\alpha} \gamma^{\lambda} (1-\gamma_5) \nu_{\alpha} Z_{\lambda} = -\frac{g}{2\cos\theta_{\mathrm{W}}} \sum_{\alpha} \bar{\nu}_{\alpha L} \gamma^{\lambda} \nu_{\alpha L} Z_{\lambda}, \tag{1.2}$$

where γ^{λ} are the Dirac γ matrices in the standard representation, $\gamma_5 \equiv \mathrm{i}\gamma^0\gamma^1\gamma^2\gamma^3$, and g is the weak $SU(2)_L$ coupling constant related to the Fermi coupling constant G_{F} and the W mass m_{W} as $G_{\mathrm{F}} = g^2/4\sqrt{2}m^2_{\mathrm{W}}$, and θ_{W} is the Weinberg mixing angle. With the Einstein notation, all terms are summed over λ, and h.c. is an abbreviation for their hermitian conjugates.

There are three active lepton flavors α engaged in the weak interactions. They match the three known charged leptons of electron e, muon μ, and tau τ, *i.e.*, $\alpha = e, \mu, \tau$.

Apparently, only left-handed components of neutrino fields ν_L take part in the SM interactions. The SM does not originally contain any ν_R singlets, and neutrinos are assumed to be massless (two-component neutrino formalism).

Please note that for many considerations in the following text, NC interactions of Eq. (1.2) are often left out by any of the common reasons: they do not discriminate between the

[2] The current limits on the fourth gen. masses of quarks and heavy charged leptons can be found in Ref. [7].

[3] Using the standard $\psi = \psi_L + \psi_R$, where $\psi_L = P_L\psi = \frac{1-\gamma_5}{2}\psi$ is the left-handed component of a fermionic field ψ and P_L is the left-hand projection operator (ψ_R and P_R accordingly).

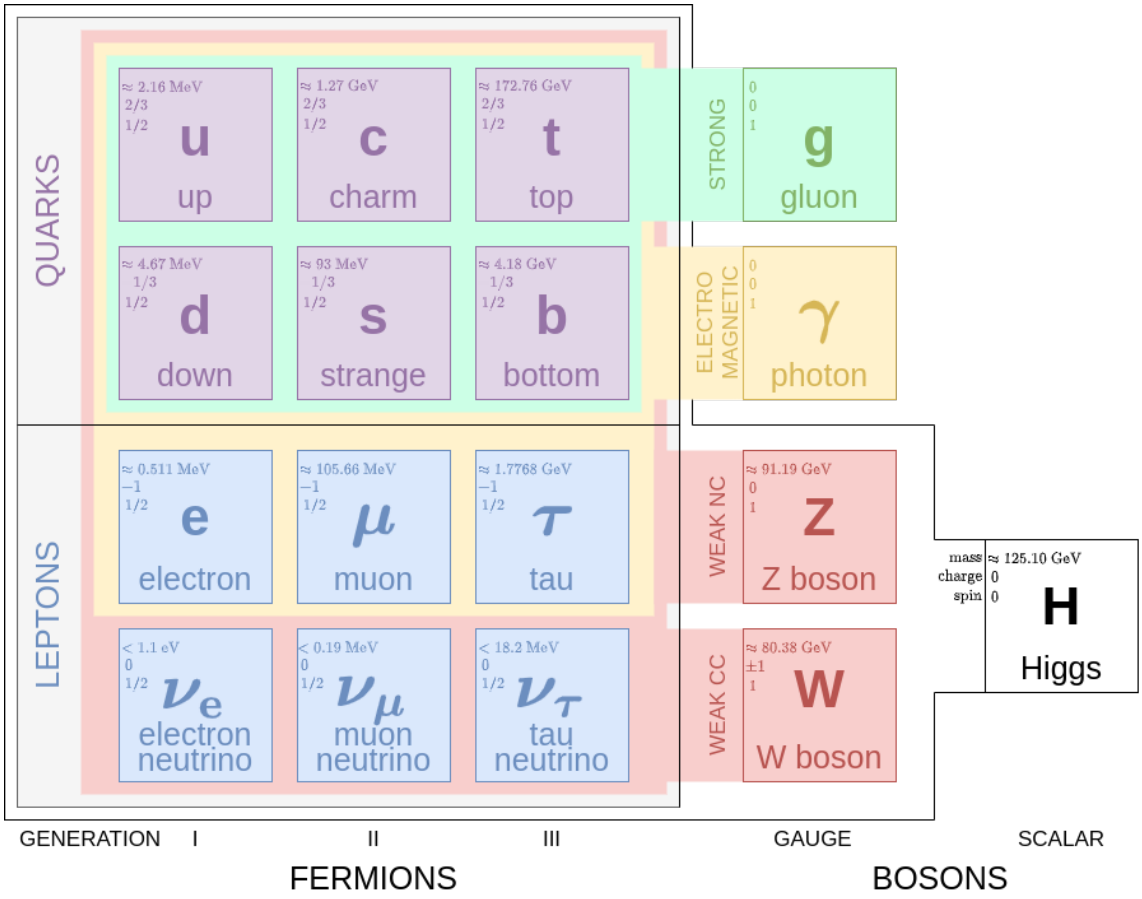

Figure 1.1: Diagram illustrating the elementary particles of the SM and their properties. The left part shows three generations of elementary fermions. Each consists of a pair (left-handed weak flavor doublet) of quarks (upper, purple) and a pair of leptons (lower, blue) to illustrate the corresponding doublets for left-handed chiral fields. Right-handed fields are singlets with vanishing coupling constants in the case of neutrinos. The right part shows the bosons of the SM, gauge bosons together with couplings to fermions: strong interaction in green, electromagnetic in yellow, and weak CC and NC in red. One scalar Higgs boson responsible for the generation of masses of fermions, $W^{\pm}$, and Z is in white. The stated masses are taken from Ref. [7].

neutrino flavors, the relevant NC part of the SM Lagrangian is analogic to the CC part, or it is in some other way unequivocal, trivial, or uninteresting.

1.1.2 Neutrino masses

Dictated by the observation of neutrino flavor transitions (see Section 1.3) and their presumable implication of non-zero neutrino masses, the SM has to be properly extended. Relevant neutrino mass terms need to be introduced into the SM Lagrangian. Theoretically, they can be constructed in many different ways. Yet, they always require new SM objects (at least one right-handed ν_R).[4]

The easiest way is to add the corresponding ν_R, SM non-interacting (sterile) singlets, to the existing ν_L (*i.e.* to add the right-handed components of hypothetical four-spinor neutrino

[4] *N.b.*, without additional particle content or ν_R, the mass terms of ν_L can be inserted into the SM Lagrangian only by breaking its gauge invariance or renormalizability (mass terms of ν_L only are not renormalizable), see Ref. [3, p. 205–208].

fields). They would immediately combine into the so-called Dirac mass terms of the form $\bar{\nu}_L \nu_R + \bar{\nu}_R \nu_L$ similarly to other fermions in the SM. It leads to [3, Chapter 6]

$$\mathcal{L}^{(\text{Dirac})}_{\text{mass},\nu} = -\sum_{\alpha,\beta} \bar{\nu}_{\alpha L} D_{\alpha\beta} \nu_{\beta R} + \text{h.c.} = -\sum_{i}^{3} m_i (\bar{\nu}_{iL} \nu_{iR} + \bar{\nu}_{iR} \nu_{iL}) = -\sum_{i}^{3} m_i \bar{\nu}_i \nu_i, \tag{1.3}$$

where α, β go over the lepton flavors e, μ, τ and D is the (Dirac-like) mass matrix, not necessarily diagonal. The neutrino masses m_i are well-defined w.r.t. the neutrino mass eigenstates ν_i. The relations between the neutrino components of the flavor doublets $\nu_{\alpha L}$ and ν_i are obtained by diagonalizing D. For the yet present gaps in understanding the true nature of neutrinos, it would be better and instructive to examine a more comprehensive approach to the problem.

In fact, Dirac masses of Eq. (1.3) can be seen as a special solution to a general Majorana case[5] (see Ref. [5, p. 27]). Let, *e.g.*,

$$\nu_L = \begin{pmatrix} \nu_{eL} \\ \nu_{\mu L} \\ \nu_{\tau L} \\ \vdots \\ \nu_{n_L L} \end{pmatrix}, \qquad \nu_R = \begin{pmatrix} \nu_{eR} \\ \nu_{\mu R} \\ \nu_{\tau R} \\ \vdots \\ \nu_{n_R R} \end{pmatrix} \tag{1.4}$$

be vectors of n_L left- and n_R right-handed components in the weak flavor space, respectively. Only ν_L would represent the active neutrinos, *i.e.* the subjects to the SM weak interactions (and $n_L \geq 3$), and ν_R are sterile.[6] Then, for $n = n_L + n_R$ with a $n \times n$ complex symmetric mass matrix M, the neutrino mass term is [3, Chapter 6]

$$\mathcal{L}^{(\text{Majorana})}_{\text{mass},\nu} = -\frac{1}{2} \bar{\boldsymbol{\nu}}_{\boldsymbol{L}} M \boldsymbol{\nu}^{C}_{\boldsymbol{R}} + \text{h.c.} = -\frac{1}{2} \sum_{i}^{n} m_i \bar{\nu}^{\text{M}}_i \nu^{\text{M}}_i, \tag{1.5}$$

where the bold symbols for the vectors of fields are defined as $\boldsymbol{\nu_L} = \left(\nu_L, \nu^C_R\right)^\top$, $\boldsymbol{\nu_R} = \left(\nu^C_L, \nu_R\right)^\top$ with ν^C being the charge conjugated field $\nu^C \equiv C\bar{\nu}^\top$, and C is the charge conjugation matrix. M is composed of three sub-matrices M_L ($n_L \times n_L$), M_R ($n_R \times n_R$) and D ($n_L \times n_R$)

$$M = \begin{pmatrix} M_L & D \\ D^\top & M_R \end{pmatrix}, \tag{1.6}$$

with the elements of Dirac (D_{ij}) and Majorana "left-handed" (M_{Lij}) and "right-handed" (M_{Rij}) masses (constants). The Lagrangian of Eq. (1.5) still produces Dirac mass terms of the form $\bar{\nu}_L D \nu_R$ (+h.c.) which could be associated with Yukawa interaction after spontaneous EW symmetry breaking similarly to the charged fermions (Higgs mechanism) [4, p. 57].

The extra Majorana mass terms of $\bar{\nu}_L M_L \nu^C_L$ and $\bar{\nu}^C_R M_R \nu_R$ (+h.c.) can appear as bare terms of the Lagrangian,[7] and they break the lepton number by 2 (two neutrino fields). However, they are allowed only if the neutrinos do not carry any additive charge to be conserved, which seems plausible for neutral neutrinos. The fields have to satisfy the Majorana condition of "particle ≡ antiparticle", see Ref. [3, p. 188–191].

In theory, the number of neutrino weak eigenstates n is not limited, but it should be $n_L \geq 3$ to account for the three observed interacting states. Let the indices of $\boldsymbol{\nu_L}, \boldsymbol{\nu_R}$ iterate first

[5] It is usually called "Majorana-Dirac", whereas "Majorana" is another special solution with vanishing Dirac mass terms ($D = 0$).

[6] It is customary to choose a specific notation for the sterile fields, but it is considered confusing by the author. It brings a particular meaning only for the actual SM.

[7] *N.b.*, they are singlets of the SM gauge group.

through the SM flavors as $e, \mu, \tau, \ldots, n_L$, and denote the rest as $\bar{e}, \bar{\mu}, \bar{\tau}, \ldots, \bar{n}_R$, *i.e.*, $\boldsymbol{\nu_L}_\alpha = \nu_{\alpha L}$ and $\boldsymbol{\nu_L}_{\bar{\alpha}} = \nu^C_{\alpha R}$ if α goes over the flavors to n, and $\bar{\alpha} = \alpha + n_L$, $\boldsymbol{\nu_L}_{\bar{\alpha}} = 0$ for $\bar{\alpha} > n$. If all the original weak flavor combinations $M_{ee}, M_{e\mu}, M_{e\tau}, \ldots, M_{\bar{e}\bar{e}}, \ldots$ of M are 0, then no $\nu_{(e,\mu,\tau)R}$ are needed in conformity with the SM (*i.e.* massless neutrinos if $n = n_L = 3$).

The second equality of Eq. (1.5) identifies the neutrino mass eigenstates ν_i^{M} with masses m_i, where

$$\nu^{\mathrm{M}} = \nu + \nu^C, \quad \nu^{\mathrm{M}} = (\nu^{\mathrm{M}})^C \tag{1.7}$$

are referred to as the Majorana neutrino fields, for they manifestly obey the Majorana condition. Unlike in the case of the charged fields of particle and antiparticle, Majorana neutrinos are described by only one two-component spinor, *i.e.* by one field.[8] There are generally n mass eigenstates with eigenvalues m_i.

Once again, one shall find the relations between the original $\nu_{\alpha L}$ weak eigenstates and ν_i^{M}. Complex and symmetric matrix M can be written as (Autonne–Takagi factorization [22])

$$M = V \begin{pmatrix} m_1 & & & \\ & m_2 & & \\ & & \ddots & \\ & & & m_n \end{pmatrix} V^\top, \tag{1.8}$$

where V is a unitary matrix of dimension n, m_i are real and non-negative masses of ν_i^{M}. *Ergo*,

$$\nu_i^{\mathrm{M}} = \sum_j^n \left(V^*_{ji} \boldsymbol{\nu_L}_j + V_{ji} \boldsymbol{\nu^C_R}_j \right) \tag{1.9}$$

and

$$\nu_\alpha^M = \nu_\alpha + \nu_\alpha^C = \sum_i^n \left[\mathfrak{Re}(V_{\alpha i} + V_{\bar{\alpha} i}) \nu_i^{\mathrm{M}} + \mathfrak{Im}(V_{\alpha i} + V_{\bar{\alpha} i})(\nu_{iL}^{\mathrm{M}} - \nu_{iR}^{\mathrm{M}}) \right],$$

$$\nu_{\alpha L} = P_L \sum_i^n V_{\alpha i} \nu_i^{\mathrm{M}}, \tag{1.10}$$

where P_L is the left projector, $V_{\bar{\alpha} i} = 0$ for $\alpha > n_R$. The sum of the charge conjugated flavor fields, ν_α^{M}, might be interpreted as a Majorana neutrino field of flavor α, and $\nu_{iL}^{\mathrm{M}}, \nu_{iR}^{\mathrm{M}}$ are the left- and right-handed components of the Majorana mass eigenstates ν_i^{M}. The neutrino parts of the weak flavor doublets $\nu_{\alpha L}$ correspond to $\alpha = e, \mu$, or τ.

From this general approach, some subordinate neutrino spectra to comprise the experimentally established SM $\nu_{eL}, \nu_{\mu L}, \nu_{\tau L}$ is to be retrieved by imposing additional assumptions on the matrix M. Examples follow:

- Removing the eligible combinations of mass terms in Eq. (1.5), *i.e.* setting the elements of M to $M_{ij} = 0$ for particular i and j, can effectively reduce the number of $\nu_{\alpha L}$ or $\nu_{\alpha R}$ of Eq. (1.4) by making them obsolete. That is how an $L - R$ asymmetric case, $n_L \neq n_R$, is deduced from a more instinctive $n_L = n_R$.

- For $M_L = 0$ and $M_R = 0$, only Dirac mass terms are allowed, *i.e.* no lepton number violation, and the resulting m_i spectrum is degenerate (degenerate ν_i^{M}). With $n_L = n_R$, the mass eigenstates can be expressed as $n/2$ pure Dirac fields with legitimate right-handed components ν_R (Eq. (1.3) recovery). The relation between $\nu_{\alpha L}$ and ν_i is provided by only $n/2 \times n/2$ matrix to diagonalize D.

[8] Neutrino $\equiv$ antineutrino, although the term "antineutrino" does not have a clear meaning here.

- For $n_R = 0$, there are no Dirac mass terms ($D = 0$), only n_L Majorana mass states and active flavor states. Note that this scenario is not allowed in the SM framework for breaking its renormalizability [3, p. 205–208]. In order to recover it, further extra particle fields ("new physics") are needed.

Specific constrictions can also lead to the popular "See-Saw" mechanism to reclaim a spectrum of the SM light neutrinos ($n_L = 3$) and several (n_R) heavy neutrinos. This See-Saw type I is formulated, *e.g.*, in Ref. [4].

1. Assume there are no left-handed Majorana mass terms, *i.e.*, $M_L = 0$ from Eq. (1.6).
2. Assume the Dirac mass terms are generated by the SM Higgs mechanism.
3. Assume the lepton number conservation is violated at a much larger scale than the EW scale, *i.e.*, the eigenvalues of M_R are much larger than the vacuum expectation of the Higgs field (the Dirac masses), formally denoted as $M_R \gg D$.

With the above,

$$M = \begin{pmatrix} 0 & D \\ D^\top & M_R \end{pmatrix} \tag{1.11}$$

and there are two weight categories of neutrinos: lighter ones with masses proportional to $D^\top M_R^{-1} D$ (three observed light neutrinos) and very heavy neutrinos with masses proportional to M_R.

Note that there are many other theoretical ways to construe neutrino masses or flavor transitions in particular. The popularity of the one revealed here is based on its sufficient generality without the need of any extra exotic SM content (notably at the EW scale) or the need for revisions of even more fundamental concepts (*e.g.* Lorentz invariance). The See-Saw mechanism is one of the simplest theoretical extensions for which the SM might be considered a good effective low energy model.

1.1.3 Lepton mixing

With n neutrino mass eigenstates denoted ν_i from now on, $\nu_1, \nu_2, \nu_3, \ldots, \nu_n$, $n \geq 3$, and three active lepton flavors $\alpha = e, \mu, \tau$, the $\mathcal{L}^{(\mathrm{CC})}_{\mathrm{int,lep}}$ of Eq. (1.1) can be recast as

$$\mathcal{L}^{(\mathrm{CC})}_{\mathrm{int,lep}} = -\frac{g}{2\sqrt{2}} \sum_{\alpha,i} \bar{l}_\alpha \gamma^\lambda (1 - \gamma_5) U_{\alpha i} \nu_i W^-_\lambda + \mathrm{h.c.}, \tag{1.12}$$

where U is a $3 \times n$ complex matrix satisfying the unitary condition $UU^\dagger = \mathbb{1}_{3\times 3}$, but not necessarily $U^\dagger U = \mathbb{1}_{n\times n}$. $U_{\alpha i}$ are immediately identified as the corresponding $V_{\alpha i}$.[9]

A $3 \times n$ complex matrix has $6n$ real parameters. The $UU^\dagger = \mathbb{1}_{3\times 3}$ represents nine independent real conditions,[10] *i.e.*, $3(2n - 3)$ parameters are independent, out of which $3(n - 2)$

[9] Mixing of charged leptons is a more general case of the neutrino only mixing. But, no Majorana mass terms are allowed for charged leptons, and the numbers of their mass and interaction eigenstates are equal. Then Eq. (1.12) is written in the basis of lepton mass eigenstates (instead of flavor states) with a general U of

$$U_{ji} \propto \sum_\alpha \left(V^l_{j\alpha}\right)^\dagger V_{\alpha i},$$

where α goes over the weak flavors (e, μ, τ for three charged leptons) and V^l is to diagonalize the would-be non-diagonal lepton mass matrix in the flavor basis, *e.g.*, see [12]. Provided charged leptons undergo the SM interactions only, their mass states are directly identified as the interaction flavor states, and there is effectively no mixing.

[10] 3 (normalization) + $2\cdot\binom{3}{2}$ (orthogonality)

parameters are rotational angles,[11] and the rest are phases. Three of $3(n-1)$ phases are physically irrelevant, for they can be arbitrarily fixed by phase redefinition of the three charged lepton fields l_α. Moreover, for degenerate neutrino mass states, the number of relevant phases is further reduced by up to $n-1$ for Dirac neutrinos in general. In conclusion, for $n \geq 3$, there are $3(n-2)$ physically independent rotational angles and $3(n-2)$ phases ($2n-5$ for Dirac neutrinos).

1.1.4 CP symmetry in lepton sector

From the form of $\mathcal{L}^{(\mathrm{CC})}_{\mathrm{int,lep}}$ in Eq. (1.12), one can deduce the conditions on CP invariance in the leptonic sector. For the sake of brevity, please consult Refs. [3, 4] for the full algebraic gymnastics. From a somewhat simplified perspective, the first and the h.c. term of Eq. (1.12) describe two CP conjugated transitions

$$l^+_\alpha \to \bar{\nu}_i + W^+, \quad l^-_\alpha \to \nu_i + W^-, \tag{1.13}$$

with amplitudes proportional to $U_{\alpha i}$ and $U^*_{\alpha i}$. One would therefore expect that CP invariance holds if $U_{\alpha i} \sim U^*_{\alpha i}$. In fact, the rigorous condition is

$$U^*_{\alpha i} = U_{\alpha i}, \quad U^*_{\alpha i} = \rho_i U_{\alpha i} \tag{1.14}$$

for Dirac and Majorana neutrinos, respectively, where $\rho_i = \pm 1$, depending on the phase factor signs of the Majorana neutrino fields ν^{M}_i.

1.2 Mixing and oscillations in three neutrinos paradigm

There is no fundamental reason or symmetry principle that would constrain the number of neutrinos to three. Nevertheless, in the sense of Occam's razor, most of the experimental observations (the invisible decay width of Z [23], flavor transitions in Section 1.3) are currently best explained by a model of three active neutrino flavor eigenstates that couple to the SM gauge bosons $W^\pm$ and Z and three neutrino mass eigenstates connected via matrix U with 3×3 elements.

Provided the theoretical grounds of the previous Section 1.1 are viable, the minimal three neutrinos spectrum is a good effective or even exact model for several possibly realized scenarios (using the notation from Subsection 1.1.2):

- There are only three Dirac neutrinos with tiny masses, $n_L = n_R = 3$, $M_L = M_R = 0$.
- There are only three pure Majorana mass states (as discussed, this scenario would still require a revision of the SM and its content), $n_L = 3, n_R = 0$.
- (See-Saw) There are three light active neutrinos and a number of heavy sterile neutrinos, *i.e.*, $n_L = 3, M_L = 0, M_R \gg D$. Then, U cannot be unitary. However, the "violation" of the unitary conditions would be of the order (formally) $\mathcal{O}(D/M_R)$, see Eq. (1.11).
- Solutions similar to the previous point of a mass spectrum with three isolated neutrinos, where the rest have masses at much different scales, could manifest as an effective three neutrinos mixing with small unitarity violation.

Throughout the text from now on, the three neutrinos paradigm (3ν-paradigm) is used in its standard formulation. The three active neutrino flavors are identified, by definition, in weak CC interactions with the corresponding charged leptons ($e \leftrightarrow \nu_e$, $\mu \leftrightarrow \nu_\mu$, $\tau \leftrightarrow \nu_\tau$).

[11] The independent parameters in a real matrix, *i.e.* $3n$ parameters minus $6 = 3 + \binom{3}{2}$ unitary conditions.

This flavor representation $\boldsymbol{\nu}_f \equiv (\nu_e, \nu_\mu, \nu_\tau)^\top$ is related to the neutrino mass representation $\boldsymbol{\nu}_m \equiv (\nu_1, \nu_2, \nu_3)^\top$ as

$$\boldsymbol{\nu}_f = U\boldsymbol{\nu}_m, \tag{1.15}$$

or in terms of the neutrino quantum states (flavor and mass eigenstates):

$$|\nu_i\rangle = \sum_\alpha U_{\alpha i}|\nu_\alpha\rangle, \qquad |\nu_\alpha\rangle = \sum_i U^*_{\alpha i}|\nu_i\rangle, \qquad (\alpha = e,\mu,\tau; \quad i = 1,2,3), \tag{1.16}$$

where $U_{\alpha i}$ are the elements of U. The three neutrino mass eigenstates $|\nu_i\rangle$ have well-defined masses m_i, and they are assumed to be orthonormal (with Kronecker δ):

$$\langle\nu_i|\nu_j\rangle = \delta_{ij}. \tag{1.17}$$

1.2.1 U_{PMNS} mixing matrix

In the 3ν-paradigm, U has up to six independent parameters. Most commonly, U is conveniently parametrized with the use of three mixing angles θ_{ij}, a complex phase δ_{CP}, and two Majorana phases a, b. It is a product of three rotational matrices $U_{ij}(\theta_{ij})$, $I_{\delta_{\text{CP}}} \equiv \text{diag}(1, 1, \exp(\text{i}\delta_{\text{CP}}))$, and $I_A \equiv \text{diag}(\exp(\text{i}a/2), \exp(\text{i}b/2), 1)$. With $\text{c}_{ij}, \text{s}_{ij} \equiv \cos\theta_{ij}, \sin\theta_{ij}$, this can be written as [3, 4, 5, 6, 7]

$$U = \begin{pmatrix} U_{e1} & U_{e2} & U_{e3} \\ U_{\mu 1} & U_{\mu 2} & U_{\mu 3} \\ U_{\tau 1} & U_{\tau 2} & U_{\tau 3} \end{pmatrix} = U_{23}(\theta_{23}) I_{\delta_{\text{CP}}} U_{13}(\theta_{13}) I^*_{\delta_{\text{CP}}} U_{12}(\theta_{12}) I_A =$$

$$= \begin{pmatrix} 1 & & \\ & c_{23} & s_{23} \\ & -s_{23} & c_{23} \end{pmatrix} \begin{pmatrix} c_{13} & & s_{13}\text{e}^{-\text{i}\delta_{\text{CP}}} \\ & 1 & \\ -s_{13}\text{e}^{+\text{i}\delta_{\text{CP}}} & & c_{13} \end{pmatrix} \begin{pmatrix} c_{12} & s_{12} & \\ -s_{12} & c_{12} & \\ & & 1 \end{pmatrix} \begin{pmatrix} \text{e}^{\text{i}\frac{a}{2}} & & \\ & \text{e}^{\text{i}\frac{b}{2}} & \\ & & 1 \end{pmatrix} =$$

$$= \begin{pmatrix} c_{13}c_{12} & c_{13}s_{12} & s_{13}\text{e}^{-\text{i}\delta_{\text{CP}}} \\ -c_{23}s_{12} - s_{13}c_{12}s_{23}\text{e}^{+\text{i}\delta_{\text{CP}}} & c_{23}c_{12} - s_{13}s_{12}s_{23}\text{e}^{+\text{i}\delta_{\text{CP}}} & c_{13}s_{23} \\ s_{23}s_{12} - s_{13}c_{12}c_{23}\text{e}^{+\text{i}\delta_{\text{CP}}} & -s_{23}c_{12} - s_{13}s_{12}c_{23}\text{e}^{+\text{i}\delta_{\text{CP}}} & c_{13}c_{23} \end{pmatrix} \times \begin{pmatrix} \text{e}^{\text{i}\frac{a}{2}} & & \\ & \text{e}^{\text{i}\frac{b}{2}} & \\ & & 1 \end{pmatrix}, \tag{1.18}$$

where $\theta_{ij} \in [0, \pi/2]$ and $\delta_{\text{CP}}, a, b \in [0, 2\pi]$. If neutrinos are Dirac-like particles, Majorana phases a and b are absorbed in their physical states, and there is effectively only one phase, δ_{CP} (or $I_A = \mathbb{1}$). Then, the neutrino mixing matrix U is completely analogous to the quark mixing matrix V_{CKM} except for the sizes of individual elements, and it is usually referred to as the Pontecorvo-Maki-Nakagawa-Sakata (PMNS, U_{PMNS}) mixing matrix:

$$U_{\text{PMNS}} = \begin{pmatrix} c_{13}c_{12} & c_{13}s_{12} & s_{13}\text{e}^{-\text{i}\delta_{\text{CP}}} \\ -c_{23}s_{12} - s_{13}c_{12}s_{23}\text{e}^{+\text{i}\delta_{\text{CP}}} & c_{23}c_{12} - s_{13}s_{12}s_{23}\text{e}^{+\text{i}\delta_{\text{CP}}} & c_{13}s_{23} \\ s_{23}s_{12} - s_{13}c_{12}c_{23}\text{e}^{+\text{i}\delta_{\text{CP}}} & -s_{23}c_{12} - s_{13}s_{12}c_{23}\text{e}^{+\text{i}\delta_{\text{CP}}} & c_{13}c_{23}. \end{pmatrix}. \tag{1.19}$$

1.2.2 Neutrino oscillations in vacuum

Supported by experimental evidence (Section 1.3), lepton flavor is not conserved in neutrino propagation. That is a prompt consequence of the neutrino mixing, which leads to neutrino flavor oscillations as a function of space-time coordinates.

A neutrino of energy E produced in a source through a weak CC interaction with a charged lepton l_α travels to a distance L, where it undergoes another CC interaction with a charged lepton l_β. *Ipso facto*, the neutrino is born as ν_α (a coherent sum $\sum_i U^*_{\alpha i}\nu_i$) and transforms into ν_β (a coherent sum $\sum_i U^*_{\beta i}\nu_i$), Fig. 1.2.

With the prevalent assumption that $|\nu\rangle$ is a plane wave [12], *i.e.*

$$|\nu_i(t)\rangle = \exp(-\mathrm{i}E_i t)|\nu_i(0)\rangle, \tag{1.20}$$

and ultrarelativistic ($m_i \ll E$), *i.e.*, the neutrino momentum $p_i \simeq p_j \equiv p \simeq E$, then $E_i \simeq p + \dfrac{m_i^2}{2E}$ is the energy of the i-th mass eigenstate, and $t \simeq L$. It is straightforward to compute the probability of the $\nu_\alpha \to \nu_\beta$ transition (for the standard derivation, see Refs. [3, 5, 8, 12], for more detailed discussions of the quantum mechanical description aspects and subtleties, *e.g.*, see Refs. [9, 10, 24]).

Let $S(t)$ be the evolution matrix for an arbitrary neutrino state $|\nu\rangle$ such that

$$|\nu(t)\rangle = S(t)|\nu(0)\rangle. \tag{1.21}$$

Then, from Eqs. (1.16) and (1.20), the elements of S in the neutrino flavor basis are

$$S_{\beta\alpha}(t) = S_{\beta\alpha}(L \simeq t, E) = \langle\nu_\beta|\nu_\alpha(L \simeq t, E)\rangle = \sum_{i=1}^{3} U^*_{\alpha i} U_{\beta i} \exp\left(-\mathrm{i}E_i L\right), \tag{1.22}$$

and the probability of $\nu_\alpha \to \nu_\beta$ is

$$\begin{aligned} P(\nu_\alpha \to \nu_\beta; L, E) &= \left|S_{\beta\alpha}(L, E)\right|^2 = \left|\sum_{i=1}^{3} U^*_{\alpha i} U_{\beta i} \exp(-\mathrm{i}E_i L)\right|^2 = \\ &= \left|\exp\left(-\mathrm{i}pL\right) \cdot \sum_{i=1}^{3} U^*_{\alpha i} U_{\beta i} \exp\left(-\mathrm{i}\frac{m_i^2}{2E} L\right)\right|^2 = \\ &= \sum_{i=1}^{3}\sum_{j=1}^{3} U^*_{\alpha i} U_{\alpha j} U_{\beta i} U^*_{\beta j} \exp\left(-\mathrm{i}\frac{\Delta m_{ij}^2}{2E} L\right), \end{aligned} \tag{1.23}$$

where Δm_{ij}^2 are the differences of squared neutrino masses

$$\Delta m_{ij}^2 = m_i^2 - m_j^2. \tag{1.24}$$

Using the orthonormality of neutrino mass eigenstates, $\langle\nu_i|\nu_j\rangle = \delta_{ij}$, one can arrive to a somewhat more popular form of Eq. (1.23):

$$\begin{aligned} P(\nu_\alpha \to \nu_\beta; L, E) = \delta_{\alpha\beta} &- 4\sum_{i>j} \mathfrak{Re}(U^*_{\alpha i} U_{\alpha j} U_{\beta i} U^*_{\beta j}) \sin^2\left(\frac{\Delta m_{ij}^2}{4E} L\right) + \\ &+ 2\sum_{i>j} \mathfrak{Im}(U^*_{\alpha i} U_{\alpha j} U_{\beta i} U^*_{\beta j}) \sin\left(\frac{\Delta m_{ij}^2}{2E} L\right). \end{aligned} \tag{1.25}$$

Not conserving the lepton flavor means $P(\nu_\alpha \to \nu_\alpha; L, E) \neq 1$ and $P(\nu_\alpha \to \nu_\beta; L, E) \neq 0$ for $\alpha \neq \beta$. From Eqs. (1.23) and (1.25), this occurs only and only if the corresponding off-diagonal elements of U and also Δm_{ij}^2 are non-zero. That means a non-trivial mixing of lepton flavor in weak CC interactions ($U_{\mathrm{PMNS}} \neq \mathbb{1}$), and that some of the neutrino mass eigenstates have non-vanishing masses (*i.e.*, neutrinos cannot be massless as previously assumed by the SM).

Furthermore, from Eq. (1.25), it is clear that $P(\nu_\alpha \to \nu_\beta; L, E)$ has oscillatory patterns. It is a function of L (or L/E in general) with oscillation lengths

$$L_{ij}^{\mathrm{osc}} = \frac{4\pi E}{|\Delta m_{ij}^2|} \tag{1.26}$$

and amplitudes proportional to the elements of $U_{\rm PMNS}$, *i.e.* the mixing parameters θ_{ij} and $\delta_{\rm CP}$. This phenomenon is known as "neutrino oscillations". A typical neutrino oscillation experiment observes a reduction in the flux of neutrinos of the produced flavor (disappearance $\nu_\alpha \to \nu_\alpha$) or an increase in the neutrino flux of different flavors (appearance $\nu_\alpha \to \nu_\beta$) as a function of reconstructed energy E at a distance L. The actual probability is then averaged over the neutrino energy spectrum in minimal intervals determined by the detector energy resolution $\langle P(\nu_\alpha \to \nu_\beta; E_{\rm min}, E_{\rm max})\rangle$.

As there are only three independent neutrino masses m_i in the 3ν-paradigm, there are consequently two independent squared mass differences Δm^2_{ij} and two typical oscillation lengths $L^{\rm osc}_{ij}$. Their estimates are later stated in Sections 1.3 and 1.4.

It is worth noting that the amplitude in Eq. (1.23) is independent of the Majorana phases a and b.[12] *Ergo*, oscillations of Dirac and Majorana neutrinos have exactly the same manifestation, and the transition probabilities are insensitive to the possible Majorana nature of neutrinos. Without losing generality, $U_{\rm PMNS}$ of Eq. (1.19) describe oscillations for both types of neutrinos, and, for the sake of brevity, let U denote the mixing matrix in general. In this context, "antineutrino" transition ($\bar\nu_\alpha \to \bar\nu_\beta$) is a charge conjugated process to the neutrino transition. It is customary to call ultrarelativistic Majorana neutrinos with negative helicity "neutrinos", $|\nu(p)\rangle \equiv |\nu(p,-)\rangle$, and Majorana neutrinos with positive helicity "antineutrinos", $|\bar\nu(p)\rangle \equiv |\nu(p,+)\rangle$, with the helicity sign $\pm$, see [3, p. 198]. The further text uses this convention and will not distinguish between Dirac and Majorana (anti)neutrinos unless stated otherwise.

To obtain equivalent oscillation probabilities to Eq. (1.23) for antineutrinos, one can employ the CPT theorem or replace $U \to U^*$:

$$P(\bar\nu_\alpha \to \bar\nu_\beta; L, E) = P(\nu_\beta \to \nu_\alpha; L, E). \tag{1.27}$$

Probabilities of CP conjugated transitions require $U = U^*$ to be equal. For one complex phase $\delta_{\rm CP}$, there is only one

$$\Delta P_{\rm CP}(L,E) = P(\nu_\alpha \to \nu_\beta; L, E) - P(\bar\nu_\alpha \to \bar\nu_\beta; L, E) = \tag{1.28}$$
$$= 2\sin\delta_{\rm CP}\cos\theta_{13}\sin 2\theta_{13}\sin 2\theta_{23}\sin 2\theta_{12}\sin\left(\frac{\Delta m^2_{31}}{E}L\right)\sin\left(\frac{\Delta m^2_{32}}{E}L\right)\sin\left(\frac{\Delta m^2_{21}}{E}L\right).$$

It vanishes with any of the oscillation parameters equal to 0 and also with $\delta_{\rm CP} = \pi$ or $\theta_{13} = \pi/2$. On the other hand, $\delta_{\rm CP} = \pi/2$ or $3\pi/2$ results in maximal CP violation w.r.t. $\delta_{\rm CP}$.

If the 3ν-paradigm provides a complete description of neutrino mixing, *i.e.*, there are three active neutrino flavor states and only three neutrino mass states, U is unitary, $\langle\nu_\alpha|\nu_\beta\rangle = \delta_{\alpha\beta}$, and

$$\sum_{\beta=e,\mu,\tau} P(\nu_\alpha \to \nu_\beta; L, E) = 1 = \sum_{\beta=e,\mu,\tau} P(\nu_\beta \to \nu_\alpha; L, E). \tag{1.29}$$

To summarize this subsection, neutrino flavor transitions in the 3ν-paradigm have oscillatory patterns that are fully described by six physical parameters: three lepton mixing angles θ_{12}, θ_{13}, and θ_{23}, one CP-violating mixing phase $\delta_{\rm CP}$, and two independent squared mass differences Δm^2_{21} and Δm^2_{32} (or Δm^2_{31}).

1.2.3 Neutrino oscillations in medium

When propagating in a medium, neutrinos can interact with its constituents through weak coherent forward scattering illustrated by Fig. 1.3. The medium remains unchanged in coherent interactions. That allows for the interference of the forward scattered and unscattered

[12] $\sum_i (U_{\rm PMNS} I_A)^*_{\alpha i}(U_{\rm PMNS} I_A)_{\beta i} = (U_{\rm PMNS} I_A I_A^\dagger U^\dagger_{\rm PMNS})_{\beta\alpha} = (U_{\rm PMNS} U^\dagger_{\rm PMNS})_{\beta\alpha} = \sum_i (U_{\rm PMNS})^*_{\alpha i}(U_{\rm PMNS})_{\beta i}$ with I_A from Eq. (1.18).

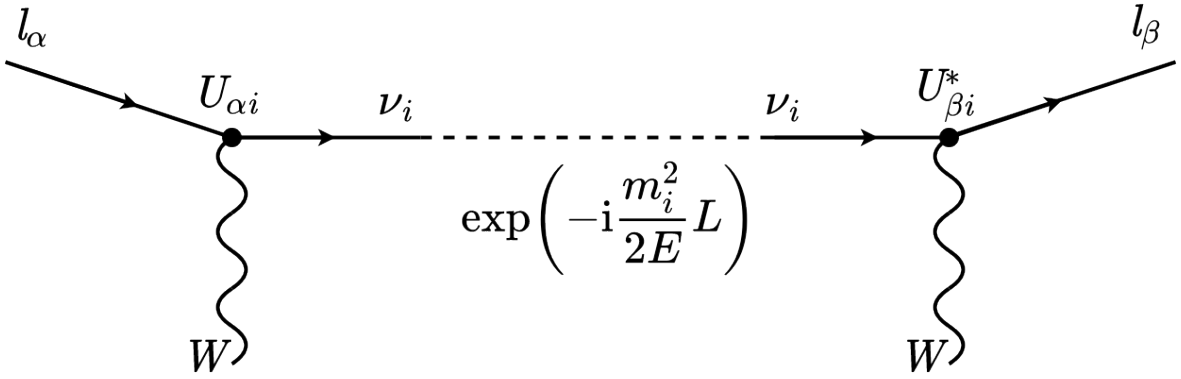

Figure 1.2: Feynmann-like diagram of a ν_i contribution to the $\nu_\alpha \to \nu_\beta$ flavor transition.

neutrinos affecting the phase velocity of the neutrino wave, *i.e.*, neutrinos have different effective masses in matter from those in vacuum. They can be expressed in terms of effective potentials of particular scattering processes, which are proportional to the Fermi coupling constant G_F and densities of the scattering targets.

Neutrino flavor transitions and oscillation probabilities depend only on the relative phases of neutrino eigenstates $(\theta_{ij}, \delta_\mathrm{CP}, \Delta m^2_{ij})$, and they will not be modified by NC interactions treating all active neutrino flavors universally [13, p. 3]. Assuming the medium is a real unpolarized matter of e, p, and n with zero average particle momenta, only $\nu_e + e \to \nu_e + e$ CC interactions are relevant. In low-energy limit ($E < m_W$, the mass of W), this is interpreted as a contribution to the ν_e potential energy given by [13]

$$V_e(x) = \sqrt{2} G_\mathrm{F} N_e(x), \tag{1.30}$$

where $N_e(x)$ is the electron density at x.[13] For $\bar{\nu}_e$, one can simply swap $V_e(x) \to -V_e(x)$.

Adding these considerations, an effective Hamiltonian $\mathcal{H}$ describing neutrino propagation in matter is [13]

$$\mathcal{H} = H + U^\dagger \begin{pmatrix} V_e(x) & & \\ & 0 & \\ & & 0 \end{pmatrix} U = \frac{1}{2E} \left[\begin{pmatrix} m_1^2 & & \\ & m_2^2 & \\ & & m_3^2 \end{pmatrix} + U^\dagger \begin{pmatrix} 2EV_e(x) & & \\ & 0 & \\ & & 0 \end{pmatrix} U \right], \tag{1.31}$$

where H is the kinetic (vacuum) Hamiltonian in the basis of the three neutrino mass eigenstates, and mixing matrix U transforms $V_e(x)$ from the flavor basis. Since the time evolution of an arbitrary neutrino state follows Schrödinger's equation

$$\mathrm{i}\frac{\mathrm{d}}{\mathrm{d}t}|\nu(t)\rangle = \mathcal{H}|\nu(t)\rangle, \qquad |\nu(t)\rangle = \exp(-\mathrm{i}\mathcal{H}t)|\nu(0)\rangle = \mathcal{S}(t)|\nu(0)\rangle, \tag{1.32}$$

the new effective matter Hamiltonian $\mathcal{H}$ needs to be diagonalized in order to identify the propagation basis (*i.e.* the instataneous neutrino mass eigenstates in matter) and to calculate the evolution matrix $\mathcal{S}$ and the transition probabilities $P(\nu_\alpha \to \nu_\beta)$. This represents an *a posteriori* understanding of matter effects in neutrino oscillations in the sense that the evolution of a neutrino state is described relative to the medium properties at particular spatial coordinates x.

There is a vast theoretical and phenomenological background to the neutrino oscillations in matter, diagonalization of $\mathcal{H}$, solving Eq. (1.32), and obtaining $P(\nu_\alpha \to \nu_\beta)$, none of which will be discussed here. For more information on this topic in general, please discuss Refs. [13, 25, 26], on adiabatic flavor transitions and Mikheev-Smirnov-Wolfenstein (MSW) effect Refs. [13, 27], on methods of $\mathcal{H}$ diagonalization or obtaining effective matter oscillation parameters Ref. [13], on analytical calculation of $P(\nu_\alpha \to \nu_\beta)$ Refs. [28, 29].

[13] $V_\mu(x), V_\tau(x) = 0$ since $N_\mu(x), N_\tau(x) = 0$, as no μ or τ are present in the medium.

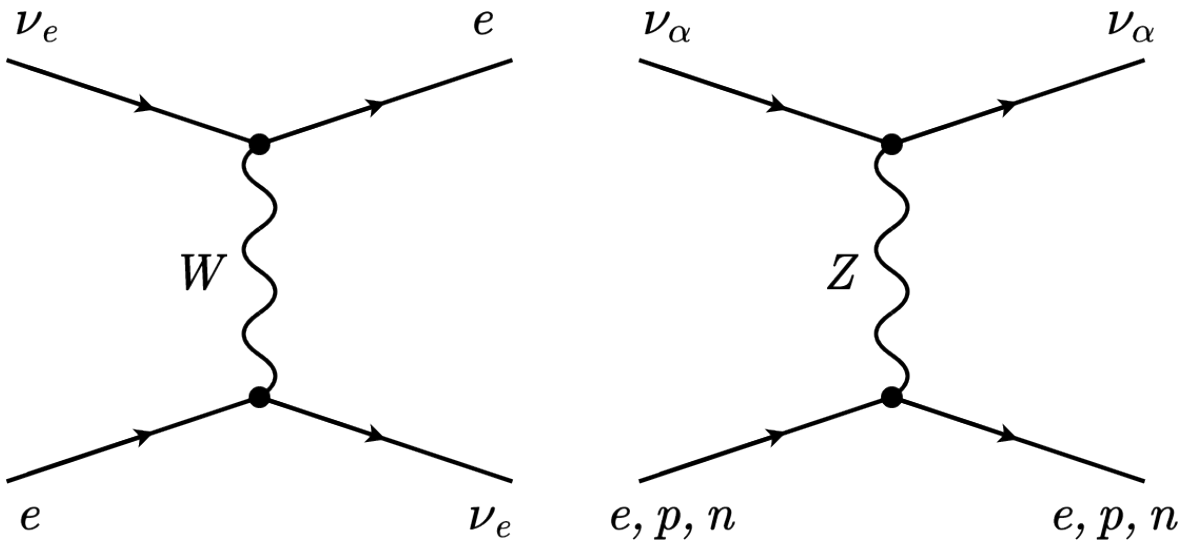

Figure 1.3: Feynmann diagrams of neutrino weak interactions in medium of CC forward scattering on e mediated by W (left) and NC scattering mediated by Z (right).

1.3 Experimental evidence of neutrino flavor transitions

There have been many direct and indirect observations of neutrino flavor transitions supporting the original hypothesis of neutrino mixing and their non-vanishing mass. Given the nature of neutrinos and weak interactions with extremely low neutrino cross sections, several experimental criteria are to be met to study neutrino oscillations:

- powerful sources providing tremendous neutrino fluxes,
- large detectors in terms of their active mass $\gtrsim$kilotons,
- detectors capable of continuous operation ($\sim$weeks or months),
- sufficient oscillation baselines L and energies E to observe the corresponding transitions,
- sufficient energy (and eventually directional or spatial) resolution of the detectors for a reliable reconstruction of neutrino interactions,
- maximal efficient background filtering (underground facilities, precise timing, *etc.*),

and preferably all of the above combined.

A common categorization of the oscillation experiments or neutrinos themselves is based on their sources (the Sun, nuclear reactors, the atmosphere, accelerators) or the investigated oscillation scale governed either by Δm^2_{21} (solar scale), $\Delta m^2_{32(1)}$ (atmospheric scale) or $\Delta m^2_{\rm s} \sim 1$ eV^2 (hypothetical light sterile neutrino scale) [7]. This section overviews basic experimental concepts and the experiments conducted, operational, or in preparation together with the important results in the 3ν-paradigm. Sensitivities to squared mass-splittings Δm^2 are quoted for the flavor transition probability maxima/minima, *i.e.* $\approx$halves the corresponding oscillation lengths.

1.3.1 Solar neutrinos

The Sun is the most powerful neutrino source available (with an average neutrino flux of about $6.5{\times}10^{10}$ cm^{-2}s^{-1} at the Earth's surface). Electron neutrinos are produced in the thermonuclear reactions in its core; they pass through all of its layers and then travel through space,

eventually reaching Earth. The ν_e fluxes are calculated based on the Standard Solar Model (SSM) in two main fusion reaction chains: *pp* and CNO (Carbon-Nitrogen-Oxygen) [30]. Typical energies of solar neutrinos are of about tenths to units of MeV coming from a distance of $L \approx 1$ AU $\approx 10^8$ km.[14]

Solar neutrinos are best known for the "solar neutrino problem", *i.e.* the observed deficit of ν_e compared to the SSM calculation. It was solved by SNO (Sudbury Neutrino Observatory) measurements of the ν_e (CC interactions) and the overall ν (NC interactions) fluxes combined with KamLAND (Kamioka Liquid Scintillator Antineutrino Detector) reactor $\bar{\nu}_e$ disappearance data. Thanks to the MSW adiabatic neutrino flavor transitions in the solar medium, $\Delta m^2_{21} \sim 7.5 \times 10^{-5}$ eV^2 and $\sin^2\theta_{12} \sim 0.3$ can be deduced from the solar neutrino experiments.

Final results were provided by Homestake [31], GALLEX (GALLium EXperiment) [32], GNO (Gallium Neutrino Observatory) [33], KamiokaNDE (Kamioka Nucleon Decay Experiment) [34], SNO [35] or KamLAND [36] (which measured both solar neutrinos and reactor neutrinos at 180 km baseline). Several experiments remain operational: Super-Kamiokande (Super-Kamioka Neutrino Detection Experiment) [37], Borexino [38], SAGE (Soviet-American Gallium Experiment) [39].

1.3.2 Atmospheric neutrinos

Atmospheric neutrinos are born in decays of pions and kaons produced in interactions of cosmic rays with the nuclei of the Earth's atmosphere. For, *e.g.*, a positively charged π^+:

$$\begin{aligned} \pi^+ &\to \mu^+ + \nu_\mu \\ &\quad \hookrightarrow e^+ + \bar{\nu}_\mu + \nu_e. \end{aligned} \tag{1.33}$$

They have a wide range of energies from about 100 MeV to more than 1 TeV and baselines L (distances of propagation before detection) from ∼10 km of the atmosphere depth for the downward going neutrinos to 1.3 $\times 10^4$ km for upward going neutrinos traveling all the way through the Earth. That makes atmospheric experiments sensitive to oscillations with $\Delta m^2 \sim 10^{-1}$ to 10^{-4} eV^2.

The observed asymmetry of up/downward going ν_μ fluxes and symmetry of ν_e is explained by the $\nu_\mu \to \nu_\tau$ oscillations, and it is used to determine the oscillation parameters of $|\Delta m^2_{32(1)}| \sim 2.5 \times 10^{-3}$ eV^2 and $\sin^2\theta_{23} \sim 0.5$.

There is a long list of past and recent experiments and their analyses of atmospheric data, and future experiments to be executed. Past: KamiokaNDE [40], MACRO (Monopole Astrophysics and Cosmic Ray Observatory) [41], Soudan2 [42], and others. Recently active: ANTARES (Astronomy with a Neutrino Telescope and Abyss environmental RESearch) [43], IceCube [44], Super-Kamiokande [45]. Preliminary results / in preparation / proposition: ORCA (Oscillation Research with Cosmics in the Abyss) and the KM3NeT (Cubic Kilometre Neutrino Telescope) [46], Baikal-GVD (Baikal Gigaton Volume Detector) [47], IceCube upgrade PINGU (Precision IceCube Next Generation Upgrade) [48], ICAL (Iron CALorimeter) [49], or multipurpose DUNE (Deep Underground Neutrino Experiment) [50] and Hyper-Kamiokande [51].

1.3.3 Accelerator neutrinos, neutrino beams

Like for atmospheric neutrinos, π and K (decaying into neutrinos) are created by colliding accelerated protons with a fixed target. By focusing charged mesons into a certain direction,

[14] A would-be best sensitive to oscillations with $\Delta m^2 \sim 10^{-10}$ eV^2.

intensive "beams" of immense neutrino fluxes are produced. Ideally, the optics of the beamlines can select (and deflect the latter) either positively or negatively charged mesons and thereby choose the dominant component of ν_μ or $\bar{\nu}_\mu$.

With energies of the accelerator neutrinos from $\sim 10^{-1}$ to 10^1 GeV, there are two commonly distinguished types of oscillation experiments: long-baseline experiments (LBL) of $L/E \sim 500$ km/GeV sensitive to $\Delta m^2 \sim 2.5 \times 10^{-3}$ eV^2 and short-baseline (SBL) of $L/E \sim 1$ km/GeV for $\Delta m^2 \sim 1$ eV^2. The former are, in a way, complementary to the atmospheric neutrino measurements with several advantages of the artificially controlled sources and beamlines (L/E tunes, beam power, timing, *etc.*). One of the consequences is better sensitivity to $\delta_{\rm CP}$ or θ_{13} in $\nu_\mu \to \nu_e$ oscillation channel. The SBL experiments are best known for the "LSND anomaly" (LA) [52, 53] of the reported ν_e CC interaction rate data/prediction excess and the hypothesis of light sterile neutrinos (an extension of 3ν-paradigm with extra mass eigenstates with Δm^2 about 1 eV^2). However, it has not been confirmed or supported by any direct observations so far.

An open list of accelerator neutrino oscillation experiments and their beamlines follows:

- LBL concluded: K2K (KEK[15] to Kamioka) on KEK-PS (KEK-Proton Synchrotron) [54], MINOS(+) (Main Injector Neutrino Oscillation Search) on NuMI (Neutrinos at the Main Injector) [55], OPERA (Oscillation Project with Emulsion-tRacking Apparatus) [56], and ICARUS (Imaging Cosmic And Rare Underground Signals) [57] on CNGS (CERN[16] Neutrinos to Gran Sasso).

- LBL in operation: T2K (Tokai to Kamioka) at J-PARC (Japan Proton Accelerator Research Complex) [58, 59], NOvA (NuMI Off-axis ν_e Appearance) on NuMI [2, 60].

- LBL in preparation: DUNE on LBNF (Long-Baseline Neutrino Facility) [50].

- SBL concluded: LSND (Liquid Scintillator Neutrino Detector) at Los Alamos [52], MiniBooNE (Mini Booster Neutrino Experiment) on BNB (Booster Neutrino Beam) [53], KARMEN (KArlsruhe Rutherford Medium Energy Neutrino experiment) at ISIS proton synchrotron source [61].

- SBL in operation/preparation: MicroBooNE and SBN (Short-Baseline Neutrino) on BNB [62], JSNS^2 (J-PARC Sterile Neutrino Search at J-PARC Spallation Neutron Source) at J-PARC [63].

1.3.4 Reactor neutrinos

In fissions of heavy isotopes that power nuclear reactors, antineutrinos of ∼MeV energies are born. Being below the threshold of μ or τ production, $\bar{\nu}_e \to \bar{\nu}_e$ is the only neutrino oscillation channel to be studied with reactor $\bar{\nu}_e$. At adequately chosen baselines L, the experiments are best sensitive to oscillations of $\Delta m^2 \sim 10^{-4}$ to 10^{-5} eV^2 at $L \sim \mathcal{O}(100$ km) (long-baseline, LBL), $\Delta m^2 \sim 10^{-2}$ to 10^{-3} eV^2 at $L \sim 1$ km (medium-baseline, MBL) and $\Delta m^2 \sim 1$ eV^2 at $L \sim 10$ m (short-baseline, SBL).

The KamLAND LBL experiment played a crucial role in resolving the solar neutrino problem with its help of reactor $\bar{\nu}_e$ data [36, 64]. Over the next years, the future JUNO (Jiangmen Underground Neutrino Observatory) LBL[17] experiment aims to provide precise measurements of oscillation parameters thanks to its exceptional neutrino energy resolution and by measuring both the $\bar{\nu}_e$ disappearance minimum of $\Delta m^2 \sim 10^{-5}$ eV^2 and oscillations of $\Delta m^2 \sim 10^{-3}$ eV^2 in the neutrino energy spectrum [65]. The famous trinity of MBL

[15] Kō Enerugī Kasokuki Kenkyū Kikō

[16] Conseil Européen pour la Recherche Nucléaire

[17] To be precise, JUNO is about 53 km away from two commercial nuclear power plants.

experiments Daya Bay [66], RENO [67], and Double Chooz [68] measured the smallest mixing angle θ_{13} with outstanding precision.

Reactor neutrino experiments also serve as $\bar{\nu}_e$ flux monitors, which proves them to be useful testing probes of the subjected nuclear physics, reactor models, and $\bar{\nu}_e$ fluxes calculations. A phenomenon called "reactor antineutrino anomaly" (RAA) refers to the reports on the observed deficit of $\bar{\nu}_e$ flux compared to predictions [69]. It is often put in close relation to "gallium anomaly" (GA) of missing ν_e from radioactive sources in gallium-based experiments (SAGE, GALLEX) [70] and LA (the previous subsection) and the "light sterile neutrino" hypothesis.

In the past few years, several new reactor experiments with "as-short-as-possible" baselines (SBL) were deployed and had started operation. Their primary purpose is to look for hints of neutrino oscillations at $\Delta m^2 \sim 1$ eV^2 scale and thereby to provide complementary tests of the 3ν-paradigm and nuclear reactor $\bar{\nu}_e$ fluxes calculations, sterile neutrinos, LA, GA, and RAA. Analyses were already published by NEOS (Neutrino Experiment for Oscillation at Short-baseline) [71], DANSS (Detector of the reactor AntiNeutrino based on Solid-state plastic Scintillator) [72], STEREO (STErile REactor neutrino Oscillation) [73], PROSPECT (PRecision Oscillation and SPECTrum experiment) [74], Neutrino-4 [75] and SoLid [76].

1.4 Status of neutrino oscillation parameters measurements

Summarizing the previous section, a global analysis of neutrino oscillation data within the 3ν-paradigm is provided by the NuFIT[18] group in Ref. [77].[19] The results can be seen in Table 1.1. A closer specification follows.

It is clear from Table 1.1 that, as advertised, there are two distinct oscillation scales of $\Delta m^2_{21} \approx 7.5 \times 10^{-5}$ eV^2 and $|\Delta m^2_{32(1)}| \approx 2.5 \times 10^{-3}$ eV^2, with $\Delta m^2_{21}/|\Delta m^2_{32(1)}| \approx 0.03$. The actual sign of the larger squared mass splitting $\Delta m^2_{32(1)}$ remains unknown, which leaves two options usually designated as

1. **Normal ordering** (NO, or "normal hierarchy", NH) of the masses of neutrino mass eigenstates for $\Delta m^2_{32} > 0$ eV^2, *i.e.*, $m^2_3 \gg m^2_2 > m^2_1$, and

2. **Inverted ordering** (IO, or "inverted hierarchy", IH) of the masses of neutrino mass eigenstates for $\Delta m^2_{32} < 0$ eV^2, *i.e.*, $m^2_2 > m^2_1 \gg m^2_3$.

Secondly, two of three mixing angles are determined with very good precisions: $\sin^2\theta_{12} \approx 0.3$ and $\sin^2\theta_{13} \approx 0.022$. On the other hand, there is an interesting ambiguity in the allowed $\sin^2\theta_{23}$ value as it is very close to the symmetric maximal possible 2–3 mixing $\sin^2\theta_{23} = 0.5$ ($\theta_{23} = 45°$).

Finally, though the recent measurements from T2K [58, 59] suggest $\delta_{\rm CP} \approx 3\pi/2$ close to the maximal *CP* violation in neutrino oscillations, the direct single-experiment measurements of $\delta_{\rm CP}$ cannot pinpoint its value precisely enough to reject $\delta_{\rm CP} = 0, \pi$ (no *CP* violation) at sufficient confidence levels ($< 3\sigma$).

Many theoretical considerations and predictions of the SM and beyond (neutrinoless double β-decay, matter *vs.* antimatter asymmetry, $U_{\rm PMNS}$ unitarity tests, sterile neutrinos hypothesis, *etc.*) would require better knowledge of the neutrino oscillation parameters.

1.5 Oscillation probabilities for long-baseline experiments

The accelerator long-baseline experiments as introduced in Subsection 1.3.3 (currently operational NOvA, T2K, future DUNE) measure neutrino oscillation parameters with ν_μ beams

[18] http://www.nu-fit.org (as of Mar 2021)

[19] Including the 2020 updates and results presented later in the text.

Table 1.1: Current status (Aug 2020) of the neutrino oscillation parameters estimates within the 3ν-paradigm as presented by the NuFIT group [77]. The estimates are reported under two different hypotheses of the neutrino mass ordering (hierarchy): normal (NO) $\Delta m^2_{3l} \equiv \Delta m^2_{31} > 0$ eV^2 (left) and inverted (IO) $\Delta m^2_{3l} \equiv \Delta m^2_{32} < 0$ eV^2 (right). The best fit of the NuFIT analysis is for NO.

	Normal ordering (best fit)		Inverted ordering	
	Best fit $\pm 1\sigma$	3σ range	Best fit $\pm 1\sigma$	3σ range
$\sin^2\theta_{12}$	0.304 ± 0.012	$0.269 - 0.343$	$0.304^{+0.013}_{-0.012}$	$0.269 - 0.343$
$\sin^2\theta_{23}$	$0.573^{+0.016}_{-0.020}$	$0.415 - 0.616$	$0.575^{+0.016}_{-0.019}$	$0.419 - 0.617$
$\sin^2\theta_{13}$	$0.02219^{+0.00062}_{-0.00063}$	$0.02032 - 0.02410$	$0.02238^{+0.00063}_{-0.00062}$	$0.02052 - 0.02428$
$\frac{\Delta m^2_{21}}{10^{-5}\ \text{eV}^2}$	$7.42^{+0.21}_{-0.20}$	$6.82 - 8.04$	$7.42^{+0.21}_{-0.20}$	$6.82 - 8.04$
$\frac{\Delta m^2_{3l}}{10^{-3}\ \text{eV}^2}$	$2.517^{+0.026}_{-0.028}$	$2.435 - 2.598$	-2.498 ± 0.028	$-2.581 - -2.414$
$\frac{\delta_{\text{CP}}}{\pi}$	$1.09^{+0.15}_{-0.13}$	$0.67 - 2.05$	$1.57^{+0.14}_{-0.17}$	$1.07 - 1.96$

in the $\nu_\mu \to \nu_\mu$ and $\nu_\mu \to \nu_e$ (or ν_τ) channels. In the 3ν-paradigm, the relevant probabilities are expressed to satisfactory accuracy as expansions in two small parameters (see Table 1.1) $\sin\theta_{13}$ and $\varepsilon \equiv \Delta m^2_{21}/\Delta m^2_{32}$.

Using $c_{ij}, s_{ij} \equiv \cos\theta_{ij}, \sin\theta_{ij}$ as previously, the disappearance probability of $\nu_\mu \to \nu_\mu$ is

$$P(\nu_\mu \to \nu_\mu; L, E) \approx 1 - c^2_{13}\sin^2(2\theta_{23})\sin^2\frac{\Delta m^2_{32}L}{4E} + \mathcal{O}(\varepsilon, s^2_{13}) \tag{1.34}$$

and one does not need to account for the matter effects in this case (of order ε^2 [29]).

On the other hand, this is not true for the appearance $\nu_\mu \to \nu_e$ channel. Assuming a constant matter density in the Earth's crust (mantle) about 2.8 (4.5) g/cm^3, *i.e.*, $N_e(x) = N_e = 6.4$ (10.3) keV[3], the oscillation probability can be written as

$$\begin{aligned} P(\nu_\mu \to \nu_e; L, E, A) \ &\approx 4s^2_{13}s^2_{23}\frac{\sin^2\Delta}{(1-A)^2} + \varepsilon^2\sin^2 2\theta_{12}c^2_{23}\frac{\sin^2 A\Delta}{A^2} + \\ &+ 8\ \varepsilon\ c_{12}s_{12}c_{23}s_{23}c^2_{13}s_{13}\cos(\Delta + \delta_{\text{CP}})\frac{\sin A\Delta}{A}\frac{\sin\Delta(1-A)}{1-A}, \end{aligned} \tag{1.35}$$

where

$$\Delta \equiv \frac{\Delta m^2_{31}L}{4E}, \quad A \equiv \sqrt{2}G_{\text{F}}N_e\frac{2E}{\Delta m^2_{31}}. \tag{1.36}$$

Unlike Eq. (1.34), ν_e appearance Eq. (1.35) is sensitive to δ_{CP}, *i.e.* to the CP violation in oscillations, and through ε, Δ and A also to the sign of $\Delta m^2_{32(1)}$, *i.e.* the neutrino mass ordering. As instinctively anticipated, these sensitivities are further improved in experiments that discriminate between neutrinos and antineutrinos, *e.g.* with ν and $\bar{\nu}$ dominated beams (NOvA, T2K). Fig. 1.4 shows $P(\nu_\mu \to \nu_e)$ at GeV energies for $L = 810$ km (NOvA).

Naturally, there are nine possible neutrino flavor transition channels $\nu_{e,\mu,\tau} \to \nu_e, \nu_\mu, \nu_\tau$. Thanks to (unitarity provided) Eq. (1.29), only four of the associated oscillation probabilities are independent, and they can be used to make out the remaining. Besides, the parametrization of U, Eq. (1.18), allows for an additional simplification, as the rotational matrix $U_{23}(\theta_{23})$ commutes with the matter Hamiltonian $\mathcal{H}$ of Eq. (1.31) (or the vacuum H). Hence, for the evolution matrices of Eqs. (1.21) and (1.32) holds

$$S = U_{23}\widetilde{S}U^\top_{23}, \tag{1.37}$$

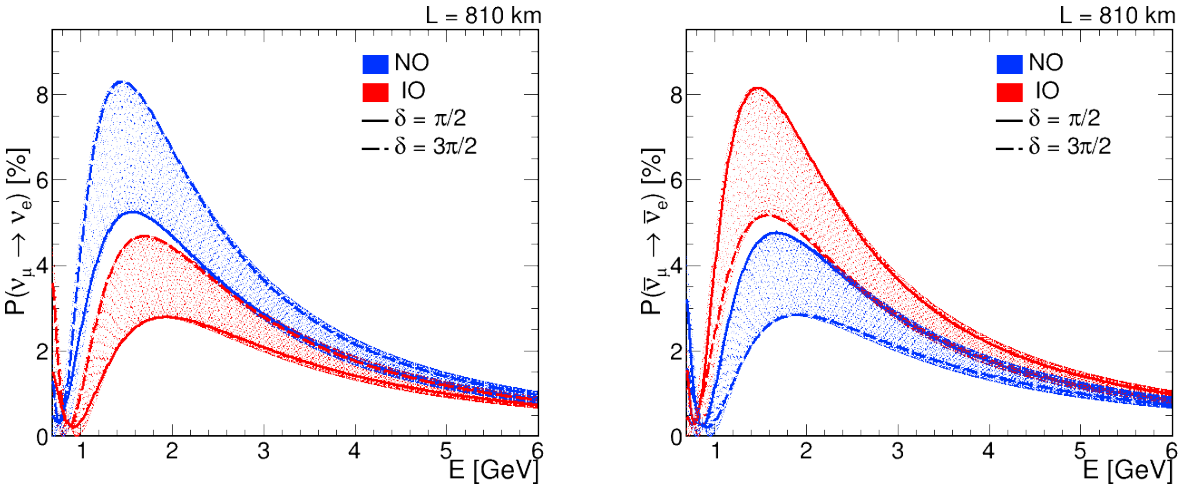

Figure 1.4: Example of $P(\nu_\mu \to \nu_e)$ (left) and $P(\bar{\nu}_\mu \to \bar{\nu}_e)$ (right) over $L = 810$ km baseline as a function of neutrino energy E for neutrino oscillation parameters from Table 1.1 and normal (blue) and inverted (red) ordering (hierarchy) of the neutrino masses for all possible values of $\delta_{\rm CP}$ (dotted bands, denoted δ) and maximal CP violation cases of $\delta_{\rm CP} = \pi/2$ (full line) and $3\pi/2$ (dashed line).

where $\widetilde{S}$ does not depend on θ_{23}. Then, using

$$\widetilde{P}(\nu_\alpha \to \nu_\beta) \equiv P(\nu_\alpha \to \nu_\beta; s^2_{23} \leftrightarrow c^2_{23}, \sin 2\theta_{23} \to -\sin 2\theta_{23}) \tag{1.38}$$

derived by replacing the θ_{23} terms as indicated, one can easily show that, *e.g.*,

$$P(\nu_\tau \to \nu_\tau) = \widetilde{P}(\nu_\mu \to \nu_\mu), \qquad P(\nu_e \to \nu_\tau) = \widetilde{P}(\nu_e \to \nu_\mu). \tag{1.39}$$

With this additional θ_{23} "symmetry", there are only two effectively independent transition probabilities left. With Eqs. (1.38) and (1.39), all of the rest are calculated from (*e.g.*) $P(\nu_\mu \to \nu_\mu)$ of Eq. (1.34) and $P(\nu_\mu \to \nu_e)$ of Eq. (1.35).[20]

The probabilities for antineutrinos are formally obtained by $A \to -A$ (or $N_e \to -N_e$) and $\delta_{\rm CP} \to -\delta_{\rm CP}$ in the formulae above.

For a more detailed explanation of this analytical approach, consult Refs. [13, 28, 29].

[20] *N.b.*, for the sake of completeness, all the trasition probabilities in terms of $P(\nu_\mu \to \nu_\mu)$ and $P(\nu_\mu \to \nu_e)$ with Eqs. (1.38) and (1.39) are:

$$\begin{aligned}
&P(\nu_\mu \to \nu_\mu), \\
&P(\nu_\mu \to \nu_e), \\
&P(\nu_\mu \to \nu_\tau) &&= 1 - P(\nu_\mu \to \nu_\mu) - P(\nu_\mu \to \nu_e), \\
&P(\nu_e \to \nu_\mu) &&= \widetilde{P}(\nu_\mu \to \nu_e) + \widetilde{P}(\nu_\mu \to \nu_\mu) - P(\nu_\mu \to \nu_\mu), \\
&P(\nu_e \to \nu_e) &&= 1 - P(\nu_\mu \to \nu_e) - \widetilde{P}(\nu_\mu \to \nu_e), \\
&P(\nu_e \to \nu_\tau) &&= P(\nu_\mu \to \nu_e) + P(\nu_\mu \to \nu_\mu) - \widetilde{P}(\nu_\mu \to \nu_\mu), \\
&P(\nu_\tau \to \nu_\mu) &&= 1 - \widetilde{P}(\nu_\mu \to \nu_\mu) - \widetilde{P}(\nu_\mu \to \nu_e), \\
&P(\nu_\tau \to \nu_e) &&= \widetilde{P}(\nu_\mu \to \nu_e), \\
&P(\nu_\tau \to \nu_\tau) &&= \widetilde{P}(\nu_\mu \to \nu_\mu).
\end{aligned}$$

2. The NOvA experiment

Chapter 2 provides basic information on the NOvA experiment. NOvA's physics interests are listed in Section 2.1. The NuMI neutrino beam is described in Section 2.2. For more details, see Refs. [78, 79] or https://targets.fnal.gov (as of Dec 2020). The NOvA detectors and the beam off-axis concept are introduced in Sections 2.3 and 2.4, or Refs. [79, 80, 81, 82].

2.1 Introduction and physics interests

NOvA (NuMI Off-axis ν_e Appearance) is a second-generation long-baseline accelerator neutrino oscillation experiment using Fermilab's NuMI (Neutrinos at the Main Injector) 700 kW beamline previously employed by MINOS and MINERvA projects. NOvA has two functionally identical detectors (near and far detector) circa 14.6 mrad off the beam axis and separated by 810 km of Earth's crust, enough for matter effects to substantially affect $P(\nu_\mu \to \nu_e)$. It observes the disappearance of ν_μ and appearance of ν_e in the ν_μ beam, which can run in both neutrino ($\nu_\mu \to \nu_\mu/\nu_e$) and antineutrino ($\bar{\nu}_\mu \to \bar{\nu}_\mu/\bar{\nu}_e$) modes ($\nu$-beam and $\bar{\nu}$-beam).

The experiment started taking data in 2014, and it is scheduled to run until 2025 with an equivalent exposure in both $\nu/\bar{\nu}$-beams, about 63×10^{20} POT (protons-on-target) in total ($\sim$2$\times$ the recent POT, Section 3.3). NOvA addresses several aspects of neutrino oscillations:

1. the size of $\sin^2 2\theta_{23}$ and $|\Delta m^2_{32}|$,
2. the CP violation, *i.e.*, $\delta_{\rm CP} \neq 0$,
3. the neutrino mass ordering, *i.e.* the sign of Δm^2_{32}, and
4. the θ_{23} ambiguity, *i.e.*, whether $\theta_{23} =, <$ or $> 45°$.

Besides that, NOvA provides essential checks on the completeness of the 3ν-paradigm in the long-baseline disappearance of NC events [83] and short-baseline neutrino oscillations [84]. There is also a rich non-oscillation physics program including neutrino cross section measurements [85, 86], cosmic μ [87], gravitational wave detection coincidences [88], light dark matter [89], supernova neutrinos [90], or slow magnetic-monopoles [91], *etc.*

2.2 The NuMI beam

NuMI is a ν_μ beam operated at Fermi National Laboratory, Illinois, USA, near Chicago (map in Fig. 2.1). Neutrinos are produced in decays of secondary mesons (π and K) from the primary interactions of accelerated, 120 GeV protons from the Main Injector (accelerator) with a graphite target. K and π decay predominantly via

$$\pi^\pm, K^\pm \to \mu^\pm + \nu_\mu/\bar{\nu}_\mu \tag{2.1}$$

and subsequent $\mu^\pm$ decays

$$\mu^\pm \to e^\pm + \nu_e/\bar{\nu}_e + \bar{\nu}_\mu/\nu_\mu. \tag{2.2}$$

The original 350 kW NuMI has been steadily improved since before NOvA started taking data. As of Mar 2020, NuMI works at around 600 kW with the capability of up to 700 kW, and it delivers about 2.5–3.0 $\times 10^{18}$ POT/day (see Fig. 2.2). That makes it currently the highest intensity artificial neutrino source. A schematic of the NuMI beamline and its main elements is in Fig. 2.5.

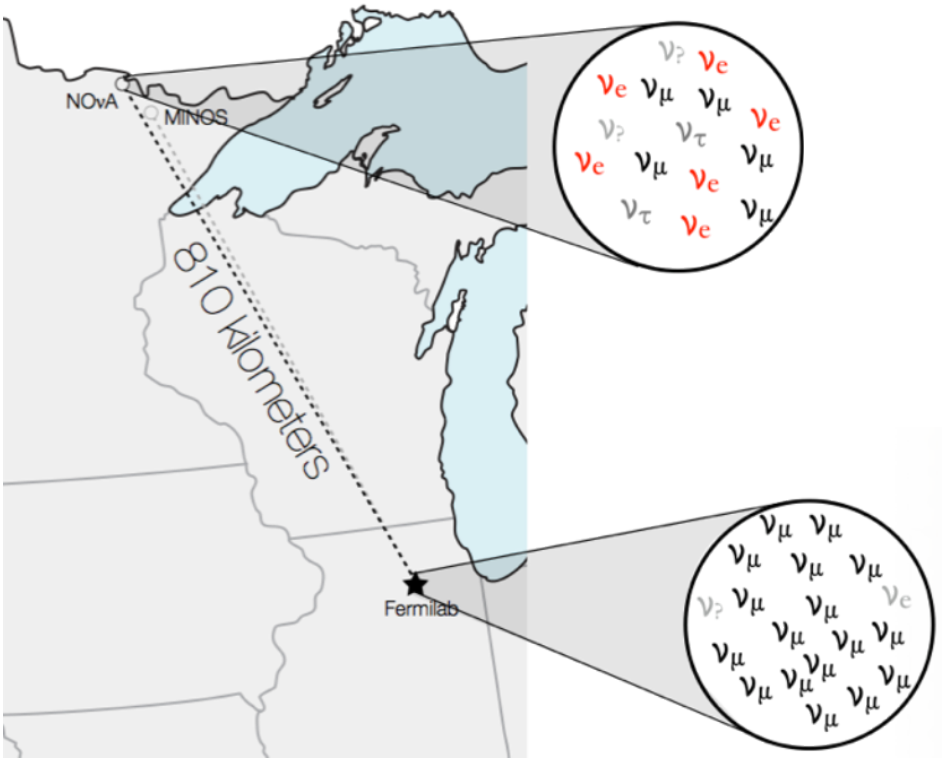

Figure 2.1: Map of the NuMI beam. A ν_μ dominated beam is produced with intrinsic $\bar{\nu}_\mu$ (or *vice versa*) and ν_e+$\bar{\nu}_e$. Over the 810 km baseline, most of the ν_μ flux disappears as ν_μ oscillate into ν_τ and ν_e. From https://images.app.goo.gl/t8NxrcgyJgbEHrvo8 (as of Feb 2021).

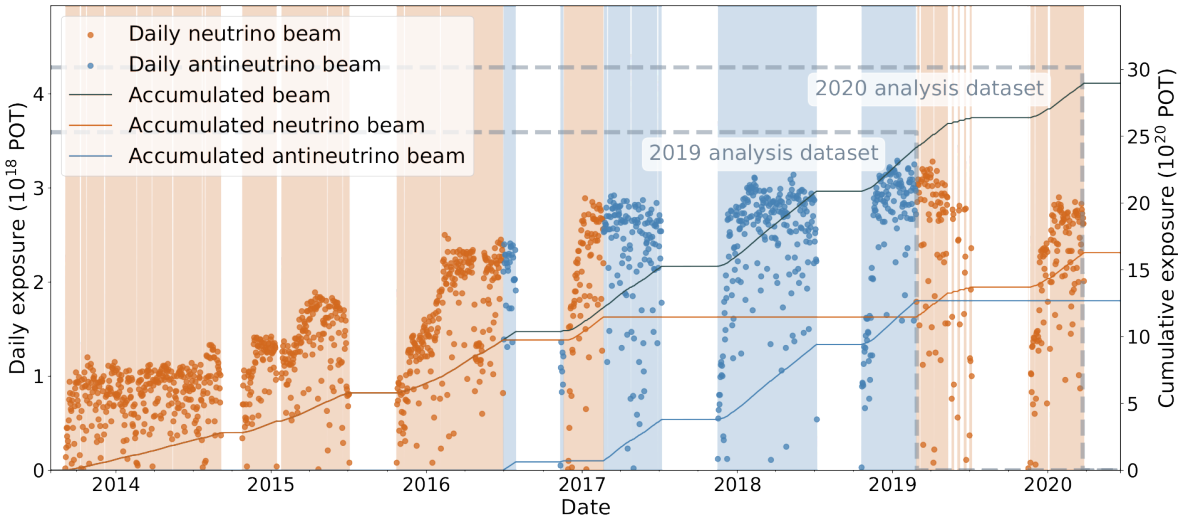

Figure 2.2: Daily (dots, left vertical axis) and cumulative (line, right vertical axis) NuMI beam exposure of the NOvA far detector over all periods of data taking with ν-beam (orange) and $\bar{\nu}$-beam (blue). 2020 and 2019 datasets [2] are highlighted. The figure is from Ref. [92].

Target: NuMI had (Nov–Dec 2019) a new high-intensity, 900 kW target installed. The target comprises 48 graphite fins enclosed in a canister with beryllium windows for the beam entrance and exit. The canister is filled with helium gas, and the fins are water-cooled. The upgrades compared to the previous target account for its size and the size of its fins, their

Figure 2.3: Schematic of the NuMI target graphite fins and four new winged fins to protect the beam components from any proton mis-steering, from Ref. [93].

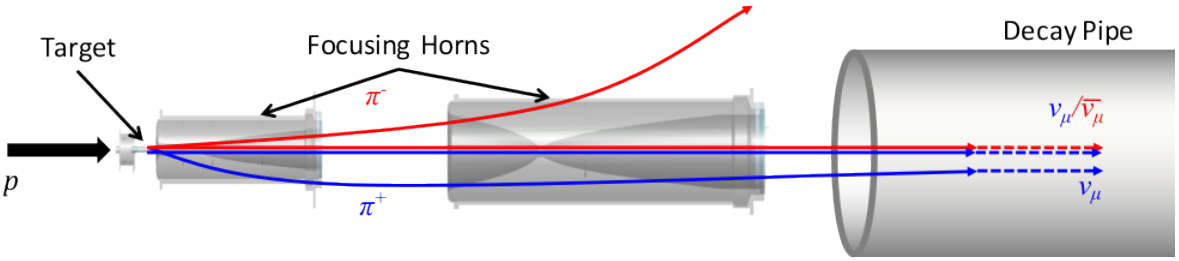

Figure 2.4: Sketch of the NuMI focusing optics in FHC mode (ν-beam). With the given polarity of the horns, positively charged mesons are focused towards the beam direction (blue), whereas the opposite charge sign particles are deflected (curved red). Although, a small portion of wrong sign particles cannot escape the beam as they travel along its axis, being almost unaffected by the magnetic field (straight red). The figure is from Ref. [94].

mutual position, and four new "winged" (baffled) fins beam upstream. The winged fins have special safeguards (wings) to protect any valuable beam components from even relatively small proton mis-steering. See Fig. 2.3.

Focusing horns: The secondary π and K escaping the target are focused into a collimated beam by two magnetic horns. They consist of cylindrically shaped outer and parabolically shaped inner conductors to function as lenses. The horns' current and their position relative to the target effectively determine the mesons momentum spectra while deflecting those with the wrong (opposite) charge sign, Fig. 2.4. With currents of up to 200 kA, the horns are pulsed and water-cooled to avoid overheating. Changing the polarity, *i.e.* currents, of the horns allows for focusing either positively or negatively charged particles. The default "forward" horn current (FHC) produces a beam of π^+, K^+ and thus "neutrino beam" (ν-beam), the switched "reversed" horn current (RHC) produces a beam of π^-, K^-, and thus "antineutrino beam" ($\bar{\nu}$-beam).

Decay pipe and absorbers: The focused mesons enter a 675 m long (one decay length of 10 GeV π), 2 m wide decay pipe (0.9 atm of He) for most of them to decay by its end via Eq. (2.1). The pipe is followed by an ionization chamber ("hadron monitor") to measure the flux and spatial profile of the remaining hadrons, which are then absorbed in an Al-Fe water-cooled beam stop. All μ left in the beam are attenuated by a 250 m rock shielding.

The whole NuMI beamline is depicted in Fig. 2.5, daily and cumulative exposures delivered to the NOvA far detector (FD) since the start of data taking are in Fig. 2.2.

Along with the predominant $\nu_\mu/\bar{\nu}_\mu$, the beam has intrinsic impurities of wrong sign $\bar{\nu}_\mu/\nu_\mu$ mainly due to imperfect focusing of the mesons and $\nu_e + \bar{\nu}_e$ mainly due to μ in-flight decays of Eq. (2.2). The simulated composition of the beam at the NOvA near detector can be seen in Fig. 2.6.

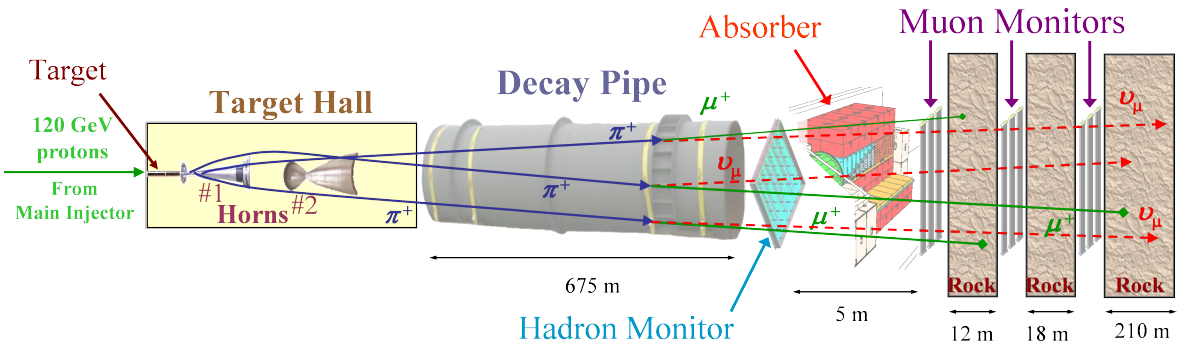

Figure 2.5: Schematic of the NuMI beamline. **From left to right:** 120 GeV protons hit the carbon target in the Target Hall, producing π and K. These are focused by two magnetic horns, then decay while traveling through the Decay Pipe. All hadrons are stopped in the Hadron Absorber, and residual muons are attenuated by nearly 250 m of rock leaving only neutrinos in the beam. The figure was taken from Ref. [95].

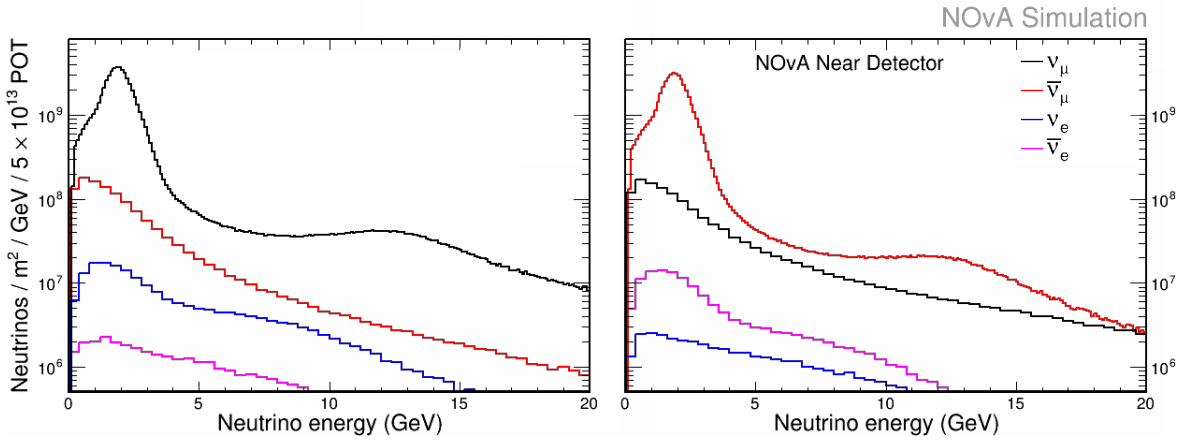

Figure 2.6: Simulated components of the neutrino flux at the NOvA near detector (Subsection 3.4.1): ν_μ (black), $\bar{\nu}_\mu$ (red), ν_e (blue) and $\bar{\nu}_e$ (magenta). **Left:** In FHC mode, ν-beam. **Right:** In RHC mode, $\bar{\nu}$-beam. The figures were taken from Ref. [97].

2.3 Off-axis concept

As π and K are spinless particles, they decay isotropically and produce monoenergetic neutrinos in their rest frame. When boosted, neutrino energy E_ν from π or K, Eq. (2.1), of energy E at a small laboratory angle ϕ is approximately

$$E_\nu = \frac{(1 - m_\mu^2/m^2)E}{1 + E^2\phi^2/m^2} \Leftarrow \begin{cases} \left(1 - \dfrac{m_\mu^2}{m_\pi^2}\right) \approx 0.427 & \text{for } \pi, \\ \left(1 - \dfrac{m_\mu^2}{m_K^2}\right) \approx 0.954 & \text{for } K, \end{cases} \tag{2.3}$$

with m the mass of the parent particle and m_μ the mass of μ (detailed derivation in, *e.g.*, Ref. [5, p. 66]). For parent π, as can be seen in Fig. 2.7 – left, E_ν of off-axis neutrinos ($\phi > 0$) is less dependent on the energy E_π of π.

Although the integrated off-axis beam flux is considerably reduced, the neutrino energy spectrum is much sharper. Depending on the angle ϕ, the flux is enhanced at lower and

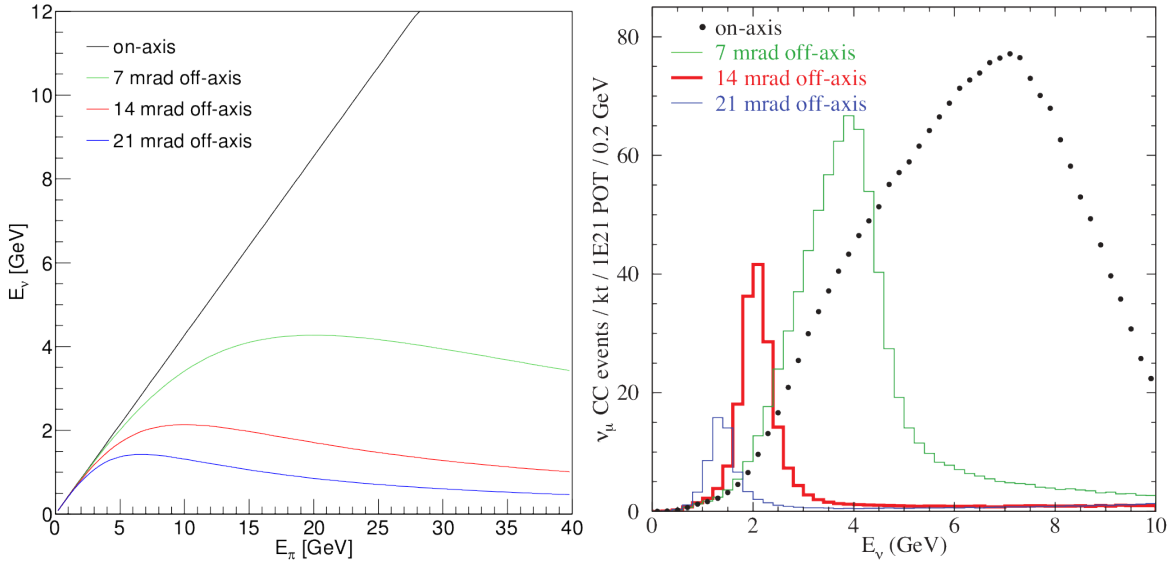

Figure 2.7: NOvA neutrino beam off-axis concept. **Left:** ν_μ energy E_ν as a function of the parent π energy E_π for several experimental off-axis angle dispositions. **Right:** Simulated NuMI neutrino flux for off-axis energy spectra, the figure is from Ref. [80]. NOvA approximately corresponds to the red lines.

suppressed at higher energies w.r.t. the on-axis geometry, Fig. 2.7 – right. The NOvA detectors sit about 14.6 mrad off the beam axis (at the red curves in Fig. 2.7). This helps to reduce backgrounds with broad energy distribution such as NC events and ν_τ CC events with a threshold over 3 GeV.

The right combination of the beam focusing optics, off-axis angle (14.6 mrad), and sufficient oscillation baseline (810 km) allows NOvA to observe the region of the first oscillation $\nu_\mu \to \nu_\mu$ disappearance minimum and $\nu_\mu \to \nu_e$ appearance maximum in a narrow energy peak around 2 GeV.

2.4 NOvA detectors

2.4.1 Detectors design

As already stated, NOvA uses two functionally equivalent detectors: Near Detector (ND) and Far Detector (FD). They are both finely segmented, highly active (∼65% active mass), liquid scintillator tracking calorimeters. They are designed to be as similar as possible aside from the size, see Fig. 2.8. The FD of 14 kt is located in Ash River, Minnesota, USA, and the ND of only 0.3 kt is located in Fermilab, Illinois, USA.

The basic detection unit of both detectors is a cell of extruded, highly reflective PVC filled with scintillator and a looped wavelength shifting (WLS) fiber attached to a pixel of an avalanche photodiode (APD), Fig. 2.9. The cell is 5.9×3.9 cm (parallel $\times$ transverse to the beam direction) with a wall thickness of about 3.3–4.8 mm. It is circa 15.5 (4) m in length for the FD (ND).

A single APD with 32 channels reads out 32 cells, a module. Twelve modules form a plane in the FD, only three modules in the ND. The planes alternate their horizontal and vertical orientation (inset in Fig. 2.8) to allow for a stereo 3D readout. In total, there are 896 planes, *i.e.* ∼344000 channels, in the FD and 214 planes, ∼20000 channels, in the ND. The high detector segmentation is vital for a satisfactory tracking resolution of neutrino interactions final states, hence, for events reconstruction and particle identification. To compensate for its

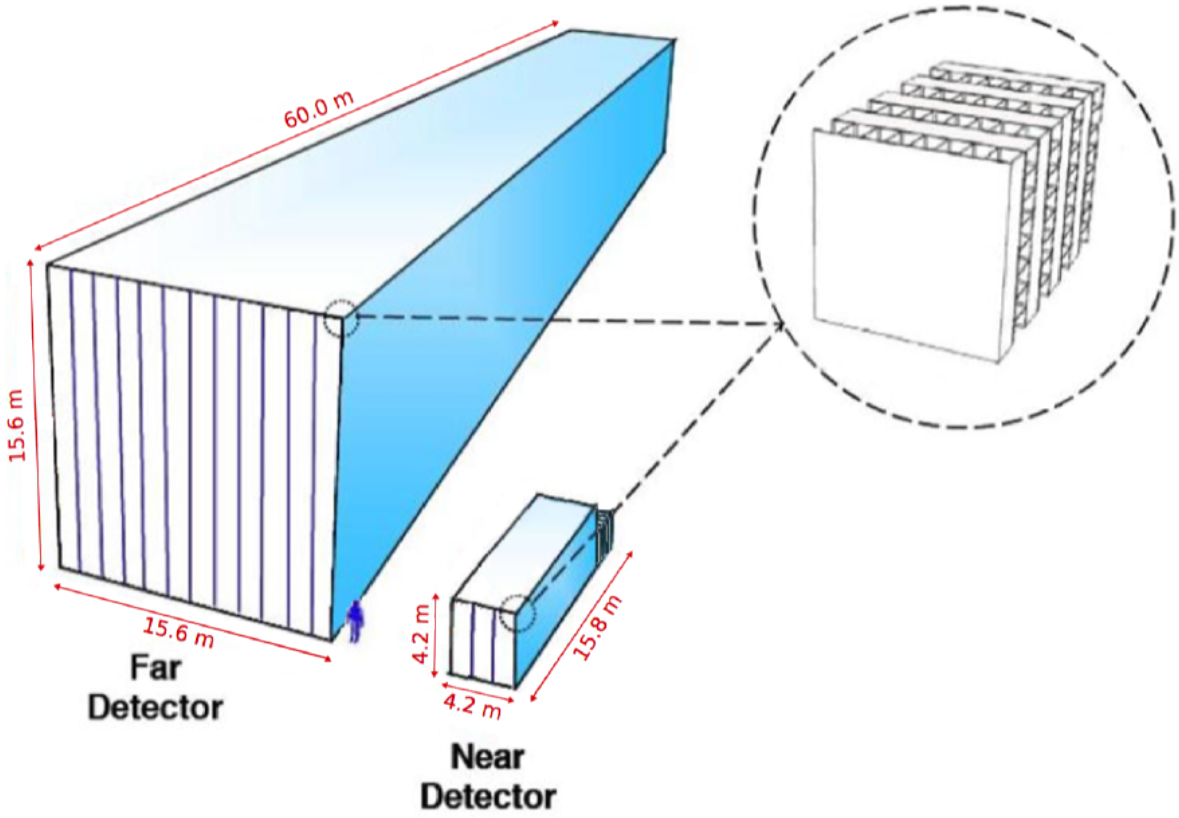

Figure 2.8: Drawing of the NOvA detectors with a human figure for scale. **Inset:** Illustration of the cellular structure of the detectors. The layers of elementary cells are oriented orthogonally to the adjacent ones to provide stereo 3D readout. The figure is from Ref. [80].

short length (∼16 m) for μ tracks from ν_μ CC, the ND is equipped with a μ-catcher of several detector planes interlayered with steel at the downstream end of the detector as in Fig. 2.8.

When charged particles travel through cells, their energy is absorbed by the scintillator and emitted as light collected by the fibers and amplified by the APDs. The scintillator is a mixture of mineral oil (95%), scintillating pseudocumene, PPO (2,5-diphenyloxazole), and bis-MSB (1,4-bis-(o-methyl-styryl)-benzene) as waveshifters from emitted UV to collected visible light of 380–450 nm (all the remaining 5%), with subpercent portion of antistatic Stadis-425 and antioxidant Vitamin E. More details can be found in Ref. [98].

32-pixel APDs serve as photodetectors. Both ends of the fibers are attached to one of the APD pixels, *i.e.* one APD per module. To reduce noise from dark currents of no light caused by thermally created electron–hole pairs, APDs are cooled to −15°C with a thermoelectric cooler and subsequent circulating water cooling system. APDs have very high quantum efficiency (85%) in comparison to conventional photomultiplier tubes (∼10–20%), which is important to detect faint light signals from the end of 16 m cells. A technical APDs description is in Ref. [80].

2.4.2 Data acquisition and triggering systems

The detectors are operated in a nonstop continuous online acquisition mode (24/7). Any collected charge above a particular threshold in a cell (an APD pixel) is recorded as a "hit" with a timestamp and the cell ID.

These APD signals are read and digitized by Front-End Boards (FEB). FEBs are instrumented with Analogue-to-Digital Converters (ADC) and other operating electronics –

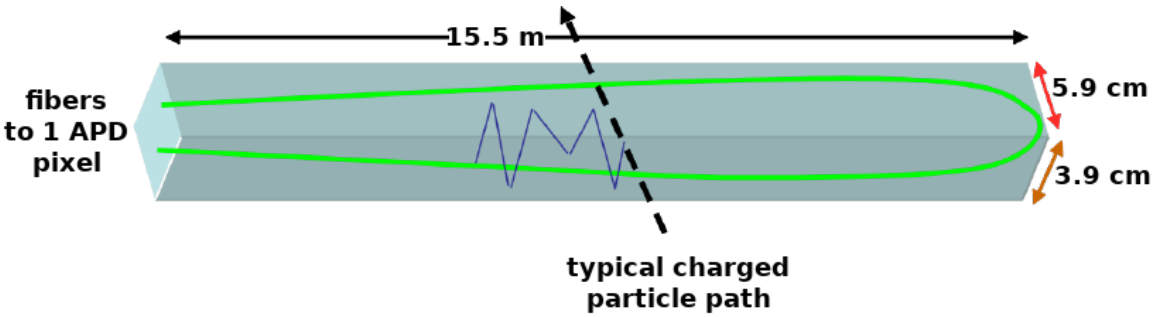

Figure 2.9: Basic NOvA detector unit, detector cell. About 15.5 m of extruded reflective PVC filled with scintillator and a looped WLS fiber attached to an APD pixel. The figure is from Ref. [80].

amplifier, gate array, APD cooler regulator, *etc.* Data from groups of 64 FEBs are collected by Data Concentrator Modules (DCM). The experiment and DCM timing is provided by series of Time Distributing Units (TDUs) controlled by a Master TDU (MTDU), which uses external GPS satellites time to synchronize all the DCMs in both detectors with the accelerator time [99].

DCMs aggregate data and send them into a circular buffer, where the data live for up to 16 minutes before they are stored on disks or discarded. To decide that, NOvA uses several types of triggering flags: specific time intervals (clock triggers), pre-defined signals and associated time intervals for readout (signal triggers), and characteristic data conditions or detector behavior (data-driven triggers or DDTs).

Concerning the NOvA neutrino oscillation analysis, the following triggers are essential in particular:

- **NuMI Data Trigger** is a GPS timestamp from the accelerator, which starts a 550 μs long readout centered on a 10 μs beam spill (218–228 μs). Any beam intrinsic neutrino interactions are expected to be well contained within this time interval. Also, more than 250 μs sidebands include the typical cosmic and other activity in the detectors around the beam spills.

- **Cosmic Data Trigger** is 10 (1) Hz in the FD (ND), again with a 550 μs readout, and mainly used for the detector calibration.

- **Activity DDT** is a trigger for any activity in the ND, 550 μs readout. The data are used for calibration and ND running conditions evaluation.

- **Energy DDT** is a FD trigger for a total charge exceeding a specified threshold deposited during a 50 μs time window.

3. The NOvA neutrino oscillation analysis

This chapter outlines the NOvA 2020 neutrino oscillation analysis within the 3ν-paradigm. It clarifies the analysis' concept in Section 3.1, lists the changes w.r.t. the previous 2019 analysis in Sections 3.2, 3.3, overviews the standard analysis steps in Sections 3.4 to 3.9 (modeling, reconstruction, calibration, event selection) and unique NOvA techniques of particle identification with machine learning algorithms in Section 3.7 and energy estimation in Section 3.8. Sections 3.10 to 3.13 explain the assembly of the final analysis predictions.

The chapter serves as a quick guide to the analysis and an interrelating reference aggregator. A special focus is given to the specific NOvA analysis features that might be not known from general neutrino or particle physics. Also, most of the relevant 2020 analysis novelties are detailed in order to provide a meaningful comparison to previously reported methods and results in Refs. [1, 2].

Where appropriate and if not stated otherwise, all studies, validations, or optimizations were performed using a reference set of neutrino oscillation parameters of

$$\Delta m^2_{32} = 2.44 \times 10^{-3}\ \text{eV}^2, \quad \sin^2\theta_{23} = 0.5, \quad \delta_{\text{CP}}/\pi = 0, \tag{3.1}$$

and

$$\Delta m^2_{21} = 7.53 \times 10^{-5}\ \text{eV}^2, \quad \sin^2\theta_{12} = 0.307, \quad \sin^2\theta_{13} = 0.0218, \tag{3.2}$$

and the experiment parameters of the oscillation baseline L and the average Earth's crust density ρ computed for the average depth of the NuMI beam in the crust using CRUST2.0 [100]

$$L = 810\ \text{km}, \quad \rho = 2.84\ \text{g/cm}^3. \tag{3.3}$$

3.1 Analysis strategy

The goal of the NOvA neutrino oscillation analysis is to study neutrino transitions over the distance between its two detectors (near, ND, and far, FD, detector, 810 km) in four individual channels: $\nu_\mu \to \nu_\mu$ or $\nu_\mu \to \nu_e$, and $\bar{\nu}_\mu \to \bar{\nu}_\mu$ or $\bar{\nu}_\mu \to \bar{\nu}_e$. That is in the disappearance ($\nu_\mu/\bar{\nu}_\mu \to \nu_\mu/\bar{\nu}_\mu$) and appearance ($\nu_\mu/\bar{\nu}_\mu \to \nu_e/\bar{\nu}_e$) oscillation channels using neutrinos (ν-beam) and antineutrinos ($\bar{\nu}$-beam). With the available external inputs from solar (Δm^2_{21}, θ_{12}) and reactor neutrino experiments (θ_{13}), constraints on the oscillation parameters $\Delta m^2_{32}, \theta_{23}$ and δ_{CP} can be deduced from the data.

The ND is used to generate, *i.e.* to correct, the FD MC predictions in order to weaken the model dependence of the analysis and to reduce the detector correlated systematic uncertainties. This course proceeds for two sets of ν-beam and $\bar{\nu}$-beam data and in two more-or-less separate, though disjunct, phases that correspond to two analysis dis/appearance channels. Both are schematically illustrated in Fig. 3.1.

The following convention is adopted throughout the text: there are two sets of data with different NuMI horn polarities, **ν-beam** and **$\bar{\nu}$-beam** (beam focusing Forward and Reversed Horn Current, FHC and RHC), two **analysis channels** of ν_μ disappearance ($\nu_\mu/\bar{\nu}_\mu \to \nu_\mu/\bar{\nu}_\mu$) and ν_e appearance ($\nu_\mu/\bar{\nu}_\mu \to \nu_e/\bar{\nu}_e$) and several **analysis samples** (fourteen in total) contributing with their **bins** (of reconstructed energy mainly) to the final likelihood construction (Section 5.1). All of them are described in this chapter.

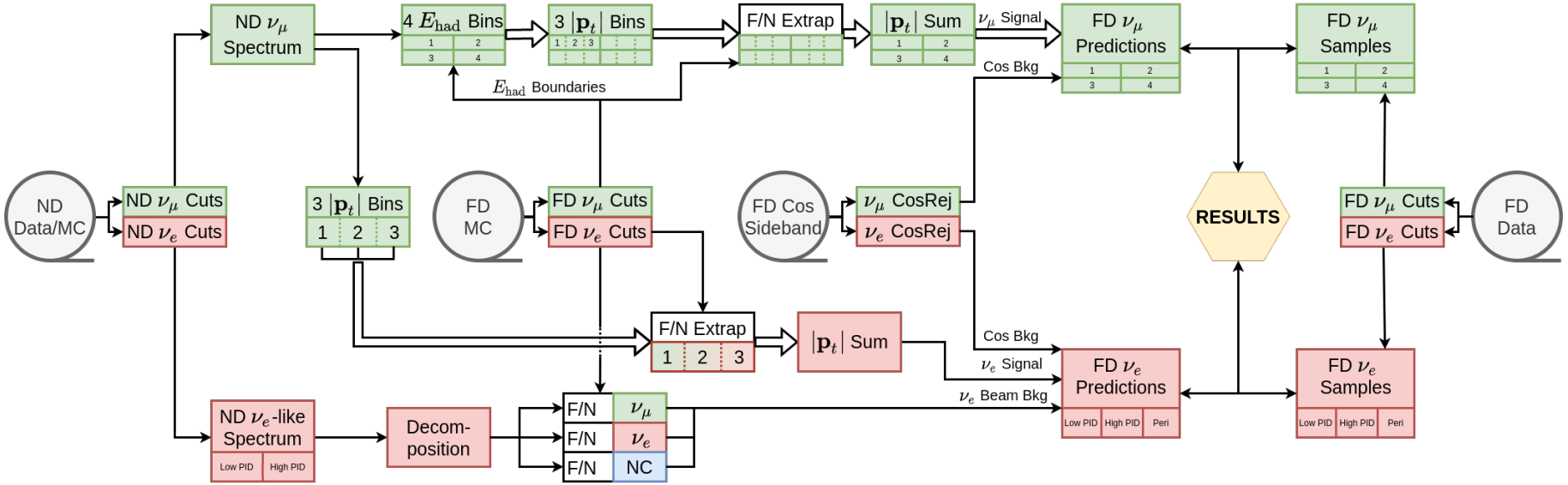

Figure 3.1: Diagram of the NOvA neutrino oscillation analysis strategy. Each block represents a relevant element of the analysis and the corresponding evaluation and validation processes. The upper part of the diagram (green) illustrates the ν_μ disappearance channel, and the bottom part (red) the ν_e appearance channel components of the analysis. The far detector (FD) simulation (MC) is adjusted by the near detector (ND) data/MC with the Far/Near "extrapolation" technique (F/N Extrap) to produce FD predictions. A comparison of this model to the FD data of selected ν_μ and ν_e candidates is used to constrain the neutrino oscillation parameters.

3.2 Improvements and changes in 2020 analysis

The NOvA 2020 analysis involved several updates and upgrades [101] compared to Ref. [2], which can be characterized as "primary" (independent strides) and "secondary" (necessary aftermaths).

Primary changes:

- New ν-beam data, an increase of approx. 50% in the total ν-beam POT – Section 3.3.
- New NuMI high-intensity 900 kW target – Subsection 3.4.1.
- Upgrade of the neutrino interactions simulation to GENIE v3.0.6 and the NOvA custom model with updated internal tunes – Subsection 3.4.2.
- Upgrade to a different version of Geant4 v10.4 (+patch 02) and multiple detector simulation updates, light model and readout simulation updates – Subsection 3.4.3, improvements of the detector calibration procedure – Section 3.6.
- New basic clustering algorithm for event reconstruction – Section 3.5, and new cosmic veto – Subsection 3.5.1.
- New additional variable of μ (or e) transverse momentum p_t relative to the beam direction used to generate FD predictions via Far/Near technique, *i.e.* "extrapolation samples" – Subsection 3.11.1.
- Multiple improvements in systematic uncertainties evaluation, implementation, and validation – Chapter 4.

Secondary changes:

- Retraining and update of all major PID algorithms – Section 3.7.
- Reoptimizing the energy estimators – Section 3.8.
- Changes and reoptimization of the event selections – Section 3.9, and decomposition techniques – Subsection 3.10.2.
- Reevaluation of systematic uncertainties – Chapter 4.

3.3 Data sets

The analysis data has accumulated over six years since the start of its taking in 2014. The total ν-beam exposure accounts for 13.60×10^{20} POT of the full FD mass equivalent[1] and 12.50×10^{20} POT for $\bar{\nu}$-beam [102]. The data collection is divided into "periods" of time intervals characterized by uniform running conditions (periods correspond to major experimental events: beam shutdowns, horns polarity switches, target replacement, *etc.*) and shorter "epochs" (epochs follow any production or analysis reasons). There are ten periods of data from 6 Feb 2014 to 14 Mar 2020; two of them are new in the 2020 analysis. With the previous 8.85×10^{20} POT ν-beam exposure [2], the new data represents about one-third of the total ν-beam POT. The cumulative exposure and the beam performance were shown in Fig. 2.2.

The last data-taking period used in the 2020 analysis was operated with the new high-intensity 900 kW NuMI target (19% of the ν-beam POT).

[1] Data taking had started before the full FD was assembled in 2014.

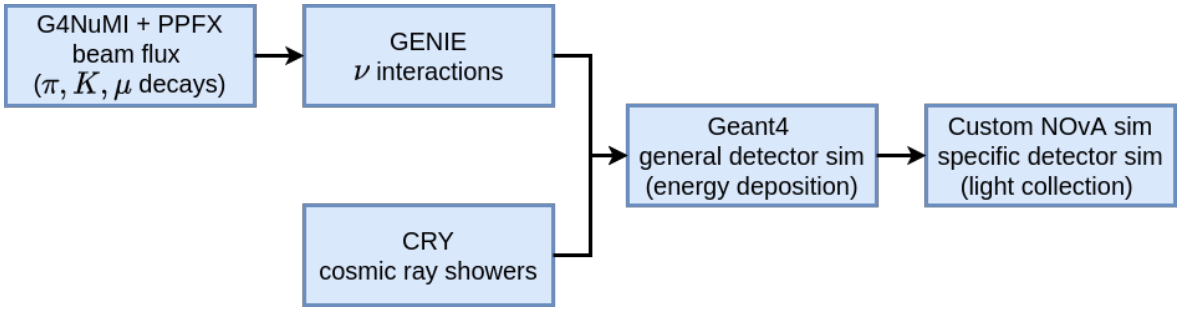

Figure 3.2: Flowchart of the NOvA simulation chain. G4NuMI package for the NuMI geometry together with PPFX [96] and external constraints on hadron production and decays predicts the total neutrino flux. GENIE v3.0.6 [103, 104] simulates neutrino interactions in and around the detectors. Geant4 v10.4 provides energy depositions of charged particles in the detectors. Custom NOvA light model and several additional methods describe the final collection of light and electronics responses. Cosmic showers and μ are generated by CRY.

3.4 NOvA simulations

To simulate neutrino fluxes and detectors response, NOvA uses a complex simulation chain consisting of several steps as depicted in Fig. 3.2.

Detailed model of the beamline geometry and Geant4, together as G4NuMI, simulates the hadron production at the beam target, their transport, and decays into neutrinos. The flux is constrained with data from hadron production experiments by the PPFX tool (Package to Predict FluX) [96], Subsection 3.4.1. With this input, neutrino interactions in the detectors and their vicinity are simulated with GENIE (Generates Events for Neutrino Interaction Experiments) [103, 104], Subsection 3.4.2. CRY (Cosmic-RaY shower generator) provides cosmic showers and cosmogenic μ [105]. Propagation, energy depositions, and interactions of particles in the detectors are simulated by Geant4 as standard [106, 107, 108]. Several custom NOvA procedures model the final signal light collection, attenuation in the fibers, background noise fluctuations, and response of APDs and FEBs [109].

3.4.1 Beam simulation

The predictions of neutrino fluxes are generated by a combination of G4NuMI and PPFX packages. G4NuMI is a Geant4 code accurately integrating the NuMI geometry and the associated physics to the particles propagated in the beamline, starting with the incoming proton beam from the Main Injector [110]. PPFX implements a correction for any hadron production mismodeling exploiting most of the relevant, available data like that from MIPP, NA49, and NA61/SHINE experiments. It serves as a constraint to the Geant4 intrinsic hadronic model [96, 111].

Due to the new higher power beam target, an austere revision of the beam simulation was necessary. The target is different from the previous one in several key aspects. The beam spot size increased (1.3 to 1.5 mm), target fins width increased (7.4 to 9.0 mm), four new beam upstream winged fins were added. These upgrades were checked in several studies (pre/post target installation data, simulation changes) to have no malign effects or defects [93, 112]. Hence, practically no essential changes were made to PPFX or G4NuMI.

3.4.2 Neutrino interactions model

In the interval of neutrino energy between 1 and 5 GeV where NOvA operates (also commonly referred to as the "transition region", see Ref. [113]), several phenomenological interaction types have significant contributions to the total cross section of $\nu-$nucleus scattering. Fig. 3.3 shows the relevant energy regions of ν_μ and $\bar{\nu}_\mu$ total CC cross sections.

- **Quasi-elastic charged current scattering** (CCQE) are interactions of the type

$$\nu + n \to l^- + p, \quad \bar{\nu} + p \to l^+ + n, \tag{3.4}$$

  where the four-momentum transferred between the leptonic and hadronic system $Q^2 = -q^2 = -(p_l - p_\nu)^2$ is low enough for nucleons to be approximated by point-like particles with no substructure like in Fermi's four body theory. CCQE interactions dominate for energies < 1 GeV.

- **Elastic neutral current scattering** (NCEL) of a neutrino and a nucleon N

$$\nu + N \to \nu + N. \tag{3.5}$$

- **Deep inelastic scattering** (DIS) of ν off a quark breaks the nucleon N and creates many hadrons (X is an arbitrary state of the hadronic system)

$$\nu + N \to l^- + X, \quad \nu + N \to \nu + X \tag{3.6}$$

  for CC and NC interactions, respectively. Contrary to CCQE, DIS dominates for energies > 5 GeV.

- **Resonant baryon production** (RES) happens as both CC and NC processes

$$\nu + N \to l^- + \Delta^+, \quad \nu + N \to \nu + N^* \tag{3.7}$$

  with nucleon N, respectively. N^* is a nucleon resonance and Δ a delta resonance, both quickly decaying, most often into a nucleon and a single-pion final state.

- **Meson exchange current** (MEC) has become a well-established interaction type recently. In analogy to electron–nucleus scattering, a weak boson mediating the interaction similar to that of Eq. (3.4) is exchanged with a pair of nucleons (2 particles – 2 holes, 2p2h) and believed to lead to their emission, *i.e.* emission of two nucleons, see Ref. [114].

- **Coherent π production** (COH) appears as the target nuclei A are heavy compared to the neutrino energies with vanishing nuclear recoil

$$\nu + A \to l^- + \pi^+ + A, \quad \nu + A \to \nu + \pi^0 + A \tag{3.8}$$

  as both CC and NC processes, respectively.

Apart from cross sections, a reliable model of neutrino induced hadron production, hadronization model, is required to calculate final state particles and their properties. Hadrons can interact on their way out of the nucleus, which is described by a model of "final state interactions" (FSI). Finally, an underlying model of the nuclear structure dynamics is needed.

All neutrino interactions are simulated with GENIE v3.0.6 (available documentation for the previous version is in Ref. [104]).[2] This is one of the major changes since all of the previous oscillation analyses and MC productions used GENIE v2.12.2. New GENIE v3.0.6 allows

[2]For more information on GENIE v3.0.6, visit http://genie-mc.org or the preliminary physics and user manual at https://genie-docdb.pp.rl.ac.uk/DocDB/0000/000002/006/man.pdf (as of Dec 2020).

Table 3.1: List of the important phenomena of neutrino–nucleus scattering and the models employed by NOvA through "comprehensive model configuration" of GENIE v3.0.6 with references and prospective internal tunes. The used acronyms stand for Partially Conserved Axial Current (PCAC), Andreopoulos-Gallagher-Kehayias-Yang (AGKY), and Koba-Nielsen-Olesen (KNO).

Phenomena		Model
Cross sections	CCQE	Valencia, Nieves et al. [121, 122]
	NCEL	Ahrens et al. [123] (GENIE default)
	DIS	Bodek-Yang [124, 125] (GENIE default)
	RES	Berger-Sehgal [126]
	MEC	Valencia MEC [114] + NOvA ND data tune [116]
	COH	Rein-Sehgal with modified PCAC formula [127, 128] (GENIE default)
Hadr.	Low-W	Empirical AGKY [104] with KNO scaling [129]
	High-W	PYTHIA/JETSET [130]
	FSI	INTRANUKE hN [131] + $\pi^+ - {}^{12}C$ data tune [120]
	Nucleus	Bodek-Ritchie (relativistic Fermi gas with short-range correlations) [132]

multiple "Comprehensive Model Configurations" (CMC) as a choice of self-consistent combinations of physics models as listed above (*i.e.* cross sections + hadronization + FSI + nucleus) and their parameters.[3] NOvA constructed and tuned its own CMC, which is summarized in Table 3.1. The main advantage of the new GENIE is the availability of the model tunes to the most recent scattering data and – halfway as a consequence – a significant simplification of the internal NOvA tuning procedures in comparison to previous years, see Ref. [115]. 2020 analysis retuned the FSI model to π^+–^{12}C scattering data [119, 120] and incorporated a fit of the MEC model to the NOvA ND data [116] similar to MINERvA tune [117, 118]. The achieved ND data/MC agreement in ν_μ CC samples can be seen in Fig. 3.4 and in Fig. 3.5 with contributions from particular cross section phenomenological models (for details on the reconstruction and selection techniques, please refer to Sections 3.5, 3.7, 3.8 and 3.9).

See NOvA's cross section group documentation in Refs. [116, 120] for a comprehensive elaboration on the individual models and comparisons to GENIE v2.12.2.

3.4.3 Detectors simulation

The "general" modeling of particles energy deposition uses Geant4. The 2020 analysis MC production updated to Geant4 v10.4 with patch 02.[4]

One improvement is the more precise calculation of Fermi's density effect correction $\delta(\beta\gamma)$ for the Bethe-Bloch formula using Sternheimer's method [134]. It was even later internally patched for the exact prescription instead of the Geant4 approximation [135, p. 13]. It affects μ ranges in steel of the ND μ-catcher and FD structure supporting pivoter stand by more than +1% compared to the previously used δ approximation, or by +0.3% in the FD alone (for 1 GeV μ). It also affects the overall ratio of $\mathrm{d}E/\mathrm{d}x$ deposited in plastic dead material and scintillator [136]. Besides that, multiple minor updates and bug fixes of the detector geometry were implemented (more precise cell sizes and their positions, detector temperatures, *etc.*), see Ref. [137].

[3] For GENIE available CMC, see https://hep.ph.liv.ac.uk/∼costasa/genie/tunes.html (as of Dec 2020).
[4] http://cern.ch/geant4-data/releases/patch_geant4.10.04.p02.tar.gz (as of Jan 2021)

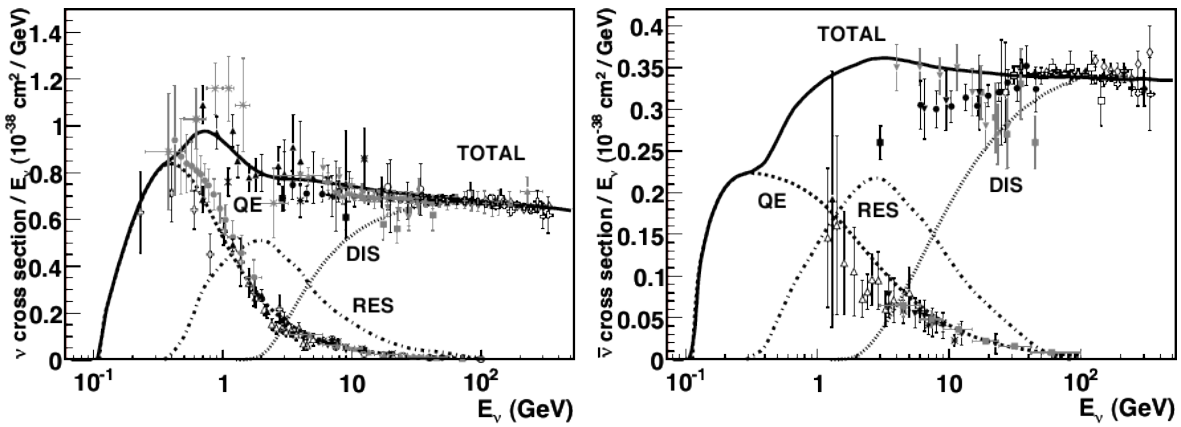

Figure 3.3: Total ν_μ (left) and $\bar{\nu}_\mu$ (right) CC cross sections per nucleon for an isoscalar target compared to multiple scattering data (from Ref. [113]). It is divided by and plotted in the neutrino energy E_ν. The contributions of the relevant processes are shown: CCQE (dashed), RES (dash-dotted), DIS (dotted).

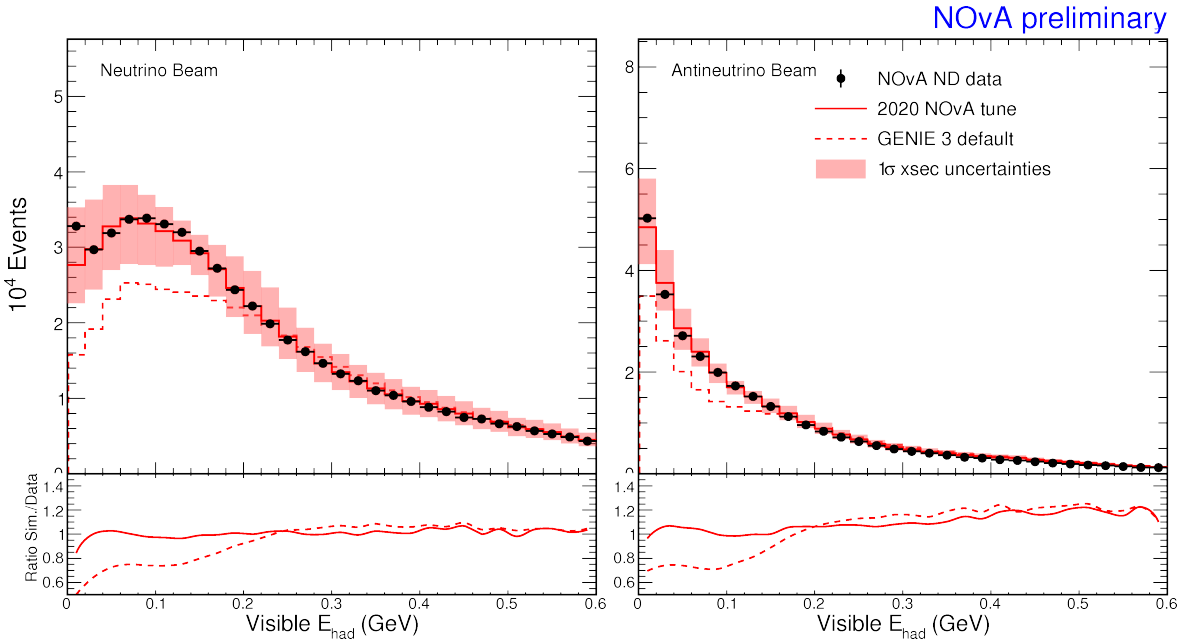

Figure 3.4: Comparisons of default GENIE v3.0.6 simulation (dashed) and internal 2020 NOvA tune (full) in distributions of visible energy of the hadronic system of ND ν_μ CC samples. FSI model and neutrino cross section Valencia MEC model are corrected by ND data (black dots). **Left:** ν-beam. **Right:** $\bar{\nu}$-beam. The plots are from Ref. [133].

Detectors light model

The second part of the detector simulation implements the collection of light, *i.e.* optical responses to scintillation and Cherenkov light produced by the charged particles. The energy depositions of particles in the detectors' cells provided by Geant4 need to be converted to scintillation light. The specific scintillator light yield (fluorescence) $\mathrm{d}S/\mathrm{d}r$ along the path of

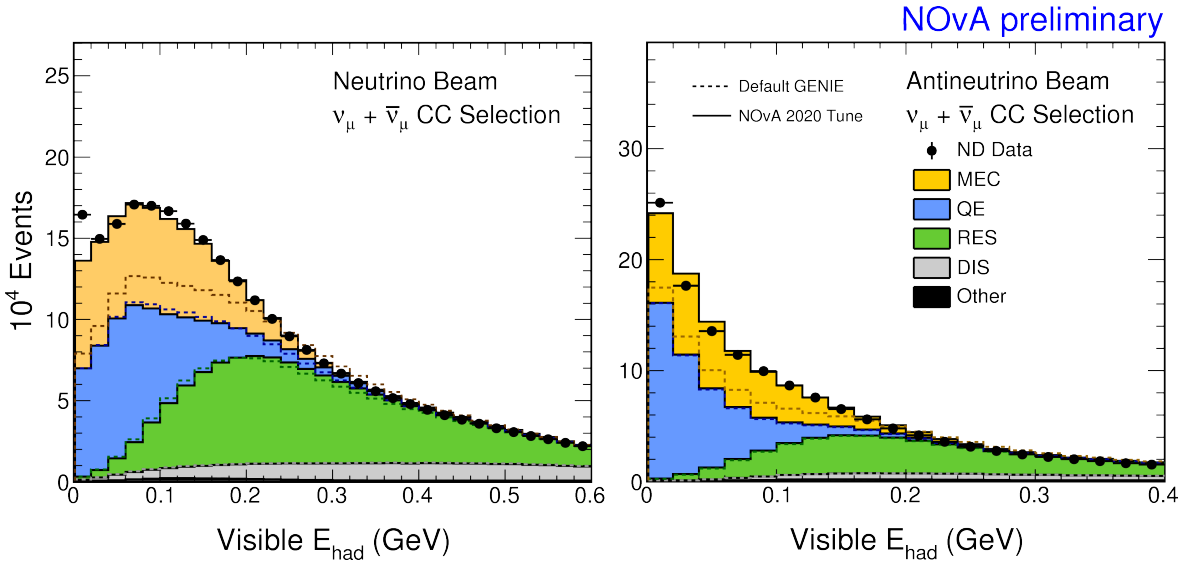

Figure 3.5: Particular phenomenological cross sections contributions in the default GENIE v3.0.6 simulation (dashed) and in the internal 2020 NOvA tune (full) in distributions of visible energy of the hadronic system of ND ν_μ CC samples. FSI model and neutrino cross section Valencia MEC model are corrected by ND data (black dots). **Left:** ν-beam. **Right:** $\bar{\nu}$-beam. The plots are from Ref. [133].

the particle with residual range r is described by the common Birks' empirical law [138]

$$\frac{\mathrm{d}S}{\mathrm{d}r} = \frac{A\dfrac{\mathrm{d}E}{\mathrm{d}r}}{1 + c_\mathrm{B}\dfrac{\mathrm{d}E}{\mathrm{d}r}}, \tag{3.9}$$

where A is the scintillator efficiency, c_B is Birks' constant, and $\mathrm{d}E/\mathrm{d}r$ is the specific energy loss of the particle. The non-linearity introduced by the c_B dependent term is speculated to occur due to recombination and quenching effects caused by damaged or ionized molecules created along the path of the particle. The Birks' parameter c_B was determined in a test bench measurement of the NOvA scintillator [139].

In addition, superluminal charged particles in the medium generate Cherenkov light [140], which is calculated from the Frank-Tamm formula [141]. Ambiguously, it could be indistinguishable from the scintillation in certain wavelength regions when collected, or reemitted and recollected by the WLS fibers.

A new tuning method was developed and employed in 2020 analysis for the full NOvA's light model [142]. The number of photons produced in the scintillator that is collected by the WLS fiber N_γ is parameterized as

$$N_\gamma = F_\mathrm{view}(Y_s E_\mathrm{Birks} + \epsilon_C C_\gamma), \tag{3.10}$$

where E_Birks, C_γ are the numbers of photons produced due to scintillation, Eq. (3.9), and Cherenkov radiation, respectively. Y_s and ϵ_C are corresponding scaling factors (efficiencies) as the intrinsic properties of the active medium of the detectors. F_view is an overall scaling factor for each of the detector views (top and side, to account for the detector cells' and prevailing μ directions) and separate for the ND and FD. All six parameters are deduced from a fit in four dedicated MC and data samples: FD/ND cosmic samples and ND μ and ND p-like (6% purity) from ν_μ CC selection samples. The fit was performed in 2D spectra of reconstructed hit distance to the track end *vs.* the number of collected pre-calibrated photoelectrons for

each of the samples and detector views. More details and the results of the tuning can be found in Ref. [142].

To simulate photon transport in the cells, through the fibers, and APD and electronics response, several custom heuristic algorithms were designed (with the help of Geant4 where appropriate), see Refs. [109, 143]. With parametrized simulation templates for a detector cell unit, they help to reduce redundancy of full detector (more than 344000 channels) Geant4 simulation and thus save computational resources.

3.5 Event reconstruction

NOvA's raw data are sets of cell "hits", collected charge with timestamps mapped to the cells spatial distribution (cells' IDs) in individual exposition windows of triggered time intervals. As the cell planes are perpendicular to one another (Subsection 2.4.1), the hits are effectively taped in two plane projections xz – top view and yz – side view, where z is the direction along the detector length, *i.e.* along about the beam direction, x is the horizontal and y the vertical direction perpendicular to z. The frame origin ($x, y, z = 0$ cm) is located in the center of the detector's front face through which the beam enters. An example of recorded data can be seen in Fig. 3.6. With available information on detector geometry and cells' relative calibration, the data are actual "photos" of the detector activity.

As usual, event reconstruction strives to isolate individual "events" of interactions (see simulated examples in Fig. 3.7) and to provide basic physics interpretation of the direct observations. It consists of several consecutive algorithms for clustering, vertexing, and tracking. The reconstruction process also accounts for events filtering (Subsection 3.7.1) to remove dominant backgrounds at the early stages of data processing. Except for the new clustering [144], a sweeping summary of the NOvA reconstruction chain is given in Ref. [145] or see the flowchart in Fig. 3.8.

First, an introduction to NOvA's standard terminology for basic reconstruction objects is in order.

Raw hits: As in Subsection 2.4.2, a raw hit is any above-threshold charge in ADC units collected by the elementary channels of a detector cell+APD pixel with a timestamp and channel ID. Raw hits also account for the electronic noise resembling the signal.

Hits (CalHits): Raw hits provided with information on geometry (xyz spatial coordinates instead of channel ID), calibration (deposited energy instead of ADC units, available after calibration procedures), and optionally on beam and detector conditions become the fundamental data objects, *i.e.* hits or calorimetric hits, CalHits. If not stated otherwise, this definition of hits is used from now on.

Slice: Spatially adjacent and in-time close hits are called a slice. Slices serve as the primary candidates of fundamental physics events (*e.g.* ν interaction). The clustering algorithm used to construct slices is shortly described in Subsection 3.5.1.

Tracks: Charged non-showering particles that lose their energy in the detector mainly via ionization form narrow tracks of hits with minimal changes in direction when scattered. They come predominantly from μ from ν_μ interactions (tracks in the beam direction) and from cosmic showers (downward going tracks, perpendicular to the beam direction). The reconstruction of tracks is described in Subsection 3.5.4.

Vertex: Spatial and temporal coordinates of the primary interaction point, from which the traces of secondary particles arise, make up a vertex, Subsection 3.5.2.

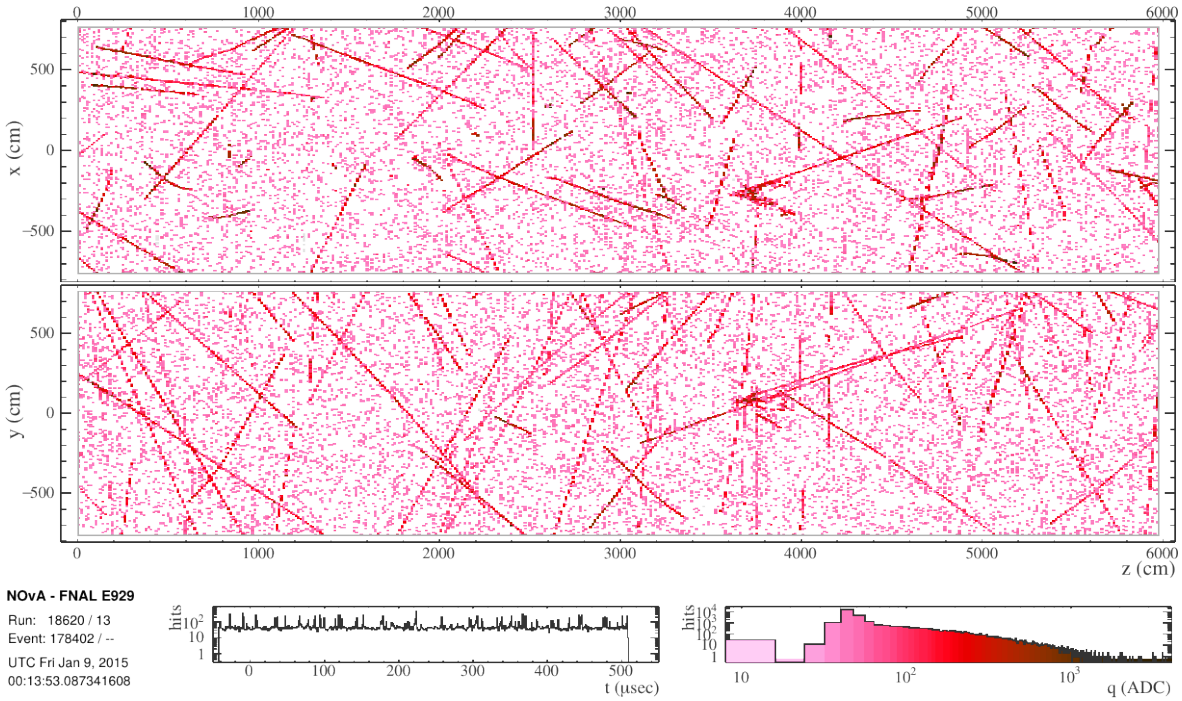

Figure 3.6: Example of the FD data collected in the NuMI trigger 550 μs window in both detector views xz top view (top panel) and yz side view (bottom panel). Color brightness corresponds to the collected charge (ADC units). NuMI beam arrives from the left in a spill centered in 218–228 μs interval. Most of the activity is cosmogenic as the detector is located on the surface.

Prong: Prong is a collection of hits in a slice to represent a single particle emerging from the interaction vertex, a single particle representation. The formation of prongs is described in Subsection 3.5.3.

3.5.1 Event clustering

One of the important changes in the NOvA 2020 neutrino oscillation analysis is the use of a new clustering algorithm called Time Density Slicer (TDSlicer). TDSlicer employs a centroid-finding algorithm as in Ref. [146] for both of the detector xz and yz views. The density of hits ρ_i around each hit i is

$$\rho_i = \sum_j \exp\left(-\frac{d_{ij}^2}{\tau^2}\right), \tag{3.11}$$

where the sum goes over all other hits j and

$$d_{ij} = ||\Delta T_{ij}| - R_{ij}/c|\,, \tag{3.12}$$

with ΔT_{ij} being the time difference between the hits i and j, and R_{ij} is their spatial distance. The scale parameter τ related to the detector timing resolution is set to 16 and 80 ns for the ND and FD [99], respectively. Additionally, an isolation score δ_i of hits is calculated as

$$\delta_i = \min_{j|\rho_j>\rho_i} d_{ij}, \tag{3.13}$$

where the width of the beam spill limits the maximum possible δ_i. Cluster centroids are identified as hits of $\rho > 3$ (10) and $\delta > 8$ (6) in the ND (FD), *i.e.* with both high density and high isolation scores.

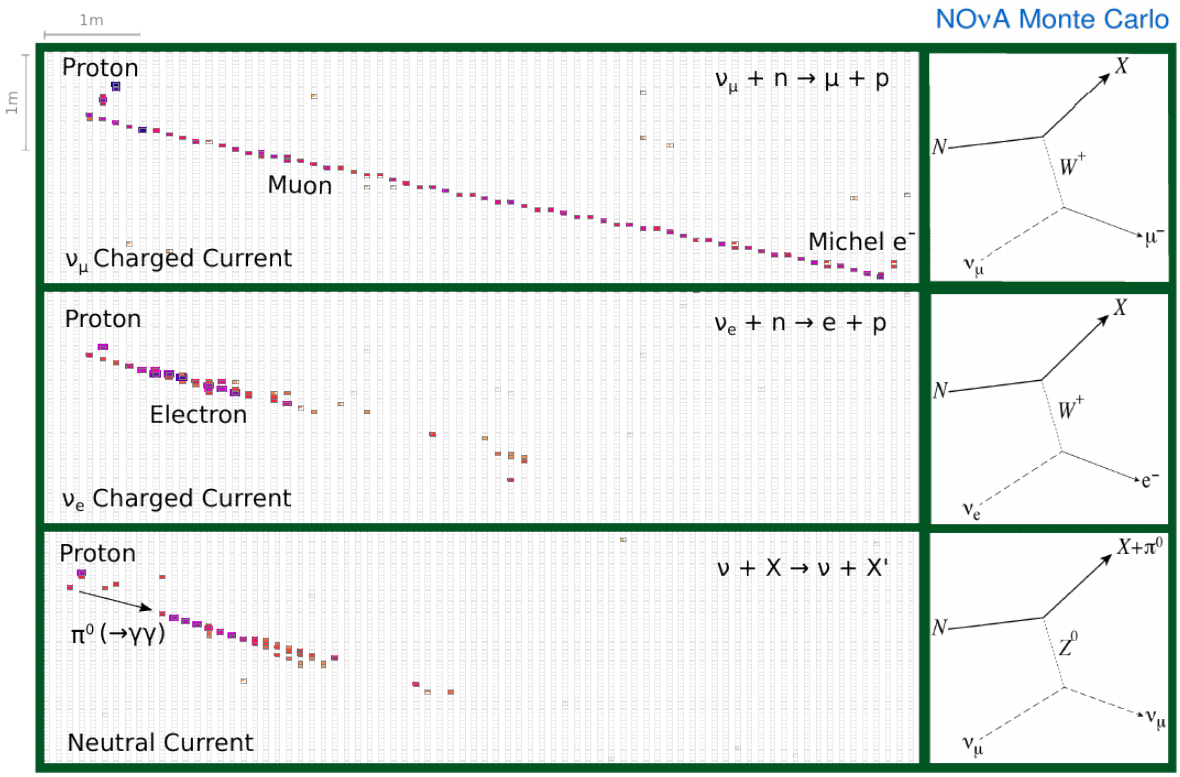

Figure 3.7: Examples of the NOvA event topologies in one of the detector's views. **From top to bottom:** ν_μ CC event with a long straight μ track decaying into Michel e, ν_e CC event with an electromagnetic shower, NC event with a π^0 production. Taken from Ref. [145].

All hits with $d_{ij} < 10\tau$ to the nearest cluster centroid are grouped. 3D clusters in xzt and yzt are made from the initial groups through Prim's algorithm, see Ref. [147], by successive addition of the hits outside the cluster that are nearest in d_{ij} to some hit already inside whilst $d_{ij} < 8\tau$ (5τ) in the ND (FD). Finally, 3D clusters from the two views are paired together simply by iteratively finding the best match of their average zt values. All hits not grouped, groups not 3D clustered and clusters not paired are considered as noise. A typical output of TDSlicer is in Fig. 3.9.

NOvA's previous clustering algorithm Slicer4D, see Ref. [148], used a method based on the DBSCAN (Density-Based Spatial Clustering of Applications with Noise [149]) algorithm of grouping hits in their light-like intervals with penalization to large x, y, or z distances. That sometimes caused accidental merges of clearly different physics interactions in one slice due to shared hits close to the edges of the ideal slices (bridges of mostly low energy hits). It biases the energy estimation, or it can make the slices fail containment cuts. The more stringent TDSlicer is expected to perform better. Besides that, TDSlicer also mitigates the pile-up effects in the ND. With increasing beam intensity and the power above 650 kW, Slicer4D is known to error, which resulted in a drop of the number of reconstructed slices relative to the beam intensity (per spill POT) by up to 12% [150]. Altogether, it was estimated that TDSlicer is responsible for an appreciable 7% increase in the ND data candidates of neutrino interactions related mainly to higher beam intensities in comparison to the Slicer4D [151, 152].

More information on TDSlicer, its implementation, tuning, and validation can be found in a dedicated technote in Ref. [144]. Validations performed w.r.t. the neutrino oscillation analysis were summarized in Ref. [101].

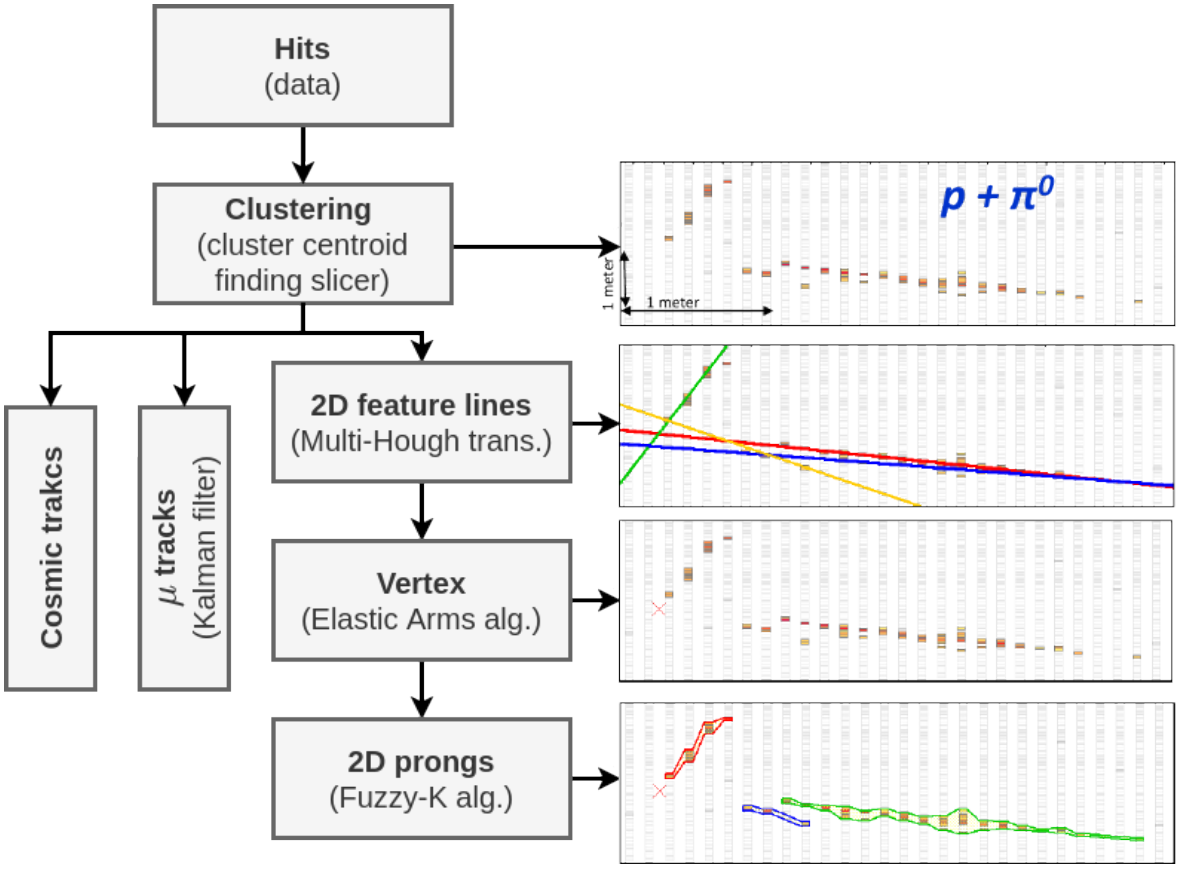

Figure 3.8: NOvA event reconstruction chain flowchart with an example of a simulated NC π^0 production event (event taken from Ref. [145]).

3.5.2 Vertex reconstruction

Finding the interaction vertex of the reconstructed slices proceeds in two main steps. First, a modified Multi-Hough transform [153] for each pair of hits in both detector views prepares primary (guide)lines of the slice. The dominant line directions are identified as peaks in Gaussian-smeared distributions of the transformed hit pairs in Hough-space [154].

The intersections of Hough lines are treated as seeds for the Elastic Arms algorithm from Ref. [155] (see also [156, 157, 158]) to find the vertex. It was adapted to the basic NOvA template of a single vertex event with multiple particles emerging from it and represented by "arms" (vectors pointing away from the vertex, compare Fig. 3.7). The vertex candidate is chosen by minimizing an energy cost function that measures the goodness of fit between the hits and the assembled arms while simultaneously penalizing unassociated hits and arms with first hits too far from the vertex [159].

3.5.3 Prongs formation

To further cluster individual particle contributions in the event slice, NOvA adopted an adjusted Fuzzy K-means algorithm [160, 161]. It allows the hits to be assigned to more than a single prong, and it incorporates a possibilistic clustering, *i.e.*, they are also not required to be assigned to any prong (noise or single hits from very short tracks).

The algorithm is used in both detector views separately. Prongs are assumed to be straight lines emerging directly from the reconstructed vertex, and they are identified as peaks in the angular distribution of energy deposits. The hits are assigned a "degree" of membership to

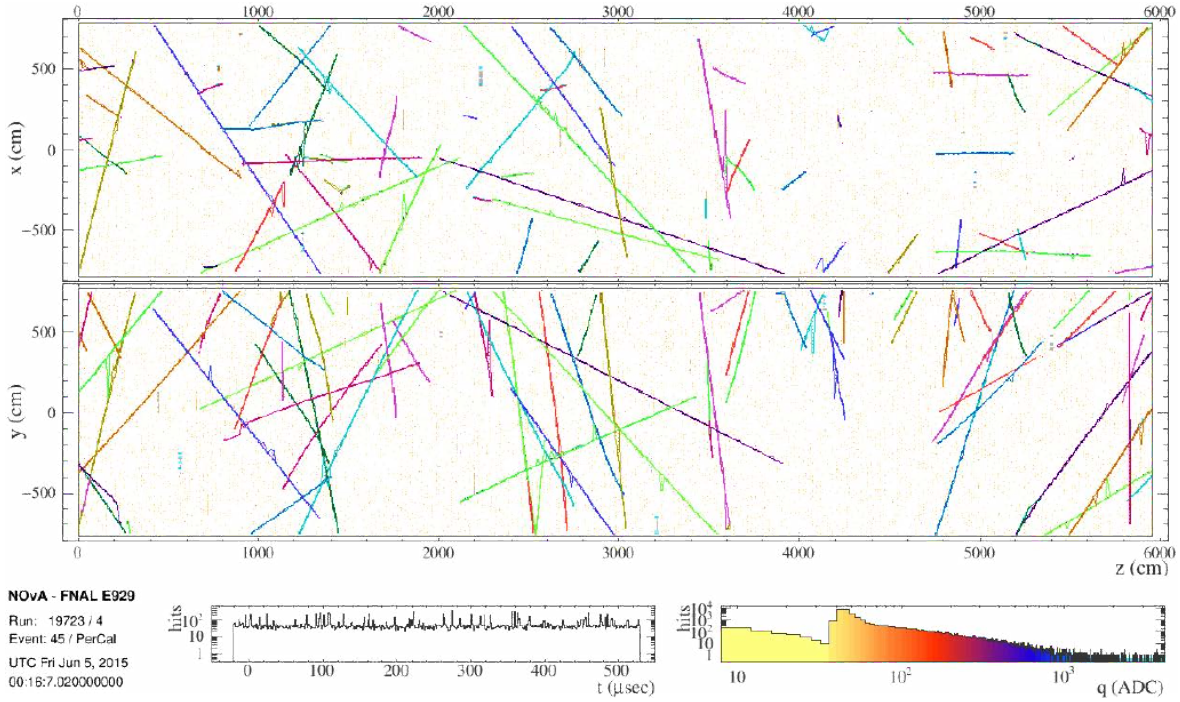

Figure 3.9: Example output of the clustering algorithm (TDSlicer). Different colors correspond to individual reconstructed slices (events). The figure was taken from Ref. [144].

a prong based on their distance to its axis in the angular space. The 2D prongs are paired with the help of Kuiper's test of the cumulative energy deposition along the z direction in both views.

The algorithm reconstructs the primary lepton in about 90% of the simulated ν CC interaction events. This efficiency improves with increasing lepton momentum. All details on the prong formation are in Ref. [162].

3.5.4 Tracking

Kalman tracks

The first tracker – primarily designed to identify tracks of μ from ν_μ CC interactions – uses a linear Kalman filter technique [163]. The process initiates with identifying track seeds, *i.e.* two hits no more than four cells apart. Again, it is done in both detector 2D views starting at the detector end opposite to the beam direction (high z, from the detector's back), where the tracks are expected to be separated much better. The hits are added if they are close enough to the track prediction, *i.e.*, close to a simple linear fit with uncertainties from the measurement of the particle location within the cell and possible scattering. Once a hit is added, both the track's position and prediction are updated. The iteration is stopped when there are no hits satisfying the filter conditions on the track projection proximity or on a probability of a gap along the track. The propagation is then reversed, front to back, to recover any missing hits. 2D views are matched according to a simplistic metric of differences in start and stop z coordinates relative to the number of overlapping cell planes in between. For details, see the Kalman tracking technote Ref. [164].

Cosmic tracks

The second tracker aims for quick processing of single-particle slices essentially caused by cosmic rays. Hits in a window of a given number of cell planes (eight by default) in the z direction are fitted with a straight line, again, starting from the back. Those consistent with the line are added to the forming track. The window is moved one plane at a time along z to add hits consistent with the original line, perform a new fit, add new hits, and move the window again until all planes in the slice have been covered. Like in most of the reconstruction methods, this is done in both detector 2D views, which are then combined to form a 3D track. Details on implementation and performance are in Ref. [165].

3.6 Detectors energy calibration

Energy calibration of the NOvA detectors has two crucial steps. The first one is a cell-by-cell relative calibration which accounts for light attenuation in the long fibers inside the detector cells (attenuation calibration). The second one is the absolute energy calibration (the calorimetric energy scale) using stopping cosmic ray μ.

Attenuation calibration principally removes natural attenuation of collected signal charge in photoelectrons per cm, PE/cm, along the cell length and possibly other effects causing variations in PE/cm. It uses cosmic ray μ data with three adjacent hits in three neighboring planes of cells (tri-cell hits, the middle cell is perpendicular to the other two) to ensure good estimates of the hit position and energy depositions. The mean PE/cm, Y, as a function of the position of the hits from the center of the cell W is expressed as [166]

$$Y = C + A\left(\exp\left(\frac{W}{X}\right) + \exp\left(-\frac{L+W}{X}\right)\right), \tag{3.14}$$

where A, C, and X are fitted parameters, L is the length of the cell. Two exponentials are for two routes of the light towards the readout in the looped fiber, Fig. 2.9 earlier.

As the above parametrization does not work well for the near and far ends of the cells along with occasional residual shapes in the center, a non-parametric LOWESS (LOcally WEighted Scatter plot Smoothing) interpolation algorithm is applied in these regions (*e.g.* 30 cm from the cell ends in the FD) to smooth the mean PE/cm profiles with the nearby hits [166]. Fig. 3.10 illuminates the procedure.

Absolute calibration [166] exploits stopping cosmic μ as standard candles to translate the corrected PE/cm provided by the attenuation calibration to specific energy losses $\mathrm{d}E/\mathrm{d}x$ of a MIP (minimum ionizing particle), which is given by the Bethe-Bloch formula [7]. The μ used for the absolute calibration are required to stop in the detectors' central regions (to avoid issues with attenuation curves shape) and to have a reconstructed Michel e[5] at the end of their track. Fig. 3.11 illustrates the absolute calibration of the FD, and the ND follows suit. Moreover, to account for the calibration drift, *i.e.* changes in APD gain, scintillator and electronics aging, or environmental conditions, the calorimetric energy scales for 2020 analysis were determined separately for shorter data-taking intervals per epoch [168].

[5] A few notes on the Michel e reconstruction and identification are in the "Michel decomposition" paragraph of Subsection 3.10.2 or Ref. [167].

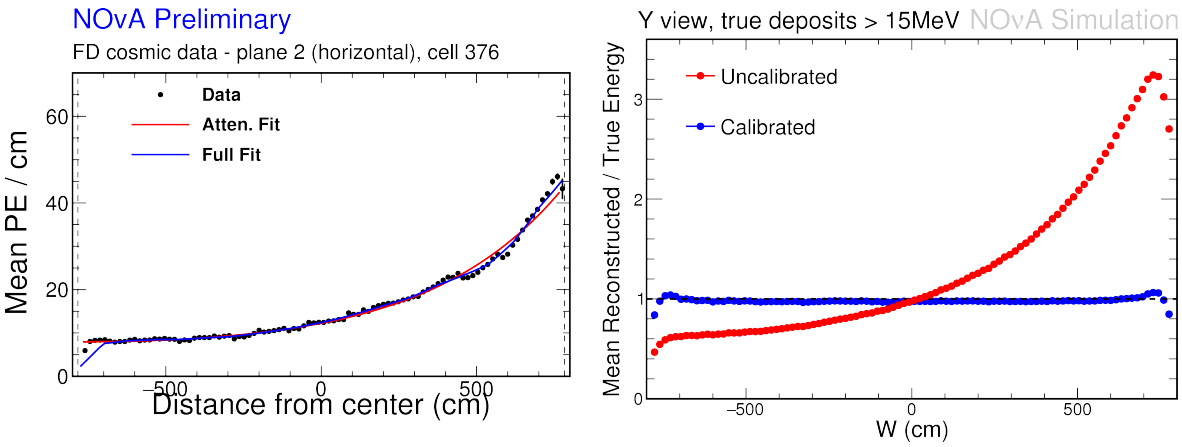

Figure 3.10: Example of the attenuation calibration procedure in horizontal cells (yz side view). **Left:** Mean number of PE/cm in a cosmic data sample w.r.t. the "distance from center" in a horizontal FD cell ($W = 0$ cm) fitted with the attenuation formula of Eq. (3.14) (red) and subsequent full fit smoothing (blue). APD pixel is on the right side of the plot. **Right:** Simulated mean reconstructed to true calorimetric energy response over all FD horizontal cells as a function of W (hit position in the cell) without (red) and with (blue) attenuation correction. The plots are from Ref. [169].

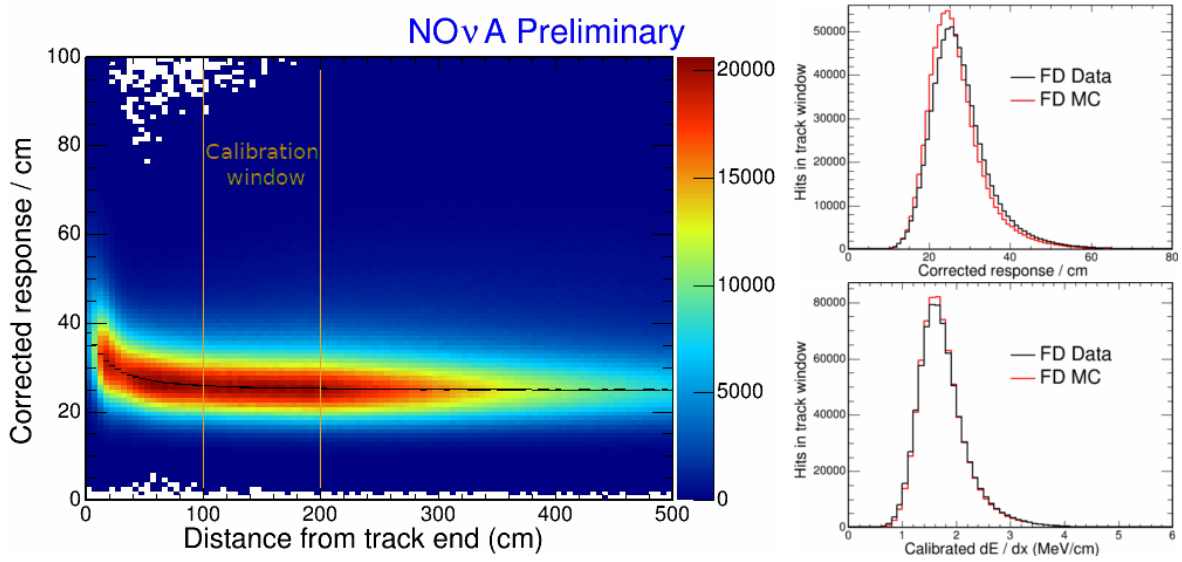

Figure 3.11: Illustration of the absolute calibration procedure. **Left:** FD attenuation corrected PE/cm response of tri-cell hits in tracks of stopping cosmic μ *vs.* their distance to the track end. The black curve shows the means of corrected PE/cm at particular distances. Only hits within the calibration window (orange vertical lines) are used for calibration. **Right:** FD data and MC of the number of hits in the calibration window as a function of corrected PE/cm (top) and the calibrated $\mathrm{d}E/\mathrm{d}x$ (bottom). The plots are from Ref. [170]

3.7 Particle identification algorithms

3.7.1 Filters

Filters are to remove obvious undesirable or background events from recorded data before the main steps of the reconstruction and thus substantially save production CPU time [171].

Cosmic veto

The FD records an order of magnitude more cosmic data than the actual beam events of ν interactions or misidentified ν-like cosmic events. To promptly remove this uninteresting activity, a CNN-based (Convolutional Neural Network) algorithm was developed. It is applied in 16 μs windows of the FD data hits distributions (pixel maps) with 1 μs overlaps to reduce events being split up. The entire nominal NuMI beam spill interval is always within one of the windows, see Appendix A and Fig. A.1. The CNN is based on the ResNet18 architecture, see Ref. [172], and it was trained on the previous production MC of cosmic sidebands in the NuMI trigger window (Subsection 3.9.2). This veto rejects ∼95% of the cosmic background while keeping >99% of relevant ν-like events [173].

Rock filter

A large number of μ in ND data comes from ν interactions in the surrounding rock (so-called "rock events"), and they are later discarded by the preselection fiducial rules (Subsection 3.9.2). The rock filter uses a simple cut on the start of the μ track or the vertex position to remove the event from processing. This potentially saves the time required for full ND data reconstruction while keeping >99% of otherwise selected events [174].

3.7.2 Reconstructed μ identification

To distinguish reconstructed Kalman tracks of μ from others (mostly from $\pi^{\pm}$), NOvA uses the so-called ReMId (Reconstructed Muon Identification) algorithm. ReMId is newly a BDTG[6] (Gradient Boosted Decision Tree [177, 178]), and its output score is based on four variables. Two log-likelihood differences of μ and π hypotheses $LL(\mu) - LL(\pi)$ of $\mathrm{d}E/\mathrm{d}x$ and "scattering" (*i.e.* the amount of angular deflection, deviations from a straight line) distributions along the track, the total track length, and the fraction of detector planes in the track with non-hadronic energy contributions.

The choice of the specified inputs follows a straightforward rationale. μ and π have different specific energy losses as MIPs, and the expected $\mathrm{d}E/\mathrm{d}x$ distributions in each point (detector plane) of the track in a π ensemble are wider and has higher mean values than that of μ. Similarly, there are more potential scattering centers for π as they, unlike μ, interact via the strong force. Next, the mean range of particles in hadronic showers is usually smaller than for a single μ. Also, μ have lower fractions of additional non-MIP energy depositions outside of the reconstructed track in the crossed detector planes away from the interaction vertex (remnants of hadronic activity towards the track end).

For the 2020 analysis, the probability distribution functions (PDF) for both likelihood calculations were updated, and the ReMId BDTG was trained using TMVA (Toolkit for Multivariate Data Analysis [179]) separately for FD, ND, and $\nu/\bar{\nu}$-beam MC samples [180]. ReMId classification efficiencies and purities were estimated to be over 90% for a large interval of ReMId output scores > 0. ReMId $\in [-1, 1]$, and higher scores signify a better agreement with the signal training sample, *i.e.* simulated events with reconstructed μ, w.r.t. the input variables while simultaneously discriminate background-like events of lower scores.

3.7.3 Cosmic rejection

The cosmic rejection algorithms are dedicated BDTs (Boosted Decision Tree) based on AdaBoost [181], prepared and validated using TMVA. All of them were trained separately for ν- and $\bar{\nu}$-beam FD MC. The 2020 analysis updates included retraining and performance optimization in relation to various sets of BDTs inputs and training sample definitions [182, 183].

[6] A k-Nearest Neighbor (k-NN) method [175] was used in the previous analyses [176].

Again, higher BDT output scores indicate better congruence with simulated signal non-cosmic events and worse with the cosmic background.

As there are two essentially different analysis samples in the ν_e appearance channel – see Subsections 3.9.5 and 3.9.6 – there are also two ν_e cosmic rejection BDTs: core CosRej BDT and peripheral CosRej BDT.

The BDTs input variables cover those expected to have an intrinsic power to discriminate between cosmic and beam ν-like electromagnetic showers like p_t/p of reconstructed transverse momentum fraction w.r.t. the beam direction, p_x/p, p_y/p, vertex coordinates, the distance of prongs to the detector edges, sparseness asymmetry, *etc.* Some of them were previously used directly for cosmic rejection cuts. The sets for the core and peripheral BDT are slightly different, however. The training was performed on FD MC cosmic and beam samples for several selections, and it was validated in order to choose the best performance within the ν_e signal regions in the FD [182].

The cosmic rejection BDT for the ν_μ disappearance channel follows a similar philosophy. The chosen input variables list basic reconstructed μ or cosmic track properties (track length, stop and start positions, the angle relative to the beam direction and y-axis, p_t/p, *etc.*) [183].

3.7.4 Convolutional visual networks

To identify and classify neutrino interactions and particles emerging from them, NOvA employs techniques from machine learning and computer vision for image recognition (apart from the mentioned cosmic veto). CVNs (Convolutional Visual Network) are convolutional neural networks[7] (CNN) with visual inputs, images, *i.e.* calibrated pixel-maps.[8] In the case of NOvA, xz and yz detectors view hit-maps of the reconstructed objects colored pixel-wise by the collected charge (Fig. 3.12) serve as inputs to CVNs to construe the typical topological features of the NOvA events, the CNN feature map. The outputs of the networks are closed sets of classification scores ranging over all eligible hypotheses of the physics events. The scores are normalized to one to provide a "probability-like" interpretation.

There are two CVNs: one for identifying the ν interaction events (event CVN or simply CVN from now on) and one for classification of the reconstructed prongs, *i.e.* single particles produced in ν interactions (prong CVN or simply pCVN from now on). Both were designed with Keras 2.1.2[9] and Tensorflow 1.12 [186]. To train and validate the networks, adequately split between the procedures, about 2.5 million events for each $\nu_\mu + \bar{\nu}_\mu$ CC, $\nu_e + \bar{\nu}_e$ CC and NC, 1.25 million $\nu_\tau + \bar{\nu}_\tau$ CC (not used for event CVN) were generated and ~ 0.75 million cosmic data events were chosen. CVN training technote is in Ref. [186], Refs. [187, 188] document the use of CVN in previous analyses.

Event identification

The event CVN architecture is a simplified MobileNetV2 [189], Fig. 3.13. It is modified to allow for two individual network inputs of two detector views. There are four recognized output event interaction classification scores of ν_μ CC, ν_e CC, NC, and cosmic. The ν_τ CC interactions were removed, as their threshold lies higher than the typical energy of the ν interactions in the oscillation analysis, and they have different topologies. The training was performed separately for ν- and $\bar{\nu}$-beam samples. To further strengthen this topological inquiry of the network and to loosen the absolute energy scale and calibration dependence, the training pixel-maps were randomly scaled by up to $\pm 10\%$ [186].

The new event CVN has about 90% efficiency and similar purity in terms of the highest classification score of the network's output, Figs. 3.14 and 3.15.

[7] First in Ref. [184], a general introduction and uses in Ref. [185].

[8] CVN(s) refers to a specific CNN(s) developed by NOvA for neutrino interactions classification.

[9] https://keras.io (as of Dec 2020)

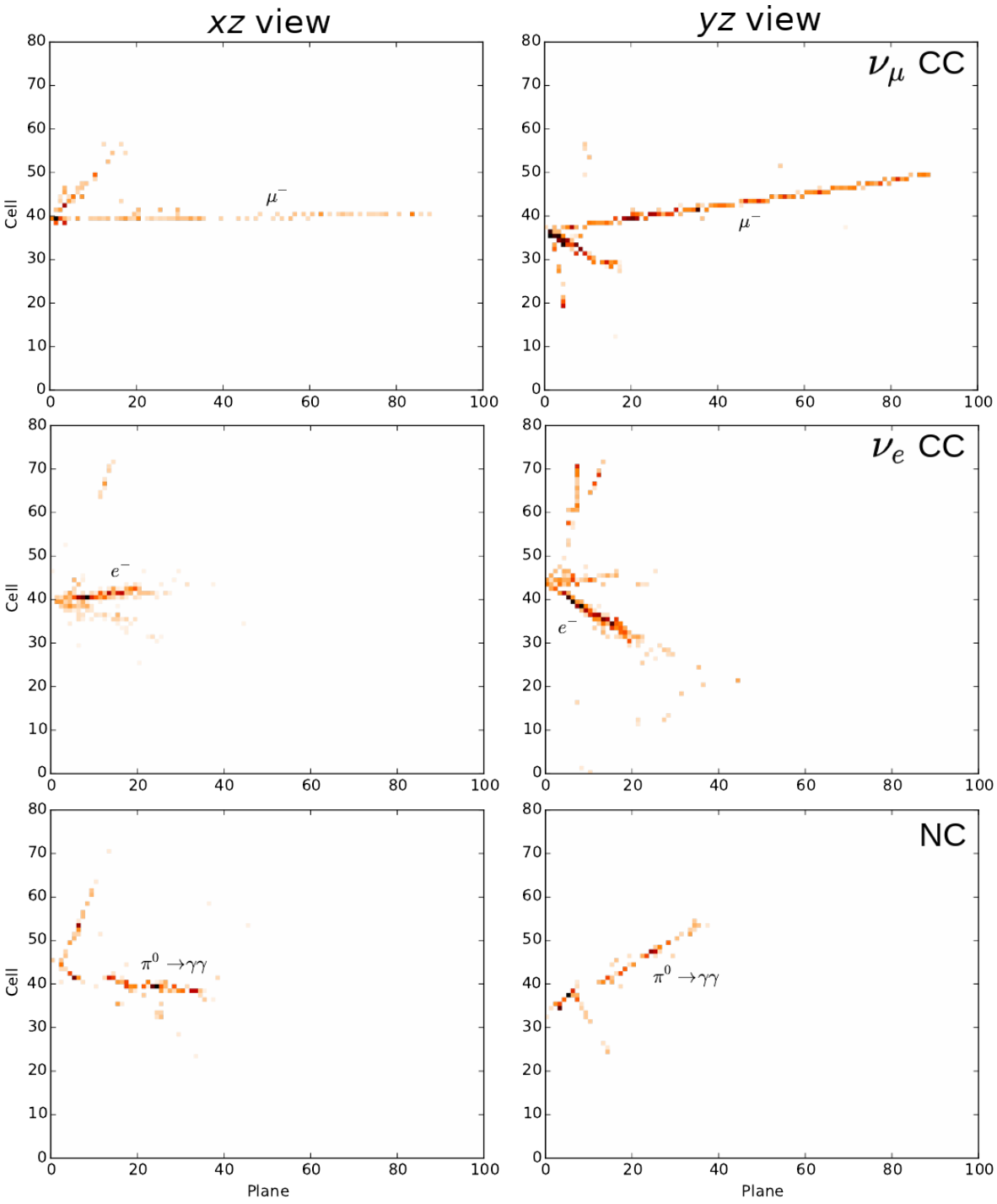

Figure 3.12: Examples of simulated CVN inputs for both detectors views, xz (top view, left) and yz (side view, right). Interactions of ν_μ CC, ν_e CC, and ν NC with π^0 production (from top to bottom). Colors denote the amount of the collected charge. The images are from Ref. [187].

Prong identification

Prong CVN is a single final state particle identifier, and its subjects – unlike reconstructed slices for the event CVN – are reconstructed prongs (Subsection 3.5.3). It utilizes both two views of the prong and corresponding two views of the event slice, *i.e.* four input pixel-maps

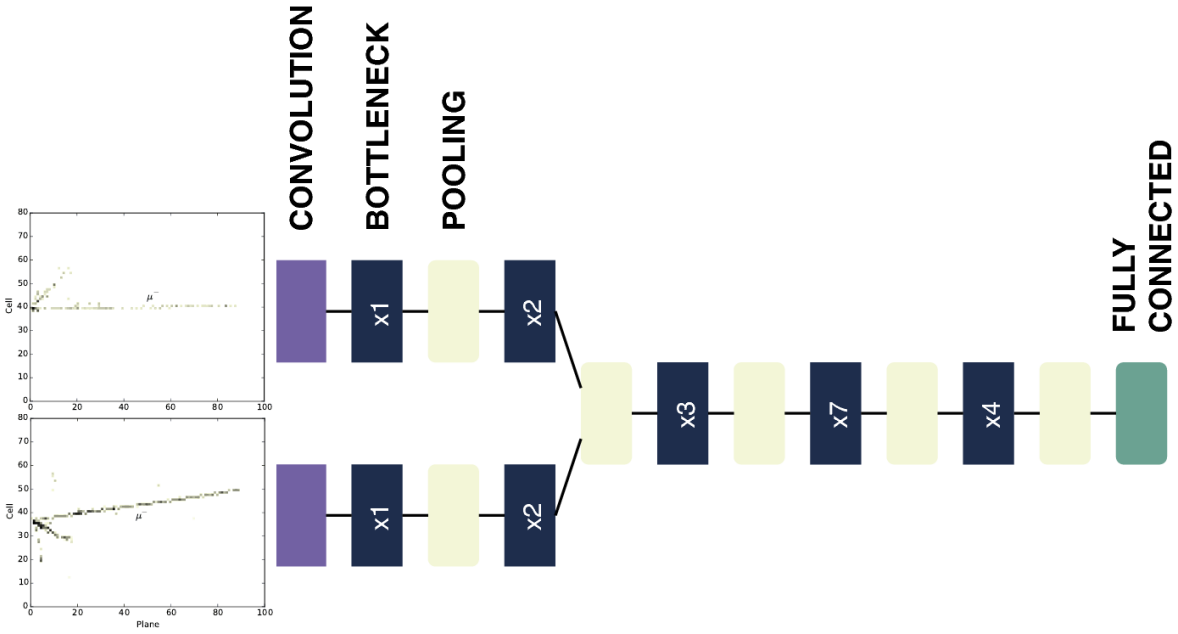

Figure 3.13: Diagram of the event CVN architecture. The network starts with two convolution layers building the initial features for the input views. The main components of the architecture are the bottleneck blocks that expand the input features, perform a depthwise convolution, and then compress the features once again. They are interlaced with pooling layers to reduce dimensionality. The fully connected output is represented by the four output scores of ν_μ, ν_e, NC, and cosmic. The picture is taken from Ref. [190]. Consult Refs. [185, Chapter 9] and [189] for terminology.

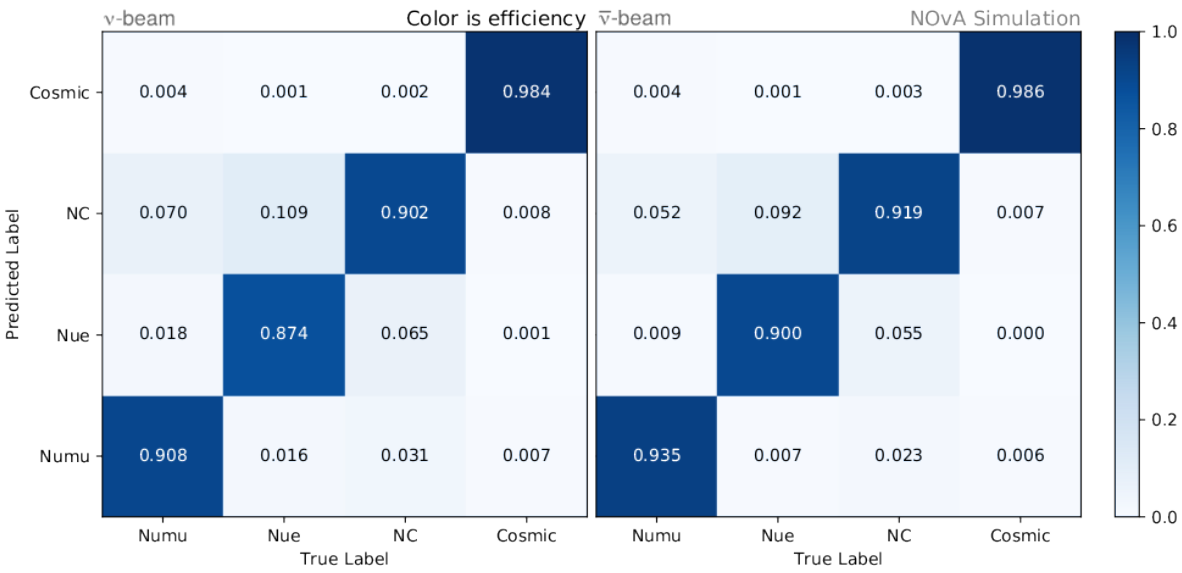

Figure 3.14: Classification efficiency of the event CVN for ν-beam (left) and $\bar{\nu}$-beam (right). The predicted label corresponds to the highest CVN output score (ν_μ CC – Numu, ν_e CC – Nue, NC or cosmic). The plots are from Ref. [190].

in total. The architecture is similar to the event CVN, and it is built on MobileNetV2 as well. The distinguished output classification scores account for μ, e, γ, p and $\pi^\pm$ labels that

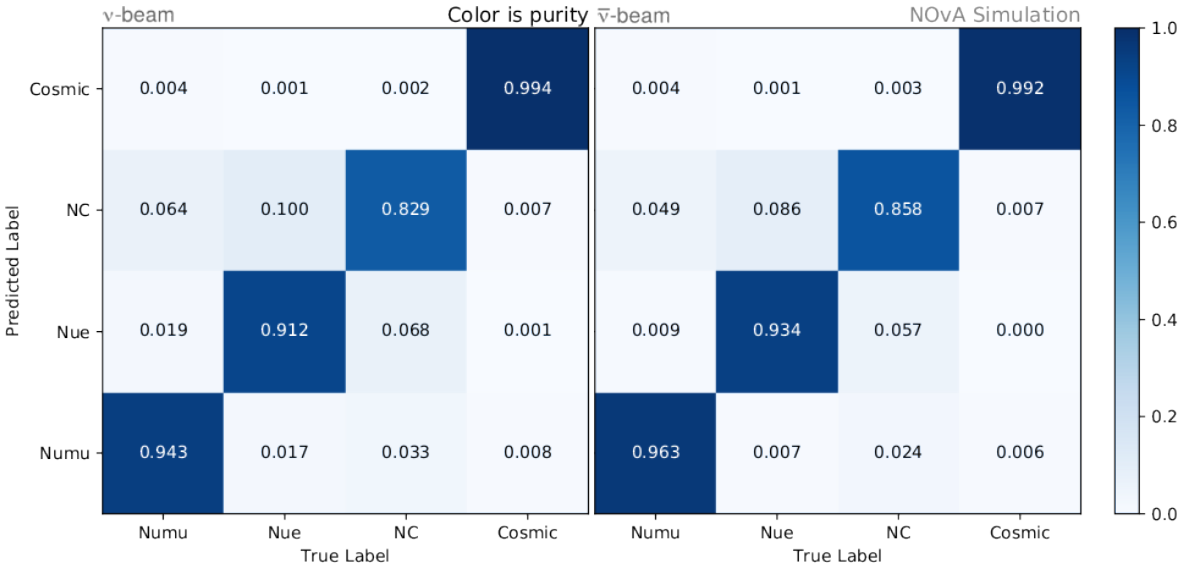

Figure 3.15: Classification purity of the event CVN for ν-beam (left) and $\bar{\nu}$-beam (right). The predicted label corresponds to the highest CVN output score (ν_μ CC – Numu, ν_e CC – Nue, NC or cosmic). The plots are from Ref. [190].

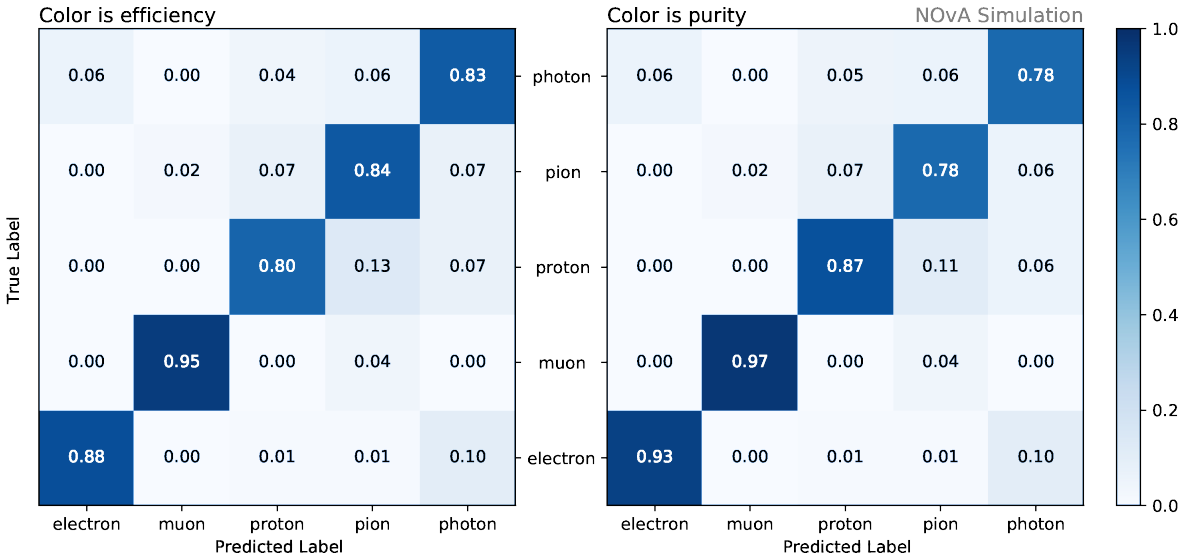

Figure 3.16: Efficiency (left) and purity (right) of the prong CVN classification in ν-beam. True label corresponds to the particle with the highest direct contribution to the total calorimetric energy deposited in the prong. The predicted label corresponds to the highest pCVN output score. The plots are from Ref. [192].

are based on the most prominent contributor that directly deposited energy in the prong (*e.g.*, a γ-like prong has most of its deposited energy originating from γ). The network was trained for ν- and $\bar{\nu}$-beam separately with roughly equal representations of the prong types in the simulated samples ($\sim$20% each).

pCVN expected efficiency is more than 80% with purity ranging from 78% (γ, π) to over 97% (μ), see Fig. 3.16. Though pCVN was trained and used for $\nu/\bar{\nu}$-beam, respectively, the actual performance of both versions was found qualitatively and quantitatively similar within the same validation samples (*e.g.* ν trained and $\bar{\nu}$ trained pCVNs in ν sample) [191].

3.8 Energy estimation

There are two basic energy estimators used in the oscillation analysis: one for ν_μ and one for ν_e CC candidates. Both were reoptimized because of the modeling and reconstruction changes [137, 171].

The estimator functions are determined for ν- and $\bar{\nu}$-beam modes separately. In the case of ν_μ also for the ND and FD and several data-taking periods because of different FD running conditions and the presence of μ-catcher in the ND. The RMS of the fractional residuals between true and estimated energies $(E_{\text{true}} - E)/E_{\text{true}}$ is interpreted as the expected energy resolution [101].

3.8.1 ν_μ energy

The energy of selected ν_μ in CC interactions is estimated as

$$E_{\nu_\mu} = E_\mu + E_{\text{had}}, \tag{3.15}$$

where E_μ is the energy of the primary μ and E_{had} is the energy of the remaining activity (hadronic shower) [193, 194].

E_μ is derived from the reconstructed μ track (Kalman) length. It uses a function resulting from a spline fit of peaks in a 2D distribution of simulated μ energy and reconstructed track length, as indicated in Fig. 3.17. Peaks are obtained from Gaussian fits in each of the track length bins. Since μ from ν_μ CC interactions are almost ideal MIPs, their tracks are rather long, and the average E_μ resolution of about 3% is directly related to the size of the detector cell planes.

E_{had} is estimated from all calorimetric energy not assigned to the μ track,[10] *i.e.* visible hadronic energy. The procedure is similar to that of E_μ, though the investigated distribution is (true ν_μ energy $-E_\mu$) *vs.* visible hadronic energy. E_{had} resolution is about 30%.

The average resolution of the total E_{ν_μ} is approximately 8–11% depending on the beam mode, detector (being worse in the ND due to the μ-catcher), and data-taking period [194]. The performance is considered slightly worse than with the previous estimator, possibly due to the changes in the ν cross section model and the new slicing algorithm. Nevertheless, for the oscillation analysis (Subsection 3.9.3), it is worth noting that the actual resolution strongly depends on the fraction of E_{had} in E_{ν_μ} for apparent reasons, and it varies from about less than 6% to more than 12%.

3.8.2 ν_e energy

Since the detectors have quite different electromagnetic and hadronic responses, the energy estimator for ν_e candidates relies on prong CVN (a single particle cluster, pCVN) ID to categorize the depositions into electromagnetic- (E_{em}) and hadronic-like (E_{had}), where the event's total calorimetric energy $E_{\text{cal}} = E_{\text{em}} + E_{\text{had}}$. E_{em} is a sum of calorimetric energies of all prongs with

$$\text{pCVN } e + \text{pCVN } \gamma \geq 0.5, \tag{3.16}$$

i.e., equivalently, if the sum of pCVN scores on e and γ is greater than or equal to the sum of the rest. All remaining prongs contribute to E_{had}.

E_{ν_e} is estimated as a quadratic function of E_{em} and E_{had}

$$E_{\nu_e} = a_0(a_1 E_{\text{em}} + a_2 E_{\text{had}} + a_3 E_{\text{em}}^2 + a_4 E_{\text{had}}^2). \tag{3.17}$$

[10] This includes hits from the μ track near the interaction vertex exceeding a certain MIP threshold, *i.e.* probably caused by hadronic activity.

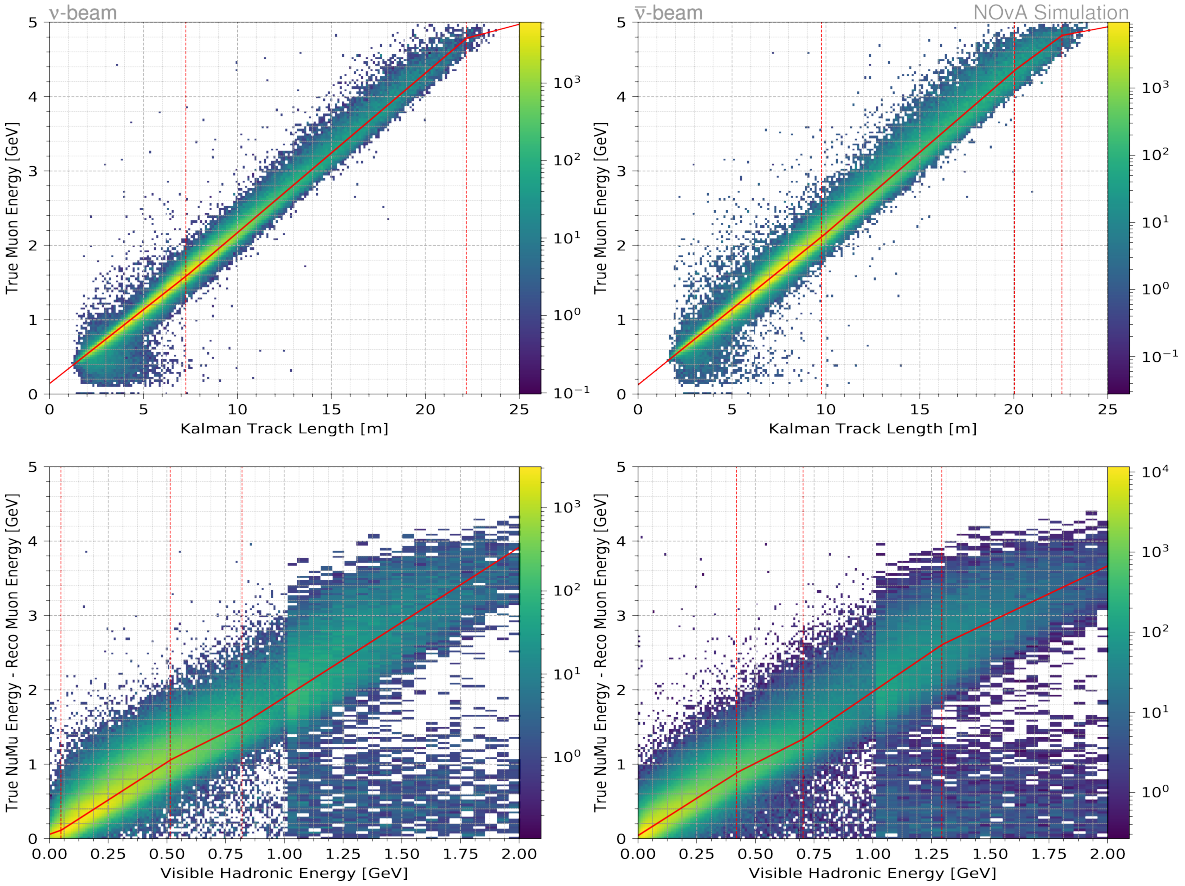

Figure 3.17: ν_μ CC energy spline plots. **Top:** μ energy E_μ spline plots. The full red line represents the spline fit of the peaks of true μ energy (vertical axis) distributions in individual track length bins (horizontal axis). The vertical dashed red lines indicate the linear segments stitch points of the spline fit. **Bottom:** Visible hadronic energy E_{had} spline plots. The procedure is similar but performed in true ν_μ energy $- E_\mu$ (vertical axis) and calorimetric energy not assigned to μ (visible hadronic energy E_{had}, horizontal axis). **Left:** ν-beam. **Right:** $\bar{\nu}$-beam. The plots are taken from Ref. [195].

The parameters are obtained through a fit to FD MC ν_e CC events with event CVN $\nu_e > 0.75$ (potential selection candidates) to minimize the variance from the true neutrino energy. To stay unbiased towards the expected position of the beam peak (around 2 GeV), FD MC is reweighted with neutrino true energy to obtain a flat spectrum first.

Final ν_e energy resolution is slightly better than in the previous analysis [101]. Estimated RMS of fractional energy residuals in FD MC are 10.7% (10.9%) / 8.8% (9.5%) in $\nu/\bar{\nu}$-beam (previously). For more details and validations, see Ref. [196].

3.9 Event selection and analysis samples

The analysis utilizes two conceptually different event selection chains for the disappearance (ν_μ selection) and appearance (ν_e selection) channel. Nevertheless, the dedicated cuts follow a standard flow of basic quality → preselection → cosmic rejection and PID (particle identification), Fig. 3.18. NOvA's cuts also split the candidate events into the analysis samples described in Subsections 3.9.3, 3.9.5, and 3.9.6.

Almost all of the selections were updated and reoptimized for the 2020 analysis. An apt summary can be found in Ref. [197]. Appendix A lists all the selection rules applied.

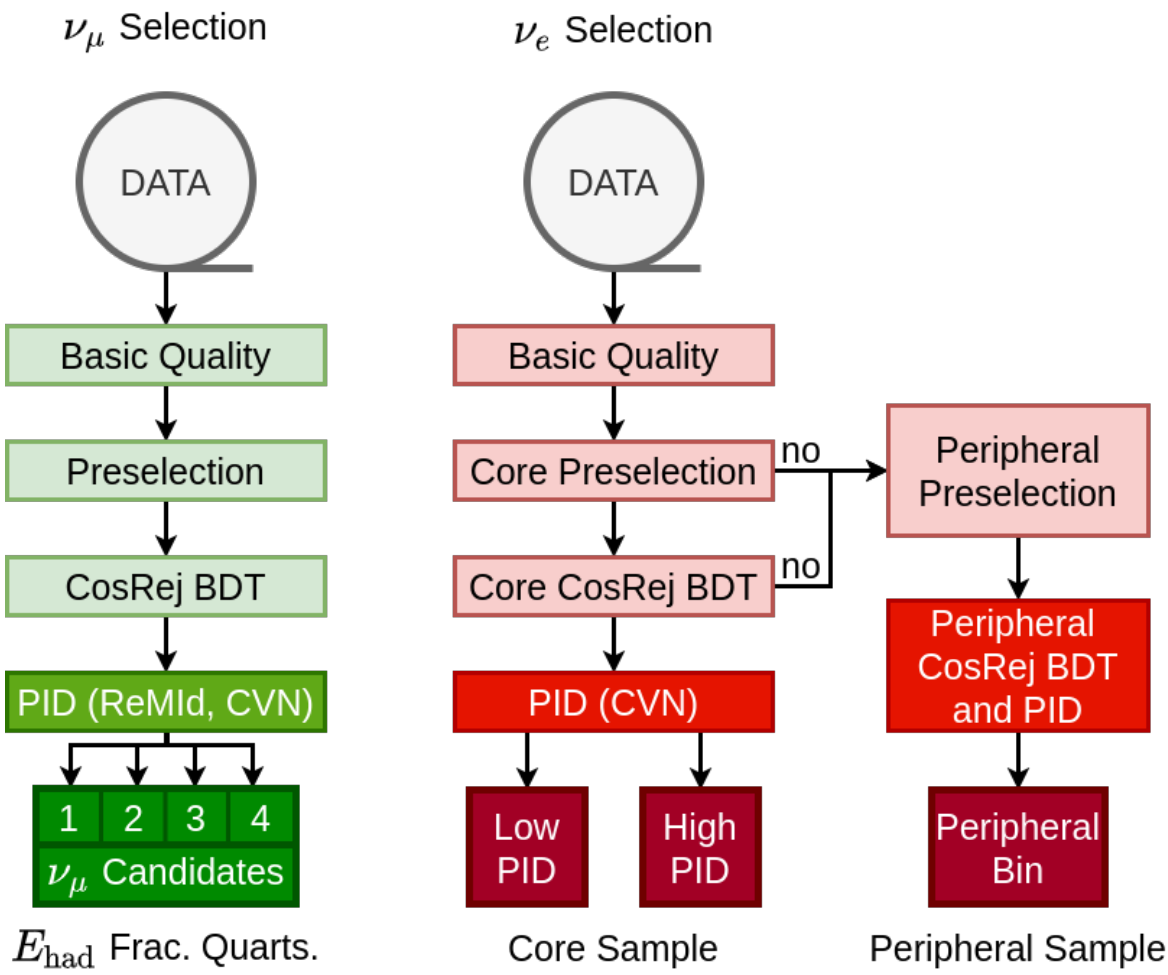

Figure 3.18: Event selection cutflows in the disappearance (left, green, ν_μ selection) and appearance (right, red, ν_e selection) channel. The splitting into the analysis samples of E_{had} fraction quartiles, low/high PID, and the peripheral sample is indicated, see Subsections 3.9.3, 3.9.5, and 3.9.6 for clarification. The selections are similar for ν- and $\bar{\nu}$-beam data, though particular cut points might differ.

3.9.1 Basic quality cuts

Detector and beam quality cuts ensure the detectors and NuMI beam good and stable running conditions (*e.g.* horizontal beam width, acceptable beam position, or magnetic horns current). Unlike other cuts which are applied event-by-event, they are spill level cuts [102, 197].

Beam and cosmic sideband timing cuts define time intervals in the NuMI triggered 550 μs data where to look for beam events and for the sidebands of cosmic activity. The standard NuMI beam window is set to 217–229 μs, and the sidebands are 25–208 μs and 238–475 μs. An issue with TDUs during period 1 that caused their timestamps to randomly jump -64 μs after resetting was corrected by adding an extra NuMI timing cut of 281–293 μs for period 1 [198].

The new CNN cosmic veto (Subsection 3.7.1) introduces an additional 16 μs time sampling of the original 550 μs window. It breaks down 550 μs into 16 μs intervals with 1 μs overlaps. Unfortunately, the effects of the sampling in these overlaps (*e.g.* breaking up real events) were not fully understood, and they were removed from the analysis. That resulted in a partial

loss of period 1 exposure (0.2% of the total ν-beam POT) and total detector livetime (about 7%). For details see Fig. A.1 in Appendix A.

3.9.2 Preselection cuts

Event quality cuts remove slices that fail to meet several reasonable criteria on basic reconstruction or provide rough filtering of backgrounds. They include cuts on a minimal (and maximal) number of hits in slices as these correspond to too low (high) energy events to originate from the beam, or they tend to be poorly reconstructed. There are also cuts on the presence of some reconstructed objects, such as at least one reconstructed track in a ν_μ event candidate and its ReMId score > 0, or one reconstructed prong in ν_e events.

Containment and fiducial cuts guarantee the interaction and all subsequent energy depositions happened inside the detector. They minimize the energy escaping from the detectors and help to sift events entering from outside (cosmic and ν interactions in front of the detectors). They include cuts on reconstructed vertex position, the distance of prongs to the detectors' edges, and alike.

Containment cuts were reoptimized for the new FD and ND MC w.r.t. three general metrics: contained/uncontained number of events, energy resolution, and escaping energy fraction $\frac{E \text{ not deposited in the detector}}{E_{\text{true}}}$, and for an additional data/MC metric in the ND. Despite the changes in geometry, simulation, and clustering, the containment cuts required very little changes and became somewhat tighter than in the previous analyses: tighter vertex position cuts for both ν_μ and ν_e ND, and the length of track projections to the nearest detector edge for ν_μ FD. For details, see Appendix A or Ref. [197].

3.9.3 ν_μ samples

As mentioned in Subsection 3.8.1, E_{ν_μ} resolution strongly depends on the fraction of the energy of the hadronic system E_{had} in the total reconstructed neutrino energy. Hence, each of the ν_μ samples (both ND and FD, $\nu/\bar{\nu}$-beam) is divided into four subsamples based on the reconstructed $E_{\text{had}}/E_{\nu_\mu}$ called the "hadronic energy fraction quartiles", E_{had}-quartiles. This can significantly enhance sensitivity to the important $\sin^2 2\theta_{23}$ [199]. Four quartiles are a reasonable compromise between the estimated gain and extra computational resources required in the subsequent steps of the analysis. The quartiles are numbered from the lowest $E_{\text{had}}/E_{\nu_\mu}$ (quartile 1) to the highest (quartile 4).

Furthermore, ν_μ samples use a variable E_{ν_μ} binning, see Fig. 3.34, respecting the oscillation "dip" region in the ν_μ spectra, where the minimum of $P(\nu_\mu \to \nu_\mu)$ from Eq. (1.34) is located. The binning is finer for 1–2 GeV and coarser elsewhere to save computational time. The lowest bin width of 0.1 GeV is about the expected best-achieved energy resolution of $\sim$6%.

The boundaries of E_{had}-quartiles (25%, 50%, and 75%) are determined for each energy bin from the population of ν_μ ($+\bar{\nu}_\mu$) CC events in FD unoscillated MC, and they can be seen in Fig. 3.19. The ν_μ CC MC populations of the quartiles are set to be the same by the definition of a quartile. Nevertheless, the final predicted and observed numbers in them might vary for obvious reasons. The average estimated energy resolution in the individual quartiles is about 6%, 8%, 10%, and 12% from the lowest to highest E_{had} fraction, respectively.

3.9.4 ν_μ PID selection

Three separate PID classifiers manage the selection of ν_μ CC candidates: ν_μ cosmic rejection BDT (Subsection 3.7.3), ReMId (Subsection 3.7.2) and event CVN ν_μ score (Subsection 3.7.4). The PID cuts were optimized for the reference oscillation parameters, FD MC,

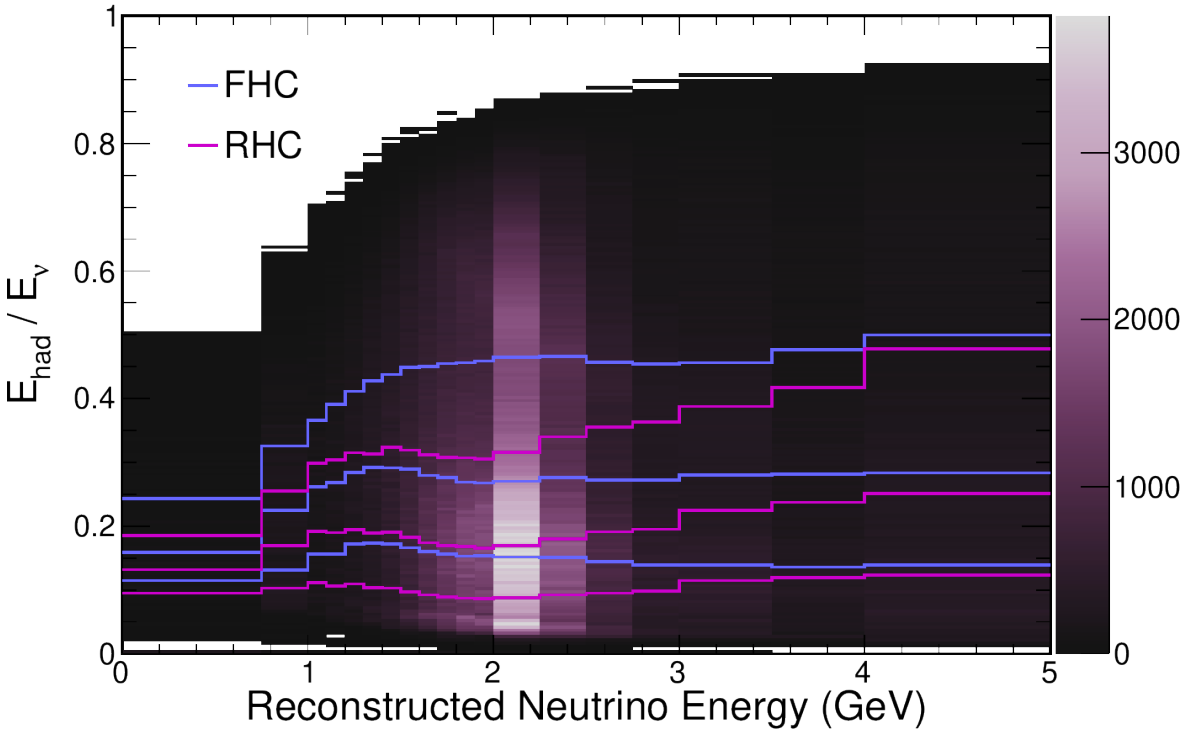

Figure 3.19: Boundaries of the E_{had} fraction quartiles ($E_{\text{had}}/E_{\nu_\mu}$, vertical axis) w.r.t. the reconstructed neutrino energy for ν-beam (blue, FHC) and $\bar{\nu}$-beam (magenta, RHC), overlayed with FD MC unoscillated $\nu_\mu + \bar{\nu}_\mu$ CC sample (ν-beam only). The plot is from Ref. [197].

and a simple figure of merit (FOM)

$$\text{FOM} = \frac{s}{\sqrt{s+b}}, \tag{3.18}$$

where the signal s accounts for all $\nu_\mu + \bar{\nu}_\mu$ CC events, background b is any other interaction (ν_e, NC, *etc.*). The combination of cosmic rejection, ReMId, and event CVN cuts to maximize the FOM is considered optimal. Stability of the FOM around individual cut points is also required.

The optimization was performed separately for ν- and $\bar{\nu}$-beam and also for several different underlying FOM specifications:

1. FOM in the "dip" region, *i.e.* for $E_{\nu_\mu} \in (1, 2)$ GeV (see Fig. 3.34),
2. FOM in the entire energy interval, *i.e.* for $E_{\nu_\mu} < 5$ GeV, and
3. separate FOMs of 1. or 2. for the quartile with the highest E_{had} fraction as it is estimated to have more background events than other quartiles.

The two latter versions did not show any additional impact, therefore the final PID selection was optimized using the first FOM definition. The ideal PID cut values were so close for ν- and $\bar{\nu}$-beam that it allowed for using identical cuts for both of them:

$$\begin{aligned} \nu_\mu \text{ CosRej BDT} &> 0.45, \\ \text{ReMId} &> 0.30, \\ \text{Event CVN } \nu_\mu &> 0.80. \end{aligned} \tag{3.19}$$

The details of the optimization procedure, methodology, and results are described in Refs. [197, 200].

3.9.5 ν_e core sample

The ν_e PID selection uses the ν_e dedicated cosmic rejection BDT (Subsection 3.7.3) and the event CVN ν_e score (Subsection 3.7.4). The sample has bins of 0.5 GeV width, and it is divided into two subsets depending on the CVN score: low and high PID. They are expected to have fundamentally different background compositions with more ν_μ and NC events in the low PID bin. The high PID bin has a better purity of signal events and intrinsic $\nu_e + \bar{\nu}_e$ background, see Table 3.5.

The optimization was initially performed with three different PID bins of unconstrained and floating boundaries, and it used a metric of

$$\mathrm{FOM}^2 = \sum_{\mathrm{PID}} \frac{s^2}{s+b}, \tag{3.20}$$

where the signal s is defined as "appeared" ν_e CC and $\bar{\nu}_e$ CC, *i.e.* originating from $\nu_\mu/\bar{\nu}_\mu$ parent, for ν- and $\bar{\nu}$-beam, respectively. The appeared $\bar{\nu}_e$ in ν-beam and ν_e in $\bar{\nu}$-beam (wrong-signed or WS background), intrinsic beam $\nu_e + \bar{\nu}_e$ and all other interactions are background b. The sum goes over the PID bins. For the lowest PID bin turned out to be background dominated with the corresponding individual FOM < 1, it was not incorporated into the analysis.

To further reduce Bremsstrahlung background from cosmic rays, the selected ν_e candidate slices are required to be enough spatially or temporally separated from other candidates or not to be near the top edge of the detector, see Appendix A.

The cut values maximizing the FOM in Eq. (3.20) for ν-beam / $\bar{\nu}$-beam were:

$$\begin{aligned} \nu_e \text{ Core CosRej BDT} &> 0.49 \;/\; 0.47, \\ \text{Event CVN } \nu_e & \\ \text{Low PID} &> 0.84 \;/\; 0.85, \\ \text{High PID} &> 0.97 \;/\; 0.97. \end{aligned} \tag{3.21}$$

The details of the procedure are illustrated in Fig. 3.20 and summarized in Ref. [197]. Events filtered by the described cutflow (basic quality, preselection, cosmic rejection, and PID, Fig. 3.18) form the so-called "core sample" of the ν_e CC candidates selection.

3.9.6 ν_e peripheral sample

Events failing the preselection or ν_e cosmic rejection cuts can still score a high event CVN ν_e PID. Such events are usually not fully contained, and they appear at the very periphery of the detector. They can be reenacted into the analysis by ν_e "peripheral sample" with different preselection, omitting containment cuts and allowing a larger interval of reconstructed energy $E_{\nu_e} \in [0, 4.5)$ GeV.

Peripheral sample PID cuts require a higher CVN ν_e score and a special, dedicated ν_e peripheral cosmic rejection BDT cut (Subsection 3.7.3). The optimization is similar to the ν_e core sample, Fig. 3.21.

As E_{ν_e} cannot be reliably estimated for not fully contained events, they are integrated into a single "counting" peripheral bin (Fig. 3.35, rightmost bin). The peripheral sample is expected to contain a significant amount of up to 10% signal events.

3.10 Near detector data constraints and decomposition

As advertised, the NOvA neutrino oscillation analysis takes advantage of its two detector design to be constrained by the ND observations. There are multiple ways how to exploit ND

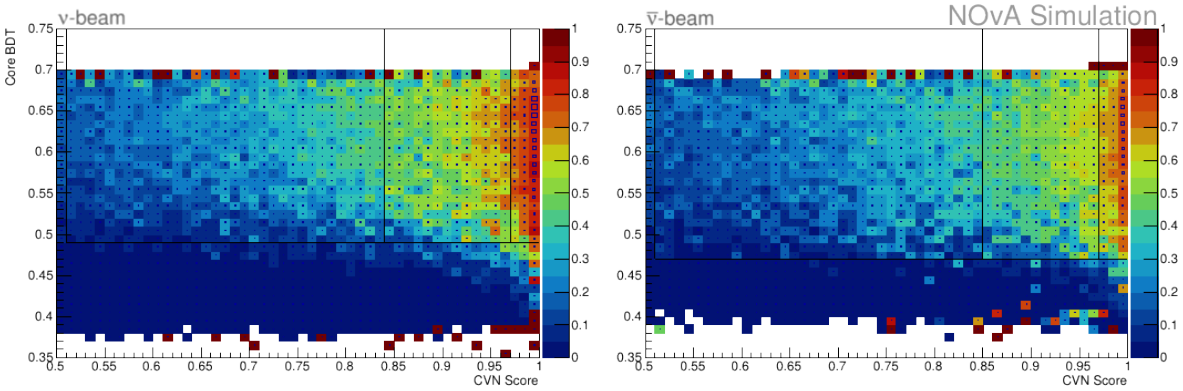

Figure 3.20: Illustration of the optimized ν_e core PID selection cuts in FD MC. Black full lines show the sample boundaries of CVN ν_e score (horizontal axes) and core cosmic rejection BDT score (vertical axes). The color represents signal ($\nu_\mu \rightarrow \nu_e$) purity, and the box size is proportional to the absolute amount of signal in each bin. **Left:** ν-beam. **Right:** $\bar{\nu}$-beam. The plots are taken from Ref. [197].

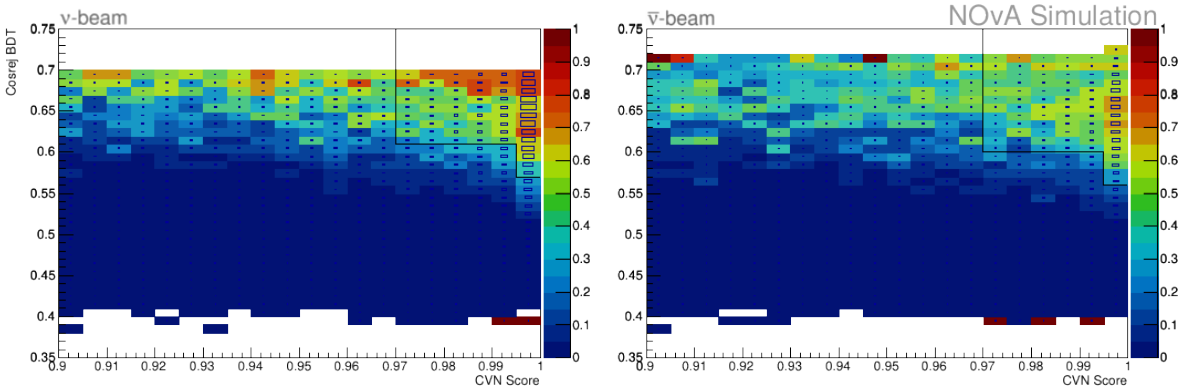

Figure 3.21: Illustration of the optimized ν_e peripheral PID selection cuts in FD MC. Black full lines show the sample boundaries of CVN ν_e score (horizontal axes) and peripheral cosmic rejection BDT score (vertical axes). The color represents signal ($\nu_\mu \rightarrow \nu_e$) purity, and the box size is proportional to the absolute amount of signal in each bin. **Left:** ν-beam. **Right:** $\bar{\nu}$-beam. The plots are taken from Ref. [197].

data in order to do so. Recall from Subsection 3.4.2 that the underlying neutrino interactions model is exerted to conform to ND data, *i.e.*, the base simulation is modified. Moreover, many ND studies were conducted to validate, tune or check the analysis elements, reconstruction algorithms, simulation outputs, *etc.*

Besides that, and primarily in fact, ND data is used to directly constrain FD MC predictions in particular analysis samples with the "Far/Near extrapolation" technique (more in Section 3.11). The basic idea of the technique can be simplistically expressed as a correction of FD MC by any ND data/MC discrepancies. FD and ND MC are closely entangled due to the detectors' functional similarity. From another point of view, by imposing equivalent FD event selections in the ND, the analysis FD samples are checked in their unoscillated states to provide information on the neutrino fluxes and interaction rates near the beam source.

To properly account for the neutrino transition probabilities $P(\nu_\alpha \rightarrow \nu_\beta)$ en-route to the FD, the constraining ND samples need to be broken down into single components of (anti)neutrino flavors (CC) and NC interactions. In NOvA, these procedures are referred

to as "decomposition", and they were designed within and in relation to the individual ND samples. The main intention of the decomposition is to estimate (anti)neutrino CC interaction rates of (anti)neutrinos with a specific flavor ν_α (or neutrino NC interactions) under selection s as a vector in neutrino reconstructed energy bins $\mathbf{N}(\nu_\alpha; s) = (N_1, N_2, \ldots)^\top$ or $\mathbf{N}(\mathrm{NC}; s)$. Here s is usually "equivalent" to one of the FD analysis sample selections.

ND selections in both channels are almost identical to the FD selections of the analysis samples (the same PID cuts, the same E_{had}-quartiles boundaries) with the following adjustments: tighter fiducial and containment cuts due to the smaller detector, specific μ-catcher cuts, no cosmic rejection as the ND is 100 m underground, and no ν_e peripheral sample.

3.10.1 Near detector ν_μ samples

The ND ν_μ CC samples are in Fig. 3.22 (4 E_{had}-quartiles) and in Fig. 3.23 (full ND ν_μ CC selection). They are expected to consist almost entirely of $\nu_\mu + \bar{\nu}_\mu$ CC events. Hence, contributions of ν_e CC and NC interactions can be neglected, and the decomposition is straightforward.

For ν_μ CC ND sample selection s_μ the $\mathbf{N}(\nu_\mu; s_\mu) = (N_1, N_2, \ldots)^\top$ (or $\mathbf{N}(\bar{\nu}_\mu; s_\mu)$ by the same token) is estimated in each reconstructed energy bin i as

$$N_i(\nu_\mu; s_\mu) = N_{\mathrm{MC},i}(\nu_\mu; s_\mu) \cdot \frac{N_{\mathrm{data},i}(s_\mu) - N_{\mathrm{MC},i}(\text{not } \nu_\mu/\bar{\nu}_\mu; s_\mu)}{N_{\mathrm{MC},i}(\nu_\mu + \bar{\nu}_\mu; s_\mu)} \approx N_{\mathrm{MC},i}(\nu_\mu; s_\mu) \cdot \frac{N_{\mathrm{data},i}(s_\mu)}{N_{\mathrm{MC},i}(s_\mu)}, \tag{3.22}$$

where $\mathbf{N_{MC}}(\nu_\mu; s_\mu)$ is a spectrum of rates of true ν_μ CC interactions in ND MC under selection s_μ, "not $\nu_\mu/\bar{\nu}_\mu$" means "not true ν_μ or $\bar{\nu}_\mu$ CC", $\mathbf{N_{data}}(s_\mu)$ is a vector of rates in ND data under selection s_μ, others accordingly. The approximation can be used as an effective simpler expression thanks to the very high $\nu_\mu + \bar{\nu}_\mu$ purities of ND ν_μ samples s_μ or in bins with only $\nu_\mu/\bar{\nu}_\mu$ CC events expected. Please note, that ν_μ decomposition is actually applied in the individual extrapolation samples (Subsection 3.11.1).

3.10.2 Near detector ν_e samples

ND ν_e samples represent a ν_e-like contents of the NuMI $\nu/\bar{\nu}$-beam and thereby constrain the beam induced background of FD ν_e samples. ND ν_e samples are mixtures of beam intrinsic $\nu_e + \bar{\nu}_e$ CC interactions, misidentified $\nu_\mu + \bar{\nu}_\mu$ CC interactions (typically with short μ tracks) and NC interactions, Fig. 3.28. Since the expected MC compositions vary significantly by their nature among the samples and in $\nu/\bar{\nu}$-beam, there are three different decomposition methods in use.

Beam ν_e decomposition (BEN)

Beam Electron Neutrino (BEN) decomposition to estimate ν_e CC intrinsic beam component relies on the fact that most of the beam ν_e originate from π^+ and K created in the target [202]

$$\begin{aligned} \pi^+ &\to \mu^+ + \nu_\mu \\ &\quad \hookrightarrow e^+ + \bar{\nu}_\mu + \nu_e \end{aligned} \tag{3.23}$$

and

$$K^+ \to \pi^0 + e^+ + \nu_e, \tag{3.24}$$

$$K^0_L \to \pi^- + e^+ + \nu_e. \tag{3.25}$$

Ad Eq. (3.23), π^+ is a common ancestor to both ν_μ and ν_e in this case. Using ND ν_μ sample which is dominated by ν_μ from π^+ (Fig. 3.24), a constraining data/MC weight on ν_μ

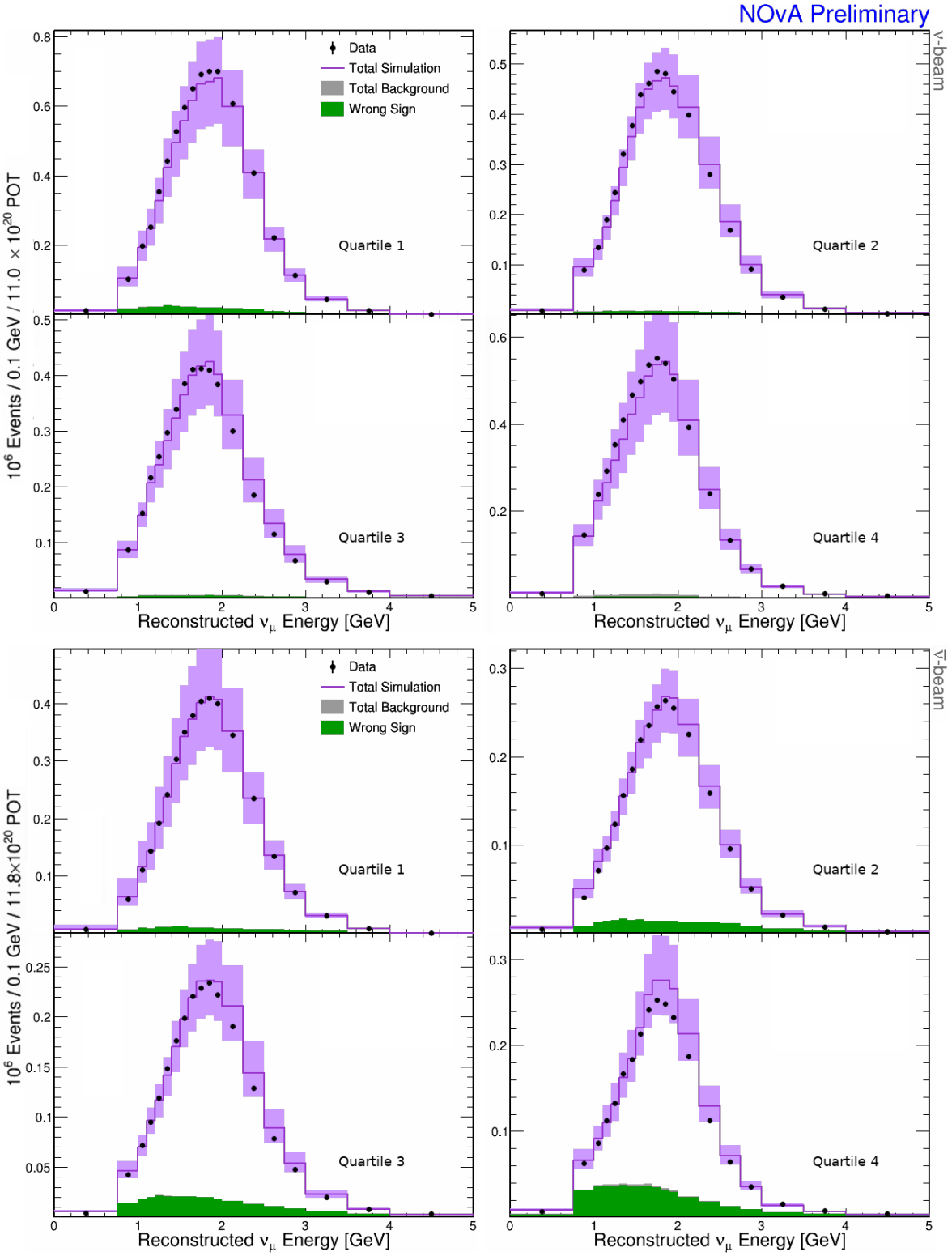

Figure 3.22: Near detector ν_μ CC selection in E_{had} fraction quartiles, *i.e.* ND ν_μ CC selected events (black dots) in bins of reconstructed neutrino energy E_{ν_μ} per 0.1 GeV overlaid with MC prediction (violet), wrong sign component of $\bar{\nu}_\mu$ in ν-beam and *vice versa* (green), and the total systematic uncertainty (band). Mostly negligible background (grey) is stacked onto the wrong sign component histogram. **Top four plots:** ν-beam, quartiles 1–4. **Bottom four plots:** $\bar{\nu}$-beam, quartiles 1–4. The plots are from Ref. [201].

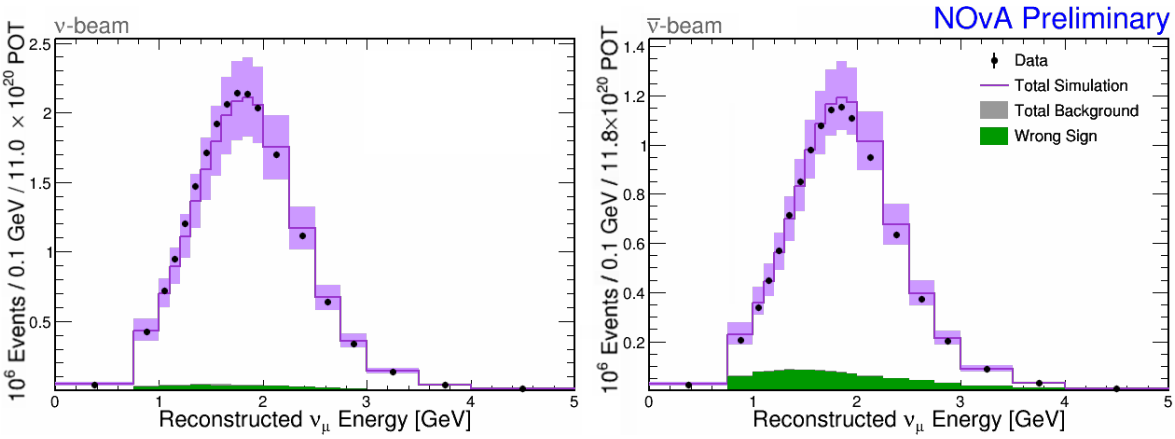

Figure 3.23: Near detector ν_μ CC full selection summed over E_{had} fraction quartiles, *i.e.* number of ND ν_μ CC selected events (black dots) in bins of reconstructed neutrino energy E_{ν_μ} per 0.1 GeV overlaid with MC prediction (violet), wrong sign component of $\bar{\nu}_\mu$ in ν-beam and *vice versa* (green), and the total systematic uncertainty (band). Mostly negligible background (grey) is stacked onto the wrong sign component histogram. **Left:** ν-beam. **Right:** $\bar{\nu}$-beam. The plots are from Ref. [201].

from π^+ in E_{ν_μ} bins is calculated. This weight is then propagated to the level of simulated true parent π^+ momentum space and applied to descendant ν_e CC in MC. A sum in bins of true ν_e energy over the momentum space provides the correction factor to the ν_e CC from the MC π^+ spectrum.

Ad Eqs. (3.24) and (3.25), K are parents of the higher energetic uncontained ν_μ CC events. ND ν_μ CC contained sample data/MC provides a normalization scale for ν_μ CC from π^+ events (Fig. 3.25). It is applied to the true ν_μ CC from π^+ events in a special ν_μ CC uncontained sample, which allows for constructing additional ν_μ from K normalization factor ($\sim +5.8\%$) in the higher energetic tail of the E_{ν_μ} distribution. This factor is used as a correction to the simulated ν_e CC from K.

To obtain the final $\mathbf{N}(\nu_e; s_e)$ in the ND sample s_e, any ν_e of different particle ancestors (and also $\bar{\nu}_e$) are estimated directly from the ND MC. They are scaled proportionally if the total $\mathbf{N}(\nu_e + \bar{\nu}_e; s_e)$ exceeds the selected ND data rate in the corresponding reconstructed energy bins $\mathbf{N_{data}}(s_e)$. Though the idea of BEN itself is not complicated, a direct expression for $\mathbf{N}(\nu_e; s_e)$ would be quite challenging and is therefore omitted for the sake of readability. Please refer to the dedicated technical notes in Refs. [202, 203] for further details.

BEN is rather not instantly applicable to $\bar{\nu}$-beam data as it cannot be effectively $\nu \to \bar{\nu}$ transformed. That is mostly due to the much larger wrong-sign component (WS, ν in $\bar{\nu}$-beam and *vice versa*) for higher energies originally negligible in ν-beam, which introduces extra degrees of freedom to the problem, compare Fig. 2.7. Though several approaches have been studied, it has not been resolved yet [204].

Michel decomposition

The second decomposition method aims to fix the ratio of $\nu_\mu + \bar{\nu}_\mu$ CC and NC interaction rates in the reconstructed energy bins of the ν_e samples, *i.e.* to estimate both $\mathbf{N}(\nu_\mu + \bar{\nu}_\mu; s_e)$ and $\mathbf{N}(\text{NC}; s_e)$. It exploits the distributions of the number of Michel e candidates N_{ME} in the selection to do so (Michel decomposition). A true ν_μ CC event contains a μ decaying into

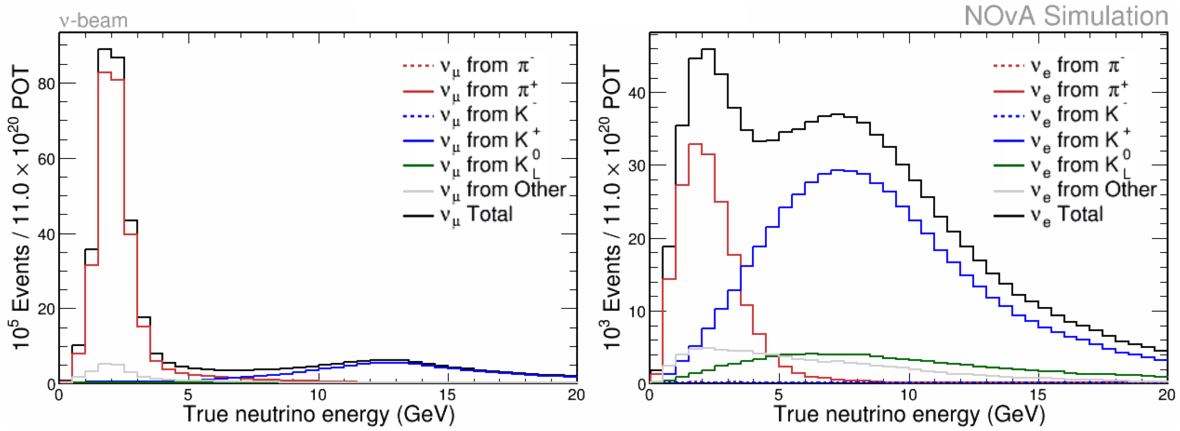

Figure 3.24: True neutrino energy spectra of ND ν_μ (left) and ν_e (right) CC events with interaction vertex contained in the detector for ν-beam, split by their ancestors at the beam target. The plots are from Ref. [205].

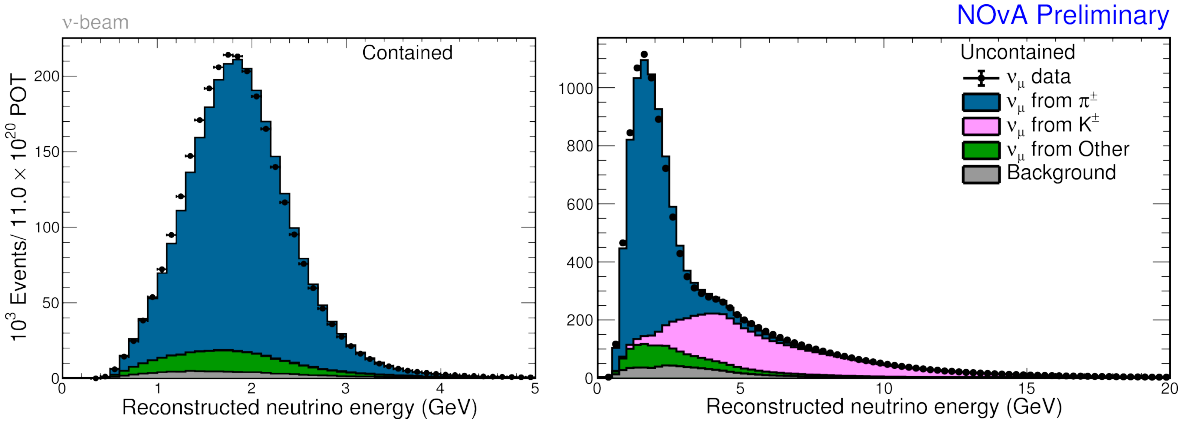

Figure 3.25: ND data (dots) and MC (stacked histograms) contained (left) and uncontained (right) selected ν_μ CC reconstructed energy spectra. The contained sample constrains the ν_μ from π weights, the uncontained sample then fixes the overall ν_μ from K scale. The plots are from Ref. [205].

an e via

$$\begin{aligned} \nu_\mu + A \to \mu^- + B \\ \hookrightarrow e^- + \bar{\nu}_e + \nu_\mu, \end{aligned} \tag{3.26}$$

where A, B are arbitrary states of the non-leptonic part of the interaction. Generally, for CC or NC interactions of any neutrino flavor ν_α, Michel e candidates can typically also occur in the decays of produced π

$$\begin{aligned} \nu_\alpha + A \to \pi^+ \ + \ \nu_\alpha/\alpha^- + B \\ \hookrightarrow \mu^+ + \ \nu_\mu \\ \hookrightarrow e^+ + \nu_e + \bar{\nu}_\mu, \end{aligned} \tag{3.27}$$

or in misidentified nuclear interactions. Nevertheless, true ν_μ CC events are expected to have about one more Michel e, Eq. (3.26), and the corresponding distributions of N_{ME} should be

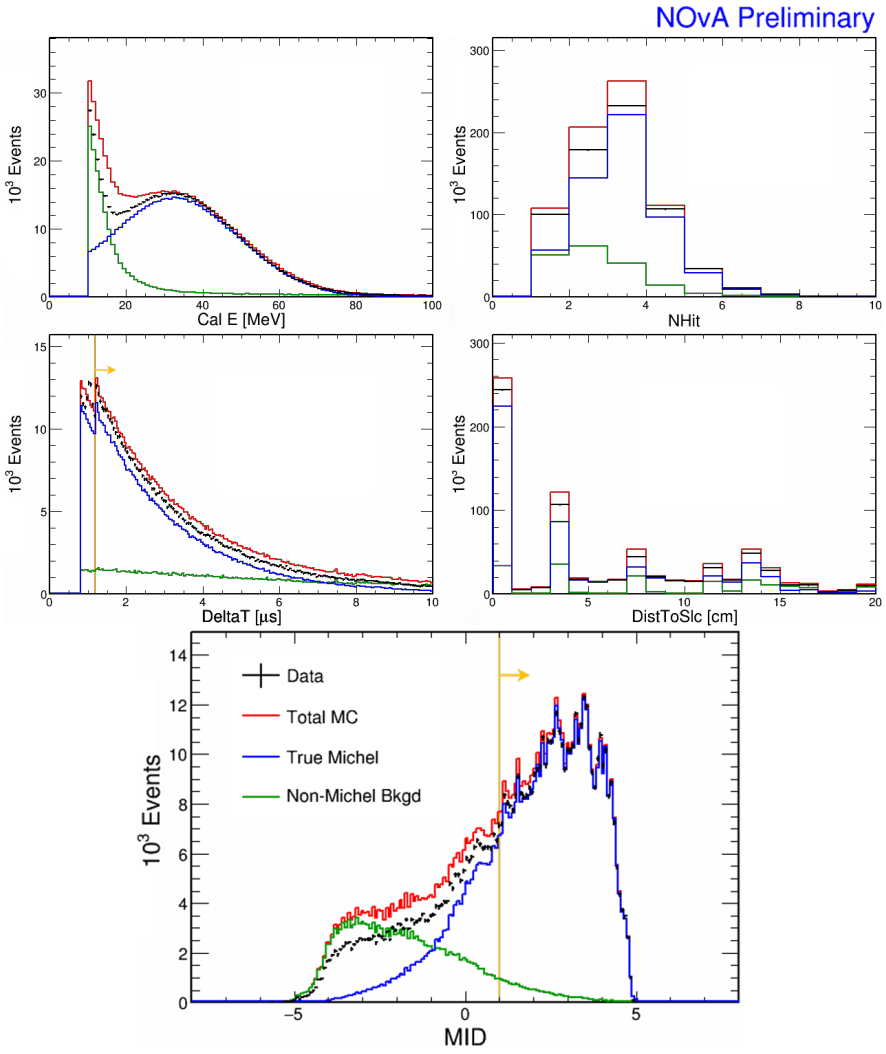

Figure 3.26: Distributions of the reconstructed variables of Michel e candidates in ND data and MC (red), true Michel e (blue), and background (green) in ND ν_e preselected sample. **Top four plots, clockwise from the top left:** Reconstructed calorimetric energy, number of reconstructed hits, spatial distance to the parent event slice, and time delay to the parent slice. **Bottom:** Output score of the Michel e classifier MID based on the variables in the left plots. The orange lines indicate the main selection criteria for ND ν_e ν-beam candidates used by the decomposition.[11]

shifted to higher values.

Michel electron candidates are reconstructed and identified thanks to the lifetime of free μ of 2.2 μs being much longer than the ND time resolution (∼10 ns). That means the hits associated with Michel e are rarely reconstructed within the common objects of tracks or event slices. A simple finding algorithm based on DBSCAN [167] looks for delayed hits in the vicinity of the hits already assigned to slices or μ-like tracks. Additionally, to filter non-Michel e delayed physics processes from mostly neutron captures, several characteristic variables serve as input to a log-likelihood Michel PID ("MID"). Their distributions are illustrated in

[11] As there are two qualitatively different samples of reconstructed Michel e candidates in combination with parent event slices or μ Kalman tracks, their selections slightly differ. Nevertheless, end-of-track Michel e are suppressed in ND ν_e samples whose events have poorly reconstructed tracks if any (misidentified ν_μ with very short μ tracks). Fig. 3.26 shows the dominant selection criteria, *i.e.* for Michel e reconstructed without a direct connection to a track.

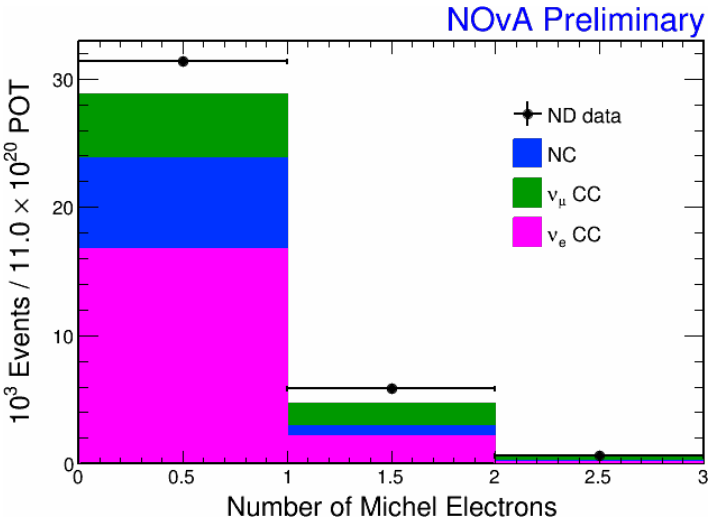

Figure 3.27: Distribution of the number of Michel e N_{ME} in the selected ND ν_e-like sample of events in ν-beam data and MC. The expected N_{ME} of $\nu_\mu(+\bar{\nu}_\mu)$ CC (green) from ND MC is shifted towards higher values of N_{ME} in comparison to NC (blue) and $\nu_e(+\bar{\nu}_e)$ CC (magenta) which have nearly degenerate shapes. The MC histograms are stacked.

Fig. 3.26, and the selections were slightly updated for 2020 analysis to get a better data/MC agreement.

With a given $\mathbf{N}(\nu_e + \bar{\nu}_e; s_e)$ provided by BEN, the decomposition condition of the sample s_e, *i.e.*, data matches the decomposed predictions in each reconstructed energy bin, is

$$\mathbf{N_{data}}(s_e) = \mathbf{N}(\nu_\mu + \bar{\nu}_\mu; s_e) + \mathbf{N}(\mathrm{NC}; s_e) + \mathbf{N}(\nu_e + \bar{\nu}_e; s_e). \tag{3.28}$$

Ergo, estimating $N_i(\nu_\mu + \bar{\nu}_\mu; s_e)$ and $N_i(\mathrm{NC}; s_e)$ bin-by-bin i is a one-dimensional problem that can be addressed with the supplementary information from the N_{ME} distributions. $N_i(\nu_\mu + \bar{\nu}_\mu; s_e)$ is estimated by maximizing a one-parameter (ν_μ scale) likelihood function for data and N_i of a Poisson experiment in the N_{ME} bins of the i-th ν_e samples reconstructed energy bin. The overall N_{ME} distribution is in Fig. 3.27.

The robustness of this method depends on the available statistics. Specifically, with lower ν_μ fractions, relatively small distortions of the other non-ν_μ CC components can have a heftier effect on the observed data of N_{ME} than a change of ν_μ rate itself. Hence, an intuitive *ad hoc* criterion of at least 20% of *a priori* predicted ν_μ CC, $N_{\mathrm{MC},i}(\nu_\mu + \bar{\nu}_\mu; s_e)$, in the energy bins to be Michel decomposed is required. Otherwise, ν_μ CC and NC interactions are only proportionally scaled. Several of the low PID energy bins are Michel decomposed as a result.

ND data are expected to contain even lower fractions of ν_μ CC (Fig. 3.28) for $\bar{\nu}$-beam, and thus, this method becomes somewhat ineffective and is abandoned.

Proportional decomposition

As BEN and Michel decomposition cannot be employed with $\bar{\nu}$-beam data, the i-th bin's ν_α flavor/NC contents of $\mathbf{N}(\nu_\alpha; s_e)$ are estimated in a simpler way by an impromptu data/MC "proportional" scaling (similar to ν_μ ND samples)

$$N_i(\nu_\alpha; s_e) = N_{\mathrm{MC},i}(\nu_\alpha; s_e) \cdot \frac{N_{\mathrm{data},i}(s_e)}{N_{\mathrm{MC},i}(s_e)}. \tag{3.29}$$

The (un)corrected spectra are again in Fig. 3.28.

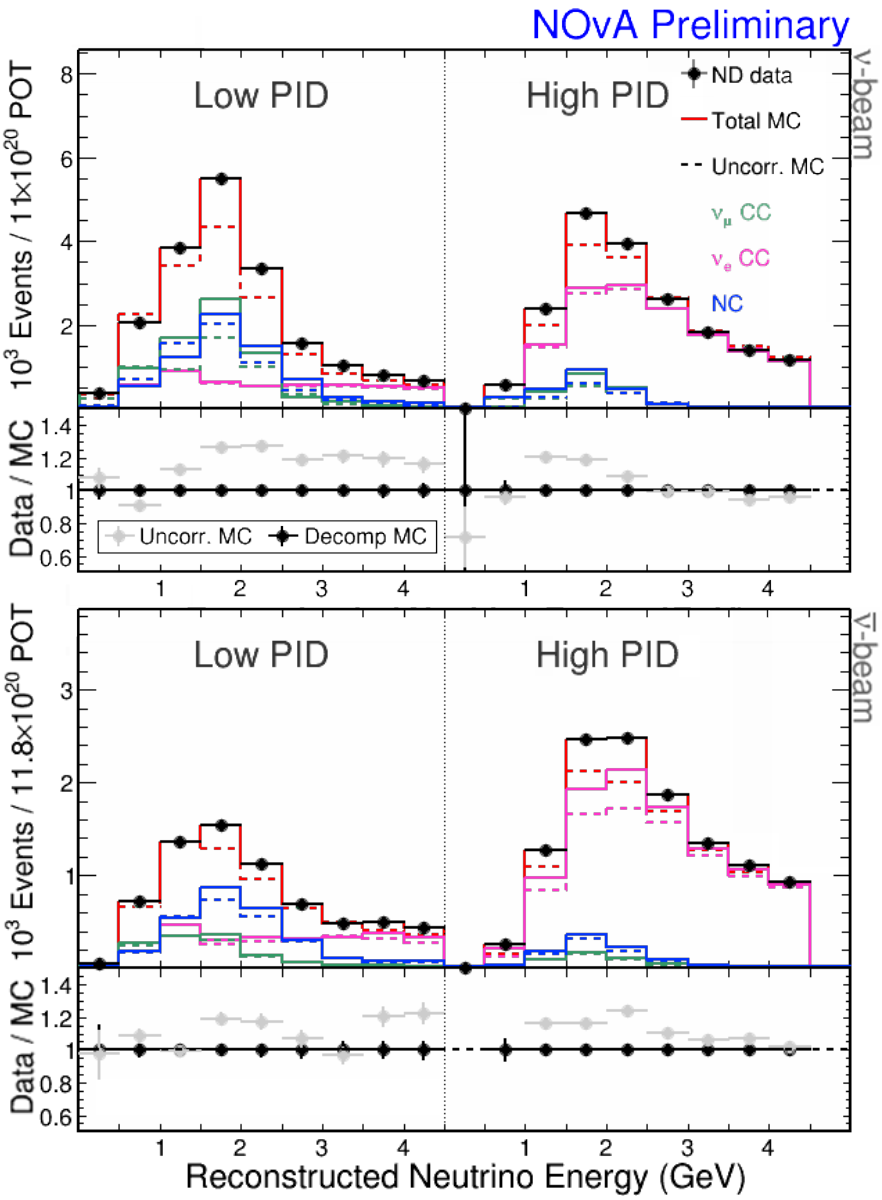

Figure 3.28: ND ν_e CC events of low and high PID score selected samples. The samples are broken down into $\nu_e + \bar{\nu}_e$ (magenta), $\nu_\mu + \bar{\nu}_\mu$ (green) and NC (blue) with the "decomposition" techniques using ND data (black dots) which corrects (full lines) the base MC prediction (dashed lines, grey dots for data/MC). **Top:** ν-beam, BEN+Michel decomposed. **Bottom:** $\bar{\nu}$-beam, proportionally decomposed. The plots are from Ref. [201].

3.11 Near to far extrapolation technique

FD analysis predictions are constrained by the results of ND decomposition – *i.e.* by the estimates on CC interactions neutrino flavor composition or NC rates in ND data $\mathbf{N}(\nu_\alpha; s)$ – with a Far/Near extrapolation technique (F/N technique). That allows for the accounting of any MC disparities commonly shared by both detectors, thus for a potential reduction or cancellation of some underlying systematic uncertainties.

The technique is a bit different for predicting signal events (disappearing $\nu_\mu/\bar{\nu}_\mu$, appearing ν_e and appearing $\bar{\nu}_e$) and beam intrinsic background for ν_e FD samples. They are referred to as "RTR" (reconstructed-true-reconstructed) and "RR" (reconstructed-reconstructed) for the

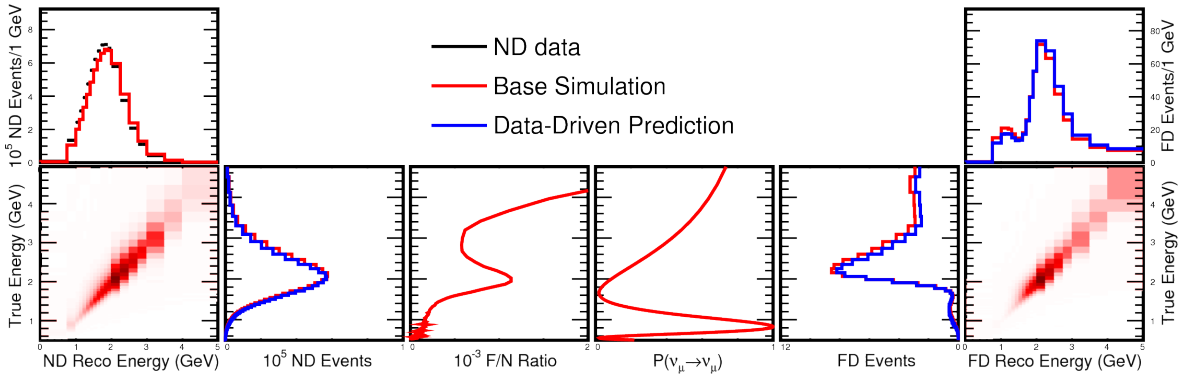

Figure 3.29: Diagram illustrating the Far/Near extrapolation technique for the disappearance channel, Eq. (3.30). **From left to right:** ND sample is decomposed and translated from reconstructed to true neutrino energy (M_N), then F/N ratio (T_true) and transition probabilities are applied ($P(\nu_\mu \to \nu_\mu)$), and finally, the spectrum is translated back to the reconstructed energy (M_F^{-1}). This ND data-driven prediction (blue) works as a correction to the base simulation (red). The diagram is from Ref. [206].

former and latter, respectively. The meaning is outlined below and illuminated by Fig. 3.29.

In the case of RTR, a vector of predicted event rates of ν_β transitioned from ν_α in individual reconstructed energy bins $\mathbf{F_p}(\nu_\alpha \to \nu_\beta; s, f)$ as a single spectrum for a particular selection f and a ND constraining selection s is given by a matrix equation

$$\mathbf{F_p}(\nu_\alpha \to \nu_\beta; s, f) = M_\mathrm{F}^{-1}(\nu_\beta/\nu_\alpha; f) \cdot P(\nu_\alpha \to \nu_\beta) \cdot T_\mathrm{true}(\nu_\beta/\nu_\alpha; f, s) \cdot M_\mathrm{N}(\nu_\alpha; s) \cdot \mathbf{N}(\nu_\alpha; s), \tag{3.30}$$

and the clarification of the individual terms follows.

$\mathbf{N}(\nu_\alpha; s)$ is the estimated rate of ν_α in ND reconstructed energy bins as a result of the ND decomposition under selection s. For, *e.g.* ν_μ ND samples, ND MC is basically corrected by the observed data $N_i(\nu_\mu; s) \approx N_{\mathrm{MC},i}(\nu_\mu; s) \cdot \dfrac{N_{\mathrm{data},i}(s)}{N_{\mathrm{MC},i}(s)}$, Eq. (3.22), where $\mathbf{N_X}(s) = (N_{\mathrm{X},1}, N_{\mathrm{X},2}, \ldots)^\top$ are the corresponding simulated or observed spectra under selection s.

$T_\mathrm{true}(\nu_\beta/\nu_\alpha; f, s)$ is a diagonal matrix representing the so-called Far/Near ratio accounting for flux and geometry differences of the detectors w.r.t. the neutrino initial and eventual flavors ν_α, ν_β and ND/FD selections s/f. It is purely simulated with no neutrino transitions applied. And, it is calculated in the bins of true neutrino energies, where ν_α are swapped for ν_β in the simulated flux for FD MC $F_\mathrm{MC}(\nu_\beta/\nu_\alpha; f; E_i^\mathrm{true})$

$$T_{\mathrm{true},ii}(\nu_\beta/\nu_\alpha; f, s) = \frac{F_{\mathrm{MC},i}(\nu_\beta/\nu_\alpha; f; E_i^\mathrm{true})}{N_{\mathrm{MC},i}(\nu_\alpha; s; E_i^\mathrm{true})}. \tag{3.31}$$

$N_\mathrm{MC}(\nu_\alpha; s; E_i^\mathrm{true})$ is the simulated ND event rate of ν_α under selection s in the i-th bin of the neutrino true simulated energy E^true.

$M_\mathrm{X}(\nu_\alpha; s)$ are, again, purely simulated migration matrices from reconstructed to true energy bins for a given neutrino ν_α and a selection s in the ND (M_N) and FD (M_F).

Finally, $P(\nu_\alpha \to \nu_\beta)$ is a diagonal matrix of $\nu_\alpha \to \nu_\beta$ transition probabilities averaged in the particular true energy bins, $P(\nu_\alpha \to \nu_\beta)_{ii} = \bar{P}(\nu_\alpha \to \nu_\beta; E_i^\mathrm{true})$.

In the case of RR, $\mathbf{F_p^r}$ is calculated similarly, but the Far/Near ratio T_reco is applied in the reconstructed neutrino energies

$$\mathbf{F_p^r}(\nu_\alpha \to \nu_\alpha; s, f) = M_\mathrm{F}^{-1}(\nu_\alpha; f) \cdot P(\nu_\alpha \to \nu_\alpha) \cdot M_\mathrm{F}(\nu_\alpha; f) \cdot T_\mathrm{reco}(\nu_\alpha/\nu_\alpha; s, f) \cdot \mathbf{N}(\nu_\alpha; s). \tag{3.32}$$

RR is designed to predict the FD beam intrinsic background in the ν_e appearance channel, *i.e.* surviving $\nu_e \to \nu_e$, $\nu_\mu \to \nu_\mu$ and antineutrinos, and NC events misidentified as ν_e CC

which are constrained by an equivalent ND selection (denoted simply as $\nu_\alpha \to \nu_\alpha$, $s \approx f$). There is no reason for the ν_e energy estimator to perform well in this sample, so RTR cannot be used.

For the purposes of the F/N technique described above, NC events are considered to be of a non-oscillating[12] neutrino flavor *sui generis*. The beam induced background of the disappearance ν_μ channel is deduced directly from FD MC with no extrapolation F/N technique as it is expected to be minor if any (Sections 3.12 and 3.13). So it is in the case of any appearing beam background ($\nu_e \to \nu_\mu/\nu_\tau$, *etc.*) in the appearance ν_e channel. There are also no ν_τ neutrinos assumed in the ND samples. ND constraints for generating FD predictions can be summarized as (listing also the beam components with no ND constraints, Section 3.12)

Disappearance channel ($\nu_\mu \to \nu_\mu$)

signal ($\nu_\mu \to \nu_\mu + \bar{\nu}_\mu \to \bar{\nu}_\mu$): RTR F/N technique constrained by ND ν_μ,

beam background: FD MC (no ND constraint),

Appearance channel ($\nu_\mu \to \nu_e$)

signal ($\nu_\mu \to \nu_e$ for ν-beam): RTR F/N technique constrained by ND ν_μ,

WS background ($\bar{\nu}_\mu \to \bar{\nu}_e$ for ν-beam): RTR F/N technique constrained by ND ν_μ,

surviving beam background and NC: RR F/N technique constrained by ND ν_e,

appearing beam background: FD MC (no ND constraint).

3.11.1 Extrapolation samples

FD predictions are generated separately for both ν- and $\bar{\nu}$-beam and for all disappearance samples of E_{had}-quartiles. The ν_e appearance channel signal and WS background predictions for all low, high PID (core) and peripheral samples use the total ν_μ CC ND selection (summed E_{had}-quartiles) as a constraint. The beam background of the FD ν_e core sample is extrapolated from the corresponding ND ν_e samples. As there is no peripheral ν_e sample in the ND, the high PID ν_e ND sample is used as a constraint for the FD ν_e peripheral beam background prediction.

To further increase the analysis robustness and to account for different acceptances and selection efficiencies of the detectors (Fig. 3.30), the signal predictions (and ν_e WS) are extrapolated individually in three different subsamples. They are based on the reconstructed transverse momentum $p_t = p\sqrt{1-\cos^2\vartheta}$ of the primary lepton in ν CC interaction candidates, where ϑ is the angle of the lepton direction to the beam direction. The extrapolation p_t samples are then summed back to form the final FD predictions in particular analysis samples.

The momentum p is reconstructed from the lepton energy. The μ energy is reconstructed from its track length, and the e energy is reconstructed from the calorimetric energy of the primary electromagnetic shower prong [207]. Similar to E_{had}-quartiles, p_t bins are designed to be three quantiles, terciles, in each reconstructed neutrino energy bin. Unlike for E_{had}-quartiles, p_t-quantiles boundaries are determined from the ND MC to ensure each ND quantile has adequate p_t coverage as FD has larger lepton p_t acceptance. In the disappearance channel, the p_t boundaries are determined separately for ν- and $\bar{\nu}$-beam and all E_{had}-quartiles, *i.e.* $2(\text{beam}) \times 3(p_t) \times 4(E_{\text{had}}) = 24$ extrapolation samples for both beam modes (12 each). In the appearance channel, the boundaries are determined over all E_{had}-quartiles. That is $2 \times 3 = 6$ extrapolation samples (3 for each beam mode). Selecting the extrapolation p_t samples is outlined in Figs. 3.31, 3.32, and 3.33.

[12] This follows from the 3ν-paradigm and Eq. (1.29).

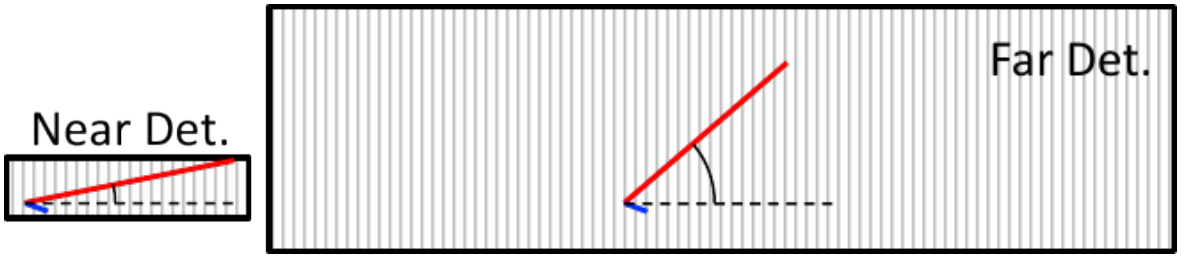

Figure 3.30: Sketch explaining different acceptance of the detectors to the neutrino CC interaction primary lepton (red line) kinematics, from Ref. [60].

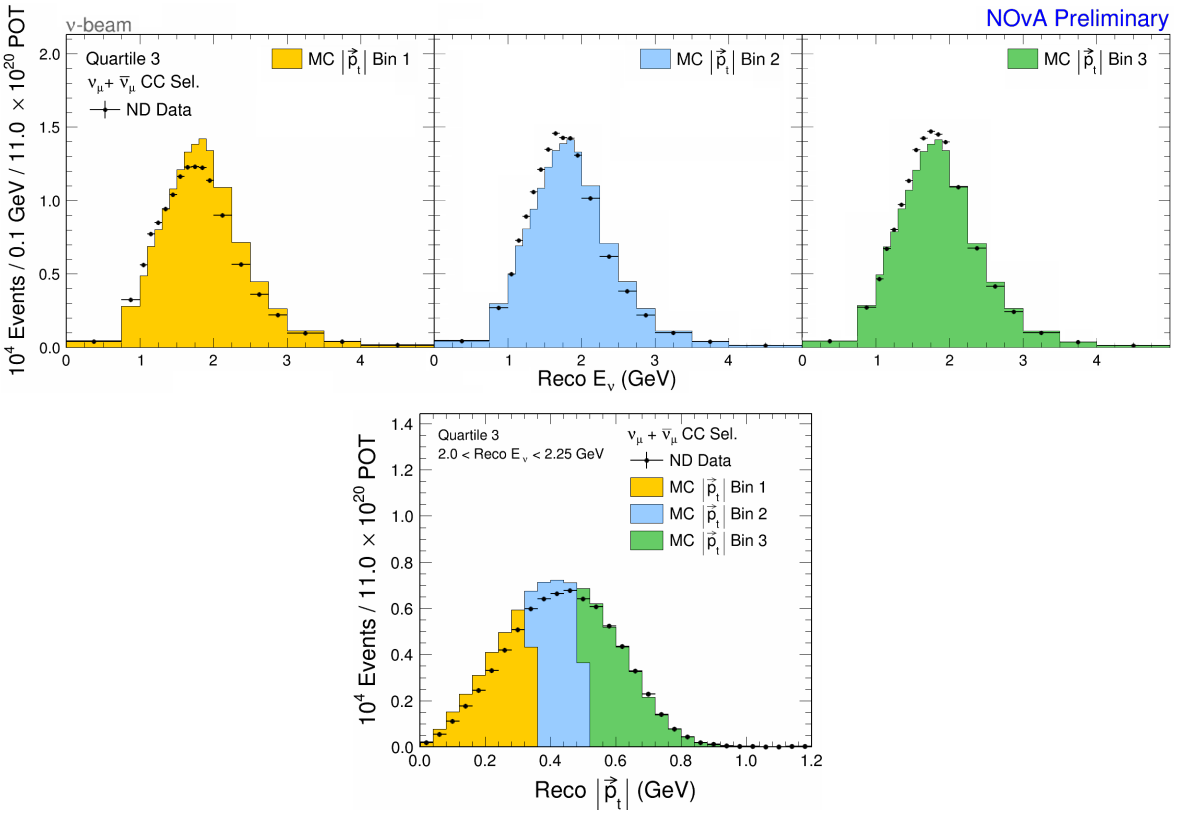

Figure 3.31: Example of the ND p_t extrapolation samples in the third E_{had}-quartile, quartile 3, of the ν_μ CC selection for ν-beam. **Top:** Three p_t bins are designed as quantiles based on the reconstructed p_t in energy bins of ND MC $\nu_\mu + \bar{\nu}_\mu$ CC selection samples. The predicted reconstructed energy spectra are identical. From low to high p_t: left – yellow, middle – blue, right – green. **Bottom:** Reconstructed p_t (denoted $|\vec{p}_t|$) in the most populous reconstructed energy bin E_{ν_μ} between 2.0 and 2.25 GeV of the third E_{had}-quartile of the ν_μ CC ND selection. The plots are from Ref. [208].

3.12 Unconstrained prediction components and cosmics

There are several components of the FD predictions estimated in different ways. Firstly, as mentioned, beam background in the disappearance channel, any appearing beam background in the appearance channel, and any ν_τ background are taken directly from the FD MC. That means, in the corresponding analysis sample a as

$$\mathbf{F}_{\mathbf{p}}^{\mathbf{MC}}(\nu_\alpha \to \nu_\beta; a) = M_{\mathrm{F}}^{-1}(\nu_\alpha; a) \cdot P(\nu_\alpha \to \nu_\beta) \cdot \mathbf{F}_{\mathbf{MC}}(\nu_\beta/\nu_\alpha; a, E^{\text{true}}), \tag{3.33}$$

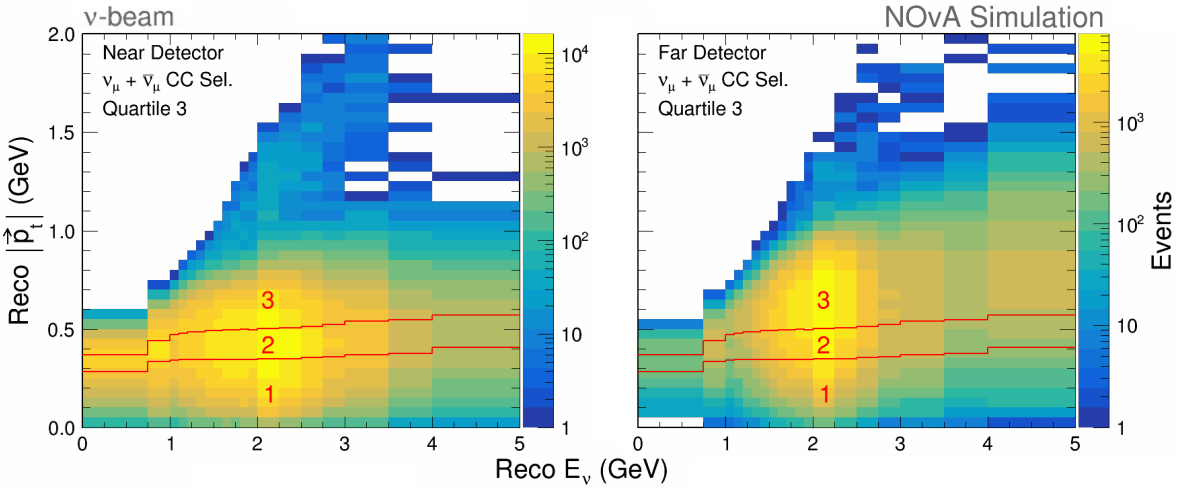

Figure 3.32: Example of the extrapolation p_t quantiles boundaries (red lines) in the third E_{had}-quartile of ν_μ CC selection for ν-beam. **Left:** 3 p_t bins are designed as quantiles based on the reconstructed p_t (vertical axis) in each of the reconstructed energy bins (horizontal axis) in the ND MC ν_μ ($+\bar{\nu}_\mu$) CC selection (overlayed). **Right:** p_t bins boundaries applied to the FD MC unoscillated ν_μ selection. Note that the p_t distribution in FD MC does not match the ND MC on the left within the bin boundaries due to the differences between the detectors. The plots are from Ref. [208].

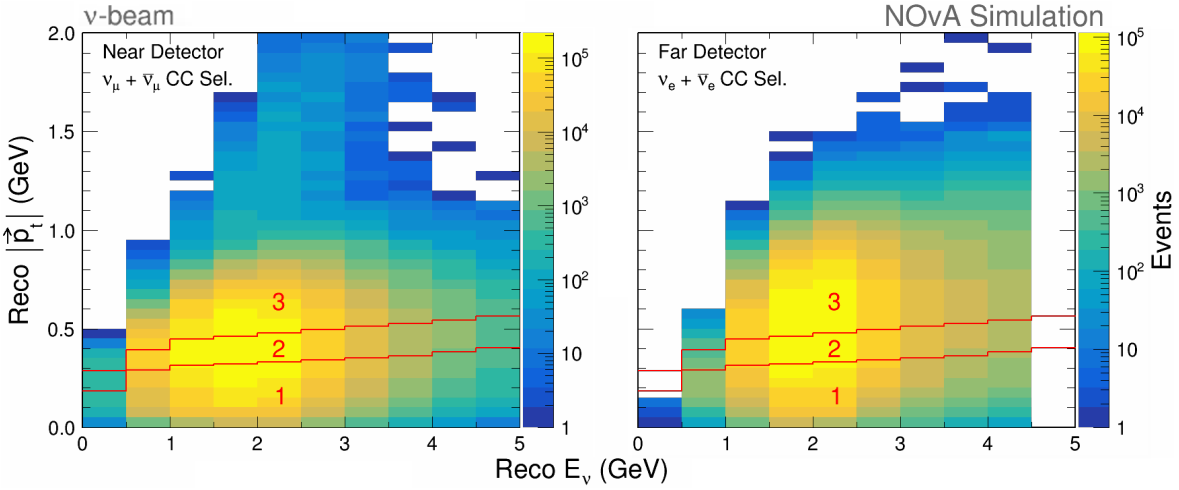

Figure 3.33: Example of the extrapolation p_t quantiles boundaries (red lines) in the $\nu_\mu \to \nu_e$ appearance samples for ν-beam. **Left:** 3 p_t bins are designed as quantiles based on the reconstructed p_t (vertical axis) in each of the reconstructed energy bins (horizontal axis) in the ND MC ν_μ ($+\bar{\nu}_\mu$) full CC selection (overlayed, summed over E_{had}-quartiles). **Right:** p_t bins boundaries applied to the FD MC ν_e CC selection in unoscillated $\nu_\mu + \bar{\nu}_\mu$ simulated flux swapped for ν_e and $\bar{\nu}_e$. Note that the p_t distribution in FD MC does not match the ND MC on the left within the bin boundaries due to differences between the detectors. The plots are from Ref. [208].

where $\mathbf{F_{MC}}$ is the unoscillated FD MC rate of ν_α swapped for ν_β in true energy bins. Eq. (3.33) does not use any F/N extrapolation technique, and such predictions are "not extrapolated".

Secondly, neutrino interactions in the rock and other materials surrounding the FD can

produce particles entering the FD active volume. These are potentially selected as candidate events. As most of the rock events are initially filtered from the MC not to waste resources during the reconstruction chain, a unique MC sample is generated to reintroduce such events into the FD predictions with no extrapolation applied [209], *i.e.* Eq. (3.33). Since the amount of the "uncontained events" in the disappearance channel is negligible, they are completely dropped from those.

Thirdly, the cosmic background is estimated from the NuMI sideband timing window around the NuMI beam window (see Appendix A and Fig. A.1). Except for the timing, standard selections are used, and the resulting spectra are scaled to the beam window total livetime. That is done again separately for all analysis samples and ν- and $\bar{\nu}$-beam [210].

3.13 Far detector predictions

The final total FD predictions of the analysis – as described in Sections 3.11 and 3.12 – are generated from the ND data constraints $\mathbf{N}$, if used, and FD MC as *in situ* data objects without specifying the neutrino oscillation parameters (only $P(\nu_\alpha \to \nu_\beta)$ in Eqs. (3.30), (3.32), and (3.33) is considered to depend on the oscillation parameters). The actual rates in the reconstructed energy bins $\mathbf{F}$ using $\mathbf{F_p}, \mathbf{F_p^r}, \mathbf{F_p^{MC}}$, cosmic background spectra, and uncontained prediction, are estimated by applying the particular neutrino transition probabilities, *i.e.* oscillation parameters, during the validation or the fitting procedure (Section 5.1).

The methods to generate the FD predictions for different analysis samples are summarized in Table 3.2 for the disappearance channel and in Table 3.3 for the appearance channel. FD predictions evaluated at NOvA's 2019 best-fit estimates of oscillation parameters, *i.e.*, $\Delta m^2_{32} = 2.48 \times 10^{-3}$ eV^2, $\sin^2\theta_{23} = 0.56, \delta_{\mathrm{CP}}/\pi = 0$, and Eq. (3.2), can be seen in Figs. 3.34, 3.35, 3.36 and Tables 3.4, 3.5.

Table 3.2: Summary of the final FD predictions assembly in the disappearance channel analysis samples. The notation is as follows: $\mathbf{F_p}$ represents RTR F/N extrapolation technique of Eq. (3.30), $\mathbf{F_p^{MC}}$ is the unconstrained MC prediction of Eq. (3.33), f are FD extrapolation selections, s are ND constraining selections decomposed by Eq. (3.22), FD/ND ν_μ corresponds to FD/ND PID selection, q_i corresponds to the i-th E_{had} fraction quartile selection, p^μ_{ij} corresponds to the j-th p_t bin in the i-th E_{had} quartile selection.

Disappearance channel FD predictions					
Analysis sample	Components		FD prediction	FD extrap. samples f	ND extrap. samples s
E_{had}-quartile q_i	Signal	$\nu_\mu \to \nu_\mu$	$\sum_{j=1}^{3} \mathbf{F_p}(\nu_\mu \to \nu_\mu; s_{ij}, f_{ij})$	f_{ij} = FD ν_μ & quartile q_i & p_t-quant. p^μ_{ij}	s_{ij} = ND ν_μ & quartile q_i & p_t-quant. p^μ_{ij}
		$\bar{\nu}_\mu \to \bar{\nu}_\mu$	$\sum_{j=1}^{3} \mathbf{F_p}(\bar{\nu}_\mu \to \bar{\nu}_\mu; s_{ij}, f_{ij})$		
	Beam backgrounds		$\mathbf{F_p^{MC}}(\nu \to \nu; \text{FD } \nu_\mu \& q_i)$	$--$	$--$
	Cosmic		scaled NuMI sideband FD ν_μ & q_i	$--$	$--$
	Uncontained		negligible	$--$	$--$

Table 3.3: Summary of the final FD predictions assembly in the appearance channel analysis samples. The notation is as follows: $\mathbf{F_p}$ represents RTR F/N extrapolation technique of Eq. (3.30), $\mathbf{F_p^r}$ represents RR F/N extrapolation technique of Eq. (3.32), $\mathbf{F_p^{MC}}$ is the unconstrained MC prediction of Eq. (3.33), f are FD extrapolation selections, s are ND constraining selections decomposed as in Subsection 3.10.2, FD/ND ν_e/ν_μ corresponds to FD/ND ν_e/ν_μ CC selection, low/high PID corresponds to lower/higher CVN ν_e output score, "peripheral" to the peripheral sample selection, p_j^e corresponds to the j-th p_t extrapolation bin selection (from the full ND MC ν_μ CC sample).

Appearance channel FD predictions						
Analysis sample	Components		FD prediction	FD extrap. samples f	ND extrap. samples s	ND decomp.
All samples	Signal	$\nu_\mu \to \nu_e$	$\sum_{j=1}^{3} \mathbf{F_p}(\nu_\mu \to \nu_e; s_j, f_j)$	f_j = FD ν_e & p_t-quant. p_j^e	s_{ij} = ND ν_μ & p_t-quant. p_j^e	ν_μ decomp.
	WS bkg.	$\bar{\nu}_\mu \to \bar{\nu}_e$	$\sum_{j=1}^{3} \mathbf{F_p}(\bar{\nu}_\mu \to \bar{\nu}_e; s_j, f_j)$			
Low/High PID (Core)	Beam bkg.	$\nu_\mu \to \nu_\mu$	$\mathbf{F_p^r}(\nu_\mu \to \nu_\mu; s, f)$	f = FD ν_e low/high PID	s = ND ν_e low/high PID	ν-beam: BEN+Michel
		$\bar{\nu}_\mu \to \bar{\nu}_\mu$	$\mathbf{F_p^r}(\bar{\nu}_\mu \to \bar{\nu}_\mu; s, f)$			
		$\nu_e \to \nu_e$	$\mathbf{F_p^r}(\nu_e \to \nu_e; s, f)$			
		$\bar{\nu}_e \to \bar{\nu}_e$	$\mathbf{F_p^r}(\bar{\nu}_e \to \bar{\nu}_e; s, f)$			$\bar{\nu}$-beam: Prop.
		NC	$\mathbf{F_p^r}(\mathrm{NC} \to \mathrm{NC}; s, f)$			
		Other	$\mathbf{F_p^{MC}}(\nu \to \nu; \text{FD } \nu_e \text{ \& PID})$	$--$	$--$	$--$
	Cosmic		scaled NuMI sideband & FD low/high PID ν_e	$--$	$--$	$--$
	Uncontained		FD ν_e low/high PID in special FD MC	$--$	$--$	$--$
Peripheral	Beam bkg.	$\nu \to \nu$ NC	$\mathbf{F_p^r}(\nu \to \nu; s, f)$	f = peripheral ν_e	s = ND ν_e & high PID ν_e	as in ND high PID
		Other	$\mathbf{F_p^{MC}}(\nu \to \nu; \text{FD } \nu_e \text{ peripheral})$	$--$	$--$	$--$
	Cosmic		scaled NuMI sideband FD & peripheral ν_e	$--$	$--$	$--$
	Uncontained		peripheral ν_e in special FD MC	$--$	$--$	$--$

Table 3.4: Integral numbers of FD predicted events in the ν_μ disappearance channel analysis samples, Q1–4 E_{had} fraction quartiles, evaluated at the NOvA 2019 best-fit point of neutrino oscillation parameters $\Delta m^2_{32} = 2.48 \times 10^{-3}$ eV^2, $\sin^2\theta_{23} = 0.56, \delta_{\text{CP}}/\pi = 0$ [2] and stated exposures for ν- and $\bar{\nu}$-beam.

Disappearance channel FD predictions at 2019 best fit								
	Components		Q1	Q2	Q3	Q4	Total	POT-eq.
ν-beam	Signal	$\nu_\mu \to \nu_\mu$	41.60	39.96	42.55	48.99	173.10	13.35×10^{20}
		$\bar{\nu}_\mu \to \bar{\nu}_\mu$	5.31	2.72	2.27	1.26	11.56	
	Bkg.	NC	0.10	0.16	0.40	1.81	2.47	
		Cosmic	0.36	0.36	0.89	3.50	5.09	
		Other	0.14	0.14	0.16	0.33	0.77	
	Total		47.52	43.34	46.27	55.88	193.00	
$\bar{\nu}$-beam	Signal	$\bar{\nu}_\mu \to \bar{\nu}_\mu$	19.98	16.78	15.60	14.11	66.47	12.33×10^{20}
		$\nu_\mu \to \nu_\mu$	3.50	4.74	6.09	9.76	24.08	
	Bkg.	NC	0.02	0.04	0.09	0.63	0.78	
		Cosmic	0.06	0.03	0.11	0.73	0.94	
		Other	0.06	0.08	0.09	0.12	0.35	
	Total		23.62	21.66	21.98	25.36	92.62	

Table 3.5: Integral numbers of FD predicted events in the ν_e appearance channel analysis samples evaluated at the NOvA 2019 best-fit point of neutrino oscillation parameters $\Delta m^2_{32} = 2.48 \times 10^{-3}$ eV^2, $\sin^2\theta_{23} = 0.56, \delta_{\text{CP}}/\pi = 0$ [2] and stated exposures for ν- and $\bar{\nu}$-beam.

Appearance channel FD predictions at 2019 best fit							
	Components		Low PID	High PID	Peripheral	Total	POT-eq.
ν-beam	Signal	$\nu_\mu \to \nu_e$	11.73	49.37	10.20	71.31	13.35×10^{20}
	WS bkg.	$\bar{\nu}_\mu \to \bar{\nu}_e$	0.18	0.65	0.20	1.03	
	Beam bkg.	$\nu_e + \bar{\nu}_e$	2.29	7.59	3.50	13.39	
		$\nu_\mu + \bar{\nu}_\mu$	0.57	0.16	0.12	0.85	
		$\nu_\tau + \bar{\nu}_\tau$	0.18	0.31	0.12	0.60	
		NC	3.66	0.22	1.68	3.22	
	Cosmic		1.32	0.22	1.68	3.22	
	Total		19.93	59.31	16.04	95.27	
$\bar{\nu}$-beam	Signal	$\bar{\nu}_\mu \to \bar{\nu}_e$	2.10	14.20	2.90	19.20	12.33×10^{20}
	WS bkg.	$\nu_\mu \to \nu_e$	0.48	1.79	0.52	2.80	
	Beam bkg.	$\nu_e + \bar{\nu}_e$	0.88	4.07	1.92	6.86	
		$\nu_\mu + \bar{\nu}_\mu$	0.10	0.04	0.05	0.20	
		$\nu_\tau + \bar{\nu}_\tau$	0.11	0.19	0.07	0.36	
		NC	1.15	0.43	0.10	1.68	
	Cosmic		0.42	0.14	0.97	1.53	
	Total		5.24	20.86	6.54	32.64	

3.14 Summary

NOvA 2020 neutrino oscillation analysis was performed on seven samples for ν-beam and seven for $\bar{\nu}$-beam data. For both beam modes, there are three ν_e appearance PID samples (2 core + 1 peripheral) and four ν_μ disappearance E_{had} fraction quartiles based on the fraction of the reconstructed hadronic energy in the selected events. The samples reconstructed energy spectra predictions for signal and ν_e intrinsic beam background are constrained by ND data/MC through F/N (Far over Near ratio) extrapolation technique. To "extrapolate" $\nu_\mu \to \nu_\mu$ and $\nu_\mu \to \nu_e$ signal, each of the ND data/MC constraining samples is further divided into three kinematic quantiles based on the reconstructed transverse momentum p_t of the primary lepton in ν CC interactions. It is motivated by the disparate acceptances of the NOvA detectors. The extrapolations are later summed back over the p_t quantiles to form the analysis predictions.

To account for different oscillation probabilities, F/N technique is applied w.r.t. individual neutrino flavors or NC events. To estimate the beam components in the ND samples, they need to be "decomposed". That is done either directly in proportion to the ND MC, or with the help of additional data-driven methods (BEN and Michel, Section 3.10). This is vital for ND ν_e-like samples, which are used to predict FD ν_e appearance background as they contain beam intrinsic $\nu_e + \bar{\nu}_e$ CC, NC, and misidentified $\nu_\mu + \bar{\nu}_\mu$ CC events. The signal constraining ND ν_μ CC samples are expected to have very high $\nu_\mu + \bar{\nu}_\mu$ purities.

Other beam induced background is derived from FD MC, and the cosmic background is estimated by scaling FD cosmic sidebands of the NuMI trigger data.

Event selections are provided by series of basic quality, event quality, fiducial, and containment cuts. The PID selection uses several cosmic BDTs (ν_μ, ν_e core, ν_e peripheral $\times$ $\nu/\bar{\nu}$-mode) to reject cosmic ν-like events, ReMId BDTG to identify reconstructed μ tracks in ν_μ CC events, and event CVN (Convolutional Visual Network) scores of ν_μ and ν_e CC. The ν_e PID samples boundaries reflect their background neutrino flavor compositions in relation to different event PID scores.

There are two energy estimators for ν_μ and ν_e channels trained separately for ν- and $\bar{\nu}$-beam. The energy of ν_μ CC selected events is determined from the μ track length and the remaining hadronic-like activity which is reconstructed calorimetrically. The ν_e energy classify the calorimetric energy depositions as electromagnetic or hadronic with the use of an auxiliary prong CVN to identify single particles emerging from interactions. The resulting estimator is a quadratic function of both categories.

The calibration of the detectors exploits cosmic μ tracks as MIPs with hits in three neighboring detector cells of perpendicular orientation. It accounts for natural attenuation of light at the far ends of the cells and for calibration drift due to time dependent detector conditions.

The basic reconstruction chain utilizes cell hits of collected charge as converted from light produced in scintillator. It begins with clustering (TDSlicer) and tracking (Kalman technique), and it continues with vertexing (Multi-Hough, Elastic Arms) and prong formation (Fuzzy K-means), respectively, for interaction and single particle representations. The very new TDSlicer is a centroid-finding algorithm with better performance in higher-intensity spills and pile-ups in comparison to the previous one.

The upgraded MC production employed the latest available generators of GENIE v3.0.6 for neutrino interaction simulation and Geant4 v10.4 for detectors modeling. Prior the analysis, underlying FSI (Final State Interactions) model was retuned to $\pi^{+-12}C$ scattering data, and the model of neutrino MEC (Meson Exchange Current) interactions was fitted to agree with NOvA ND ν_μ CC data. Also, a newly optimized model of detector light collection exploiting several dedicated data and MC samples was adopted.

The total NuMI exposure for the 2020 analysis is about 13.60×10^{20} POT in ν-mode and 12.50×10^{20} POT in $\bar{\nu}$-mode, which accounts for approximately 50% increase of ν-beam

(+22% total) data to Ref. [2]. With all the analysis changes, the expected gain at 2019 best fit is about +60% both ν-beam ν_μ CC disappearance and ν_e CC appearance events, +20% $\bar{\nu}$-beam $\bar{\nu}_e$ CC events, and a partial loss of −2% $\bar{\nu}$-beam $\bar{\nu}_\mu$ CC events.

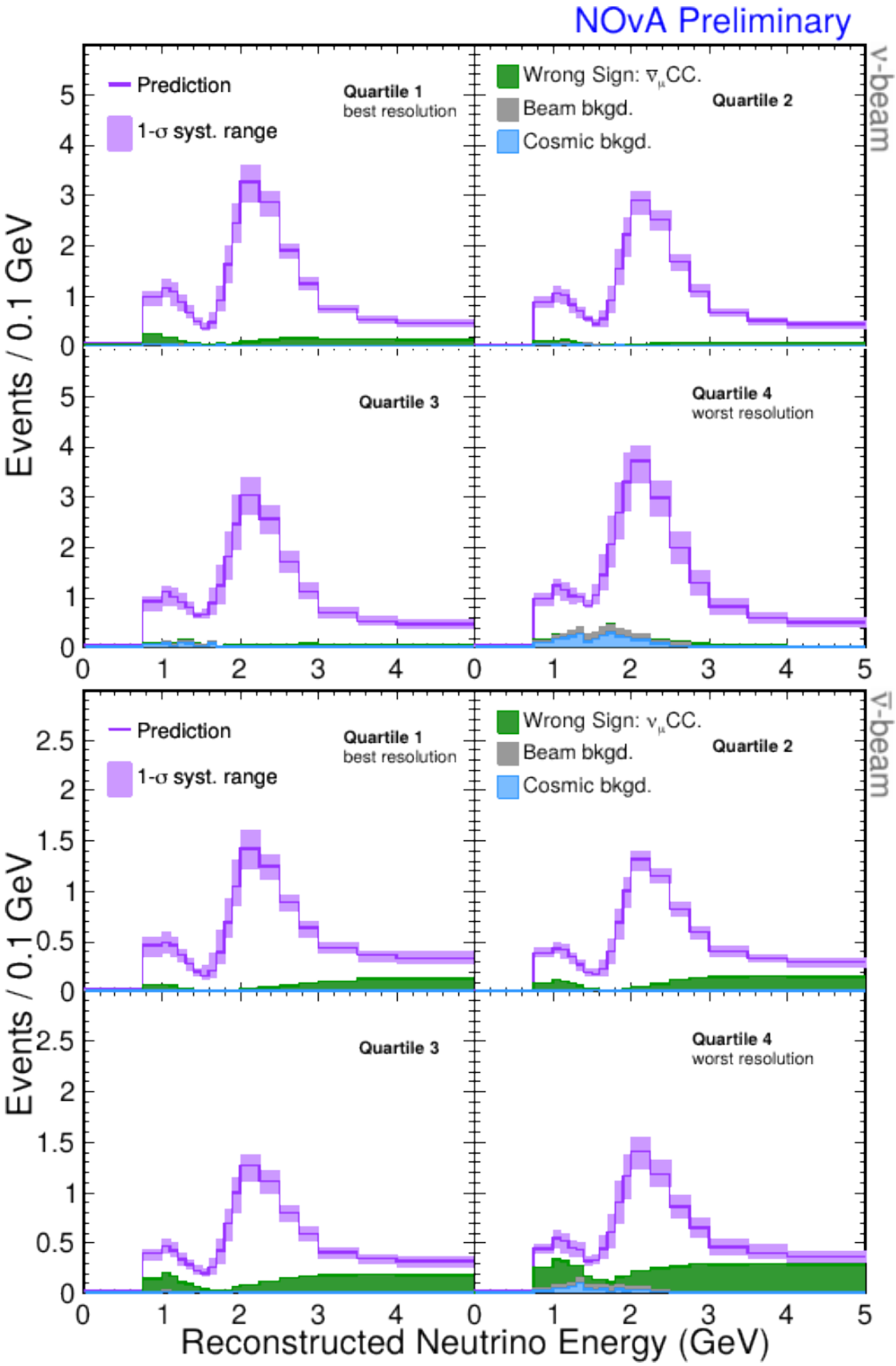

Figure 3.34: Far detector ν_μ disappearance channel predicted spectra at 2019 best-fit point of neutrino oscillation parameters $\Delta m^2_{32} = 2.48 \times 10^{-3}$ eV^2, $\sin^2\theta_{23} = 0.56, \delta_{\rm CP}/\pi = 0$ for ν-(top) and $\bar{\nu}$-beam (bottom), exposures from Table 3.4. The plots are from Ref. [101].

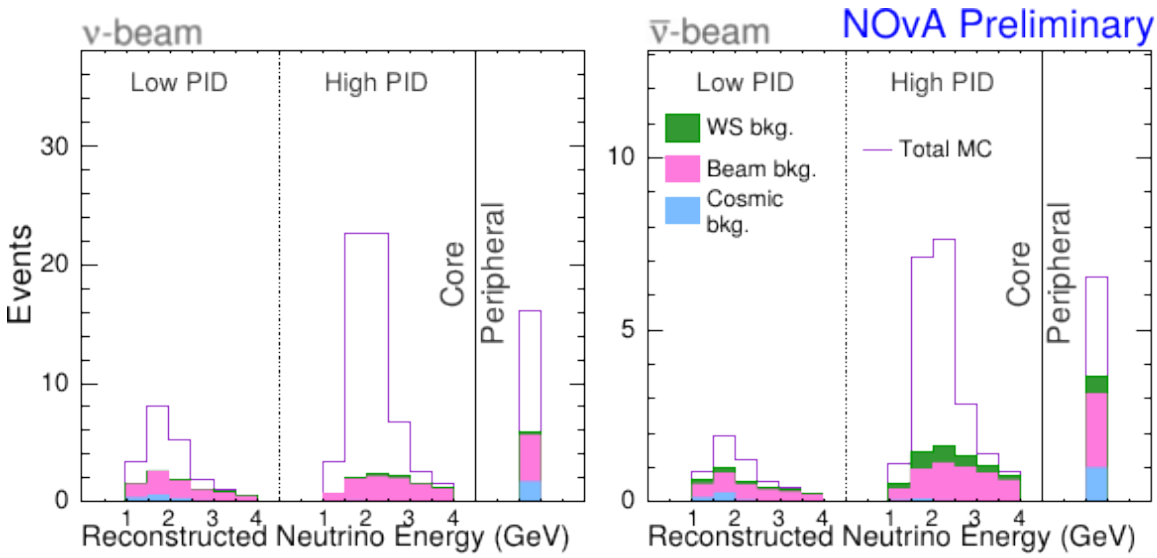

Figure 3.35: Far detector ν_e appearance channel predicted spectra at 2019 best-fit point of neutrino oscillation parameters $\Delta m^2_{32} = 2.48 \times 10^{-3}$ eV^2, $\sin^2\theta_{23} = 0.56, \delta_{\rm CP}/\pi = 0$ for ν- (left) and $\bar{\nu}$-beam (right), exposures from Table 3.5. Note the shape and area of the spectra would change with different oscillation parameters. The plots are from Ref. [101].

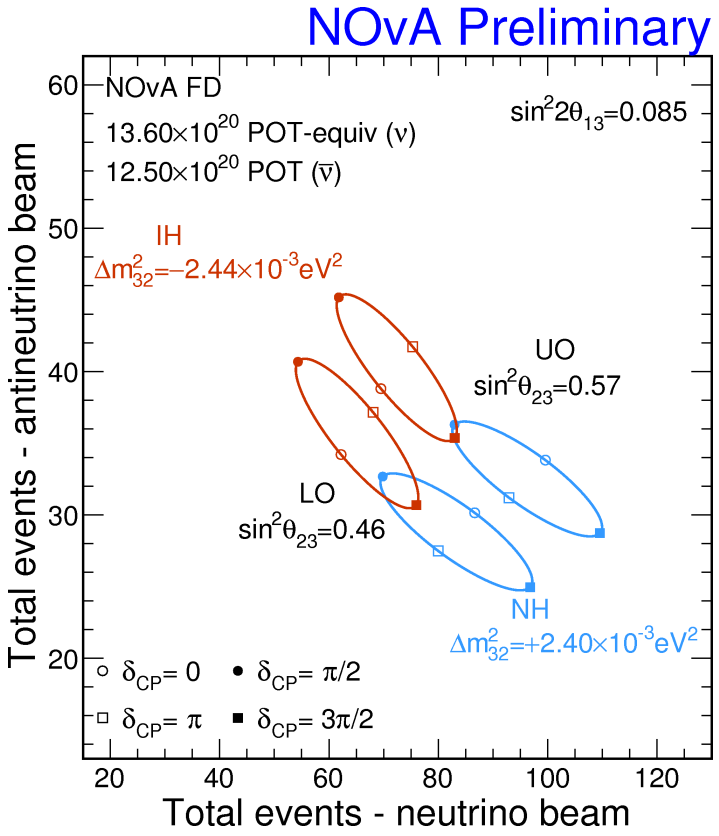

Figure 3.36: Far detector ν_e appearance channel predicted number of selected events in ν- (horizontal axis) *vs.* $\bar{\nu}$-beam (vertical axis) evaluated at different neutrino oscillation parameters corresponding to normal (NH, blue) and inverted (IH, red) neutrino mass ordering (hierarchy), lower (LO, $\sin^2\theta_{23} < 0.5$) or upper (UO, $\sin^2\theta_{23} > 0.5$) θ_{23} octant and all possible values of $\delta_{\rm CP}$. The figure is from Ref. [211].

4. Systematic uncertainties

The following chapter explains, in brief, the treatment of systematic uncertainties in the NOvA neutrino oscillation analysis in Section 4.1, and it reviews and categorizes all of those actually considered in Sections 4.2–4.8. The conclusion is dedicated to a short discussion on the topic.

4.1 Introduction

There are over one hundred separate systematic "unknowns" studied for the NOvA neutrino oscillation analysis. However, nearly 50% of them are related to the neutrino cross sections and interaction models, see Section 4.5. In the end, about seventy individual uncertainties represented by 67 systematic nuisance parameters were considered, see Section 5.1.

The treatment of systematic uncertainties remained analogous in methodology to the previous oscillation analyses [1, 2] with adequate updates and improvements (new extrapolation samples from Section 3.11, better automatization, *etc.*).

In general, both ND and FD MC are modified as positive and negative shifts in terms of the standard deviation ($\pm1\sigma$, $\pm2\sigma$) of the uncertainty relative to the base simulation by

1. reweighting the nominal MC w.r.t. the neutrino interaction type ($\pm1\sigma$, $\pm2\sigma$ shifts, *e.g.* neutrino interaction uncertainties),

2. recalculating the simulated event variables in accordance with the tenet of the particular uncertainty ($\pm1\sigma$, $\pm2\sigma$ shifts, *e.g.* reconstruction uncertainties), or

3. creating a new altered MC events sample by adjusting the simulation parameters (only $\pm1\sigma$ shifts for detector calibration and response uncertainties).

Uncertainties on the final FD predictions in the analysis samples as vectors of neutrino rates in bins of reconstructed energy $\mathbf{F} = (F_1, F_2, \ldots)^\top$ are evaluated by repeating the event selections, decomposition, and F/N technique of Sections 3.9, 3.10, and 3.11, respectively. For each investigated uncertainty, corresponding $\pm1\sigma$ ($\pm2\sigma$) shifted FD predictions are generated. This approach has a preeminent effect of reducing or even canceling any ND to FD correlated uncertainties thanks to the detectors functional similarity and the F/N ratio expressed by Eq. (3.31).

Let $\mathbf{F}(\boldsymbol{\theta})$ be the FD prediction evaluated for a fixed set of neutrino oscillation parameters $\boldsymbol{\theta}$. Then for a given uncertainty, to get the systematically shifted FD predictions at any possible multiples of σ, $\mathbf{F}(\boldsymbol{\theta}, \varsigma)$ are parameterized w.r.t. ς of units of a standard deviation σ. The generated 0σ, $\pm1\sigma$, $\pm2\sigma$ (*i.e.*, $\varsigma = 0, \pm1, \pm2$) shifts are then interpolated in $F_i(\boldsymbol{\theta}, \varsigma)/F_i(\boldsymbol{\theta}, 0)$ for all bins of reconstructed energy i and for any combination of oscillation parameters $\boldsymbol{\theta}$ with a cubic spline at analysis time [212]. The ς act as the aforementioned systematic nuisance parameter of the subsequent fitting procedure.

The sections of this chapter present the systematic uncertainties included in the NOvA 2020 neutrino oscillation analysis. The sources of the uncertainties, motivations for their introduction, and preliminary estimations of the "effects" on the FD predictions are discussed using parameters from Eqs. (3.1), (3.2), and (3.3). The uncertainties were reported as relative changes in integral numbers of predicted events in the analysis samples or channels (*i.e.* summed over subject samples) or as $\pm1\sigma$ shifted spectra in the neutrino reconstructed energy or as a χ^2 test value to the nominal predictions in Ref. [213]. The final evaluations for the best-fit predictions are later summarized in Section 5.3 and closely detailed in Appendix C or Ref. [214]. Exceptions from this general approach may apply where specified.

4.2 Detectors calibration

Uncertainties of the calibration procedure and the detector model (Section 4.3) are addressed by adjusting ($\pm 1\sigma$) the relevant parameters (such as the absolute energy scale) and resimulating both ND and FD MC samples. There are four different calibration uncertainties correlated between the analysis samples and ν- and $\bar{\nu}$-beam data.

4.2.1 Detectors absolute energy scale

Absolute calibration energy scale uncertainty covers the overall (over all detector channels) data/MC discrepancies in the energy response that were observed in several dedicated control samples (cosmic μ, beam μ, Michel e, π^0, and p candidates) to be up to about 4–5% (for ND p) [168]. The deemed and simulated uncertainty is $\pm 5\%$ on the reported calorimetric energy. As it is not possible to resolve whether data/MC discrepancies extend from one detector to the other, it is implemented as both fully ND and FD correlated (**absolute calibration**) and anticorrelated (detectors **relative calibration**) in order to take this possibility into account.

Among other reasons, by being rather conservative, this calibration uncertainty accounts for one of the largest ones in the analysis with up to 5–7% effect on the total number of predicted ν_μ CC events and even larger in individual E_{had}-quartiles. Moreover, any miscalibration scale shifts the neutrino reconstructed energy axis, which is crucial for identifying neutrino oscillation minima (ν_μ disappearance channel dip) and maxima (ν_e appearance channel peak) and hence for constraining the oscillation parameters.

Nevertheless, the calibration uncertainty could be reduced by further possible improvements of the detector model and calibration techniques with the help of the NOvA Test Beam program [215].

4.2.2 Calibration shape

Calibration shape systematic uncertainty is motivated by a different energy response at the detector cells' ends and in their middle (see Fig. 3.10, low/high W position in the cell). It is based on a polynomial fit of the ratio of reconstructed to true energy as a function of W in the peripheral regions of the cells. The resulting functional form is used to simulate a shifted MC to cover the reco/true differences. For the exact nature of these effects is not understood, this $+1\sigma$ shift is reflected to obtain the negative pulls on predictions as well. The uncertainty is treated as fully correlated between the detectors, as it is expected to have a common source. The uncertainty on the total number of predicted events is about 1–3%, being more prominent in the ν_μ lowest and highest E_{had} fraction quartiles and the ν_e peripheral sample.

4.2.3 Calibration drift

Calibration drift (detector aging) uncertainty is grounded in the observed decrease of the average number of reconstructed hits in candidate events since the start of data taking [168] as a result of the scintillator aging, presumably. The simulation uses a gradient of 4.5% loss of light yield per year. The process cannot be reversed (no possible light enhancement), so the corresponding effect is only a one-directional shift of the prediction ($+1\sigma$ shift, whereas the negative σ shift is identical to the nominal prediction). A variation of up to 0.5% in the total number of expected events strongly depends on the analysis sample. Generally, lower light yield leads to lower reconstructed energy of particle showers, *i.e.*, it affects mainly ν_e CC events and ν_μ with higher visible E_{had}.

4.3 Detectors response

Detector response systematic uncertainties cover potential detectors mismodeling and light collection discrepancies.

4.3.1 Detectors light levels

Two separate light level uncertainties for the ND and FD (*i.e.* two systematic nuisance parameters) were designed uncorrelated between the detectors, as there are also two separate detector light model tunes (Subsection 3.4.3). The uncertainties consist of shifts in the view scaling factors F_{view}, Eq. (3.10), and a reciprocal normalization shift of the absolute calibration [137]. The ND F_{view} was varied by $\pm 10\%$ for both xz (top) and yz (side) views, FD F_{view} by $\pm 16\%$ in the xz view, and $\mp 6\%$ in the yz view. The sizes of the shifts were determined from differences acquired in an additional iteration update of the light model tuning procedure. The expected effect on the total number of FD predicted events is about 1–2% and slightly larger for the ν_μ disappearance samples.

4.3.2 Cherenkov light production

Cherenkov light uncertainty was motivated by the observed $\sim$5% data/MC discrepancy in $\mathrm{d}E/\mathrm{d}x$ of candidate p (whereas only $\sim$1.5% data/MC, *e.g.* for μ). With a constraint of equal light response for μ in the relevant $\beta\gamma$ region of a MIP, the scintillator yield (Y_s) and Cherenkov efficiency (ϵ_C) from Eq. (3.10) were adjusted to diminish the original p discrepancy under 1%. Y_s was reduced by 4.4%, ϵ_C increased by 83% (*i.e.* to ϵ_C about 0.86) [137].[1] The (re)simulated shifted sample was then used to estimate the uncertainty ($+1\sigma$). As this is only a one-sided effect of reducing scintillation to Cherenkov light ratio, so is the implemented uncertainty (compare to the calibration drift). Finally, because the scintillator is nearly identical in both detectors due to similar blends, the uncertainty is assumed to be fully correlated between them. The estimated 1σ deviation in the total number of FD predicted events is up to 2% among the analysis samples.

4.4 Neutron uncertainty

The so-called neutron uncertainty is enforced by an observed ND data/MC discrepancy in a low energy neutron-rich sample of mostly $\bar{\nu}_\mu$ CC candidate events (predominantly in $\bar{\nu}$-beam) as illustrated in Fig. 4.1. Neutron induced prongs of hit clusters originating from primary neutrons are selected with a set of cuts requiring a spatial displacement from the interaction vertex (neutron free path) and a discriminating photon pCVN score [216]. The achieved selection purity and efficiency are about 60% and 71%, respectively. There is (Fig. 4.1) an apparent MC excess for low reconstructed calorimetric energies $\lesssim$30 MeV and a deficit for mid-energies of up to 150 MeV. They are likely rooted in a mismodeled detector response to fast neutrons of kinetic energies $\gtrsim$1 MeV, but the issue has not been tracked down yet [217].

The associated uncertainty is evaluated by artificially inflating the calorimetric energy contributions of pseudorandomly chosen neutrons with low energy deposits. The truth-level primary neutrons simulated visible energy under 40 MeV was scaled by a factor of 3.6 for 33.3% (1 in 3) of them and added to the reconstructed calorimetric energy. The energy is subtracted from the events accordingly to get the opposite potential systematic shift. The achieved data *vs.* MC congruence with the upscaling is in Fig. 4.1, right, blue line.

[1] This enlarged ϵ_C was also close to the reiterated light model tuning optimum described in Subsection 4.3.1.

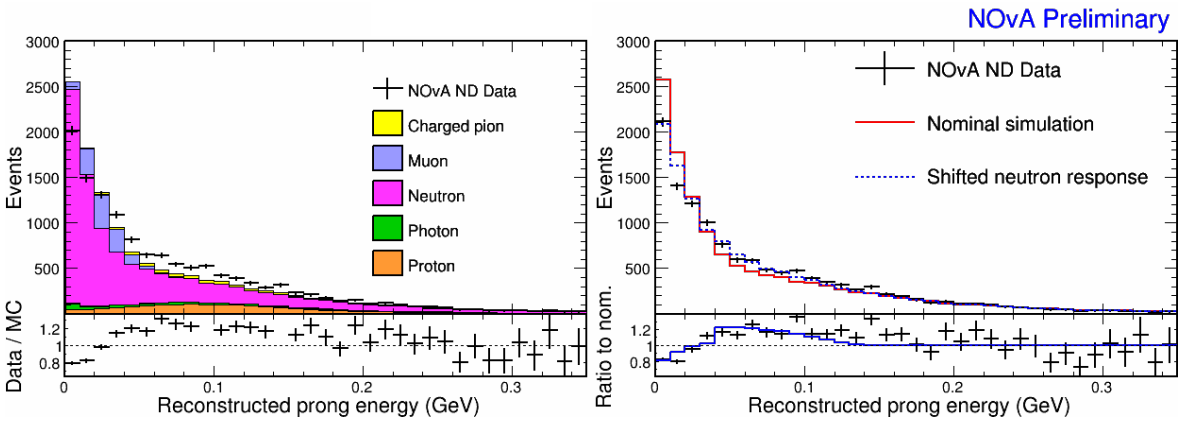

Figure 4.1: **Left:** Total reconstructed energy of neutron candidate prongs in ND $\bar{\nu}$-beam data and MC true categories (stacked colors). The data/MC disagreement is imminent. **Right:** ND $\bar{\nu}$-beam data (black), nominal simulation (red), and the shifted neutron response with pseudorandom energy scaling (blue) to cover the discrepancies, *i.e.* the neutron uncertainty. The plots are from Ref. [218].

As a consequence, the uncertainty in $\bar{\nu}_\mu$ CC events reconstructed energy is approximately 1%, and the total number of predicted FD events of the $\bar{\nu}$-beam disappearance samples varies by ∼3–5%. But, it can also considerably affect other samples.

4.5 Neutrino cross sections

Neutrino cross section and interaction uncertainties count as by far the biggest systematic category in terms of the individual implemented systematic pulls (72 in total). Many of them are natively provided by the GENIE software in the form of physics parameters tweaks and events reweighting (GENIE package ReWeight [104, Chapter 9]), *i.e.* by applying eligible weights to the simulated events in order to obtain $\pm1\sigma$ shifted spectra. NOvA employs a similar strategy for any extra uncertainties developed or modified by the NOvA Cross Section Tuning group with the NOvARwgt package.[2]

The following paragraphs summarize the uncertainties implemented and used in the NOvA neutrino oscillation analysis. Due to their essentially informative character, please review Subsection 3.4.2 for the notation and abbreviations and skim through the quoted references for details on underlying models and their parametrization, if interested.

First, a number of systematic uncertainties are derived directly from GENIE [104]:[3]

- form factor axial mass M_A^{NCEL} for NCEL (±25%) [123],
- strange axial form factor scale η for NCEL (±30%) [123],
- axial M_A^{CCRES} and vector M_V^{CCRES} masses for CC RES ν production (±20% and ±10%),
- axial M_A^{NCRES} and vector M_V^{NCRES} masses for NC RES ν production (±20%, ±10%),
- A, B empirical param. for higher twist ξ_w scaling in Bodek-Yang model (±25%) [124],
- valence quark correction parameters C_{1v} (±30%), C_{2v} (±40%) in Bodek-Yang model,
- π kinematics for $N{+}\pi$ final states in AGKY model [104],

[2] https://github.com/novaexperiment/NOvARwgt-public (as of Jan 2021)
[3] Or visit https://genie-docdb.pp.rl.ac.uk/DocDB/0000/000002/006/man.pdf (as of Dec 2020).

- branching ratios for radiative (±50%) and single η resonance decays (±50%),
- π angular distribution in $\Delta \to N + \pi$ decays [126],
- and CCQE axial form factor normalization (z-expansion parameter, +20%/−15%).

Second, some uncertainties were evaluated by the NOvA Cross Section Tuning group, either for not being included in GENIE or because of a principally distinct approach [116].

CCQE cross sections are calculated from the isovector axial nucleon form factor with the ***z*-expansion** formalism described in Ref. [122]. There are five z-expansion parameters: a normalization (GENIE inherent above) and four axial vector form factor shape variation parameters with their errors estimated from a set of experimental and theoretical uncertainties. To properly account for strong correlations of the shape parameters, custom weights were derived from eigenvectors of their covariance matrix based on Ref. [122], see Ref. [116].

The CCQE model [121] uses the random phase approximation (**CCQE RPA**) method to account for long-range nuclear correlation effects. Ref. [219] summarizes the physics motivation and prescriptions for two systematic uncertainties related to the RPA corrections:[4]

1. ±25% on RPA correction suppression of CCQE for low transferred four-momentum invariant Q^2 based on comparisons of direct RPA predictions with μ capture data and
2. an uncertainty on RPA correction enhancement of CCQE from differences of relativistic and non-relativistic calculations (high Q^2).

A similar phenomenon of low Q^2 suppression is expected in **resonance production** (π production through the lowest Δ resonance for NOvA ν energies). The new GENIE v3.0.6 calculation within the selected Berger-Sehgal RES model [126], Table 3.1, has much better agreement with the available data [116] than the older versions. Nevertheless, a specific parametrization from the MINOS experiment [220] increasing the overall suppression correction was used as a sensible bound ($\pm 1\sigma$) on the viable systematic effects.

There are three uncertainties for the internal meson exchange current interaction (**MEC**) tune associated with its spectral shape in transferred four-momentum (q_0, q) dependence, neutrino energy dependence (E_ν), and compositions of the initial state, *i.e.* struck nucleon pair [116]. The shape uncertainty is determined from artificially distorted interaction spectra to be more "non-MEC" like and to contain higher fractions of CCQE or RES events. The accountable systematic shifts of CCQE z-expansion coefficients shift, M_A^{CCRES} and M_V^{CCRES} variations and alike are applied, and the ND data tune is repeated [116]. These new MEC spectra are taken as the signified systematic pulls. The E_ν dependence uncertainty is estimated by comparing several MEC models [221, 222] with the one in use (Valencia MEC [114]), and it is implemented as a functional weight encapsulating the observed differences. Similarly, the uncertainty in the fraction of struck nucleon pairs of $np/(np+nn)$ for ν and $np/(np+pp)$ for $\bar{\nu}$ are taken to cover the variations of the available models (−5%/+15%) [116].

Errors on nonresonant interactions with π production in deep inelastic scattering (**DIS**) are based on the original GENIE ±50% with a custom extension in the regions of hadronic invariant mass $W > 3$ GeV to linearly decrease from 50% at $W = 3$ GeV to 5% at $W = 5$ GeV. This lower normalization uncertainty for larger W is suggested by measurements at very high E_ν (*e.g.* Refs. [223, 224]). Also, the DIS "formation zone"[5] uncertainty is rejigged to be consistent with Ref. [225].

Coherent π production (**COH CC/NC**) uses a ±20% scale for both NC and CC cross sections to embrace the uncertainties from measurements in Refs. [85, 226] conservatively.

[4] CCQE RPA uncertainties are maintained by NOvA because of the discrepancies between the GENIE implementation and the original Ref. [219].

[5] The constant distance in a decreasing exponential sampling distribution for hadrons' pre-hadronization propagation.

Inspired by Ref. [227] and based on Ref. [228] extra E_ν flat scale uncertainties were placed on ν_e/ν_μ cross section ratios. One is $\nu/\bar{\nu}$ uncorrelated (*i.e.* two parameters) 2% error due to **radiative corrections**. An additional 2% for **second class currents** is fully anticorrelated between ν_e and $\bar{\nu}_e$.

A 60% uncertainty on $\boldsymbol{\nu_\tau}$ **CC** cross section (excluding $\nu_\tau - e$ scatt.) was estimated from the OPERA result $(1.2\pm0.6)\times\sigma_{\rm SM}$ [56] of the SM prediction $\sigma_{\rm SM}$.

The final state interactions (**FSI**) model (INTRANUKE hN) uncertainties are computed by varying the tuned parameters [120] w.r.t. the data/MC discrepancies and previous work by T2K/DUET [119]. The π mean free path ($\pm30\%$) is the mean distance of π before they undergo an interaction in the nuclear structure. The probabilities of different (re)interaction categories are expressed by the "fate fraction" scales on π absorption (up to 40% uncertainty), π charge exchange (20%), and quasielastic scattering (30%). Their correlations are taken into account by finding the eigenvalues and eigenvectors of their covariance matrix (from the fit) and by constructing a set of uncorrelated fate fraction scales. See the details in Ref. [120].

4.5.1 Major uncertainties

All the neutrino interaction uncertainties listed above were classified as major (significant) or inferior (insignificant) based on a χ^2 test score of the nominal and $\pm1\sigma$ shifted FD predictions at reference oscillation parameters values, *i.e.* Eqs. (3.2), (3.1), and (3.3).[6] If $\chi^2 < 0.005$ for all reconstructed neutrino energy distributions of (one at a time) signal, background, and total FD predictions in all oscillation channels [213], the uncertainty is inferior. It is considered major otherwise.

The major uncertainties are conservatively treated as uncorrelated (E_ν bin-to-bin), and hence, they are represented by independent systematic pulls and nuisance parameters. There are the following major neutrino interaction uncertainties (with the quoted number of corresponding systematic parameters, 25 in total):

- z-expansion CCQE norm. (1) and uncorrelated axial vector shape variations (4),
- $M_A^{\rm NCRES}, M_A^{\rm CCRES}, M_V^{\rm NCRES}$ and $M_V^{\rm CCRES}$ uncertainties (4),
- high Q^2 enhancement and low Q^2 suppression for RPA shape in CCQE (2),
- RES low Q^2 suppression uncertainty (1),
- normalization of 1π final states in DIS CC of ν on n (1),
- π mean free path in FSI (1),
- the largest of the 3 FSI uncorrelated "fate fraction" shifts (1),
- E_ν and (q_0, q) dependence of MEC for ν and $\bar{\nu}$ (4),
- fraction of MEC on np pairs for ν and $\bar{\nu}$ (2),
- ν_e/ν_μ and $\bar{\nu}_e/\bar{\nu}_\mu$ cross section ratio uncertainty due to radiative corrections (2),
- ν_e/ν_μ and $\bar{\nu}_e/\bar{\nu}_\mu$ anticorrelated cross section ratio uncertainty due to possible second-class currents (1), and

[6] *N.b.*, χ^2 over all reconstructed energy E_ν bins of the oscillation channel, *i.e.* in all analysis samples of the channel in ν- or $\bar{\nu}$-beam at once.

$$\chi^2 = \sum_{i=1}^{N} \frac{(F_i - S_i)^2}{F_i},$$

where F_i is the predicted nominal number of events, S_i the (+ or −) 1σ shifted number of predicted events in the i-th E_ν bin of the oscillation channel ($\nu_\mu \to \nu_\mu, \nu_\mu \to \nu_e, \bar{\nu}_\mu \to \bar{\nu}_\mu, \bar{\nu}_\mu \to \bar{\nu}_e$) with N bins in total.

- ν_τ scale uncertainty (1).

The resulting error on the total number of predicted events for most of the listed uncertainties is <1%. The ν_e/ν_μ cross section ratio uncertainties, as an exception, naturally behave as detectors effectively uncorrelated ±2% on ν_e events.

4.5.2 Inferior uncertainties

All neutrino interaction uncertainties excluded from the list in the preceding subsection are considered inferior (47 in total), and they are approximated by a principal component analysis (PCA).[7] The PCA uses a simulated ensemble of pseudorandomly generated normally distributed[8] prediction shifts (universes) in neutrino true energy bins of ND and F/N (Far/Near) basis for several ν_e (QE, non-QE, ν_μ CC, NC) and ν_μ (QE, non-QE, NC) selection samples (as quoted respectively).

The principal components (PCs) of the simulated ensemble are constructed through eigenvector decomposition of a covariance matrix of the casted vectors in bins of the examined samples and energy. The PC shifts are later translated back to the ND and FD basis of the initially exploited neutrino interaction types and energy. The corresponding ratios to the nominal MC prediction are then used as weights to estimate the uncertainty.

The application of PCs has some key advantages over the original systematic shifts [230]:

1. PCs are by construction orthogonal and therefore linearly uncorrelated in the source data (PCs help to account for possible neutrino energy correlations of the considered uncertainties without overestimating when later directly summed in quadrature).

2. Interaction type classification and F/N basis allow for capturing more of the modeled physics correlated between the detectors and samples (extra cancellation of uncertainties smeared by the analysis and extrapolation selections).

3. Only a few of the total number of PCs usually account for a large majority of the variance in the ensemble, and, while neglecting the rest, they can be used to reduce the initial data dimensionality (*i.e.* the consequent number of systematic nuisance parameters and computational demands of the final fitting).

Based on a reciprocal RMS (root mean square) coverage of the simulated ensemble variations and the selected PCs summed in quadrature w.r.t. the nominal prediction in F/N basis (Fig. 4.2), and on the sensitivity comparisons of pseudo experiments resembling the analysis procedure (more in Appendix B), twelve PCs with an *ad hoc* +35% normalization scale to make up for the neglected ones were used in the end [233].

4.6 Beam flux

Neutrino flux uncertainties in the NOvA detectors are derived from the beam focusing uncertainties [235] and uncertainties on hadron production at the beam target from the PPFX package, which applies corrections and constraints on proton interaction cross sections from NA49 and MIPP measurements [96]. Similar to neutrino cross section uncertainties, they behave as weights propagated through the simulation and then approximated with PCA.

Variations of the beam optics (Figs. 2.5, 2.4) G4NuMI package simulation parameters of the focusing horns current and position, target position and position of the proton beam on

[7] General notes on the PCA can be found in, *e.g.*, Ref. [229], a simpler tutorial in Ref. [230], for PCA in the NOvA neutrino oscillation analyses see Refs. [231, 232, 233, 234], or see Appendix B.

[8] *N.b.*, the shifts in fractions of σ of the included uncertainties w.r.t. to the nominal prediction ($\sigma = 0$, *i.e.* mean) are normally distributed in the ensemble.

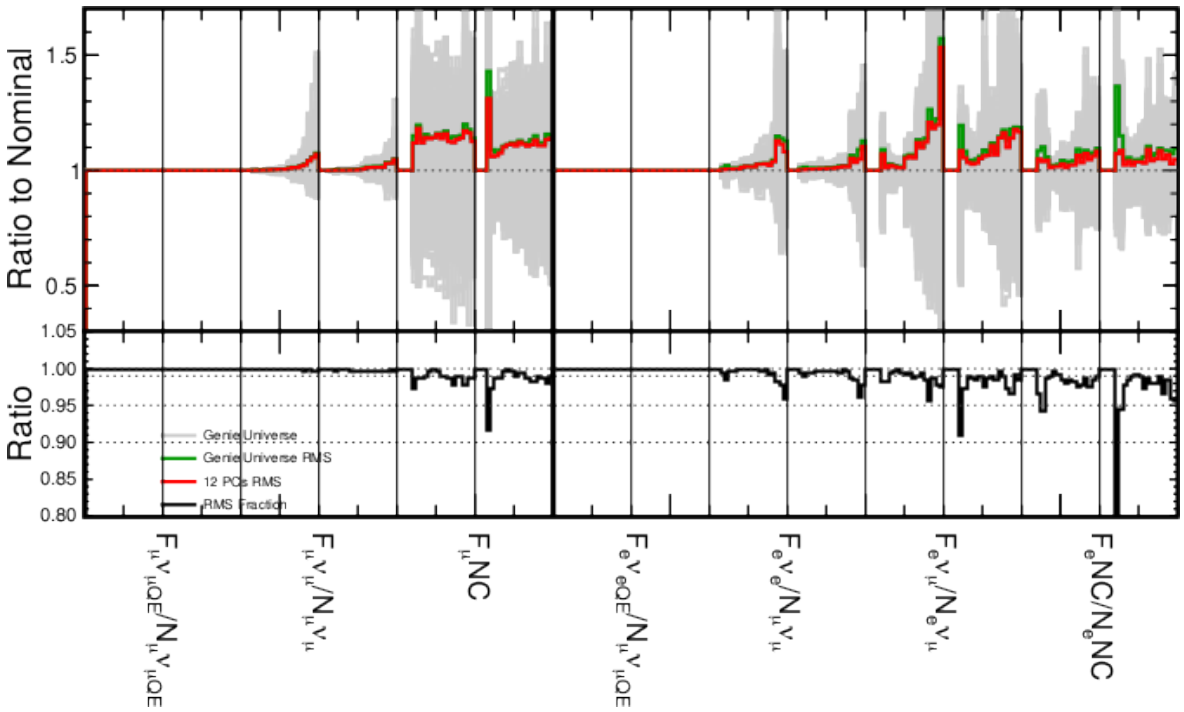

Figure 4.2: Coverage for the first twelve PCs in the F/N basis expressed w.r.t. the nominal MC and generated ensemble of inferior neutrino cross section uncertainties. F and N denote the Far and Near basis, their μ/e index corresponds to ν_μ disappearance / ν_e appearance selection with ν_x quasielastic (ν_xQE), non-quasielastic CC (ν_x) or NC interactions, each sample is divided into two columns for ν-beam (left) and $\bar{\nu}$-beam (right) MC. *N.b.*, FD ν_μ NC background is unconstrained (not constrained by any ND selection or $F/N = 1$), FD ν_e signal is constrained by ND ν_μ. The ratios of the simulated ensemble to the nominal MC (grey, "Genie Universe") are overlayed with the RMS w.r.t. the nominal (green, effectively added to 1) and the RMS of the largest twelve constructed PCs (red). The RMS ratio (green to red) is in the bottom plot (black). Only five bins have RMS fraction (coverage) <95% with twelve PCs.

the target, beam spot size, *etc.*, are used to produce the relative weights to the nominal simulated neutrino flux to evaluate the uncertainties. PPFX package constructs complementary uncertainties on hadron production as illustrated in Fig. 4.3, and the weights are applied w.r.t. the produced hadron kinematics. The largest effects on the overall neutrino flux come from the horn positions (up to 10%, but away from the NOvA flux peak at neutrino energy 2 GeV) and from the incident nucleon interactions not directly covered by any available data and thus remaining unconstrained (up to 8%, denoted "nucleon-A" in Fig. 4.3) [96].

The flux PCA is identical in its methodology to the neutrino cross section PCA (Subsection 4.5.2, Appendix B or Ref. [231]),[9] but it employs different samples: true simulated neutrino flavors (ν_μ, ν_e, $\bar{\nu}_\mu$, $\bar{\nu}_e$)×(ν-beam, $\bar{\nu}$-beam) in ND+F/N basis of neutrino energies. Once again, advocated by the overall coverage in F/N basis and sensitivity pseudo experiments, only the five largest PCs with a +25% scale enter the neutrino oscillation analysis. With supplementary cancellation by the F/N technique, beam flux uncertainties account for the lowest ones with <1% variations on the total number of FD predicted events.

[9]However, it has wider applicability in other NOvA analyses using the NuMI beam data.

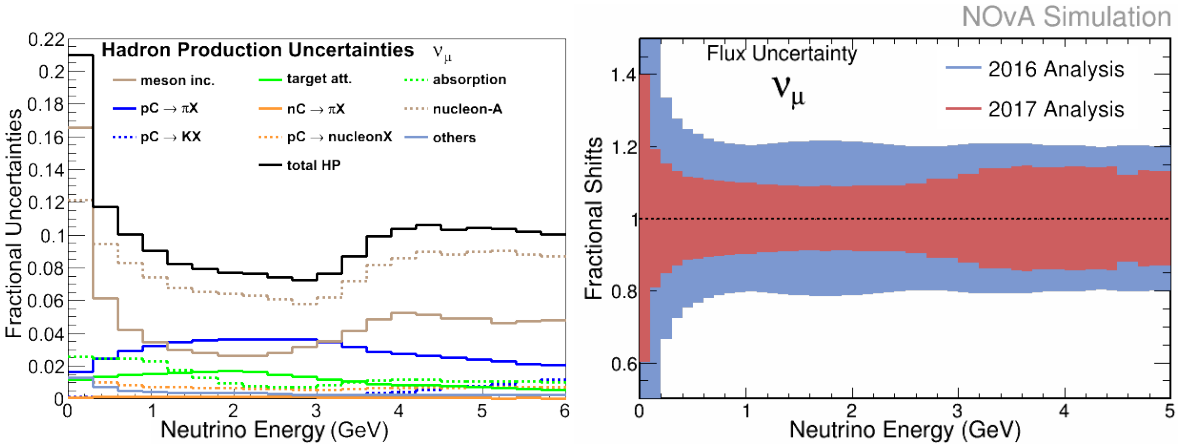

Figure 4.3: **Left:** Hadron production fractional uncertainties for ν_μ in the NOvA ND as derived from PPFX as a function of the neutrino energy. The total (black) is a sum of the individual interaction uncertainties (shown in colors) in quadrature. The largest contribution comes from uncertainties on nucleon incident interactions unconstrained by any data (nucleon-A, dotted brown). **Right:** The total fractional uncertainty on ν_μ flux in the NOvA ND from hadron production and beam focusing uncertainties added in quadrature. The 2020 analysis uses their last update from 2017 (red) – compared to the 2016 version (blue). As they possibly include high bin-to-bin correlations, they are treated with PCA. The plots are from Ref. [97].

4.7 Lepton reconstruction

The NOvA neutrino oscillation analysis suffers from two possible systematic uncertainties linked to the reconstruction of primary leptons in the neutrino CC interactions. First, uncertainty on μ energy scale affects the ν_μ energy reconstruction, Eq. (2.3). Second, uncertainty on the reconstructed primary lepton angle w.r.t. the beam direction might influence the composition of the extrapolation samples, p_t-quantiles (Subsection 3.11.1).

4.7.1 Muon energy scale

Primary μ energy error hails from the uncertainties on its reconstructed range, which is measured by means of crossed and hit detector cells (about 4 cm × 6 cm). Ref. [135] provides an extensive, collaboration-wide 2020 updated evaluation of these (an older version using similar methodology is in Ref. [236]) with a list of investigated unknowns of

- detectors masses: scintillator, PVC, glue, paint and ND μ-catcher steel,
- detectors elemental composition,
- Bethe-Bloch formula accuracy [7, Subsection 34.2.3],
- elements' and compounds' mean excitation energy (ionization potential) for $\mathrm{d}E/\mathrm{d}x$ calculation,
- Fermi's density effect correction $\delta(\beta\gamma)$ by Sternheimer's method and its further non-specific Geant4 calculation uncertainties of μ ranges for NOvA's detectors materials (Geant4 *vs.* tabulated values from Ref. [237]),
- hadronic modeling and hadronic *vs.* μ hit overlaps in events topology,

- extra corrections for coulombic interactions between nucleus and outgoing $\mu^{\pm}$, *i.e.* GENIE μ energy calculation,
- ND thermalized neutron pile-up hits over the course of an average 10 μs beam spill potentially "lengthening" the μ tracks, and
- various smaller effects (multiple scattering, μ decay, noise modeling, and detectors alignment).

Due to its obvious functional and structural dissimilarities to the main ND section, μ-catcher was treated as a separate additional detector to assess the uncertainty. Overall, it is represented by three uncorrelated independent errors for FD (0.15%), ND main section (0.13%) and μ-catcher (0.48%), a fully correlated FD/ND/μ-catcher error (0.74%/0.74%/ 0.13%, respectively), and a ND only neutron pile-up error (0.46 cm for the main detector, 1.3 cm for the μ-catcher in the total μ range). The correlated part is dominated by uncertainties in $\delta(\beta\gamma)$ calculation and differences in the μ range in Geant4 *vs.* Ref. [237], while the uncorrelated parts are governed by the mass accounting.

The expected detector uncorrelated uncertainties on the total number of predicted events are $\sim$0.5% in the ν_μ disappearance samples and $\sim$2.0% for the fully correlated. They are significantly lower $\lesssim$0.5% in the ν_e samples.[10]

4.7.2 Primary lepton angle reconstruction

Besides calibration, detector model, neutron uncertainty, and μ energy scale, any shift in the primary lepton angle ϑ to the beam direction can also bias the reconstructed p_t and thus move the boundaries of p_t-quantiles. The uncertainty in ϑ of the μ stems primarily from the detectors geometry and plane misalignments or tilts. They were originally studied by comparing MC (ND+FD) and data (ND) samples with standard and tweaked detector geometries based on assembly records [238] and were estimated to be about 2.5 mrad. It is a matter of concern that these misalignments are, in fact, correlated between the planes, and the actual uncertainty is larger [208]. Therefore, the systematics is designed as a conservative rotation of the ND xz and yz projections of the primary μ direction by $\pm$10 mrad. Similarly, FD μ and e are rotated by the same amount. The uncertainties are treated as detectors and their views uncorrelated, fully correlated between the beam modes, *i.e.* four nuisance parameters in total.

The effect is up to $\sim$0.5% of the total number of predicted events in the individual analysis samples and dominated by the ND xz projection uncertainty (*i.e.* horizontally along the beam direction, as instinctively anticipated). It is about negligible in ν_e appearance samples and ν_μ higher E_{had} fraction quartiles which is understandable.

4.8 Near-Far uncorrelated uncertainties

The last systematics category lists several uncertainties generally considered uncorrelated between the detectors. Either they are directly associated with only one of the detectors (*e.g.* FD prediction scales, detector mass), uncorrelated between the detectors by their nature (exposure POT counting), or they affect FD total predictions through the F/N extrapolation technique itself only (acceptance and Michel e tagging).

The following paragraphs describe the uncertainties on the differences in the detectors ν_μ and ν_e acceptance (2 systematic nuisance parameters), Michel e tagging (1), overall normalization (3), cosmic (1), and uncontained (1) prediction scales.

[10] Obviously, errors on μ range will not apply on ν_e CC events' final state particles.

4.8.1 Detectors' ν_μ and ν_e acceptance differences

Detectors' ν_μ and ν_e acceptance difference uncertainty probes the plausibility of the F/N extrapolation technique (Section 3.11) and ND constraints on FD predictions. In other words, there is a reasonable requirement for the ND samples to be representative reflections of FD samples, *i.e.* to share common features with them, *e.g.* the interactions phase space and underlying kinematic variables distributions. As demonstrated few times [239, 240], such distributions of transferred four-momentum Q^2, relative transverse momentum p_t/p, primary lepton angle to the beam direction $\cos\vartheta$ and others do not match between ND MC ν_μ constraining sample and FD MC ν_e signal sample, see Fig. 4.4. That could lead to additional uncertainties illconstrained by the ND data or other detectors correlated uncertainties.[11]

In order to estimate them, ND ν_μ MC and data samples are reweighted to match the shape of FD MC ν_e signal w.r.t. some kinematic variables to see the aftereffect on F/N extrapolated FD predictions. In a simplified case of Eqs. (3.22), (3.30), and (3.33) (using the notation in the quoted equations of ND ν_μ selection s_μ and FD ν_e f_e, $M_N = \mathbb{1}$ and $\mathbf{N_{MC}}(\nu_\mu; s_\mu) = \mathbf{N_{MC}}(s_\mu)$ – "pure ND constraints"), FD F/N extrapolated prediction of ν_e signal event rates $\mathbf{F_p}$ in bin i is

$$F_{\mathrm{p},i}(\nu_\mu \to \nu_e; f_e, s_\mu) = F^{\mathrm{MC}}_{\mathrm{p},i}(\nu_\mu \to \nu_e; f_e) \cdot \frac{N_{\mathrm{data},i}(s_\mu)}{N_{\mathrm{MC},i}(s_\mu)}, \tag{4.1}$$

and with any reweighted ND samples $\mathbf{N^{rwt}_{data}}, \mathbf{N^{rwt}_{MC}}$ spectra in reconstructed neutrino energy (omitting selection and bin specifications, using formal ratios),

$$\frac{\mathbf{F^{rwt}_p}}{\mathbf{F_p}} = \frac{\mathbf{F^{MC}_p}}{\mathbf{F^{MC}_p}} \cdot \frac{\dfrac{\mathbf{N^{rwt}_{data}}}{\mathbf{N^{rwt}_{MC}}}}{\dfrac{\mathbf{N_{data}}}{\mathbf{N_{MC}}}} = \left(\frac{\mathbf{N^{rwt}_{data}}}{\mathbf{N^{rwt}_{MC}}}\right) \Big/ \left(\frac{\mathbf{N_{data}}}{\mathbf{N_{MC}}}\right) \neq 1 \tag{4.2}$$

holds for the predictions $\mathbf{F^{rwt}_p}$ constrained by the reweighted ND samples. The last inequality of Eq. (4.2) articulates the uncertainty cause as the reweighted ND samples could lead to distorted FD predictions.

The eventual uncertainty is evaluated separately for ν- and $\bar{\nu}$-beam (and for ν_e peripheral sample) by reweighting of the variable with the largest relative effect on the total number of predicted appearance channel signal+WS background ($\nu_e + \bar{\nu}_e$ from $\nu_\mu + \bar{\nu}_\mu$) events of $\mathbf{F^{rwt}_p}$ *vs.* $\mathbf{F_p}$ (reweighted in p_t/p for ν-beam, $\cos\vartheta$ for $\bar{\nu}$-beam), Fig. 4.4. $\mathbf{F^{rwt}_p}$ spectrum relative differences serve as estimates for $\pm1\sigma$ uncertainties. The expected error is about 0.4–1.0% on the total number of predicted appearance signal+WS events, and it differs among the extrapolation p_t-quantiles [239].

Although Eq. (4.2) also applies to the disappearance ν_μ FD sample (not fully overlapped phase spaces of FD ν_μ CC and ND ν_μ CC), the effect should be smaller or even negligible because the samples themselves have much closer physical resemblance than FD ν_e *vs.* ND ν_μ CC, which are fundamentally different interactions with disparate selections, *etc.* Moreover, the use of extrapolation samples (E_{had}-quartiles, p_t-quantiles) already mitigates the discrepancies. *Ergo*, no acceptance uncertainty is considered for the ν_μ disappearance.

4.8.2 Michel e tagging

The ability to reconstruct Michel e clusters, *i.e.* to "tag" Michel e, suffers from intrinsic uncertainties on decaying μ^- atomic binding fractions and nuclear capture rates, Michel e energy (what atom μ^- binds to), and primarily from ambiguities concerning Michel e hits

[11] The actual differences in ND *vs.* FD kinematic acceptances were, among others, the motivation for introducing additional extrapolation samples of p_t-quantiles.

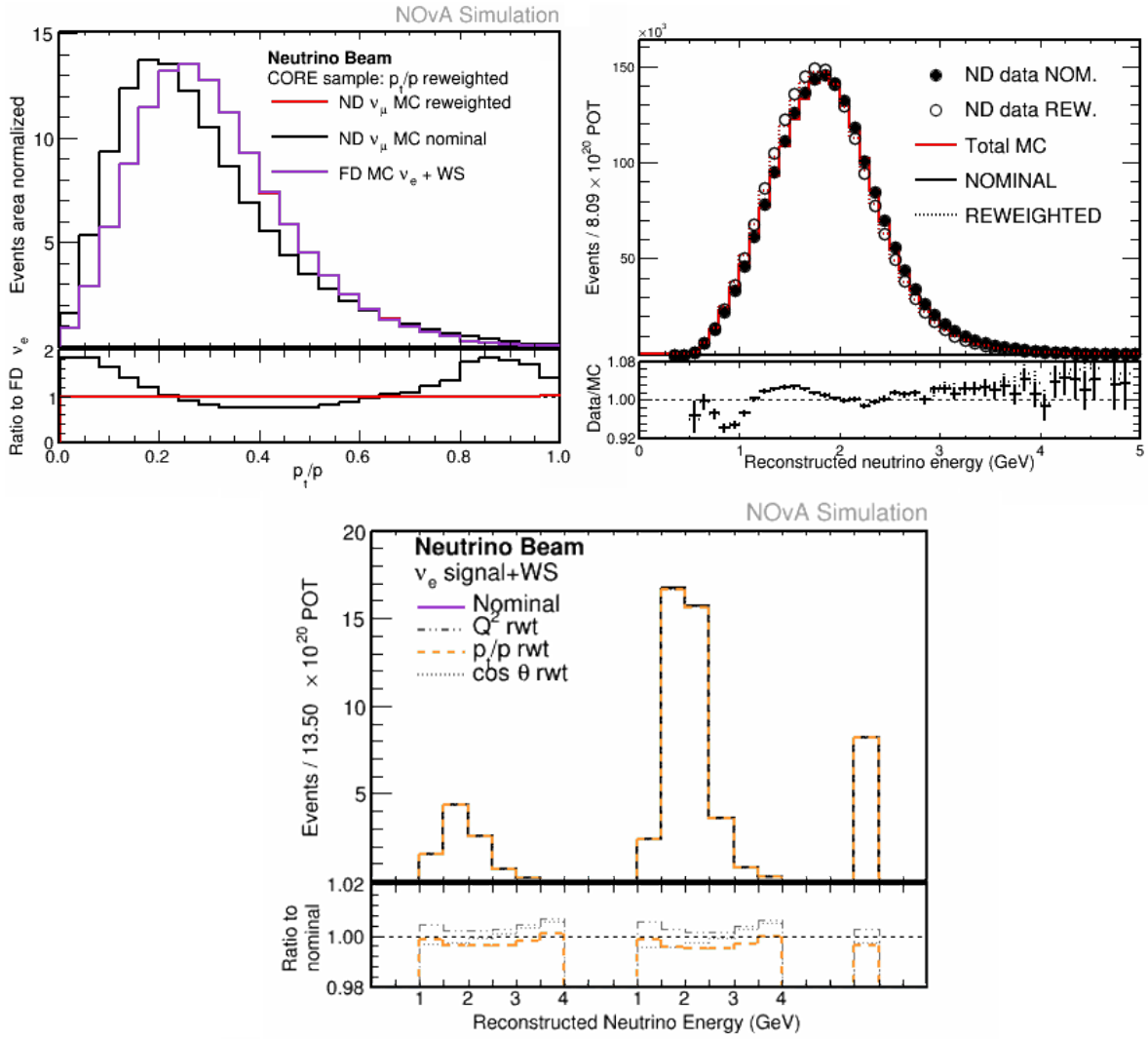

Figure 4.4: **Top left:** Differences in selected FD MC ν_e CC (magenta) and ND MC ν_μ CC (black) ν-beam reconstructed p_t/p distributions. **Top right:** Nominal (full) and FD MC ν_e p_t/p reweighted (blank+dotted) ND ν_μ CC ν-beam constraining sample. **Bottom:** Nominal (magenta) and F/N extrapolated ν_e signal+WS ν-beam prediction for three different kinematic reweightings. p_t/p weight (orange, dashed) was selected to construct the ND ν_μ *vs.* FD ν_e acceptance uncertainty. From left to right, the three histograms correspond to the ν_e low, high PID, and peripheral sample, respectively. *N.b.*, for simplicity's sake, the plot shows only the overall effect in the ν_e appearance analysis samples, whereas the weights are implemented on the level of extrapolation p_t-quantiles, hence, differ from the displayed ones.

overlapping with the parent μ tracks [241]. The uncertainty on the observed tagging efficiency should be conservatively about 5%.

In order to use the general approach and to properly modify the Michel e reconstruction itself, an adjusted MC sample would be needed (such as calibration or light model adjusted samples). That would inconveniently exploit extra computational resources (time in particular), and, therefore, an alternative method is adopted. Instead of Michel e tagging efficiency (MC reconstructed *vs.* simulated), the 5% variation is implemented on the level of the actual selection efficiency (MC true selected *vs.* simulated). Then, pseudorandomly chosen Michel e are forced to fail or pass the selection criteria. To mimic a $\pm$5% variation of the tagging efficiency, 8% of tagged Michel e were forced to be selected ($+1\sigma$ shift), and 5% of them were

discarded (-1σ) [242].

Michel e tagging efficiency affects the expected fractions of $\nu_\mu(+\bar{\nu}_\mu)$ CC and NC events in Michel decomposed bins of ν_e ND sample to constrain FD ν_e appearance background predictions (*i.e.* only low PID sample of ν-beam data), see Subsection 3.10.2. Ultimately, the estimated uncertainty on the total number of predicted background events of the ν_e ν-beam low PID sample is about $\pm 4\%$, or $\pm 1.5\%$ of all predicted events in this sample.

4.8.3 Normalization uncertainties

Normalization systematics fold in the uncertainties on the overall scale of the predicted events, arising from detectors mass accounting, simulation "mismatch", POT accounting, and context (or pile-up) uncertainty on ND selection efficiency.

Detectors' fully uncorrelated FD **mass uncertainty** was estimated to 0.19% along with μ energy scale studies in Ref. [135] based on the available records of the detectors assembly techniques. Inaccurate scintillator density (various blends), filling, and leaks are the principal causes of this systematic error.

Simulation mismatch uncertainty of 0.8% accounts for the fact that an unresolved bug in NOvA software caused Geant4 to skip some primary particles generated in previous simulation steps (missing primary leptons in simulated interactions). It appears to affect the FD MC only ($\lesssim$0.005% of ND MC events) in about 0.6% events relevant for neutrino oscillation analysis with a reasonably flat distribution in their true energy [243]. Instead of an applicable MC correction, an adequately inflated 0.8% systematic uncertainty was implemented, as the bug was not entirely understood nor studied sufficiently.

The mass and simulation uncertainties are treated as intrinsically uncorrelated, *i.e.* added in quadrature to 0.82%, and correlated between all analysis samples and both ν- and $\bar{\nu}$-mode.

The total exposure **POT counting** (ND *vs.* FD) can be skewed by any potential calibration drift of the main beam monitoring toroid w.r.t. the beam intensity or time [244] or possible timing issues (such as described in Subsection 3.9.1). This is secured by a chary 0.55% scale uncertainty[12] virtually uncorrelated between the beam modes but taken of equal size.

The ND selection efficiency for ν_μ and ν_e-like candidate events depends quite dramatically on the intensity of the NuMI beam pulses. With higher intensities, more interactions appear in the ND, which makes it more difficult for reconstruction and particle identification algorithms to succeed. These so-called **context (pile-up) effects**[13] have different manifestations in data and MC (ostensibly originating from mismodeled neutrino fluxes, interactions, detector response, *etc.*), and they are evaluated by inserting single simulated events into the standard MC and data spills, single event overlays [245]. The recognized difference in selection efficiency within the modified data and MC samples is then applied as a systematic uncertainty. It was estimated to 0.21/0.41% correlated between the ND ν_μ/ν_e selection in ν-beam and 0.48/0.53% in $\bar{\nu}$-beam, beam uncorrelated. Subsequent uncertainties on the FD predictions are taken according to the ND constraining samples, *i.e.* ND ν_μ for both FD ν_μ and ν_e signal, ND ν_e for FD ν_e background.

Added in quadrature, POT counting and context together constitute two ν- and $\bar{\nu}$-beam uncorrelated normalization uncertainties: 0.59/0.69% for ν-beam and 0.73/0.76% for $\bar{\nu}$-beam, which are fully correlated in their ND selection context parts of ν_μ (FD $\nu_\mu + \nu_e$ signal) / ν_e (FD ν_e beam background).

[12] The toroid has, in fact, a very stable calibration with practically no drifts observed [244].

[13] The observed pile-up effects were among the motivations for the new clustering algorithm, TDSlicer (Subsection 3.5.1).

4.8.4 Cosmic and rock prediction scales

The uncertainties on the uncontained (rock) and cosmic predictions are not, *de facto*, systematic, but they are treated similarly throughout the analysis. It suits the physics unknowns behind them.

As noted in Section 3.12, a special dedicated MC sample is used to predict ν_e CC event candidates caused by particles entering the detector from neutrino interactions in the surrounding rock (ν_e appearance only). Since the number is almost negligible and there is no way of constraining it, a **rock rate** uncertainty of 100% was included leading to up to 0.7% uncertainty on the total number of ν_e appearance channel events prediction ($\sim$2–3% in the peripheral sample, $\lesssim$0.5% otherwise).

Though the actual systematic uncertainty on the spectra extracted from cosmic trigger data is very low, if any, possible statistical fluctuations caused by the stochastic nature of cosmic events affect the final predictions. Shifted **cosmic background** predictions are constructed as lower (-1σ) and upper ($+1\sigma$) Poisson error bounds (68.27% confidence level limit of Poisson distribution) in each bin of the corresponding cosmic trigger spectra unscaled to the NuMI beam window livetime, *i.e.* in real detector livetime. That implies about 0.5–1.0% uncertainty on the total number of predicted events. It is significant, *i.e.* >1%, in ν_e low PID and peripheral samples and the highest E_{had} fraction quartile of the ν_μ disappearance channel.

4.9 Summary and notes

Overall, when summed in quadrature over the categories, the expected systematic (statistical[14]) uncertainties on the total numbers of predicted events are 6.5%/6.8% (7%/10%) in the ν_μ disappearance channel and 3.6%/3.8% (10%/17%) in the ν_e appearance channel for $\nu/\bar{\nu}$-beam. For a more detailed evaluation concerning the later obtained best-fit point of the oscillation parameters, see Appendix C.

There are several concerns regarding the treatment of the systematic errors in the NOvA neutrino oscillation analysis. Firstly, many of the uncertainties introduced above are estimated on fairly conservative grounds (absolute calibration scale, most importantly). Hence, potential improvements through eventual (and ongoing) studies (NOvA Test Beam) are far from being depleted.

As a matter of fact, the analysis framework[15] does not allow for a straightforward way to deal with possible correlations. The systematic nuisance parameters have to be "decorrelated" (*e.g.* PCA of flux and cross section uncertainties in F/N basis, uncorrelated "fate fraction" scales for FSI) upon implementing into the analysis. That is certainly not true for the whole set in its entirety because of the inadequate effort and time that would be required to do so. Although, this is believed to rather overestimate the final uncertainties, as they are not generally expected to be anticorrelated. Quite the contrary, some uncertainties are suspected of having common sources leading to "double counting", *e.g.* calibration and detector response, normalization, and μ energy scale. The necessary investigations are on the agenda of the future NOvA analyses.

Additionally, some uncertainties were designed to "bracket" the related discrepancies and unknowns because their true sources remain unrecognized, *e.g.* calibration shape, normalization, neutron uncertainty, or they might be considered not perfectly understood, *e.g.* ND/FD acceptance differences. This could, again, catalyze double counting and ultimate overestimation.

[14] Estimated statistical uncertainties strongly depend on the oscillation parameters. They are evaluated at 2019 best fit, Eqs. (3.1) and (3.2).

[15] CAFAna (Common Analysis Files Analysis framework) [212]

Though the analysis is mainly limited by the experiment's statistics, with about twice the exposure, in the end, further reduction of the systematic uncertainties is still one of the most apparent ways to improve it. Statistics are determined by the beam operation time, its power, and the FD active mass. Given the current status, none of them could be enhanced easily (or at all) compared to the initial plans.

5. Results and constraints on neutrino oscillation parameters

This chapter describes the NOvA neutrino oscillation analysis fitting procedure and the oscillation parameters estimation in Section 5.1. It overviews the best-fit predictions compared to the observed FD data, Section 5.2, and the final calculations of the systematic uncertainties, Section 5.3. It explains the construction of the parameters confidence regions (limits) with Feldman-Cousins corrections, Section 5.4, and shows the resulting constraints, Section 5.5.

The NOvA neutrino oscillation analysis follows a strict blinding policy, and any results stated in this chapter were obtained with no *ex post* interventions into any of its elements, *i.e.* through a direct evaluation only. The observations are interpreted within the 3ν-paradigm in terms of the frequentist inference [246].

5.1 Best-fit estimates

The best-fit estimates of oscillation parameters $\boldsymbol{\theta}$ are found by minimizing a log-likelihood ratio $\lambda(\boldsymbol{\theta}, \boldsymbol{\varsigma})$ [7] for n bins of independent Poisson distributed random variables of binned FD data $\mathbf{D} = (D_1, \ldots, D_n)^\top$ and a saturated model $\mathbf{F}(\boldsymbol{\theta}, \boldsymbol{\varsigma})$ of predictions (constructed as in Sections 3.11 to 3.13) with Gaussian penalty terms for systematic parameters $\boldsymbol{\varsigma}$ in units of standard deviation σ

$$-2 \ln \lambda(\boldsymbol{\theta}, \boldsymbol{\varsigma}) = 2 \sum_{i=1}^{n} \left(F_i(\boldsymbol{\theta}, \boldsymbol{\varsigma}) - D_i + D_i \ln \frac{D_i}{F_i(\boldsymbol{\theta}, \boldsymbol{\varsigma})} \right) + \sum_{j=1}^{m} \varsigma_j^2, \tag{5.1}$$

where i runs over the reconstructed energy bin indices ($n = 178$ in total) of all the analysis samples, *i.e.* all analysis bins, and j runs over the systematic nuisance parameters and external constraints (*i.e.* one as later specified, $m = 67 + 1$).

The minimum of expression in Eq. (5.1) is also often loosely interpreted as χ^2 for it asymptotically obeys χ^2 distribution with $n-k$ degrees of freedom provided certain conditions (see Wilks' theorem in Ref. [247]), where k is the number of estimated parameters $\boldsymbol{\theta}$.

The NOvA neutrino oscillation analysis is performed within the 3ν-paradigm described in Section 1.2. Eq. (5.1) is minimized w.r.t. three neutrino oscillation parameters $\theta_{23}, \Delta m^2_{32}, \delta_{\text{CP}}$, all systematic nuisance parameters $\boldsymbol{\varsigma}$, and one additional parameter with a Gaussian penalty term similar to ς_j for an external constraint on mixing angle θ_{13} from reactor neutrino experiments as in Ref. [248]:

$$\sin^2 2\theta_{13} = 0.085 \pm 0.003. \tag{5.2}$$

All remaining oscillation [248] and experimental parameters are taken as fixed

$$\Delta m^2_{21} = 7.53 \times 10^{-5} \text{ eV}^2, \quad \sin^2 2\theta_{21} = 0.851, \tag{5.3}$$

and

$$L = 810 \text{ km}, \quad \rho = 2.84 \text{ g/cm}^3. \tag{5.4}$$

The Eq. (5.1) minimization is carried out with the help of Minuit2 library of the MINUIT software [249]. Using NOvA FD data, the found **best-fit estimates** are

$$\begin{aligned} \Delta m^2_{32} &= 2.41 \times 10^{-3} \text{ eV}^2, \\ \sin^2 \theta_{23} &= 0.57, \\ \delta_{\text{CP}} &= 0.82\pi. \end{aligned} \tag{5.5}$$

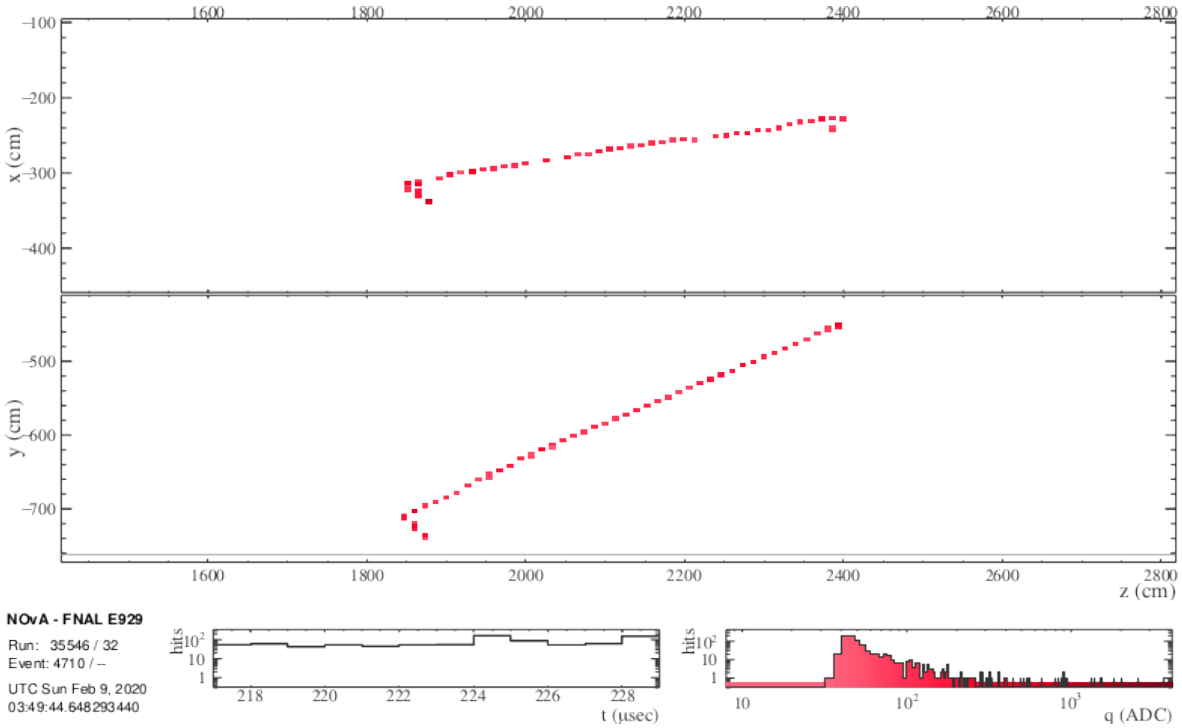

Figure 5.1: Example of a FD event display of a selected ν_μ CC candidate in ν-beam data [250] (the gray line is one of the detector edges). Long μ track is clearly distinguishable from the very short shower-like hadronic activity near the interaction vertex.

5.2 Far detector data

There were 211 candidates selected in FD ν-beam data for the ν_μ disappearance channel, 105 candidates in $\bar{\nu}$-beam data. There were 82 candidates in ν-beam data for the ν_e appearance channel, 33 for $\bar{\nu}$-beam. Using the best-fit parameters of Eq. (5.5), the expected total signal+background is 213.7+8.6 for ν_μ disapp. ν-beam, 103.2+2.2 for $\bar{\nu}_\mu$ disapp. $\bar{\nu}$-beam, 59.0+26.8 for ν_e app. ν-beam and 19.2+14.0 for $\bar{\nu}_e$ app. $\bar{\nu}$-beam. That represents over 4σ direct evidence of $\bar{\nu}_\mu \to \bar{\nu}_e$ transition, best among recent neutrino oscillation experiments.

Two examples of selected event displays are in Figs. 5.1, 5.2. Reconstructed neutrino energy spectra in all analysis samples ($\nu/\bar{\nu}$-beam ν_μ disappearance E_{had}-quartiles and ν_e appearance PID samples) overlayed with the best-fit FD predictions including systematic uncertainty bands are in Figs. 5.3, 5.4, and 5.5. They are also summarized in Tables 5.1 and 5.2. Checks on the selected events accumulation over the experiment's operation are in Fig. 5.6, and their distributions in the NuMI beam timing window are in Fig. 5.7. A pedagogical plot in Fig. 5.8 illustrates the results in the total ν-beam *vs.* $\bar{\nu}$-beam ν_e appearance channel selected events space.

5.3 Overview of systematic uncertainties

To further scrutinize the systematic uncertainties, they were evaluated using the neutrino oscillation parameters estimates, including the systematic pulls. To this end, $\pm 1\sigma$ limits relative to the best-fit predictions were calculated for all of the uncertainties in the analysis (Chapter 4), eventually summed in quadrature in their categories. Apart from the 1σ systematic bands to be seen in the reconstructed energy plots, overall uncertainties on the integrated predictions in the analysis samples and the expected impact on the uncertainties

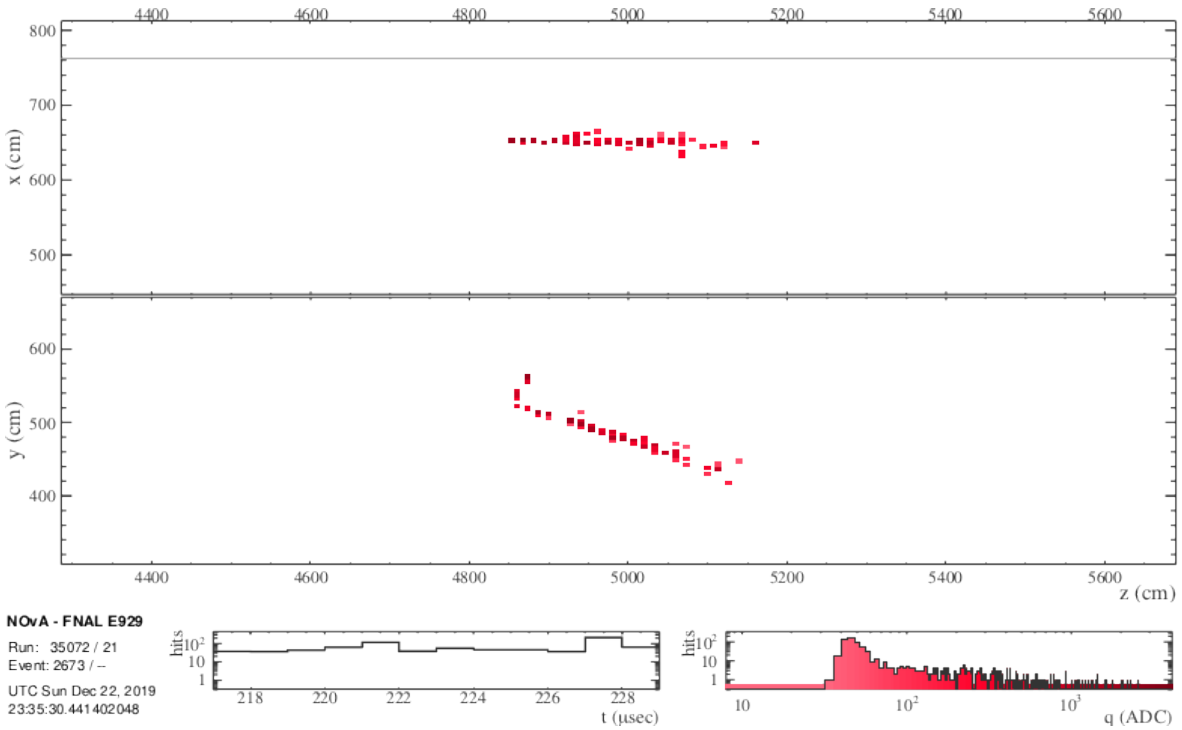

Figure 5.2: Example of a FD event display of a selected ν_e CC candidate in ν-beam data [250] (the gray line is one of the detector edges). The large electromagnetic shower is clearly distinguishable from the short hadronic-like activity emerging in different directions from the interaction vertex.

of the oscillation parameters estimates are shown.

5.3.1 Uncertainties on far detector predictions

The summary for the ν_μ disappearance channel is in Figs. 5.9, 5.10, and 5.11. Fig. 5.9 displays the uncertainties on the total number of predicted events, Fig. 5.10 provides a feasible comparison of the E_{had} fraction quartiles subsets, and Fig. 5.11 confronts the expected uncertainties with and w/o the F/N extrapolation technique using Eq. (3.33). Equivalent plots for the ν_e appearance channel are in Figs. 5.12, 5.13, and 5.14, respectively.

One can directly make several important first-order conclusions for the total integrated number of events. Firstly, ν_μ disappearance channel systematic uncertainties are already comparable to the statistical ones, with only about 41% of the total expected NOvA exposure (until 2025). The ν_e appearance channel uncertainties are governed by the low statistics, which is mainly due to the more than significant reduction of neutrino fluxes and cross sections[1] errors through the F/N extrapolation technique. On the other hand, ν_μ disappearance uncertainties are primarily trimmed by flux and cross section PCAs, which employ F/N ratios as well (Sections 4.5, 4.6). The subsequent F/N extrapolation effects are therefore lower.

Secondly, the analysis samples comparisons and the differences in the individual uncertainties give an *ex post* confirmation of the original rationale for their implementation. The intrinsic kinematic construction determines the errors within them (uncertainties on lepton reconstruction and calibration in E_{had} fraction ν_μ quartiles) or background composition (ν_e samples).

[1]The main contributions to the neutrino interaction uncertainties are the ν_μ/ν_e CC cross section ratios and the second class currents uncertainties unaffected by any FD to ND functional similarities.

Table 5.1: Integral numbers of FD data (bold) and predicted events in the ν_μ disappearance channel analysis samples, Q1–4 E_{had} fraction quartiles, evaluated at the NOvA 2020 best-fit point of neutrino oscillation parameters $\Delta m^2_{32} = 2.41 \times 10^{-3}$ eV^2, $\sin^2\theta_{23} = 0.57, \delta_{\text{CP}}/\pi = 0.82$ (+systematic parameters) and stated exposures for ν- and $\bar{\nu}$-beam.

Disappearance channel FD data and predictions at 2020 best fit								
	Components		Q1	Q2	Q3	Q4	Total	POT-eq.
ν-beam	Signal	$\nu_\mu \to \nu_\mu$	45.92	45.66	49.60	59.87	201.05	13.60×10^{20}
		$\bar{\nu}_\mu \to \bar{\nu}_\mu$	5.79	2.76	2.55	1.53	12.63	
	Bkg.	NC	0.11	0.17	0.42	1.87	2.57	
		Cosmic	0.35	0.35	0.86	3.40	4.96	
		Other	0.21	0.24	0.25	0.40	1.10	
	Total		52.38	49.18	53.68	67.07	222.31	
	Data		**48**	**48**	**40**	**75**	**211**	
$\bar{\nu}$-beam	Signal	$\bar{\nu}_\mu \to \bar{\nu}_\mu$	23.06	19.03	17.78	17.31	77.18	12.50×10^{20}
		$\nu_\mu \to \nu_\mu$	4.03	4.99	6.11	10.92	26.05	
	Bkg.	NC	0.02	0.04	0.10	0.65	0.81	
		Cosmic	0.06	0.03	0.11	0.74	0.94	
		Other	0.08	0.10	0.11	0.15	0.44	
	Total		27.25	24.19	24.21	29.77	105.42	
	Data		**26**	**23**	**27**	**29**	**105**	

5.3.2 Uncertainties on neutrino oscillation parameters

To appraise the systematics concerning the overall uncertainties on the estimated neutrino oscillation parameters (*i.e.* allowed CL intervals), the analysis is resimulated, and all predictions, including ND MC, are evaluated at the best fit. Then, for the statistic only case, and for any desired combination of systematic uncertainties (*e.g.* $\varsigma_{\text{calibration}}, \varsigma_{\text{flux}}$), the intervals, for which the profiled $\Delta\chi^2(\theta)$ does not exceed a critical value, are located around the best-fit value of a particular parameter θ. For the comparisons have an illustrative purpose of ordering the systematics importance and both limited and incomplete interpretation, applying Feldman-Cousins corrections (as explained in Section 5.4) would be rather exaggerated. The critical value is taken as 1 in loose relation to $\chi^2 = 1$ with one degree of freedom and corresponding p-value 0.3173 of significance (68.27% CL), *i.e.* to the classical 1σ error bounds.

The systematic and statistical uncertainties are assumed to be added in quadrature, so $\sigma^2 = \sigma^2_{\text{stat}} + \sum_j \sigma^2_{\text{syst},j}$, where σ_{stat} is obtained in the statistic only case ($\boldsymbol{\varsigma} = 0$). The results might be understood as the impact of the systematic uncertainties or their categories in the vicinity of the neutrino oscillation parameters' best-fit estimates.

It is evident from Table 5.3 and Fig. 5.15 that the largest systematic uncertainty comes from the detector calibration category, strictly speaking from its ND/FD anticorrelated term, see Subsection 4.2.1. Its reduction by better calibration procedure or detector model and alike is vital for more precise $\sin^2\theta_{23}$ measurement or $\sin^2\theta_{23}$ ($\lesseqgtr 0.5$) octant determination. To properly interpret the comparisons to the reported statistical uncertainties, one should keep in mind the potential "degenerate-like" solutions of the NOvA $\nu_e/\bar{\nu}_e$ appearance problem with different combinations of the θ_{23} octant, δ_{CP} and neutrino masses ordering (hierarchy) hypotheses. An illuminating, first-order explanation was given by the bi-counting (ν_e *vs.* $\bar{\nu}_e$) plots in Figs. 3.36 and 5.8.

Table 5.2: Integral numbers of FD data (bold) and predicted events in the ν_e appearance channel analysis samples evaluated at the NOvA 2020 best-fit point of neutrino oscillation parameters $\Delta m^2_{32} = 2.41 \times 10^{-3}$ eV^2, $\sin^2\theta_{23} = 0.57, \delta_{\rm CP}/\pi = 0.82$ (+systematic parameters) and stated exposures for ν- and $\bar{\nu}$-beam.

Appearance channel FD data and predictions at 2020 best fit							
	Components		Low PID	High PID	Peripheral	Total	POT-eq.
ν-beam	Signal	$\nu_\mu \to \nu_e$	10.21	40.49	8.27	58.97	13.60×10^{20}
	WS bkg.	$\bar{\nu}_\mu \to \bar{\nu}_e$	0.19	0.66	0.19	1.04	
	Beam bkg.	$\nu_e + \bar{\nu}_e$	2.49	7.85	3.74	14.08	
		$\nu_\mu + \bar{\nu}_\mu$	1.12	0.31	0.28	1.72	
		$\nu_\tau + \bar{\nu}_\tau$	0.16	0.26	0.10	0.52	
		NC	4.42	1.52	0.37	6.31	
	Cosmic		1.28	0.21	1.64	3.13	
	Total		19.88	51.29	14.60	85.77	
	Data		**16**	**50**	**16**	**82**	
$\bar{\nu}$-beam	Signal	$\bar{\nu}_\mu \to \bar{\nu}_e$	2.21	14.13	2.83	19.18	12.50×10^{20}
	WS bkg.	$\nu_\mu \to \nu_e$	0.42	1.43	0.40	2.25	
	Beam bkg.	$\nu_e + \bar{\nu}_e$	1.14	4.16	1.98	7.29	
		$\nu_\mu + \bar{\nu}_\mu$	0.17	0.06	0.12	0.35	
		$\nu_\tau + \bar{\nu}_\tau$	0.08	0.17	0.07	0.32	
		NC	1.64	0.44	0.13	2.21	
	Cosmic		0.43	0.14	0.98	1.55	
	Total		6.10	20.53	6.51	33.14	
	Data		**13**	**18**	**2**	**33**	

Table 5.3: Simulated impact of the individual uncertainty sources (systematic uncertainty categories) on the resulting errors of the neutrino oscillation parameters estimates around the NOvA 2020 best-fit point. Note the comparisons are simulated, and they use a Gaussian approximation with no FC corrections. Hence, they might not be in general agreement with Table 5.4.

	Parameters					
Uncertainty source	$\sin^2\theta_{23}$		$\delta_{\rm CP}/\pi$		$\Delta m^2_{32}(\times 10^{-3}{\rm eV}^2)$	
Beam flux	-0.001	$+0.001$	-0.010	$+0.002$	-0.002	$+0.001$
Detector calibration	-0.025	$+0.005$	-0.173	$+0.028$	-0.019	$+0.019$
Detector response	-0.002	$+0.002$	-0.004	$+0.004$	-0.009	$+0.007$
Lepton reconstruction	-0.002	$+0.003$	-0.016	$+0.006$	-0.015	$+0.009$
Near-Far uncor.	-0.002	$+0.002$	-0.028	$+0.012$	-0.005	$+0.001$
Neutrino cross sections	-0.003	$+0.003$	-0.070	$+0.044$	-0.012	$+0.007$
Neutron uncertainty	-0.008	$+0.005$	-0.042	$+0.001$	-0.017	$+0.011$
Systematic uncertainty	-0.027	$+0.008$	-0.194	$+0.054$	-0.034	$+0.025$
Statistical uncertainty	-0.033	$+0.022$	-0.872	$+0.210$	-0.055	$+0.043$

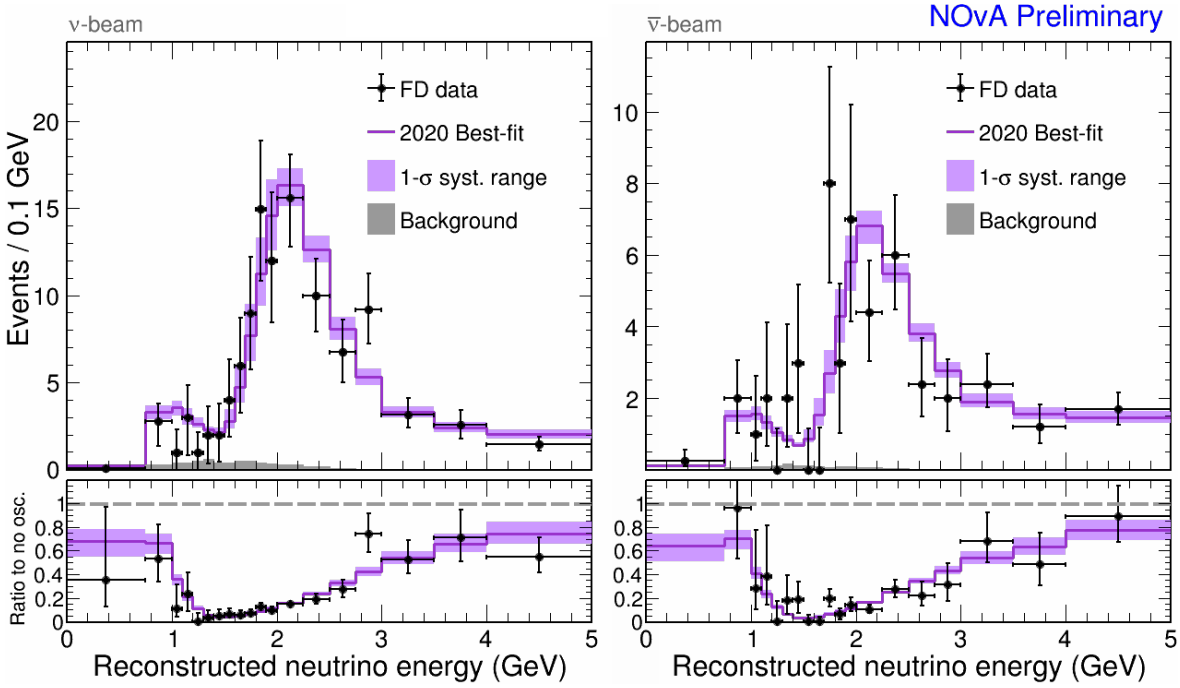

Figure 5.3: Reconstructed energy spectra of the FD ν_μ disappearance channel data selected candidates (black) summed together over individual analysis samples (E_{had} fraction quartiles), overlayed with the best-fit prediction (magenta), and also expressed as a ratio to "no oscillation" hypothesis, *i.e.*, $P(\nu_\mu \to \nu_\mu) = 1$. **Left:** ν-beam data, **Right:** $\bar{\nu}$-beam data. 1σ systematic bands are constructed from the individual uncertainties 1σ limits around the prediction summed in quadrature. Statistical uncertainties are Poisson and FC corrected for the bins with low statistics. The plots are from Ref. [251].

5.4 Confidence regions with Feldman-Cousins corrections

The requirements of Wilks' theorem might be unmet because of the low statistics, physical boundaries of the parametric space of interest, *etc.*, and its application is questionable. A straightforward Gaussian approximation and classical construction of confidence regions from differences of $-2\ln\lambda$, Eq. (5.1), to its minimum relative to the estimated parameters is therefore problematic (Eq. (5.1) as χ^2). Such regions can sometimes include the true values of the parameters at rates significantly off the intended confidence levels (CL).[2] Hence, Feldman-Cousins "Unified Approach" (FC corrections) is employed as in Ref. [254] to determine the CL regions for the reported estimates.

At each point $\boldsymbol{\theta} = (\theta_{23}, \Delta m^2_{32}, \delta_{\text{CP}})$ of the parametric space many $\sim \mathcal{O}(10^3)$ mock experiments are simulated with statistically fluctuated numbers of events in the analyzed bins. Then, with λ of Eq. (5.1),

$$\Delta\chi^2(\boldsymbol{\theta}) = -2\ln\frac{\lambda(\boldsymbol{\theta})}{\lambda(\boldsymbol{\theta}_{\text{BF}})} \tag{5.6}$$

are calculated, where $\boldsymbol{\theta}_{\text{BF}}$ are the best-fit parameters estimates for the corresponding experiment. For a given confidence level α (*e.g.* 90%), a critical value $\Delta\chi^2_{\text{c}}(\boldsymbol{\theta}, \alpha)$ for any $\boldsymbol{\theta}$ is such that for α experiments $\Delta\chi^2(\boldsymbol{\theta}) < \Delta\chi^2_{\text{c}}(\boldsymbol{\theta}, \alpha)$. These "corrected" $\Delta\chi^2_{\text{c}}(\boldsymbol{\theta}, \alpha)$ values are adopted in the comparisons with $\Delta\chi^2$ of Eq. (5.6) for the real data when constructing eligible confidence limits.

In order to get the coverage of the most probable systematic pulls $\boldsymbol{\varsigma}$, as well as any

[2] In the sense of the Neyman construction of CL intervals from Ref. [246].

Table 5.4: NOvA 2020 best-fit estimates of $\Delta m^2_{32}, \sin^2\theta_{23}$, and $\delta_{\rm CP}$ neutrino oscillation parameters and their 1σ CL allowed intervals when profiled over the rest of the parameters. The best fit corresponds to the normal ordering of neutrino masses.

		1σ allowed range	
Parameter	Best fit	Normal Ordering	Inverted Ordering
$\frac{\lvert\Delta m^2_{32}\rvert}{10^{-3}\ \mathrm{eV}^2}$	2.41	$[2.336, 2.482]$	$[2.386, 2.521]$
$\sin^2\theta_{23}$	0.57	$[0.431, 0.487] \cup [0.530, 0.602]$	$[0.433, 0.492] \cup [0.526, 0.595]$
$\frac{\delta_{\rm CP}}{\pi}$	0.82	$[-0.18, 1.06]$	$[1.26, 1.73]$

parameters not considered directly, Eq. (5.2), they are fitted to the data for any $\boldsymbol{\theta}$ prior throwing the mock experiments.

5.5 Constraints on neutrino oscillation parameters

The resulting contraints on the neutrino oscillation parameters are found by evaluating

$$\min_{\boldsymbol{\theta}_{\rm n},\boldsymbol{\varsigma}_{\rm n}} \Delta\chi^2(\boldsymbol{\theta},\boldsymbol{\theta}_{\rm n},\boldsymbol{\varsigma}_{\rm n}) = \min_{\boldsymbol{\theta}_{\rm n},\boldsymbol{\varsigma}_{\rm n}} \left(-2\ln\frac{\lambda(\boldsymbol{\theta},\boldsymbol{\theta}_{\rm n},\boldsymbol{\varsigma}_{\rm n})}{\lambda(\boldsymbol{\theta}_{\rm BF},\boldsymbol{\varsigma}_{\rm BF})}\right), \tag{5.7}$$

i.e. by profiling over any nuisance parameters $\boldsymbol{\theta}_{\rm n}$ and systematic parameters $\boldsymbol{\varsigma}_{\rm n}$, where $\boldsymbol{\theta}$ are the parameters of interest and $\boldsymbol{\theta}_{\rm BF}, \boldsymbol{\varsigma}_{\rm BF}$ are the best-fit estimates. They are compared to the FC corrected $\Delta\chi^2_{\rm c}(\boldsymbol{\theta})$ to be presented as contours of 2D allowed regions for two parameters of interest at different CL, usually in terms of 1σ, 2σ, 3σ as 68.27%, 95.45%, 99.73% CL, respectively. For one parameter of interest, there are simple 1D single-parameter significance profiles.

For estimating $\delta_{\rm CP}$, θ_{23} and the determination of the neutrino mass ordering ($\Delta m^2_{32} \gtrless 0$) are closely related matters of the ν_e appearance channel (see the instructive Fig. 5.8), their constraints are reported for the normal and inverted mass ordering (hierarchy, NO/H or IO/H) separately. They are profiled in $\Delta m^2_{32} > 0$ (NO, NH) or < 0 (IO, IH) hyperplanes of the parametric space.

Table 5.4 contains a summary of the best-fit estimates on Δm^2_{32}, θ_{23}, and $\delta_{\rm CP}$ parameters and their 1σ CL allowed ranges. Fig. 5.16 shows the 90% CL region in Δm^2_{32} *vs.* $\sin^2\theta_{23}$ with comparisons to the latest results of T2K [59], MINOS+ [55], IceCube [44], and Super-Kamiokande [255] neutrino oscillation experiments. They are all in excellent agreement. Fig. 5.17 indicates the 1σ, 2σ, and 3σ allowed regions in $\sin^2\theta_{23}$ *vs.* $\delta_{\rm CP}$ plane for the normal and inverted neutrino mass ordering (hierarchy). Figs. 5.18 and 5.19 display the $\delta_{\rm CP}$ and $\sin^2\theta_{23}$ significance profiles, respectively, and separately for NO (NH) and IO (IH) hypothesis.

To summarize, there is a large region of the parametric space around $\delta_{\rm CP} \sim \pi/2$ rejected with $>3\sigma$ significance for IO (IH), Fig. 5.17. Nevertheless, the overall constraints on $\delta_{\rm CP}$ are relatively weak, with any possible value of $[0, 2\pi]$ interval allowed within 2σ, Fig. 5.18. As the best-fit estimates correspond to the NO (NH) and $\theta_{23} > 45°$, rejection significances for hypotheses of IO (IH) and $\theta_{23} < 45°$ were determined from the distributions of $\Delta\chi^2(\boldsymbol{\theta})$ of the FC generated mock experiments by comparing to the profiled $\min\Delta\chi^2$ of the hypothesis to be rejected. They are both disfavored at about 1σ. The results are overall consistent with the 2019 analysis in Ref. [2] within 1σ.

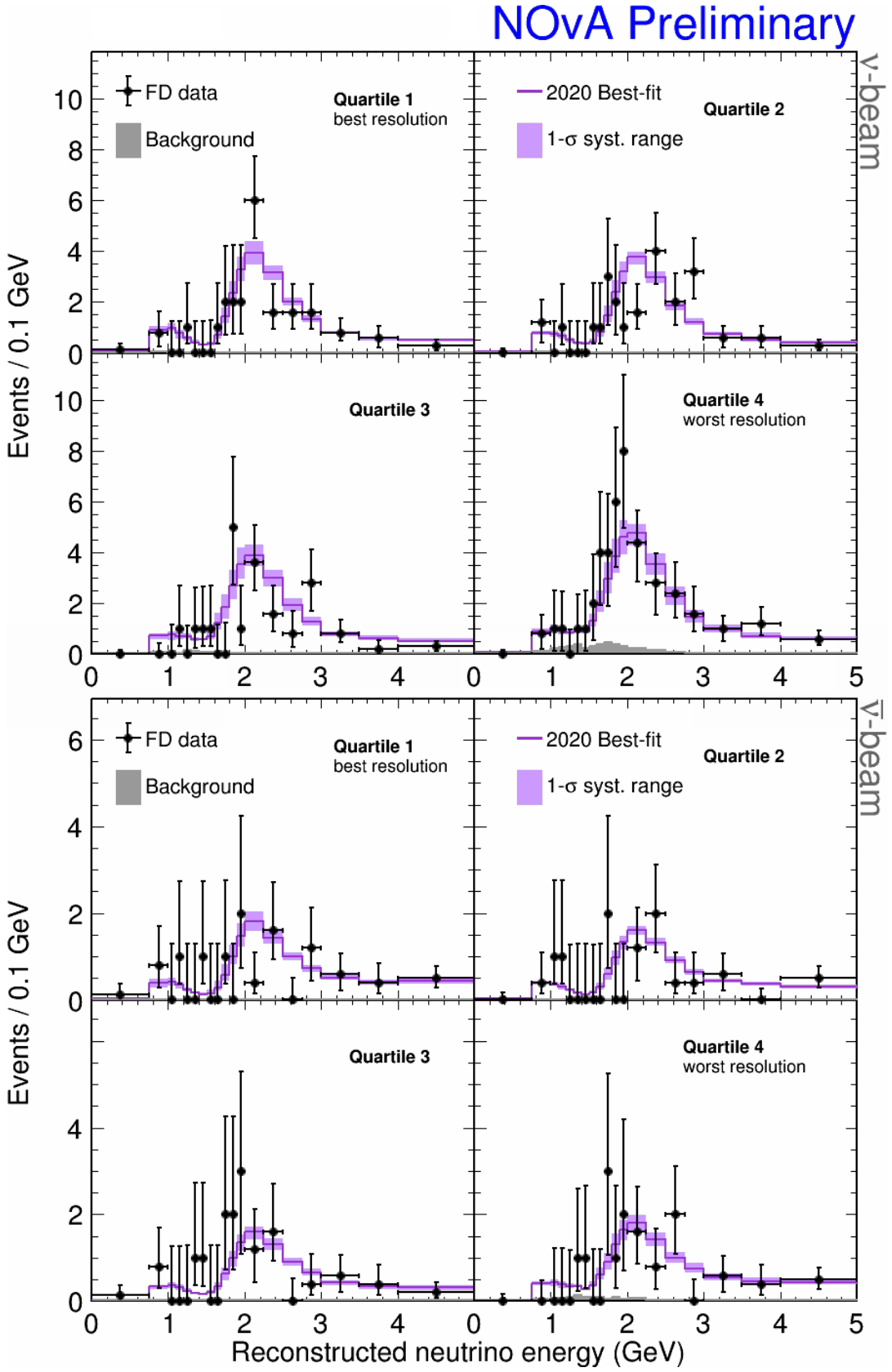

Figure 5.4: Reconstructed energy spectra of the FD ν_μ disappearance channel data selected candidates (black) in individual analysis samples (E_{had} fraction quartiles) overlayed with the best-fit prediction (magenta). **Top:** ν-beam data, four quartiles. **Bottom:** $\bar{\nu}$-beam data, four quartiles. 1σ systematic bands are constructed from the individual uncertainties 1σ limits around the prediction summed in quadrature. Statistical uncertainties are Poisson and FC corrected for the bins with low statistics. The plots are from Ref. [251].

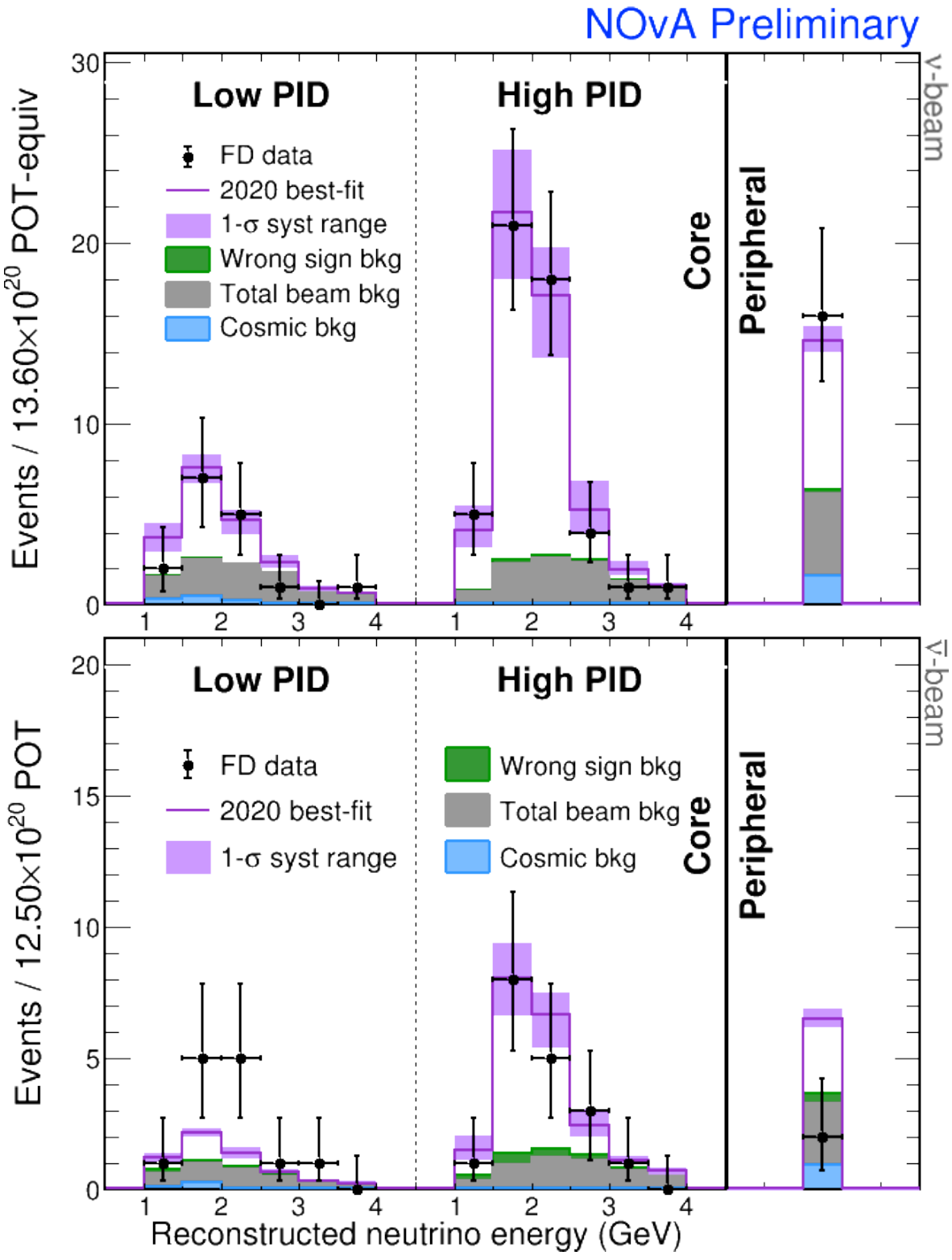

Figure 5.5: Reconstructed energy spectra of the FD ν_e appearance channel data selected candidates (black) overlayed with the best-fit prediction (magenta). The spectra are split into individual low, high ν_e CC PID and peripheral analysis samples. **Top:** ν-beam data. **Bottom:** $\bar{\nu}$-beam data. 1σ systematic bands are constructed from the individual uncertainties 1σ limits around the prediction summed in quadrature. Statistical uncertainties are Poisson and FC corrected for the bins with low statistics. The plots are from [252]

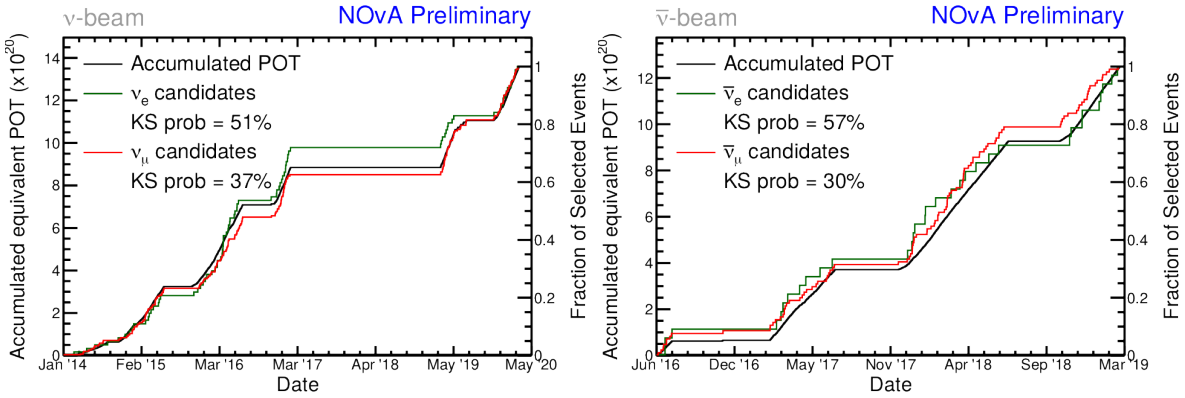

Figure 5.6: Accumulated POT exposure (black) in ν-beam (left) and $\bar{\nu}$-beam (right) modes and the fractions of the ν_μ CC (red) and ν_e CC (green) selected candidates over the time of NOvA's operation. The quoted KS probabilities are Kolmogorov-Smirnov test scores to the generating POT cumulative distributions. The plots are from Ref. [253].

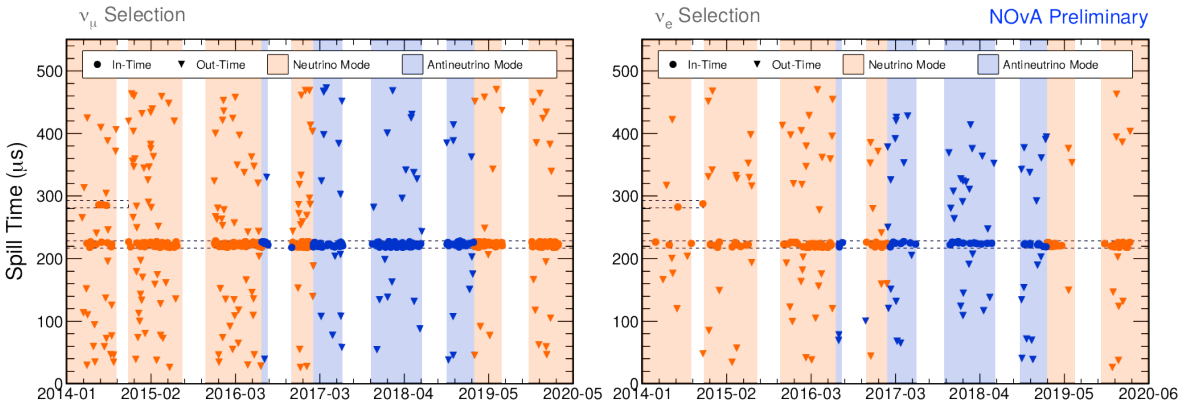

Figure 5.7: The beam spill time distributions of the selected neutrino candidates (dots within dashed lines of the NuMI timing window) and the out-of-time selected cosmic events (triangles in the NuMI timing sidebands) used to estimate the cosmic background over the time of NOvA's operation. The background colors indicate the NuMI ν-beam mode (orange), $\bar{\nu}$-beam mode (blue), and shutdown (white). The early additional beam window is included due to a bug in the timing system (Subsection 3.9.1). **Left:** In the ν_μ disappearance channel (ν_μ CC selection). **Right:** In the ν_e appearance channel (ν_e CC selection). The plots are from Ref. [253].

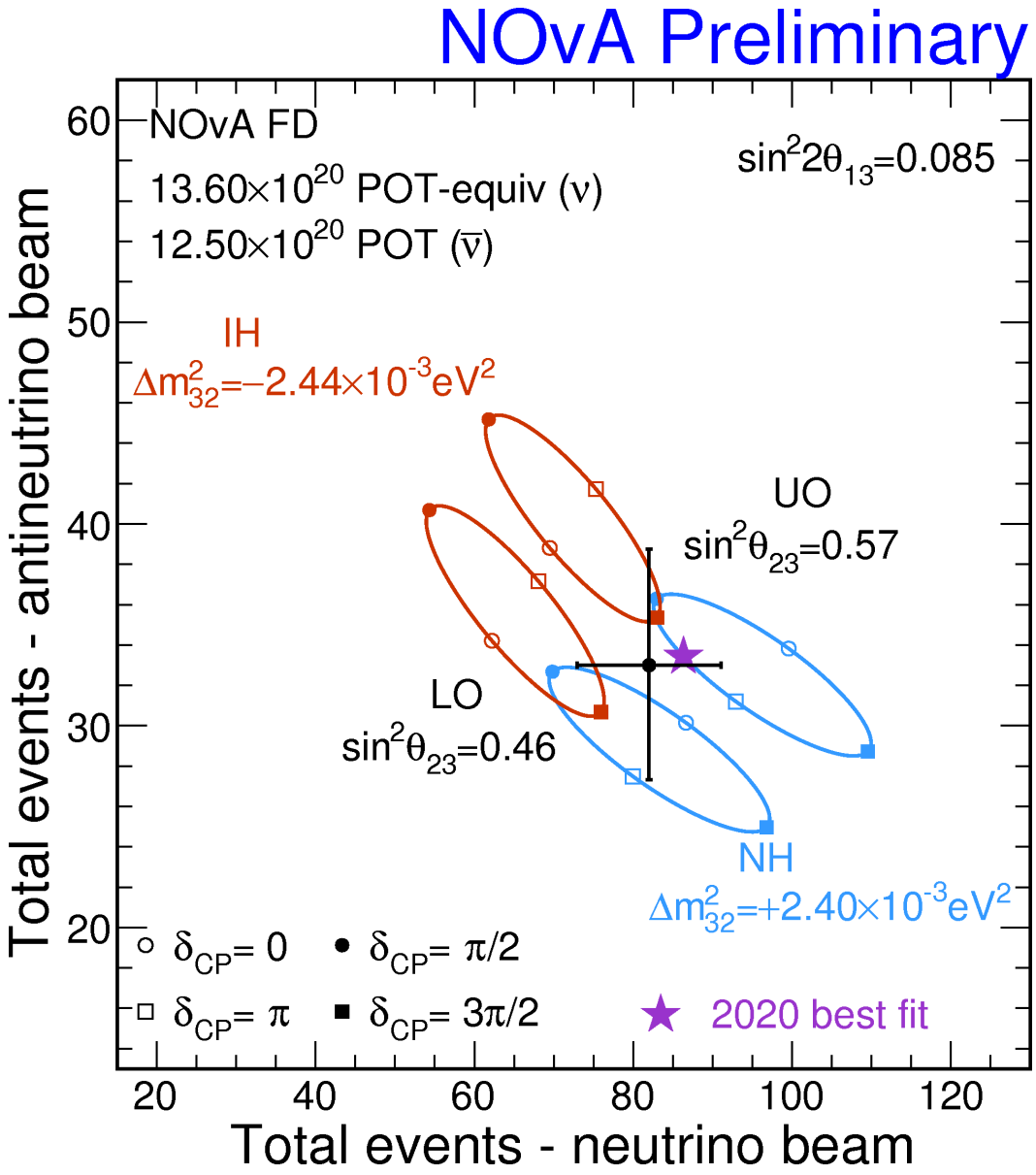

Figure 5.8: Far detector ν_e appearance channel predicted number of selected events in ν-beam (horizontal axis) *vs.* $\bar{\nu}$-beam (vertical axis) evaluated at different neutrino oscillation parameters corresponding to normal (NH, blue) and inverted (IH, red) neutrino mass ordering (hierarchy), lower (LO, $\sin^2\theta_{23} < 0.5$) or upper (UO, $\sin^2\theta_{23} > 0.5$) θ_{23} octant and all possible values of $\delta_{\rm CP}$. The predictions are overlayed with the observed data point (black dot) and the NOvA 2020 best-fit prediction (star). The figure is from Ref. [211].

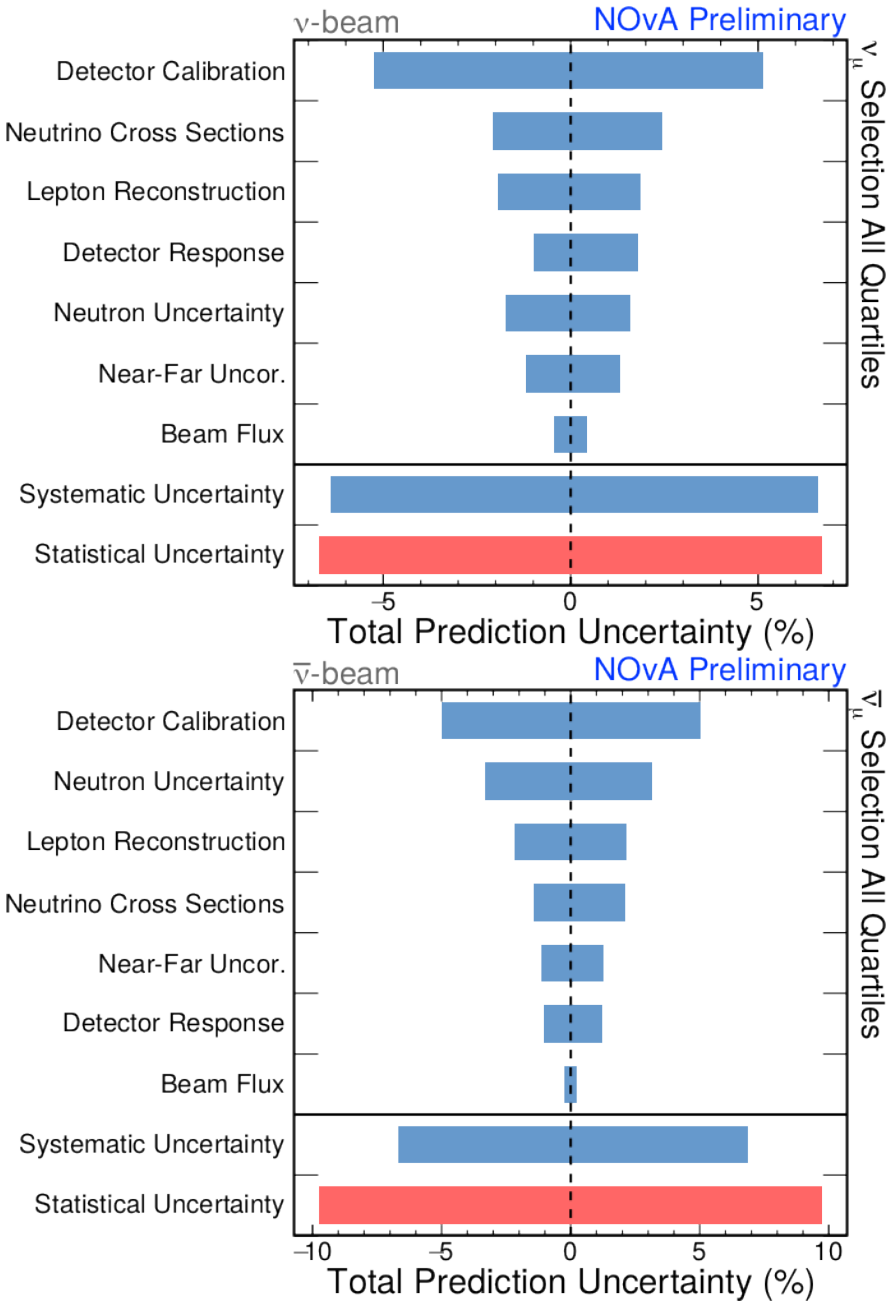

Figure 5.9: Comparisons of the relative systematic (blue) and statistical (red) uncertainties on the total number of predicted events in the ν_μ disappearance channel for ν-beam (top) and $\bar{\nu}$-beam (bottom) evaluated in the NOvA 2020 best-fit point and summed over E_{had} fraction quartiles (note the differences in axes' ranges). The uncertainties are summed in quadrature within the categories and for the total.

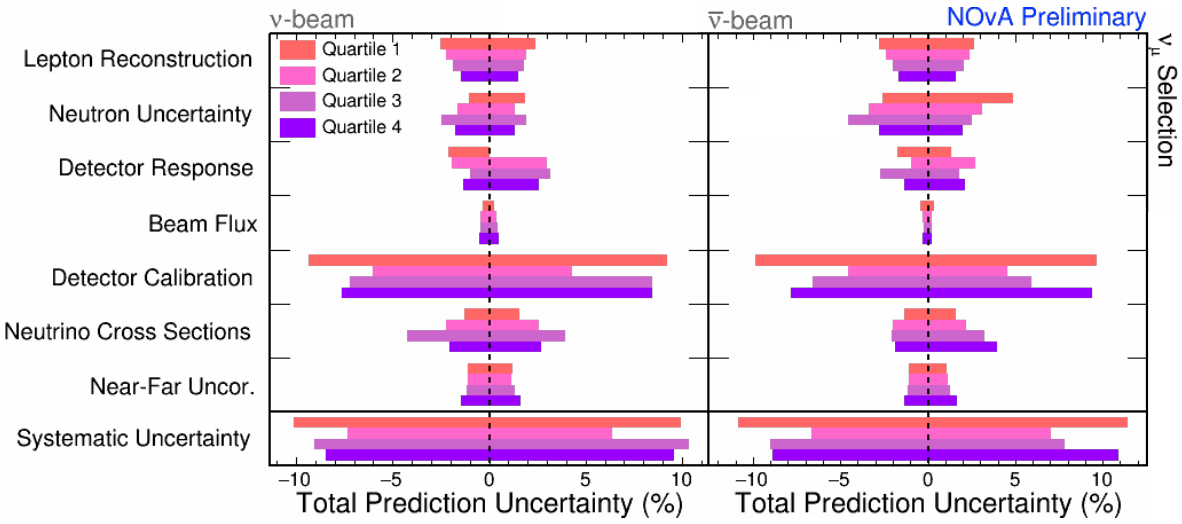

Figure 5.10: Comparisons of the relative systematic uncertainties on the total number of predicted events in the individual ν_μ disappearance channel E_{had} fraction quartiles for ν-beam (left) and $\bar{\nu}$-beam (right) evaluated in the NOvA 2020 best-fit point. The uncertainties are summed in quadrature within the categories and for the total.

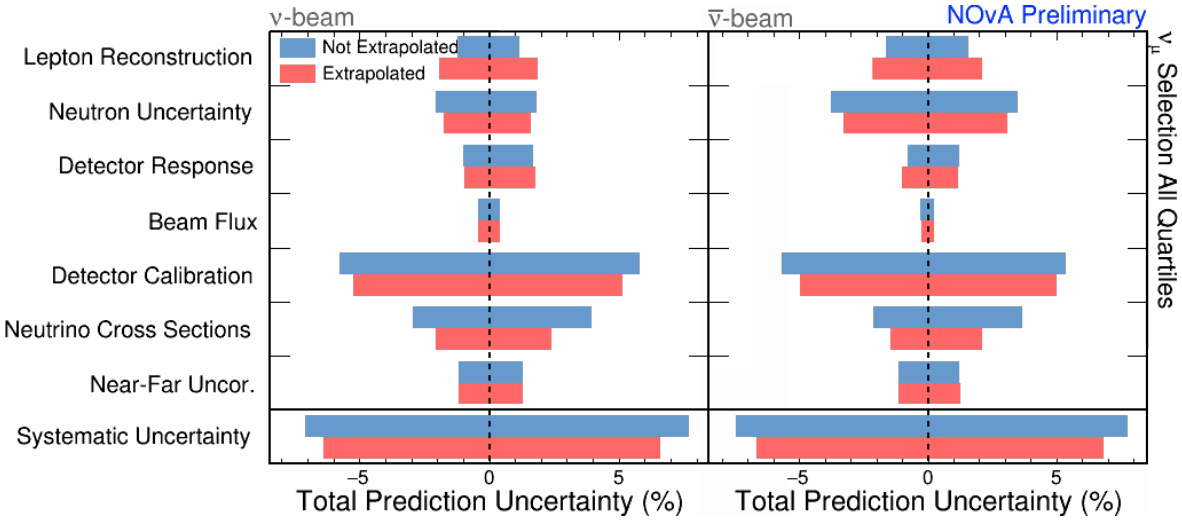

Figure 5.11: Comparisons of the relative systematic uncertainties on the total number of predicted events in the ν_μ disappearance channel for ν-beam (top) and $\bar{\nu}$-beam (bottom) evaluated in the NOvA 2020 best-fit point and summed over E_{had} fraction quartiles (note the differences in axes' ranges) with (red) and w/o (blue) the use of the F/N extrapolation technique and ND data constraints. The uncertainties are summed in quadrature within the categories and for the total.

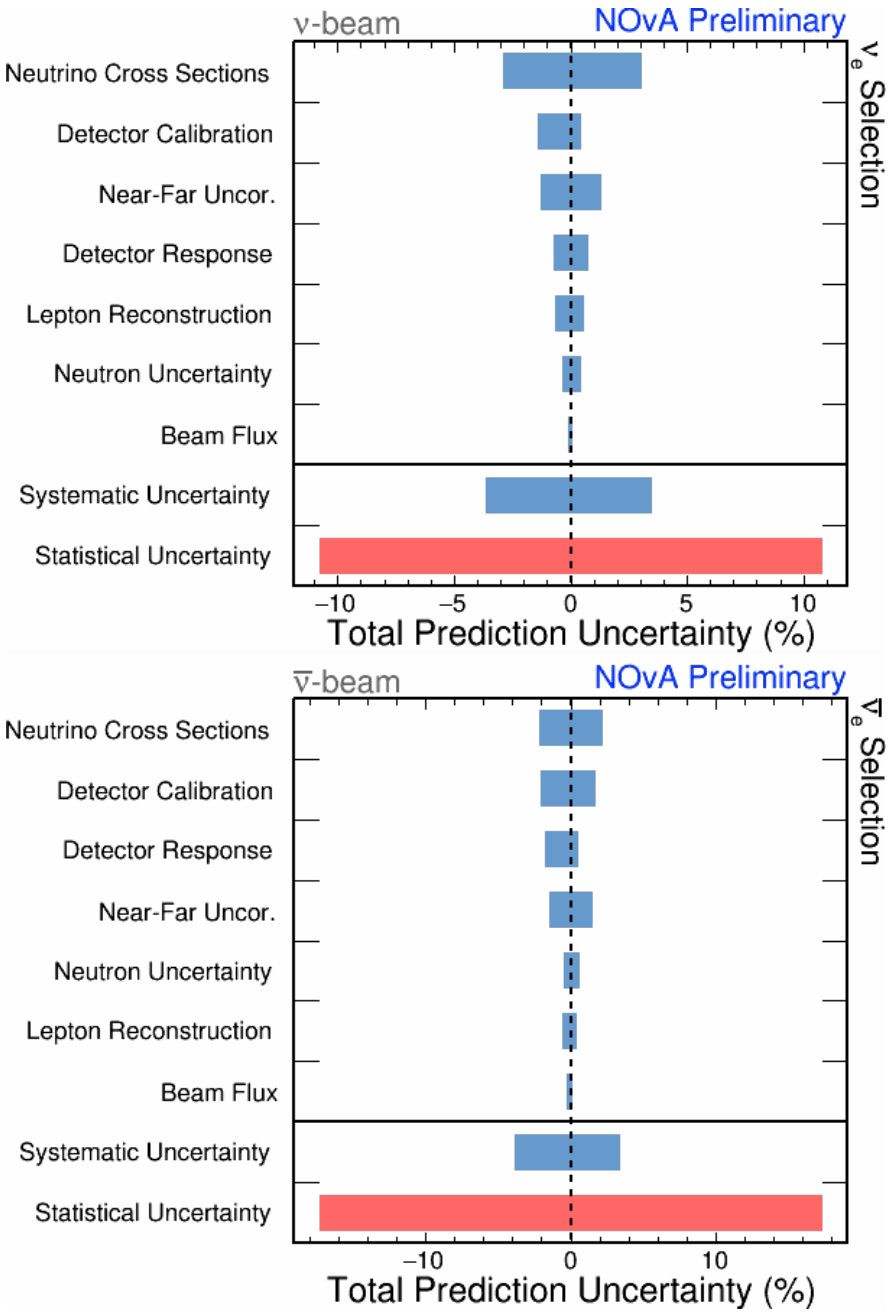

Figure 5.12: Comparisons of the relative systematic (blue) and statistical (red) uncertainties on the total number of predicted events in the ν_e appearance channel for ν-beam (top) and $\bar{\nu}$-beam (bottom) evaluated in the NOvA 2020 best-fit point and summed over PID and peripheral samples (note the differences in axes' ranges). The uncertainties are summed in quadrature within the categories and for the total.

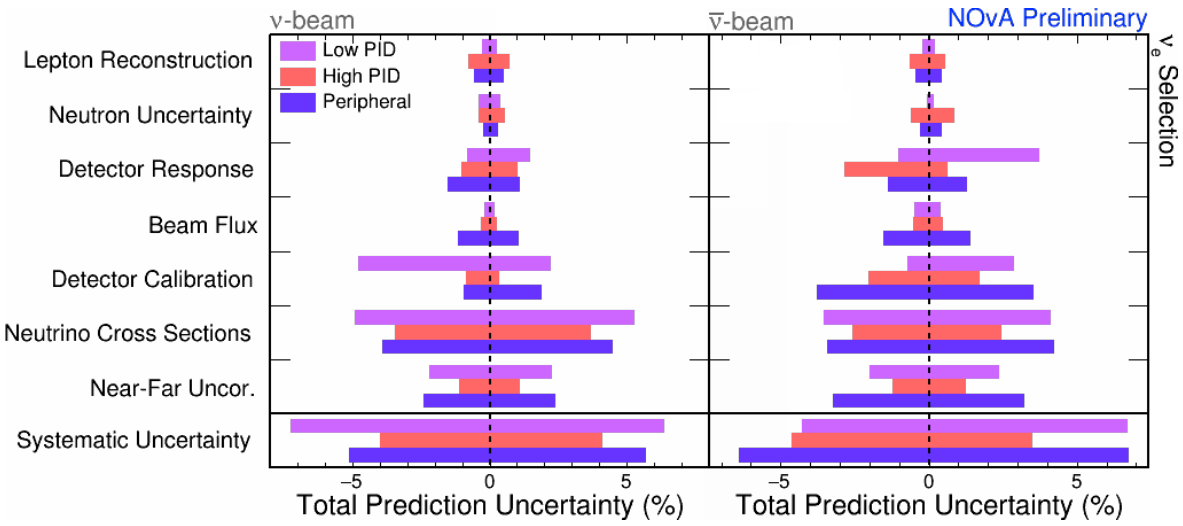

Figure 5.13: Comparisons of the relative systematic uncertainties on the total number of predicted events in the individual ν_e appearance channel samples for ν-beam (left) and $\bar{\nu}$-beam (right) evaluated in the NOvA 2020 best-fit point (note the differences in axes' ranges). The uncertainties are summed in quadrature within the categories and for the total.

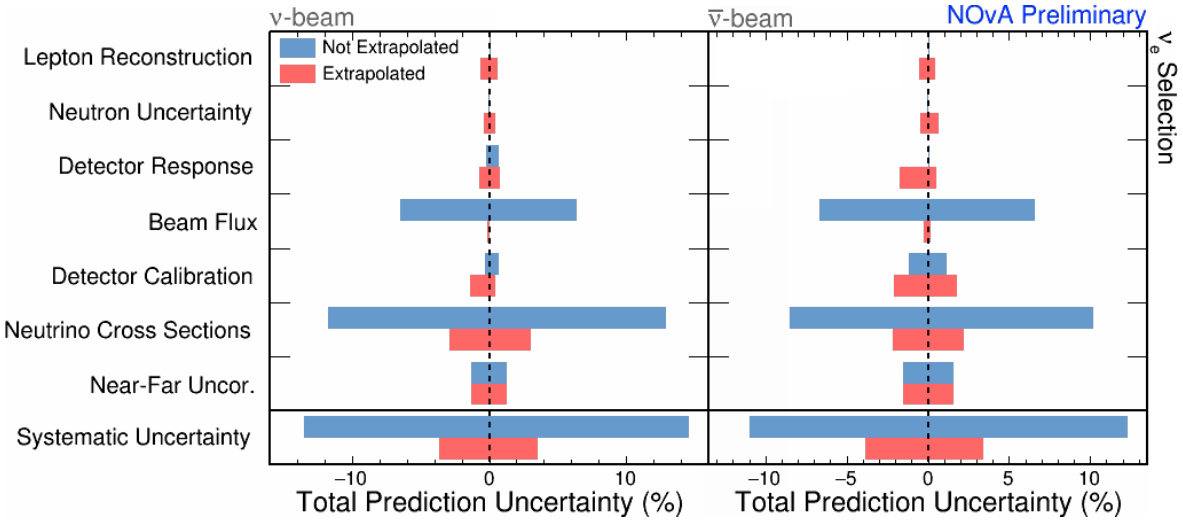

Figure 5.14: Comparisons of the relative systematic uncertainties on the total number of predicted events in the ν_e appearance channel for ν-beam (top) and $\bar{\nu}$-beam (bottom) evaluated in the NOvA 2020 best-fit point (note the differences in axes' ranges) with (red) and w/o (blue) the use of the F/N extrapolation technique and ND data constraints. The uncertainties are summed in quadrature within the categories and for the total.

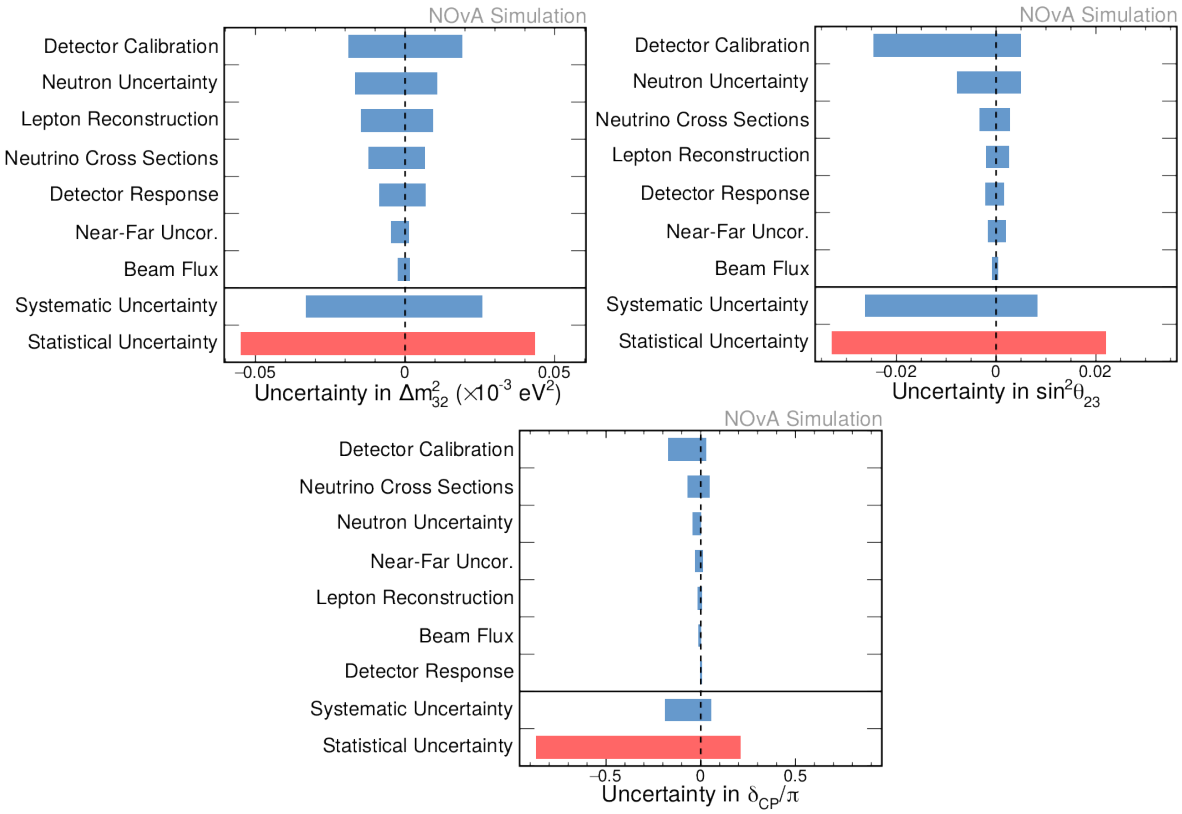

Figure 5.15: Estimated 1σ uncertainties on the neutrino oscillation parameters simulated around the NOvA 2020 best-fit point and their expected impact w.r.t. to the particular sources. **Clockwise from top left:** uncertainty on Δm^2_{32}, $\sin^2\theta_{23}$ and δ_{CP}.

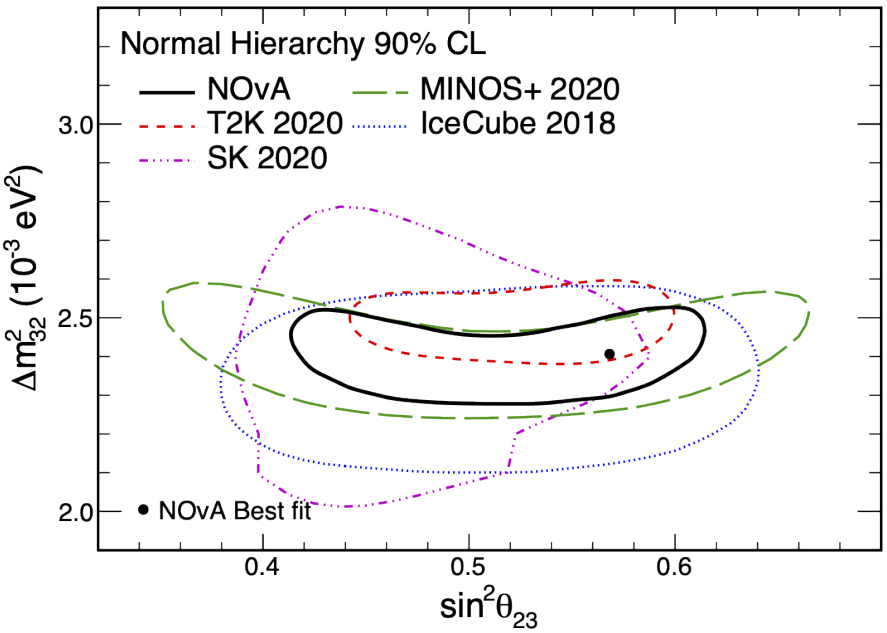

Figure 5.16: NOvA 2020 90% CL contour for Δm^2_{32} *vs.* $\sin^2\theta_{23}$ in the $\Delta m^2_{32} > 0$ hyperplane (black, full) and the best-fit point of $\Delta m^2_{32} = 2.41 \times 10^{-3}$ eV^2, $\sin^2\theta_{23} = 0.57$ (black dot), compared to the latest results from T2K (red, short-dashed), MINOS+ (green, long-dashed), IceCube (blue, dotted), and Super-Kamiokande (magenta, dash-dotted, SK), references in the text. The plot is from Ref. [256].

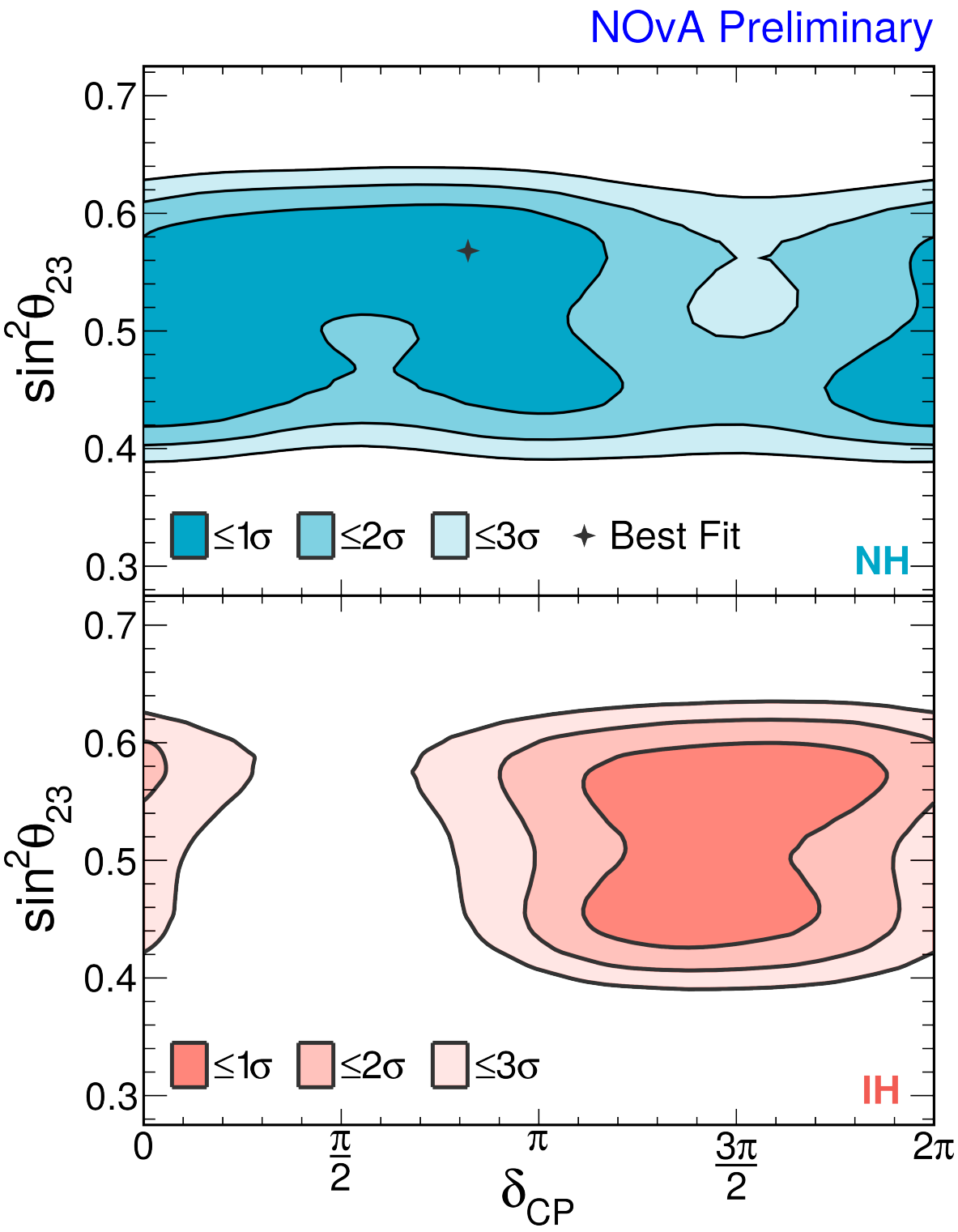

Figure 5.17: NOvA 2020 1σ, 2σ, and 3σ (68.27%, 95.45%, 99.73%) CL contours for $\sin^2\theta_{23}$ *vs.* $\delta_{\rm CP}$ for the normal (NH, blue, top) and inverted (IH, red, bottom) hierarchy (ordering) of the neutrino masses (Δm^2_{32} >0 and <0 hyperplanes). They are profiled over $|\Delta m^2_{32}|$ and the external reactor neutrino oscillation constraint $\sin^2 2\theta_{13} = 0.085\pm0.003$ [248] (with a Gaussian penalty) and systematics. The best fit corresponds to $\sin^2\theta_{23} = 0.57$ and $\delta_{\rm CP} = 0.82\pi$. A large portion of the parametric space around $\delta_{\rm CP} \sim \pi/2$ for IH is rejected at $>3\sigma$. The plots are from Ref. [257].

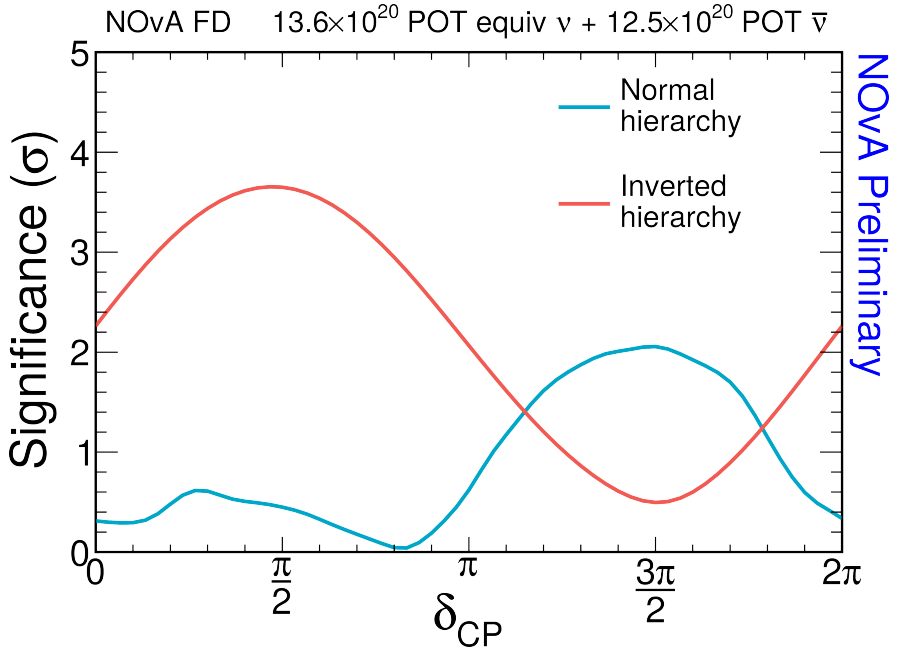

Figure 5.18: NOvA 2020 δ_{CP} significance for the normal (blue) and inverted (red) hierarchy (ordering) of the neutrino masses. It is profiled over $\sin^2\theta_{23}$, the reactor constraint $\sin^2 2\theta_{13} = 0.0085 \pm 0.003$, systematics and the corresponding Δm^2_{32} hyperplane. Best fit: $\delta_{\text{CP}} = 0.82\pi$, and any value $\delta_{\text{CP}} \in [0, 2\pi]$ is allowed within 2σ. The plot is from Ref. [257].

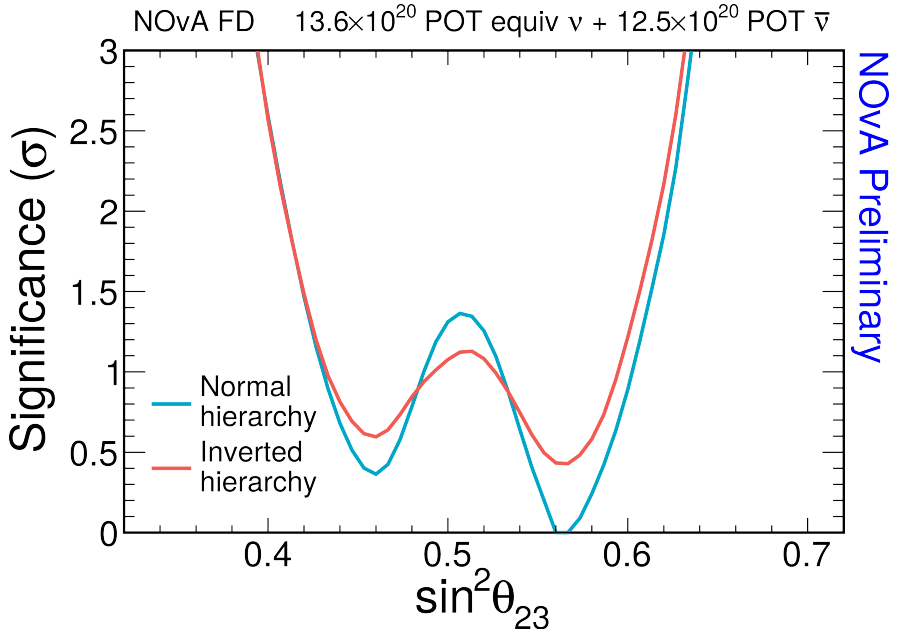

Figure 5.19: NOvA 2020 $\sin^2\theta_{23}$ significance for the normal (blue) and inverted (red) hierarchy (ordering) of the neutrino masses. It is profiled over δ_{CP}, the reactor constraint $\sin^2 2\theta_{13} = 0.0085 \pm 0.003$, systematics and the corresponding Δm^2_{32} hyperplane. Best fit: $\sin^2\theta_{23} = 0.57$, and $\sin^2\theta_{23} < 0.5$ is disfavored at about 1σ. The plot is from Ref. [257].

Conclusion

The NOvA experiment presented new results of the neutrino oscillation analysis within the model of three active neutrinos in 2020. This update used new data with about 50% more ν-beam mode of NuMI POT (protons-on-target) and its high-intensity upgrade to 700 kW power. In total, the data represents 13.60 $\times 10^{20}$ POT of ν-beam and 12.50 $\times 10^{20}$ POT of $\bar{\nu}$-beam accounting for about 41% of the total exposure expected until 2025. The text overviewed the important analysis novelties and the work done for estimating and validating the systematic uncertainties. Although statistical uncertainties currently dominate, understanding the major sources of systematic uncertainties, their correlations, and proper evaluation are vital for both the interpretation and precision of the results and also for further improvements of the analysis.

There were 211 candidate events observed in the ν-beam ν_μ disappearance, 105 in the $\bar{\nu}$-beam $\bar{\nu}_\mu$, 82 in the ν-beam ν_e appearance, and 33 in the $\bar{\nu}$-beam $\bar{\nu}_e$ appearance channel. Exploiting the NOvA two detector design with the Near to Far Detector extrapolation technique (F/N technique) to generate the analysis predictions, three neutrino oscillation parameters were estimated and constrained. With external inputs on the neutrino squared mass-splitting Δm^2_{21} and mixing angle θ_{12} from the solar experiments, and on the mixing angle θ_{13} from the reactor experiments, the best fit corresponds to

$$\begin{aligned} \sin^2\theta_{23} &= 0.57^{+0.05}_{-0.07}, \\ \Delta m^2_{32} &= (2.41 \pm 0.07) \times 10^{-3}\ \text{eV}^2, \\ \delta_{\text{CP}} &= 0.82\pi, \end{aligned} \tag{5.8}$$

and the normal ordering of the neutrino masses. The parameter δ_{CP} is only poorly constrained with all possible values $[0, 2\pi]$ allowed within 2σ CL. The rest are in good agreement with other neutrino oscillation measurements. The results reject the hypothesis of the inverted mass ordering of the neutrino masses and δ_{CP} around $\pi/2$ at $>3\sigma$ CL. Overall, both lower octant of $\theta_{23} < 45^\circ$ and inverted ordering are disfavored at about 1σ CL. The significances and constraints in the neutrino oscillation parametric space of $\sin^2\theta_{23}$ *vs.* Δm^2_{32}, $\sin^2\theta_{23}$ *vs.* δ_{CP}, δ_{CP}, and $\sin^2\theta_{23}$ alone were detailed in Figs. 5.16, 5.17, 5.18, and 5.19, respectively.

Appendices

A. Event selection details

This appendix archives all the selection criteria employed in the analysis. They are grouped in tables by their category and eventually by the analysis channel. Where appropriate, they are also divided into columns for the Near Detector (ND), Far Detector (FD), or beam modes ($\nu/\bar{\nu}$-mode), or their applicability is quoted in the table's header. Every line in the tables corresponds to a cut to be met by the stated reconstructed variable. The notation is as follows: || is a logical OR, & a logical AND w.r.t. the preceding line(s), # is the cardinality of the set (*e.g.*, "# hits" is the total number of hits in the event), X means the cut is not applied. Abbreviations and acronyms as in Chapter 3: cosmic rejection BDT score (CosRej BDT), Reconstructed Muon Identification score (ReMId), event or prong convolutional visual network score (CVN or pCVN), *etc.*

Beam and detector quality cuts

Table A.1: Basic quality cuts. The special DCM (Data Concentrator Module) metrics ensure their proper time synchronization by the matching hits on the edges, and they filter possible remnants in the cases of failure.

Beam quality cuts ($\nu + \bar{\nu}$-beam)		**Detector quality cuts** ($\nu + \bar{\nu}$-beam)	ND	FD
Δt of spill	< 0.5 s			
Spill intensity	$> 2 \times 10^{12}$ POT	missing DCM	X	False
|Horn current|	$\in (198, 202)$ A	DCM edge match	X	> 0.2
Beam vs. target	$x, y \in (-2, 2)$ mm	3hits || missing DCM	False	X
Beam width	$x, y \in (0.57, 1.58)$ mm			

Timing cuts

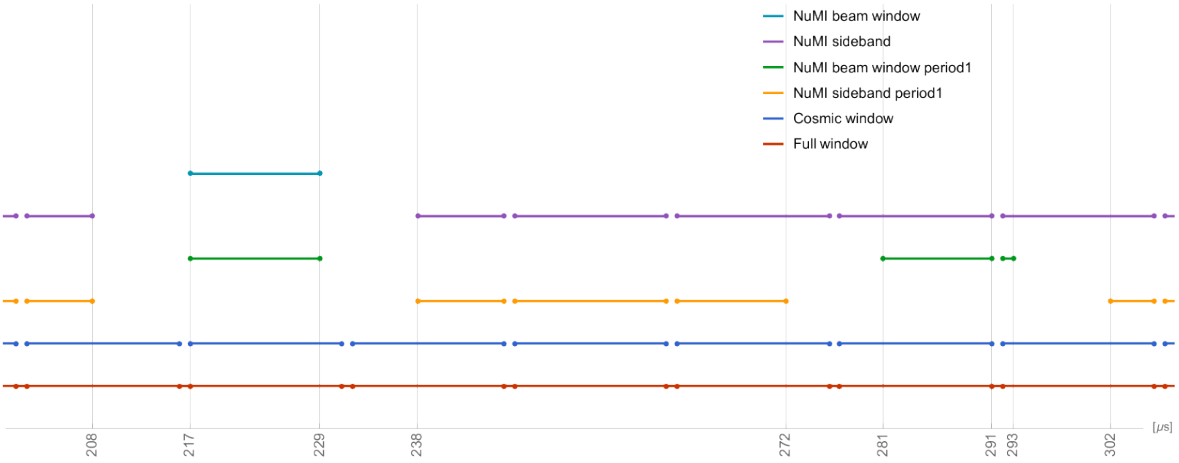

Figure A.1: Different timing cuts in the NuMI triggered time interval 0–550 μs (horizontal axis). The NuMI beam window cut (light blue) of 12 μs is centered around 223 μs in the NuMI trigger data (full window, red), and it is isolated from the NuMI cosmic sidebands (purple). The additional 16 μs time sampling (dots and spaces) is from the new cosmic veto (Subsection 3.7.1). The special windows for period 1 of the data taking (green and yellow) are due to an error in the timing system (Subsection 3.9.1). Taken from Ref. [197].

Event quality cuts

Table A.2: Event quality and veto cuts for the ν_μ disappearance (left) and ν_e appearance (right) channel.

ν_μ event quality cuts (All ND, FD, $\nu + \bar{\nu}$-beam)	
# hits	> 20
# consecutive planes	> 4
# tracks	> 0
ReMID	> 0
E_{cal} in μ-catcher	< 0.03 GeV
E_{ν_μ}	$\in (0, 5)$ GeV

ν_e event quality cuts		
($\nu + \bar{\nu}$-beam)	ND	FD
Vertex	True	
# hits	$\in (20, 200)$	$\in (30, 150)$
# prongs	> 0	
Longest prong	$\in (100, 500)$ cm	
E_{ν_e}	$\in [0, 4.5)$ GeV	$\in (1, 4)$ GeV

Event containment

Table A.3: Event containment cuts for the ν_μ disappearance channel in ND (left) and FD (right). Prongs x, y, z are the positions of any hit in the prong. Prongs dist. (distance) is the distance of any hit from the detector's edge in any prong. Proj.fw.(bw.) is the projected number of cells from the track end (start) to the detector's edge.

ν_μ ND containment cuts ($\nu + \bar{\nu}$-beam)		
	Coord.	$\in$ [cm]
Prongs	x	$(-180, 180)$
	y	$(-180, 180)$
	z	(40,1525)
First plane num.		> 1
Last plane num.		< 212
# μ-catcher tracks		$= 1$
Track proj.fw. cells		> 5
Track proj.bw. cells		> 10
Track z start		< 1100 cm
&		
Track z stop		< 1275 cm
$\|\|$ y at boundary		< 55 cm

ν_μ FD containment cuts ($\nu + \bar{\nu}$-beam)		
	Edge	Distance [cm]
Prongs dist.	Top	> 60
	Bottom	> 12
	East	> 16
	West	> 12
	Front	> 18
	Back	> 18
Track proj.fw. cells		> 6
Track proj.bw. cells		> 6
CosTrack proj.fw. cells		> 0
CosTrack proj.bw. cells		> 7
# planes to front		> 2
# planes to back		> 3

Table A.4: Event containment cuts for the ν_e disappearance channel in the ND (left) and FD (right). Prongs x, y, z are the positions of any hit in the prong. Prongs dist. (distance) is the distance of any hit from the detector's edge in any prong.

ν_e ND containment cuts ($\nu + \bar{\nu}$-beam)		
	Coord.	$\in$ [cm]
Vertex	x	$(-100, 160)$
	y	$(-160, 100)$
	z	(150,900)
Prongs	x	$(-150, 170)$
	y	$(-170, 150)$
	z	(100,1225)
# empty front planes		> 10

ν_e FD containment cuts ($\nu + \bar{\nu}$-beam)		
	Edge	Distance [cm]
Prongs dist.	Top	> 63
	Bottom	> 12
	East	> 12
	West	> 12
	Front	> 18
	Back	> 18

Event PID cuts

Table A.5: Event PID cuts for the ν_μ disappearance (top) and the ν_e appearance channel (bottom). The vetoes on the "nearest candidate" or "distance to top" to filter cosmic events are applied together with the ν_e CC PID selection.

ν_μ PID cuts ($\nu + \bar{\nu}$-beam)	
ν_μ CosRej BDT	> 0.45
ReMID	> 0.30
CVN ν_μ	> 0.80

ν_e core PID cuts	ν-beam	$\bar{\nu}$-beam
ν_e Core CosRej BDT	> 0.45	> 0.47
CVN ν_e		
Low PID	> 0.84	> 0.85
High PID	> 0.97	
	&	
Nearest candidate	dist. > 500 cm $\|\|$ $\Delta t > 100$ ns	
$\|\|$ dist. to top	$> 400/50$ cm for Low/High PID	

ν_e peripheral sample cuts

Table A.6: Preselection (top) and PID (bottom) cuts of the ν_e appearance peripheral sample. The vetoes on the "nearest candidate" or "distance to top" to filter cosmic events are applied together with the PID selection.

ν_e peripheral preselection cuts (peripheral event quality, $\nu + \bar{\nu}$-beam)	
E_{ν_e}	$\in [0, 4.5)$ GeV

ν_e peripheral PID cuts		
	ν-beam	$\bar{\nu}$-beam
CVN ν_e	> 0.97	
ν_e Peri CosRej BDT	> 0.61	> 0.60
	||	
CVN ν_e	> 0.995	
ν_e Peri CosRej BDT	> 0.57	> 0.56
	&	
Nearest candidate	dist. > 500 cm || $\Delta t > 100$ ns	
|| dist. to top	$> 400/50$ cm for Low/High PID	

B. Principal component analysis

This appendix explains the principal component analysis (PCA) concept and main ideas and how it is employed when evaluating some systematic uncertainties of the NOvA neutrino oscillation analysis. For more rigorous details, consult Ref. [229], for a short PCA manual, see Ref. [230].

B.1 Overview

Classic PCA is a heuristic tool to reduce the dimensionality of multivariate data while keeping as much as possible of the variation present in it. That is realized by a **linear** transformation to a new set of variables, the principal components (PCs), representing the data underlying structures and intrinsic properties (or "eigenproperties"). PCs are **uncorrelated** and ordered by the amount of the variation in data they retain. As a consequence, it is often possible to neglect the unimportant ones and, to some accuracy, simplify or "minimize the redundancy" and decorrelate the representation of the initial information, see illustrative Fig. B.1.

Provided several assumptions are valid [230]:

- linearity, *i.e.*, PCs are linear combinations of the original variables (basis),
- large variances have important structures in the data, and
- PCs are orthogonal,

PCs can be derived with a straightforward eigenvector decomposition of the data covariance matrix. Let $\mathbf{X} \equiv (X_1, X_2, \ldots, X_n)^\top$ be a vector of n random variables X (bins), each with finite variance and expected value, then

$$C = \mathrm{cov}(\mathbf{X}, \mathbf{X}) = \mathrm{E}(\mathbf{X}\mathbf{X}^\top) - \mathrm{E}(\mathbf{X})\mathrm{E}(\mathbf{X})^\top \tag{B.1}$$

is the covariance matrix, where $\mathrm{E}(\cdot)$ denotes the expected value operator, $\mathrm{cov}(\cdot)$ the "covariance" operator.

Covariance matrix C, by construction, is a real symmetric matrix, *i.e.*, its eigenvalues are real. Its eigenvectors form an orthonormal basis, and the matrix can be diagonalized by an orthonormal transformation. That can be characterized by an orthonormal matrix $V = (\mathbf{v}_1\ \mathbf{v}_2 \ldots \mathbf{v}_n)$ with $\mathbf{v}_i$ being the eigenvectors of C. Hence, $VV^\top = V^\top V = \mathbb{1}$, which implies $V^\top = V^{-1}$. Then, $C = V\Lambda V^\top$, where $\Lambda = \mathrm{diag}(\lambda_1, \lambda_2, \ldots)$ with λ_i the eigenvalues of C, see [230].

B.2 Application in the NOvA analysis

The NOvA neutrino oscillation analysis utilizes PCA when estimating systematic uncertainties that are expected to be intrinsically related. PCA is performed on a simulated ensemble of many pseudorandomly generated, normally distributed systematic shifts of the nominal prediction in the chosen basis (see below). The largest identified PCs are to replace the original systematics when properly translated to the neutrino reconstructed energy basis used in the analysis. There are two essential motivations.

1. Reducing the number of systematic nuisance parameters in the analysis fitting procedure speed up its convergence.
2. PCs are, unlike the original systematic uncertainties, uncorrelated and thus do not overestimate the actual uncertainty.

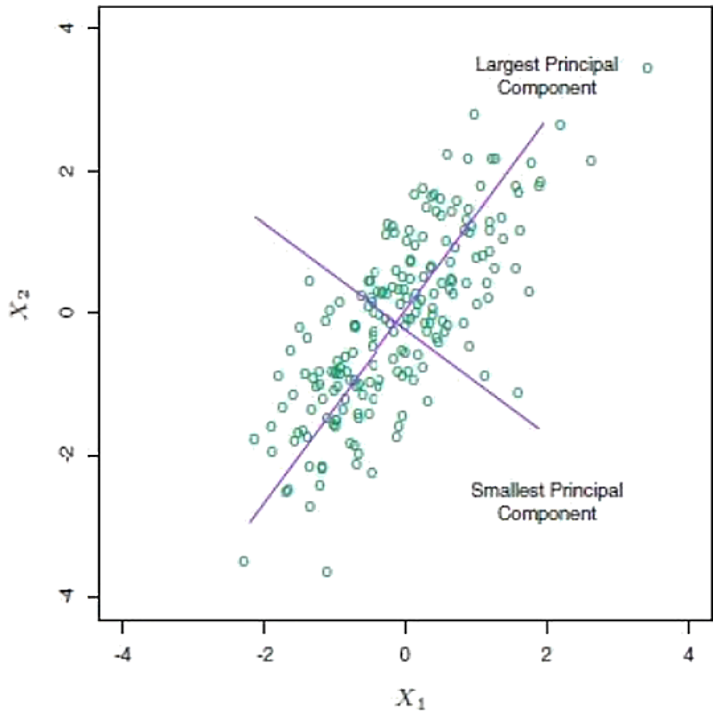

Figure B.1: Example of PCA on a data ensemble of two random variables X_1, X_2. There are two orthogonal PCs (principal components, blue) that can be ordered by the amount of variance they retain (their "length") as indicated. The plot is from https://docs.tibco.com/pub/sfire-dsc/6.5.0/doc/html/TIB_sfire-dsc_user-guide/ (as of Mar 2020).

B.2.1 General approach and building the covariance matrix

The NOvA PCA adopts the covariance matrix eigenvector decomposition method. The investigated ensembles are populated by systematic "universes", where a single universe is created by setting each of the included systematic parameters in units of standard deviation σ to a random number from a normal distribution $\mathcal{N}(0,1)$. Let $\mathbf{N}_i$ be a vector of simulated event rates in the chosen basis (*e.g.* neutrino energy) of the i-th systematic universe, and $\mathbf{N}_0$ is the nominal prediction (central value). The covariance matrix is constructed as

$$C = \frac{1}{k-1} \sum_{i=1}^{k} \left(\mathbf{N}_i - \mathbf{N}_0\right) \left(\mathbf{N}_i - \mathbf{N}_0\right)^\top , \tag{B.2}$$

where k is the number of universes $\mathcal{O}(1000)$ in the ensemble, and C is defined relative to the central value (instead of mean) to lower bias from asymmetrical uncertainties.

For $\mathbf{\Delta} \equiv \mathbf{N}_{\text{data}} - \mathbf{N}_{\text{MC}}$, where $\mathbf{N}_{\text{data}}$ is a vector of observed data rates, and $\mathbf{N}_{\text{MC}}$ is a vector of predicted rates, the systematic "pulls" to the likelihood function are of the form

$$\chi^2 = \mathbf{\Delta}^\top C^{-1} \mathbf{\Delta}. \tag{B.3}$$

With the knowledge of the preceding section ($C = V \Lambda V^\top, V^\top = V^{-1}, \Lambda = \text{diag}(\lambda_1, \ldots)$), this is written as

$$\chi^2 = \left(V^{-1}\mathbf{\Delta}\right)^\top \Lambda^{-1} \left(V^{-1}\mathbf{\Delta}\right), \tag{B.4}$$

and χ^2 equals 1, if $\mathbf{\Delta} = \sqrt{\lambda_j}\mathbf{v}_j$ for any $\lambda_j, \mathbf{v}_j$ eigenvalues and eigenvectors of C, respectively, since $\mathbf{v}_i^\top \mathbf{v}_j = \delta_{ij}$. *Ergo*, the behavior of C is fully preserved, and the corresponding independent pulls are uncorrelated.

B.2.2 Cross section uncertainties

As described in Subsection 4.5.2, inferior cross section (interaction) systematic uncertainties are substituted with PCs. The basis of the PCA consists of 28 samples, each with 20 0.25 GeV bins of neutrino energy (0-5 GeV), *i.e.*, the basis has 560 bins. The first half of the bins captures the Near Detector (ND) analysis selections, and the second half is for the F/N (Far over Near) extrapolation ratio with Far Detector (FD) selections. To further encompass the effect of uncertainties on the relevant interactions, the samples are divided into seven subsamples:

- CCQE ν_μ events,
- CC non-QE ν_μ events,
- ν_μ background NC events,
- CCQE ν_e events,
- CC non-QE ν_e events,
- ν_e background CC ν_μ events,
- ν_e background NC events.

Finally, each of the interaction subsets has its ν-beam and $\bar{\nu}$-beam simulated part.

Figs. B.2, B.3 illustrate the PCA process with the covariance matrix built, its eigenvalues spectrum, and the total explained variance of the ensemble as a function of the number of selected PCs. To reduce the number of PCs needed, they are artificially scaled up by an *ad hoc* factor of 35% to make up for the neglected. The final check compares the expected sensitivities obtained with the original ensemble and a newly created ensemble from PCs – example in Fig. B.4 – for an arbitrarily chosen set of neutrino oscillation parameters, see Fig. B.5.

B.2.3 Flux uncertainties

The PCA of flux uncertainties is very similar, although the chosen basis is different. The included uncertainties list beam focusing and all the hadron production uncertainties of PPFX [232]. There are 16 PCA samples with 40 0.25 GeV bins of neutrino energy (0-10 GeV). Alike, there are ND and F/N, and $\nu/\bar{\nu}$-beam parts. They are divided into subsamples of (anti)neutrino flavors:[1]

- ν_μ events,
- $\bar{\nu}_\mu$ events,
- ν_e events,
- $\bar{\nu}_e$ events.

By the very same arguments (explained variance of the ensemble, comparable sensitivity), the five largest PCs scaled up by 20% were employed in the end [231].

[1] *N.b.*, no (unoscillated) ν_τ are assumed in the beam.

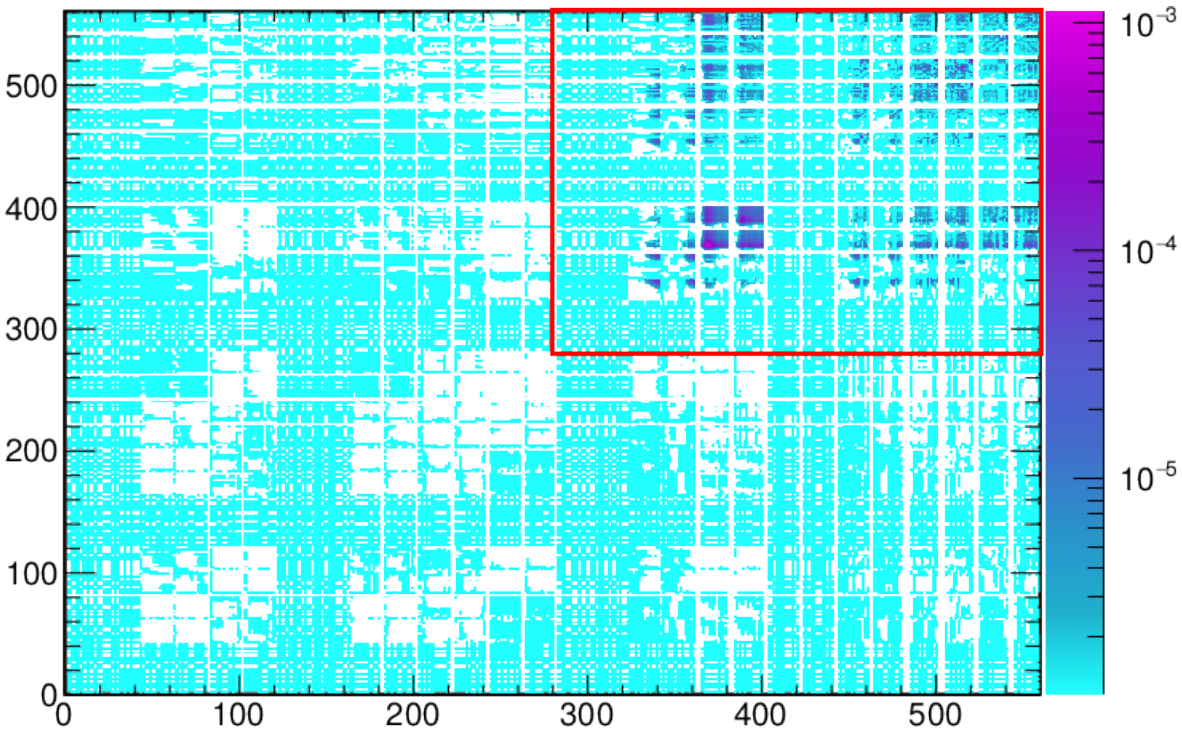

Figure B.2: Bin-bin covariance matrix for inferior cross section uncertainties built from the generated ensemble of randomly shifted universes. The basis of 560 bins is defined as follows: ND sample (bin 1–280), F/N sample (281–560), each sample is divided into seven subsamples of CCQE ν_μ (1–40), CC non-QE ν_μ (41–80), ν_μ bkg. NC (81–120), CCQE ν_e (121–160), CC non-QE ν_e (161–200), ν_e bkg. CC ν_μ (201–240) and ν_e bkg. NC (241–280). Each subsample has its ν-beam (1–20) and $\bar{\nu}$-beam (21–40) part of 20 0.25 GeV bins of neutrino energy 0–5 GeV. The red rectangle shows the F/N segment of the covariance matrix, directly affecting the F/N extrapolation technique.

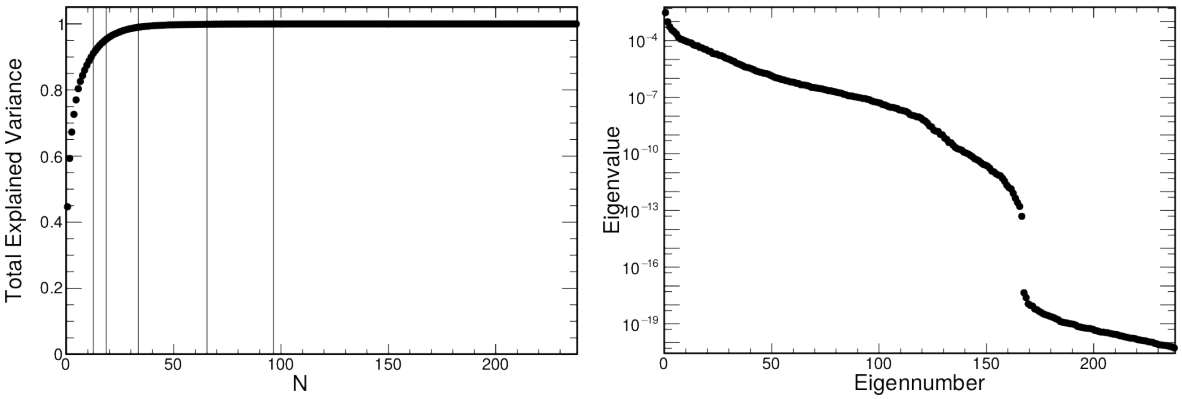

Figure B.3: **Left:** Cumulative total explained variance in the generated ensemble of cross section universes as a function of the number N of the selected PCs when ordered. The vertical lines denote the N needed to reach (from left to right) 90% (12 PCs), 95% (19), 99% (34), 99.9% (66) and 99.99% (97) coverage. **Right:** The first 240 largest eigenvalues of the cross section ensemble covariance matrix. The eigenvalues for PC 167 and up are $<10^{-16}$, and they are considered 0 in the diagonalization.

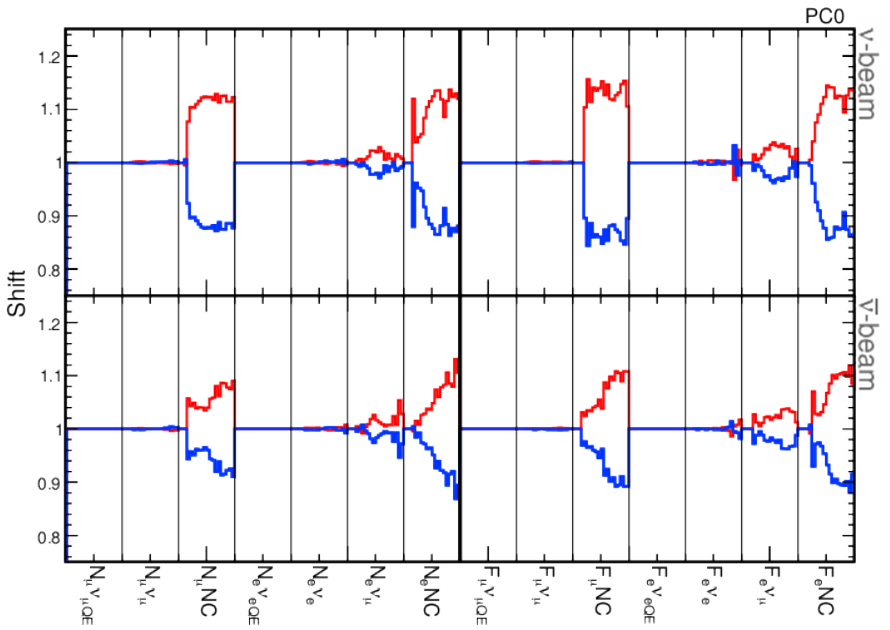

Figure B.4: Largest (the first) PC of the generated cross section uncertainties ensemble when translated to the ND (N, left) and FD (F, right) bases of the selected interaction event types (left to right: CCQE ν_μ, CC non-QE ν_μ, ν_μ bkg. NC, CCQE ν_e, CC non-QE ν_e, ν_e bkg. CC ν_μ, ν_e bkg. NC) for ν-beam (top) and $\bar{\nu}$-beam (bottom). Each sample (column) has 20 0.25 GeV bins of neutrino energy (0–5 GeV). These histograms represent the actual fractional systematic uncertainties ($\pm 1\sigma$ shifts in red/blue) implemented into the analysis and applied as weights to the simulated events.

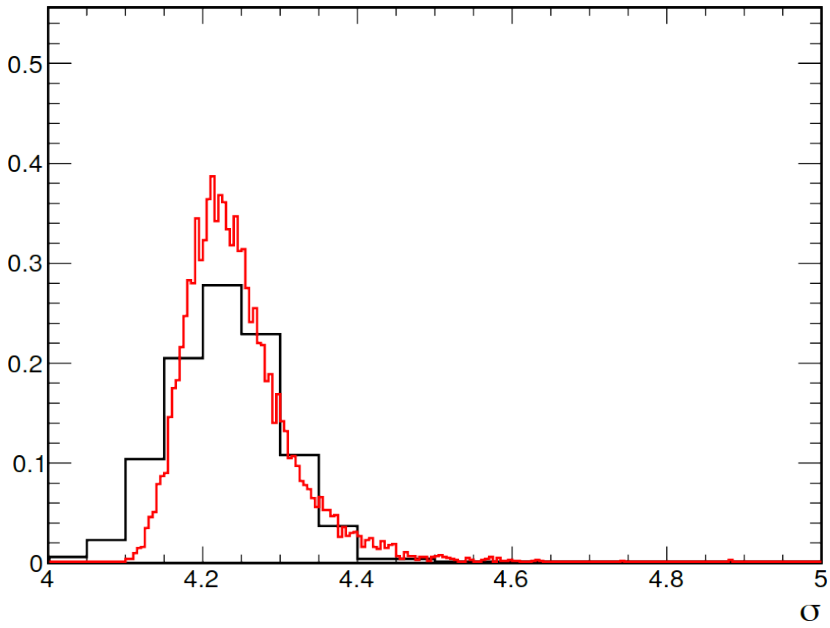

Figure B.5: Example of a sensitivity comparison of 10000 individual systematic universes simulated from 12 PCs with 35% up-scale (red) and the original 1000 cross section uncertainty universes (black). $\sigma = \sqrt{\chi^2}$ of fake data and a hypothesis of $-\Delta m^2_{32}$ as a representative combination for neutrino mass ordering determination. The vertical axis has arbitrary units on the number of the simulated universes with given sensitivity, and the histograms are area normalized.

C. Detailed overview of systematic uncertainties

This appendix examines the considered systematic uncertainties of the analysis as specified in Chapter 4 and shows their effect within the relevant analysis samples. The overview is organized into four parts for two analysis channels in two beam modes: ν_μ disappearance, $\bar{\nu}_\mu$ disappearance, ν_e appearance, $\bar{\nu}_e$ appearance. Each is divided into the relevant analysis samples of four E_{had} fraction quartiles or three PID+peripheral bins and a total prediction sample summed over them. For each sample, there is a table of all considered uncorrelated systematics expressed as fractional $\pm 1\sigma$ uncertainties on the total integral numbers of predicted events relative to the nominal prediction (Tables C.1-C.18), and there are plots of signal, background, and total prediction uncertainty summed over the general systematic categories as in Chapter 4.

There are plots of 1σ allowed intervals for the five "largest" systematic categories in terms of ratios to the nominal predictions to capture the uncertainties in the neutrino reconstructed energy spectra.

All uncertainties were evaluated using the best-fit point of the neutrino oscillation parameters, Eq. (5.5), and systematic nuisance parameters.

C.1 Disappearance ν_μ channel, ν-beam

ν_μ E_{had} fraction quartile 1

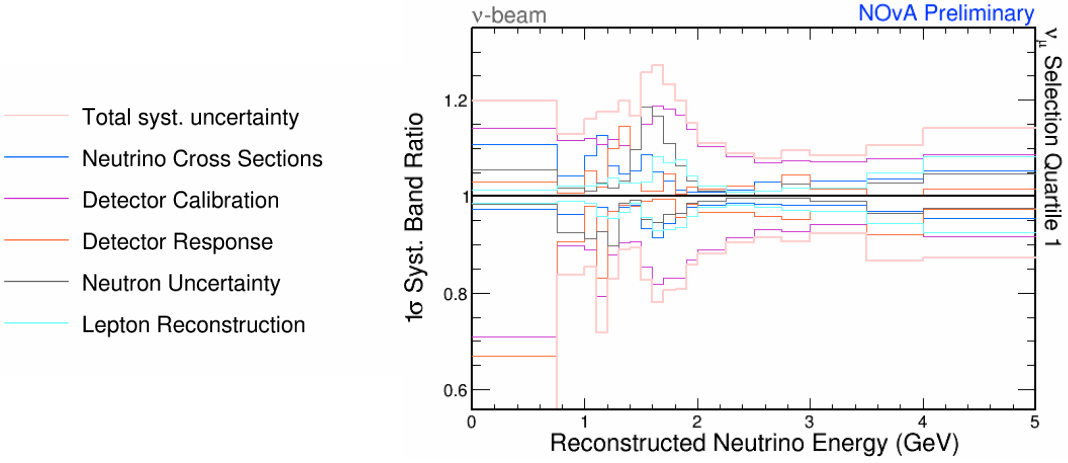

Figure C.1: 1σ systematic bands relative to the nominal prediction for the ν-beam ν_μ disapp. quartile 1 in the reconstructed neutrino energy.

Table C.1: Relative 1σ systematic uncertainties on the integral numbers of predicted events for the ν_μ disapp. ν-beam quartile 1.

Systematic summary for ν_μ disappearance ν-beam quartile 1 (%)

Systematic	Total pred		Signal		Total bkg		Beam bkg		ν_μ signal		$\bar{\nu}_\mu$ signal		ν_μ app.		NC		ν_e CC		ν_τ CC		Cosmics	
CCQE z-exp.ax.vec. 1	-0.07	+0.07	-0.05	+0.06	-1.11	+1.19	-2.31	+2.47	-0.04	+0.04	-0.16	+0.22	-3.64	+3.88	-0.00	+0.00	-0.02	+0.02	-3.30	+3.54	-0.00	+0.00
CCQE z-exp.ax.vec. 2	-0.08	+0.09	-0.07	+0.08	-0.88	+0.93	-1.83	+1.93	-0.06	+0.06	-0.14	+0.18	-2.87	+3.03	-0.00	+0.00	-0.07	+0.07	-2.63	+2.79	-0.00	+0.00
CCQE z-exp.ax.vec. 3	-0.18	+0.19	-0.17	+0.18	-0.79	+0.84	-1.63	+1.73	-0.17	+0.17	-0.19	+0.26	-2.50	+2.65	-0.00	+0.00	-0.31	+0.38	-2.38	+2.55	-0.00	+0.00
CCQE z-exp.ax.vec. 4	-0.04	+0.04	-0.04	+0.04	-0.10	+0.11	-0.21	+0.22	-0.04	+0.04	-0.04	+0.04	-0.32	+0.32	-0.00	+0.00	-0.12	+0.13	-0.32	+0.33	-0.00	+0.00
M_A^{CCRES}	-0.15	+0.22	-0.16	+0.23	-0.43	+0.41	-0.88	+0.86	-0.16	+0.21	-0.15	+0.41	-1.17	+1.13	-0.00	+0.00	-15.12	+15.45	-1.23	+1.21	-0.00	+0.00
M_V^{CCRES}	-0.13	+0.14	-0.14	+0.15	-0.28	+0.33	-0.57	+0.67	-0.14	+0.14	-0.14	+0.27	-0.73	+0.85	-0.00	+0.00	-14.09	+16.82	-0.78	+0.92	-0.00	+0.00
M_A^{NCRES}	-0.01	+0.02	-0.01	+0.01	-2.15	+2.36	-4.45	+4.89	-0.01	+0.01	-0.03	+0.02	-0.00	+0.00	-13.62	+14.94	-0.00	+0.00	-0.00	+0.00	-0.00	+0.00
M_V^{NCRES}	-0.00	+0.00	-0.00	+0.00	-0.69	+0.81	-1.43	+1.67	-0.00	+0.00	-0.00	+0.00	-0.00	+0.00	-4.36	+5.10	-0.00	+0.00	-0.00	+0.00	-0.00	+0.00
CCQE z-exp.norm.	-0.23	+0.27	-0.19	+0.23	-2.64	+3.52	-5.46	+7.28	-0.09	+0.11	-1.00	+1.17	-8.58	+11.44	-0.00	+0.00	-0.19	+0.25	-7.85	+10.46	-0.00	+0.00
RPA high Q^2 enh.	-0.10	+0.13	-0.10	+0.13	-0.34	+0.38	-0.71	+0.80	-0.12	+0.16	-0.11	+0.14	-1.28	+1.44	-0.00	+0.00	-0.04	+0.05	-0.88	+1.00	-0.00	+0.00
RPA low Q^2 supp.	-0.12	+0.11	-0.13	+0.12	-0.45	+0.48	-0.94	+0.99	-0.03	+0.02	-0.91	+0.92	-1.74	+1.82	-0.00	+0.00	-0.00	+0.00	-1.15	+1.21	-0.00	+0.00
RES low Q^2 supp.	-0.00	+0.13	-0.00	+0.13	-0.35	+0.00	-0.72	+0.00	-0.00	+0.08	-0.00	+0.58	-0.49	+0.00	-1.32	+0.00	-0.15	+0.00	-0.39	+0.00	-0.00	+0.00
DIS CC $\nu n \to 1\pi$	-0.12	+0.12	-0.12	+0.13	-0.22	+0.22	-0.46	+0.46	-0.03	+0.03	-0.84	+0.86	-0.66	+0.66	-0.00	+0.00	-9.43	+9.43	-0.59	+0.59	-0.00	+0.00
FSI π free path	-0.06	+0.03	-0.05	+0.02	-1.19	+0.79	-2.47	+1.64	-0.10	+0.06	-0.32	+0.37	-0.34	+0.21	-6.83	+4.64	-10.01	+2.90	-0.23	+0.11	-0.00	+0.00
FSI fate fraction	-0.02	+0.00	-0.02	+0.00	-0.05	+0.19	-0.10	+0.40	-0.05	+0.05	-0.57	+0.33	-0.20	+0.25	-0.00	+0.81	-1.12	+0.00	-0.13	+0.18	-0.00	+0.00
MEC E_ν shape	-0.03	+0.09	-0.04	+0.11	-1.00	+0.53	-2.07	+1.09	-0.33	+0.32	-2.90	+3.61	-3.70	+2.04	-0.00	+0.00	-0.00	+0.00	-2.64	+1.31	-0.00	+0.00
MEC $E_{\bar{\nu}}$ shape	-0.11	+0.05	-0.11	+0.05	-0.10	+0.03	-0.21	+0.05	-0.25	+0.26	-3.00	+2.43	-0.11	+0.03	-0.00	+0.00	-0.00	+0.00	-0.49	+0.12	-0.00	+0.00
MEC ν (q_0, q) response	-0.00	+0.58	-0.00	+0.64	-4.35	+5.39	-9.00	+11.16	-0.67	+1.01	-5.80	+11.03	-16.78	+17.52	-0.00	+0.00	-0.00	+0.00	-10.87	+16.08	-0.00	+0.00
MEC $\bar{\nu}$ (q_0, q) response	-0.12	+0.34	-0.12	+0.34	-0.10	+0.88	-0.20	+1.81	-0.32	+0.67	-6.39	+5.56	-0.47	+0.71	-0.00	+0.00	-0.00	+0.00	-0.16	+4.29	-0.00	+0.00
MEC ν init. np frac.	-0.06	+0.19	-0.06	+0.20	-0.22	+0.07	-0.45	+0.15	-0.05	+0.16	-0.14	+0.45	-0.88	+0.29	-0.00	+0.00	-0.00	+0.00	-0.50	+0.17	-0.00	+0.00
MEC $\bar{\nu}$ init. np frac.	-0.00	+0.02	-0.00	+0.02	-0.07	+0.22	-0.15	+0.46	-0.00	+0.02	-0.01	+0.00	-0.05	+0.14	-0.00	+0.00	-0.00	+0.00	-0.38	+1.13	-0.00	+0.00
XSecs PC00	-0.05	+0.05	-0.02	+0.02	-1.96	+1.96	-4.07	+4.07	-0.02	+0.02	-0.04	+0.04	-0.04	+0.04	-12.36	+12.36	-0.00	+0.00	-0.03	+0.03	-0.00	+0.00
XSecs PC01	-0.08	+0.08	-0.08	+0.08	-0.32	+0.32	-0.66	+0.66	-0.08	+0.08	-0.12	+0.12	-0.04	+0.04	-1.94	+1.94	-0.00	+0.00	-0.04	+0.04	-0.00	+0.00
XSecs PC02	-1.10	+1.24	-1.12	+1.26	-0.27	+0.27	-0.57	+0.57	-1.05	+1.17	-1.69	+1.96	-0.81	+0.81	-0.14	+0.14	-0.00	+0.00	-0.75	+0.75	-0.00	+0.00
XSecs PC03	-0.25	+0.26	-0.25	+0.26	-0.04	+0.04	-0.08	+0.08	-0.23	+0.24	-0.42	+0.44	-0.34	+0.34	-0.88	+0.88	-0.00	+0.00	-0.30	+0.30	-0.00	+0.00
XSecs PC04	-0.28	+0.29	-0.29	+0.30	-0.22	+0.22	-0.45	+0.45	-0.28	+0.28	-0.38	+0.39	-0.28	+0.28	-0.84	+0.84	-0.00	+0.00	-0.24	+0.24	-0.00	+0.00
XSecs PC05	-0.10	+0.10	-0.10	+0.10	-0.07	+0.07	-0.15	+0.15	-0.10	+0.10	-0.13	+0.13	-0.10	+0.10	-0.27	+0.27	-0.00	+0.00	-0.09	+0.09	-0.00	+0.00
XSecs PC06	-0.16	+0.16	-0.16	+0.17	-0.00	+0.00	-0.01	+0.01	-0.16	+0.16	-0.24	+0.24	-0.20	+0.20	-0.36	+0.36	-0.00	+0.00	-0.13	+0.13	-0.00	+0.00
XSecs PC07	-0.05	+0.05	-0.05	+0.06	-0.16	+0.16	-0.34	+0.34	-0.05	+0.05	-0.09	+0.09	-0.09	+0.09	-0.88	+0.88	-0.00	+0.00	-0.07	+0.07	-0.00	+0.00
XSecs PC08	-0.16	+0.16	-0.16	+0.16	-0.05	+0.05	-0.11	+0.11	-0.16	+0.16	-0.15	+0.15	-0.17	+0.17	-0.04	+0.04	-0.00	+0.00	-0.12	+0.12	-0.00	+0.00
XSecs PC09	-0.08	+0.08	-0.09	+0.09	-0.00	+0.00	-0.02	+0.02	-0.08	+0.08	-0.10	+0.10	-0.12	+0.12	-0.25	+0.25	-0.00	+0.00	-0.08	+0.08	-0.00	+0.00
XSecs PC10	-0.13	+0.13	-0.13	+0.13	-0.00	+0.00	-0.00	+0.00	-0.13	+0.13	-0.18	+0.18	-0.06	+0.06	-0.14	+0.14	-0.00	+0.00	-0.05	+0.05	-0.00	+0.00
XSecs PC11	-0.01	+0.01	-0.01	+0.01	-0.00	+0.00	-0.02	+0.02	-0.00	+0.00	-0.04	+0.04	-0.03	+0.03	-0.12	+0.12	-0.00	+0.00	-0.04	+0.04	-0.00	+0.00
ν_τ scale	-0.16	+0.16	-0.00	+0.00	-12.12	+12.12	-25.09	+25.09	-0.00	+0.00	-0.00	+0.00	-32.97	+32.97	-0.00	+0.00	-0.00	+0.00	-41.18	+41.18	-0.00	+0.00
Flux PC00	-0.10	+0.09	-0.08	+0.08	-0.94	+0.94	-1.95	+1.94	-0.12	+0.12	-1.71	+1.67	-2.22	+2.21	-1.10	+1.10	-2.47	+2.49	-2.48	+2.46	-0.00	+0.00
Flux PC01	-0.06	+0.03	-0.08	+0.06	-1.89	+1.85	-3.91	+3.83	-0.45	+0.46	-3.16	+2.85	-3.92	+3.83	-3.28	+3.27	-4.26	+4.30	-4.45	+4.31	-0.00	+0.00
Flux PC02	-0.21	+0.19	-0.19	+0.18	-1.13	+1.08	-2.35	+2.24	-0.12	+0.12	-0.76	+0.62	-2.67	+2.52	-1.88	+1.86	-4.64	+4.62	-2.47	+2.32	-0.00	+0.00
Flux PC03	-0.06	+0.05	-0.03	+0.01	-2.85	+2.84	-5.91	+5.87	-0.07	+0.09	-0.93	+0.69	-6.22	+6.18	-5.19	+5.18	-6.96	+6.96	-6.28	+6.21	-0.00	+0.00
Flux PC04	-0.19	+0.19	-0.19	+0.19	-0.16	+0.16	-0.33	+0.32	-0.16	+0.16	-0.38	+0.38	-0.54	+0.54	-0.14	+0.14	-0.15	+0.14	-0.57	+0.56	-0.00	+0.00
Absolute calib.	-3.88	+2.56	-3.90	+2.57	-2.42	+2.19	-5.02	+4.53	-4.11	+2.86	-2.25	+0.25	-5.65	+5.56	-5.40	+5.56	-15.29	+0.00	-4.05	+2.92	-0.00	+0.00
ND/FD relative calib.	-8.13	+8.52	-8.22	+8.62	-1.18	+1.12	-2.45	+2.33	-8.48	+8.94	-6.17	+6.08	-2.81	+2.79	-2.72	+2.76	-5.30	+0.69	-1.88	+1.60	-0.00	+0.00
Calibration shape	-2.45	+2.45	-2.48	+2.48	-0.15	+0.15	-0.32	+0.32	-2.58	+2.58	-1.70	+1.70	-0.71	+0.71	-1.29	+1.29	-9.63	+9.63	-0.15	+0.15	-0.00	+0.00
Calibration drift	-0.00	+0.37	-0.00	+0.39	-0.93	+0.00	-1.93	+0.00	-0.00	+0.60	-1.27	+0.00	-5.07	+0.00	-1.59	+0.00	-94.46	+0.00	-0.00	+1.46	-0.00	+0.00
Light level FD	-1.37	+0.00	-1.36	+0.00	-1.94	+0.00	-4.01	+0.00	-1.48	+0.00	-2.58	+0.00	-4.91	+0.00	-4.76	+0.00	-78.19	+0.00	-1.74	+0.00	-0.00	+0.00
Light level ND	-1.56	+0.00	-1.58	+0.00	-0.00	+0.00	-0.00	+0.00	-1.67	+0.00	-0.88	+0.00	-0.00	+0.00	-0.00	+0.00	-0.00	+0.00	-0.00	+0.00	-0.00	+0.00
Cherenkov	-0.21	+0.00	-0.21	+0.00	-0.00	+0.09	-0.00	+0.20	-0.00	+0.10	-2.70	+0.00	-0.00	+0.83	-0.87	+0.00	-83.68	+0.00	-0.00	+1.74	-0.00	+0.00
E_μ ND uncorr.	-0.44	+0.42	-0.45	+0.43	-0.00	+0.00	-0.00	+0.00	-0.43	+0.41	-0.57	+0.55	-0.00	+0.00	-0.00	+0.00	-0.00	+0.00	-0.00	+0.00	-0.00	+0.00
E_μ μ-catcher uncorr.	-0.54	+0.55	-0.55	+0.56	-0.00	+0.00	-0.00	+0.00	-0.51	+0.52	-0.87	+0.88	-0.00	+0.00	-0.00	+0.00	-0.00	+0.00	-0.00	+0.00	-0.00	+0.00
E_μ n pile-up	-1.27	+0.00	-1.29	+0.00	-0.00	+0.00	-0.00	+0.00	-1.23	+0.00	-1.75	+0.00	-0.00	+0.00	-0.00	+0.00	-0.00	+0.00	-0.00	+0.00	-0.00	+0.00
E_μ correlated	-2.05	+2.28	-2.08	+2.32	-0.39	+0.36	-0.81	+0.75	-1.89	+2.09	-3.57	+4.15	-0.17	+0.25	-1.44	+1.24	-0.00	+0.67	-0.78	+0.71	-0.00	+0.00
E_μ FD uncorr.	-0.11	+0.09	-0.11	+0.09	-0.06	+0.08	-0.12	+0.17	-0.11	+0.10	-0.08	+0.00	-0.04	+0.03	-0.22	+0.34	-0.00	+0.00	-0.15	+0.19	-0.00	+0.00
Lepton angle xz ND	-0.39	+0.25	-0.40	+0.26	-0.00	+0.00	-0.00	+0.00	-0.42	+0.27	-0.25	+0.18	-0.00	+0.00	-0.00	+0.00	-0.00	+0.00	-0.00	+0.00	-0.00	+0.00
Lepton angle yz ND	-0.09	+0.00	-0.09	+0.00	-0.00	+0.00	-0.00	+0.00	-0.10	+0.00	-0.06	+0.00	-0.00	+0.00	-0.00	+0.00	-0.00	+0.00	-0.00	+0.00	-0.00	+0.00
Lepton angle xz FD	-0.00	+0.00	-0.00	+0.00	-0.00	+0.00	-0.00	+0.00	-0.00	+0.00	-0.00	+0.00	-0.00	+0.00	-0.00	+0.00	-0.00	+0.00	-0.00	+0.00	-0.00	+0.00
Lepton angle yz FD	-0.00	+0.00	-0.00	+0.00	-0.00	+0.00	-0.00	+0.00	-0.00	+0.00	-0.00	+0.01	-0.00	+0.00	-0.00	+0.00	-0.00	+0.00	-0.00	+0.00	-0.00	+0.00
Neutron systematic	-1.06	+1.84	-1.04	+1.82	-2.96	+3.37	-6.12	+6.98	-0.69	+1.64	-3.86	+3.26	-6.20	+4.97	-7.67	+11.04	-2.35	+5.50	-4.74	+5.02	-0.00	+0.00
Normalization beam corr.	-0.84	+0.84	-0.85	+0.85	-0.43	+0.43	-0.89	+0.89	-0.85	+0.85	-0.79	+0.79	-0.96	+0.96	-0.79	+0.79	-1.09	+1.09	-0.92	+0.92	-0.00	+0.00
Normalization ν-beam	-0.61	+0.61	-0.61	+0.61	-0.31	+0.31	-0.64	+0.64	-0.62	+0.62	-0.57	+0.57	-0.69	+0.69	-0.57	+0.57	-0.78	+0.78	-0.66	+0.66	-0.00	+0.00
Cosmic scale	-0.32	+0.59	-0.00	+0.00	-25.40	+46.18	-0.00	+0.00	-0.00	+0.00	-0.00	+0.00	-0.00	+0.00	-0.00	+0.00	-0.00	+0.00	-0.00	+0.00	-49.15	+89.37
Quadrature	-10.10	+9.93	-10.20	+10.01	-29.46	+48.67	-30.90	+31.77	-10.49	+10.37	-14.42	+16.18	-41.10	+41.23	-24.09	+25.25	-152.03	+28.97	-45.07	+47.22	-49.15	+89.37

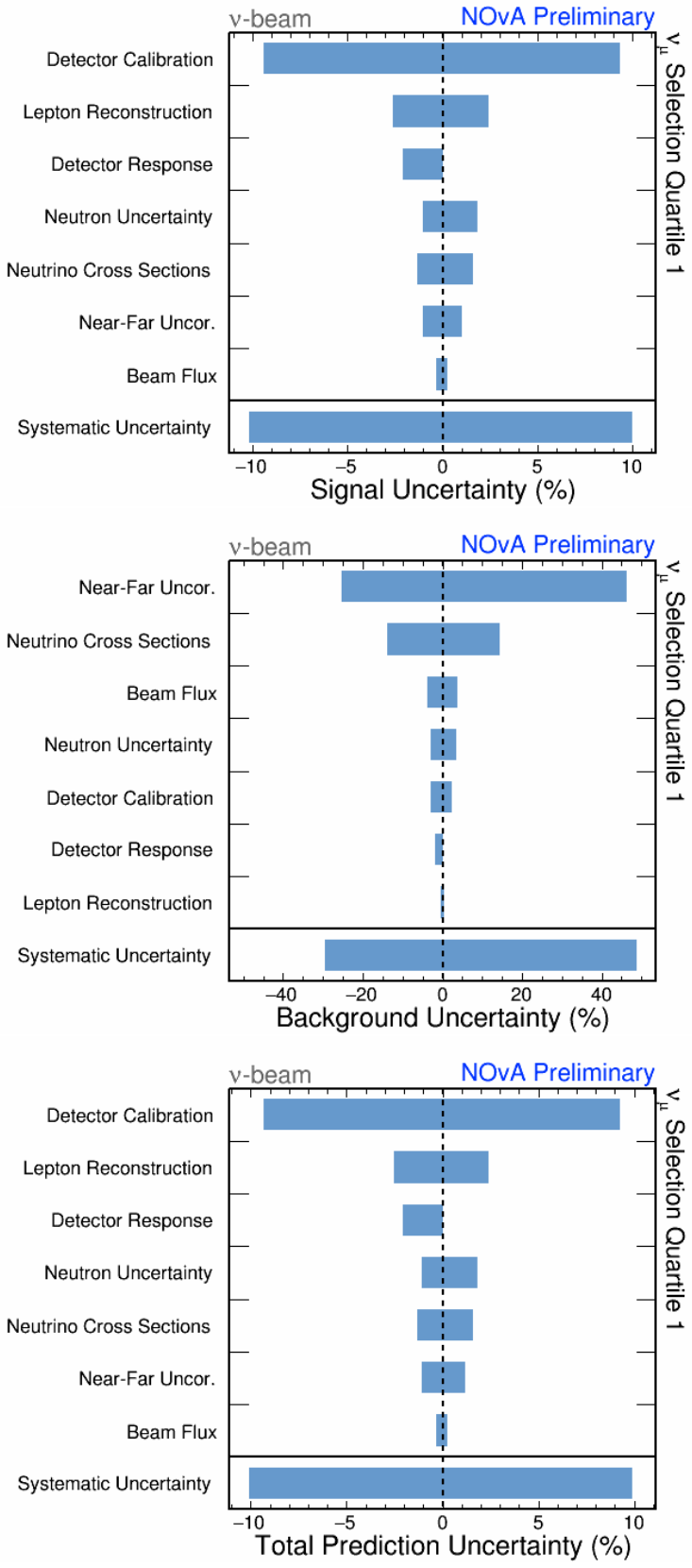

Figure C.2: Relative 1σ systematic uncertainties on the integral number of signal (top), background (middle), and total (bottom) predicted events in the ν_μ disapp. ν-beam quartile 1.

ν_μ E_{had} fraction quartile 2

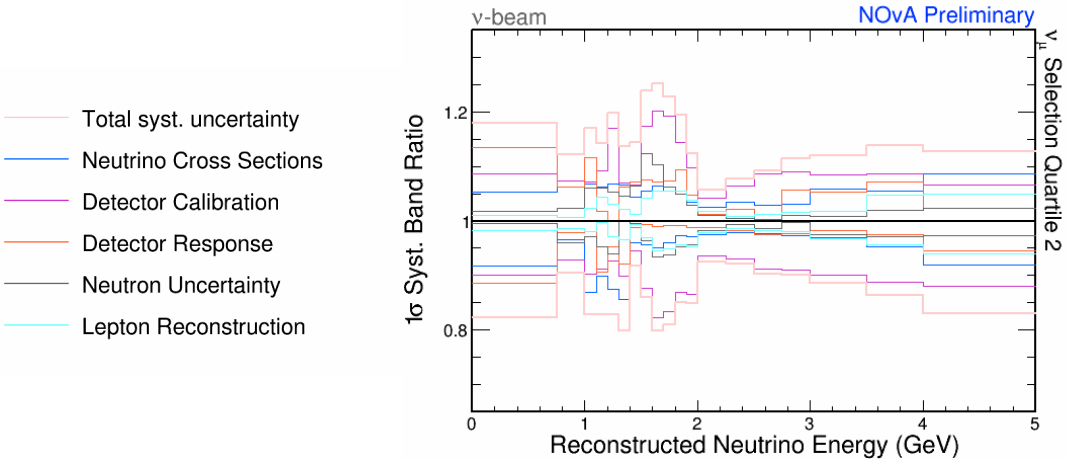

Figure C.3: 1σ systematic bands relative to the nominal prediction for the ν-beam ν_μ disapp. quartile 2 in the reconstructed neutrino energy.

Table C.2: Relative 1σ systematic uncertainties on the integral numbers of predicted events for the ν_μ disapp. ν-beam quartile 2.

Systematic summary for ν_μ disappearance ν-beam quartile 2 (%)

Systematic	Total pred		Signal		Total bkg		Beam bkg		ν_μ signal		ν_μ signal		ν_μ app.		NC		ν_e CC		ν_τ CC		Cosmics	
CCQE z-exp.ax.vec. 1	-0.20	+0.20	-0.19	+0.19	-0.71	+0.75	-1.32	+1.40	-0.22	+0.22	-0.22	+0.25	-2.42	+2.57	-0.00	+0.00	-0.10	+0.10	-2.22	+2.36	-0.00	+0.00
CCQE z-exp.ax.vec. 2	-0.20	+0.20	-0.19	+0.19	-0.62	+0.66	-1.16	+1.22	-0.22	+0.22	-0.18	+0.20	-2.13	+2.24	-0.00	+0.00	-0.07	+0.08	-1.95	+2.06	-0.00	+0.00
CCQE z-exp.ax.vec. 3	-0.58	+0.63	-0.57	+0.62	-0.92	+1.02	-1.71	+1.89	-0.62	+0.66	-0.00	+0.13	-3.03	+3.31	-0.00	+0.00	-0.38	+0.44	-2.97	+3.28	-0.00	+0.00
CCQE z-exp.ax.vec. 4	-0.14	+0.14	-0.14	+0.14	-0.18	+0.18	-0.33	+0.34	-0.14	+0.15	-0.00	+0.02	-0.57	+0.58	-0.00	+0.00	-0.11	+0.11	-0.59	+0.60	-0.00	+0.00
M_A^{CCRES}	-0.05	+0.37	-0.02	+0.34	-2.11	+2.23	-3.92	+4.14	-0.00	+0.24	-0.18	+2.06	-6.02	+6.09	-0.00	+0.00	-8.85	+9.90	-7.33	+7.95	-0.00	+0.00
M_V^{CCRES}	-0.04	+0.24	-0.02	+0.21	-1.52	+1.88	-2.82	+3.49	-0.00	+0.13	-0.28	+1.61	-4.29	+5.16	-0.00	+0.00	-6.77	+8.33	-5.30	+6.66	-0.00	+0.00
M_A^{NCRES}	-0.03	+0.04	-0.02	+0.01	-2.91	+3.51	-5.41	+6.52	-0.02	+0.01	-0.03	+0.03	-0.00	+0.00	-12.80	+15.43	-0.00	+0.00	-0.00	+0.00	-0.00	+0.00
M_V^{NCRES}	-0.01	+0.01	-0.00	+0.00	-0.99	+1.22	-1.84	+2.26	-0.00	+0.00	-0.00	+0.00	-0.00	+0.00	-4.36	+5.35	-0.00	+0.00	-0.00	+0.00	-0.00	+0.00
CCQE z-exp.norm.	-0.75	+0.91	-0.74	+0.89	-1.79	+2.39	-3.33	+4.44	-0.78	+0.94	-0.04	+0.06	-5.97	+7.97	-0.00	+0.00	-0.36	+0.48	-5.70	+7.60	-0.00	+0.00
RPA high Q^2 enh.	-0.52	+0.55	-0.53	+0.55	-0.27	+0.34	-0.50	+0.63	-0.57	+0.59	-0.17	+0.11	-0.98	+1.22	-0.00	+0.00	-0.00	+0.29	-0.81	+1.02	-0.00	+0.00
RPA low Q^2 supp.	-0.04	+0.04	-0.04	+0.04	-0.06	+0.06	-0.11	+0.12	-0.02	+0.03	-0.36	+0.36	-0.21	+0.23	-0.00	+0.00	-0.06	+0.06	-0.17	+0.18	-0.00	+0.00
RES low Q^2 supp.	-0.00	+0.16	-0.00	+0.17	-0.47	+0.00	-0.87	+0.00	-0.00	+0.12	-0.00	+0.92	-0.98	+0.00	-0.82	+0.00	-0.37	+0.00	-0.84	+0.00	-0.00	+0.00
DIS CC $\nu n \to 1\pi$	-0.06	+0.06	-0.05	+0.06	-0.46	+0.46	-0.85	+0.85	-0.18	+0.18	-1.95	+2.04	-1.31	+1.31	-0.00	+0.00	-11.72	+11.72	-1.41	+1.41	-0.00	+0.00
FSI π free path	-0.58	+0.31	-0.57	+0.30	-1.18	+1.13	-2.19	+2.10	-0.57	+0.29	-0.59	+0.47	-0.03	+0.23	-5.22	+4.72	-4.59	+1.80	-0.00	+0.17	-0.00	+0.00
FSI fate fraction	-0.34	+0.28	-0.34	+0.28	-0.00	+0.23	-0.00	+0.42	-0.34	+0.26	-0.50	+0.56	-0.16	+0.21	-0.00	+0.89	-0.02	+0.77	-0.08	+0.18	-0.00	+0.00
MEC E_ν shape	-0.21	+0.38	-0.21	+0.39	-0.50	+0.27	-0.92	+0.50	-0.09	+0.27	-2.34	+2.32	-1.85	+1.03	-0.00	+0.00	-0.00	+0.00	-1.44	+0.77	-0.00	+0.00
MEC $E_{\bar{\nu}}$ shape	-0.04	+0.06	-0.04	+0.07	-0.04	+0.04	-0.07	+0.07	-0.10	+0.07	-1.92	+2.82	-0.06	+0.10	-0.00	+0.00	-0.00	+0.00	-0.17	+0.13	-0.00	+0.00
MEC ν (q_0, q) response	-0.00	+0.52	-0.00	+0.56	-2.07	+0.49	-3.85	+0.91	-0.00	+0.36	-4.46	+5.57	-6.77	+1.55	-0.00	+0.00	-0.00	+0.00	-6.72	+1.62	-0.00	+0.00
MEC $\bar{\nu}$ (q_0, q) response	-0.17	+0.00	-0.17	+0.00	-0.21	+0.00	-0.40	+0.00	-0.10	+0.07	-4.15	+1.23	-0.18	+0.00	-0.00	+0.00	-0.00	+0.00	-1.08	+0.00	-0.00	+0.00
MEC ν init. np frac.	-0.27	+0.09	-0.28	+0.10	-0.08	+0.25	-0.15	+0.46	-0.27	+0.09	-0.48	+0.16	-0.25	+0.75	-0.00	+0.00	-0.00	+0.00	-0.28	+0.84	-0.00	+0.00
MEC $\bar{\nu}$ init. np frac.	-0.02	+0.00	-0.02	+0.00	-0.08	+0.03	-0.16	+0.05	-0.02	+0.05	-1.10	+0.37	-0.15	+0.05	-0.00	+0.00	-0.00	+0.00	-0.37	+0.12	-0.00	+0.00
XSecs PC00	-0.07	+0.07	-0.03	+0.03	-2.79	+2.79	-5.18	+5.18	-0.03	+0.03	-0.10	+0.10	-0.04	+0.04	-12.20	+12.20	-0.00	+0.00	-0.03	+0.03	-0.00	+0.00
XSecs PC01	-0.11	+0.11	-0.12	+0.12	-0.45	+0.45	-0.84	+0.84	-0.11	+0.11	-0.19	+0.19	-0.05	+0.05	-1.91	+1.91	-0.00	+0.00	-0.06	+0.06	-0.00	+0.00
XSecs PC02	-1.61	+1.90	-1.64	+1.93	-0.33	+0.33	-0.62	+0.62	-1.58	+1.84	-2.74	+3.45	-0.90	+0.90	-0.14	+0.14	-0.00	+0.00	-1.02	+1.02	-0.00	+0.00
XSecs PC03	-0.38	+0.40	-0.39	+0.41	-0.08	+0.08	-0.15	+0.15	-0.37	+0.39	-0.65	+0.70	-0.38	+0.38	-0.89	+0.89	-0.00	+0.00	-0.40	+0.40	-0.00	+0.00
XSecs PC04	-0.40	+0.41	-0.41	+0.42	-0.29	+0.29	-0.54	+0.54	-0.41	+0.42	-0.50	+0.53	-0.30	+0.30	-0.86	+0.86	-0.00	+0.00	-0.32	+0.32	-0.00	+0.00
XSecs PC05	-0.15	+0.15	-0.16	+0.16	-0.09	+0.09	-0.17	+0.17	-0.15	+0.15	-0.20	+0.20	-0.11	+0.11	-0.25	+0.25	-0.00	+0.00	-0.12	+0.12	-0.00	+0.00
XSecs PC06	-0.23	+0.24	-0.24	+0.24	-0.03	+0.03	-0.06	+0.06	-0.23	+0.24	-0.31	+0.31	-0.20	+0.20	-0.38	+0.38	-0.00	+0.00	-0.17	+0.17	-0.00	+0.00
XSecs PC07	-0.08	+0.08	-0.08	+0.08	-0.24	+0.24	-0.44	+0.44	-0.08	+0.08	-0.12	+0.12	-0.09	+0.09	-0.92	+0.92	-0.00	+0.00	-0.09	+0.09	-0.00	+0.00
XSecs PC08	-0.24	+0.24	-0.24	+0.24	-0.03	+0.03	-0.05	+0.05	-0.24	+0.25	-0.19	+0.20	-0.17	+0.17	-0.10	+0.10	-0.00	+0.00	-0.16	+0.16	-0.00	+0.00
XSecs PC09	-0.13	+0.13	-0.13	+0.13	-0.01	+0.01	-0.03	+0.03	-0.13	+0.13	-0.13	+0.13	-0.12	+0.12	-0.22	+0.22	-0.00	+0.00	-0.11	+0.11	-0.00	+0.00
XSecs PC10	-0.18	+0.19	-0.19	+0.19	-0.00	+0.00	-0.00	+0.00	-0.18	+0.18	-0.27	+0.28	-0.07	+0.07	-0.10	+0.10	-0.00	+0.00	-0.07	+0.07	-0.00	+0.00
XSecs PC11	-0.02	+0.02	-0.02	+0.02	-0.03	+0.03	-0.05	+0.05	-0.02	+0.02	-0.06	+0.06	-0.03	+0.03	-0.17	+0.17	-0.00	+0.00	-0.05	+0.05	-0.00	+0.00
ν_τ scale	-0.17	+0.17	-0.00	+0.00	-10.85	+10.85	-20.15	+20.15	-0.00	+0.00	-0.00	+0.00	-32.98	+32.98	-0.00	+0.00	-0.00	+0.00	-37.01	+37.01	-0.00	+0.00
Flux PC00	-0.06	+0.06	-0.05	+0.05	-0.89	+0.89	-1.66	+1.65	-0.06	+0.06	-1.84	+1.78	-1.97	+1.96	-1.10	+1.10	-0.87	+0.88	-2.15	+2.14	-0.00	+0.00
Flux PC01	-0.13	+0.11	-0.16	+0.15	-1.89	+1.86	-3.52	+3.46	-0.35	+0.35	-3.32	+2.96	-3.50	+3.43	-3.28	+3.26	-3.20	+3.19	-3.85	+3.76	-0.00	+0.00
Flux PC02	-0.32	+0.30	-0.31	+0.29	-1.11	+1.07	-2.07	+1.98	-0.25	+0.24	-1.24	+1.11	-2.31	+2.18	-1.89	+1.86	-1.79	+1.78	-2.13	+1.98	-0.00	+0.00
Flux PC03	-0.13	+0.12	-0.09	+0.07	-2.93	+2.92	-5.45	+5.43	-0.03	+0.03	-1.05	+0.79	-5.61	+5.59	-5.17	+5.16	-5.07	+5.07	-5.69	+5.65	-0.00	+0.00
Flux PC04	-0.21	+0.21	-0.21	+0.21	-0.14	+0.14	-0.26	+0.26	-0.19	+0.19	-0.42	+0.42	-0.53	+0.53	-0.13	+0.13	-0.44	+0.44	-0.58	+0.58	-0.00	+0.00
Absolute calib.	-5.30	+3.48	-5.37	+3.51	-0.39	+1.60	-0.73	+2.97	-5.42	+3.47	-4.67	+4.16	-0.00	+1.07	-2.55	+5.87	-19.80	+15.66	-0.00	+0.68	-0.00	+0.00
ND/FD relative calib.	-2.67	+2.32	-2.72	+2.36	-0.35	+0.65	-0.64	+1.20	-2.61	+2.23	-4.55	+4.56	-0.00	+0.28	-1.69	+2.52	-9.36	+8.35	-0.00	+0.20	-0.00	+0.00
Calibration shape	-0.92	+0.92	-0.93	+0.93	-0.55	+0.55	-1.03	+1.03	-0.91	+0.91	-1.25	+1.25	-0.69	+0.69	-1.73	+1.73	-5.88	+5.88	-0.28	+0.28	-0.00	+0.00
Calibration drift	-0.36	+0.00	-0.39	+0.00	-0.00	+1.43	-0.00	+2.66	-0.64	+0.00	-0.00	+3.63	-0.00	+4.25	-0.00	+1.91	-15.47	+0.00	-0.00	+2.74	-0.00	+0.00
Light level FD	-0.00	+1.60	-0.00	+1.61	-0.00	+0.99	-0.00	+1.84	-0.00	+1.52	-0.00	+3.00	-0.00	+2.78	-0.00	+2.87	-7.77	+22.06	-0.00	+2.18	-0.00	+0.00
Light level ND	-1.95	+0.00	-1.98	+0.00	-0.00	+0.00	-0.00	+0.00	-1.92	+0.00	-2.82	+0.00	-0.00	+0.00	-0.00	+0.00	-0.00	+0.00	-0.00	+0.00	-0.00	+0.00
Cherenkov	-0.00	+2.54	-0.00	+2.54	-0.00	+2.13	-0.00	+3.96	-0.00	+2.57	-0.00	+2.04	-0.00	+5.18	-0.00	+3.22	-7.33	+0.00	-0.00	+4.21	-0.00	+0.00
E_μ ND uncorr.	-0.30	+0.34	-0.30	+0.34	-0.00	+0.00	-0.00	+0.00	-0.30	+0.33	-0.43	+0.55	-0.00	+0.00	-0.00	+0.00	-0.00	+0.00	-0.00	+0.00	-0.00	+0.00
E_μ μ-catcher uncorr.	-0.31	+0.36	-0.32	+0.36	-0.00	+0.00	-0.00	+0.00	-0.30	+0.34	-0.67	+0.81	-0.00	+0.00	-0.00	+0.00	-0.00	+0.00	-0.00	+0.00	-0.00	+0.00
E_μ n pile-up	-0.93	+0.00	-0.94	+0.00	-0.00	+0.00	-0.00	+0.00	-0.91	+0.00	-1.45	+0.00	-0.00	+0.00	-0.00	+0.00	-0.00	+0.00	-0.00	+0.00	-0.00	+0.00
E_μ correlated	-1.83	+1.81	-1.87	+1.84	-0.30	+0.31	-0.56	+0.57	-1.78	+1.74	-3.35	+3.51	-0.12	+0.00	-0.97	+1.11	-1.54	+1.38	-0.35	+0.31	-0.00	+0.00
E_μ FD uncorr.	-0.00	+0.03	-0.00	+0.03	-0.16	+0.07	-0.29	+0.14	-0.00	+0.04	-0.08	+0.23	-0.16	+0.08	-0.46	+0.15	-0.00	+0.00	-0.18	+0.17	-0.00	+0.00
Lepton angle xz ND	-0.67	+0.46	-0.68	+0.46	-0.00	+0.00	-0.00	+0.00	-0.67	+0.46	-0.85	+0.47	-0.00	+0.00	-0.00	+0.00	-0.00	+0.00	-0.00	+0.00	-0.00	+0.00
Lepton angle yz ND	-0.17	+0.00	-0.17	+0.00	-0.00	+0.00	-0.00	+0.00	-0.17	+0.00	-0.27	+0.00	-0.00	+0.00	-0.00	+0.00	-0.00	+0.00	-0.00	+0.00	-0.00	+0.00
Lepton angle xz FD	-0.00	+0.00	-0.00	+0.00	-0.00	+0.00	-0.00	+0.00	-0.00	+0.00	-0.02	+0.01	-0.00	+0.00	-0.00	+0.00	-0.00	+0.00	-0.00	+0.00	-0.00	+0.00
Lepton angle yz FD	-0.00	+0.00	-0.00	+0.00	-0.00	+0.00	-0.00	+0.00	-0.00	+0.00	-0.00	+0.00	-0.00	+0.00	-0.00	+0.00	-0.00	+0.00	-0.00	+0.00	-0.00	+0.00
Neutron systematic	-1.64	+1.35	-1.66	+1.38	-0.26	+0.00	-0.48	+0.00	-1.88	+1.63	-2.85	+1.98	-1.06	+0.51	-1.96	+0.62	-7.23	+7.30	-1.61	+0.83	-0.00	+0.00
Normalization beam corr.	-0.82	+0.82	-0.82	+0.82	-0.44	+0.44	-0.82	+0.82	-0.82	+0.82	-0.85	+0.85	-0.84	+0.84	-0.78	+0.78	-0.77	+0.77	-0.85	+0.85	-0.00	+0.00
Normalization ν-beam	-0.59	+0.59	-0.59	+0.59	-0.32	+0.32	-0.59	+0.59	-0.59	+0.59	-0.61	+0.61	-0.61	+0.61	-0.56	+0.56	-0.56	+0.56	-0.61	+0.61	-0.00	+0.00
Cosmic scale	-0.36	+0.58	-0.00	+0.00	-23.46	+38.30	-0.00	+0.00	-0.00	+0.00	-0.00	+0.00	-0.00	+0.00	-0.00	+0.00	-0.00	+0.00	-0.00	+0.00	-50.84	+82.99
Quadrature	-7.34	+6.40	-7.44	+6.44	-26.82	+40.62	-24.14	+25.15	-7.45	+6.35	-12.42	+13.05	-36.16	+36.79	-20.65	+23.57	-35.30	+35.23	-40.20	+40.64	-50.84	+82.99

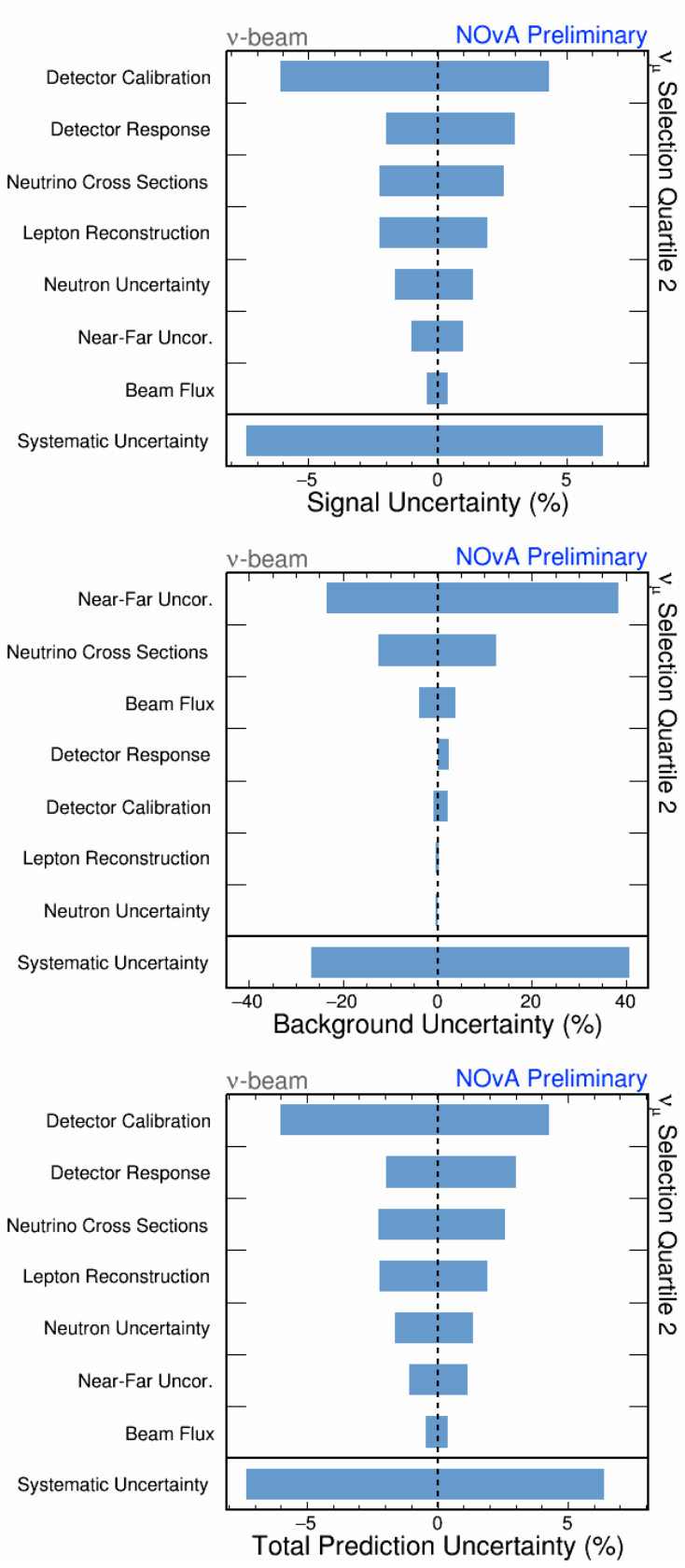

Figure C.4: Relative 1σ systematic uncertainties on the integral number of signal (top), background (middle), and total (bottom) predicted events in the ν_μ disapp. ν-beam quartile 2.

ν_μ E_{had} fraction quartile 3

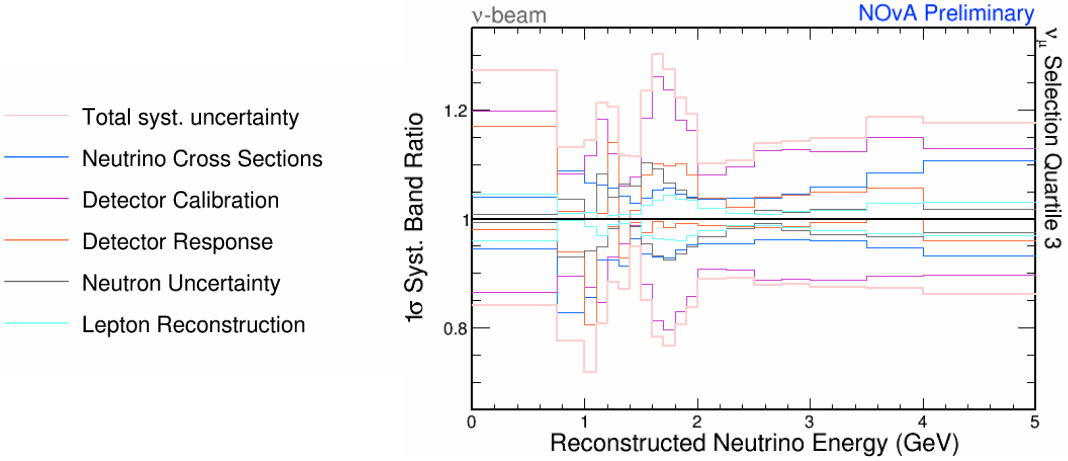

Figure C.5: 1σ systematic bands relative to the nominal prediction for the ν-beam ν_μ disapp. quartile 3 in the reconstructed neutrino energy.

Table C.3: Relative 1σ systematic uncertainties on the integral numbers of predicted events for the ν_μ disapp. ν-beam quartile 3.

Systematic summary for ν_μ disappearance ν-beam quartile 3 (%)

Systematic	Total pred		Signal		Total bkg		Beam bkg		ν_μ signal		$\bar{\nu}_\mu$ signal		ν_μ app.		NC		ν_e CC		ν_τ CC		Cosmics	
CCQE z-exp.ax.vec. 1	-0.15	+0.15	-0.15	+0.15	-0.18	+0.19	-0.40	+0.42	-0.17	+0.17	-0.22	+0.22	-1.28	+1.35	-0.00	+0.00	-0.05	+0.05	-1.03	+1.09	-0.00	+0.00
CCQE z-exp.ax.vec. 2	-0.13	+0.13	-0.12	+0.13	-0.15	+0.16	-0.34	+0.36	-0.14	+0.14	-0.17	+0.17	-1.11	+1.16	-0.00	+0.00	-0.04	+0.04	-0.87	+0.92	-0.00	+0.00
CCQE z-exp.ax.vec. 3	-0.70	+0.79	-0.70	+0.80	-0.39	+0.44	-0.89	+1.01	-0.75	+0.84	-0.17	+0.27	-2.80	+3.16	-0.00	+0.00	-0.06	+0.06	-2.31	+2.65	-0.00	+0.00
CCQE z-exp.ax.vec. 4	-0.19	+0.20	-0.20	+0.20	-0.10	+0.10	-0.22	+0.23	-0.21	+0.21	-0.04	+0.05	-0.68	+0.70	-0.00	+0.00	-0.01	+0.01	-0.58	+0.60	-0.00	+0.00
M_A^{CCRES}	-0.59	+2.01	-0.54	+1.98	-2.29	+2.95	-5.22	+6.72	-0.60	+1.80	-0.00	+5.44	-13.63	+16.59	-0.00	+0.00	-8.16	+9.03	-14.98	+20.22	-0.00	+0.00
M_0^{CCRES}	-0.31	+1.08	-0.27	+1.04	-1.66	+2.27	-3.78	+5.17	-0.34	+0.98	-0.00	+2.28	-10.03	+13.27	-0.00	+0.00	-6.32	+7.82	-10.68	+15.03	-0.00	+0.00
M_A^{NCRES}	-0.07	+0.09	-0.03	+0.02	-3.04	+4.14	-6.93	+9.42	-0.03	+0.02	-0.03	+0.02	-0.00	+0.00	-11.06	+15.04	-0.00	+0.00	-0.00	+0.00	-0.00	+0.00
M_0^{NCRES}	-0.02	+0.03	-0.00	+0.00	-1.05	+1.36	-2.40	+3.10	-0.00	+0.00	-0.00	+0.00	-0.00	+0.00	-3.83	+4.95	-0.00	+0.00	-0.00	+0.00	-0.00	+0.00
CCQE z-exp.norm.	-0.74	+0.94	-0.74	+0.95	-0.56	+0.75	-1.28	+1.71	-0.79	+1.01	-0.35	+0.28	-3.99	+5.32	-0.00	+0.00	-0.05	+0.07	-3.37	+4.49	-0.00	+0.00
RPA high Q^2 enh.	-0.29	+0.48	-0.30	+0.49	-0.10	+0.13	-0.23	+0.30	-0.33	+0.52	-0.21	+0.19	-0.79	+1.03	-0.00	+0.00	-0.04	+0.04	-0.53	+0.70	-0.00	+0.00
RPA low Q^2 supp.	-0.03	+0.03	-0.03	+0.04	-0.01	+0.01	-0.03	+0.03	-0.03	+0.03	-0.15	+0.15	-0.08	+0.08	-0.00	+0.00	-0.00	+0.00	-0.06	+0.06	-0.00	+0.00
RES low Q^2 supp.	-0.00	+0.23	-0.00	+0.25	-0.22	+0.00	-0.50	+0.00	-0.00	+0.22	-0.00	+0.68	-0.71	+0.00	-0.45	+0.00	-0.17	+0.00	-0.51	+0.00	-0.00	+0.00
DIS CC $\nu n \to 1\pi$	-0.57	+0.54	-0.57	+0.54	-0.52	+0.52	-1.18	+1.18	-0.76	+0.72	-2.97	+3.19	-2.50	+2.50	-0.00	+0.00	-10.44	+10.44	-2.85	+2.85	-0.00	+0.00
FSI π free path	-1.30	+0.92	-1.30	+0.92	-1.34	+1.15	-3.05	+2.63	-1.30	+0.91	-1.26	+1.02	-0.39	+0.60	-5.17	+4.33	-1.30	+1.25	-0.29	+0.64	-0.00	+0.00
FSI fate fraction	-0.68	+0.79	-0.70	+0.81	-0.03	+0.10	-0.08	+0.23	-0.69	+0.78	-0.94	+1.42	-0.62	+0.20	-0.00	+0.26	-1.90	+0.00	-0.35	+0.22	-0.00	+0.00
MEC E_ν shape	-0.00	+0.16	-0.00	+0.16	-0.12	+0.10	-0.26	+0.24	-0.00	+0.13	-1.06	+0.83	-0.90	+0.81	-0.00	+0.00	-0.08	+0.33	-0.62	+0.53	-0.00	+0.00
MEC $E_{\bar{\nu}}$ shape	-0.00	+0.02	-0.00	+0.02	-0.01	+0.00	-0.03	+0.00	-0.05	+0.03	-0.72	+1.43	-0.02	+0.02	-0.00	+0.00	-0.00	+0.00	-0.13	+0.04	-0.00	+0.00
MEC ν (q_0, q) response	-3.25	+1.49	-3.36	+1.55	-0.61	+0.24	-1.39	+0.55	-3.50	+1.57	-0.63	+1.20	-5.26	+2.57	-0.00	+0.00	-0.19	+0.00	-2.87	+0.77	-0.00	+0.00
MEC $\bar{\nu}$ (q_0, q) response	-0.00	+0.00	-0.00	+0.00	-0.14	+0.05	-0.32	+0.11	-0.00	+0.02	-0.35	+0.09	-0.26	+0.20	-0.00	+0.00	-0.00	+0.00	-1.47	+0.38	-0.00	+0.00
MEC ν init. np frac.	-0.14	+0.05	-0.15	+0.05	-0.00	+0.00	-0.00	+0.00	-0.15	+0.05	-0.07	+0.02	-0.01	+0.00	-0.00	+0.00	-0.12	+0.04	-0.00	+0.00	-0.00	+0.00
MEC $\bar{\nu}$ init. np frac.	-0.00	+0.03	-0.00	+0.03	-0.06	+0.02	-0.14	+0.05	-0.00	+0.03	-0.01	+0.04	-0.05	+0.02	-0.00	+0.00	-0.00	+0.00	-0.67	+0.22	-0.00	+0.00
XSecs PC00	-0.10	+0.10	-0.00	+0.00	-3.31	+3.31	-7.54	+7.54	-0.00	+0.00	-0.09	+0.09	-0.06	+0.06	-12.00	+12.00	-0.00	+0.00	-0.04	+0.04	-0.00	+0.00
XSecs PC01	-0.10	+0.10	-0.11	+0.12	-0.51	+0.51	-1.17	+1.17	-0.11	+0.11	-0.20	+0.20	-0.06	+0.06	-1.83	+1.83	-0.00	+0.00	-0.08	+0.08	-0.00	+0.00
XSecs PC02	-1.65	+1.99	-1.71	+2.05	-0.23	+0.23	-0.53	+0.53	-1.65	+1.97	-2.87	+3.69	-1.14	+1.14	-0.18	+0.18	-0.00	+0.00	-1.25	+1.25	-0.00	+0.00
XSecs PC03	-0.39	+0.41	-0.39	+0.42	-0.26	+0.26	-0.58	+0.58	-0.38	+0.40	-0.65	+0.71	-0.47	+0.47	-1.20	+1.20	-0.00	+0.00	-0.49	+0.49	-0.00	+0.00
XSecs PC04	-0.38	+0.39	-0.40	+0.42	-0.39	+0.39	-0.88	+0.88	-0.40	+0.41	-0.46	+0.48	-0.39	+0.39	-1.19	+1.19	-0.00	+0.00	-0.39	+0.39	-0.00	+0.00
XSecs PC05	-0.15	+0.15	-0.16	+0.16	-0.11	+0.11	-0.25	+0.25	-0.16	+0.16	-0.21	+0.21	-0.14	+0.14	-0.31	+0.31	-0.00	+0.00	-0.15	+0.15	-0.00	+0.00
XSecs PC06	-0.25	+0.26	-0.25	+0.26	-0.13	+0.13	-0.30	+0.30	-0.25	+0.26	-0.30	+0.30	-0.25	+0.25	-0.60	+0.60	-0.00	+0.00	-0.20	+0.20	-0.00	+0.00
XSecs PC07	-0.07	+0.07	-0.08	+0.08	-0.39	+0.39	-0.90	+0.90	-0.08	+0.08	-0.11	+0.11	-0.11	+0.11	-1.37	+1.37	-0.00	+0.00	-0.11	+0.11	-0.00	+0.00
XSecs PC08	-0.25	+0.26	-0.26	+0.26	-0.06	+0.06	-0.13	+0.13	-0.26	+0.27	-0.17	+0.17	-0.22	+0.22	-0.32	+0.32	-0.00	+0.00	-0.20	+0.20	-0.00	+0.00
XSecs PC09	-0.14	+0.14	-0.15	+0.15	-0.04	+0.04	-0.10	+0.10	-0.15	+0.15	-0.13	+0.13	-0.15	+0.15	-0.24	+0.24	-0.00	+0.00	-0.13	+0.13	-0.00	+0.00
XSecs PC10	-0.19	+0.19	-0.19	+0.19	-0.01	+0.01	-0.03	+0.03	-0.19	+0.19	-0.27	+0.27	-0.08	+0.08	-0.09	+0.09	-0.00	+0.00	-0.08	+0.08	-0.00	+0.00
XSecs PC11	-0.00	+0.00	-0.00	+0.00	-0.10	+0.10	-0.22	+0.22	-0.00	+0.00	-0.06	+0.06	-0.04	+0.04	-0.38	+0.38	-0.00	+0.00	-0.06	+0.06	-0.00	+0.00
ν_e scale	-0.15	+0.15	-0.00	+0.00	-5.27	+5.27	-12.00	+12.00	-0.00	+0.00	-0.00	+0.00	-31.07	+31.07	-0.00	+0.00	-0.00	+0.00	-36.88	+36.88	-0.00	+0.00
Flux PC00	-0.05	+0.05	-0.03	+0.03	-0.68	+0.67	-1.54	+1.53	-0.05	+0.05	-1.73	+1.67	-1.95	+1.95	-1.25	+1.25	-1.38	+1.37	-2.17	+2.16	-0.00	+0.00
Flux PC01	-0.15	+0.14	-0.20	+0.19	-1.52	+1.50	-3.47	+3.42	-0.35	+0.36	-3.08	+2.74	-3.44	+3.37	-3.34	+3.32	-3.83	+3.75	-3.87	+3.77	-0.00	+0.00
Flux PC02	-0.35	+0.34	-0.34	+0.32	-0.87	+0.84	-1.98	+1.91	-0.30	+0.28	-1.19	+1.09	-2.34	+2.22	-1.86	+1.82	-1.51	+1.41	-2.14	+1.99	-0.00	+0.00
Flux PC03	-0.16	+0.15	-0.09	+0.08	-2.34	+2.33	-5.34	+5.32	-0.04	+0.05	-0.99	+0.76	-5.53	+5.50	-5.20	+5.19	-5.43	+5.40	-5.62	+5.57	-0.00	+0.00
Flux PC04	-0.22	+0.22	-0.22	+0.22	-0.09	+0.09	-0.21	+0.21	-0.22	+0.22	-0.35	+0.35	-0.53	+0.53	-0.02	+0.02	-0.19	+0.19	-0.59	+0.59	-0.00	+0.00
Absolute calib.	-5.77	+7.08	-5.92	+7.25	-0.91	+1.41	-2.07	+3.22	-5.87	+7.13	-6.87	+9.52	-0.37	+0.90	-3.77	+5.22	-5.29	+2.69	-0.29	+1.43	-0.00	+0.00
ND/FD relative calib.	-4.08	+4.45	-4.21	+4.60	-0.52	+0.64	-1.18	+1.46	-4.14	+4.50	-5.58	+6.38	-0.25	+0.38	-2.07	+2.43	-2.31	+1.67	-0.29	+0.57	-0.00	+0.00
Calibration shape	-1.31	+1.31	-1.33	+1.33	-0.55	+0.55	-1.26	+1.26	-1.43	+1.43	-0.50	+0.50	-0.33	+0.33	-1.79	+1.79	-0.84	+0.84	-0.56	+0.56	-0.00	+0.00
Calibration drift	-0.00	+0.42	-0.00	+0.44	-0.29	+0.00	-0.65	+0.00	-0.00	+0.36	-0.00	+1.88	-1.28	+0.00	-0.00	+0.37	-30.42	+0.00	-0.00	+0.07	-0.00	+0.00
Light level FD	-0.00	+1.30	-0.00	+1.35	-0.36	+0.03	-0.81	+0.06	-0.00	+1.39	-1.46	+0.52	-0.00	+1.84	-1.08	+0.00	-22.15	+0.00	-0.00	+1.38	-0.00	+0.00
Light level ND	-0.97	+1.15	-1.00	+1.18	-0.00	+0.00	-0.00	+0.00	-1.02	+1.16	-0.69	+1.69	-0.00	+0.00	-0.00	+0.00	-0.00	+0.00	-0.00	+0.00	-0.00	+0.00
Cherenkov	-0.00	+2.68	-0.00	+2.74	-0.00	+0.77	-0.00	+1.75	-0.00	+2.59	-0.00	+5.61	-0.93	+0.00	-0.00	+3.79	-15.65	+0.00	-0.65	+0.00	-0.00	+0.00
E_μ ND uncorr.	-0.23	+0.23	-0.24	+0.24	-0.00	+0.00	-0.00	+0.00	-0.24	+0.23	-0.25	+0.27	-0.00	+0.00	-0.00	+0.00	-0.00	+0.00	-0.00	+0.00	-0.00	+0.00
E_μ μ-catcher uncorr.	-0.09	+0.12	-0.09	+0.12	-0.00	+0.00	-0.00	+0.00	-0.09	+0.11	-0.28	+0.31	-0.00	+0.00	-0.00	+0.00	-0.00	+0.00	-0.00	+0.00	-0.00	+0.00
E_μ n pile-up	-0.62	+0.00	-0.64	+0.00	-0.00	+0.00	-0.00	+0.00	-0.63	+0.00	-0.86	+0.00	-0.00	+0.00	-0.00	+0.00	-0.00	+0.00	-0.00	+0.00	-0.00	+0.00
E_μ correlated	-1.65	+1.70	-1.71	+1.75	-0.27	+0.35	-0.61	+0.79	-1.65	+1.70	-2.91	+2.72	-0.27	+1.18	-1.32	+1.38	-1.71	+1.47	-0.31	+0.34	-0.00	+0.00
E_μ FD uncorr.	-0.06	+0.06	-0.06	+0.06	-0.00	+0.04	-0.00	+0.08	-0.05	+0.05	-0.22	+0.33	-0.17	+0.31	-0.06	+0.23	-0.52	+0.10	-0.18	+0.10	-0.00	+0.00
Lepton angle xz ND	-0.50	+0.55	-0.52	+0.57	-0.00	+0.00	-0.00	+0.00	-0.52	+0.56	-0.57	+0.72	-0.00	+0.00	-0.00	+0.00	-0.00	+0.00	-0.00	+0.00	-0.00	+0.00
Lepton angle yz ND	-0.08	+0.02	-0.08	+0.02	-0.00	+0.00	-0.00	+0.00	-0.08	+0.02	-0.09	+0.02	-0.00	+0.00	-0.00	+0.00	-0.00	+0.00	-0.00	+0.00	-0.00	+0.00
Lepton angle xz FD	-0.00	+0.00	-0.00	+0.00	-0.00	+0.00	-0.00	+0.00	-0.00	+0.00	-0.00	+0.00	-0.00	+0.00	-0.00	+0.00	-0.00	+0.00	-0.00	+0.00	-0.00	+0.00
Lepton angle yz FD	-0.00	+0.00	-0.00	+0.00	-0.00	+0.00	-0.00	+0.00	-0.00	+0.00	-0.00	+0.00	-0.00	+0.00	-0.00	+0.00	-0.00	+0.00	-0.00	+0.00	-0.00	+0.00
Neutron systematic	-2.48	+1.93	-2.56	+1.99	-0.00	+0.12	-0.00	+0.28	-2.65	+2.05	-0.71	+0.74	-1.01	+2.42	-1.10	+0.91	-0.61	+2.13	-0.95	+1.77	-0.00	+0.00
Normalization beam corr.	-0.79	+0.79	-0.80	+0.80	-0.36	+0.36	-0.81	+0.81	-0.80	+0.80	-0.78	+0.78	-0.85	+0.85	-0.79	+0.79	-0.88	+0.88	-0.86	+0.86	-0.00	+0.00
Normalization ν-beam	-0.57	+0.57	-0.58	+0.58	-0.26	+0.26	-0.58	+0.58	-0.58	+0.58	-0.56	+0.56	-0.61	+0.61	-0.57	+0.57	-0.63	+0.63	-0.62	+0.62	-0.00	+0.00
Cosmic scale	-0.59	+0.90	-0.00	+0.00	-20.78	+31.42	-0.00	+0.00	-0.00	+0.00	-0.00	+0.00	-0.00	+0.00	-0.00	+0.00	-0.00	+0.00	-0.00	+0.00	-37.04	+56.00
Quadrature	-9.04	+10.32	-9.26	+10.53	-22.44	+32.78	-19.30	+21.28	-9.30	+10.36	-11.42	+16.10	-37.07	+39.23	-19.67	+22.80	-44.37	+17.86	-42.41	+45.82	-37.04	+56.00

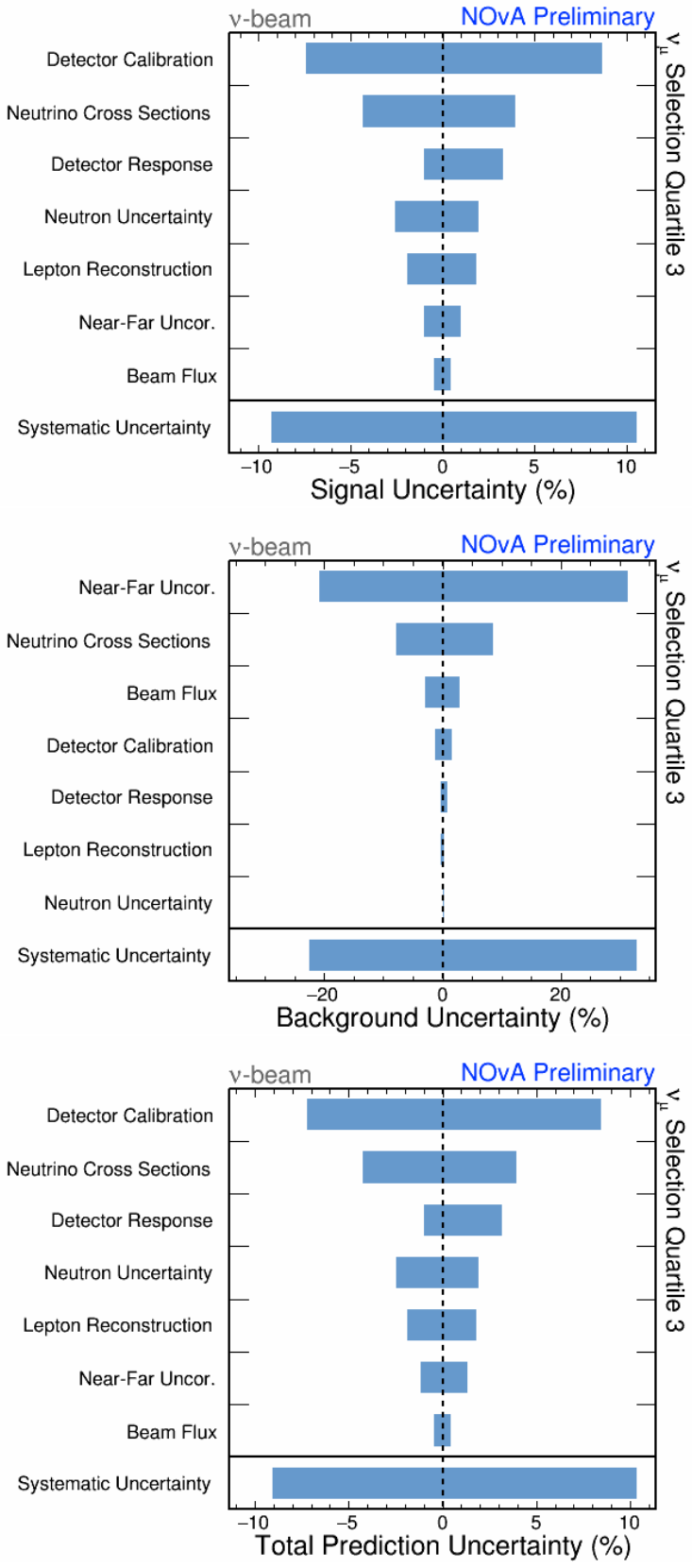

Figure C.6: Relative 1σ systematic uncertainties on the integral number of signal (top), background (middle), and total (bottom) predicted events in the ν_μ disapp. ν-beam quartile 3.

ν_μ E_{had} fraction quartile 4

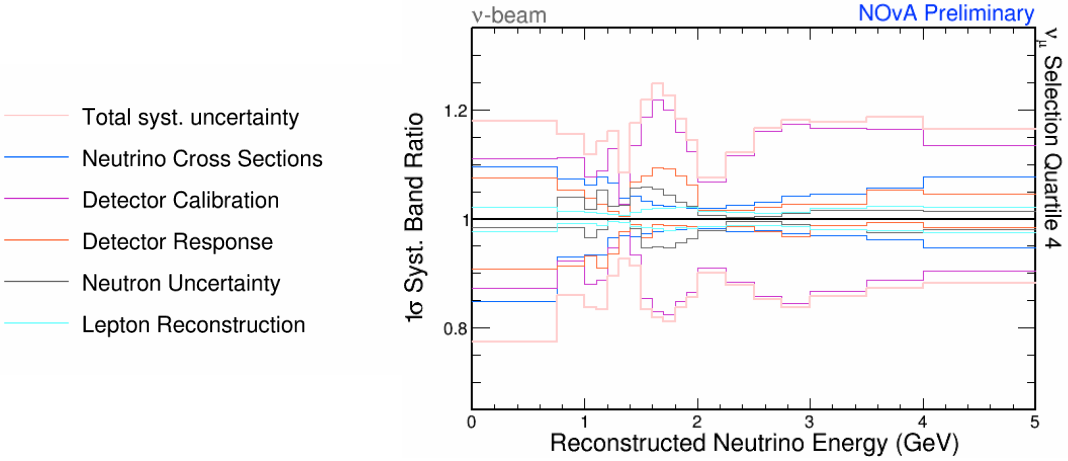

Figure C.7: 1σ systematic bands relative to the nominal prediction for the ν-beam ν_μ disapp. quartile 4 in the reconstructed neutrino energy.

Table C.4: Relative 1σ systematic uncertainties on the integral numbers of predicted events for the ν_μ disapp. ν-beam quartile 4.

Systematic Summary for fhc NuMu Quartile 4 (%)

Systematic	Total pred		Signal		Total bkg		Beam bkg		ν_μ signal		$\bar{\nu}_\mu$ signal		ν_μ app.		NC		ν_e CC		ν_τ CC		Cosmics	
CCQE z-exp.ax.vec. 1	-0.00	+0.00	-0.00	+0.00	-0.02	+0.02	-0.05	+0.06	-0.00	+0.00	-0.10	+0.09	-0.49	+0.52	-0.00	+0.00	-0.08	+0.09	-0.46	+0.49	-0.00	+0.00
CCQE z-exp.ax.vec. 2	-0.00	+0.00	-0.00	+0.00	-0.01	+0.02	-0.04	+0.04	-0.00	+0.00	-0.07	+0.07	-0.34	+0.37	-0.00	+0.00	-0.03	+0.04	-0.32	+0.36	-0.00	+0.00
CCQE z-exp.ax.vec. 3	-0.13	+0.16	-0.14	+0.16	-0.08	+0.09	-0.19	+0.23	-0.15	+0.17	-0.20	+0.24	-1.73	+2.02	-0.00	+0.00	-0.45	+0.53	-1.39	+1.71	-0.00	+0.00
CCQE z-exp.ax.vec. 4	-0.04	+0.05	-0.05	+0.05	-0.02	+0.02	-0.06	+0.06	-0.05	+0.05	-0.06	+0.06	-0.50	+0.53	-0.00	+0.00	-0.14	+0.15	-0.40	+0.44	-0.00	+0.00
M_A^{CCRES}	-0.37	+1.51	-0.31	+1.52	-1.00	+1.40	-2.50	+3.50	-0.38	+1.36	-0.00	+7.72	-17.27	+24.19	-0.00	+0.00	-11.53	+14.15	-16.00	+25.12	-0.00	+0.00
M_A^{CCRES}	-0.00	+0.44	-0.00	+0.39	-0.71	+1.00	-1.79	+2.51	-0.00	+0.40	-0.02	+4.58	-12.38	+17.47	-0.00	+0.00	-8.73	+11.37	-10.83	+16.31	-0.00	+0.00
M_A^{NCRES}	-0.27	+0.41	-0.14	+0.08	-4.13	+6.30	-10.35	+15.79	-0.14	+0.08	-0.11	+0.06	-0.00	+0.00	-12.50	+19.07	-0.00	+0.00	-0.00	+0.00	-0.00	+0.00
M_A^{NCRES}	-0.09	+0.12	-0.04	+0.03	-1.37	+1.86	-3.43	+4.65	-0.04	+0.03	-0.03	+0.02	-0.00	+0.00	-4.14	+5.62	-0.00	+0.00	-0.00	+0.00	-0.00	+0.00
CCQE z-exp.norm.	-0.10	+0.13	-0.10	+0.14	-0.08	+0.11	-0.20	+0.27	-0.11	+0.14	-0.14	+0.11	-1.99	+2.65	-0.00	+0.00	-0.17	+0.23	-1.82	+2.42	-0.00	+0.00
RPA high Q^2 enh.	-0.00	+0.04	-0.00	+0.05	-0.00	+0.02	-0.02	+0.04	-0.00	+0.05	-0.11	+0.08	-0.19	+0.32	-0.00	+0.00	-0.04	+0.15	-0.13	+0.22	-0.00	+0.00
RPA low Q^2 supp.	-0.00	+0.00	-0.00	+0.00	-0.00	+0.00	-0.00	+0.00	-0.00	+0.00	-0.04	+0.04	-0.02	+0.02	-0.00	+0.00	-0.01	+0.01	-0.02	+0.02	-0.00	+0.00
RES low Q^2 supp.	-0.00	+0.09	-0.00	+0.10	-0.08	+0.00	-0.20	+0.00	-0.00	+0.10	-0.00	+0.30	-0.27	+0.00	-0.18	+0.00	-0.38	+0.00	-0.18	+0.00	-0.00	+0.00
DIS CC $\nu n \to 1\pi$	-0.80	+0.74	-0.83	+0.77	-0.41	+0.41	-1.03	+1.03	-0.97	+0.89	-4.20	+4.68	-4.39	+4.39	-0.00	+0.00	-8.00	+8.00	-4.69	+4.69	-0.00	+0.00
FSI π free path	-0.88	+0.55	-0.82	+0.50	-1.61	+1.06	-4.02	+2.65	-0.82	+0.51	-0.85	+0.00	-0.37	+0.86	-4.33	+2.88	-7.17	+4.11	-0.18	+0.49	-0.00	+0.00
FSI fate fraction	-0.37	+0.29	-0.40	+0.33	-0.19	+0.00	-0.47	+0.00	-0.40	+0.32	-0.47	+0.68	-0.63	+0.20	-0.41	+0.00	-1.12	+0.00	-0.43	+0.10	-0.00	+0.00
MEC E_ν shape	-0.12	+0.24	-0.13	+0.26	-0.01	+0.01	-0.03	+0.03	-0.14	+0.28	-0.66	+0.37	-0.24	+0.21	-0.00	+0.00	-0.00	+0.00	-0.36	+0.35	-0.00	+0.00
MEC $E_{\bar{\nu}}$ shape	-0.00	+0.01	-0.00	+0.02	-0.00	+0.00	-0.00	+0.00	-0.02	+0.01	-0.61	+1.56	-0.00	+0.00	-0.00	+0.00	-0.00	+0.00	-0.05	+0.00	-0.00	+0.00
MEC ν (q_0, q) response	-0.23	+0.00	-0.26	+0.00	-0.04	+0.02	-0.09	+0.06	-0.25	+0.00	-0.44	+0.57	-0.57	+1.07	-0.00	+0.00	-0.00	+0.00	-1.27	+0.14	-0.00	+0.00
MEC $\bar{\nu}$ (q_0, q) response	-0.02	+0.00	-0.02	+0.00	-0.00	+0.02	-0.00	+0.04	-0.00	+0.02	-0.96	+0.00	-0.00	+0.02	-0.00	+0.00	-0.00	+0.00	-0.00	+0.82	-0.00	+0.00
MEC ν init. np frac.	-0.00	+0.00	-0.00	+0.00	-0.00	+0.00	-0.00	+0.02	-0.00	+0.00	-0.08	+0.03	-0.03	+0.08	-0.00	+0.00	-0.00	+0.00	-0.10	+0.29	-0.00	+0.00
MEC $\bar{\nu}$ init. np frac.	-0.01	+0.00	-0.02	+0.00	-0.00	+0.00	-0.02	+0.00	-0.00	+0.00	-0.96	+0.32	-0.06	+0.02	-0.00	+0.00	-0.00	+0.00	-0.38	+0.13	-0.00	+0.00
XSecs PC00	-0.25	+0.25	-0.10	+0.10	-4.01	+4.01	-10.04	+10.04	-0.10	+0.10	-0.06	+0.06	-0.06	+0.06	-12.12	+12.12	-0.00	+0.00	-0.05	+0.05	-0.00	+0.00
XSecs PC01	-0.06	+0.06	-0.12	+0.12	-0.61	+0.61	-1.52	+1.52	-0.12	+0.12	-0.20	+0.20	-0.08	+0.08	-1.83	+1.83	-0.00	+0.00	-0.09	+0.09	-0.00	+0.00
XSecs PC02	-1.41	+1.74	-1.55	+1.92	-0.13	+0.13	-0.32	+0.32	-1.53	+1.88	-2.59	+3.36	-1.41	+1.41	-0.21	+0.21	-0.00	+0.00	-1.49	+1.49	-0.00	+0.00
XSecs PC03	-0.32	+0.34	-0.31	+0.33	-0.44	+0.44	-1.09	+1.09	-0.30	+0.32	-0.53	+0.58	-0.58	+0.58	-1.39	+1.39	-0.00	+0.00	-0.58	+0.58	-0.00	+0.00
XSecs PC04	-0.28	+0.29	-0.35	+0.36	-0.48	+0.48	-1.20	+1.20	-0.35	+0.36	-0.42	+0.43	-0.48	+0.48	-1.39	+1.39	-0.00	+0.00	-0.47	+0.47	-0.00	+0.00
XSecs PC05	-0.12	+0.12	-0.14	+0.15	-0.12	+0.12	-0.30	+0.30	-0.14	+0.14	-0.20	+0.21	-0.18	+0.18	-0.34	+0.34	-0.00	+0.00	-0.18	+0.18	-0.00	+0.00
XSecs PC06	-0.21	+0.22	-0.21	+0.21	-0.23	+0.23	-0.58	+0.58	-0.21	+0.21	-0.27	+0.27	-0.31	+0.31	-0.73	+0.73	-0.00	+0.00	-0.24	+0.24	-0.00	+0.00
XSecs PC07	-0.00	+0.01	-0.06	+0.06	-0.55	+0.55	-1.37	+1.37	-0.06	+0.06	-0.10	+0.10	-0.14	+0.14	-1.64	+1.64	-0.00	+0.00	-0.13	+0.13	-0.00	+0.00
XSecs PC08	-0.20	+0.20	-0.20	+0.21	-0.15	+0.15	-0.38	+0.38	-0.21	+0.21	-0.12	+0.13	-0.26	+0.26	-0.49	+0.49	-0.00	+0.00	-0.23	+0.23	-0.00	+0.00
XSecs PC09	-0.15	+0.15	-0.15	+0.15	-0.08	+0.08	-0.20	+0.20	-0.15	+0.15	-0.16	+0.16	-0.18	+0.18	-0.27	+0.27	-0.00	+0.00	-0.16	+0.16	-0.00	+0.00
XSecs PC10	-0.17	+0.18	-0.19	+0.19	-0.02	+0.02	-0.06	+0.06	-0.19	+0.19	-0.26	+0.26	-0.11	+0.11	-0.08	+0.08	-0.00	+0.00	-0.10	+0.10	-0.00	+0.00
XSecs PC11	-0.00	+0.00	-0.00	+0.00	-0.16	+0.16	-0.41	+0.41	-0.00	+0.00	-0.05	+0.05	-0.05	+0.05	-0.50	+0.50	-0.00	+0.00	-0.07	+0.07	-0.00	+0.00
ν_τ scale	-0.11	+0.11	-0.00	+0.00	-1.36	+1.36	-3.40	+3.40	-0.00	+0.00	-0.00	+0.00	-30.71	+30.71	-0.00	+0.00	-0.00	+0.00	-36.13	+36.13	-0.00	+0.00
Flux PC00	-0.07	+0.06	-0.02	+0.02	-0.56	+0.56	-1.41	+1.40	-0.02	+0.02	-1.70	+1.65	-2.01	+2.00	-1.35	+1.35	-1.06	+1.05	-2.21	+2.20	-0.00	+0.00
Flux PC01	-0.09	+0.09	-0.23	+0.22	-1.39	+1.38	-3.48	+3.45	-0.31	+0.31	-3.05	+2.75	-3.60	+3.52	-3.44	+3.42	-3.42	+3.37	-3.98	+3.87	-0.00	+0.00
Flux PC02	-0.36	+0.35	-0.33	+0.31	-0.75	+0.73	-1.87	+1.82	-0.31	+0.29	-1.05	+0.95	-2.15	+2.02	-1.87	+1.83	-1.65	+1.60	-1.94	+1.78	-0.00	+0.00
Flux PC03	-0.26	+0.26	-0.09	+0.09	-2.13	+2.12	-5.32	+5.31	-0.07	+0.07	-1.00	+0.77	-5.51	+5.48	-5.31	+5.30	-5.17	+5.16	-5.58	+5.53	-0.00	+0.00
Flux PC04	-0.22	+0.22	-0.24	+0.24	-0.05	+0.05	-0.12	+0.12	-0.23	+0.23	-0.32	+0.32	-0.54	+0.54	-0.10	+0.10	-0.32	+0.32	-0.61	+0.60	-0.00	+0.00
Absolute calib.	-5.28	+6.11	-5.66	+6.59	-1.17	+0.94	-2.92	+2.36	-5.64	+6.50	-6.73	+9.81	-2.94	+0.59	-2.77	+2.83	-10.31	+4.48	-2.89	+1.49	-0.00	+0.00
ND/FD relative calib.	-4.93	+5.32	-5.43	+5.87	-0.55	+0.50	-1.39	+1.25	-5.39	+5.81	-6.93	+8.21	-1.18	+0.59	-1.39	+1.41	-4.43	+2.97	-1.27	+0.92	-0.00	+0.00
Calibration shape	-2.41	+2.41	-2.65	+2.65	-0.12	+0.12	-0.29	+0.29	-2.60	+2.60	-4.29	+4.29	-0.24	+0.24	-0.27	+0.27	-1.12	+1.12	-0.06	+0.06	-0.00	+0.00
Calibration drift	-0.00	+0.29	-0.00	+0.33	-0.22	+0.00	-0.54	+0.00	-0.00	+0.22	-0.00	+4.89	-0.67	+0.00	-0.29	+0.00	-3.31	+0.00	-0.67	+0.00	-0.00	+0.00
Light level FD	-1.27	+0.22	-1.36	+0.27	-0.38	+0.00	-0.94	+0.00	-1.40	+0.26	-0.06	+0.65	-1.74	+0.25	-1.05	+0.00	-2.57	+1.11	-1.28	+0.00	-0.00	+0.00
Light level ND	-0.45	+1.71	-0.49	+1.87	-0.00	+0.00	-0.00	+0.00	-0.54	+1.85	-0.00	+2.54	-0.00	+0.00	-0.00	+0.00	-0.00	+0.00	-0.00	+0.00	-0.00	+0.00
Cherenkov	-0.00	+1.94	-0.00	+2.06	-0.00	+0.66	-0.00	+1.66	-0.00	+2.00	-0.00	+4.47	-1.07	+0.00	-0.00	+1.90	-0.00	+3.54	-2.05	+0.00	-0.00	+0.00
E_μ ND uncorr.	-0.11	+0.11	-0.12	+0.12	-0.00	+0.00	-0.00	+0.00	-0.12	+0.12	-0.14	+0.11	-0.00	+0.00	-0.00	+0.00	-0.00	+0.00	-0.00	+0.00	-0.00	+0.00
E_μ μ-catcher uncorr.	-0.00	+0.00	-0.01	+0.00	-0.00	+0.00	-0.00	+0.00	-0.01	+0.00	-0.02	+0.00	-0.00	+0.00	-0.00	+0.00	-0.00	+0.00	-0.00	+0.00	-0.00	+0.00
E_μ n pile-up	-0.24	+0.00	-0.26	+0.00	-0.00	+0.00	-0.00	+0.00	-0.26	+0.00	-0.21	+0.00	-0.00	+0.00	-0.00	+0.00	-0.00	+0.00	-0.00	+0.00	-0.00	+0.00
E_μ correlated	-1.40	+1.46	-1.51	+1.57	-0.23	+0.21	-0.57	+0.54	-1.50	+1.56	-1.96	+2.29	-1.20	+1.03	-0.53	+0.52	-0.17	+0.19	-1.21	+0.82	-0.00	+0.00
E_μ FD uncorr.	-0.16	+0.16	-0.17	+0.17	-0.04	+0.04	-0.10	+0.09	-0.17	+0.17	-0.24	+0.09	-0.22	+0.23	-0.10	+0.08	-0.01	+0.05	-0.23	+0.16	-0.00	+0.00
Lepton angle xz ND	-0.23	+0.20	-0.25	+0.21	-0.00	+0.00	-0.00	+0.00	-0.25	+0.21	-0.25	+0.22	-0.00	+0.00	-0.00	+0.00	-0.00	+0.00	-0.00	+0.00	-0.00	+0.00
Lepton angle yz ND	-0.05	+0.00	-0.06	+0.00	-0.00	+0.00	-0.00	+0.00	-0.06	+0.00	-0.07	+0.00	-0.00	+0.00	-0.00	+0.00	-0.00	+0.00	-0.00	+0.00	-0.00	+0.00
Lepton angle xz FD	-0.00	+0.00	-0.00	+0.00	-0.00	+0.00	-0.00	+0.00	-0.00	+0.00	-0.00	+0.04	-0.00	+0.00	-0.00	+0.00	-0.00	+0.00	-0.00	+0.00	-0.00	+0.00
Lepton angle yz FD	-0.00	+0.00	-0.00	+0.00	-0.00	+0.00	-0.00	+0.00	-0.00	+0.00	-0.00	+0.03	-0.00	+0.00	-0.00	+0.00	-0.00	+0.00	-0.00	+0.00	-0.00	+0.00
Neutron systematic	-1.73	+1.32	-1.92	+1.47	-0.36	+0.33	-0.90	+0.82	-1.96	+1.47	-0.40	+1.52	-1.70	+1.60	-0.86	+0.79	-0.35	+0.19	-1.55	+1.46	-0.00	+0.00
Normalization beam corr.	-0.73	+0.73	-0.77	+0.77	-0.32	+0.32	-0.81	+0.81	-0.77	+0.77	-0.73	+0.73	-0.86	+0.86	-0.80	+0.80	-0.83	+0.83	-0.87	+0.87	-0.00	+0.00
Normalization ν-beam	-0.52	+0.52	-0.55	+0.55	-0.23	+0.23	-0.58	+0.58	-0.55	+0.55	-0.52	+0.52	-0.62	+0.62	-0.58	+0.58	-0.59	+0.59	-0.62	+0.62	-0.00	+0.00
Cosmic scale	-1.13	+1.36	-0.00	+0.00	-13.39	+16.08	-0.00	+0.00	-0.00	+0.00	-0.00	+0.00	-0.00	+0.00	-0.00	+0.00	-0.00	+0.00	-0.00	+0.00	-22.29	+26.77
Quadrature	-8.46	+9.61	-9.08	+10.30	-15.21	+18.28	-18.05	+21.80	-9.06	+10.17	-12.65	+19.27	-38.70	+43.88	-20.22	+24.94	-22.68	+22.31	-42.29	+47.95	-22.29	+26.77

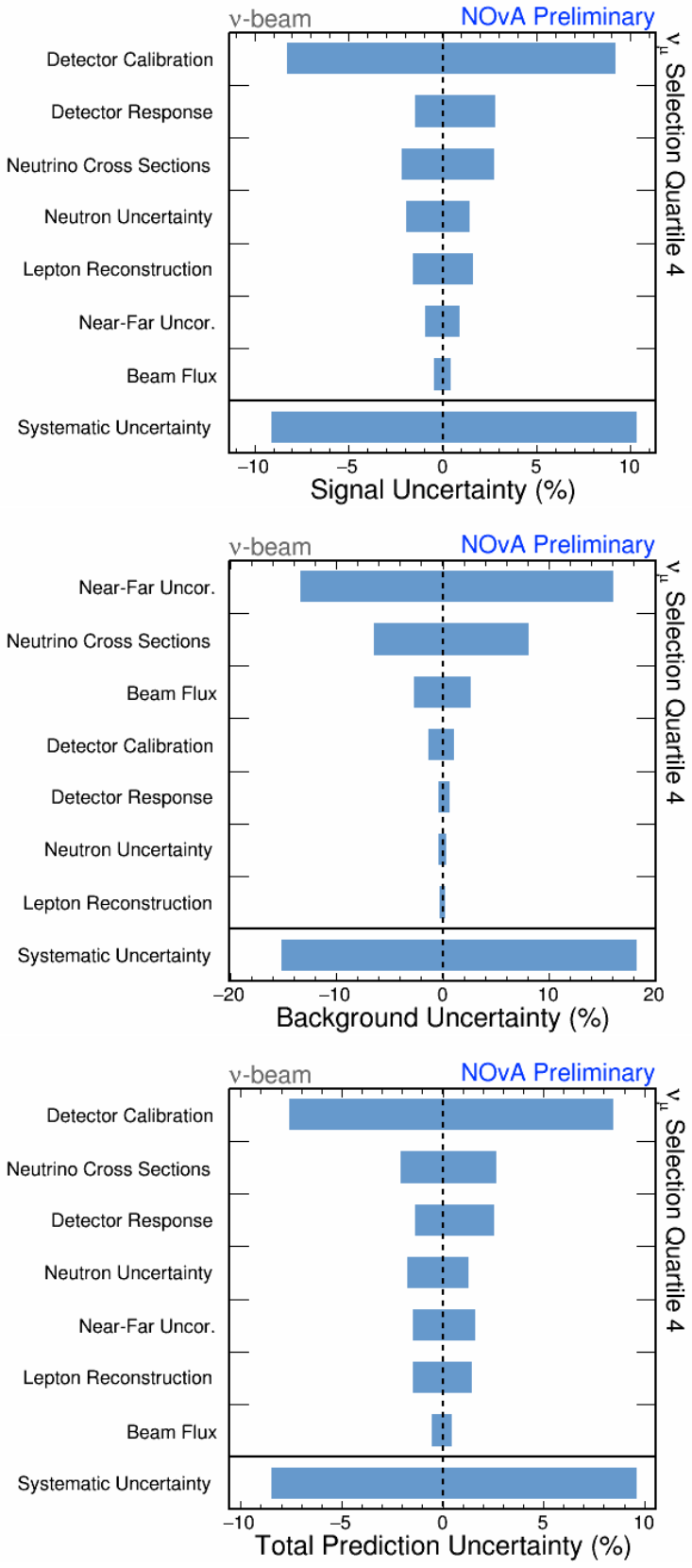

Figure C.8: Relative 1σ systematic uncertainties on the integral number of signal (top), background (middle), and total (bottom) predicted events in the ν_μ disapp. ν-beam quartile 4.

Summed all ν_μ quartiles

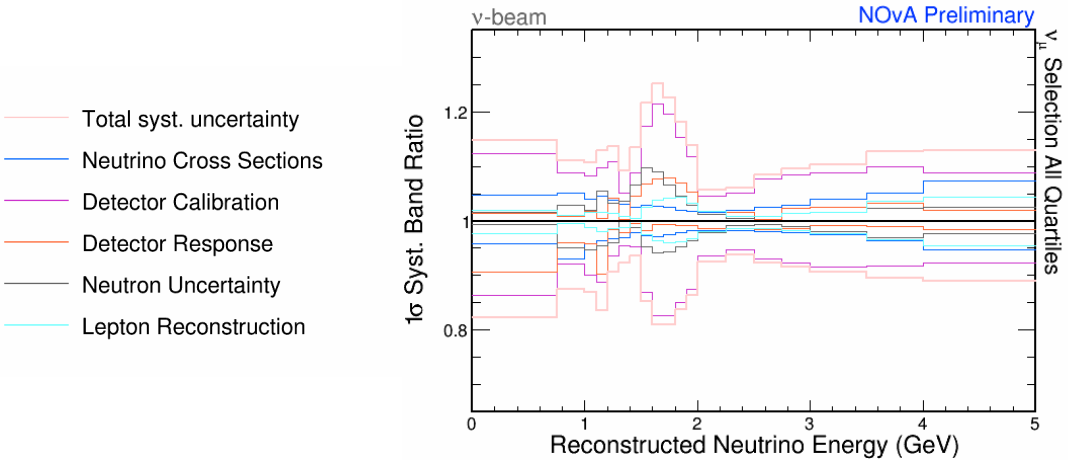

Figure C.9: 1σ systematic bands relative to the nominal prediction for the ν-beam ν_μ disapp. all quartiles in the reconstructed neutrino energy.

Table C.5: Relative 1σ systematic uncertainties on the integral numbers of predicted events for the ν_μ disapp. ν-beam all quartiles.

Systematic summary for ν_μ disappearance ν-beam all quartiles (%)

Systematic	Total pred		Signal		Total bkg		Beam bkg		ν_μ signal		$\bar{\nu}_\mu$ signal		ν_μ app.		NC		ν_e CC		ν_τ CC		Cosmics	
CCQE z-exp.ax.vec. 1	-0.10	+0.10	-0.09	+0.10	-0.19	+0.21	-0.46	+0.49	-0.10	+0.10	-0.00	+0.04	-1.90	+2.02	-0.00	+0.00	-0.08	+0.08	-1.75	+1.87	-0.00	+0.00
CCQE z-exp.ax.vec. 2	-0.09	+0.09	-0.09	+0.09	-0.16	+0.17	-0.37	+0.40	-0.10	+0.10	-0.00	+0.02	-1.56	+1.65	-0.00	+0.00	-0.03	+0.04	-1.44	+1.53	-0.00	+0.00
CCQE z-exp.ax.vec. 3	-0.38	+0.42	-0.38	+0.43	-0.26	+0.29	-0.61	+0.69	-0.41	+0.45	-0.00	+0.07	-2.51	+2.78	-0.00	+0.00	-0.42	+0.49	-2.28	+2.57	-0.00	+0.00
CCQE z-exp.ax.vec. 4	-0.10	+0.10	-0.10	+0.10	-0.06	+0.06	-0.13	+0.14	-0.11	+0.11	-0.00	+0.00	-0.52	+0.54	-0.00	+0.00	-0.13	+0.14	-0.48	+0.50	-0.00	+0.00
M_A^{CCRES}	-0.21	+0.99	-0.17	+0.96	-1.28	+1.67	-3.01	+3.93	-0.22	+0.87	-0.00	+2.41	-9.84	+12.45	-0.00	+0.00	-11.23	+13.67	-9.91	+13.61	-0.00	+0.00
M_V^{CCRES}	-0.02	+0.41	-0.00	+0.38	-0.92	+1.25	-2.16	+2.94	-0.03	+0.36	-0.00	+0.82	-7.09	+9.52	-0.00	+0.00	-8.55	+11.08	-6.92	+9.75	-0.00	+0.00
M_A^{NCRES}	-0.11	+0.16	-0.05	+0.04	-3.68	+5.37	-8.66	+12.63	-0.05	+0.04	-0.04	+0.03	-0.00	+0.00	-12.33	+17.99	-0.00	+0.00	-0.00	+0.00	-0.00	+0.00
M_V^{NCRES}	-0.04	+0.05	-0.02	+0.01	-1.23	+1.63	-2.89	+3.84	-0.02	+0.01	-0.01	+0.00	-0.00	+0.00	-4.11	+5.47	-0.00	+0.00	-0.00	+0.00	-0.00	+0.00
CCQE z-exp.norm.	-0.43	+0.53	-0.42	+0.53	-0.51	+0.69	-1.21	+1.61	-0.43	+0.53	-0.40	+0.46	-5.01	+6.68	-0.00	+0.00	-0.16	+0.22	-4.68	+6.25	-0.00	+0.00
RPA high Q^2 enh.	-0.21	+0.28	-0.21	+0.29	-0.07	+0.09	-0.17	+0.22	-0.23	+0.31	-0.14	+0.14	-0.79	+0.99	-0.00	+0.00	-0.03	+0.14	-0.59	+0.74	-0.00	+0.00
RPA low Q^2 supp.	-0.05	+0.04	-0.05	+0.05	-0.04	+0.05	-0.10	+0.11	-0.02	+0.02	-0.53	+0.53	-0.48	+0.50	-0.00	+0.00	-0.01	+0.01	-0.34	+0.36	-0.00	+0.00
RES low Q^2 supp.	-0.00	+0.15	-0.00	+0.16	-0.16	+0.00	-0.37	+0.00	-0.00	+0.13	-0.00	+0.64	-0.61	+0.00	-0.32	+0.00	-0.36	+0.00	-0.49	+0.00	-0.00	+0.00
DIS CC $\nu n \to 1\pi$	-0.36	+0.34	-0.36	+0.34	-0.42	+0.42	-0.99	+0.99	-0.51	+0.48	-1.92	+2.05	-2.28	+2.28	-0.00	+0.00	-8.27	+8.27	-2.37	+2.37	-0.00	+0.00
FSI π free path	-0.72	+0.46	-0.69	+0.44	-1.49	+1.06	-3.50	+2.50	-0.72	+0.46	-0.32	+0.16	-0.09	+0.30	-4.63	+3.31	-6.66	+3.83	-0.06	+0.27	-0.00	+0.00
FSI fate fraction	-0.35	+0.33	-0.37	+0.35	-0.10	+0.00	-0.22	+0.00	-0.38	+0.36	-0.20	+0.23	-0.22	+0.02	-0.18	+0.00	-1.16	+0.00	-0.10	+0.03	-0.00	+0.00
MEC E_ν shape	-0.00	+0.11	-0.00	+0.12	-0.15	+0.09	-0.35	+0.21	-0.02	+0.15	-2.14	+2.37	-1.61	+0.99	-0.00	+0.00	-0.00	+0.03	-1.26	+0.74	-0.00	+0.00
MEC $E_{\bar{\nu}}$ shape	-0.04	+0.04	-0.04	+0.04	-0.01	+0.00	-0.03	+0.01	-0.10	+0.09	-2.01	+2.21	-0.05	+0.04	-0.00	+0.00	-0.00	+0.00	-0.21	+0.07	-0.00	+0.00
MEC ν (q_0, q) response	-0.70	+0.53	-0.72	+0.55	-0.24	+0.11	-0.56	+0.25	-1.01	+0.66	-1.13	+3.90	-2.57	+0.90	-0.00	+0.00	-0.02	+0.00	-1.96	+1.08	-0.00	+0.00
MEC $\bar{\nu}$ (q_0, q) response	-0.04	+0.04	-0.04	+0.04	-0.00	+0.04	-0.01	+0.10	-0.05	+0.13	-2.72	+1.45	-0.10	+0.08	-0.00	+0.00	-0.00	+0.00	-0.02	+0.63	-0.00	+0.00
MEC ν init. np frac.	-0.05	+0.02	-0.05	+0.02	-0.00	+0.00	-0.00	+0.02	-0.06	+0.02	-0.02	+0.08	-0.00	+0.00	-0.00	+0.00	-0.01	+0.00	-0.06	+0.17	-0.00	+0.00
MEC $\bar{\nu}$ init. np frac.	-0.00	+0.00	-0.00	+0.00	-0.00	+0.00	-0.02	+0.00	-0.00	+0.02	-0.35	+0.12	-0.03	+0.01	-0.00	+0.00	-0.00	+0.00	-0.09	+0.03	-0.00	+0.00
XSecs PC00	-0.13	+0.13	-0.01	+0.01	-3.62	+3.62	-8.52	+8.52	-0.02	+0.02	-0.05	+0.05	-0.05	+0.05	-12.12	+12.12	-0.00	+0.00	-0.04	+0.04	-0.00	+0.00
XSecs PC01	-0.08	+0.08	-0.11	+0.11	-0.56	+0.56	-1.31	+1.31	-0.11	+0.11	-0.16	+0.16	-0.06	+0.06	-1.84	+1.84	-0.00	+0.00	-0.07	+0.07	-0.00	+0.00
XSecs PC02	-1.44	+1.72	-1.51	+1.79	-0.18	+0.18	-0.42	+0.42	-1.46	+1.73	-2.27	+2.80	-1.08	+1.08	-0.20	+0.20	-0.00	+0.00	-1.13	+1.13	-0.00	+0.00
XSecs PC03	-0.33	+0.35	-0.33	+0.35	-0.34	+0.34	-0.81	+0.81	-0.32	+0.34	-0.53	+0.57	-0.45	+0.45	-1.31	+1.31	-0.00	+0.00	-0.44	+0.44	-0.00	+0.00
XSecs PC04	-0.33	+0.34	-0.36	+0.37	-0.43	+0.43	-1.00	+1.00	-0.36	+0.37	-0.43	+0.44	-0.37	+0.37	-1.30	+1.30	-0.00	+0.00	-0.35	+0.35	-0.00	+0.00
XSecs PC05	-0.13	+0.13	-0.14	+0.14	-0.11	+0.11	-0.26	+0.26	-0.14	+0.14	-0.17	+0.17	-0.14	+0.14	-0.32	+0.32	-0.00	+0.00	-0.14	+0.14	-0.00	+0.00
XSecs PC06	-0.21	+0.22	-0.22	+0.22	-0.18	+0.18	-0.42	+0.42	-0.21	+0.22	-0.27	+0.27	-0.24	+0.24	-0.67	+0.67	-0.00	+0.00	-0.18	+0.18	-0.00	+0.00
XSecs PC07	-0.05	+0.05	-0.07	+0.07	-0.46	+0.46	-1.09	+1.09	-0.07	+0.07	-0.10	+0.10	-0.11	+0.11	-1.52	+1.52	-0.00	+0.00	-0.10	+0.10	-0.00	+0.00
XSecs PC08	-0.21	+0.21	-0.21	+0.22	-0.10	+0.10	-0.24	+0.24	-0.22	+0.22	-0.16	+0.16	-0.21	+0.21	-0.41	+0.41	-0.00	+0.00	-0.18	+0.18	-0.00	+0.00
XSecs PC09	-0.13	+0.13	-0.13	+0.13	-0.06	+0.06	-0.15	+0.15	-0.13	+0.13	-0.12	+0.12	-0.15	+0.15	-0.26	+0.26	-0.00	+0.00	-0.12	+0.12	-0.00	+0.00
XSecs PC10	-0.17	+0.17	-0.18	+0.18	-0.02	+0.02	-0.04	+0.04	-0.17	+0.17	-0.23	+0.23	-0.08	+0.08	-0.09	+0.09	-0.00	+0.00	-0.08	+0.08	-0.00	+0.00
XSecs PC11	-0.01	+0.01	-0.00	+0.00	-0.13	+0.13	-0.30	+0.30	-0.00	+0.00	-0.05	+0.05	-0.04	+0.04	-0.44	+0.44	-0.00	+0.00	-0.05	+0.05	-0.00	+0.00
ν_e scale	-0.14	+0.14	-0.00	+0.00	-3.72	+3.72	-8.74	+8.74	-0.00	+0.00	-0.00	+0.00	-31.88	+31.88	-0.00	+0.00	-0.00	+0.00	-37.77	+37.77	-0.00	+0.00
Flux PC00	-0.07	+0.07	-0.05	+0.04	-0.64	+0.64	-1.51	+1.50	-0.06	+0.06	-1.74	+1.69	-2.03	+2.02	-1.31	+1.31	-1.10	+1.09	-2.25	+2.23	-0.00	+0.00
Flux PC01	-0.11	+0.09	-0.17	+0.16	-1.50	+1.48	-3.52	+3.48	-0.36	+0.37	-3.17	+2.84	-3.61	+3.53	-3.41	+3.39	-3.46	+3.41	-4.03	+3.92	-0.00	+0.00
Flux PC02	-0.31	+0.30	-0.29	+0.28	-0.83	+0.80	-1.96	+1.89	-0.25	+0.24	-0.99	+0.86	-2.36	+2.23	-1.87	+1.84	-1.66	+1.61	-2.17	+2.02	-0.00	+0.00
Flux PC03	-0.16	+0.15	-0.07	+0.06	-2.29	+2.28	-5.39	+5.37	-0.02	+0.02	-0.98	+0.73	-5.71	+5.67	-5.28	+5.27	-5.21	+5.19	-5.79	+5.74	-0.00	+0.00
Flux PC04	-0.21	+0.21	-0.21	+0.21	-0.07	+0.07	-0.17	+0.17	-0.20	+0.20	-0.37	+0.38	-0.54	+0.53	-0.07	+0.07	-0.31	+0.31	-0.59	+0.58	-0.00	+0.00
Absolute calib.	-5.07	+4.93	-5.23	+5.08	-1.15	+1.18	-2.71	+2.78	-5.29	+5.14	-4.25	+4.13	-0.68	+0.68	-3.03	+3.53	-10.05	+4.40	-0.07	+0.04	-0.00	+0.00
ND/FD relative calib.	-1.05	+1.28	-1.12	+1.35	-0.58	+0.59	-1.36	+1.38	-1.18	+1.41	-0.17	+0.45	-0.34	+0.34	-1.58	+1.70	-4.32	+2.91	-0.03	+0.02	-0.00	+0.00
Calibration shape	-0.67	+0.67	-0.70	+0.70	-0.06	+0.06	-0.14	+0.14	-0.74	+0.74	-0.09	+0.09	-0.48	+0.48	-0.16	+0.16	-1.08	+1.08	-0.20	+0.20	-0.00	+0.00
Calibration drift	-0.00	+0.19	-0.00	+0.21	-0.14	+0.00	-0.33	+0.00	-0.00	+0.15	-0.00	+1.18	-0.66	+0.00	-0.09	+0.00	-6.59	+0.00	-0.00	+0.92	-0.00	+0.00
Light level FD	-0.04	+0.13	-0.03	+0.14	-0.34	+0.00	-0.81	+0.00	-0.06	+0.21	-0.92	+0.54	-0.92	+0.00	-0.86	+0.00	-4.99	+0.00	-0.15	+0.44	-0.00	+0.00
Light level ND	-0.97	+0.37	-1.01	+0.38	-0.00	+0.00	-0.00	+0.00	-1.02	+0.40	-0.87	+0.13	-0.00	+0.00	-0.00	+0.00	-0.00	+0.00	-0.00	+0.00	-0.00	+0.00
Cherenkov	-0.00	+1.74	-0.00	+1.78	-0.00	+0.77	-0.00	+1.80	-0.00	+1.84	-0.00	+0.88	-0.00	+0.93	-0.00	+2.18	-0.00	+0.98	-0.00	+0.86	-0.00	+0.00
E_μ ND uncorr.	-0.26	+0.26	-0.27	+0.27	-0.00	+0.00	-0.00	+0.00	-0.26	+0.26	-0.42	+0.44	-0.00	+0.00	-0.00	+0.00	-0.00	+0.00	-0.00	+0.00	-0.00	+0.00
E_μ μ-catcher uncorr.	-0.22	+0.23	-0.23	+0.24	-0.00	+0.00	-0.00	+0.00	-0.20	+0.22	-0.60	+0.64	-0.00	+0.00	-0.00	+0.00	-0.00	+0.00	-0.00	+0.00	-0.00	+0.00
E_μ n pile-up	-0.73	+0.00	-0.76	+0.00	-0.00	+0.00	-0.00	+0.00	-0.72	+0.00	-1.32	+0.00	-0.00	+0.00	-0.00	+0.00	-0.00	+0.00	-0.00	+0.00	-0.00	+0.00
E_μ correlated	-1.71	+1.79	-1.78	+1.86	-0.03	+0.04	-0.08	+0.09	-1.69	+1.76	-3.19	+3.50	-0.34	+0.51	-0.04	+0.04	-0.00	+0.00	-0.12	+0.00	-0.00	+0.00
E_μ FD uncorr.	-0.03	+0.04	-0.04	+0.04	-0.00	+0.00	-0.02	+0.02	-0.03	+0.04	-0.09	+0.09	-0.09	+0.11	-0.00	+0.00	-0.00	+0.00	-0.02	+0.00	-0.00	+0.00
Lepton angle xz ND	-0.43	+0.35	-0.45	+0.37	-0.00	+0.00	-0.00	+0.00	-0.45	+0.37	-0.45	+0.36	-0.00	+0.00	-0.00	+0.00	-0.00	+0.00	-0.00	+0.00	-0.00	+0.00
Lepton angle yz ND	-0.08	+0.00	-0.09	+0.00	-0.00	+0.00	-0.00	+0.00	-0.09	+0.00	-0.11	+0.00	-0.00	+0.00	-0.00	+0.00	-0.00	+0.00	-0.00	+0.00	-0.00	+0.00
Lepton angle xz FD	-0.00	+0.00	-0.00	+0.00	-0.00	+0.00	-0.00	+0.00	-0.00	+0.00	-0.00	+0.00	-0.00	+0.00	-0.00	+0.00	-0.00	+0.00	-0.00	+0.00	-0.00	+0.00
Lepton angle yz FD	-0.00	+0.00	-0.00	+0.00	-0.00	+0.00	-0.00	+0.00	-0.00	+0.00	-0.00	+0.01	-0.00	+0.00	-0.00	+0.00	-0.00	+0.00	-0.00	+0.00	-0.00	+0.00
Neutron systematic	-1.74	+1.60	-1.80	+1.66	-0.04	+0.02	-0.08	+0.06	-1.82	+1.69	-1.53	+1.20	-0.26	+0.19	-0.05	+0.02	-0.00	+0.01	-0.12	+0.17	-0.00	+0.00
Normalization beam corr.	-0.79	+0.79	-0.81	+0.81	-0.35	+0.35	-0.82	+0.82	-0.81	+0.81	-0.79	+0.79	-0.88	+0.88	-0.80	+0.80	-0.83	+0.83	-0.87	+0.87	-0.00	+0.00
Normalization ν-beam	-0.57	+0.57	-0.58	+0.58	-0.25	+0.25	-0.59	+0.59	-0.58	+0.58	-0.57	+0.57	-0.63	+0.63	-0.58	+0.58	-0.60	+0.60	-0.63	+0.63	-0.00	+0.00
Cosmic scale	-0.64	+0.90	-0.00	+0.00	-16.52	+23.08	-0.00	+0.00	-0.00	+0.00	-0.00	+0.00	-0.00	+0.00	-0.00	+0.00	-0.00	+0.00	-0.00	+0.00	-28.72	+40.15
Quadrature	-6.39	+6.59	-6.56	+6.72	-18.21	+24.69	-18.05	+20.59	-6.65	+6.78	-8.85	+9.78	-35.74	+37.26	-20.14	+24.23	-23.39	+21.60	-40.98	+42.77	-28.72	+40.15

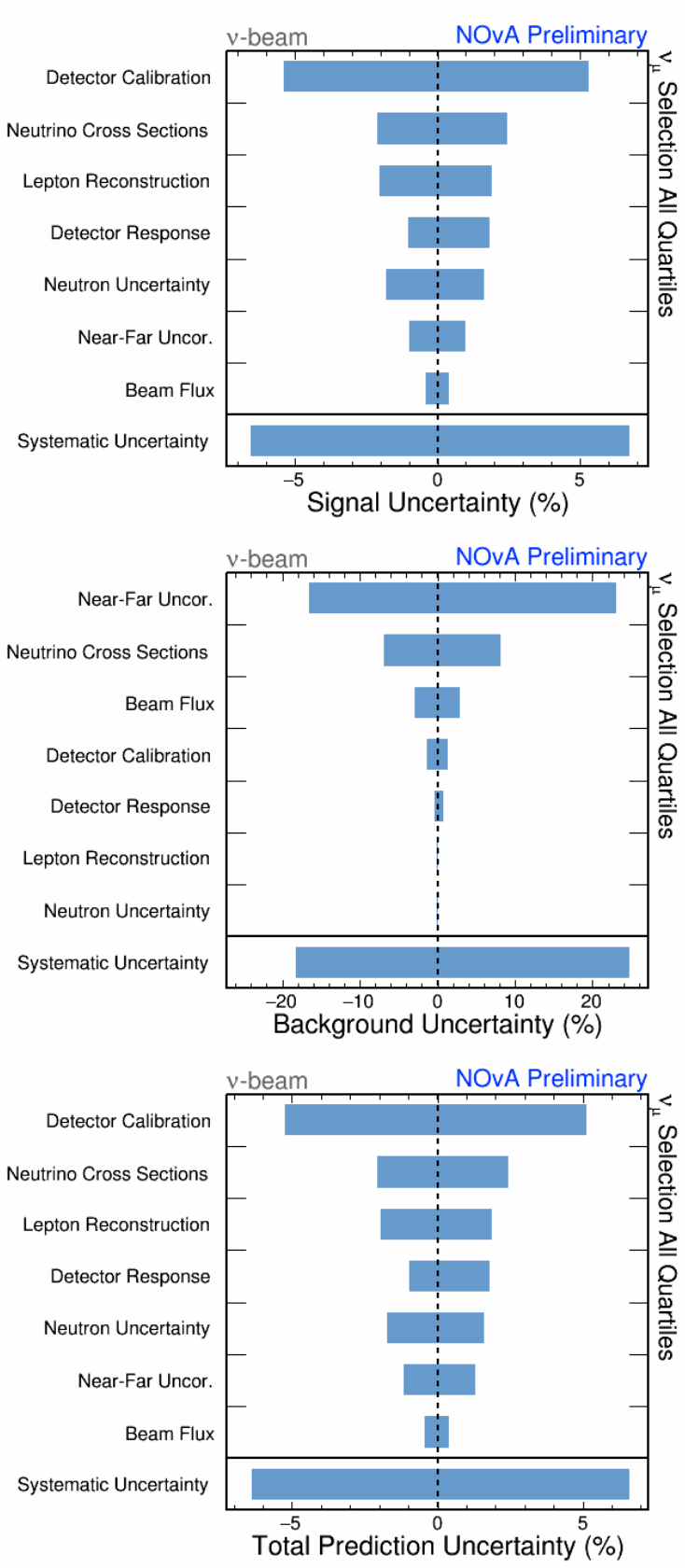

Figure C.10: Relative 1σ syst. uncertainties on the integral number of signal (top), background (middle), and total (bottom) predicted events in the ν_μ disapp. ν-beam all quartiles.

C.2 Disappearance $\bar{\nu}_\mu$ channel, $\bar{\nu}$-beam

$\bar{\nu}_\mu$ E_{had} fraction quartile 1

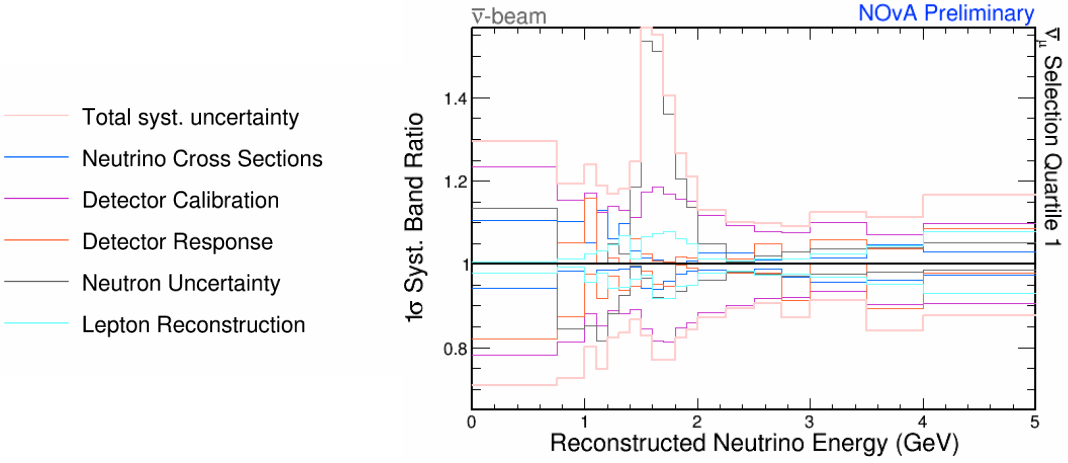

Figure C.11: 1σ systematic bands relative to the nominal prediction for the $\bar{\nu}$-beam $\bar{\nu}_\mu$ disapp. quartile 1 in the reconstructed neutrino energy.

Table C.6: Relative 1σ systematic uncertainties on the integral numbers of predicted events for the $\bar{\nu}_\mu$ disapp. $\bar{\nu}$-beam quartile 1.

Systematic summary for ν_μ disappearance $\bar{\nu}$-beam quartile 1 (%)

Systematic	Total pred		Signal		Total bkg		Beam bkg		$\bar{\nu}_\mu$ signal		ν_μ signal		ν_μ app.		NC		ν_e CC		ν_τ CC		Cosmics	
CCQE z-exp.ax.vec. 1	-0.05	+0.06	-0.04	+0.05	-1.71	+1.86	-2.77	+3.01	-0.04	+0.04	-0.09	+0.09	-3.49	+3.79	-0.00	+0.00	-0.00	+0.00	-3.42	+3.71	-0.00	+0.00
CCQE z-exp.ax.vec. 2	-0.06	+0.06	-0.05	+0.06	-1.34	+1.43	-2.16	+2.31	-0.05	+0.05	-0.09	+0.09	-2.71	+2.90	-0.00	+0.00	-0.00	+0.00	-2.68	+2.87	-0.00	+0.00
CCQE z-exp.ax.vec. 3	-0.10	+0.12	-0.10	+0.11	-1.14	+1.25	-1.84	+2.02	-0.09	+0.10	-0.14	+0.16	-2.26	+2.47	-0.00	+0.00	-0.00	+0.00	-2.31	+2.54	-0.00	+0.00
CCQE z-exp.ax.vec. 4	-0.02	+0.02	-0.02	+0.02	-0.15	+0.15	-0.24	+0.24	-0.02	+0.02	-0.03	+0.03	-0.28	+0.29	-0.00	+0.00	-0.00	+0.00	-0.30	+0.31	-0.00	+0.00
M_A^{CCRES}	-0.21	+0.27	-0.22	+0.27	-0.48	+0.69	-0.77	+1.12	-0.20	+0.25	-0.32	+0.43	-0.74	+1.03	-0.00	+0.00	-12.71	+33.63	-0.92	+1.16	-0.00	+0.00
M_V^{CCRES}	-0.17	+0.16	-0.17	+0.16	-0.29	+0.45	-0.47	+0.72	-0.16	+0.14	-0.25	+0.24	-0.44	+0.64	-0.00	+0.00	-8.24	+21.00	-0.57	+0.77	-0.00	+0.00
M_A^{NCRES}	-0.00	+0.00	-0.00	+0.00	-1.57	+1.80	-2.54	+2.90	-0.00	+0.00	-0.00	+0.00	-0.00	+0.00	-13.39	+15.29	-0.00	+0.00	-0.00	+0.00	-0.00	+0.00
M_V^{NCRES}	-0.00	+0.00	-0.00	+0.00	-0.07	+0.15	-0.11	+0.24	-0.00	+0.00	-0.00	+0.00	-0.00	+0.00	-0.60	+1.27	-0.00	+0.00	-0.00	+0.00	-0.00	+0.00
CCQE z-exp.norm.	-0.18	+0.21	-0.15	+0.18	-4.33	+5.78	-7.00	+9.33	-0.12	+0.15	-0.30	+0.36	-8.87	+11.82	-0.00	+0.00	-0.00	+0.00	-8.62	+11.50	-0.00	+0.00
RPA high Q^2 enh.	-0.07	+0.07	-0.07	+0.07	-0.35	+0.39	-0.57	+0.63	-0.05	+0.05	-0.15	+0.17	-0.77	+0.85	-0.00	+0.00	-0.00	+0.00	-0.67	+0.74	-0.00	+0.00
RPA low Q^2 supp.	-0.04	+0.04	-0.04	+0.04	-0.50	+0.50	-0.81	+0.81	-0.03	+0.03	-0.11	+0.12	-1.14	+1.14	-0.00	+0.00	-0.00	+0.00	-0.93	+0.93	-0.00	+0.00
RES low Q^2 supp.	-0.00	+0.11	-0.00	+0.11	-0.23	+0.00	-0.38	+0.00	-0.00	+0.09	-0.00	+0.23	-0.13	+0.00	-1.38	+0.00	-0.00	+0.00	-0.16	+0.00	-0.00	+0.00
DIS CC $\nu n \to 1\pi$	-0.00	+0.00	-0.00	+0.00	-0.08	+0.08	-0.14	+0.14	-0.00	+0.00	-0.01	+0.00	-0.15	+0.15	-0.00	+0.00	-0.08	+0.08	-0.18	+0.18	-0.00	+0.00
FSI π free path	-0.07	+0.03	-0.06	+0.03	-0.87	+0.49	-1.41	+0.80	-0.06	+0.03	-0.06	+0.00	-0.01	+0.02	-7.12	+3.98	-11.18	+7.24	-0.00	+0.01	-0.00	+0.00
FSI fate fraction	-0.07	+0.10	-0.07	+0.10	-0.13	+0.02	-0.22	+0.03	-0.07	+0.10	-0.08	+0.09	-0.02	+0.05	-1.17	+0.16	-4.20	+0.09	-0.00	+0.04	-0.00	+0.00
MEC E_ν shape	-0.12	+0.03	-0.11	+0.03	-0.28	+0.11	-0.45	+0.19	-0.10	+0.03	-0.20	+0.04	-0.59	+0.29	-0.00	+0.00	-0.00	+0.00	-0.54	+0.20	-0.00	+0.00
MEC $E_{\bar{\nu}}$ shape	-0.00	+0.11	-0.00	+0.11	-0.94	+0.39	-1.51	+0.64	-0.00	+0.12	-0.00	+0.14	-2.11	+0.98	-0.00	+0.00	-0.00	+0.00	-1.76	+0.68	-0.00	+0.00
MEC ν (q_0, q) response	-0.72	+1.06	-0.71	+1.05	-2.13	+1.40	-3.43	+2.26	-0.62	+0.88	-1.25	+2.04	-4.39	+2.49	-0.00	+0.00	-0.00	+0.00	-4.21	+3.00	-0.00	+0.00
MEC $\bar{\nu}$ (q_0, q) response	-0.89	+0.98	-0.88	+0.95	-2.05	+6.73	-3.32	+10.88	-0.93	+1.16	-0.57	+0.00	-4.07	+14.36	-0.00	+0.00	-0.00	+0.00	-4.16	+13.06	-0.00	+0.00
MEC ν init. np frac.	-0.06	+0.02	-0.06	+0.02	-0.45	+0.15	-0.73	+0.24	-0.04	+0.02	-0.15	+0.05	-1.06	+0.35	-0.00	+0.00	-0.00	+0.00	-0.82	+0.27	-0.00	+0.00
MEC $\bar{\nu}$ init. np frac.	-0.01	+0.04	-0.00	+0.03	-0.35	+1.04	-0.56	+1.69	-0.00	+0.02	-0.03	+0.11	-0.78	+2.34	-0.00	+0.00	-0.00	+0.00	-0.65	+1.96	-0.00	+0.00
XSecs PC00	-0.03	+0.03	-0.02	+0.02	-0.77	+0.77	-1.25	+1.25	-0.01	+0.01	-0.07	+0.07	-0.02	+0.02	-6.48	+6.48	-0.00	+0.00	-0.02	+0.02	-0.00	+0.00
XSecs PC01	-0.02	+0.02	-0.01	+0.01	-0.79	+0.79	-1.27	+1.27	-0.00	+0.00	-0.04	+0.04	-0.00	+0.00	-6.71	+6.71	-0.00	+0.00	-0.00	+0.00	-0.00	+0.00
XSecs PC02	-0.19	+0.21	-0.19	+0.21	-0.19	+0.19	-0.31	+0.31	-0.14	+0.16	-0.46	+0.52	-0.23	+0.23	-0.38	+0.38	-0.00	+0.00	-0.33	+0.33	-0.00	+0.00
XSecs PC03	-0.00	+0.01	-0.00	+0.01	-0.00	+0.00	-0.00	+0.00	-0.00	+0.00	-0.04	+0.04	-0.10	+0.10	-0.54	+0.54	-0.00	+0.00	-0.14	+0.14	-0.00	+0.00
XSecs PC04	-0.29	+0.30	-0.29	+0.30	-0.19	+0.19	-0.31	+0.31	-0.26	+0.27	-0.50	+0.52	-0.19	+0.19	-0.76	+0.76	-0.00	+0.00	-0.21	+0.21	-0.00	+0.00
XSecs PC05	-0.02	+0.02	-0.02	+0.02	-0.00	+0.00	-0.01	+0.01	-0.01	+0.01	-0.03	+0.03	-0.00	+0.00	-0.06	+0.06	-0.00	+0.00	-0.00	+0.00	-0.00	+0.00
XSecs PC06	-0.10	+0.11	-0.11	+0.11	-0.08	+0.08	-0.13	+0.13	-0.09	+0.09	-0.19	+0.19	-0.06	+0.06	-0.46	+0.46	-0.00	+0.00	-0.05	+0.05	-0.00	+0.00
XSecs PC07	-0.24	+0.25	-0.24	+0.25	-0.14	+0.14	-0.22	+0.22	-0.22	+0.22	-0.40	+0.41	-0.13	+0.13	-1.65	+1.65	-0.00	+0.00	-0.11	+0.11	-0.00	+0.00
XSecs PC08	-0.02	+0.02	-0.02	+0.02	-0.10	+0.10	-0.16	+0.16	-0.01	+0.01	-0.08	+0.08	-0.00	+0.00	-0.80	+0.80	-0.00	+0.00	-0.00	+0.00	-0.00	+0.00
XSecs PC09	-0.15	+0.15	-0.15	+0.15	-0.05	+0.05	-0.09	+0.09	-0.13	+0.13	-0.25	+0.25	-0.10	+0.10	-0.07	+0.07	-0.00	+0.00	-0.09	+0.09	-0.00	+0.00
XSecs PC10	-0.16	+0.16	-0.16	+0.16	-0.06	+0.06	-0.10	+0.10	-0.14	+0.14	-0.29	+0.29	-0.10	+0.10	-0.13	+0.13	-0.00	+0.00	-0.09	+0.09	-0.00	+0.00
XSecs PC11	-0.22	+0.22	-0.22	+0.22	-0.05	+0.05	-0.09	+0.09	-0.20	+0.20	-0.35	+0.35	-0.12	+0.12	-0.03	+0.03	-0.00	+0.00	-0.09	+0.09	-0.00	+0.00
ν_τ scale	-0.12	+0.12	-0.00	+0.00	-20.06	+20.06	-32.41	+32.41	-0.00	+0.00	-0.00	+0.00	-38.10	+38.10	-0.00	+0.00	-0.00	+0.00	-41.65	+41.65	-0.00	+0.00
Flux PC00	-0.10	+0.10	-0.09	+0.09	-1.63	+1.62	-2.63	+2.62	-0.09	+0.09	-0.10	+0.09	-2.83	+2.82	-2.15	+2.15	-1.45	+1.27	-2.71	+2.70	-0.00	+0.00
Flux PC01	-0.06	+0.04	-0.08	+0.06	-2.75	+2.70	-4.44	+4.36	-0.07	+0.06	-0.11	+0.07	-4.59	+4.51	-4.35	+4.32	-1.66	+1.15	-4.42	+4.32	-0.00	+0.00
Flux PC02	-0.32	+0.30	-0.32	+0.29	-1.43	+1.38	-2.31	+2.22	-0.20	+0.18	-1.00	+0.96	-2.23	+2.12	-1.49	+1.49	-9.65	+9.83	-2.57	+2.46	-0.00	+0.00
Flux PC03	-0.04	+0.00	-0.06	+0.03	-3.29	+3.26	-5.31	+5.26	-0.10	+0.07	-0.22	+0.15	-5.35	+5.30	-4.84	+4.80	-5.99	+5.72	-5.45	+5.40	-0.00	+0.00
Flux PC04	-0.22	+0.22	-0.22	+0.22	-0.10	+0.10	-0.16	+0.16	-0.18	+0.19	-0.41	+0.41	-0.32	+0.32	-0.43	+0.43	-0.41	+0.41	-0.28	+0.28	-0.00	+0.00
Absolute calib.	-5.52	+4.44	-5.53	+4.45	-2.64	+2.81	-4.27	+4.54	-5.41	+4.48	-6.21	+4.30	-4.59	+4.27	-7.73	+7.04	-0.00	+34.03	-3.29	+3.79	-0.00	+0.00
ND/FD relative calib.	-7.87	+8.29	-7.91	+8.33	-1.34	+1.38	-2.17	+2.24	-8.30	+8.80	-5.71	+5.60	-2.26	+2.18	-3.78	+3.61	-3.21	+12.41	-1.71	+1.83	-0.00	+0.00
Calibration shape	-2.24	+2.24	-2.25	+2.25	-0.09	+0.09	-0.15	+0.15	-2.30	+2.30	-1.98	+1.98	-0.55	+0.55	-0.63	+0.63	-20.61	+20.61	-0.00	+0.00	-0.00	+0.00
Calibration drift	-0.35	+0.00	-0.35	+0.00	-0.67	+0.00	-1.09	+0.00	-0.90	+0.00	-0.00	+2.80	-0.00	+0.11	-4.04	+0.00	-141.79	+0.00	-0.00	+1.16	-0.00	+0.00
Light level FD	-1.04	+0.00	-1.04	+0.00	-1.58	+0.00	-2.56	+0.00	-1.02	+0.00	-1.29	+0.00	-2.99	+0.00	-7.45	+0.00	-136.91	+0.00	-1.31	+0.61	-0.00	+0.00
Light level ND	-0.00	+1.33	-0.00	+1.33	-0.00	+0.00	-0.00	+0.00	-0.00	+0.86	-0.00	+4.06	-0.00	+0.00	-0.00	+0.00	-0.00	+0.00	-0.00	+0.00	-0.00	+0.00
Cherenkov	-1.35	+0.00	-1.37	+0.00	-0.00	+1.39	-0.00	+2.24	-1.32	+0.00	-1.62	+0.00	-0.00	+0.59	-0.00	+8.31	-0.00	+6.12	-0.00	+0.89	-0.00	+0.00
E_μ ND uncorr.	-0.43	+0.52	-0.43	+0.53	-0.00	+0.00	-0.00	+0.00	-0.40	+0.46	-0.60	+0.90	-0.00	+0.00	-0.00	+0.00	-0.00	+0.00	-0.00	+0.00	-0.00	+0.00
E_μ μ-catcher uncorr.	-0.67	+0.75	-0.68	+0.76	-0.00	+0.00	-0.00	+0.00	-0.59	+0.64	-1.19	+1.46	-0.00	+0.00	-0.00	+0.00	-0.00	+0.00	-0.00	+0.00	-0.00	+0.00
E_μ n pile-up	-1.41	+0.00	-1.42	+0.00	-0.00	+0.00	-0.00	+0.00	-1.29	+0.00	-2.16	+0.00	-0.00	+0.00	-0.00	+0.00	-0.00	+0.00	-0.00	+0.00	-0.00	+0.00
E_μ correlated	-2.27	+2.47	-2.29	+2.49	-0.40	+0.59	-0.65	+0.95	-2.08	+2.19	-3.46	+4.16	-0.22	+0.44	-1.66	+1.43	-0.44	+0.00	-0.52	+1.07	-0.00	+0.00
E_μ FD uncorr.	-0.15	+0.10	-0.15	+0.10	-0.07	+0.13	-0.12	+0.21	-0.13	+0.09	-0.28	+0.18	-0.06	+0.12	-0.00	+0.00	-0.11	+0.00	-0.20	+0.34	-0.00	+0.00
Lepton angle xz ND	-0.20	+0.20	-0.20	+0.20	-0.00	+0.00	-0.00	+0.00	-0.22	+0.20	-0.10	+0.21	-0.00	+0.00	-0.00	+0.00	-0.00	+0.00	-0.00	+0.00	-0.00	+0.00
Lepton angle yz ND	-0.09	+0.00	-0.09	+0.00	-0.00	+0.00	-0.00	+0.00	-0.10	+0.00	-0.11	+0.00	-0.00	+0.00	-0.00	+0.00	-0.00	+0.00	-0.00	+0.00	-0.00	+0.00
Lepton angle xz FD	-0.00	+0.00	-0.00	+0.00	-0.00	+0.00	-0.00	+0.00	-0.00	+0.00	-0.03	+0.00	-0.00	+0.00	-0.00	+0.00	-0.00	+0.00	-0.00	+0.00	-0.00	+0.00
Lepton angle yz FD	-0.00	+0.01	-0.00	+0.01	-0.00	+0.00	-0.00	+0.00	-0.00	+0.00	-0.03	+0.03	-0.00	+0.00	-0.00	+0.00	-0.00	+0.00	-0.00	+0.00	-0.00	+0.00
Neutron systematic	-2.59	+4.87	-2.57	+4.83	-6.61	+11.29	-10.68	+18.24	-2.72	+5.12	-1.71	+3.18	-11.34	+12.64	-14.26	+44.26	-0.02	+0.22	-9.09	+11.99	-0.00	+0.00
Normalization beam corr.	-0.79	+0.79	-0.79	+0.79	-0.53	+0.53	-0.86	+0.86	-0.80	+0.80	-0.75	+0.75	-0.87	+0.87	-0.78	+0.78	-1.21	+1.21	-0.87	+0.87	-0.00	+0.00
Normalization $\bar{\nu}$-beam	-0.71	+0.71	-0.71	+0.71	-0.47	+0.47	-0.76	+0.76	-0.71	+0.71	-0.66	+0.66	-0.78	+0.78	-0.70	+0.70	-1.08	+1.08	-0.78	+0.78	-0.00	+0.00
Cosmic scale	-0.15	+0.32	-0.00	+0.00	-24.09	+52.92	-0.00	+0.00	-0.00	+0.00	-0.00	+0.00	-0.00	+0.00	-0.00	+0.00	-0.00	+0.00	-0.00	+0.00	-63.24	+138.88
Quadrature	-10.87	+11.39	-10.91	+11.41	-33.20	+58.82	-36.90	+41.50	-11.13	+11.79	-10.31	+10.79	-42.76	+45.71	-26.98	+49.86	-199.48	+59.44	-45.15	+48.07	-63.24	+138.88

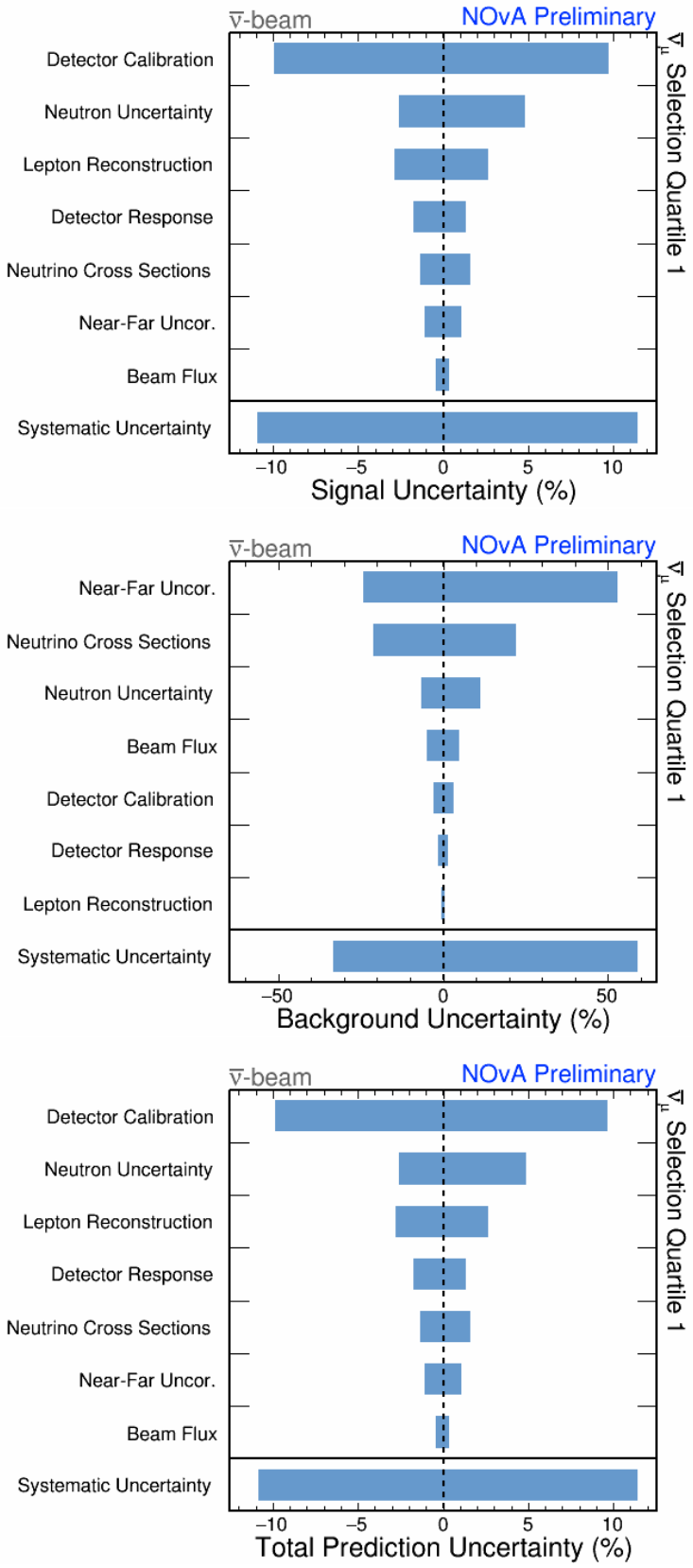

Figure C.12: Relative 1σ systematic uncertainties on the integral number of signal (top), background (middle), and total (bottom) predicted events in the $\bar{\nu}_\mu$ disapp. $\bar{\nu}$-beam quartile 1.

$\bar{\nu}_\mu$ E_{had} fraction quartile 2

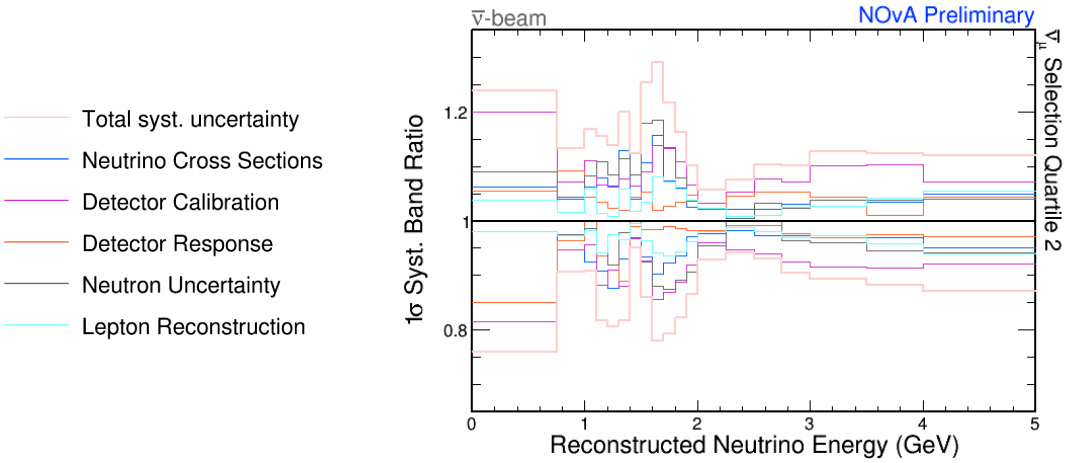

Figure C.13: 1σ systematic bands relative to the nominal prediction for the $\bar{\nu}$-beam $\bar{\nu}_\mu$ disapp. quartile 2 in the reconstructed neutrino energy.

Table C.7: Relative 1σ systematic uncertainties on the integral numbers of predicted events for the $\bar{\nu}_\mu$ disapp. $\bar{\nu}$-beam quartile 2.

Systematic summary for ν_μ disappearance $\bar{\nu}$-beam quartile 2 (%)

Systematic	Total pred		Signal		Total bkg		Beam bkg		$\bar{\nu}_\mu$ signal		ν_μ signal		ν_μ app.		NC		ν_e CC		ν_τ CC		Cosmics	
CCQE z-exp.ax.vec. 1	-0.30	+0.32	-0.29	+0.31	-1.64	+1.78	-2.01	+2.19	-0.29	+0.31	-0.32	+0.34	-2.92	+3.18	-0.00	+0.00	-0.00	+0.00	-2.75	+2.99	-0.00	+0.00
CCQE z-exp.ax.vec. 2	-0.28	+0.30	-0.27	+0.29	-1.38	+1.49	-1.70	+1.84	-0.26	+0.28	-0.29	+0.30	-2.47	+2.66	-0.00	+0.00	-0.00	+0.00	-2.33	+2.51	-0.00	+0.00
CCQE z-exp.ax.vec. 3	-0.43	+0.51	-0.43	+0.50	-1.60	+1.83	-1.97	+2.26	-0.41	+0.47	-0.51	+0.60	-2.78	+3.15	-0.00	+0.00	-0.00	+0.00	-2.73	+3.13	-0.00	+0.00
CCQE z-exp.ax.vec. 4	-0.09	+0.09	-0.09	+0.09	-0.27	+0.29	-0.34	+0.35	-0.08	+0.08	-0.11	+0.12	-0.47	+0.48	-0.00	+0.00	-0.00	+0.00	-0.47	+0.49	-0.00	+0.00
M_A^{CCRES}	-0.15	+0.38	-0.17	+0.40	-2.34	+2.64	-2.88	+3.25	-0.31	+0.48	-0.00	+0.37	-3.42	+3.77	-0.00	+0.00	-0.02	+0.01	-4.28	+4.87	-0.00	+0.00
M_V^{CCRES}	-0.15	+0.22	-0.17	+0.23	-1.65	+2.18	-2.03	+2.69	-0.29	+0.31	-0.05	+0.28	-2.37	+3.10	-0.00	+0.00	-0.00	+0.00	-3.03	+4.03	-0.00	+0.00
M_A^{NCRES}	-0.01	+0.02	-0.01	+0.00	-3.38	+4.37	-4.17	+5.38	-0.01	+0.00	-0.01	+0.00	-0.00	+0.00	-14.91	+19.26	-0.00	+0.00	-0.00	+0.00	-0.00	+0.00
M_V^{NCRES}	-0.00	+0.00	-0.00	+0.00	-0.08	+0.28	-0.10	+0.35	-0.00	+0.00	-0.00	+0.00	-0.00	+0.00	-0.36	+1.26	-0.00	+0.00	-0.00	+0.00	-0.00	+0.00
CCQE z-exp.norm.	-1.01	+1.23	-0.98	+1.20	-4.25	+5.66	-5.23	+6.98	-0.95	+1.15	-1.11	+1.38	-7.49	+9.98	-0.00	+0.00	-0.00	+0.00	-7.18	+9.57	-0.00	+0.00
RPA high Q^2 enh.	-0.41	+0.49	-0.41	+0.49	-0.33	+0.39	-0.40	+0.48	-0.39	+0.46	-0.51	+0.59	-0.60	+0.71	-0.00	+0.00	-0.00	+0.00	-0.54	+0.65	-0.00	+0.00
RPA low Q^2 supp.	-0.00	+0.00	-0.00	+0.00	-0.18	+0.18	-0.22	+0.22	-0.00	+0.00	-0.06	+0.05	-0.34	+0.34	-0.00	+0.00	-0.00	+0.00	-0.30	+0.30	-0.00	+0.00
RES low Q^2 supp.	-0.00	+0.09	-0.00	+0.10	-0.55	+0.00	-0.68	+0.00	-0.00	+0.09	-0.00	+0.14	-0.50	+0.00	-1.14	+0.00	-1.38	+0.00	-0.50	+0.00	-0.00	+0.00
DIS CC $\nu n \to 1\pi$	-0.06	+0.07	-0.06	+0.06	-0.19	+0.19	-0.24	+0.24	-0.04	+0.04	-0.17	+0.17	-0.28	+0.28	-0.00	+0.00	-0.00	+0.00	-0.36	+0.36	-0.00	+0.00
FSI π free path	-0.36	+0.25	-0.35	+0.25	-1.28	+0.79	-1.58	+0.97	-0.27	+0.20	-0.65	+0.43	-0.13	+0.31	-6.59	+3.86	-3.27	+0.00	-0.15	+0.40	-0.00	+0.00
FSI fate fraction	-0.12	+0.16	-0.12	+0.16	-0.23	+0.15	-0.28	+0.19	-0.11	+0.14	-0.15	+0.26	-0.04	+0.04	-0.91	+0.54	-1.84	+2.61	-0.04	+0.06	-0.00	+0.00
MEC E_ν shape	-0.08	+0.12	-0.08	+0.12	-0.54	+0.23	-0.67	+0.29	-0.06	+0.11	-0.15	+0.16	-0.99	+0.43	-0.00	+0.00	-0.00	+0.00	-0.91	+0.39	-0.00	+0.00
MEC $E_{\bar{\nu}}$ shape	-0.27	+0.31	-0.27	+0.32	-0.75	+0.31	-0.93	+0.38	-0.27	+0.29	-0.27	+0.41	-1.41	+0.57	-0.00	+0.00	-0.00	+0.00	-1.23	+0.51	-0.00	+0.00
MEC ν (q_0, q) response	-0.42	+0.03	-0.40	+0.03	-3.79	+0.60	-4.67	+0.75	-0.24	+0.04	-0.98	+0.00	-7.07	+1.32	-0.00	+0.00	-0.00	+0.00	-6.23	+0.91	-0.00	+0.00
MEC $\bar{\nu}$ (q_0, q) response	-0.91	+0.39	-0.91	+0.41	-2.66	+0.00	-3.28	+0.00	-1.21	+0.51	-0.00	+0.25	-5.00	+0.00	-0.00	+0.00	-0.00	+0.00	-4.36	+0.00	-0.00	+0.00
MEC ν init. np frac.	-0.03	+0.08	-0.03	+0.09	-0.60	+0.20	-0.74	+0.25	-0.02	+0.06	-0.06	+0.19	-1.29	+0.43	-0.00	+0.00	-0.00	+0.00	-0.91	+0.30	-0.00	+0.00
MEC $\bar{\nu}$ init. np frac.	-0.27	+0.85	-0.28	+0.85	-0.04	+0.01	-0.05	+0.02	-0.30	+0.92	-0.19	+0.60	-0.12	+0.04	-0.00	+0.00	-0.00	+0.00	-0.05	+0.02	-0.00	+0.00
XSecs PC00	-0.05	+0.05	-0.03	+0.03	-1.55	+1.55	-1.90	+1.90	-0.02	+0.02	-0.11	+0.11	-0.02	+0.02	-6.76	+6.76	-0.00	+0.00	-0.02	+0.02	-0.00	+0.00
XSecs PC01	-0.04	+0.04	-0.03	+0.03	-1.56	+1.56	-1.92	+1.92	-0.02	+0.02	-0.09	+0.09	-0.00	+0.00	-6.87	+6.87	-0.00	+0.00	-0.00	+0.00	-0.00	+0.00
XSecs PC02	-0.44	+0.52	-0.45	+0.53	-0.30	+0.30	-0.36	+0.36	-0.31	+0.36	-0.99	+1.18	-0.29	+0.29	-0.40	+0.40	-0.00	+0.00	-0.38	+0.38	-0.00	+0.00
XSecs PC03	-0.05	+0.05	-0.05	+0.05	-0.04	+0.04	-0.05	+0.05	-0.03	+0.03	-0.12	+0.13	-0.12	+0.12	-0.57	+0.57	-0.00	+0.00	-0.16	+0.16	-0.00	+0.00
XSecs PC04	-0.54	+0.57	-0.55	+0.57	-0.34	+0.34	-0.42	+0.42	-0.46	+0.48	-0.87	+0.92	-0.25	+0.25	-0.82	+0.82	-0.00	+0.00	-0.27	+0.27	-0.00	+0.00
XSecs PC05	-0.02	+0.02	-0.02	+0.02	-0.02	+0.02	-0.02	+0.02	-0.01	+0.01	-0.03	+0.03	-0.00	+0.00	-0.07	+0.07	-0.00	+0.00	-0.00	+0.00	-0.00	+0.00
XSecs PC06	-0.20	+0.20	-0.20	+0.20	-0.16	+0.16	-0.19	+0.19	-0.16	+0.16	-0.35	+0.36	-0.08	+0.08	-0.51	+0.51	-0.00	+0.00	-0.07	+0.07	-0.00	+0.00
XSecs PC07	-0.44	+0.46	-0.45	+0.46	-0.32	+0.32	-0.39	+0.39	-0.38	+0.39	-0.69	+0.71	-0.17	+0.17	-1.83	+1.83	-0.00	+0.00	-0.16	+0.16	-0.00	+0.00
XSecs PC08	-0.05	+0.05	-0.05	+0.05	-0.22	+0.22	-0.27	+0.27	-0.02	+0.02	-0.15	+0.16	-0.02	+0.02	-0.92	+0.92	-0.00	+0.00	-0.01	+0.01	-0.00	+0.00
XSecs PC09	-0.27	+0.27	-0.27	+0.28	-0.10	+0.10	-0.13	+0.13	-0.23	+0.23	-0.43	+0.44	-0.14	+0.14	-0.12	+0.12	-0.00	+0.00	-0.12	+0.12	-0.00	+0.00
XSecs PC10	-0.29	+0.30	-0.30	+0.30	-0.11	+0.11	-0.13	+0.13	-0.25	+0.25	-0.49	+0.50	-0.13	+0.13	-0.14	+0.14	-0.00	+0.00	-0.12	+0.12	-0.00	+0.00
XSecs PC11	-0.39	+0.40	-0.39	+0.40	-0.07	+0.07	-0.09	+0.09	-0.35	+0.35	-0.57	+0.58	-0.15	+0.15	-0.04	+0.04	-0.00	+0.00	-0.14	+0.14	-0.00	+0.00
ν_τ scale	-0.18	+0.18	-0.00	+0.00	-26.43	+26.43	-32.56	+32.56	-0.00	+0.00	-0.00	+0.00	-44.31	+44.31	-0.00	+0.00	-0.00	+0.00	-45.75	+45.75	-0.00	+0.00
Flux PC00	-0.09	+0.09	-0.08	+0.07	-2.12	+2.11	-2.61	+2.60	-0.08	+0.08	-0.08	+0.07	-2.82	+2.81	-2.18	+2.18	-4.16	+4.08	-2.76	+2.74	-0.00	+0.00
Flux PC01	-0.06	+0.03	-0.08	+0.06	-3.70	+3.63	-4.56	+4.48	-0.07	+0.05	-0.15	+0.09	-4.70	+4.61	-4.33	+4.31	-7.19	+6.94	-4.61	+4.51	-0.00	+0.00
Flux PC02	-0.13	+0.10	-0.12	+0.09	-2.19	+2.14	-2.70	+2.64	-0.07	+0.04	-0.72	+0.67	-3.00	+2.92	-1.71	+1.71	-0.63	+0.60	-3.12	+3.04	-0.00	+0.00
Flux PC03	-0.13	+0.09	-0.17	+0.13	-4.83	+4.77	-5.95	+5.88	-0.21	+0.18	-0.06	+0.00	-6.32	+6.23	-4.99	+4.95	-7.18	+6.90	-6.33	+6.24	-0.00	+0.00
Flux PC04	-0.19	+0.20	-0.20	+0.20	-0.08	+0.08	-0.10	+0.10	-0.15	+0.15	-0.39	+0.39	-0.32	+0.31	-0.42	+0.42	-0.16	+0.16	-0.30	+0.30	-0.00	+0.00
Absolute calib.	-3.54	+3.37	-3.56	+3.39	-0.91	+1.14	-1.12	+1.40	-3.54	+3.23	-3.65	+3.98	-0.31	+0.22	-3.40	+4.80	-0.75	+4.83	-0.21	+0.00	-0.00	+0.00
ND/FD relative calib.	-2.73	+2.84	-2.76	+2.87	-0.48	+0.54	-0.60	+0.67	-2.38	+2.42	-4.20	+4.56	-0.15	+0.12	-1.87	+2.22	-0.88	+1.90	-0.08	+0.03	-0.00	+0.00
Calibration shape	-0.94	+0.94	-0.95	+0.95	-0.05	+0.05	-0.06	+0.06	-1.07	+1.07	-0.48	+0.48	-0.00	+0.00	-0.36	+0.36	-19.31	+19.31	-0.15	+0.15	-0.00	+0.00
Calibration drift	-0.00	+0.81	-0.00	+0.82	-0.00	+0.09	-0.00	+0.12	-0.00	+1.07	-0.16	+0.00	-0.00	+1.27	-2.17	+0.00	-121.26	+0.00	-0.00	+1.33	-0.00	+0.00
Light level FD	-0.00	+1.34	-0.00	+1.35	-1.10	+0.00	-1.36	+0.00	-0.00	+1.39	-0.00	+1.22	-0.62	+1.00	-3.89	+0.00	-115.69	+0.00	-0.43	+1.05	-0.00	+0.00
Light level ND	-0.96	+0.00	-0.96	+0.00	-0.00	+0.00	-0.00	+0.00	-0.82	+0.00	-1.70	+0.58	-0.00	+0.00	-0.00	+0.00	-0.00	+0.00	-0.00	+0.00	-0.00	+0.00
Cherenkov	-0.00	+2.35	-0.00	+2.38	-1.30	+0.00	-1.60	+0.00	-0.00	+2.53	-0.00	+1.80	-0.21	+0.00	-5.38	+0.00	-106.67	+0.00	-0.00	+0.29	-0.00	+0.00
E_μ ND uncorr.	-0.31	+0.39	-0.32	+0.39	-0.00	+0.00	-0.00	+0.00	-0.26	+0.35	-0.53	+0.55	-0.00	+0.00	-0.00	+0.00	-0.00	+0.00	-0.00	+0.00	-0.00	+0.00
E_μ μ-catcher uncorr.	-0.41	+0.42	-0.41	+0.42	-0.00	+0.00	-0.00	+0.00	-0.30	+0.33	-0.84	+0.75	-0.00	+0.00	-0.00	+0.00	-0.00	+0.00	-0.00	+0.00	-0.00	+0.00
E_μ n pile-up	-1.06	+0.00	-1.07	+0.00	-0.00	+0.00	-0.00	+0.00	-0.89	+0.00	-1.74	+0.00	-0.00	+0.00	-0.00	+0.00	-0.00	+0.00	-0.00	+0.00	-0.00	+0.00
E_μ correlated	-2.04	+2.30	-2.05	+2.32	-0.49	+0.29	-0.61	+0.36	-1.92	+2.19	-2.54	+2.82	-0.61	+0.09	-0.97	+1.11	-0.00	+0.00	-0.40	+0.06	-0.00	+0.00
E_μ FD uncorr.	-0.02	+0.03	-0.02	+0.03	-0.20	+0.00	-0.25	+0.00	-0.04	+0.06	-0.11	+0.04	-0.15	+0.00	-0.55	+0.05	-0.00	+0.00	-0.13	+0.00	-0.00	+0.00
Lepton angle xz ND	-0.41	+0.46	-0.41	+0.46	-0.00	+0.00	-0.00	+0.00	-0.36	+0.38	-0.61	+0.77	-0.00	+0.00	-0.00	+0.00	-0.00	+0.00	-0.00	+0.00	-0.00	+0.00
Lepton angle yz ND	-0.15	+0.06	-0.15	+0.06	-0.00	+0.00	-0.00	+0.00	-0.14	+0.02	-0.21	+0.20	-0.00	+0.00	-0.00	+0.00	-0.00	+0.00	-0.00	+0.00	-0.00	+0.00
Lepton angle xz FD	-0.00	+0.00	-0.00	+0.00	-0.00	+0.00	-0.00	+0.00	-0.00	+0.00	-0.00	+0.00	-0.00	+0.00	-0.00	+0.00	-0.00	+0.00	-0.00	+0.00	-0.00	+0.00
Lepton angle yz FD	-0.01	+0.01	-0.01	+0.01	-0.00	+0.00	-0.00	+0.00	-0.02	+0.01	-0.00	+0.01	-0.00	+0.00	-0.00	+0.00	-0.00	+0.00	-0.00	+0.00	-0.00	+0.00
Neutron systematic	-3.38	+3.08	-3.39	+3.12	-2.59	+0.00	-3.20	+0.00	-3.42	+3.17	-3.31	+2.95	-3.23	+1.14	-10.59	+0.00	-0.88	+3.65	-3.15	+1.16	-0.00	+0.00
Normalization beam corr.	-0.82	+0.82	-0.82	+0.82	-0.71	+0.71	-0.88	+0.88	-0.83	+0.83	-0.82	+0.82	-0.91	+0.91	-0.80	+0.80	-1.10	+1.10	-0.90	+0.90	-0.00	+0.00
Normalization $\bar{\nu}$-beam	-0.73	+0.73	-0.73	+0.73	-0.63	+0.63	-0.78	+0.78	-0.73	+0.73	-0.73	+0.73	-0.81	+0.81	-0.71	+0.71	-0.98	+0.98	-0.80	+0.80	-0.00	+0.00
Cosmic scale	-0.08	+0.19	-0.00	+0.00	-11.90	+27.23	-0.00	+0.00	-0.00	+0.00	-0.00	+0.00	-0.00	+0.00	-0.00	+0.00	-0.00	+0.00	-0.00	+0.00	-63.17	+144.52
Quadrature	-6.65	+7.05	-6.68	+7.10	-31.20	+39.57	-35.53	+35.38	-6.46	+6.91	-8.04	+8.34	-47.24	+46.90	-24.43	+23.82	-199.96	+23.13	-48.43	+48.31	-63.17	+144.52

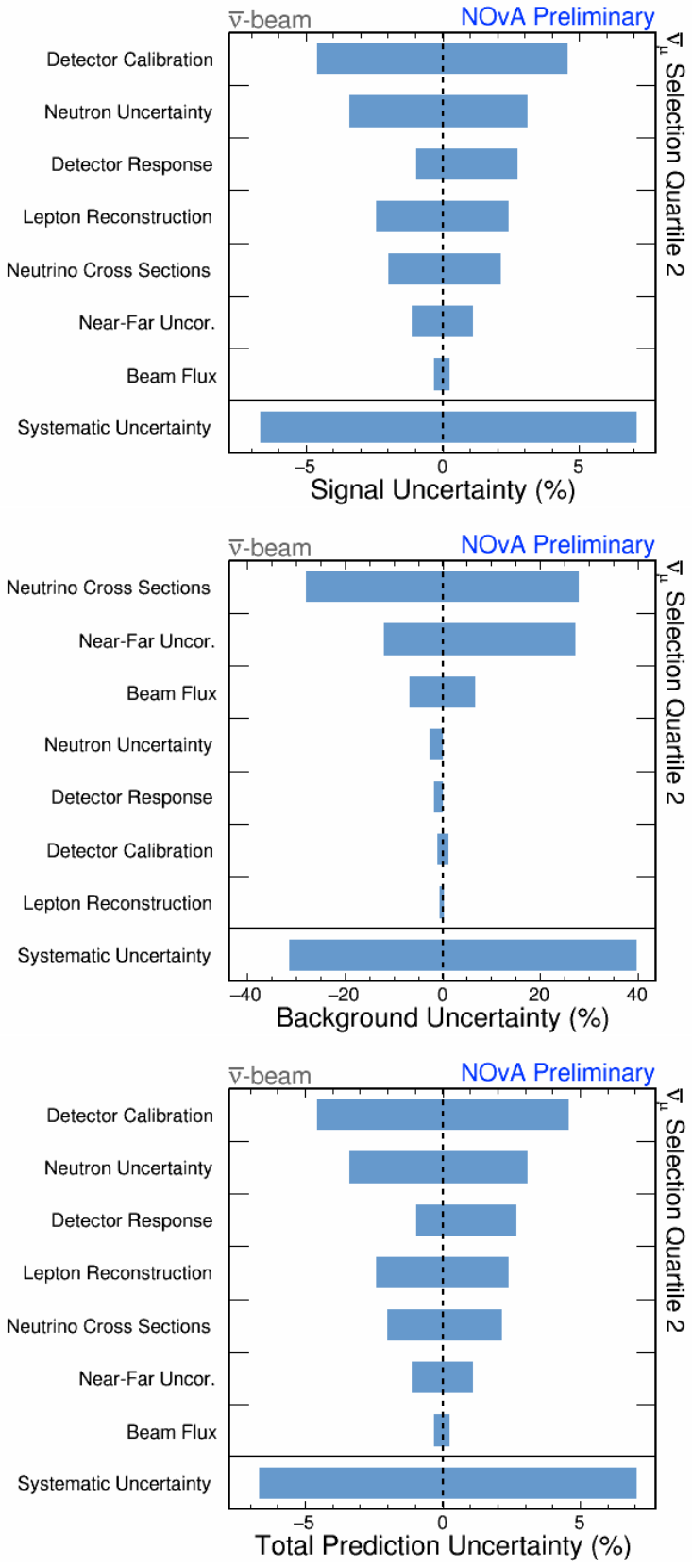

Figure C.14: Relative 1σ systematic uncertainties on the integral number of signal (top), background (middle), and total (bottom) predicted events in the $\bar{\nu}_\mu$ disapp. $\bar{\nu}$-beam quartile 2.

$\bar{\nu}_\mu$ E_{had} fraction quartile 3

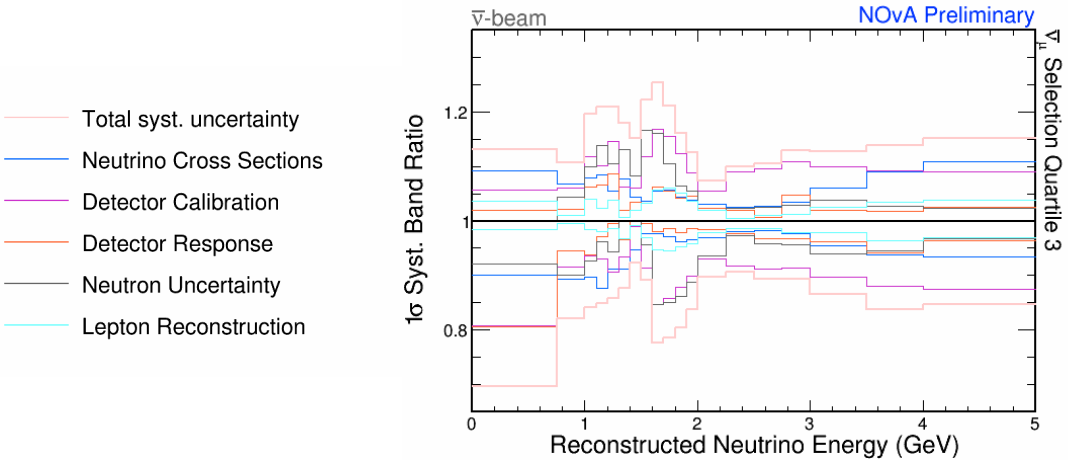

Figure C.15: 1σ systematic bands relative to the nominal prediction for the $\bar{\nu}$-beam $\bar{\nu}_\mu$ disapp. quartile 3 in the reconstructed neutrino energy.

Table C.8: Relative 1σ systematic uncertainties on the integral numbers of predicted events for the $\bar{\nu}_\mu$ disapp. $\bar{\nu}$-beam quartile 3.

Systematic summary for ν_μ disappearance $\bar{\nu}$-beam quartile 3 (%)

Systematic	Total pred		Signal		Total bkg		Beam bkg		$\bar{\nu}_\mu$ signal		ν_μ signal		ν_μ app.		NC		ν_e CC		ν_τ CC		Cosmics	
CCQE z-exp.ax.vec. 1	-0.17	+0.19	-0.17	+0.18	-0.62	+0.67	-0.94	+1.02	-0.19	+0.21	-0.10	+0.11	-1.78	+1.93	-0.00	+0.00	-0.02	+0.02	-1.71	+1.85	-0.00	+0.00
CCQE z-exp.ax.vec. 2	-0.16	+0.17	-0.15	+0.17	-0.54	+0.58	-0.82	+0.89	-0.18	+0.20	-0.08	+0.09	-1.57	+1.69	-0.00	+0.00	-0.03	+0.04	-1.49	+1.61	-0.00	+0.00
CCQE z-exp.ax.vec. 3	-0.38	+0.51	-0.37	+0.50	-0.90	+1.09	-1.38	+1.66	-0.41	+0.54	-0.28	+0.39	-2.67	+3.20	-0.00	+0.00	-0.07	+0.10	-2.48	+2.98	-0.00	+0.00
CCQE z-exp.ax.vec. 4	-0.10	+0.11	-0.10	+0.10	-0.20	+0.21	-0.30	+0.32	-0.10	+0.11	-0.08	+0.09	-0.58	+0.61	-0.00	+0.00	-0.03	+0.04	-0.54	+0.57	-0.00	+0.00
M_A^{CCRES}	-0.93	+2.19	-0.90	+2.15	-3.35	+4.75	-5.10	+7.24	-0.46	+1.44	-2.18	+4.24	-8.95	+12.24	-0.00	+0.00	-0.00	+1.95	-9.61	+13.78	-0.00	+0.00
M_V^{CCRES}	-0.57	+1.28	-0.54	+1.25	-2.34	+3.51	-3.57	+5.34	-0.29	+0.86	-1.26	+2.38	-6.32	+9.26	-0.00	+0.00	-0.53	+3.71	-6.67	+10.05	-0.00	+0.00
M_A^{NCRES}	-0.03	+0.05	-0.02	+0.02	-3.57	+5.28	-5.44	+8.04	-0.02	+0.01	-0.02	+0.02	-0.00	+0.00	-12.01	+17.75	-0.00	+0.00	-0.00	+0.00	-0.00	+0.00
M_V^{NCRES}	-0.00	+0.00	-0.00	+0.00	-0.03	+0.32	-0.05	+0.48	-0.00	+0.00	-0.00	+0.00	-0.00	+0.00	-0.11	+1.06	-0.00	+0.00	-0.00	+0.00	-0.00	+0.00
CCQE z-exp.norm.	-0.84	+1.06	-0.82	+1.04	-1.87	+2.49	-2.85	+3.80	-0.92	+1.16	-0.55	+0.69	-5.44	+7.25	-0.00	+0.00	-0.00	+0.00	-5.16	+6.87	-0.00	+0.00
RPA high Q^2 enh.	-0.41	+0.50	-0.41	+0.50	-0.14	+0.18	-0.22	+0.28	-0.48	+0.57	-0.20	+0.29	-0.43	+0.55	-0.00	+0.00	-0.00	+0.00	-0.39	+0.50	-0.00	+0.00
RPA low Q^2 supp.	-0.00	+0.00	-0.00	+0.00	-0.02	+0.02	-0.04	+0.04	-0.01	+0.01	-0.02	+0.02	-0.07	+0.07	-0.00	+0.00	-0.00	+0.00	-0.06	+0.06	-0.00	+0.00
RES low Q^2 supp.	-0.00	+0.18	-0.00	+0.19	-0.37	+0.00	-0.57	+0.00	-0.00	+0.17	-0.00	+0.24	-0.60	+0.00	-0.59	+0.00	-0.19	+0.00	-0.54	+0.00	-0.00	+0.00
DIS CC $\nu n \to 1\pi$	-0.28	+0.28	-0.28	+0.27	-0.31	+0.31	-0.48	+0.48	-0.18	+0.18	-0.56	+0.55	-0.78	+0.78	-0.00	+0.00	-4.59	+4.59	-0.88	+0.88	-0.00	+0.00
FSI π free path	-0.61	+0.41	-0.60	+0.40	-1.36	+0.84	-2.08	+1.29	-0.48	+0.30	-0.97	+0.70	-0.40	+0.34	-5.01	+3.27	-2.45	+4.77	-0.38	+0.38	-0.00	+0.00
FSI fate fraction	-0.12	+0.00	-0.12	+0.00	-0.00	+0.04	-0.00	+0.06	-0.10	+0.00	-0.20	+0.07	-0.11	+0.04	-0.00	+0.24	-1.82	+11.20	-0.12	+0.03	-0.00	+0.00
MEC E_ν shape	-0.00	+0.06	-0.00	+0.06	-0.32	+0.16	-0.48	+0.24	-0.00	+0.03	-0.06	+0.14	-0.94	+0.48	-0.00	+0.00	-0.00	+0.00	-0.87	+0.44	-0.00	+0.00
MEC $E_{\bar{\nu}}$ shape	-0.09	+0.20	-0.09	+0.21	-0.21	+0.09	-0.32	+0.14	-0.11	+0.22	-0.01	+0.17	-0.58	+0.24	-0.00	+0.00	-0.00	+0.00	-0.59	+0.27	-0.00	+0.00
MEC ν (q_0, q) response	-0.31	+0.17	-0.30	+0.18	-1.25	+0.00	-1.90	+0.00	-0.27	+0.17	-0.38	+0.22	-4.26	+0.00	-0.00	+0.00	-0.00	+0.00	-3.18	+0.00	-0.00	+0.00
MEC $\bar{\nu}$ (q_0, q) response	-0.10	+0.08	-0.10	+0.10	-1.79	+0.00	-2.73	+0.00	-0.30	+0.30	-1.25	+1.26	-4.69	+0.22	-0.00	+0.00	-0.00	+0.00	-5.18	+0.00	-0.00	+0.00
MEC ν init. np frac.	-0.15	+0.05	-0.15	+0.05	-0.05	+0.15	-0.07	+0.22	-0.15	+0.05	-0.16	+0.05	-0.16	+0.47	-0.00	+0.00	-0.00	+0.00	-0.13	+0.39	-0.00	+0.00
MEC $\bar{\nu}$ init. np frac.	-0.22	+0.68	-0.22	+0.69	-0.33	+0.11	-0.50	+0.17	-0.24	+0.76	-0.16	+0.50	-1.02	+0.34	-0.00	+0.00	-0.00	+0.00	-0.89	+0.30	-0.00	+0.00
XSecs PC00	-0.07	+0.07	-0.04	+0.04	-2.27	+2.27	-3.46	+3.46	-0.01	+0.01	-0.11	+0.11	-0.03	+0.03	-7.61	+7.61	-0.00	+0.00	-0.03	+0.03	-0.00	+0.00
XSecs PC01	-0.06	+0.06	-0.03	+0.04	-1.85	+1.85	-2.81	+2.81	-0.01	+0.01	-0.09	+0.09	-0.00	+0.00	-6.21	+6.21	-0.00	+0.00	-0.00	+0.00	-0.00	+0.00
XSecs PC02	-0.51	+0.62	-0.52	+0.63	-0.25	+0.25	-0.39	+0.39	-0.35	+0.42	-1.02	+1.27	-0.34	+0.34	-0.41	+0.41	-0.00	+0.00	-0.39	+0.39	-0.00	+0.00
XSecs PC03	-0.03	+0.04	-0.03	+0.04	-0.11	+0.11	-0.17	+0.17	-0.02	+0.02	-0.07	+0.08	-0.14	+0.14	-0.55	+0.55	-0.00	+0.00	-0.16	+0.16	-0.00	+0.00
XSecs PC04	-0.58	+0.61	-0.60	+0.63	-0.38	+0.38	-0.59	+0.59	-0.51	+0.53	-0.85	+0.90	-0.29	+0.29	-0.94	+0.94	-0.00	+0.00	-0.29	+0.29	-0.00	+0.00
XSecs PC05	-0.03	+0.03	-0.03	+0.03	-0.02	+0.02	-0.04	+0.04	-0.02	+0.02	-0.05	+0.05	-0.00	+0.00	-0.08	+0.08	-0.00	+0.00	-0.00	+0.00	-0.00	+0.00
XSecs PC06	-0.23	+0.24	-0.24	+0.24	-0.27	+0.27	-0.42	+0.42	-0.19	+0.19	-0.39	+0.40	-0.09	+0.09	-0.82	+0.82	-0.00	+0.00	-0.08	+0.08	-0.00	+0.00
XSecs PC07	-0.52	+0.53	-0.52	+0.53	-0.76	+0.76	-1.16	+1.16	-0.44	+0.45	-0.74	+0.77	-0.20	+0.20	-2.79	+2.79	-0.00	+0.00	-0.18	+0.18	-0.00	+0.00
XSecs PC08	-0.06	+0.06	-0.06	+0.06	-0.42	+0.42	-0.64	+0.64	-0.02	+0.02	-0.19	+0.19	-0.01	+0.01	-1.41	+1.41	-0.00	+0.00	-0.00	+0.00	-0.00	+0.00
XSecs PC09	-0.31	+0.31	-0.31	+0.32	-0.14	+0.14	-0.22	+0.22	-0.26	+0.27	-0.46	+0.47	-0.16	+0.16	-0.30	+0.30	-0.00	+0.00	-0.14	+0.14	-0.00	+0.00
XSecs PC10	-0.34	+0.34	-0.34	+0.35	-0.14	+0.14	-0.21	+0.21	-0.28	+0.28	-0.53	+0.54	-0.15	+0.15	-0.30	+0.30	-0.00	+0.00	-0.14	+0.14	-0.00	+0.00
XSecs PC11	-0.45	+0.46	-0.46	+0.47	-0.02	+0.02	-0.03	+0.03	-0.40	+0.41	-0.62	+0.63	-0.18	+0.18	-0.14	+0.14	-0.00	+0.00	-0.16	+0.16	-0.00	+0.00
ν_τ scale	-0.22	+0.22	-0.00	+0.00	-16.24	+16.24	-24.74	+24.74	-0.00	+0.00	-0.00	+0.00	-44.47	+44.47	-0.00	+0.00	-0.00	+0.00	-45.99	+45.99	-0.00	+0.00
Flux PC00	-0.11	+0.11	-0.09	+0.08	-1.64	+1.63	-2.49	+2.48	-0.08	+0.08	-0.12	+0.11	-2.72	+2.69	-2.22	+2.22	-2.60	+2.61	-2.72	+2.69	-0.00	+0.00
Flux PC01	-0.05	+0.01	-0.03	+0.00	-2.97	+2.92	-4.52	+4.45	-0.03	+0.00	-0.05	+0.00	-4.53	+4.42	-4.47	+4.44	-5.18	+5.15	-4.57	+4.46	-0.00	+0.00
Flux PC02	-0.03	+0.00	-0.03	+0.00	-1.69	+1.66	-2.58	+2.53	-0.20	+0.17	-0.55	+0.48	-3.34	+3.26	-1.70	+1.69	-2.10	+1.46	-3.30	+3.22	-0.00	+0.00
Flux PC03	-0.10	+0.05	-0.15	+0.10	-3.96	+3.90	-6.03	+5.95	-0.22	+0.19	-0.16	+0.05	-6.62	+6.51	-5.30	+5.25	-5.68	+5.63	-6.65	+6.54	-0.00	+0.00
Flux PC04	-0.20	+0.20	-0.20	+0.20	-0.05	+0.04	-0.07	+0.07	-0.14	+0.14	-0.40	+0.40	-0.34	+0.33	-0.24	+0.24	-0.18	+0.18	-0.33	+0.32	-0.00	+0.00
Absolute calib.	-4.53	+3.62	-4.57	+3.67	-1.07	+0.49	-1.64	+0.75	-4.49	+3.95	-4.80	+2.84	-1.30	+0.00	-2.78	+2.96	-6.84	+9.03	-1.10	+0.00	-0.00	+0.00
ND/FD relative calib.	-4.70	+4.66	-4.76	+4.73	-0.46	+0.32	-0.71	+0.49	-4.60	+4.60	-5.25	+5.10	-0.37	+0.00	-1.41	+1.46	-3.69	+4.24	-0.35	+0.00	-0.00	+0.00
Calibration shape	-0.77	+0.77	-0.78	+0.78	-0.01	+0.01	-0.02	+0.02	-0.09	+0.09	-2.80	+2.80	-0.58	+0.58	-0.53	+0.53	-10.14	+10.14	-0.44	+0.44	-0.00	+0.00
Calibration drift	-0.45	+0.00	-0.47	+0.00	-0.00	+1.15	-0.00	+1.75	-0.33	+0.00	-0.91	+0.00	-2.27	+0.00	-0.00	+6.30	-27.93	+0.00	-1.64	+0.00	-0.00	+0.00
Light level FD	-0.00	+0.32	-0.00	+0.32	-0.00	+1.15	-0.00	+1.75	-0.00	+0.38	-0.00	+0.33	-0.21	+0.06	-0.00	+4.14	-59.36	+0.00	-0.00	+0.54	-0.00	+0.00
Light level ND	-2.70	+0.00	-2.74	+0.00	-0.00	+0.00	-0.00	+0.00	-2.45	+0.00	-3.59	+0.00	-0.00	+0.00	-0.00	+0.00	-0.00	+0.00	-0.00	+0.00	-0.00	+0.00
Cherenkov	-0.00	+1.77	-0.00	+1.79	-0.00	+0.53	-0.00	+0.81	-0.00	+1.97	-0.00	+1.27	-1.52	+0.00	-0.00	+3.68	-43.19	+0.00	-1.16	+0.00	-0.00	+0.00
E_μ ND uncorr.	-0.23	+0.20	-0.23	+0.21	-0.00	+0.00	-0.00	+0.00	-0.23	+0.18	-0.26	+0.28	-0.00	+0.00	-0.00	+0.00	-0.00	+0.00	-0.00	+0.00	-0.00	+0.00
E_μ μ-catcher uncorr.	-0.17	+0.14	-0.17	+0.15	-0.00	+0.00	-0.00	+0.00	-0.12	+0.09	-0.33	+0.31	-0.00	+0.00	-0.00	+0.00	-0.00	+0.00	-0.00	+0.00	-0.00	+0.00
E_μ n pile-up	-0.64	+0.00	-0.64	+0.00	-0.00	+0.00	-0.00	+0.00	-0.57	+0.00	-0.88	+0.00	-0.00	+0.00	-0.00	+0.00	-0.00	+0.00	-0.00	+0.00	-0.00	+0.00
E_μ correlated	-1.81	+2.00	-1.83	+2.03	-0.18	+0.00	-0.28	+0.00	-1.90	+1.98	-1.64	+2.18	-0.41	+0.39	-1.06	+0.52	-2.21	+0.00	-0.45	+0.39	-0.00	+0.00
E_μ FD uncorr.	-0.11	+0.12	-0.11	+0.12	-0.00	+0.09	-0.00	+0.13	-0.16	+0.14	-0.00	+0.04	-0.08	+0.20	-0.00	+0.30	-1.27	+0.00	-0.10	+0.19	-0.00	+0.00
Lepton angle xz ND	-0.46	+0.43	-0.47	+0.44	-0.00	+0.00	-0.00	+0.00	-0.43	+0.37	-0.57	+0.62	-0.00	+0.00	-0.00	+0.00	-0.00	+0.00	-0.00	+0.00	-0.00	+0.00
Lepton angle yz ND	-0.15	+0.00	-0.16	+0.00	-0.00	+0.00	-0.00	+0.00	-0.10	+0.00	-0.33	+0.12	-0.00	+0.00	-0.00	+0.00	-0.00	+0.00	-0.00	+0.00	-0.00	+0.00
Lepton angle xz FD	-0.00	+0.00	-0.00	+0.00	-0.00	+0.00	-0.00	+0.00	-0.00	+0.00	-0.00	+0.00	-0.00	+0.00	-0.00	+0.00	-0.00	+0.00	-0.00	+0.00	-0.00	+0.00
Lepton angle yz FD	-0.00	+0.00	-0.00	+0.00	-0.00	+0.00	-0.00	+0.00	-0.00	+0.00	-0.00	+0.01	-0.00	+0.00	-0.00	+0.00	-0.00	+0.00	-0.00	+0.00	-0.00	+0.00
Neutron systematic	-4.58	+2.55	-4.65	+2.60	-1.09	+0.93	-1.66	+1.41	-5.18	+2.90	-3.11	+1.73	-3.02	+3.13	-0.00	+0.20	-4.74	+0.00	-3.30	+2.38	-0.00	+0.00
Normalization beam corr.	-0.83	+0.83	-0.83	+0.83	-0.55	+0.55	-0.84	+0.84	-0.82	+0.82	-0.86	+0.86	-0.89	+0.89	-0.78	+0.78	-0.84	+0.84	-0.89	+0.89	-0.00	+0.00
Normalization $\bar{\nu}$-beam	-0.74	+0.74	-0.74	+0.74	-0.49	+0.49	-0.75	+0.75	-0.73	+0.73	-0.76	+0.76	-0.79	+0.79	-0.70	+0.70	-0.75	+0.75	-0.80	+0.80	-0.00	+0.00
Cosmic scale	-0.29	+0.68	-0.00	+0.00	-21.71	+51.22	-0.00	+0.00	-0.00	+0.00	-0.00	+0.00	-0.00	+0.00	-0.00	+0.00	-0.00	+0.00	-0.00	+0.00	-63.17	+149.02
Quadrature	-9.02	+7.86	-9.12	+7.90	-28.63	+54.80	-28.43	+29.67	-9.10	+7.84	-10.05	+9.22	-47.83	+48.75	-18.62	+23.96	-80.40	+21.39	-49.32	+50.59	-63.17	+149.02

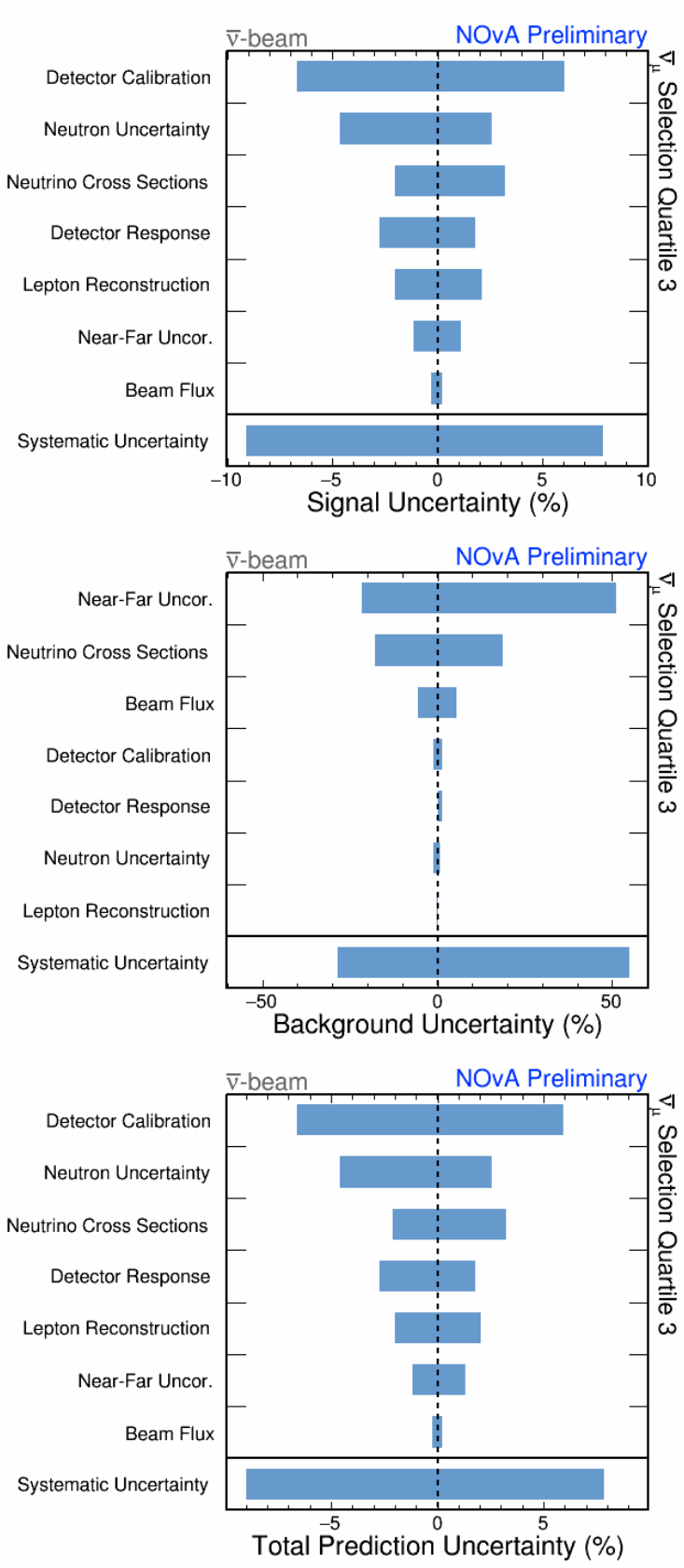

Figure C.16: Relative 1σ systematic uncertainties on the integral number of signal (top), background (middle), and total (bottom) predicted events in the $\bar{\nu}_\mu$ disapp. $\bar{\nu}$-beam quartile 3.

$\bar{\nu}_\mu$ E_{had} fraction quartile 4

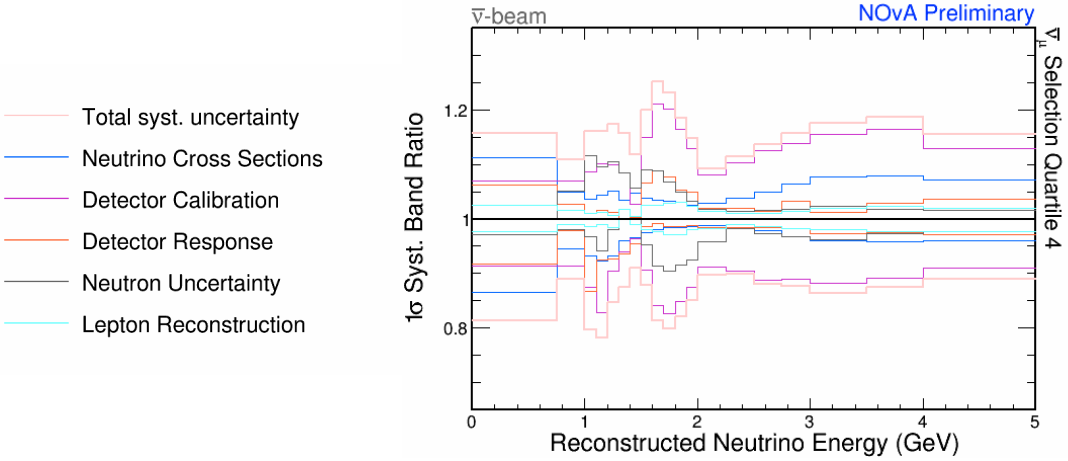

Figure C.17: 1σ systematic bands relative to the nominal prediction for the $\bar{\nu}$-beam $\bar{\nu}_\mu$ disapp. quartile 4 in the reconstructed neutrino energy.

Table C.9: Relative 1σ systematic uncertainties on the integral numbers of predicted events for the $\bar{\nu}_\mu$ disapp. $\bar{\nu}$-beam quartile 4.

Systematic Summary for rhc NuMu Quartile 4 (%)

Systematic	Total pred		Signal		Total bkg		Beam bkg		$\bar{\nu}_\mu$ signal		ν_μ signal		ν_μ app.		NC		ν_e CC		ν_τ CC		Cosmics	
CCQE z-exp.ax.vec. 1	-0.06	+0.06	-0.05	+0.06	-0.07	+0.08	-0.13	+0.15	-0.05	+0.05	-0.07	+0.07	-0.85	+0.92	-0.00	+0.00	-0.12	+0.14	-0.87	+0.94	-0.00	+0.00
CCQE z-exp.ax.vec. 2	-0.04	+0.05	-0.04	+0.05	-0.05	+0.06	-0.10	+0.12	-0.04	+0.04	-0.05	+0.05	-0.71	+0.77	-0.00	+0.00	-0.27	+0.36	-0.72	+0.79	-0.00	+0.00
CCQE z-exp.ax.vec. 3	-0.10	+0.17	-0.10	+0.17	-0.16	+0.21	-0.30	+0.40	-0.10	+0.19	-0.10	+0.15	-1.91	+2.50	-0.00	+0.00	-0.62	+0.94	-1.74	+2.28	-0.00	+0.00
CCQE z-exp.ax.vec. 4	-0.03	+0.04	-0.03	+0.04	-0.04	+0.05	-0.08	+0.09	-0.03	+0.04	-0.03	+0.03	-0.51	+0.56	-0.00	+0.00	-0.31	+0.38	-0.45	+0.50	-0.00	+0.00
M_A^{CCRES}	-0.97	+3.49	-0.96	+3.55	-1.25	+2.34	-2.40	+4.49	-0.69	+3.00	-1.39	+4.42	-14.38	+24.24	-0.00	+0.00	-4.85	+17.04	-14.07	+25.26	-0.00	+0.00
M_A^{CCRES}	-0.00	+1.13	-0.00	+1.11	-0.81	+1.44	-1.56	+2.76	-0.05	+1.27	-0.00	+0.85	-9.86	+16.19	-0.00	+0.00	-2.38	+8.45	-9.10	+15.50	-0.00	+0.00
M_A^{NCRES}	-0.19	+0.34	-0.16	+0.08	-5.14	+9.44	-9.88	+18.14	-0.16	+0.08	-0.16	+0.08	-0.00	+0.00	-12.20	+22.39	-0.00	+0.00	-0.00	+0.00	-0.00	+0.00
M_A^{NCRES}	-0.00	+0.02	-0.01	+0.00	-0.03	+0.65	-0.06	+1.25	-0.01	+0.00	-0.01	+0.00	-0.00	+0.00	-0.08	+1.54	-0.00	+0.00	-0.00	+0.00	-0.00	+0.00
CCQE z-exp.norm.	-0.27	+0.35	-0.27	+0.35	-0.27	+0.36	-0.52	+0.70	-0.31	+0.40	-0.21	+0.26	-3.38	+4.51	-0.00	+0.00	-0.06	+0.07	-3.23	+4.31	-0.00	+0.00
RPA high Q^2 enh.	-0.07	+0.12	-0.07	+0.12	-0.01	+0.02	-0.03	+0.04	-0.09	+0.15	-0.05	+0.08	-0.16	+0.25	-0.00	+0.00	-0.06	+0.07	-0.14	+0.21	-0.00	+0.00
RPA low Q^2 supp.	-0.00	+0.00	-0.00	+0.00	-0.00	+0.00	-0.00	+0.00	-0.00	+0.00	-0.01	+0.00	-0.03	+0.03	-0.00	+0.00	-0.00	+0.00	-0.03	+0.03	-0.00	+0.00
RES low Q^2 supp.	-0.00	+0.12	-0.00	+0.14	-0.15	+0.00	-0.30	+0.00	-0.00	+0.13	-0.00	+0.14	-0.33	+0.00	-0.30	+0.00	-0.34	+0.00	-0.28	+0.00	-0.00	+0.00
DIS CC $\nu n \to 1\pi$	-0.77	+0.74	-0.80	+0.76	-0.25	+0.25	-0.47	+0.47	-0.47	+0.45	-1.31	+1.26	-1.62	+1.62	-0.00	+0.00	-5.97	+5.97	-1.89	+1.89	-0.00	+0.00
FSI π free path	-0.49	+0.41	-0.41	+0.38	-1.97	+0.96	-3.78	+1.84	-0.38	+0.29	-0.45	+0.53	-0.26	+0.54	-4.60	+2.20	-4.60	+2.85	-0.18	+0.54	-0.00	+0.00
FSI fate fraction	-0.21	+0.02	-0.21	+0.04	-0.32	+0.00	-0.62	+0.00	-0.21	+0.00	-0.22	+0.16	-0.09	+0.00	-0.74	+0.00	-0.70	+0.00	-0.03	+0.00	-0.00	+0.00
MEC E_ν shape	-0.09	+0.13	-0.09	+0.14	-0.03	+0.02	-0.05	+0.04	-0.06	+0.09	-0.14	+0.22	-0.30	+0.20	-0.00	+0.00	-0.00	+0.00	-0.35	+0.23	-0.00	+0.00
MEC $E_{\bar{\nu}}$ shape	-0.02	+0.06	-0.03	+0.06	-0.01	+0.00	-0.02	+0.00	-0.00	+0.04	-0.06	+0.09	-0.14	+0.04	-0.00	+0.00	-0.00	+0.01	-0.16	+0.04	-0.00	+0.00
MEC ν (q_0, q) response	-0.25	+0.00	-0.27	+0.00	-0.27	+0.20	-0.52	+0.38	-0.35	+0.03	-0.14	+0.00	-3.39	+3.14	-0.00	+0.00	-0.00	+0.00	-3.19	+2.05	-0.00	+0.00
MEC $\bar{\nu}$ (q_0, q) response	-0.61	+0.16	-0.65	+0.18	-0.13	+0.03	-0.24	+0.05	-0.70	+0.20	-0.58	+0.14	-1.57	+0.38	-0.00	+0.00	-0.02	+0.09	-1.51	+0.27	-0.00	+0.00
MEC ν init. np frac.	-0.00	+0.01	-0.00	+0.02	-0.00	+0.00	-0.02	+0.00	-0.00	+0.00	-0.01	+0.04	-0.05	+0.02	-0.00	+0.00	-0.00	+0.00	-0.14	+0.05	-0.00	+0.00
MEC $\bar{\nu}$ init. np frac.	-0.04	+0.01	-0.04	+0.01	-0.02	+0.00	-0.04	+0.01	-0.02	+0.00	-0.07	+0.02	-0.26	+0.09	-0.00	+0.00	-0.00	+0.00	-0.23	+0.08	-0.00	+0.00
XSecs PC00	-0.15	+0.15	-0.04	+0.04	-3.62	+3.62	-6.95	+6.95	-0.06	+0.06	-0.00	+0.00	-0.03	+0.03	-8.58	+8.58	-0.00	+0.00	-0.03	+0.03	-0.00	+0.00
XSecs PC01	-0.12	+0.12	-0.00	+0.00	-2.53	+2.53	-4.86	+4.86	-0.03	+0.03	-0.03	+0.03	-0.01	+0.01	-5.99	+5.99	-0.00	+0.00	-0.00	+0.00	-0.00	+0.00
XSecs PC02	-0.53	+0.67	-0.57	+0.72	-0.21	+0.21	-0.41	+0.41	-0.30	+0.37	-1.00	+1.29	-0.28	+0.28	-0.44	+0.44	-0.00	+0.00	-0.36	+0.36	-0.00	+0.00
XSecs PC03	-0.04	+0.04	-0.03	+0.03	-0.24	+0.24	-0.46	+0.46	-0.00	+0.00	-0.07	+0.08	-0.12	+0.12	-0.60	+0.60	-0.00	+0.00	-0.15	+0.15	-0.00	+0.00
XSecs PC04	-0.48	+0.50	-0.53	+0.56	-0.48	+0.48	-0.92	+0.92	-0.42	+0.44	-0.71	+0.75	-0.30	+0.30	-1.08	+1.08	-0.00	+0.00	-0.30	+0.30	-0.00	+0.00
XSecs PC05	-0.04	+0.04	-0.03	+0.03	-0.04	+0.04	-0.08	+0.08	-0.01	+0.01	-0.07	+0.07	-0.02	+0.02	-0.10	+0.10	-0.00	+0.00	-0.00	+0.00	-0.00	+0.00
XSecs PC06	-0.20	+0.20	-0.24	+0.24	-0.45	+0.45	-0.87	+0.87	-0.16	+0.16	-0.36	+0.37	-0.10	+0.10	-1.06	+1.06	-0.00	+0.00	-0.09	+0.09	-0.00	+0.00
XSecs PC07	-0.51	+0.52	-0.46	+0.47	-1.44	+1.44	-2.77	+2.77	-0.35	+0.36	-0.63	+0.65	-0.23	+0.23	-3.46	+3.46	-0.00	+0.00	-0.20	+0.20	-0.00	+0.00
XSecs PC08	-0.04	+0.04	-0.08	+0.08	-0.76	+0.76	-1.47	+1.47	-0.00	+0.00	-0.21	+0.21	-0.02	+0.02	-1.81	+1.81	-0.00	+0.00	-0.01	+0.01	-0.00	+0.00
XSecs PC09	-0.26	+0.26	-0.28	+0.29	-0.17	+0.17	-0.33	+0.33	-0.20	+0.21	-0.40	+0.41	-0.18	+0.18	-0.38	+0.38	-0.00	+0.00	-0.16	+0.16	-0.00	+0.00
XSecs PC10	-0.29	+0.29	-0.31	+0.32	-0.18	+0.18	-0.34	+0.34	-0.21	+0.22	-0.47	+0.48	-0.17	+0.17	-0.39	+0.39	-0.00	+0.00	-0.15	+0.15	-0.00	+0.00
XSecs PC11	-0.41	+0.42	-0.43	+0.44	-0.05	+0.05	-0.10	+0.10	-0.35	+0.36	-0.56	+0.57	-0.21	+0.21	-0.16	+0.16	-0.00	+0.00	-0.18	+0.18	-0.00	+0.00
ν_τ scale	-0.19	+0.19	-0.00	+0.00	-3.64	+3.64	-6.99	+6.99	-0.00	+0.00	-0.00	+0.00	-42.54	+42.54	-0.00	+0.00	-0.00	+0.00	-44.55	+44.55	-0.00	+0.00
Flux PC00	-0.11	+0.10	-0.05	+0.04	-1.23	+1.22	-2.36	+2.35	-0.06	+0.05	-0.03	+0.02	-2.55	+2.52	-2.32	+2.32	-2.44	+2.40	-2.54	+2.51	-0.00	+0.00
Flux PC01	-0.12	+0.08	-0.05	+0.00	-2.37	+2.34	-4.55	+4.50	-0.03	+0.00	-0.08	+0.00	-4.17	+4.06	-4.63	+4.59	-4.46	+4.30	-4.22	+4.11	-0.00	+0.00
Flux PC02	-0.14	+0.10	-0.21	+0.17	-1.14	+1.13	-2.19	+2.17	-0.44	+0.42	-0.23	+0.16	-3.40	+3.35	-1.95	+1.94	-2.17	+1.98	-3.40	+3.35	-0.00	+0.00
Flux PC03	-0.03	+0.00	-0.20	+0.13	-3.03	+2.99	-5.83	+5.75	-0.30	+0.26	-0.08	+0.00	-6.44	+6.32	-5.72	+5.65	-5.27	+5.14	-6.52	+6.40	-0.00	+0.00
Flux PC04	-0.16	+0.16	-0.17	+0.17	-0.03	+0.03	-0.06	+0.06	-0.10	+0.10	-0.29	+0.30	-0.36	+0.35	-0.13	+0.13	-0.24	+0.23	-0.35	+0.34	-0.00	+0.00
Absolute calib.	-5.73	+7.49	-5.98	+7.85	-1.24	+1.08	-2.38	+2.07	-6.49	+7.88	-5.18	+7.79	-0.95	+1.40	-2.86	+2.48	-9.68	+6.66	-0.87	+1.51	-0.00	+0.00
ND/FD relative calib.	-4.52	+5.04	-4.80	+5.35	-0.60	+0.56	-1.15	+1.07	-4.35	+4.61	-5.53	+6.53	-0.53	+0.64	-1.38	+1.29	-4.46	+3.71	-0.52	+0.67	-0.00	+0.00
Calibration shape	-2.71	+2.71	-2.86	+2.86	-0.14	+0.14	-0.27	+0.27	-2.92	+2.92	-2.77	+2.77	-0.08	+0.08	-0.38	+0.38	-1.07	+1.07	-0.05	+0.05	-0.00	+0.00
Calibration drift	-0.40	+0.00	-0.39	+0.00	-0.72	+0.00	-1.38	+0.00	-0.41	+0.00	-0.35	+0.00	-0.85	+0.00	-1.58	+0.00	-0.27	+0.00	-0.46	+0.00	-0.00	+0.00
Light level FD	-0.79	+0.00	-0.79	+0.00	-0.65	+0.00	-1.25	+0.00	-0.54	+0.00	-1.20	+0.00	-0.36	+0.00	-0.66	+0.00	-22.42	+0.00	-0.12	+0.09	-0.00	+0.00
Light level ND	-1.12	+1.31	-1.19	+1.39	-0.00	+0.00	-0.00	+0.00	-1.22	+1.16	-1.13	+1.74	-0.00	+0.00	-0.00	+0.00	-0.00	+0.00	-0.00	+0.00	-0.00	+0.00
Cherenkov	-0.00	+1.71	-0.00	+1.77	-0.00	+0.59	-0.00	+1.13	-0.00	+2.20	-0.00	+1.08	-1.11	+0.00	-0.00	+1.79	-5.07	+0.00	-1.04	+0.00	-0.00	+0.00
E_μ ND uncorr.	-0.08	+0.09	-0.08	+0.10	-0.00	+0.00	-0.00	+0.00	-0.07	+0.07	-0.10	+0.15	-0.00	+0.00	-0.00	+0.00	-0.00	+0.00	-0.00	+0.00	-0.00	+0.00
E_μ μ-catcher uncorr.	-0.00	+0.03	-0.00	+0.03	-0.00	+0.00	-0.00	+0.00	-0.03	+0.04	-0.00	+0.03	-0.00	+0.00	-0.00	+0.00	-0.00	+0.00	-0.00	+0.00	-0.00	+0.00
E_μ n pile-up	-0.21	+0.00	-0.22	+0.00	-0.00	+0.00	-0.00	+0.00	-0.17	+0.00	-0.30	+0.00	-0.00	+0.00	-0.00	+0.00	-0.00	+0.00	-0.00	+0.00	-0.00	+0.00
E_μ correlated	-1.57	+1.55	-1.65	+1.63	-0.18	+0.25	-0.35	+0.47	-1.64	+1.63	-1.67	+1.62	-1.05	+1.25	-0.22	+0.34	-0.00	+0.05	-1.13	+1.26	-0.00	+0.00
E_μ FD uncorr.	-0.22	+0.20	-0.23	+0.21	-0.03	+0.03	-0.07	+0.06	-0.24	+0.24	-0.20	+0.17	-0.15	+0.18	-0.05	+0.04	-0.00	+0.00	-0.19	+0.19	-0.00	+0.00
Lepton angle xz ND	-0.38	+0.20	-0.40	+0.21	-0.00	+0.00	-0.00	+0.00	-0.32	+0.15	-0.53	+0.31	-0.00	+0.00	-0.00	+0.00	-0.00	+0.00	-0.00	+0.00	-0.00	+0.00
Lepton angle yz ND	-0.16	+0.00	-0.17	+0.00	-0.00	+0.00	-0.00	+0.00	-0.14	+0.00	-0.21	+0.00	-0.00	+0.00	-0.00	+0.00	-0.00	+0.00	-0.00	+0.00	-0.00	+0.00
Lepton angle xz FD	-0.00	+0.00	-0.00	+0.00	-0.00	+0.00	-0.00	+0.00	-0.00	+0.00	-0.00	+0.00	-0.00	+0.00	-0.00	+0.00	-0.00	+0.00	-0.00	+0.00	-0.00	+0.00
Lepton angle yz FD	-0.00	+0.00	-0.00	+0.00	-0.00	+0.00	-0.00	+0.00	-0.00	+0.00	-0.00	+0.00	-0.00	+0.00	-0.00	+0.00	-0.00	+0.00	-0.00	+0.00	-0.00	+0.00
Neutron systematic	-2.77	+1.99	-2.95	+2.13	-0.60	+0.58	-1.14	+1.12	-3.68	+2.50	-1.80	+1.53	-1.62	+2.57	-1.11	+0.92	-0.59	+0.00	-1.54	+2.41	-0.00	+0.00
Normalization beam corr.	-0.75	+0.75	-0.77	+0.77	-0.42	+0.42	-0.82	+0.82	-0.77	+0.77	-0.77	+0.77	-0.86	+0.86	-0.81	+0.81	-0.79	+0.79	-0.86	+0.86	-0.00	+0.00
Normalization $\bar{\nu}$-beam	-0.67	+0.67	-0.69	+0.69	-0.38	+0.38	-0.73	+0.73	-0.69	+0.69	-0.68	+0.68	-0.76	+0.76	-0.72	+0.72	-0.70	+0.70	-0.77	+0.77	-0.00	+0.00
Cosmic scale	-0.93	+1.31	-0.00	+0.00	-17.92	+25.25	-0.00	+0.00	-0.00	+0.00	-0.00	+0.00	-0.00	+0.00	-0.00	+0.00	-0.00	+0.00	-0.00	+0.00	-37.35	+52.64
Quadrature	-8.87	+10.90	-9.26	+11.32	-20.28	+28.14	-18.24	+23.84	-9.57	+10.97	-9.10	+12.14	-47.25	+52.79	-19.43	+26.68	-28.11	+22.84	-48.82	+54.63	-37.35	+52.64

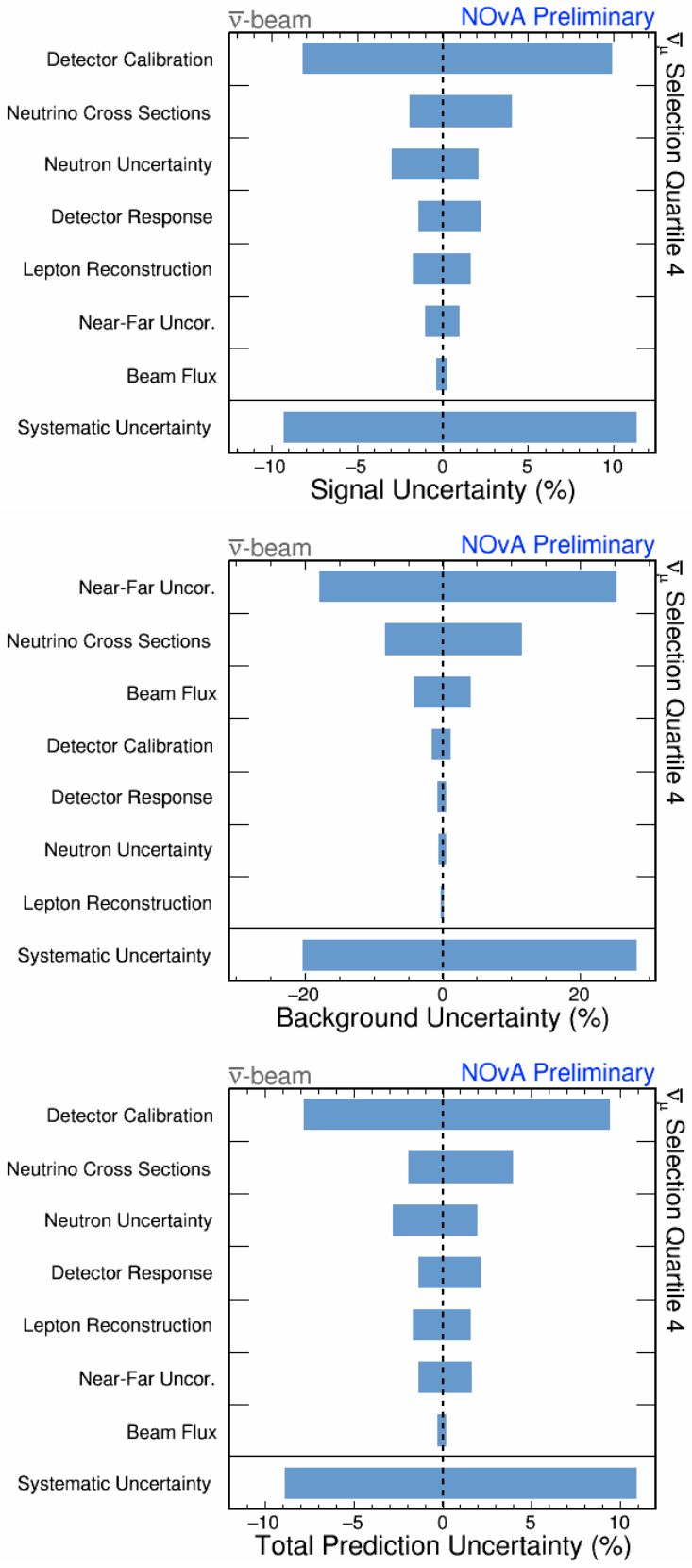

Figure C.18: Relative 1σ systematic uncertainties on the integral number of signal (top), background (middle), and total (bottom) predicted events in the $\bar{\nu}_\mu$ disapp. $\bar{\nu}$-beam quartile 4.

Summed all $\bar{\nu}_\mu$ quartiles

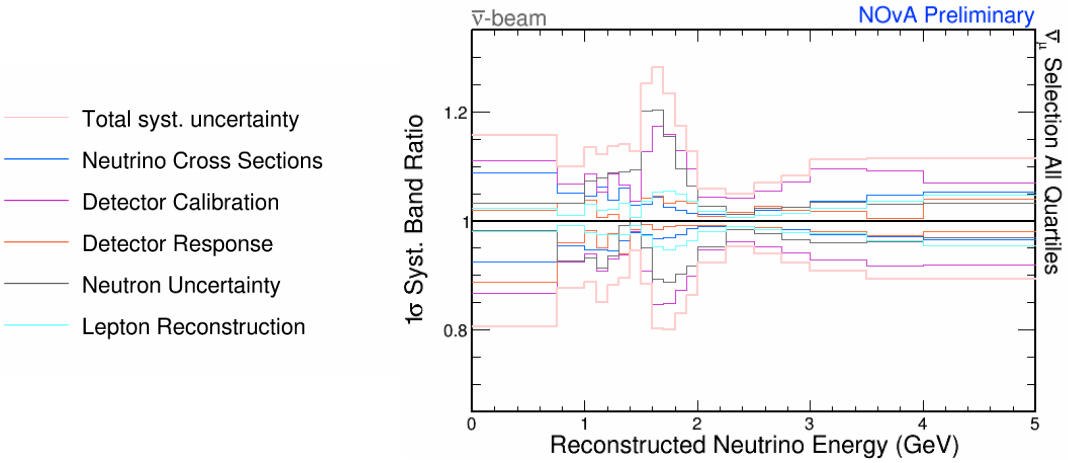

Figure C.19: 1σ systematic bands relative to the nominal prediction for the $\bar{\nu}$-beam $\bar{\nu}_\mu$ disapp. all quartiles in the reconstructed neutrino energy.

Table C.10: Relative 1σ systematic uncertainties on the integral numbers of predicted events for the $\bar{\nu}_\mu$ disapp. $\bar{\nu}$-beam all quartiles.

Systematic summary for ν_μ disappearance $\bar{\nu}$-beam all quartiles (%)

Systematic	Total pred		Signal		Total bkg		Beam bkg		$\bar{\nu}_\mu$ signal		ν_μ signal		ν_μ app.		NC		ν_e CC		ν_τ CC		Cosmics	
CCQE z-exp.ax.vec. 1	-0.14	+0.15	-0.13	+0.14	-0.39	+0.43	-0.69	+0.75	-0.14	+0.15	-0.13	+0.13	-2.16	+2.34	-0.00	+0.00	-0.11	+0.13	-2.00	+2.17	-0.00	+0.00
CCQE z-exp.ax.vec. 2	-0.13	+0.14	-0.12	+0.13	-0.32	+0.35	-0.57	+0.61	-0.13	+0.14	-0.11	+0.12	-1.78	+1.92	-0.00	+0.00	-0.26	+0.34	-1.66	+1.79	-0.00	+0.00
CCQE z-exp.ax.vec. 3	-0.24	+0.31	-0.24	+0.31	-0.45	+0.54	-0.79	+0.95	-0.24	+0.31	-0.23	+0.29	-2.38	+2.82	-0.00	+0.00	-0.58	+0.89	-2.28	+2.72	-0.00	+0.00
CCQE z-exp.ax.vec. 4	-0.06	+0.06	-0.06	+0.06	-0.09	+0.10	-0.16	+0.17	-0.06	+0.06	-0.06	+0.06	-0.47	+0.50	-0.00	+0.00	-0.29	+0.35	-0.45	+0.48	-0.00	+0.00
M_A^{CCRES}	-0.33	+1.40	-0.30	+1.37	-1.58	+2.59	-2.78	+4.55	-0.07	+0.87	-1.01	+2.87	-7.40	+11.24	-0.00	+0.00	-4.80	+16.84	-8.18	+12.99	-0.00	+0.00
M_V^{CCRES}	-0.04	+0.53	-0.02	+0.51	-1.06	+1.72	-1.86	+3.02	-0.00	+0.37	-0.18	+0.93	-5.11	+7.91	-0.00	+0.00	-2.45	+8.55	-5.48	+8.66	-0.00	+0.00
M_A^{NCRES}	-0.06	+0.11	-0.05	+0.03	-4.51	+7.87	-7.92	+13.81	-0.05	+0.03	-0.08	+0.04	-0.00	+0.00	-12.33	+21.52	-0.00	+0.00	-0.00	+0.00	-0.00	+0.00
M_V^{NCRES}	-0.00	+0.00	-0.00	+0.00	-0.04	+0.54	-0.07	+0.94	-0.00	+0.00	-0.00	+0.00	-0.00	+0.00	-0.10	+1.46	-0.00	+0.00	-0.00	+0.00	-0.00	+0.00
CCQE z-exp.norm.	-0.55	+0.68	-0.53	+0.66	-1.11	+1.48	-1.95	+2.60	-0.55	+0.69	-0.48	+0.59	-6.09	+8.11	-0.00	+0.00	-0.05	+0.07	-5.66	+7.54	-0.00	+0.00
RPA high Q^2 enh.	-0.23	+0.28	-0.23	+0.28	-0.08	+0.10	-0.14	+0.17	-0.24	+0.29	-0.19	+0.24	-0.47	+0.57	-0.00	+0.00	-0.06	+0.07	-0.40	+0.49	-0.00	+0.00
RPA low Q^2 supp.	-0.01	+0.01	-0.01	+0.01	-0.06	+0.06	-0.10	+0.10	-0.00	+0.00	-0.04	+0.04	-0.36	+0.36	-0.00	+0.00	-0.00	+0.00	-0.26	+0.26	-0.00	+0.00
RES low Q^2 supp.	-0.00	+0.13	-0.00	+0.13	-0.22	+0.00	-0.39	+0.00	-0.00	+0.12	-0.00	+0.18	-0.39	+0.00	-0.40	+0.00	-0.34	+0.00	-0.38	+0.00	-0.00	+0.00
DIS CC $\nu n \to 1\pi$	-0.30	+0.29	-0.30	+0.29	-0.24	+0.24	-0.42	+0.42	-0.16	+0.15	-0.71	+0.69	-0.77	+0.77	-0.00	+0.00	-5.73	+5.73	-0.94	+0.94	-0.00	+0.00
FSI π free path	-0.38	+0.27	-0.35	+0.26	-1.74	+0.89	-3.06	+1.57	-0.28	+0.19	-0.55	+0.47	-0.21	+0.32	-4.80	+2.45	-4.69	+2.98	-0.20	+0.37	-0.00	+0.00
FSI fate fraction	-0.13	+0.06	-0.13	+0.06	-0.21	+0.00	-0.37	+0.00	-0.12	+0.03	-0.18	+0.15	-0.03	+0.00	-0.54	+0.00	-0.72	+0.11	-0.02	+0.00	-0.00	+0.00
MEC E_ν shape	-0.07	+0.09	-0.07	+0.09	-0.13	+0.06	-0.22	+0.11	-0.05	+0.06	-0.13	+0.16	-0.69	+0.34	-0.00	+0.00	-0.00	+0.00	-0.66	+0.32	-0.00	+0.00
MEC $E_{\bar{\nu}}$ shape	-0.04	+0.12	-0.04	+0.12	-0.17	+0.07	-0.29	+0.12	-0.05	+0.12	-0.00	+0.12	-0.99	+0.43	-0.00	+0.00	-0.00	+0.01	-0.82	+0.33	-0.00	+0.00
MEC ν (q_0, q) response	-0.42	+0.31	-0.42	+0.32	-0.45	+0.00	-0.79	+0.00	-0.39	+0.32	-0.53	+0.31	-2.31	+0.00	-0.00	+0.00	-0.00	+0.00	-2.37	+0.00	-0.00	+0.00
MEC $\bar{\nu}$ (q_0, q) response	-0.34	+0.11	-0.34	+0.11	-0.37	+0.01	-0.64	+0.02	-0.24	+0.03	-0.62	+0.36	-1.89	+0.83	-0.00	+0.00	-0.02	+0.09	-1.91	+0.00	-0.00	+0.00
MEC ν init. np frac.	-0.03	+0.00	-0.03	+0.00	-0.06	+0.02	-0.11	+0.04	-0.03	+0.01	-0.00	+0.00	-0.43	+0.14	-0.00	+0.00	-0.00	+0.00	-0.30	+0.10	-0.00	+0.00
MEC $\bar{\nu}$ init. np frac.	-0.11	+0.35	-0.11	+0.36	-0.00	+0.01	-0.00	+0.02	-0.13	+0.40	-0.07	+0.22	-0.05	+0.16	-0.00	+0.00	-0.00	+0.00	-0.00	+0.03	-0.00	+0.00
XSecs PC00	-0.08	+0.08	-0.01	+0.01	-3.05	+3.05	-5.35	+5.35	-0.00	+0.00	-0.06	+0.06	-0.02	+0.02	-8.33	+8.33	-0.00	+0.00	-0.02	+0.02	-0.00	+0.00
XSecs PC01	-0.06	+0.06	-0.02	+0.02	-2.22	+2.22	-3.90	+3.90	-0.00	+0.00	-0.06	+0.06	-0.00	+0.00	-6.08	+6.08	-0.00	+0.00	-0.00	+0.00	-0.00	+0.00
XSecs PC02	-0.42	+0.51	-0.43	+0.52	-0.22	+0.22	-0.39	+0.39	-0.26	+0.31	-0.92	+1.15	-0.28	+0.28	-0.43	+0.43	-0.00	+0.00	-0.37	+0.37	-0.00	+0.00
XSecs PC03	-0.03	+0.04	-0.03	+0.03	-0.19	+0.19	-0.33	+0.33	-0.01	+0.02	-0.07	+0.08	-0.12	+0.12	-0.59	+0.59	-0.00	+0.00	-0.15	+0.15	-0.00	+0.00
XSecs PC04	-0.47	+0.49	-0.49	+0.51	-0.43	+0.43	-0.76	+0.76	-0.40	+0.42	-0.74	+0.78	-0.26	+0.26	-1.04	+1.04	-0.00	+0.00	-0.27	+0.27	-0.00	+0.00
XSecs PC05	-0.02	+0.02	-0.02	+0.02	-0.04	+0.04	-0.06	+0.06	-0.01	+0.01	-0.05	+0.05	-0.00	+0.00	-0.10	+0.10	-0.00	+0.00	-0.00	+0.00	-0.00	+0.00
XSecs PC06	-0.18	+0.19	-0.19	+0.20	-0.38	+0.38	-0.66	+0.66	-0.15	+0.15	-0.34	+0.35	-0.08	+0.08	-0.99	+0.99	-0.00	+0.00	-0.08	+0.08	-0.00	+0.00
XSecs PC07	-0.43	+0.44	-0.41	+0.42	-1.16	+1.16	-2.04	+2.04	-0.34	+0.35	-0.64	+0.65	-0.19	+0.19	-3.26	+3.26	-0.00	+0.00	-0.17	+0.17	-0.00	+0.00
XSecs PC08	-0.04	+0.04	-0.06	+0.06	-0.62	+0.62	-1.09	+1.09	-0.02	+0.02	-0.17	+0.17	-0.01	+0.01	-1.70	+1.70	-0.00	+0.00	-0.01	+0.01	-0.00	+0.00
XSecs PC09	-0.24	+0.25	-0.25	+0.26	-0.16	+0.16	-0.27	+0.27	-0.20	+0.20	-0.40	+0.41	-0.15	+0.15	-0.35	+0.35	-0.00	+0.00	-0.13	+0.13	-0.00	+0.00
XSecs PC10	-0.27	+0.27	-0.28	+0.28	-0.16	+0.16	-0.28	+0.28	-0.21	+0.22	-0.46	+0.47	-0.14	+0.14	-0.36	+0.36	-0.00	+0.00	-0.13	+0.13	-0.00	+0.00
XSecs PC11	-0.37	+0.37	-0.37	+0.38	-0.02	+0.02	-0.04	+0.04	-0.32	+0.32	-0.54	+0.55	-0.17	+0.17	-0.14	+0.14	-0.00	+0.00	-0.15	+0.15	-0.00	+0.00
ν_e scale	-0.18	+0.18	-0.00	+0.00	-8.44	+8.44	-14.82	+14.82	-0.00	+0.00	-0.00	+0.00	-42.44	+42.44	-0.00	+0.00	-0.00	+0.00	-44.71	+44.71	-0.00	+0.00
Flux PC00	-0.10	+0.10	-0.08	+0.07	-1.38	+1.38	-2.43	+2.42	-0.08	+0.07	-0.07	+0.06	-2.72	+2.70	-2.30	+2.30	-2.44	+2.39	-2.67	+2.65	-0.00	+0.00
Flux PC01	-0.03	+0.00	-0.06	+0.03	-2.59	+2.55	-4.54	+4.48	-0.05	+0.03	-0.09	+0.02	-4.48	+4.38	-4.59	+4.56	-4.43	+4.27	-4.45	+4.34	-0.00	+0.00
Flux PC02	-0.09	+0.06	-0.07	+0.03	-1.32	+1.30	-2.32	+2.28	-0.11	+0.08	-0.52	+0.46	-3.03	+2.95	-1.90	+1.89	-2.34	+2.16	-3.16	+3.08	-0.00	+0.00
Flux PC03	-0.07	+0.02	-0.15	+0.10	-3.33	+3.28	-5.84	+5.76	-0.20	+0.17	-0.12	+0.01	-6.21	+6.12	-5.62	+5.55	-5.31	+5.18	-6.32	+6.22	-0.00	+0.00
Flux PC04	-0.19	+0.19	-0.20	+0.20	-0.00	+0.00	-0.00	+0.00	-0.14	+0.14	-0.35	+0.36	-0.34	+0.33	-0.17	+0.17	-0.22	+0.22	-0.32	+0.31	-0.00	+0.00
Absolute calib.	-4.90	+4.87	-4.97	+4.95	-1.30	+1.13	-2.27	+1.98	-4.98	+4.81	-4.96	+5.36	-0.95	+0.40	-2.99	+2.75	-8.39	+6.61	-0.32	+0.11	-0.00	+0.00
ND/FD relative calib.	-0.84	+1.11	-0.87	+1.15	-0.63	+0.58	-1.10	+1.03	-0.00	+0.21	-3.49	+3.92	-0.41	+0.27	-1.47	+1.41	-3.97	+3.53	-0.13	+0.08	-0.00	+0.00
Calibration shape	-0.22	+0.22	-0.23	+0.23	-0.10	+0.10	-0.18	+0.18	-0.21	+0.21	-0.29	+0.29	-0.25	+0.25	-0.25	+0.25	-2.01	+2.01	-0.14	+0.14	-0.00	+0.00
Calibration drift	-0.12	+0.00	-0.12	+0.00	-0.38	+0.00	-0.67	+0.00	-0.17	+0.00	-0.00	+0.04	-0.51	+0.00	-0.73	+0.00	-5.85	+0.00	-0.08	+0.00	-0.00	+0.00
Light level FD	-0.13	+0.00	-0.13	+0.00	-0.56	+0.00	-0.99	+0.00	-0.05	+0.00	-0.41	+0.00	-0.90	+0.00	-0.75	+0.12	-27.23	+0.00	-0.24	+0.47	-0.00	+0.00
Light level ND	-0.99	+0.50	-1.01	+0.51	-0.00	+0.00	-0.00	+0.00	-0.88	+0.26	-1.41	+1.24	-0.00	+0.00	-0.00	+0.00	-0.00	+0.00	-0.00	+0.00	-0.00	+0.00
Cherenkov	-0.00	+1.08	-0.00	+1.09	-0.00	+0.50	-0.00	+0.87	-0.00	+1.18	-0.00	+0.84	-0.63	+0.00	-0.00	+1.84	-6.89	+0.00	-0.42	+0.00	-0.00	+0.00
E_μ ND uncorr.	-0.26	+0.30	-0.26	+0.30	-0.00	+0.00	-0.00	+0.00	-0.25	+0.28	-0.30	+0.37	-0.00	+0.00	-0.00	+0.00	-0.00	+0.00	-0.00	+0.00	-0.00	+0.00
E_μ μ-catcher uncorr.	-0.30	+0.32	-0.30	+0.33	-0.00	+0.00	-0.00	+0.00	-0.27	+0.29	-0.41	+0.45	-0.00	+0.00	-0.00	+0.00	-0.00	+0.00	-0.00	+0.00	-0.00	+0.00
E_μ n pile-up	-0.81	+0.00	-0.83	+0.00	-0.00	+0.00	-0.00	+0.00	-0.77	+0.00	-1.00	+0.00	-0.00	+0.00	-0.00	+0.00	-0.00	+0.00	-0.00	+0.00	-0.00	+0.00
E_μ correlated	-1.91	+2.07	-1.95	+2.11	-0.06	+0.08	-0.11	+0.14	-1.90	+2.02	-2.11	+2.37	-0.29	+0.27	-0.03	+0.06	-0.03	+0.00	-0.27	+0.31	-0.00	+0.00
E_μ FD uncorr.	-0.07	+0.05	-0.07	+0.05	-0.00	+0.01	-0.01	+0.03	-0.07	+0.06	-0.04	+0.01	-0.05	+0.06	-0.00	+0.02	-0.04	+0.00	-0.04	+0.04	-0.00	+0.00
Lepton angle xz ND	-0.36	+0.31	-0.37	+0.32	-0.00	+0.00	-0.00	+0.00	-0.33	+0.27	-0.49	+0.45	-0.00	+0.00	-0.00	+0.00	-0.00	+0.00	-0.00	+0.00	-0.00	+0.00
Lepton angle yz ND	-0.08	+0.00	-0.08	+0.00	-0.00	+0.00	-0.00	+0.00	-0.07	+0.00	-0.13	+0.00	-0.00	+0.00	-0.00	+0.00	-0.00	+0.00	-0.00	+0.00	-0.00	+0.00
Lepton angle xz FD	-0.00	+0.00	-0.00	+0.00	-0.00	+0.00	-0.00	+0.00	-0.00	+0.00	-0.00	+0.00	-0.00	+0.00	-0.00	+0.00	-0.00	+0.00	-0.00	+0.00	-0.00	+0.00
Lepton angle yz FD	-0.00	+0.00	-0.00	+0.00	-0.00	+0.00	-0.00	+0.00	-0.00	+0.00	-0.00	+0.00	-0.00	+0.00	-0.00	+0.00	-0.00	+0.00	-0.00	+0.00	-0.00	+0.00
Neutron systematic	-3.28	+3.11	-3.35	+3.18	-0.08	+0.07	-0.15	+0.13	-3.67	+3.54	-2.38	+2.10	-0.75	+0.86	-0.09	+0.04	-0.71	+0.00	-0.00	+0.05	-0.00	+0.00
Normalization beam corr.	-0.80	+0.80	-0.80	+0.80	-0.47	+0.47	-0.83	+0.83	-0.81	+0.81	-0.79	+0.79	-0.88	+0.88	-0.80	+0.80	-0.81	+0.81	-0.88	+0.88	-0.00	+0.00
Normalization $\bar{\nu}$-beam	-0.71	+0.71	-0.72	+0.72	-0.42	+0.42	-0.74	+0.74	-0.72	+0.72	-0.71	+0.71	-0.78	+0.78	-0.72	+0.72	-0.72	+0.72	-0.79	+0.79	-0.00	+0.00
Cosmic scale	-0.39	+0.65	-0.00	+0.00	-18.48	+31.27	-0.00	+0.00	-0.00	+0.00	-0.00	+0.00	-0.00	+0.00	-0.00	+0.00	-0.00	+0.00	-0.00	+0.00	-42.95	+72.68
Quadrature	-6.67	+6.83	-6.77	+6.90	-21.97	+34.12	-20.87	+23.97	-6.80	+6.73	-7.60	+8.51	-45.00	+46.38	-19.32	+25.86	-32.55	+22.72	-47.23	+48.91	-42.95	+72.68

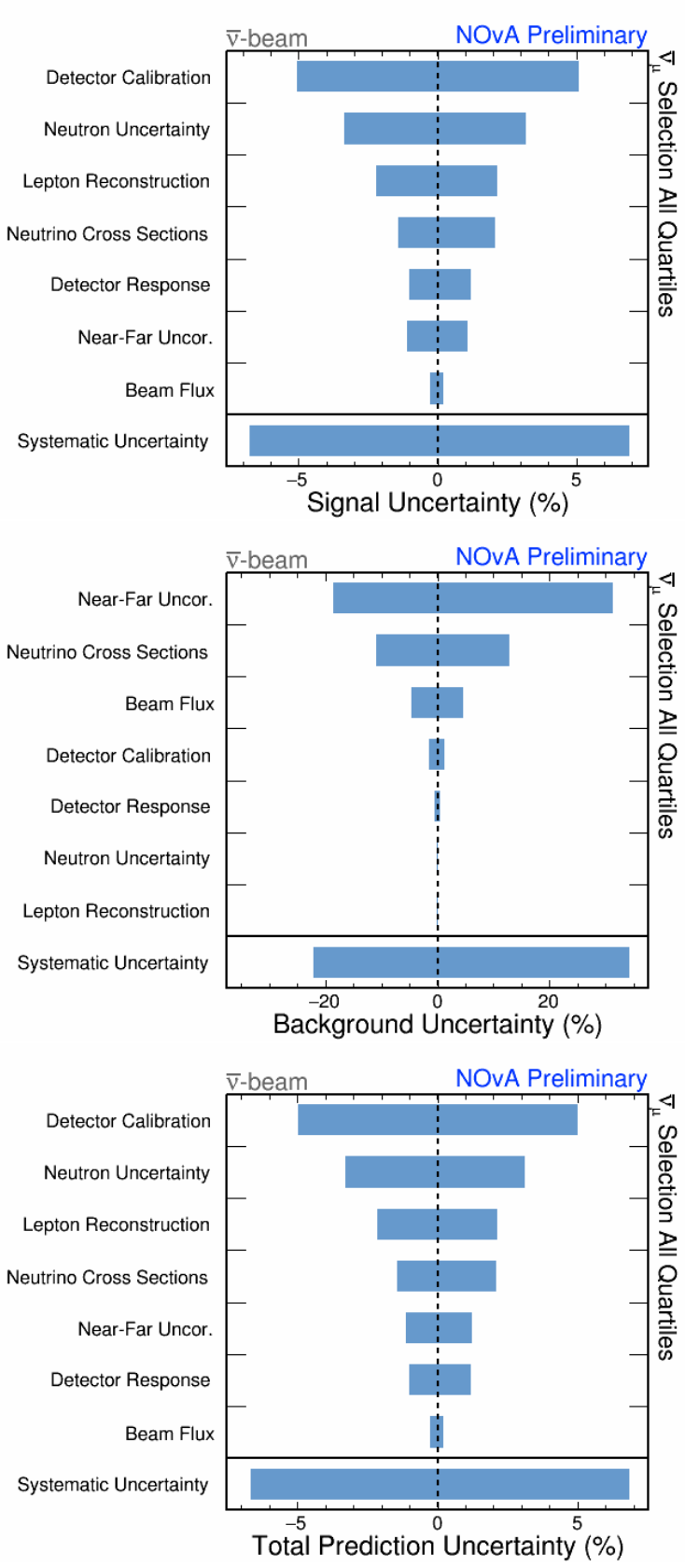

Figure C.20: Relative 1σ syst. uncertainties on the integral number of signal (top), background (middle), and total (bottom) predicted events in the $\bar{\nu}_\mu$ disapp. $\bar{\nu}$-beam all quartiles.

C.3 Appearance ν_e channel, ν-beam

Low PID sample

Table C.11: Relative 1σ systematic uncertainties on the integral numbers of predicted events for the ν_e app. ν-beam low PID sample.

Systematic summary for ν_e appearance ν-beam low PID sample (%)

Systematic	Total pred		ν_e signal		Total bkg		Beam bkg		$\bar{\nu}_e$ WS		Beam ν_e CC		NC		ν_μ CC		ν_τ CC		Cosmics	
CCQE z-exp.ax.vec. 1	-0.45	+0.43	-0.80	+0.77	-0.07	+0.07	-0.08	+0.08	-0.01	+0.05	-0.12	+0.13	-0.18	+0.18	-0.08	+0.07	-1.91	+2.04	-0.00	+0.00
CCQE z-exp.ax.vec. 2	-0.34	+0.33	-0.60	+0.59	-0.05	+0.06	-0.06	+0.06	-0.00	+0.03	-0.09	+0.09	-0.15	+0.14	-0.06	+0.06	-1.62	+1.72	-0.00	+0.00
CCQE z-exp.ax.vec. 3	-0.00	+0.02	-0.00	+0.04	-0.00	+0.01	-0.00	+0.01	-0.00	+0.07	-0.28	+0.34	-0.36	+0.35	-0.22	+0.22	-3.22	+3.67	-0.00	+0.00
CCQE z-exp.ax.vec. 4	-0.05	+0.05	-0.08	+0.08	-0.03	+0.02	-0.04	+0.02	-0.00	+0.00	-0.10	+0.11	-0.05	+0.02	-0.01	+0.02	-0.74	+0.77	-0.00	+0.00
M_A^{CCRES}	-3.07	+3.39	-4.99	+5.28	-1.05	+1.40	-1.21	+1.61	-0.00	+2.31	-6.38	+7.13	-1.72	+1.54	-0.11	+0.92	-8.55	+12.55	-0.00	+0.00
M_V^{CCRES}	-2.48	+2.93	-4.08	+4.71	-0.81	+1.05	-0.93	+1.21	-0.00	+1.68	-4.82	+6.01	-1.42	+1.01	-0.03	+0.32	-5.87	+8.73	-0.00	+0.00
M_A^{NCRES}	-0.14	+0.22	-0.06	+0.04	-0.33	+0.50	-0.38	+0.58	-0.07	+0.05	-0.53	+0.36	-0.79	+1.36	-0.55	+0.17	-0.00	+0.00	-0.00	+0.00
M_V^{NCRES}	-0.03	+0.05	-0.02	+0.01	-0.08	+0.12	-0.09	+0.13	-0.02	+0.02	-0.15	+0.11	-0.16	+0.25	-0.33	+0.35	-0.00	+0.00	-0.00	+0.00
CCQE z-exp.norm.	-1.12	+0.91	-1.98	+1.61	-0.22	+0.16	-0.25	+0.19	-0.54	+0.68	-0.03	+0.06	-0.88	+0.65	-0.37	+0.47	-5.56	+7.41	-0.00	+0.00
RPA high Q^2 enh.	-0.25	+0.28	-0.37	+0.43	-0.12	+0.11	-0.14	+0.13	-0.08	+0.05	-0.00	+0.09	-0.35	+0.28	-0.11	+0.14	-0.00	+0.00	-0.00	+0.00
RPA low Q^2 supp.	-0.40	+0.41	-0.68	+0.68	-0.10	+0.11	-0.12	+0.13	-0.45	+0.43	-0.23	+0.23	-0.09	+0.14	-0.16	+0.09	-0.00	+0.00	-0.00	+0.00
RES low Q^2 supp.	-0.00	+0.13	-0.00	+0.20	-0.00	+0.06	-0.00	+0.07	-0.00	+0.51	-0.15	+0.00	-0.00	+0.18	-0.00	+0.07	-0.02	+0.00	-0.00	+0.00
DIS CC $\nu n \to 1\pi$	-0.73	+0.73	-1.65	+1.58	-0.16	+0.23	-0.19	+0.27	-2.01	+2.10	-1.23	+1.18	-1.57	+1.87	-2.78	+2.29	-1.46	+1.46	-0.00	+0.00
FSI π free path	-1.21	+0.70	-1.13	+0.75	-1.29	+0.66	-1.49	+0.76	-0.64	+0.00	-0.00	+0.02	-3.14	+1.44	-0.10	+1.35	-0.00	+0.25	-0.00	+0.00
FSI fate fraction	-0.63	+0.41	-0.35	+0.21	-0.92	+0.61	-1.06	+0.71	-0.26	+0.48	-0.47	+0.14	-2.35	+1.65	-1.65	+2.44	-0.11	+0.30	-0.00	+0.00
MEC E_ν shape	-0.58	+0.87	-0.89	+1.42	-0.26	+0.29	-0.30	+0.33	-2.26	+2.67	-0.00	+0.17	-0.59	+0.50	-0.24	+0.23	-0.47	+0.07	-0.00	+0.00
MEC $E_{\bar{\nu}}$ shape	-0.00	+0.02	-0.06	+0.07	-0.05	+0.05	-0.05	+0.06	-2.48	+2.10	-0.16	+0.14	-0.06	+0.11	-0.00	+0.00	-0.15	+0.02	-0.00	+0.00
MEC ν (q_0, q) response	-0.30	+0.31	-0.50	+1.73	-1.19	+0.00	-1.38	+0.00	-0.13	+0.88	-0.97	+0.00	-2.60	+0.00	-0.00	+1.67	-0.00	+1.95	-0.00	+0.00
MEC $\bar{\nu}$ (q_0, q) response	-0.03	+0.00	-0.06	+0.07	-0.14	+0.06	-0.16	+0.07	-0.82	+0.00	-0.59	+0.42	-0.55	+0.51	-0.13	+0.21	-0.00	+0.46	-0.00	+0.00
MEC ν init. np frac.	-0.26	+0.08	-0.41	+0.14	-0.10	+0.02	-0.11	+0.03	-0.02	+0.07	-0.28	+0.09	-0.03	+0.00	-0.16	+0.08	-0.57	+0.19	-0.00	+0.00
MEC $\bar{\nu}$ init. np frac.	-0.03	+0.00	-0.00	+0.00	-0.07	+0.02	-0.08	+0.02	-0.15	+0.44	-0.02	+0.06	-0.22	+0.06	-0.00	+0.00	-0.02	+0.07	-0.00	+0.00
ν_e/ν_μ radiative corr.	-1.03	+1.03	-1.98	+1.98	-0.02	+0.02	-0.03	+0.03	-0.00	+0.00	-1.64	+1.64	-0.79	+0.79	-0.33	+0.32	-0.00	+0.00	-0.00	+0.00
$\bar{\nu}_e/\bar{\nu}_\mu$ radiative corr.bar	-0.01	+0.01	-0.00	+0.00	-0.03	+0.03	-0.03	+0.03	-1.99	+1.99	-0.14	+0.14	-0.09	+0.09	-0.03	+0.03	-0.00	+0.00	-0.00	+0.00
Second class currents	-1.03	+1.03	-1.98	+1.98	-0.03	+0.02	-0.04	+0.03	-1.99	+1.99	-1.50	+1.50	-0.62	+0.61	-0.34	+0.32	-0.00	+0.00	-0.00	+0.00
XSecs PC00	-0.51	+0.69	-0.00	+0.00	-1.06	+1.42	-1.22	+1.64	-0.04	+0.04	-0.83	+1.00	-1.76	+2.43	-0.34	+0.47	-0.02	+0.02	-0.00	+0.00
XSecs PC01	-0.18	+0.19	-0.09	+0.09	-0.28	+0.30	-0.32	+0.35	-0.10	+0.10	-0.00	+0.00	-0.57	+0.64	-0.14	+0.08	-0.00	+0.00	-0.00	+0.00
XSecs PC02	-0.67	+0.73	-1.03	+1.11	-0.28	+0.34	-0.33	+0.40	-1.42	+1.57	-0.83	+0.85	-0.67	+0.72	-1.45	+1.68	-0.04	+0.04	-0.00	+0.00
XSecs PC03	-0.11	+0.13	-0.21	+0.21	-0.46	+0.48	-0.53	+0.55	-0.35	+0.36	-0.21	+0.23	-0.95	+0.96	-0.13	+0.24	-0.06	+0.06	-0.00	+0.00
XSecs PC04	-0.28	+0.28	-0.36	+0.37	-0.19	+0.19	-0.21	+0.22	-0.42	+0.43	-0.36	+0.36	-0.63	+0.65	-0.19	+0.16	-0.00	+0.00	-0.00	+0.00
XSecs PC05	-0.40	+0.41	-0.17	+0.17	-0.65	+0.65	-0.74	+0.75	-0.16	+0.16	-0.08	+0.08	-0.36	+0.36	-4.33	+4.39	-0.00	+0.00	-0.00	+0.00
XSecs PC06	-0.03	+0.04	-0.08	+0.08	-0.02	+0.02	-0.02	+0.03	-0.18	+0.18	-0.16	+0.16	-0.12	+0.13	-0.61	+0.64	-0.00	+0.00	-0.00	+0.00
XSecs PC07	-0.10	+0.11	-0.05	+0.05	-0.16	+0.17	-0.18	+0.20	-0.07	+0.07	-0.13	+0.15	-0.23	+0.25	-0.18	+0.18	-0.02	+0.02	-0.00	+0.00
XSecs PC08	-0.29	+0.32	-0.22	+0.22	-0.83	+0.90	-0.96	+1.03	-0.26	+0.27	-0.51	+0.54	-1.23	+1.34	-1.22	+1.30	-0.02	+0.02	-0.00	+0.00
XSecs PC09	-0.33	+0.32	-0.06	+0.06	-0.61	+0.60	-0.70	+0.69	-0.09	+0.09	-0.22	+0.22	-1.53	+1.51	-0.27	+0.27	-0.00	+0.00	-0.00	+0.00
XSecs PC10	-0.23	+0.23	-0.27	+0.27	-0.18	+0.19	-0.21	+0.21	-0.25	+0.25	-0.00	+0.00	-0.55	+0.55	-0.62	+0.64	-0.00	+0.00	-0.00	+0.00
XSecs PC11	-0.59	+0.58	-0.00	+0.00	-1.21	+1.20	-1.40	+1.38	-0.01	+0.01	-0.15	+0.15	-2.60	+2.56	-0.12	+0.15	-0.02	+0.02	-0.00	+0.00
ν_τ scale	-0.52	+0.52	-0.00	+0.00	-1.08	+1.08	-1.24	+1.24	-0.00	+0.00	-0.00	+0.00	-0.00	+0.00	-0.07	+0.07	-63.13	+63.13	-0.00	+0.00
Flux PC00	-0.02	+0.00	-0.09	+0.09	-0.14	+0.11	-0.16	+0.13	-1.40	+1.36	-0.89	+0.83	-0.26	+0.22	-0.42	+0.44	-2.00	+2.00	-0.00	+0.00
Flux PC01	-0.09	+0.06	-0.14	+0.14	-0.04	+0.00	-0.04	+0.00	-2.92	+2.67	-0.18	+0.00	-0.11	+0.09	-0.58	+0.61	-4.34	+4.31	-0.00	+0.00
Flux PC02	-0.07	+0.03	-0.19	+0.19	-0.36	+0.27	-0.41	+0.31	-1.33	+1.17	-0.45	+0.26	-0.21	+0.13	-0.69	+0.68	-2.13	+2.07	-0.00	+0.00
Flux PC03	-0.11	+0.12	-0.11	+0.11	-0.12	+0.12	-0.14	+0.14	-0.96	+0.64	-0.59	+0.59	-0.20	+0.22	-0.02	+0.00	-6.57	+6.59	-0.00	+0.00
Flux PC04	-0.10	+0.10	-0.00	+0.00	-0.19	+0.19	-0.22	+0.22	-0.29	+0.29	-0.46	+0.46	-0.14	+0.14	-0.02	+0.02	-0.43	+0.43	-0.00	+0.00
Absolute calib.	-4.54	+1.97	-1.71	+1.23	-7.52	+2.76	-8.67	+3.18	-0.00	+1.10	-5.03	+3.93	-14.55	+0.00	-0.00	+18.35	-0.06	+0.12	-0.00	+0.00
ND/FD relative calib.	-1.39	+0.81	-0.73	+0.58	-3.48	+2.44	-4.01	+2.81	-0.02	+0.16	-1.25	+0.93	-7.50	+3.67	-2.51	+9.29	-0.04	+0.05	-0.00	+0.00
Calibration shape	-0.72	+0.72	-0.18	+0.18	-1.68	+1.68	-1.93	+1.93	-0.56	+0.56	-0.26	+0.26	-2.99	+2.99	-2.00	+2.00	-0.01	+0.01	-0.00	+0.00
Calibration drift	-0.19	+0.00	-0.44	+0.00	-0.00	+0.06	-0.00	+0.07	-0.00	+1.97	-2.41	+0.00	-2.87	+0.00	-0.00	+16.84	-0.13	+0.00	-0.00	+0.00
Light level FD	-0.81	+0.29	-0.00	+0.98	-2.10	+0.00	-2.43	+0.00	-0.00	+1.69	-4.50	+0.00	-0.90	+0.00	-4.68	+1.27	-0.14	+0.00	-0.00	+0.00
Light level ND	-0.00	+0.43	-0.74	+0.00	-0.00	+0.93	-0.00	+1.07	-0.69	+0.00	-0.28	+1.11	-0.00	+2.56	-2.71	+1.55	-0.00	+0.00	-0.00	+0.00
Cherenkov	-0.00	+1.39	-0.00	+0.36	-0.00	+2.47	-0.00	+2.85	-0.85	+0.00	-0.00	+0.69	-0.00	+3.76	-0.00	+5.13	-0.02	+0.00	-0.00	+0.00
E_μ ND uncorr.	-0.04	+0.04	-0.07	+0.08	-0.00	+0.00	-0.00	+0.00	-0.07	+0.07	-0.04	+0.04	-0.02	+0.02	-0.01	+0.01	-0.00	+0.00	-0.00	+0.00
E_μ μ-catcher uncorr.	-0.00	+0.00	-0.00	+0.00	-0.00	+0.00	-0.00	+0.00	-0.11	+0.11	-0.04	+0.05	-0.02	+0.02	-0.02	+0.02	-0.00	+0.00	-0.00	+0.00
E_μ n pile-up	-0.10	+0.00	-0.18	+0.00	-0.00	+0.00	-0.01	+0.00	-0.24	+0.00	-0.11	+0.00	-0.00	+0.04	-0.00	+0.03	-0.00	+0.00	-0.00	+0.00
E_μ correlated	-0.22	+0.24	-0.42	+0.45	-0.02	+0.02	-0.02	+0.02	-0.41	+0.45	-0.25	+0.25	-0.10	+0.10	-0.08	+0.08	-0.00	+0.00	-0.00	+0.00
Lepton angle xz ND	-0.08	+0.06	-0.16	+0.11	-0.00	+0.00	-0.00	+0.00	-0.18	+0.14	-0.00	+0.00	-0.00	+0.00	-0.00	+0.00	-0.00	+0.00	-0.00	+0.00
Lepton angle yz ND	-0.04	+0.00	-0.07	+0.00	-0.00	+0.00	-0.00	+0.00	-0.05	+0.00	-0.00	+0.00	-0.00	+0.00	-0.00	+0.00	-0.00	+0.00	-0.00	+0.00
Lepton angle xz FD	-0.00	+0.00	-0.00	+0.00	-0.00	+0.00	-0.00	+0.00	-0.01	+0.00	-0.00	+0.00	-0.00	+0.00	-0.00	+0.00	-0.00	+0.00	-0.00	+0.00
Lepton angle yz FD	-0.00	+0.00	-0.00	+0.00	-0.00	+0.00	-0.00	+0.00	-0.00	+0.00	-0.00	+0.00	-0.00	+0.00	-0.00	+0.00	-0.00	+0.00	-0.00	+0.00
Neutron systematic	-0.40	+0.38	-0.24	+0.40	-0.58	+0.37	-0.67	+0.42	-0.36	+0.00	-0.59	+0.67	-0.92	+0.40	-0.00	+0.14	-0.10	+0.22	-0.00	+0.00
Normalization beam corr.	-0.75	+0.75	-0.81	+0.81	-0.68	+0.68	-0.79	+0.79	-0.82	+0.82	-0.80	+0.80	-0.80	+0.80	-0.66	+0.66	-0.87	+0.87	-0.00	+0.00
Normalization ν-beam	-0.58	+0.58	-0.58	+0.58	-0.57	+0.57	-0.66	+0.66	-0.59	+0.59	-0.67	+0.67	-0.68	+0.68	-0.56	+0.56	-0.73	+0.73	-0.00	+0.00
Acceptance ν_μ/ν_e ND/FD	-0.17	+0.17	-0.33	+0.33	-0.00	+0.00	-0.00	+0.00	-0.27	+0.27	-0.00	+0.00	-0.00	+0.00	-0.00	+0.00	-0.00	+0.00	-0.00	+0.00
Michel e tagging	-1.45	+1.46	-0.00	+0.00	-2.99	+3.00	-3.44	+3.45	-0.00	+0.00	-0.00	+0.00	-8.66	+8.78	-8.79	+8.38	-0.00	+0.00	-0.00	+0.00
Rock scale	-0.29	+0.29	-0.06	+0.06	-0.53	+0.53	-0.62	+0.62	-0.00	+0.00	-0.14	+0.14	-0.48	+0.48	-2.40	+2.40	-0.00	+0.00	-0.00	+0.00
Cosmic scale	-1.28	+1.43	-0.00	+0.00	-2.63	+2.93	-0.00	+0.00	-0.00	+0.00	-0.00	+0.00	-0.00	+0.00	-0.00	+0.00	-0.00	+0.00	-19.87	+22.11
Quadrature	-7.29	+6.37	-8.21	+8.74	-10.25	+7.30	-11.42	+7.71	-6.61	+7.60	-11.43	+10.83	-20.32	+12.53	-12.61	+29.35	-64.92	+66.13	-19.87	+22.11

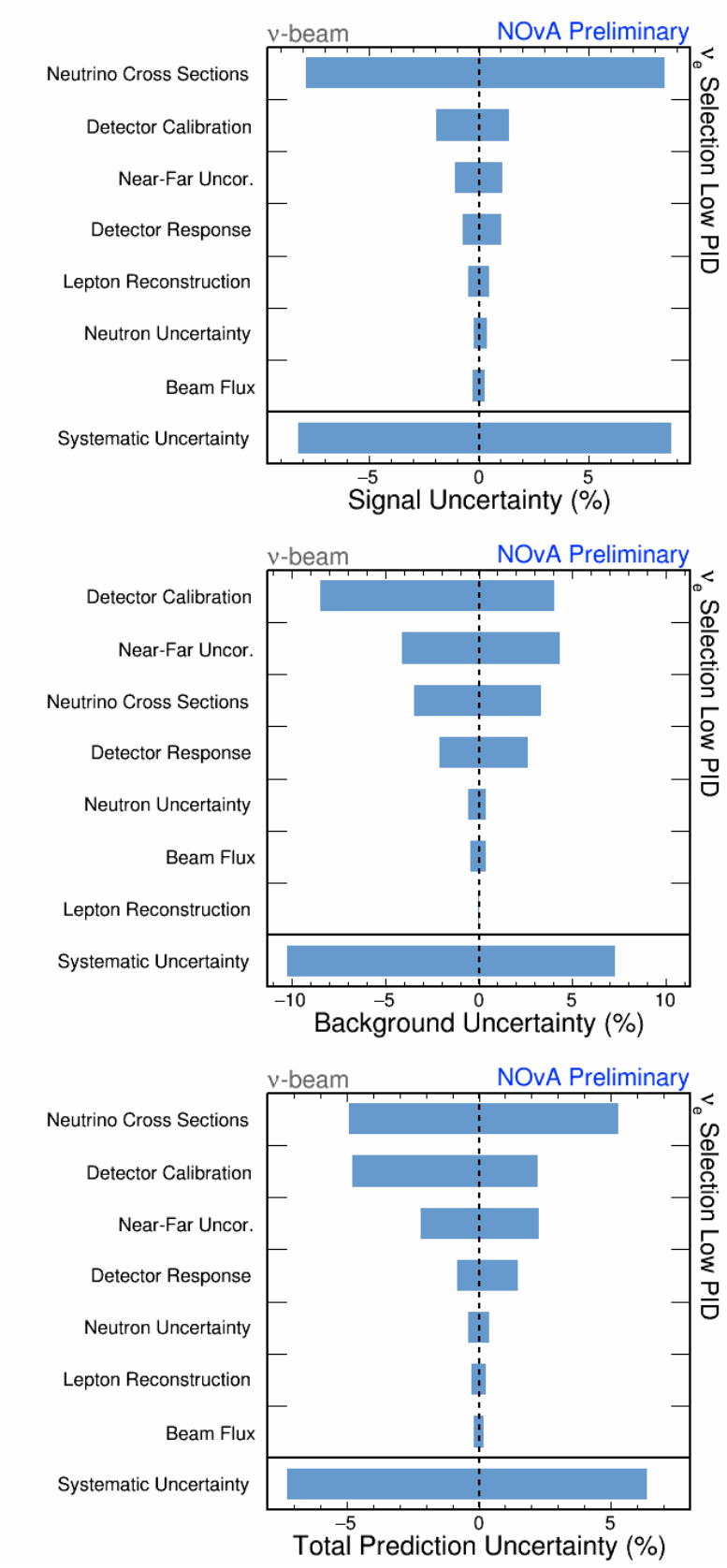

Figure C.21: Relative 1σ syst. uncertainties on the integral number of signal (top), background (middle), and total (bottom) predicted events in the ν_e app. ν-beam low PID sample.

High PID sample

Table C.12: Relative 1σ systematic uncertainties on the integral numbers of predicted events for the ν_e app. ν-beam high PID sample.

Systematic summary for ν_e appearance ν-beam high PID sample (%)

Systematic	Total pred		ν_e signal		Total bkg		Beam bkg		$\bar{\nu}_e$ WS		Beam ν_e CC		NC		ν_μ CC		ν_τ CC		Cosmics	
CCQE z-exp.ax.vec. 1	-0.42	+0.43	-0.49	+0.50	-0.14	+0.15	-0.14	+0.15	-0.78	+0.87	-0.61	+0.63	-2.64	+2.53	-2.45	+2.35	-2.92	+3.12	-0.00	+0.00
CCQE z-exp.ax.vec. 2	-0.37	+0.38	-0.44	+0.45	-0.13	+0.14	-0.13	+0.14	-0.59	+0.65	-0.52	+0.54	-2.15	+2.08	-2.01	+1.94	-2.46	+2.61	-0.00	+0.00
CCQE z-exp.ax.vec. 3	-0.74	+0.80	-0.85	+0.91	-0.36	+0.40	-0.36	+0.41	-0.41	+0.52	-0.84	+0.90	-2.31	+2.20	-2.18	+2.07	-3.75	+4.18	-0.00	+0.00
CCQE z-exp.ax.vec. 4	-0.16	+0.17	-0.18	+0.18	-0.09	+0.09	-0.09	+0.09	-0.04	+0.05	-0.17	+0.17	-0.34	+0.34	-0.32	+0.32	-0.76	+0.78	-0.00	+0.00
M_A^{CCRES}	-0.68	+1.01	-1.32	+1.63	-1.30	+1.72	-1.32	+1.75	-2.13	+4.27	-2.91	+2.98	-3.94	+4.89	-0.00	+1.84	-5.84	+7.78	-0.00	+0.00
M_V^{CCRES}	-0.72	+0.83	-1.27	+1.30	-0.96	+1.36	-0.97	+1.38	-2.34	+3.32	-2.22	+2.72	-4.38	+3.87	-0.08	+0.39	-4.15	+5.85	-0.00	+0.00
M_A^{NCRES}	-0.12	+0.13	-0.05	+0.03	-0.70	+0.82	-0.71	+0.84	-0.05	+0.03	-0.33	+0.23	-6.72	+8.29	-3.49	+2.52	-0.00	+0.00	-0.00	+0.00
M_V^{NCRES}	-0.04	+0.05	-0.01	+0.01	-0.24	+0.29	-0.24	+0.30	-0.02	+0.01	-0.10	+0.08	-2.26	+2.83	-1.09	+0.81	-0.00	+0.00	-0.00	+0.00
CCQE z-exp.norm.	-1.22	+1.52	-1.44	+1.77	-0.42	+0.56	-0.43	+0.57	-2.42	+3.01	-1.56	+1.97	-7.76	+6.25	-7.30	+5.89	-7.58	+10.11	-0.00	+0.00
RPA high Q^2 enh.	-0.64	+0.76	-0.77	+0.90	-0.13	+0.24	-0.14	+0.25	-0.30	+0.29	-0.70	+0.95	-2.78	+2.33	-2.66	+2.25	-0.00	+0.00	-0.00	+0.00
RPA low Q^2 supp.	-0.06	+0.06	-0.12	+0.12	-0.15	+0.14	-0.16	+0.14	-0.02	+0.00	-0.07	+0.05	-1.15	+1.16	-1.05	+1.04	-0.00	+0.00	-0.00	+0.00
RES low Q^2 supp.	-0.00	+0.13	-0.00	+0.11	-0.00	+0.21	-0.00	+0.22	-0.00	+0.82	-0.00	+0.18	-0.00	+0.13	-0.00	+0.48	-0.03	+0.00	-0.00	+0.00
DIS CC $\nu n \to 1\pi$	-0.41	+0.44	-0.46	+0.48	-0.25	+0.28	-0.26	+0.28	-2.12	+2.22	-0.10	+0.12	-2.24	+2.41	-9.22	+8.72	-0.81	+0.81	-0.00	+0.00
FSI π free path	-0.39	+0.25	-0.37	+0.22	-0.49	+0.33	-0.50	+0.34	-0.39	+0.01	-0.29	+0.21	-1.27	+1.00	-3.05	+1.38	-0.14	+0.40	-0.00	+0.00
FSI fate fraction	-0.05	+0.00	-0.08	+0.00	-0.10	+0.06	-0.10	+0.06	-0.29	+0.48	-0.15	+0.00	-0.00	+0.64	-0.62	+0.20	-0.00	+0.11	-0.00	+0.00
MEC E_ν shape	-0.30	+0.08	-0.43	+0.12	-0.09	+0.17	-0.09	+0.17	-1.59	+2.36	-0.46	+0.25	-1.23	+2.41	-0.11	+1.84	-1.24	+0.16	-0.00	+0.00
MEC E_ν shape	-0.00	+0.00	-0.05	+0.07	-0.24	+0.16	-0.25	+0.16	-3.11	+1.89	-0.17	+0.12	-0.28	+0.46	-0.15	+0.39	-0.21	+0.03	-0.00	+0.00
MEC ν (q_0, q) response	-0.46	+0.00	-0.82	+0.00	-1.66	+1.35	-1.69	+1.37	-0.00	+0.55	-2.68	+1.01	-0.00	+4.73	-0.00	+4.20	-8.59	+0.00	-0.00	+0.00
MEC $\bar{\nu}$ (q_0, q) response	-0.00	+0.11	-0.03	+0.05	-0.00	+0.32	-0.00	+0.33	-2.94	+0.94	-0.00	+0.37	-0.65	+1.69	-0.75	+1.38	-1.72	+2.09	-0.00	+0.00
MEC ν init. np frac.	-0.09	+0.27	-0.05	+0.15	-0.24	+0.72	-0.24	+0.73	-0.02	+0.05	-0.28	+0.85	-0.12	+0.36	-0.27	+0.82	-0.36	+1.09	-0.00	+0.00
MEC $\bar{\nu}$ init. np frac.	-0.02	+0.00	-0.00	+0.01	-0.14	+0.05	-0.15	+0.05	-0.86	+0.29	-0.08	+0.03	-0.10	+0.04	-0.16	+0.05	-0.65	+0.22	-0.00	+0.00
ν_e/ν_μ radiative corr.	-1.68	+1.68	-2.06	+2.06	-0.24	+0.24	-0.24	+0.24	-0.00	+0.00	-1.20	+1.20	-3.73	+3.73	-3.87	+3.87	-0.00	+0.00	-0.00	+0.00
$\bar{\nu}_e/\bar{\nu}_\mu$ radiative corr.	-0.03	+0.03	-0.00	+0.00	-0.12	+0.12	-0.12	+0.12	-2.00	+2.00	-0.08	+0.08	-0.34	+0.35	-0.36	+0.36	-0.00	+0.00	-0.00	+0.00
Second class currents	-1.65	+1.65	-2.06	+2.06	-0.12	+0.12	-0.12	+0.12	-2.00	+2.00	-1.12	+1.12	-3.41	+3.37	-3.54	+3.48	-0.00	+0.00	-0.00	+0.00
XSecs PC00	-0.05	+0.05	-0.02	+0.02	-0.32	+0.29	-0.33	+0.29	-0.02	+0.02	-0.34	+0.40	-4.98	+4.37	-2.59	+3.04	-0.00	+0.00	-0.00	+0.00
XSecs PC01	-0.08	+0.08	-0.10	+0.10	-0.00	+0.00	-0.00	+0.00	-0.13	+0.13	-0.06	+0.06	-0.54	+0.53	-0.75	+0.76	-0.00	+0.00	-0.00	+0.00
XSecs PC02	-1.18	+1.26	-1.36	+1.45	-0.51	+0.56	-0.52	+0.57	-1.81	+2.00	-0.07	+0.11	-2.69	+2.78	-1.13	+0.84	-0.00	+0.00	-0.00	+0.00
XSecs PC03	-0.29	+0.30	-0.34	+0.35	-0.11	+0.13	-0.11	+0.13	-0.45	+0.46	-0.11	+0.12	-1.92	+2.05	-3.88	+3.61	-0.00	+0.00	-0.00	+0.00
XSecs PC04	-0.41	+0.42	-0.49	+0.50	-0.12	+0.12	-0.12	+0.12	-0.56	+0.57	-0.02	+0.02	-0.44	+0.44	-0.38	+0.38	-0.00	+0.00	-0.00	+0.00
XSecs PC05	-0.22	+0.22	-0.21	+0.21	-0.23	+0.24	-0.24	+0.24	-0.20	+0.21	-0.00	+0.00	-0.60	+0.61	-4.72	+4.78	-0.00	+0.00	-0.00	+0.00
XSecs PC06	-0.21	+0.21	-0.21	+0.22	-0.19	+0.19	-0.19	+0.20	-0.27	+0.28	-0.01	+0.02	-1.42	+1.43	-0.46	+0.45	-0.00	+0.00	-0.00	+0.00
XSecs PC07	-0.07	+0.07	-0.09	+0.09	-0.00	+0.00	-0.00	+0.01	-0.10	+0.10	-0.04	+0.04	-0.07	+0.07	-0.58	+0.56	-0.00	+0.00	-0.00	+0.00
XSecs PC08	-0.24	+0.24	-0.32	+0.32	-0.06	+0.07	-0.06	+0.07	-0.33	+0.34	-0.13	+0.14	-0.34	+0.34	-1.09	+1.16	-0.00	+0.00	-0.00	+0.00
XSecs PC09	-0.14	+0.14	-0.14	+0.14	-0.14	+0.14	-0.14	+0.14	-0.15	+0.15	-0.10	+0.10	-1.67	+1.66	-0.87	+0.87	-0.00	+0.00	-0.00	+0.00
XSecs PC10	-0.24	+0.24	-0.28	+0.28	-0.10	+0.10	-0.10	+0.10	-0.28	+0.28	-0.09	+0.09	-0.08	+0.08	-0.03	+0.03	-0.00	+0.00	-0.00	+0.00
XSecs PC11	-0.05	+0.05	-0.00	+0.00	-0.25	+0.25	-0.26	+0.26	-0.00	+0.00	-0.05	+0.05	-1.36	+1.33	-0.97	+0.95	-0.00	+0.00	-0.00	+0.00
ν_τ scale	-0.34	+0.34	-0.00	+0.00	-1.62	+1.62	-1.65	+1.65	-0.00	+0.00	-0.00	+0.00	-0.00	+0.00	-0.05	+0.05	-68.18	+68.18	-0.00	+0.00
Flux PC00	-0.12	+0.12	-0.14	+0.14	-0.04	+0.02	-0.04	+0.02	-1.56	+1.53	-0.36	+0.30	-2.28	+2.37	-3.20	+3.39	-2.42	+2.42	-0.00	+0.00
Flux PC01	-0.23	+0.21	-0.16	+0.16	-0.48	+0.38	-0.49	+0.39	-3.25	+3.00	-0.71	+0.58	-1.26	+1.28	-3.08	+3.34	-4.83	+4.80	-0.00	+0.00
Flux PC02	-0.09	+0.06	-0.18	+0.18	-1.12	+0.95	-1.14	+0.97	-0.96	+0.82	-1.06	+0.90	-0.88	+0.62	-4.12	+3.75	-2.22	+2.14	-0.00	+0.00
Flux PC03	-0.13	+0.13	-0.08	+0.09	-0.30	+0.29	-0.31	+0.30	-1.06	+0.75	-0.60	+0.60	-0.49	+0.56	-0.50	+0.59	-7.21	+7.24	-0.00	+0.00
Flux PC04	-0.00	+0.00	-0.03	+0.03	-0.13	+0.13	-0.14	+0.13	-0.24	+0.25	-0.27	+0.27	-0.51	+0.50	-0.80	+0.79	-0.72	+0.72	-0.00	+0.00
Absolute calib.	-0.69	+0.00	-1.39	+0.64	-2.86	+1.92	-2.91	+1.96	-4.25	+2.02	-4.63	+4.61	-10.02	+6.56	-5.28	+0.00	-0.02	+0.00	-0.00	+0.00
ND/FD relative calib.	-0.48	+0.22	-1.07	+0.78	-1.88	+1.69	-1.92	+1.73	-0.97	+0.03	-2.02	+2.05	-2.62	+1.85	-1.73	+0.00	-0.00	+0.00	-0.00	+0.00
Calibration shape	-0.22	+0.22	-0.11	+0.11	-0.65	+0.66	-0.66	+0.67	-0.53	+0.53	-0.39	+0.39	-2.24	+2.29	-0.66	+0.66	-0.00	+0.00	-0.00	+0.00
Calibration drift	-0.00	+0.14	-0.00	+0.32	-0.51	+0.00	-0.52	+0.00	-0.00	+2.24	-0.23	+0.00	-3.88	+0.00	-0.00	+2.18	-0.00	+0.02	-0.00	+0.00
Light level FD	-0.05	+1.00	-0.39	+0.53	-0.00	+2.77	-0.00	+2.83	-1.34	+0.00	-0.00	+4.03	-0.40	+0.55	-5.30	+0.00	-0.03	+0.00	-0.00	+0.00
Light level ND	-1.02	+0.08	-0.82	+0.00	-1.79	+0.66	-1.83	+0.67	-0.96	+0.00	-1.77	+0.00	-2.65	+5.02	-2.59	+8.62	-0.00	+0.00	-0.00	+0.00
Cherenkov	-0.00	+0.18	-0.28	+0.00	-0.00	+1.94	-0.00	+1.98	-0.00	+0.89	-0.00	+3.23	-3.29	+0.00	-0.00	+0.15	-0.04	+0.00	-0.00	+0.00
E_μ ND uncorr.	-0.11	+0.12	-0.14	+0.15	-0.01	+0.01	-0.01	+0.01	-0.15	+0.15	-0.03	+0.03	-0.09	+0.09	-0.11	+0.11	-0.00	+0.00	-0.00	+0.00
E_μ μ-catcher uncorr.	-0.02	+0.02	-0.02	+0.02	-0.01	+0.01	-0.01	+0.01	-0.13	+0.13	-0.03	+0.03	-0.10	+0.09	-0.12	+0.11	-0.00	+0.00	-0.00	+0.00
E_μ n pile-up	-0.29	+0.00	-0.36	+0.00	-0.04	+0.00	-0.04	+0.00	-0.45	+0.00	-0.07	+0.00	-0.00	+0.24	-0.00	+0.27	-0.00	+0.00	-0.00	+0.00
E_μ correlated	-0.68	+0.71	-0.84	+0.88	-0.07	+0.08	-0.08	+0.08	-0.90	+0.93	-0.16	+0.16	-0.56	+0.57	-0.64	+0.65	-0.00	+0.00	-0.00	+0.00
Lepton angle xz ND	-0.24	+0.16	-0.30	+0.20	-0.01	+0.00	-0.01	+0.00	-0.21	+0.16	-0.00	+0.00	-0.00	+0.00	-0.00	+0.00	-0.00	+0.00	-0.00	+0.00
Lepton angle yz ND	-0.13	+0.02	-0.16	+0.03	-0.00	+0.00	-0.00	+0.00	-0.06	+0.00	-0.00	+0.00	-0.00	+0.00	-0.00	+0.00	-0.00	+0.00	-0.00	+0.00
Lepton angle xz FD	-0.00	+0.00	-0.00	+0.00	-0.00	+0.00	-0.00	+0.00	-0.00	+0.00	-0.00	+0.00	-0.00	+0.00	-0.00	+0.00	-0.00	+0.00	-0.00	+0.00
Lepton angle yz FD	-0.00	+0.00	-0.00	+0.00	-0.00	+0.00	-0.00	+0.00	-0.00	+0.00	-0.00	+0.00	-0.00	+0.00	-0.00	+0.00	-0.00	+0.00	-0.00	+0.00
Neutron systematic	-0.38	+0.57	-0.41	+0.65	-0.28	+0.27	-0.28	+0.27	-1.30	+1.06	-0.58	+0.52	-1.24	+1.48	-0.22	+0.56	-0.16	+0.13	-0.00	+0.00
Normalization beam corr.	-0.83	+0.83	-0.84	+0.84	-0.79	+0.79	-0.80	+0.80	-0.82	+0.82	-0.82	+0.82	-0.75	+0.75	-0.61	+0.61	-0.93	+0.93	-0.00	+0.00
Normalization ν-beam	-0.62	+0.62	-0.61	+0.61	-0.66	+0.66	-0.67	+0.67	-0.59	+0.59	-0.69	+0.69	-0.63	+0.63	-0.51	+0.51	-0.78	+0.78	-0.00	+0.00
Acceptance ν_μ/ν_e ND/FD	-0.34	+0.34	-0.43	+0.43	-0.02	+0.02	-0.02	+0.02	-0.37	+0.37	-0.00	+0.00	-0.00	+0.00	-0.00	+0.00	-0.00	+0.00	-0.00	+0.00
Michel e tagging	-0.00	+0.00	-0.00	+0.00	-0.00	+0.00	-0.00	+0.00	-0.00	+0.00	-0.00	+0.00	-0.00	+0.00	-0.00	+0.00	-0.00	+0.00	-0.00	+0.00
Rock scale	-0.07	+0.07	-0.01	+0.01	-0.28	+0.28	-0.29	+0.29	-0.03	+0.03	-0.04	+0.04	-0.62	+0.62	-5.65	+5.65	-0.00	+0.00	-0.00	+0.00
Cosmic scale	-0.16	+0.24	-0.00	+0.00	-0.78	+1.13	-0.00	+0.00	-0.00	+0.00	-0.00	+0.00	-0.00	+0.00	-0.00	+0.00	-0.00	+0.00	-40.05	+58.28
Quadrature	-3.98	+4.13	-5.09	+5.03	-5.39	+5.89	-5.44	+5.90	-9.82	+9.74	-7.80	+9.11	-20.14	+19.21	-19.97	+19.87	-70.39	+70.53	-40.05	+58.28

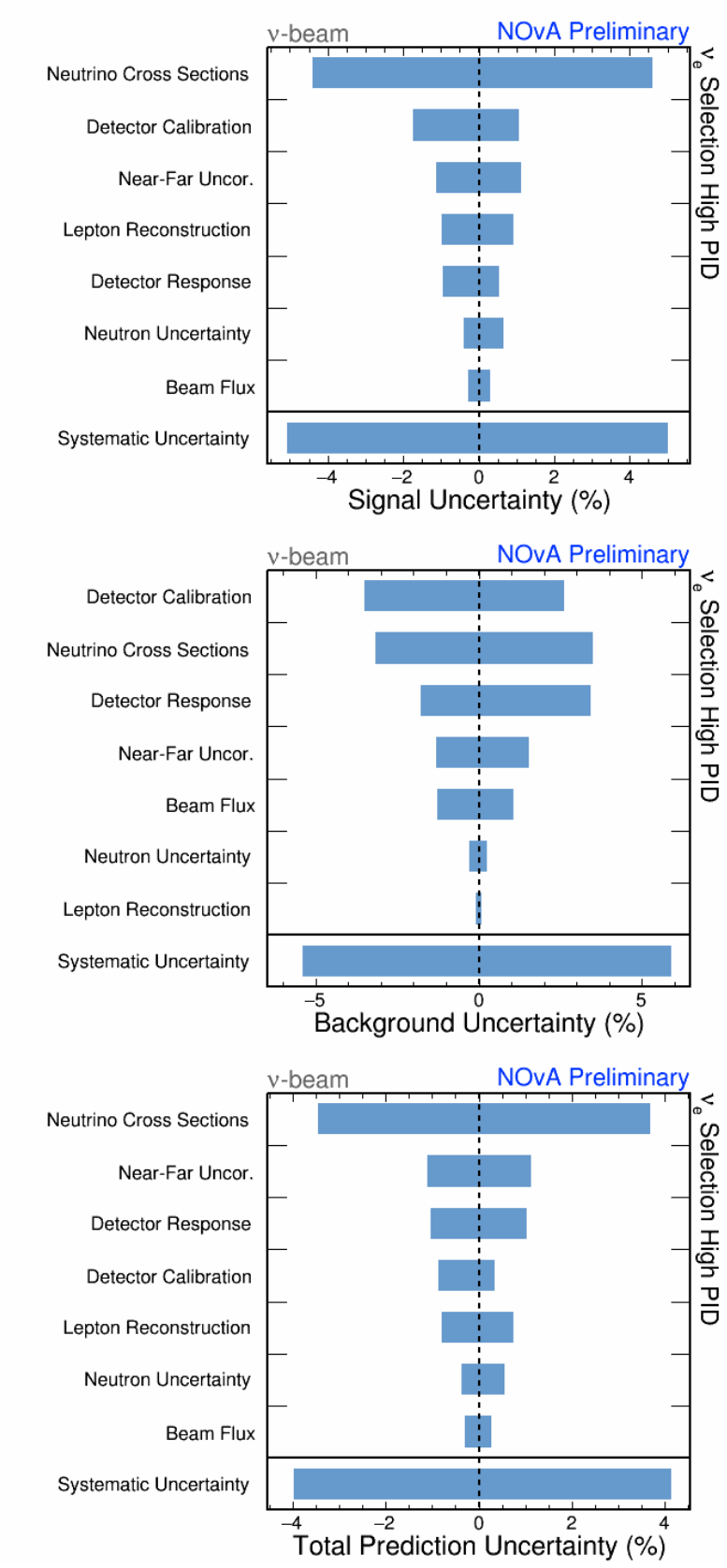

Figure C.22: Relative 1σ syst. uncertainties on the integral number of signal (top), background (middle), and total (bottom) predicted events in the ν_e app. ν-beam high PID sample.

Peripheral sample

Table C.13: Relative 1σ systematic uncertainties on the integral numbers of predicted events for the ν_e app. ν-beam peripheral sample.

Systematic summary for ν_e appearance ν-beam peripheral sample (%)

Systematic	Total pred		ν_e signal		Total bkg		Beam bkg		$\bar{\nu}_e$ WS		Beam ν_e CC		NC		ν_μ CC		ν_τ CC		Cosmics	
CCQE z-exp.ax.vec. 1	-0.56	+0.58	-0.57	+0.59	-0.54	+0.58	-0.73	+0.78	-0.70	+0.79	-1.10	+1.17	-2.58	+2.48	-0.64	+0.61	-2.47	+2.64	-0.00	+0.00
CCQE z-exp.ax.vec. 2	-0.49	+0.50	-0.51	+0.53	-0.45	+0.48	-0.61	+0.64	-0.55	+0.61	-0.92	+0.96	-2.10	+2.03	-0.52	+0.50	-2.05	+2.18	-0.00	+0.00
CCQE z-exp.ax.vec. 3	-0.84	+0.91	-0.94	+1.01	-0.71	+0.79	-0.95	+1.06	-0.44	+0.57	-1.32	+1.45	-2.29	+2.18	-0.39	+0.38	-3.46	+3.90	-0.00	+0.00
CCQE z-exp.ax.vec. 4	-0.17	+0.18	-0.20	+0.20	-0.15	+0.15	-0.20	+0.20	-0.06	+0.06	-0.26	+0.27	-0.34	+0.34	-0.04	+0.04	-0.74	+0.77	-0.00	+0.00
M_A^{CCRES}	-1.04	+1.78	-1.25	+1.60	-4.48	+5.75	-6.05	+7.76	-0.12	+2.55	-7.80	+9.52	-3.82	+4.96	-2.24	+3.59	-8.38	+11.65	-0.00	+0.00
M_V^{CCRES}	-0.64	+1.14	-1.24	+1.29	-3.15	+4.25	-4.26	+5.74	-0.87	+2.11	-5.56	+7.30	-4.32	+3.86	-1.32	+1.79	-5.91	+8.49	-0.00	+0.00
M_A^{NCRES}	-0.01	+0.01	-0.05	+0.03	-0.02	+0.04	-0.02	+0.05	-0.05	+0.03	-0.14	+0.10	-2.79	+3.88	-2.38	+1.90	-0.00	+0.00	-0.00	+0.00
M_V^{NCRES}	-0.00	+0.00	-0.02	+0.01	-0.00	+0.00	-0.00	+0.00	-0.01	+0.00	-0.05	+0.03	-0.91	+1.17	-0.81	+0.64	-0.00	+0.00	-0.00	+0.00
CCQE z-exp.norm.	-1.51	+1.93	-1.57	+1.94	-1.43	+1.92	-1.93	+2.59	-2.21	+2.78	-2.85	+3.75	-7.60	+6.15	-1.79	+1.42	-6.68	+8.90	-0.00	+0.00
RPA high Q^2 enh.	-0.73	+0.89	-0.87	+1.04	-0.55	+0.71	-0.74	+0.96	-0.38	+0.43	-1.17	+1.50	-2.76	+2.30	-0.56	+0.46	-0.00	+0.00	-0.00	+0.00
RPA low Q^2 supp.	-0.09	+0.09	-0.07	+0.07	-0.12	+0.12	-0.16	+0.16	-0.08	+0.06	-0.34	+0.34	-1.12	+1.13	-0.33	+0.34	-0.00	+0.00	-0.00	+0.00
RES low Q^2 supp.	-0.00	+0.02	-0.00	+0.20	-0.22	+0.00	-0.30	+0.00	-0.00	+0.79	-0.44	+0.00	-0.00	+0.39	-0.14	+0.00	-0.04	+0.00	-0.00	+0.00
DIS CC $\nu n \to 1\pi$	-0.43	+0.44	-0.33	+0.35	-1.45	+1.46	-1.96	+1.97	-2.35	+2.47	-2.38	+2.39	-1.66	+1.77	-4.39	+4.24	-1.55	+1.55	-0.00	+0.00
FSI π free path	-0.68	+0.46	-0.91	+0.64	-0.37	+0.23	-0.50	+0.31	-0.71	+0.39	-0.52	+0.32	-0.39	+0.54	-0.49	+0.00	-0.12	+0.31	-0.00	+0.00
FSI fate fraction	-0.05	+0.05	-0.11	+0.10	-0.00	+0.03	-0.00	+0.05	-0.32	+0.46	-0.05	+0.00	-0.00	+0.79	-0.03	+0.31	-0.02	+0.11	-0.00	+0.00
MEC E_ν shape	-0.18	+0.00	-0.22	+0.00	-0.14	+0.00	-0.18	+0.00	-1.23	+1.92	-0.45	+0.00	-0.94	+2.19	-0.46	+0.72	-0.64	+0.06	-0.00	+0.00
MEC $E_{\bar{\nu}}$ shape	-0.03	+0.00	-0.05	+0.07	-0.17	+0.06	-0.23	+0.09	-2.25	+1.14	-0.21	+0.08	-0.23	+0.40	-0.10	+0.09	-0.18	+0.02	-0.00	+0.00
MEC ν (q_0, q) response	-0.72	+0.18	-0.54	+0.00	-0.95	+0.92	-1.28	+1.25	-0.00	+0.43	-1.55	+0.91	-0.00	+3.55	-3.31	+4.11	-1.39	+0.00	-0.00	+0.00
MEC $\bar{\nu}$ (q_0, q) response	-0.18	+0.00	-0.03	+0.06	-0.48	+0.00	-0.65	+0.00	-0.00	+1.51	-0.79	+0.00	-0.55	+1.33	-2.82	+0.00	-2.63	+0.00	-0.00	+0.00
MEC ν init. np frac.	-0.01	+0.00	-0.04	+0.13	-0.20	+0.07	-0.27	+0.09	-0.00	+0.02	-0.46	+0.15	-0.16	+0.49	-0.34	+1.02	-0.51	+0.17	-0.00	+0.00
MEC $\bar{\nu}$ init. np frac.	-0.04	+0.01	-0.00	+0.01	-0.10	+0.03	-0.13	+0.04	-0.02	+0.07	-0.22	+0.07	-0.10	+0.03	-0.18	+0.54	-0.24	+0.73	-0.00	+0.00
ν_e/ν_μ radiative corr.	-1.47	+1.47	-2.05	+2.05	-0.71	+0.71	-0.96	+0.96	-0.00	+0.00	-1.65	+1.65	-3.66	+3.66	-1.18	+1.18	-0.00	+0.00	-0.00	+0.00
$\bar{\nu}_e/\bar{\nu}_\mu$ radiative corr.	-0.06	+0.06	-0.00	+0.00	-0.15	+0.15	-0.20	+0.20	-1.98	+1.98	-0.19	+0.19	-0.33	+0.33	-0.11	+0.11	-0.00	+0.00	-0.00	+0.00
Second class currents	-1.41	+1.41	-2.05	+2.05	-0.56	+0.56	-0.76	+0.76	-1.98	+1.98	-1.46	+1.46	-3.35	+3.30	-1.07	+1.06	-0.00	+0.00	-0.00	+0.00
XSecs PC00	-0.30	+0.34	-0.16	+0.16	-0.49	+0.57	-0.66	+0.76	-0.08	+0.08	-0.17	+0.19	-4.74	+5.49	-2.49	+2.90	-0.00	+0.00	-0.00	+0.00
XSecs PC01	-0.12	+0.12	-0.14	+0.14	-0.09	+0.09	-0.12	+0.13	-0.33	+0.33	-0.04	+0.04	-0.77	+0.78	-0.31	+0.31	-0.00	+0.00	-0.00	+0.00
XSecs PC02	-1.70	+1.85	-2.54	+2.76	-0.62	+0.67	-0.83	+0.90	-4.80	+5.72	-0.44	+0.47	-3.02	+3.16	-0.76	+0.78	-0.00	+0.00	-0.00	+0.00
XSecs PC03	-0.68	+0.70	-0.93	+0.95	-0.35	+0.37	-0.47	+0.50	-1.59	+1.66	-0.21	+0.21	-2.25	+2.38	-1.09	+1.17	-0.00	+0.00	-0.00	+0.00
XSecs PC04	-0.56	+0.58	-0.90	+0.92	-0.13	+0.13	-0.17	+0.17	-1.30	+1.34	-0.13	+0.13	-0.34	+0.35	-0.22	+0.22	-0.00	+0.00	-0.00	+0.00
XSecs PC05	-0.22	+0.23	-0.35	+0.35	-0.07	+0.07	-0.09	+0.09	-0.53	+0.53	-0.05	+0.05	-0.29	+0.29	-0.01	+0.01	-0.00	+0.00	-0.00	+0.00
XSecs PC06	-0.42	+0.43	-0.66	+0.67	-0.11	+0.11	-0.15	+0.15	-0.65	+0.65	-0.11	+0.11	-0.39	+0.39	-0.07	+0.06	-0.00	+0.00	-0.00	+0.00
XSecs PC07	-0.21	+0.21	-0.23	+0.23	-0.17	+0.18	-0.23	+0.24	-0.32	+0.33	-0.08	+0.08	-1.42	+1.48	-0.70	+0.73	-0.00	+0.00	-0.00	+0.00
XSecs PC08	-0.29	+0.31	-0.63	+0.64	-0.13	+0.15	-0.17	+0.20	-0.63	+0.64	-0.03	+0.03	-1.96	+2.11	-1.17	+1.25	-0.00	+0.00	-0.00	+0.00
XSecs PC09	-0.24	+0.24	-0.40	+0.40	-0.02	+0.02	-0.03	+0.03	-0.43	+0.43	-0.05	+0.05	-0.25	+0.25	-0.19	+0.19	-0.00	+0.00	-0.00	+0.00
XSecs PC10	-0.15	+0.16	-0.26	+0.26	-0.01	+0.01	-0.02	+0.02	-0.40	+0.40	-0.03	+0.03	-0.16	+0.17	-0.17	+0.17	-0.00	+0.00	-0.00	+0.00
XSecs PC11	-0.05	+0.05	-0.00	+0.00	-0.10	+0.11	-0.14	+0.14	-0.18	+0.18	-0.03	+0.03	-1.00	+1.03	-0.50	+0.52	-0.00	+0.00	-0.00	+0.00
ν_τ scale	-0.46	+0.46	-0.00	+0.00	-1.06	+1.06	-1.43	+1.43	-0.00	+0.00	-0.00	+0.00	-0.00	+0.00	-0.02	+0.02	-65.10	+65.10	-0.00	+0.00
Flux PC00	-0.40	+0.39	-0.20	+0.20	-1.17	+1.15	-1.59	+1.56	-1.66	+1.62	-2.09	+2.04	-2.39	+2.48	-0.07	+0.09	-2.40	+2.40	-0.00	+0.00
Flux PC01	-0.72	+0.66	-0.25	+0.26	-2.00	+1.86	-2.70	+2.51	-3.24	+2.95	-3.23	+2.99	-2.02	+2.08	-1.00	+1.00	-4.56	+4.53	-0.00	+0.00
Flux PC02	-0.09	+0.00	-0.09	+0.09	-0.33	+0.14	-0.45	+0.18	-1.02	+0.91	-0.26	+0.00	-2.22	+1.82	-0.28	+0.27	-2.01	+1.94	-0.00	+0.00
Flux PC03	-0.77	+0.76	-0.07	+0.08	-1.89	+1.84	-2.55	+2.48	-1.03	+0.76	-2.95	+2.87	-0.47	+0.53	-0.98	+1.01	-6.38	+6.36	-0.00	+0.00
Flux PC04	-0.11	+0.11	-0.00	+0.00	-0.26	+0.26	-0.36	+0.36	-0.28	+0.29	-0.45	+0.45	-0.44	+0.43	-0.07	+0.06	-0.80	+0.80	-0.00	+0.00
Absolute calib.	-0.83	+0.00	-2.27	+1.28	-3.57	+2.90	-4.83	+3.91	-4.12	+5.58	-6.40	+5.49	-5.94	+4.69	-3.81	+1.28	-0.01	+0.00	-0.00	+0.00
ND/FD relative calib.	-0.31	+0.04	-1.34	+0.97	-1.99	+1.84	-2.68	+2.49	-1.23	+1.41	-3.12	+2.91	-2.34	+2.23	-1.16	+0.69	-0.00	+0.00	-0.00	+0.00
Calibration shape	-0.28	+0.28	-0.00	+0.00	-0.66	+0.66	-0.89	+0.89	-0.00	+0.00	-1.24	+1.24	-0.49	+0.49	-2.24	+2.24	-0.04	+0.04	-0.00	+0.00
Calibration drift	-0.00	+1.90	-0.00	+0.00	-0.00	+4.37	-0.00	+5.89	-2.60	+0.00	-0.00	+8.00	-3.65	+0.00	-1.49	+0.00	-0.06	+0.00	-0.00	+0.00
Light level FD	-1.41	+1.07	-1.43	+1.66	-1.39	+0.31	-1.88	+0.41	-1.90	+3.32	-1.59	+0.48	-3.14	+0.64	-4.70	+0.00	-0.00	+0.10	-0.00	+0.00
Light level ND	-0.56	+0.11	-0.76	+0.00	-0.31	+0.32	-0.42	+0.44	-0.78	+0.39	-0.17	+0.00	-2.87	+4.73	-0.32	+1.09	-0.00	+0.00	-0.00	+0.00
Cherenkov	-0.00	+0.22	-1.33	+0.00	-0.00	+2.25	-0.00	+3.04	-0.99	+0.00	-0.00	+4.37	-1.49	+0.00	-4.82	+0.00	-0.00	+0.02	-0.00	+0.00
E_μ ND uncorr.	-0.08	+0.09	-0.14	+0.15	-0.00	+0.00	-0.00	+0.00	-0.22	+0.24	-0.00	+0.00	-0.10	+0.10	-0.03	+0.03	-0.00	+0.00	-0.00	+0.00
E_μ μ-catcher uncorr.	-0.02	+0.02	-0.04	+0.04	-0.00	+0.00	-0.00	+0.00	-0.26	+0.27	-0.00	+0.00	-0.11	+0.10	-0.02	+0.02	-0.00	+0.00	-0.00	+0.00
E_μ n pile-up	-0.21	+0.00	-0.36	+0.00	-0.01	+0.00	-0.02	+0.00	-0.69	+0.00	-0.02	+0.00	-0.00	+0.25	-0.00	+0.07	-0.00	+0.00	-0.00	+0.00
E_μ correlated	-0.48	+0.50	-0.82	+0.86	-0.03	+0.03	-0.04	+0.04	-1.38	+1.41	-0.05	+0.05	-0.58	+0.59	-0.16	+0.16	-0.00	+0.00	-0.00	+0.00
Lepton angle xz ND	-0.17	+0.12	-0.30	+0.20	-0.00	+0.00	-0.01	+0.00	-0.27	+0.19	-0.00	+0.00	-0.00	+0.00	-0.00	+0.00	-0.00	+0.00	-0.00	+0.00
Lepton angle yz ND	-0.09	+0.02	-0.16	+0.03	-0.00	+0.00	-0.00	+0.00	-0.07	+0.00	-0.00	+0.00	-0.00	+0.00	-0.00	+0.00	-0.00	+0.00	-0.00	+0.00
Lepton angle xz FD	-0.00	+0.00	-0.00	+0.00	-0.00	+0.00	-0.00	+0.00	-0.01	+0.00	-0.00	+0.00	-0.00	+0.00	-0.00	+0.00	-0.00	+0.00	-0.00	+0.00
Lepton angle yz FD	-0.00	+0.00	-0.00	+0.00	-0.00	+0.00	-0.00	+0.00	-0.02	+0.00	-0.00	+0.00	-0.00	+0.00	-0.00	+0.00	-0.00	+0.00	-0.00	+0.00
Neutron systematic	-0.23	+0.32	-0.29	+0.48	-0.16	+0.10	-0.21	+0.14	-1.49	+1.44	-0.35	+0.24	-1.25	+1.21	-0.26	+0.56	-0.04	+0.00	-0.00	+0.00
Normalization beam corr.	-0.72	+0.72	-0.84	+0.84	-0.56	+0.56	-0.76	+0.76	-0.81	+0.81	-0.79	+0.79	-0.62	+0.62	-0.45	+0.45	-0.89	+0.89	-0.00	+0.00
Normalization ν-beam	-0.55	+0.55	-0.61	+0.61	-0.47	+0.47	-0.63	+0.63	-0.59	+0.59	-0.66	+0.66	-0.52	+0.52	-0.38	+0.38	-0.75	+0.75	-0.00	+0.00
Acceptance ν_μ/ν_e ND/FD	-0.22	+0.22	-0.38	+0.38	-0.00	+0.00	-0.00	+0.00	-0.19	+0.19	-0.00	+0.00	-0.00	+0.00	-0.00	+0.00	-0.00	+0.00	-0.00	+0.00
Michel e tagging	-0.00	+0.00	-0.00	+0.00	-0.00	+0.00	-0.00	+0.00	-0.00	+0.00	-0.00	+0.00	-0.00	+0.00	-0.00	+0.00	-0.00	+0.00	-0.00	+0.00
Rock scale	-2.05	+2.05	-0.87	+0.87	-3.60	+3.60	-4.86	+4.86	-0.69	+0.69	-0.92	+0.92	-17.07	+17.07	-45.27	+45.27	-0.00	+0.00	-0.00	+0.00
Cosmic scale	-0.90	+0.90	-0.00	+0.00	-2.08	+2.08	-0.00	+0.00	-0.00	+0.00	-0.00	+0.00	-0.00	+0.00	-0.00	+0.00	-0.00	+0.00	-8.01	+8.01
Quadrature	-5.11	+5.70	-6.44	+6.24	-9.27	+11.19	-12.19	+14.84	-10.42	+12.02	-14.17	+17.99	-24.13	+24.01	-46.79	+46.22	-67.05	+68.03	-8.01	+8.01

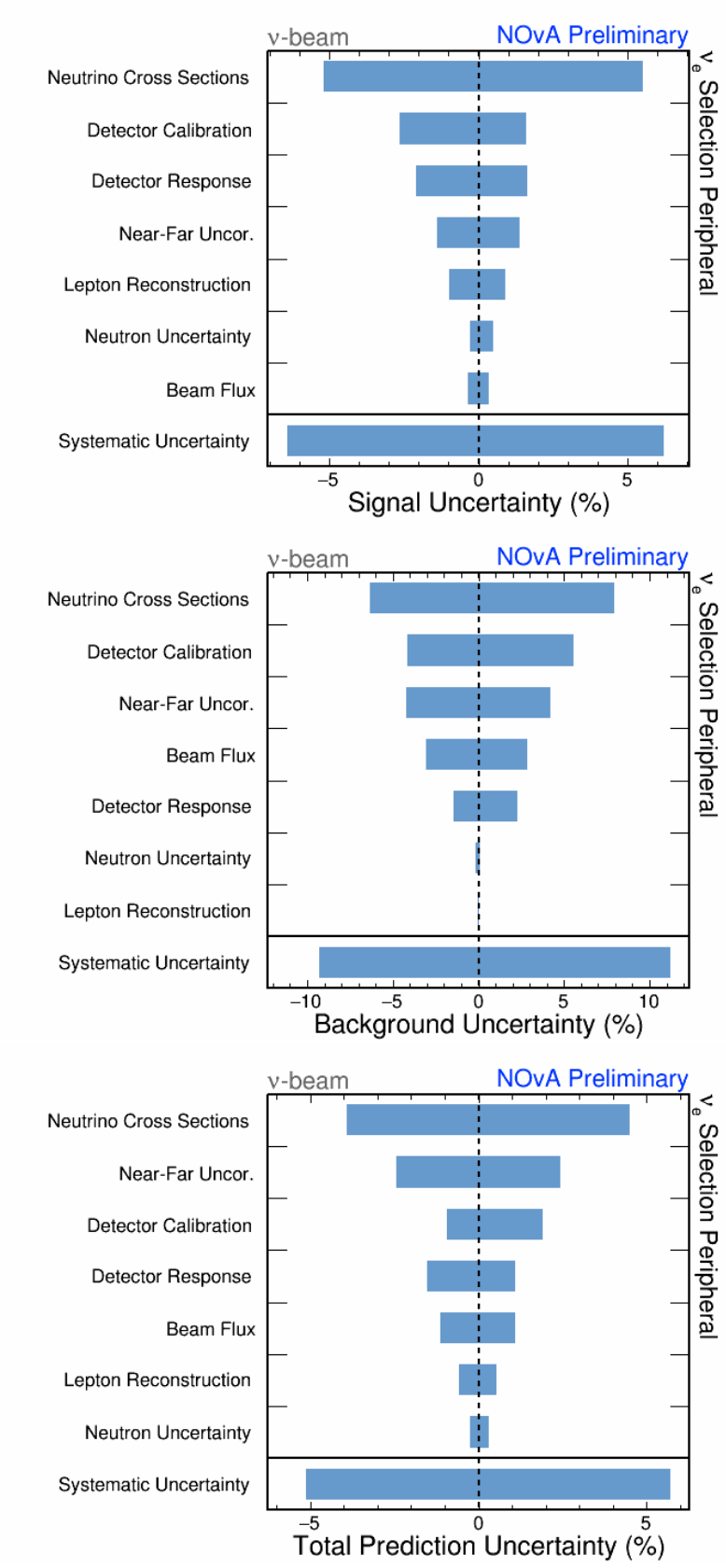

Figure C.23: Relative 1σ syst. uncertainties on the integral number of signal (top), background (middle), and total (bottom) predicted events in the ν_e app. ν-beam peripheral bin.

All prediction

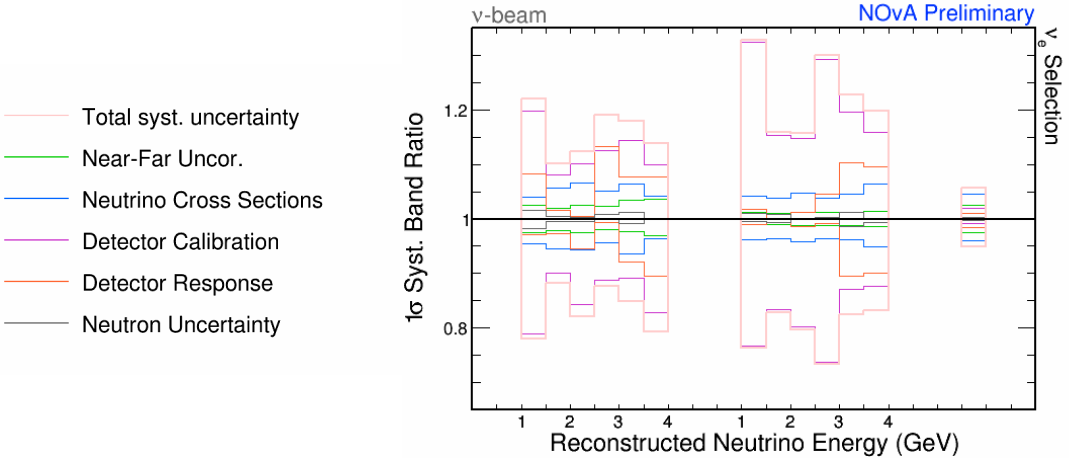

Figure C.24: 1σ systematic bands relative to the nominal prediction for the ν-beam ν_e app. samples in the reconstructed neutrino energy. Bins correspond to low, high PID and peripheral sample from left to right, respectively.

Table C.14: Relative 1σ systematic uncertainties on the integral numbers of predicted events for the ν_e app. ν-beam all samples.

Systematic summary for ν_e appearance ν-beam all samples (%)

Systematic	Total pred		ν_e signal		Total bkg		Beam bkg		$\bar{\nu}_e$ WS		Beam ν_e CC		NC		ν_μ CC		ν_τ CC		Cosmics	
CCQE z-exp.ax.vec. 1	-0.24	+0.25	-0.29	+0.29	-0.16	+0.17	-0.18	+0.19	-0.61	+0.69	-0.61	+0.64	-0.91	+0.88	-0.50	+0.47	-2.52	+2.68	-0.00	+0.00
CCQE z-exp.ax.vec. 2	-0.23	+0.24	-0.27	+0.28	-0.14	+0.15	-0.16	+0.17	-0.47	+0.52	-0.52	+0.54	-0.74	+0.72	-0.41	+0.39	-2.12	+2.25	-0.00	+0.00
CCQE z-exp.ax.vec. 3	-0.58	+0.64	-0.71	+0.77	-0.31	+0.35	-0.35	+0.40	-0.33	+0.44	-0.87	+0.95	-0.94	+0.90	-0.31	+0.29	-3.53	+3.96	-0.00	+0.00
CCQE z-exp.ax.vec. 4	-0.14	+0.14	-0.17	+0.17	-0.08	+0.08	-0.09	+0.09	-0.04	+0.04	-0.18	+0.19	-0.14	+0.11	-0.05	+0.06	-0.75	+0.78	-0.00	+0.00
M_A^{CCRES}	-0.28	+0.68	-0.17	+0.48	-1.96	+2.56	-2.22	+2.89	-1.05	+3.59	-4.82	+5.45	-2.38	+2.55	-0.41	+1.53	-7.19	+10.03	-0.00	+0.00
M_V^{CCRES}	-0.19	+0.44	-0.23	+0.37	-1.42	+1.93	-1.61	+2.19	-1.52	+2.79	-3.57	+4.52	-2.30	+1.86	-0.00	+0.26	-5.03	+7.27	-0.00	+0.00
M_A^{NCRES}	-0.10	+0.13	-0.05	+0.03	-0.41	+0.52	-0.46	+0.59	-0.05	+0.04	-0.31	+0.22	-2.33	+3.17	-0.91	+0.41	-0.00	+0.00	-0.00	+0.00
M_V^{NCRES}	-0.03	+0.04	-0.02	+0.01	-0.13	+0.16	-0.14	+0.18	-0.02	+0.01	-0.09	+0.07	-0.71	+0.92	-0.10	+0.04	-0.00	+0.00	-0.00	+0.00
CCQE z-exp.norm.	-0.78	+0.98	-0.93	+1.15	-0.45	+0.60	-0.51	+0.68	-2.03	+2.53	-1.62	+2.09	-2.93	+2.32	-1.30	+1.05	-6.77	+9.03	-0.00	+0.00
RPA high Q^2 enh.	-0.44	+0.55	-0.58	+0.70	-0.14	+0.22	-0.16	+0.25	-0.25	+0.25	-0.70	+0.94	-1.08	+0.89	-0.48	+0.41	-0.00	+0.00	-0.00	+0.00
RPA low Q^2 supp.	-0.04	+0.04	-0.03	+0.03	-0.07	+0.07	-0.08	+0.08	-0.10	+0.08	-0.09	+0.08	-0.41	+0.44	-0.18	+0.14	-0.00	+0.00	-0.00	+0.00
RES low Q^2 supp.	-0.00	+0.11	-0.00	+0.14	-0.00	+0.06	-0.00	+0.06	-0.00	+0.76	-0.04	+0.00	-0.00	+0.18	-0.00	+0.11	-0.03	+0.00	-0.00	+0.00
DIS CC $\nu n \to 1\pi$	-0.00	+0.02	-0.09	+0.09	-0.15	+0.18	-0.17	+0.21	-2.14	+2.24	-0.79	+0.79	-1.74	+2.00	-4.20	+3.77	-1.16	+1.16	-0.00	+0.00
FSI π free path	-0.63	+0.39	-0.58	+0.37	-0.75	+0.42	-0.85	+0.48	-0.49	+0.08	-0.30	+0.21	-2.53	+1.28	-0.00	+0.25	-0.02	+0.27	-0.00	+0.00
FSI fate fraction	-0.18	+0.09	-0.13	+0.05	-0.30	+0.18	-0.34	+0.20	-0.29	+0.48	-0.11	+0.00	-1.45	+1.16	-1.19	+1.68	-0.00	+0.12	-0.00	+0.00
MEC E_ν shape	-0.12	+0.00	-0.10	+0.00	-0.16	+0.16	-0.18	+0.18	-1.65	+2.34	-0.35	+0.15	-0.77	+1.06	-0.00	+0.29	-0.88	+0.11	-0.00	+0.00
MEC $E_{\bar{\nu}}$ shape	-0.00	+0.00	-0.05	+0.07	-0.15	+0.10	-0.17	+0.11	-2.83	+1.79	-0.18	+0.11	-0.12	+0.21	-0.05	+0.09	-0.18	+0.03	-0.00	+0.00
MEC ν (q_0, q) response	-0.47	+0.00	-0.32	+0.00	-0.93	+0.33	-1.05	+0.37	-0.00	+0.59	-1.99	+0.63	-0.48	+0.53	-0.04	+2.53	-3.87	+0.00	-0.00	+0.00
MEC $\bar{\nu}$ (q_0, q) response	-0.02	+0.03	-0.03	+0.05	-0.03	+0.03	-0.04	+0.03	-1.94	+0.76	-0.03	+0.07	-0.00	+0.17	-0.69	+0.16	-1.34	+0.94	-0.00	+0.00
MEC ν init. np frac.	-0.03	+0.10	-0.02	+0.05	-0.07	+0.21	-0.08	+0.23	-0.02	+0.05	-0.10	+0.30	-0.06	+0.12	-0.05	+0.21	-0.09	+0.26	-0.00	+0.00
MEC $\bar{\nu}$ init. np frac.	-0.03	+0.00	-0.00	+0.01	-0.11	+0.03	-0.12	+0.04	-0.45	+0.15	-0.09	+0.03	-0.18	+0.05	-0.02	+0.06	-0.15	+0.05	-0.00	+0.00
ν_e/ν_μ radiative corr.	-1.49	+1.49	-2.04	+2.04	-0.27	+0.27	-0.31	+0.31	-0.00	+0.00	-1.40	+1.40	-1.67	+1.67	-1.10	+1.10	-0.00	+0.00	-0.00	+0.00
$\bar{\nu}_e/\bar{\nu}_\mu$ radiative corr.	-0.03	+0.03	-0.00	+0.00	-0.09	+0.09	-0.11	+0.11	-1.99	+1.99	-0.12	+0.12	-0.17	+0.17	-0.10	+0.11	-0.00	+0.00	-0.00	+0.00
Second class currents	-1.47	+1.46	-2.04	+2.04	-0.19	+0.19	-0.22	+0.21	-1.99	+1.99	-1.28	+1.28	-1.45	+1.43	-1.03	+1.01	-0.00	+0.00	-0.00	+0.00
XSecs PC00	-0.14	+0.19	-0.04	+0.04	-0.38	+0.52	-0.43	+0.59	-0.03	+0.03	-0.38	+0.45	-0.46	+0.83	-1.10	+1.33	-0.00	+0.00	-0.00	+0.00
XSecs PC01	-0.11	+0.11	-0.10	+0.10	-0.12	+0.13	-0.14	+0.15	-0.16	+0.16	-0.04	+0.04	-0.32	+0.36	-0.28	+0.24	-0.00	+0.00	-0.00	+0.00
XSecs PC02	-1.15	+1.24	-1.47	+1.57	-0.45	+0.51	-0.51	+0.57	-2.28	+2.60	-0.00	+0.04	-1.29	+1.36	-0.92	+1.02	-0.02	+0.02	-0.00	+0.00
XSecs PC03	-0.26	+0.27	-0.40	+0.41	-0.03	+0.05	-0.03	+0.05	-0.64	+0.67	-0.04	+0.05	-0.04	+0.08	-0.35	+0.38	-0.02	+0.02	-0.00	+0.00
XSecs PC04	-0.41	+0.41	-0.52	+0.54	-0.14	+0.15	-0.16	+0.17	-0.67	+0.68	-0.02	+0.02	-0.57	+0.59	-0.09	+0.07	-0.00	+0.00	-0.00	+0.00
XSecs PC05	-0.26	+0.26	-0.22	+0.23	-0.34	+0.35	-0.39	+0.39	-0.25	+0.26	-0.00	+0.00	-0.41	+0.41	-3.68	+3.74	-0.00	+0.00	-0.00	+0.00
XSecs PC06	-0.20	+0.21	-0.25	+0.26	-0.09	+0.10	-0.11	+0.11	-0.32	+0.33	-0.00	+0.00	-0.27	+0.28	-0.33	+0.35	-0.00	+0.00	-0.00	+0.00
XSecs PC07	-0.10	+0.10	-0.10	+0.10	-0.10	+0.11	-0.11	+0.12	-0.14	+0.14	-0.06	+0.07	-0.23	+0.24	-0.13	+0.13	-0.00	+0.00	-0.00	+0.00
XSecs PC08	-0.12	+0.13	-0.34	+0.35	-0.35	+0.38	-0.40	+0.44	-0.37	+0.38	-0.15	+0.16	-0.90	+0.98	-1.19	+1.27	-0.00	+0.00	-0.00	+0.00
XSecs PC09	-0.20	+0.20	-0.16	+0.16	-0.28	+0.28	-0.32	+0.32	-0.19	+0.19	-0.08	+0.08	-1.46	+1.44	-0.37	+0.37	-0.00	+0.00	-0.00	+0.00
XSecs PC10	-0.22	+0.22	-0.27	+0.28	-0.11	+0.11	-0.12	+0.12	-0.30	+0.30	-0.06	+0.06	-0.40	+0.40	-0.44	+0.45	-0.00	+0.00	-0.00	+0.00
XSecs PC11	-0.16	+0.16	-0.00	+0.00	-0.51	+0.51	-0.58	+0.58	-0.03	+0.03	-0.05	+0.05	-2.09	+2.05	-0.00	+0.01	-0.00	+0.00	-0.00	+0.00
ν_τ scale	-0.40	+0.40	-0.00	+0.00	-1.29	+1.29	-1.46	+1.46	-0.00	+0.00	-0.00	+0.00	-0.00	+0.00	-0.05	+0.05	-65.99	+65.99	-0.00	+0.00
Flux PC00	-0.00	+0.00	-0.14	+0.14	-0.32	+0.30	-0.36	+0.33	-1.55	+1.51	-0.91	+0.86	-0.87	+0.87	-0.86	+0.91	-2.29	+2.29	-0.00	+0.00
Flux PC01	-0.04	+0.02	-0.17	+0.17	-0.33	+0.23	-0.37	+0.26	-3.18	+2.93	-0.54	+0.37	-0.50	+0.49	-0.77	+0.83	-4.62	+4.59	-0.00	+0.00
Flux PC02	-0.09	+0.05	-0.17	+0.17	-0.66	+0.51	-0.75	+0.58	-1.04	+0.90	-0.74	+0.54	-0.49	+0.35	-1.15	+1.08	-2.15	+2.08	-0.00	+0.00
Flux PC03	-0.02	+0.03	-0.08	+0.09	-0.28	+0.27	-0.32	+0.30	-1.04	+0.73	-0.35	+0.32	-0.28	+0.32	-0.05	+0.06	-6.85	+6.86	-0.00	+0.00
Flux PC04	-0.04	+0.04	-0.02	+0.02	-0.19	+0.18	-0.21	+0.21	-0.26	+0.26	-0.35	+0.35	-0.05	+0.05	-0.15	+0.15	-0.65	+0.64	-0.00	+0.00
Absolute calib.	-1.25	+0.04	-1.06	+0.32	-4.71	+2.45	-5.33	+2.78	-3.41	+2.50	-5.17	+4.72	-8.35	+0.00	-0.00	+10.47	-0.03	+0.03	-0.00	+0.00
ND/FD relative calib.	-0.61	+0.27	-0.82	+0.54	-0.35	+0.00	-0.39	+0.00	-0.84	+0.31	-2.17	+2.08	-4.68	+1.81	-1.53	+5.57	-0.01	+0.02	-0.00	+0.00
Calibration shape	-0.01	+0.01	-0.10	+0.10	-0.19	+0.19	-0.21	+0.21	-0.23	+0.23	-0.50	+0.50	-1.52	+1.53	-1.56	+1.56	-0.00	+0.00	-0.00	+0.00
Calibration drift	-0.00	+0.36	-0.00	+0.14	-0.00	+0.85	-0.00	+0.96	-0.00	+1.30	-0.00	+1.57	-3.16	+0.00	-0.00	+11.17	-0.04	+0.00	-0.00	+0.00
Light level FD	-0.20	+0.60	-0.30	+0.67	-0.00	+0.43	-0.00	+0.49	-0.26	+0.00	-0.00	+1.58	-0.87	+0.00	-4.44	+0.00	-0.06	+0.00	-0.00	+0.00
Light level ND	-0.71	+0.17	-0.80	+0.00	-0.52	+0.68	-0.58	+0.77	-0.87	+0.06	-1.08	+0.00	-0.00	+2.20	-2.29	+2.75	-0.00	+0.00	-0.00	+0.00
Cherenkov	-0.00	+0.47	-0.32	+0.00	-0.00	+2.21	-0.00	+2.50	-0.00	+0.22	-0.00	+3.08	-0.00	+1.76	-0.00	+2.59	-0.02	+0.00	-0.00	+0.00
E_μ scale ND uncorr.	-0.09	+0.10	-0.13	+0.14	-0.00	+0.00	-0.00	+0.00	-0.15	+0.15	-0.02	+0.02	-0.04	+0.04	-0.03	+0.03	-0.00	+0.00	-0.00	+0.00
E_μ μ-catcher uncorr.	-0.02	+0.02	-0.02	+0.02	-0.00	+0.00	-0.00	+0.00	-0.15	+0.15	-0.02	+0.03	-0.04	+0.04	-0.04	+0.03	-0.00	+0.00	-0.00	+0.00
E_μ n pile-up	-0.23	+0.00	-0.33	+0.00	-0.02	+0.00	-0.02	+0.00	-0.45	+0.00	-0.06	+0.00	-0.00	+0.10	-0.00	+0.08	-0.00	+0.00	-0.00	+0.00
E_μ correlated	-0.54	+0.57	-0.76	+0.80	-0.04	+0.04	-0.05	+0.05	-0.90	+0.93	-0.15	+0.14	-0.24	+0.24	-0.20	+0.20	-0.00	+0.00	-0.00	+0.00
Lepton angle xz ND	-0.19	+0.13	-0.27	+0.19	-0.00	+0.00	-0.00	+0.00	-0.21	+0.16	-0.00	+0.00	-0.00	+0.00	-0.00	+0.00	-0.00	+0.00	-0.00	+0.00
Lepton angle yz ND	-0.10	+0.02	-0.14	+0.03	-0.00	+0.00	-0.00	+0.00	-0.05	+0.00	-0.00	+0.00	-0.00	+0.00	-0.00	+0.00	-0.00	+0.00	-0.00	+0.00
Lepton angle xz FD	-0.00	+0.00	-0.00	+0.00	-0.00	+0.00	-0.00	+0.00	-0.00	+0.00	-0.00	+0.00	-0.00	+0.00	-0.00	+0.00	-0.00	+0.00	-0.00	+0.00
Lepton angle yz FD	-0.00	+0.00	-0.00	+0.00	-0.00	+0.00	-0.00	+0.00	-0.00	+0.00	-0.00	+0.00	-0.00	+0.00	-0.00	+0.00	-0.00	+0.00	-0.00	+0.00
Neutron systematic	-0.36	+0.48	-0.36	+0.58	-0.36	+0.26	-0.40	+0.30	-1.16	+0.88	-0.52	+0.47	-0.22	+0.00	-0.00	+0.21	-0.12	+0.13	-0.00	+0.00
Normalization beam corr.	-0.79	+0.79	-0.84	+0.84	-0.70	+0.70	-0.79	+0.79	-0.82	+0.82	-0.81	+0.81	-0.78	+0.78	-0.62	+0.62	-0.90	+0.90	-0.00	+0.00
Normalization ν-beam	-0.60	+0.60	-0.60	+0.60	-0.58	+0.58	-0.66	+0.66	-0.59	+0.59	-0.68	+0.68	-0.65	+0.65	-0.52	+0.52	-0.76	+0.76	-0.00	+0.00
Acceptance ν_μ/ν_e ND/FD	-0.28	+0.28	-0.40	+0.40	-0.01	+0.01	-0.01	+0.01	-0.32	+0.32	-0.00	+0.00	-0.00	+0.00	-0.00	+0.00	-0.00	+0.00	-0.00	+0.00
Michel e tagging	-0.34	+0.34	-0.00	+0.00	-1.08	+1.08	-1.22	+1.22	-0.00	+0.00	-0.00	+0.00	-6.07	+6.16	-5.75	+5.48	-0.00	+0.00	-0.00	+0.00
Rock scale	-0.46	+0.46	-0.14	+0.14	-1.16	+1.16	-1.31	+1.31	-0.14	+0.14	-0.29	+0.29	-1.49	+1.49	-10.09	+10.09	-0.00	+0.00	-0.00	+0.00
Cosmic scale	-0.55	+0.63	-0.00	+0.00	-1.75	+2.00	-0.00	+0.00	-0.00	+0.00	-0.00	+0.00	-0.00	+0.00	-0.00	+0.00	-0.00	+0.00	-15.01	+17.15
Quadrature	-3.63	+3.53	-4.32	+4.25	-6.38	+5.90	-6.95	+6.28	-8.60	+9.11	-9.25	+10.31	-14.24	+10.46	-14.53	+21.61	-67.82	+68.56	-15.01	+17.15

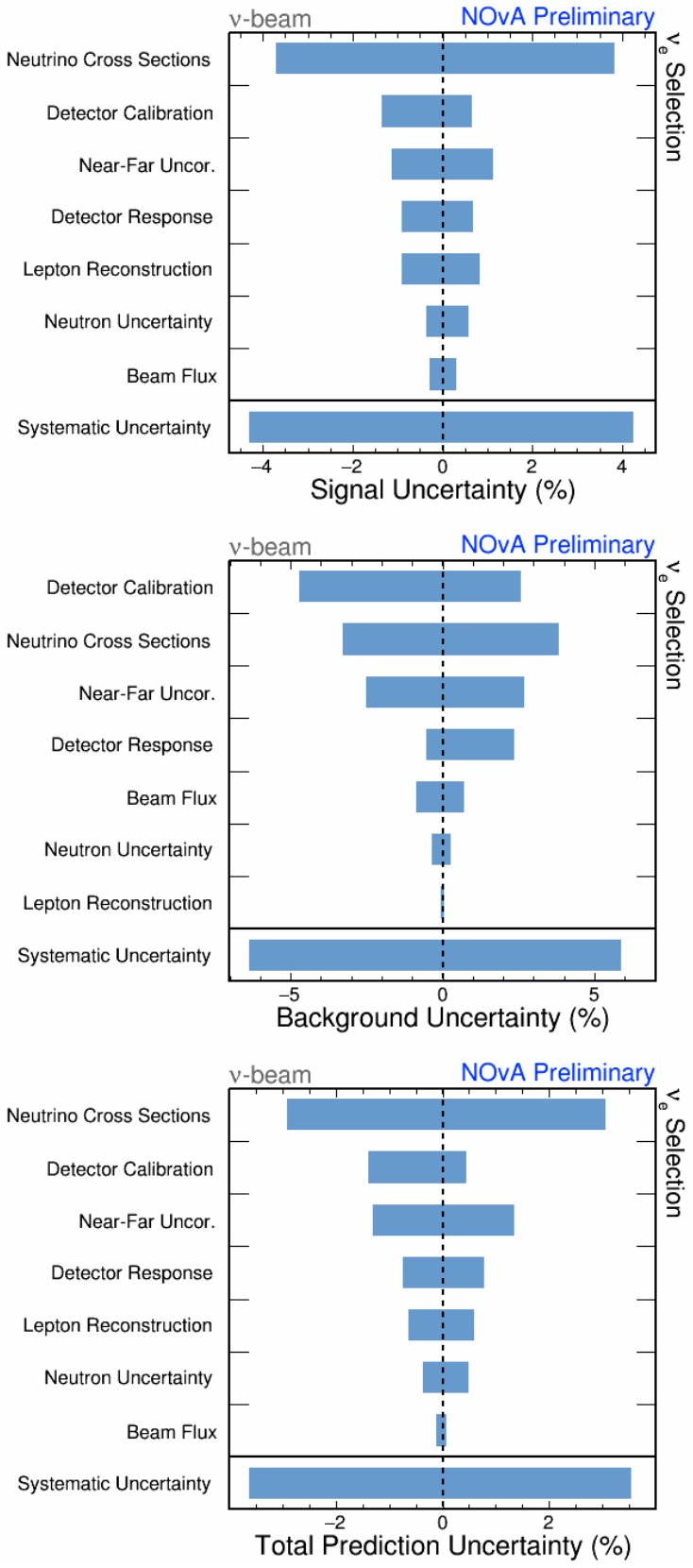

Figure C.25: Relative 1σ syst. uncertainties on the integral number of signal (top), background (middle), and total (bottom) predicted events in the ν_e app. ν-beam all samples.

C.4 Appearance $\bar{\nu}_e$ channel, $\bar{\nu}$-beam

Low PID sample

Table C.15: Relative 1σ systematic uncertainties on the integral numbers of predicted events for the $\bar{\nu}_e$ app. $\bar{\nu}$-beam low PID sample.

Systematic summary for ν_e appearance $\bar{\nu}$-beam low PID sample (%)

Systematic	Total pred		$\bar{\nu}_e$ Signal		Total bkg		Beam bkg		ν_e WS		Beam ν_e CC		NC		ν_μ CC		ν_τ CC		Cosmics	
CCQE z-exp.ax.vec. 1	-0.44	+0.43	-1.00	+0.97	-0.13	+0.12	-0.14	+0.14	-0.87	+0.84	-0.17	+0.19	-0.29	+0.27	-0.26	+0.24	-1.95	+2.11	-0.00	+0.00
CCQE z-exp.ax.vec. 2	-0.32	+0.31	-0.72	+0.70	-0.09	+0.09	-0.10	+0.10	-0.62	+0.61	-0.14	+0.15	-0.22	+0.20	-0.20	+0.19	-1.67	+1.79	-0.00	+0.00
CCQE z-exp.ax.vec. 3	-0.07	+0.12	-0.25	+0.34	-0.00	+0.03	-0.00	+0.04	-0.19	+0.27	-0.21	+0.29	-0.23	+0.19	-0.17	+0.16	-2.77	+3.39	-0.00	+0.00
CCQE z-exp.ax.vec. 4	-0.01	+0.02	-0.00	+0.01	-0.02	+0.02	-0.02	+0.02	-0.01	+0.02	-0.05	+0.06	-0.03	+0.03	-0.02	+0.02	-0.61	+0.65	-0.00	+0.00
M_A^{CCRES}	-1.35	+2.50	-2.53	+4.83	-0.68	+1.17	-0.77	+1.31	-2.58	+4.67	-3.92	+5.42	-3.86	+2.12	-0.00	+9.27	-8.18	+13.02	-0.00	+0.00
M_V^{CCRES}	-1.22	+2.07	-2.58	+4.46	-0.45	+0.71	-0.51	+0.80	-2.29	+3.89	-2.98	+4.27	-2.95	+1.60	-0.00	+2.75	-5.61	+8.99	-0.00	+0.00
M_A^{NCRES}	-0.84	+1.24	-0.05	+0.03	-1.34	+1.97	-1.50	+2.21	-0.06	+0.03	-5.09	+3.04	-5.62	+8.81	-5.24	+2.88	-0.00	+0.00	-0.00	+0.00
M_V^{NCRES}	-0.00	+0.09	-0.00	+0.00	-0.00	+0.14	-0.00	+0.16	-0.00	+0.00	-0.26	+0.00	-0.00	+0.41	-0.25	+0.00	-0.00	+0.00	-0.00	+0.00
CCQE z-exp.norm.	-1.05	+0.88	-2.47	+2.06	-0.25	+0.21	-0.28	+0.24	-2.11	+1.75	-0.75	+0.98	-1.03	+0.80	-0.91	+0.70	-5.92	+7.89	-0.00	+0.00
RPA high Q^2 enh.	-0.12	+0.13	-0.24	+0.24	-0.06	+0.07	-0.07	+0.07	-0.19	+0.19	-0.22	+0.31	-0.28	+0.24	-0.25	+0.22	-0.00	+0.00	-0.00	+0.00
RPA low Q^2 supp.	-0.28	+0.28	-0.56	+0.58	-0.11	+0.11	-0.13	+0.13	-0.47	+0.48	-0.11	+0.11	-0.20	+0.20	-0.16	+0.16	-0.00	+0.00	-0.00	+0.00
RES low Q^2 supp.	-0.18	+0.00	-0.47	+0.00	-0.01	+0.00	-0.01	+0.00	-0.41	+0.00	-0.50	+0.00	-0.00	+0.40	-0.00	+0.33	-0.00	+0.00	-0.00	+0.00
DIS CC $\nu n \to 1\pi$	-0.06	+0.06	-0.23	+0.23	-0.04	+0.04	-0.04	+0.04	-0.41	+0.41	-0.06	+0.06	-0.60	+0.62	-3.30	+3.20	-0.56	+0.56	-0.00	+0.00
FSI π free path	-0.53	+0.24	-0.56	+0.16	-0.52	+0.29	-0.58	+0.32	-0.37	+0.10	-0.84	+0.71	-1.49	+1.14	-1.51	+0.98	-0.00	+0.29	-0.00	+0.00
FSI fate fraction	-0.02	+0.04	-0.12	+0.01	-0.00	+0.06	-0.00	+0.06	-0.09	+0.07	-0.00	+0.39	-0.10	+0.03	-0.61	+0.07	-0.16	+0.22	-0.00	+0.00
MEC E_ν shape	-0.02	+0.08	-0.02	+0.03	-0.02	+0.11	-0.02	+0.12	-0.09	+0.10	-0.22	+0.46	-0.09	+0.14	-0.06	+0.16	-0.50	+0.08	-0.00	+0.00
MEC $E_{\bar{\nu}}$ shape	-0.41	+0.70	-0.94	+1.49	-0.11	+0.25	-0.12	+0.28	-0.90	+1.34	-0.48	+0.54	-0.37	+0.55	-0.23	+0.51	-0.27	+0.04	-0.00	+0.00
MEC ν (q_0, q) response	-0.24	+0.00	-0.19	+0.13	-0.45	+0.00	-0.50	+0.00	-0.21	+0.03	-0.84	+0.00	-0.23	+0.15	-0.24	+0.14	-4.47	+0.00	-0.00	+0.00
MEC $\bar{\nu}$ (q_0, q) response	-1.99	+0.88	-3.06	+3.07	-1.38	+0.00	-1.55	+0.00	-2.72	+2.79	-1.88	+0.00	-1.04	+0.00	-1.84	+0.18	-1.72	+0.00	-0.00	+0.00
MEC ν init. np frac.	-0.01	+0.03	-0.00	+0.00	-0.02	+0.06	-0.02	+0.06	-0.02	+0.00	-0.06	+0.18	-0.00	+0.00	-0.08	+0.03	-0.17	+0.51	-0.00	+0.00
MEC $\bar{\nu}$ init. np frac.	-0.18	+0.06	-0.03	+0.00	-0.26	+0.09	-0.29	+0.10	-0.00	+0.01	-0.32	+0.11	-0.31	+0.11	-0.76	+0.26	-0.33	+0.11	-0.00	+0.00
ν_e/ν_μ radiative corr.	-0.14	+0.14	-0.30	+0.30	-0.05	+0.05	-0.05	+0.05	-0.44	+0.44	-0.27	+0.27	-0.16	+0.16	-0.21	+0.21	-0.00	+0.00	-0.00	+0.00
$\bar{\nu}_e/\bar{\nu}_\mu$ radiative corr.	-0.73	+0.73	-1.70	+1.70	-0.18	+0.18	-0.20	+0.20	-1.56	+1.56	-0.63	+0.63	-0.37	+0.37	-0.41	+0.41	-0.00	+0.00	-0.00	+0.00
Second class currents	-0.59	+0.59	-1.40	+1.40	-0.13	+0.13	-0.15	+0.15	-1.12	+1.12	-0.36	+0.36	-0.20	+0.21	-0.20	+0.20	-0.00	+0.00	-0.00	+0.00
XSecs PC00	-0.48	+0.55	-0.06	+0.06	-0.73	+0.82	-0.82	+0.93	-0.05	+0.05	-3.91	+4.37	-1.43	+1.30	-2.61	+2.97	-0.00	+0.00	-0.00	+0.00
XSecs PC01	-0.18	+0.19	-0.04	+0.04	-0.26	+0.28	-0.29	+0.31	-0.02	+0.02	-2.12	+2.26	-1.14	+1.07	-1.91	+2.05	-0.00	+0.00	-0.00	+0.00
XSecs PC02	-0.06	+0.07	-0.10	+0.10	-0.04	+0.04	-0.05	+0.05	-0.08	+0.10	-0.23	+0.23	-0.24	+0.24	-2.00	+1.97	-0.01	+0.01	-0.00	+0.00
XSecs PC03	-0.37	+0.38	-0.02	+0.02	-0.59	+0.61	-0.67	+0.68	-0.04	+0.05	-0.74	+0.76	-1.21	+1.25	-3.25	+3.17	-0.02	+0.02	-0.00	+0.00
XSecs PC04	-0.13	+0.14	-0.26	+0.26	-0.36	+0.37	-0.41	+0.41	-0.32	+0.33	-0.73	+0.74	-0.40	+0.40	-0.32	+0.33	-0.00	+0.00	-0.00	+0.00
XSecs PC05	-0.12	+0.12	-0.03	+0.03	-0.16	+0.17	-0.18	+0.19	-0.04	+0.04	-0.59	+0.60	-0.21	+0.21	-2.35	+2.32	-0.00	+0.00	-0.00	+0.00
XSecs PC06	-0.03	+0.03	-0.16	+0.17	-0.05	+0.05	-0.06	+0.06	-0.16	+0.16	-0.24	+0.24	-0.33	+0.33	-0.03	+0.03	-0.00	+0.00	-0.00	+0.00
XSecs PC07	-0.07	+0.08	-0.29	+0.29	-0.05	+0.05	-0.05	+0.06	-0.30	+0.31	-1.13	+1.15	-0.69	+0.68	-0.75	+0.77	-0.00	+0.00	-0.00	+0.00
XSecs PC08	-0.30	+0.32	-0.00	+0.00	-0.47	+0.50	-0.53	+0.57	-0.02	+0.02	-2.09	+2.22	-0.44	+0.43	-0.72	+0.76	-0.00	+0.00	-0.00	+0.00
XSecs PC09	-0.37	+0.38	-0.17	+0.17	-0.48	+0.50	-0.54	+0.56	-0.18	+0.18	-1.03	+1.07	-0.32	+0.33	-0.52	+0.54	-0.00	+0.00	-0.00	+0.00
XSecs PC10	-0.21	+0.21	-0.17	+0.18	-0.23	+0.23	-0.25	+0.26	-0.19	+0.19	-0.37	+0.38	-0.28	+0.29	-0.50	+0.49	-0.00	+0.00	-0.00	+0.00
XSecs PC11	-0.10	+0.10	-0.25	+0.25	-0.01	+0.01	-0.01	+0.02	-0.26	+0.26	-0.92	+0.94	-0.69	+0.68	-0.66	+0.68	-0.00	+0.00	-0.00	+0.00
ν_τ scale	-0.89	+0.89	-0.00	+0.00	-1.40	+1.40	-1.58	+1.58	-0.00	+0.00	-0.00	+0.00	-0.00	+0.00	-0.09	+0.09	-65.98	+65.98	-0.00	+0.00
Flux PC00	-0.07	+0.06	-0.08	+0.08	-0.07	+0.05	-0.07	+0.06	-0.04	+0.04	-0.12	+0.07	-0.18	+0.18	-0.11	+0.11	-2.50	+2.50	-0.00	+0.00
Flux PC01	-0.29	+0.27	-0.21	+0.21	-0.34	+0.30	-0.38	+0.34	-0.19	+0.16	-1.32	+1.22	-0.11	+0.11	-0.35	+0.29	-5.08	+5.03	-0.00	+0.00
Flux PC02	-0.26	+0.19	-0.21	+0.16	-0.29	+0.21	-0.32	+0.23	-0.37	+0.31	-0.54	+0.29	-0.07	+0.07	-0.19	+0.18	-3.10	+3.10	-0.00	+0.00
Flux PC03	-0.24	+0.22	-0.08	+0.04	-0.33	+0.32	-0.37	+0.36	-0.04	+0.00	-1.40	+1.48	-0.17	+0.13	-0.28	+0.17	-7.11	+7.04	-0.00	+0.00
Flux PC04	-0.09	+0.09	-0.07	+0.07	-0.11	+0.10	-0.12	+0.12	-0.17	+0.18	-0.42	+0.41	-0.07	+0.06	-0.19	+0.19	-0.08	+0.08	-0.00	+0.00
Absolute calib.	-0.54	+0.29	-0.10	+0.82	-0.80	+0.00	-0.89	+0.00	-0.00	+1.89	-2.58	+1.22	-1.43	+0.00	-2.61	+0.71	-0.05	+0.00	-0.00	+0.00
ND/FD relative calib.	-0.42	+0.35	-0.52	+0.63	-0.37	+0.18	-0.42	+0.20	-0.00	+0.57	-0.78	+0.38	-0.30	+0.00	-1.54	+1.15	-0.01	+0.00	-0.00	+0.00
Calibration shape	-0.22	+0.22	-0.53	+0.53	-0.05	+0.05	-0.05	+0.05	-0.47	+0.47	-1.37	+1.37	-0.80	+0.80	-1.32	+1.32	-0.06	+0.06	-0.00	+0.00
Calibration drift	-0.00	+2.83	-0.00	+0.77	-0.00	+4.00	-0.00	+4.49	-0.00	+0.55	-0.00	+7.26	-0.00	+4.22	-0.00	+0.69	-0.13	+0.00	-0.00	+0.00
Light level FD	-1.02	+0.58	-1.04	+1.56	-1.01	+0.03	-1.13	+0.03	-0.63	+2.11	-2.70	+0.00	-0.17	+0.00	-2.84	+0.00	-0.07	+0.00	-0.00	+0.00
Light level ND	-0.00	+3.68	-0.64	+0.00	-0.00	+5.88	-0.00	+6.60	-0.72	+0.00	-0.00	+6.11	-0.00	+8.85	-0.00	+8.27	-0.00	+0.00	-0.00	+0.00
Cherenkov	-0.00	+0.07	-0.21	+0.00	-0.00	+0.22	-0.00	+0.25	-0.00	+0.12	-0.00	+0.24	-0.00	+0.83	-4.69	+0.00	-0.11	+0.00	-0.00	+0.00
E_μ ND uncorr.	-0.03	+0.04	-0.06	+0.08	-0.00	+0.01	-0.01	+0.01	-0.09	+0.10	-0.00	+0.00	-0.00	+0.00	-0.00	+0.00	-0.00	+0.00	-0.00	+0.00
E_μ μ-catcher uncorr.	-0.00	+0.00	-0.00	+0.00	-0.00	+0.00	-0.01	+0.01	-0.09	+0.09	-0.00	+0.00	-0.00	+0.00	-0.00	+0.00	-0.00	+0.00	-0.00	+0.00
E_μ n pile-up	-0.07	+0.00	-0.15	+0.00	-0.03	+0.00	-0.03	+0.00	-0.29	+0.00	-0.00	+0.00	-0.00	+0.00	-0.00	+0.00	-0.00	+0.00	-0.00	+0.00
E_μ correlated	-0.17	+0.19	-0.36	+0.40	-0.06	+0.07	-0.07	+0.08	-0.54	+0.62	-0.00	+0.00	-0.00	+0.00	-0.00	+0.00	-0.00	+0.00	-0.00	+0.00
Lepton angle xz ND	-0.11	+0.06	-0.25	+0.12	-0.04	+0.02	-0.04	+0.02	-0.35	+0.20	-0.00	+0.00	-0.00	+0.00	-0.00	+0.00	-0.00	+0.00	-0.00	+0.00
Lepton angle yz ND	-0.07	+0.01	-0.17	+0.04	-0.02	+0.00	-0.02	+0.00	-0.15	+0.00	-0.00	+0.00	-0.00	+0.00	-0.00	+0.00	-0.00	+0.00	-0.00	+0.00
Lepton angle xz FD	-0.00	+0.00	-0.00	+0.00	-0.00	+0.00	-0.00	+0.00	-0.00	+0.00	-0.00	+0.00	-0.00	+0.00	-0.00	+0.00	-0.00	+0.00	-0.00	+0.00
Lepton angle yz FD	-0.00	+0.00	-0.00	+0.00	-0.00	+0.00	-0.00	+0.00	-0.00	+0.00	-0.00	+0.00	-0.00	+0.00	-0.00	+0.00	-0.00	+0.00	-0.00	+0.00
Neutron systematic	-0.06	+0.17	-0.00	+0.19	-0.20	+0.25	-0.23	+0.29	-0.54	+0.59	-0.36	+0.62	-0.07	+0.00	-0.22	+0.37	-0.00	+0.14	-0.00	+0.00
Normalization beam corr.	-0.69	+0.69	-0.82	+0.82	-0.62	+0.62	-0.69	+0.69	-0.82	+0.82	-0.69	+0.69	-0.65	+0.65	-0.62	+0.62	-0.90	+0.90	-0.00	+0.00
Normalization $\bar{\nu}$-beam	-0.63	+0.63	-0.73	+0.73	-0.57	+0.57	-0.64	+0.64	-0.73	+0.73	-0.64	+0.64	-0.61	+0.61	-0.57	+0.57	-0.84	+0.84	-0.00	+0.00
Acceptance $\bar{\nu}_\mu/\bar{\nu}_e$ ND/FD	-0.15	+0.15	-0.38	+0.38	-0.02	+0.02	-0.03	+0.03	-0.22	+0.22	-0.00	+0.00	-0.00	+0.00	-0.00	+0.00	-0.00	+0.00	-0.00	+0.00
Rock scale	-0.48	+0.48	-0.08	+0.08	-0.71	+0.71	-0.79	+0.79	-0.07	+0.07	-0.33	+0.33	-0.52	+0.52	-8.49	+8.49	-0.00	+0.00	-0.00	+0.00
Cosmic scale	-1.67	+2.12	-0.00	+0.00	-2.62	+3.33	-0.00	+0.00	-0.00	+0.00	-0.00	+0.00	-0.00	+0.00	-0.00	+0.00	-0.00	+0.00	-23.88	+30.37
Quadrature	-4.27	+6.71	-6.41	+8.51	-4.34	+8.55	-3.89	+8.85	-5.85	+8.16	-10.39	+13.89	-8.43	+13.89	-13.90	+17.17	-67.96	+69.13	-23.88	+30.37

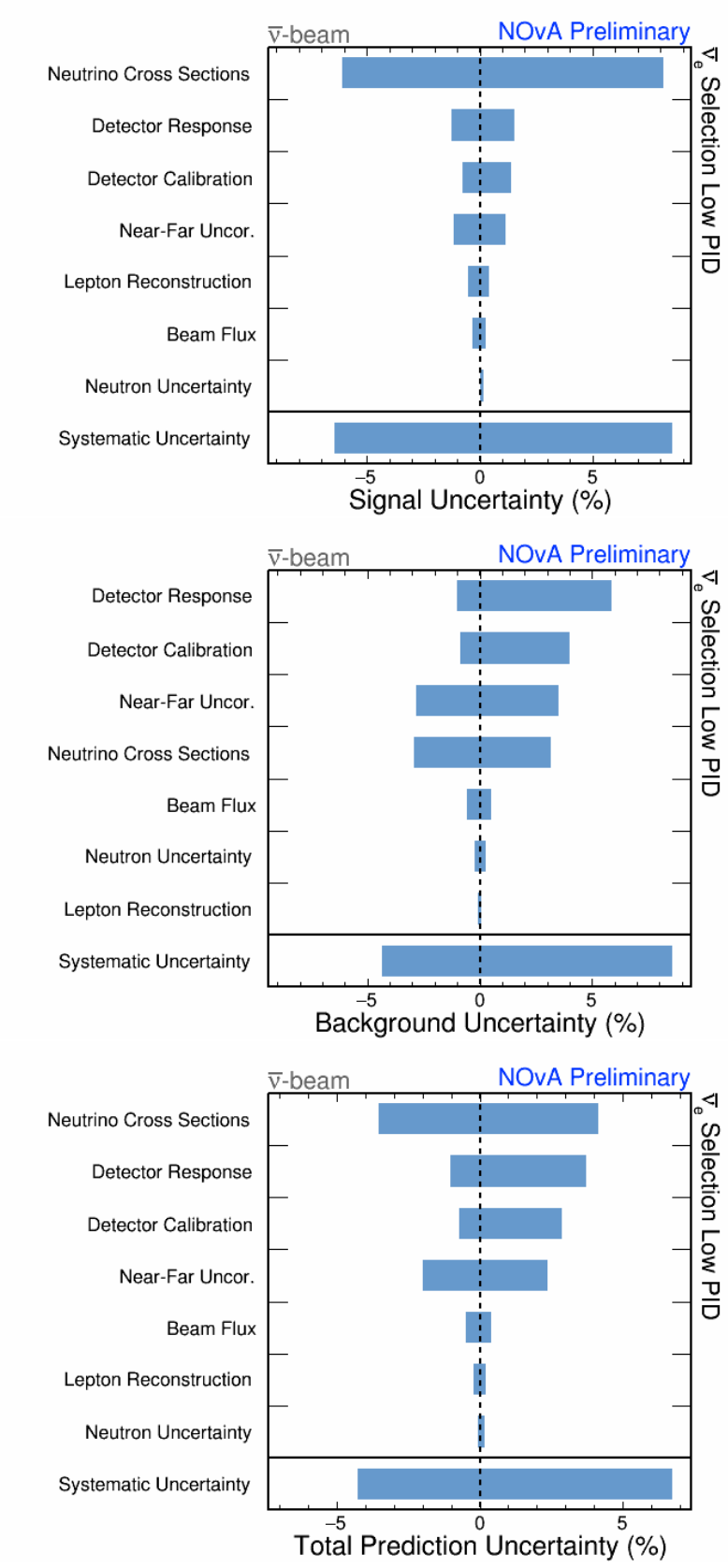

Figure C.26: Relative 1σ syst. uncertainties on the integral number of signal (top), background (middle), and total (bottom) predicted events in the $\bar{\nu}_e$ app. $\bar{\nu}$-beam low PID sample.

High PID sample

Table C.16: Relative 1σ systematic uncertainties on the integral numbers of predicted events for the $\bar{\nu}_e$ app. $\bar{\nu}$-beam high PID sample.

Systematic summary for ν_e appearance $\bar{\nu}$-beam high PID sample (%)

Systematic	Total pred		$\bar{\nu}_e$ Signal		Total bkg		Beam bkg		ν_e WS		Beam ν_e CC		NC		ν_μ CC		ν_τ CC		Cosmics	
CCQE z-exp.ax.vec. 1	-0.20	+0.22	-0.28	+0.30	-0.01	+0.02	-0.01	+0.02	-0.33	+0.35	-0.03	+0.04	-2.13	+2.05	-1.56	+1.50	-2.88	+3.13	-0.00	+0.00
CCQE z-exp.ax.vec. 2	-0.18	+0.20	-0.25	+0.27	-0.04	+0.05	-0.04	+0.05	-0.28	+0.30	-0.05	+0.06	-1.62	+1.56	-1.19	+1.14	-2.43	+2.62	-0.00	+0.00
CCQE z-exp.ax.vec. 3	-0.30	+0.36	-0.36	+0.43	-0.15	+0.20	-0.16	+0.21	-0.41	+0.49	-0.12	+0.16	-1.44	+1.34	-1.01	+0.95	-3.26	+3.83	-0.00	+0.00
CCQE z-exp.ax.vec. 4	-0.06	+0.07	-0.07	+0.07	-0.04	+0.04	-0.04	+0.05	-0.08	+0.09	-0.03	+0.03	-0.18	+0.17	-0.12	+0.11	-0.63	+0.67	-0.00	+0.00
M_A^{CCRES}	-0.48	+0.45	-0.94	+0.75	-0.22	+0.53	-0.22	+0.54	-0.50	+0.50	-0.86	+1.17	-5.08	+4.68	-0.00	+7.10	-4.43	+6.37	-0.00	+0.00
M_V^{CCRES}	-0.57	+0.46	-1.01	+0.76	-0.20	+0.40	-0.21	+0.40	-0.71	+0.57	-0.77	+1.09	-4.13	+3.15	-0.00	+3.50	-3.14	+4.76	-0.00	+0.00
M_A^{NCRES}	-0.05	+0.08	-0.05	+0.02	-0.21	+0.37	-0.22	+0.38	-0.05	+0.02	-1.25	+0.68	-9.65	+17.41	-1.16	+0.61	-0.00	+0.00	-0.00	+0.00
M_V^{NCRES}	-0.00	+0.00	-0.00	+0.00	-0.00	+0.03	-0.00	+0.03	-0.00	+0.00	-0.05	+0.00	-0.00	+0.61	-0.05	+0.00	-0.00	+0.00	-0.00	+0.00
CCQE z-exp.norm.	-0.70	+0.85	-0.99	+1.19	-0.06	+0.11	-0.06	+0.11	-1.10	+1.33	-0.06	+0.07	-6.77	+5.66	-5.08	+4.24	-7.92	+10.55	-0.00	+0.00
RPA high Q^2 enh.	-0.29	+0.33	-0.39	+0.45	-0.06	+0.07	-0.06	+0.08	-0.43	+0.51	-0.11	+0.13	-1.64	+1.42	-1.26	+1.10	-0.00	+0.00	-0.00	+0.00
RPA low Q^2 supp.	-0.03	+0.03	-0.04	+0.04	-0.19	+0.19	-0.19	+0.20	-0.08	+0.07	-0.17	+0.18	-1.22	+1.25	-0.95	+0.97	-0.00	+0.00	-0.00	+0.00
RES low Q^2 supp.	-0.00	+0.08	-0.00	+0.00	-0.00	+0.25	-0.00	+0.25	-0.00	+0.05	-0.00	+0.20	-0.00	+1.41	-0.00	+1.16	-0.02	+0.00	-0.00	+0.00
DIS CC $\nu n \to 1\pi$	-0.02	+0.02	-0.05	+0.05	-0.04	+0.04	-0.05	+0.04	-0.00	+0.00	-0.05	+0.04	-0.59	+0.59	-5.41	+5.33	-0.31	+0.31	-0.00	+0.00
FSI π free path	-0.27	+0.25	-0.17	+0.22	-0.48	+0.34	-0.49	+0.35	-0.14	+0.22	-0.38	+0.15	-2.65	+2.51	-3.10	+2.77	-0.27	+0.38	-0.00	+0.00
FSI fate fraction	-0.05	+0.10	-0.06	+0.09	-0.03	+0.12	-0.03	+0.12	-0.02	+0.07	-0.00	+0.22	-0.63	+0.00	-0.37	+0.53	-0.05	+0.00	-0.00	+0.00
MEC E_ν shape	-0.04	+0.00	-0.03	+0.00	-0.08	+0.03	-0.09	+0.03	-0.11	+0.05	-0.13	+0.08	-0.45	+0.58	-0.22	+0.40	-0.61	+0.08	-0.00	+0.00
MEC $E_\bar{\nu}$ shape	-0.25	+0.05	-0.26	+0.05	-0.23	+0.06	-0.24	+0.06	-0.15	+0.00	-0.53	+0.25	-1.42	+2.25	-0.67	+1.29	-0.84	+0.11	-0.00	+0.00
MEC ν (q_0, q) response	-0.33	+0.08	-0.11	+0.02	-0.83	+0.19	-0.85	+0.20	-0.26	+0.08	-1.03	+0.28	-0.00	+0.13	-0.00	+0.31	-4.28	+0.00	-0.00	+0.00
MEC $\bar{\nu}$ (q_0, q) response	-0.84	+0.00	-0.68	+0.00	-1.20	+0.00	-1.23	+0.00	-0.53	+0.00	-1.66	+0.03	-0.00	+1.41	-0.67	+0.70	-4.02	+1.46	-0.00	+0.00
MEC ν init. np frac.	-0.00	+0.03	-0.00	+0.00	-0.04	+0.11	-0.04	+0.11	-0.00	+0.01	-0.06	+0.17	-0.25	+0.08	-0.06	+0.02	-0.16	+0.47	-0.00	+0.00
MEC $\bar{\nu}$ init. np frac.	-0.02	+0.06	-0.04	+0.13	-0.09	+0.03	-0.09	+0.03	-0.08	+0.25	-0.18	+0.06	-0.01	+0.05	-0.04	+0.12	-1.25	+0.42	-0.00	+0.00
ν_e/ν_μ radiative corr.	-0.13	+0.13	-0.18	+0.18	-0.01	+0.02	-0.02	+0.02	-0.30	+0.30	-0.02	+0.02	-0.48	+0.49	-0.44	+0.45	-0.00	+0.00	-0.00	+0.00
$\bar{\nu}_e/\bar{\nu}_\mu$ radiative corr.	-1.42	+1.42	-1.85	+1.85	-0.46	+0.46	-0.47	+0.47	-1.74	+1.74	-0.29	+0.28	-1.43	+1.47	-1.16	+1.19	-0.00	+0.00	-0.00	+0.00
Second class currents	-1.29	+1.29	-1.67	+1.67	-0.45	+0.45	-0.46	+0.46	-1.44	+1.44	-0.31	+0.30	-0.96	+0.97	-0.73	+0.74	-0.00	+0.00	-0.00	+0.00
XSecs PC00	-0.09	+0.10	-0.06	+0.06	-0.17	+0.17	-0.17	+0.18	-0.05	+0.05	-1.00	+1.03	-7.19	+7.02	-0.91	+0.90	-0.00	+0.00	-0.00	+0.00
XSecs PC01	-0.05	+0.06	-0.04	+0.04	-0.08	+0.08	-0.08	+0.08	-0.02	+0.02	-0.59	+0.60	-4.63	+4.55	-0.36	+0.36	-0.00	+0.00	-0.00	+0.00
XSecs PC02	-0.02	+0.02	-0.05	+0.05	-0.05	+0.06	-0.05	+0.06	-0.16	+0.18	-0.03	+0.03	-0.32	+0.32	-2.64	+2.61	-0.00	+0.00	-0.00	+0.00
XSecs PC03	-0.06	+0.06	-0.00	+0.00	-0.22	+0.22	-0.22	+0.22	-0.06	+0.06	-0.29	+0.29	-0.80	+0.81	-4.64	+4.59	-0.00	+0.00	-0.00	+0.00
XSecs PC04	-0.29	+0.29	-0.38	+0.39	-0.08	+0.08	-0.08	+0.08	-0.48	+0.49	-0.07	+0.07	-0.17	+0.17	-0.08	+0.08	-0.00	+0.00	-0.00	+0.00
XSecs PC05	-0.04	+0.04	-0.05	+0.05	-0.03	+0.03	-0.03	+0.03	-0.04	+0.04	-0.13	+0.13	-0.40	+0.40	-4.10	+4.09	-0.00	+0.00	-0.00	+0.00
XSecs PC06	-0.13	+0.13	-0.21	+0.21	-0.06	+0.06	-0.06	+0.06	-0.22	+0.22	-0.04	+0.04	-1.08	+1.08	-0.40	+0.40	-0.00	+0.00	-0.00	+0.00
XSecs PC07	-0.30	+0.31	-0.40	+0.41	-0.09	+0.09	-0.09	+0.10	-0.43	+0.44	-0.25	+0.25	-2.19	+2.19	-0.33	+0.34	-0.00	+0.00	-0.00	+0.00
XSecs PC08	-0.00	+0.00	-0.00	+0.00	-0.01	+0.01	-0.01	+0.01	-0.02	+0.02	-0.40	+0.41	-3.58	+3.54	-1.20	+1.18	-0.00	+0.00	-0.00	+0.00
XSecs PC09	-0.22	+0.22	-0.26	+0.26	-0.13	+0.13	-0.14	+0.14	-0.27	+0.28	-0.22	+0.23	-1.01	+1.00	-0.41	+0.40	-0.00	+0.00	-0.00	+0.00
XSecs PC10	-0.20	+0.20	-0.25	+0.25	-0.08	+0.08	-0.08	+0.08	-0.28	+0.28	-0.06	+0.06	-0.23	+0.23	-0.83	+0.82	-0.00	+0.00	-0.00	+0.00
XSecs PC11	-0.30	+0.30	-0.36	+0.37	-0.16	+0.16	-0.17	+0.17	-0.38	+0.39	-0.12	+0.12	-2.18	+2.19	-0.21	+0.21	-0.00	+0.00	-0.00	+0.00
ν_τ scale	-0.55	+0.55	-0.00	+0.00	-1.75	+1.75	-1.79	+1.79	-0.00	+0.00	-0.00	+0.00	-0.00	+0.00	-0.04	+0.04	-66.36	+66.36	-0.00	+0.00
Flux PC00	-0.16	+0.15	-0.09	+0.09	-0.31	+0.29	-0.32	+0.29	-0.05	+0.05	-0.52	+0.48	-0.44	+0.47	-0.25	+0.26	-2.65	+2.65	-0.00	+0.00
Flux PC01	-0.39	+0.35	-0.22	+0.22	-0.76	+0.66	-0.78	+0.67	-0.20	+0.18	-1.34	+1.19	-0.25	+0.23	-0.71	+0.63	-4.95	+4.91	-0.00	+0.00
Flux PC02	-0.08	+0.01	-0.12	+0.10	-0.48	+0.31	-0.49	+0.32	-0.05	+0.02	-0.54	+0.29	-0.40	+0.42	-0.07	+0.09	-3.32	+3.33	-0.00	+0.00
Flux PC03	-0.33	+0.32	-0.23	+0.23	-0.55	+0.54	-0.57	+0.55	-0.20	+0.17	-1.16	+1.17	-0.90	+0.74	-1.20	+0.99	-7.00	+6.94	-0.00	+0.00
Flux PC04	-0.00	+0.00	-0.01	+0.01	-0.02	+0.01	-0.02	+0.01	-0.09	+0.09	-0.06	+0.05	-0.56	+0.56	-0.46	+0.47	-0.13	+0.13	-0.00	+0.00
Absolute calib.	-0.62	+0.00	-0.48	+0.09	-2.18	+0.00	-2.23	+0.00	-0.62	+3.02	-3.11	+0.00	-11.14	+6.11	-6.12	+1.30	-0.00	+0.00	-0.00	+0.00
ND/FD relative calib.	-1.16	+0.88	-0.24	+0.00	-3.71	+3.36	-3.79	+3.43	-1.67	+2.56	-6.04	+5.33	-4.73	+3.58	-3.29	+2.52	-0.00	+0.00	-0.00	+0.00
Calibration shape	-1.48	+1.48	-0.29	+0.29	-4.09	+4.09	-4.18	+4.18	-0.31	+0.31	-5.43	+5.43	-8.64	+8.64	-3.32	+3.32	-0.00	+0.00	-0.00	+0.00
Calibration drift	-0.45	+0.00	-0.00	+0.14	-1.75	+0.00	-1.79	+0.00	-0.18	+0.00	-1.96	+0.00	-6.27	+0.00	-0.15	+0.00	-0.00	+0.01	-0.00	+0.00
Light level FD	-0.01	+0.02	-0.56	+0.48	-1.10	+1.30	-1.12	+1.33	-0.48	+0.41	-1.68	+2.18	-1.12	+1.27	-10.48	+0.00	-0.00	+0.02	-0.00	+0.00
Light level ND	-2.85	+0.00	-0.74	+0.00	-7.50	+0.00	-7.67	+0.00	-0.82	+0.00	-10.16	+0.00	-9.39	+0.00	-7.78	+0.00	-0.00	+0.00	-0.00	+0.00
Cherenkov	-0.00	+0.62	-0.00	+0.04	-0.00	+1.92	-0.00	+1.96	-0.00	+0.10	-0.00	+2.61	-0.00	+3.71	-6.78	+0.00	-0.00	+0.03	-0.00	+0.00
E_μ ND uncorr.	-0.09	+0.10	-0.11	+0.13	-0.04	+0.04	-0.04	+0.04	-0.17	+0.18	-0.00	+0.00	-0.00	+0.00	-0.00	+0.00	-0.00	+0.00	-0.00	+0.00
E_μ μ-catcher uncorr.	-0.02	+0.02	-0.01	+0.01	-0.03	+0.03	-0.03	+0.03	-0.12	+0.12	-0.00	+0.00	-0.00	+0.00	-0.00	+0.00	-0.00	+0.00	-0.00	+0.00
E_μ n pile-up	-0.22	+0.00	-0.28	+0.00	-0.11	+0.00	-0.11	+0.00	-0.48	+0.00	-0.00	+0.00	-0.00	+0.00	-0.00	+0.00	-0.00	+0.00	-0.00	+0.00
E_μ correlated	-0.52	+0.55	-0.66	+0.69	-0.22	+0.24	-0.22	+0.24	-0.98	+1.05	-0.00	+0.00	-0.00	+0.00	-0.00	+0.00	-0.00	+0.00	-0.00	+0.00
Lepton angle xz ND	-0.21	+0.10	-0.27	+0.13	-0.08	+0.05	-0.09	+0.05	-0.37	+0.21	-0.00	+0.00	-0.00	+0.00	-0.00	+0.00	-0.00	+0.00	-0.00	+0.00
Lepton angle yz ND	-0.15	+0.04	-0.19	+0.06	-0.04	+0.00	-0.04	+0.00	-0.17	+0.00	-0.00	+0.00	-0.00	+0.00	-0.00	+0.00	-0.00	+0.00	-0.00	+0.00
Lepton angle xz FD	-0.00	+0.00	-0.00	+0.00	-0.00	+0.00	-0.00	+0.00	-0.00	+0.00	-0.00	+0.00	-0.00	+0.00	-0.00	+0.00	-0.00	+0.00	-0.00	+0.00
Lepton angle yz FD	-0.00	+0.00	-0.00	+0.00	-0.00	+0.00	-0.00	+0.00	-0.00	+0.00	-0.00	+0.00	-0.00	+0.00	-0.00	+0.00	-0.00	+0.00	-0.00	+0.00
Neutron systematic	-0.59	+0.87	-0.71	+1.03	-0.34	+0.52	-0.35	+0.53	-1.20	+1.54	-0.17	+0.32	-0.48	+0.57	-0.10	+0.12	-0.29	+0.09	-0.00	+0.00
Normalization beam corr.	-0.85	+0.85	-0.83	+0.83	-0.88	+0.88	-0.90	+0.90	-0.84	+0.84	-0.92	+0.92	-0.95	+0.95	-0.76	+0.76	-0.91	+0.91	-0.00	+0.00
Normalization $\bar{\nu}$-beam	-0.76	+0.76	-0.74	+0.74	-0.81	+0.81	-0.83	+0.83	-0.75	+0.75	-0.85	+0.85	-0.88	+0.88	-0.71	+0.71	-0.84	+0.84	-0.00	+0.00
Acceptance $\bar{\nu}_\mu/\bar{\nu}_e$ ND/FD	-0.33	+0.33	-0.45	+0.45	-0.06	+0.06	-0.06	+0.06	-0.28	+0.28	-0.00	+0.00	-0.00	+0.00	-0.00	+0.00	-0.00	+0.00	-0.00	+0.00
Rock scale	-0.10	+0.10	-0.01	+0.01	-0.28	+0.28	-0.28	+0.28	-0.02	+0.02	-0.05	+0.05	-1.31	+1.31	-16.79	+16.79	-0.00	+0.00	-0.00	+0.00
Cosmic scale	-0.25	+0.36	-0.00	+0.00	-0.81	+1.16	-0.00	+0.00	-0.00	+0.00	-0.00	+0.00	-0.00	+0.00	-0.00	+0.00	-0.00	+0.00	-36.56	+52.22
Quadrature	-4.62	+3.49	-3.83	+3.68	-10.28	+6.48	-10.48	+6.52	-4.17	+5.49	-14.14	+8.92	-25.74	+25.28	-26.20	+21.95	-68.21	+68.60	-36.56	+52.22

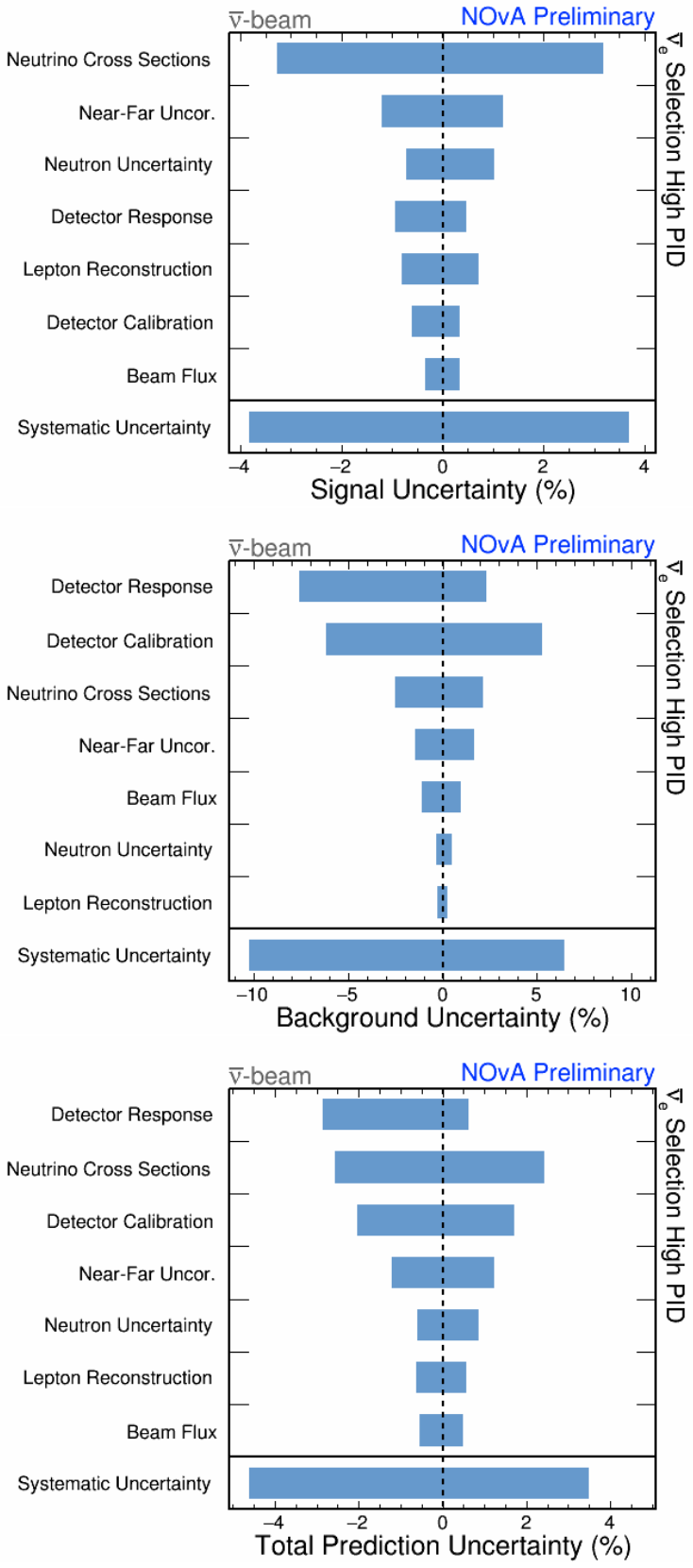

Figure C.27: Relative 1σ syst. uncertainties on the integral number of signal (top), background (middle), and total (bottom) predicted events in the $\bar{\nu}_e$ app. $\bar{\nu}$-beam high PID sample.

Peripheral sample

Table C.17: Relative 1σ systematic uncertainties on the integral numbers of predicted events for the $\bar{\nu}_e$ app. $\bar{\nu}$-beam peripheral sample.

Systematic summary for ν_e appearance $\bar{\nu}$-beam peripheral sample (%)

Systematic	Total pred		$\bar{\nu}_e$ Signal		Total bkg		Beam bkg		ν_e WS		Beam ν_e CC		NC		ν_μ CC		ν_τ CC		Cosmics	
CCQE z-exp.ax.vec. 1	-0.46	+0.50	-0.29	+0.31	-0.58	+0.64	-0.80	+0.87	-0.29	+0.31	-1.05	+1.15	-1.67	+1.60	-0.25	+0.24	-2.51	+2.74	-0.00	+0.00
CCQE z-exp.ax.vec. 2	-0.39	+0.42	-0.26	+0.28	-0.49	+0.53	-0.66	+0.72	-0.26	+0.28	-0.86	+0.93	-1.27	+1.22	-0.17	+0.17	-2.11	+2.28	-0.00	+0.00
CCQE z-exp.ax.vec. 3	-0.49	+0.59	-0.39	+0.46	-0.56	+0.69	-0.77	+0.94	-0.39	+0.46	-0.93	+1.13	-1.14	+1.06	-0.07	+0.11	-2.82	+3.38	-0.00	+0.00
CCQE z-exp.ax.vec. 4	-0.09	+0.10	-0.08	+0.08	-0.10	+0.11	-0.14	+0.15	-0.08	+0.08	-0.16	+0.17	-0.14	+0.14	-0.05	+0.05	-0.55	+0.59	-0.00	+0.00
M_A^{CCRES}	-1.85	+2.62	-0.24	+0.17	-3.41	+4.82	-4.66	+6.58	-0.24	+0.17	-6.29	+8.67	-4.18	+3.91	-1.27	+3.23	-7.18	+11.17	-0.00	+0.00
M_V^{CCRES}	-1.17	+1.71	-0.49	+0.34	-2.34	+3.40	-3.19	+4.63	-0.49	+0.34	-4.36	+6.27	-3.37	+2.61	-0.64	+1.32	-4.81	+7.49	-0.00	+0.00
M_A^{NCRES}	-0.02	+0.03	-0.05	+0.03	-0.00	+0.03	-0.00	+0.04	-0.05	+0.03	-0.58	+0.33	-4.86	+10.21	-0.66	+0.38	-0.00	+0.00	-0.00	+0.00
M_V^{NCRES}	-0.00	+0.00	-0.00	+0.00	-0.01	+0.01	-0.01	+0.02	-0.00	+0.00	-0.02	+0.00	-0.02	+0.64	-0.03	+0.00	-0.00	+0.00	-0.00	+0.00
CCQE z-exp.norm.	-1.32	+1.71	-0.92	+1.12	-1.62	+2.16	-2.21	+2.95	-0.92	+1.12	-2.90	+3.85	-5.31	+4.44	-0.72	+0.64	-6.99	+9.32	-0.00	+0.00
RPA high Q^2 enh.	-0.48	+0.60	-0.38	+0.46	-0.56	+0.70	-0.76	+0.96	-0.38	+0.47	-1.02	+1.28	-1.29	+1.12	-0.14	+0.21	-0.00	+0.00	-0.00	+0.00
RPA low Q^2 supp.	-0.09	+0.09	-0.00	+0.00	-0.16	+0.17	-0.22	+0.23	-0.00	+0.00	-0.38	+0.39	-0.96	+0.98	-0.26	+0.27	-0.00	+0.00	-0.00	+0.00
RES low Q^2 supp.	-0.10	+0.00	-0.00	+0.07	-0.23	+0.00	-0.32	+0.00	-0.00	+0.07	-0.54	+0.00	-0.00	+1.18	-0.00	+0.31	-0.02	+0.00	-0.00	+0.00
DIS CC $\nu n \to 1\pi$	-0.42	+0.42	-0.00	+0.00	-0.75	+0.75	-1.02	+1.02	-0.00	+0.00	-1.22	+1.22	-0.49	+0.49	-2.82	+2.81	-0.79	+0.79	-0.00	+0.00
FSI π free path	-0.51	+0.45	-0.67	+0.54	-0.40	+0.38	-0.54	+0.52	-0.67	+0.54	-0.47	+0.47	-2.20	+1.74	-0.05	+0.44	-0.00	+0.31	-0.00	+0.00
FSI fate fraction	-0.03	+0.13	-0.12	+0.12	-0.00	+0.13	-0.00	+0.18	-0.12	+0.12	-0.00	+0.26	-0.23	+0.08	-0.39	+0.50	-0.02	+0.11	-0.00	+0.00
MEC E_ν shape	-0.05	+0.00	-0.09	+0.03	-0.09	+0.00	-0.12	+0.00	-0.09	+0.03	-0.19	+0.00	-0.33	+0.45	-0.12	+0.10	-0.47	+0.06	-0.00	+0.00
MEC $E_{\bar{\nu}}$ shape	-0.15	+0.00	-0.25	+0.00	-0.20	+0.00	-0.27	+0.00	-0.25	+0.00	-0.49	+0.02	-1.01	+1.66	-0.41	+0.54	-0.59	+0.06	-0.00	+0.00
MEC ν (q_0, q) response	-0.30	+0.00	-0.00	+0.08	-0.60	+0.00	-0.82	+0.00	-0.00	+0.08	-1.23	+0.00	-0.00	+0.26	-0.16	+2.88	-4.75	+0.00	-0.00	+0.00
MEC $\bar{\nu}$ (q_0, q) response	-0.20	+0.26	-0.53	+0.00	-0.00	+0.86	-0.00	+1.18	-0.53	+0.00	-0.00	+1.73	-0.22	+1.18	-2.48	+0.25	-2.64	+0.00	-0.00	+0.00
MEC ν init. np frac.	-0.03	+0.01	-0.01	+0.00	-0.05	+0.02	-0.07	+0.02	-0.01	+0.00	-0.07	+0.02	-0.17	+0.06	-0.07	+0.20	-0.61	+0.20	-0.00	+0.00
MEC $\bar{\nu}$ init. np frac.	-0.03	+0.10	-0.03	+0.10	-0.03	+0.10	-0.05	+0.14	-0.03	+0.10	-0.06	+0.19	-0.05	+0.02	-0.00	+0.00	-0.65	+0.22	-0.00	+0.00
ν_e/ν_μ radiative corr.	-0.27	+0.27	-0.25	+0.25	-0.29	+0.29	-0.40	+0.40	-0.25	+0.25	-0.52	+0.52	-0.40	+0.41	-0.11	+0.11	-0.00	+0.00	-0.00	+0.00
$\bar{\nu}_e/\bar{\nu}_\mu$ radiative corr.bar	-1.17	+1.17	-1.77	+1.77	-0.72	+0.72	-0.98	+0.98	-1.77	+1.77	-1.07	+1.06	-1.12	+1.15	-0.38	+0.39	-0.00	+0.00	-0.00	+0.00
Second class currents	-0.90	+0.90	-1.52	+1.52	-0.42	+0.42	-0.58	+0.58	-1.52	+1.52	-0.54	+0.54	-0.72	+0.73	-0.27	+0.28	-0.00	+0.00	-0.00	+0.00
XSecs PC00	-0.19	+0.20	-0.09	+0.09	-0.28	+0.28	-0.38	+0.39	-0.09	+0.09	-0.40	+0.41	-1.04	+1.07	-0.44	+0.45	-0.00	+0.00	-0.00	+0.00
XSecs PC01	-0.13	+0.13	-0.05	+0.05	-0.19	+0.19	-0.26	+0.26	-0.05	+0.05	-0.28	+0.28	-0.68	+0.70	-0.30	+0.31	-0.00	+0.00	-0.00	+0.00
XSecs PC02	-0.37	+0.41	-0.67	+0.75	-0.13	+0.14	-0.18	+0.19	-0.67	+0.75	-0.08	+0.08	-0.42	+0.43	-0.08	+0.08	-0.00	+0.00	-0.00	+0.00
XSecs PC03	-0.17	+0.18	-0.21	+0.22	-0.14	+0.15	-0.20	+0.20	-0.21	+0.22	-0.18	+0.18	-0.48	+0.49	-0.19	+0.20	-0.00	+0.00	-0.00	+0.00
XSecs PC04	-0.47	+0.48	-0.91	+0.93	-0.14	+0.14	-0.18	+0.19	-0.91	+0.93	-0.04	+0.04	-0.33	+0.34	-0.04	+0.04	-0.00	+0.00	-0.00	+0.00
XSecs PC05	-0.05	+0.05	-0.05	+0.05	-0.05	+0.05	-0.07	+0.07	-0.05	+0.06	-0.07	+0.07	-0.17	+0.17	-0.08	+0.08	-0.00	+0.00	-0.00	+0.00
XSecs PC06	-0.18	+0.18	-0.33	+0.33	-0.07	+0.07	-0.09	+0.09	-0.33	+0.33	-0.05	+0.05	-0.14	+0.14	-0.05	+0.05	-0.00	+0.00	-0.00	+0.00
XSecs PC07	-0.38	+0.39	-0.76	+0.77	-0.09	+0.09	-0.13	+0.13	-0.76	+0.77	-0.00	+0.00	-0.14	+0.14	-0.00	+0.00	-0.00	+0.00	-0.00	+0.00
XSecs PC08	-0.08	+0.08	-0.00	+0.00	-0.13	+0.13	-0.18	+0.18	-0.00	+0.00	-0.20	+0.20	-0.50	+0.50	-0.22	+0.22	-0.00	+0.00	-0.00	+0.00
XSecs PC09	-0.34	+0.35	-0.54	+0.55	-0.19	+0.19	-0.25	+0.26	-0.54	+0.55	-0.19	+0.19	-0.56	+0.57	-0.20	+0.21	-0.00	+0.00	-0.00	+0.00
XSecs PC10	-0.30	+0.30	-0.51	+0.51	-0.13	+0.14	-0.18	+0.18	-0.51	+0.51	-0.12	+0.12	-0.36	+0.37	-0.13	+0.13	-0.00	+0.00	-0.00	+0.00
XSecs PC11	-0.38	+0.39	-0.73	+0.74	-0.12	+0.12	-0.16	+0.16	-0.73	+0.75	-0.05	+0.05	-0.22	+0.22	-0.05	+0.05	-0.00	+0.00	-0.00	+0.00
ν_τ scale	-0.68	+0.68	-0.00	+0.00	-1.21	+1.21	-1.65	+1.65	-0.00	+0.00	-0.00	+0.00	-0.00	+0.00	-0.02	+0.02	-66.40	+66.40	-0.00	+0.00
Flux PC00	-0.58	+0.57	-0.05	+0.04	-1.07	+1.05	-1.46	+1.43	-0.05	+0.04	-1.90	+1.86	-0.35	+0.37	-0.49	+0.49	-2.49	+2.50	-0.00	+0.00
Flux PC01	-0.88	+0.80	-0.18	+0.16	-1.68	+1.56	-2.30	+2.13	-0.18	+0.16	-2.89	+2.67	-0.21	+0.21	-1.43	+1.39	-4.66	+4.63	-0.00	+0.00
Flux PC02	-0.53	+0.39	-0.17	+0.16	-1.05	+0.81	-1.44	+1.11	-0.17	+0.16	-1.82	+1.38	-0.20	+0.25	-0.51	+0.52	-3.40	+3.42	-0.00	+0.00
Flux PC03	-0.96	+0.93	-0.23	+0.22	-1.86	+1.82	-2.54	+2.48	-0.23	+0.22	-3.09	+3.03	-0.85	+0.70	-2.00	+1.92	-6.90	+6.83	-0.00	+0.00
Flux PC04	-0.03	+0.03	-0.03	+0.03	-0.03	+0.03	-0.04	+0.04	-0.03	+0.03	-0.07	+0.07	-0.30	+0.30	-0.07	+0.07	-0.17	+0.17	-0.00	+0.00
Absolute calib.	-1.79	+1.38	-0.19	+0.00	-3.02	+2.46	-4.12	+3.35	-0.19	+0.00	-5.88	+5.17	-6.37	+4.20	-3.46	+0.78	-0.00	+0.00	-0.00	+0.00
ND/FD relative calib.	-1.42	+1.37	-0.64	+0.49	-2.89	+2.92	-3.94	+3.98	-0.65	+0.49	-5.10	+5.25	-3.64	+3.18	-1.87	+1.37	-0.00	+0.00	-0.00	+0.00
Calibration shape	-2.98	+2.98	-1.45	+1.45	-4.15	+4.15	-5.66	+5.66	-1.46	+1.46	-6.90	+6.90	-6.11	+6.11	-1.85	+1.85	-0.00	+0.00	-0.00	+0.00
Calibration drift	-0.22	+0.00	-1.49	+0.00	-0.00	+0.75	-0.00	+1.02	-1.49	+0.00	-0.00	+1.95	-0.02	+0.00	-4.27	+0.00	-0.03	+0.00	-0.00	+0.00
Light level FD	-0.53	+1.24	-1.32	+0.89	-0.00	+1.50	-0.00	+2.05	-1.32	+0.90	-0.00	+2.28	-0.00	+3.94	-0.02	+1.28	-0.03	+0.00	-0.00	+0.00
Light level ND	-1.27	+0.00	-0.81	+0.00	-1.63	+0.00	-2.22	+0.00	-0.81	+0.00	-2.23	+0.00	-7.71	+0.00	-2.27	+0.00	-0.00	+0.00	-0.00	+0.00
Cherenkov	-0.00	+0.43	-1.23	+0.00	-0.00	+1.70	-0.00	+2.32	-1.23	+0.00	-0.00	+3.29	-0.00	+5.40	-3.69	+0.00	-0.02	+0.00	-0.00	+0.00
E_μ ND uncorr.	-0.06	+0.07	-0.12	+0.15	-0.01	+0.02	-0.02	+0.02	-0.13	+0.15	-0.00	+0.00	-0.00	+0.00	-0.00	+0.00	-0.00	+0.00	-0.00	+0.00
E_μ μ-catcher uncorr.	-0.04	+0.03	-0.07	+0.06	-0.00	+0.00	-0.01	+0.00	-0.07	+0.06	-0.00	+0.00	-0.00	+0.00	-0.00	+0.00	-0.00	+0.00	-0.00	+0.00
E_μ n pile-up	-0.18	+0.00	-0.36	+0.00	-0.04	+0.00	-0.05	+0.00	-0.36	+0.00	-0.00	+0.00	-0.00	+0.00	-0.00	+0.00	-0.00	+0.00	-0.00	+0.00
E_μ correlated	-0.38	+0.41	-0.76	+0.83	-0.08	+0.09	-0.11	+0.12	-0.76	+0.83	-0.00	+0.00	-0.00	+0.00	-0.00	+0.00	-0.00	+0.00	-0.00	+0.00
Lepton angle xz ND	-0.16	+0.08	-0.31	+0.16	-0.03	+0.02	-0.05	+0.02	-0.31	+0.16	-0.00	+0.00	-0.00	+0.00	-0.00	+0.00	-0.00	+0.00	-0.00	+0.00
Lepton angle yz ND	-0.09	+0.02	-0.18	+0.04	-0.02	+0.00	-0.03	+0.00	-0.18	+0.04	-0.00	+0.00	-0.00	+0.00	-0.00	+0.00	-0.00	+0.00	-0.00	+0.00
Lepton angle xz FD	-0.00	+0.00	-0.00	+0.00	-0.00	+0.00	-0.00	+0.00	-0.00	+0.00	-0.00	+0.00	-0.00	+0.00	-0.00	+0.00	-0.00	+0.00	-0.00	+0.00
Lepton angle yz FD	-0.00	+0.00	-0.00	+0.00	-0.00	+0.00	-0.00	+0.00	-0.00	+0.00	-0.00	+0.00	-0.00	+0.00	-0.00	+0.00	-0.00	+0.00	-0.00	+0.00
Neutron systematic	-0.31	+0.43	-0.66	+0.88	-0.03	+0.08	-0.04	+0.12	-0.66	+0.88	-0.00	+0.05	-0.28	+0.40	-0.18	+0.09	-0.03	+0.03	-0.00	+0.00
Normalization beam corr.	-0.70	+0.70	-0.83	+0.83	-0.60	+0.60	-0.82	+0.82	-0.83	+0.83	-0.84	+0.84	-0.74	+0.74	-0.44	+0.44	-0.91	+0.91	-0.00	+0.00
Normalization $\bar{\nu}$-beam	-0.63	+0.63	-0.74	+0.74	-0.55	+0.55	-0.76	+0.76	-0.74	+0.74	-0.78	+0.78	-0.69	+0.69	-0.40	+0.40	-0.84	+0.84	-0.00	+0.00
Acceptance $\bar{\nu}_\mu/\bar{\nu}_e$ ND/FD	-0.14	+0.14	-0.29	+0.29	-0.03	+0.03	-0.04	+0.04	-0.29	+0.29	-0.00	+0.00	-0.00	+0.00	-0.00	+0.00	-0.00	+0.00	-0.00	+0.00
Rock scale	-2.80	+2.80	-1.68	+1.68	-3.65	+3.65	-4.98	+4.98	-1.54	+1.54	-1.57	+1.57	-21.69	+21.69	-58.64	+58.64	-0.00	+0.00	-0.00	+0.00
Cosmic scale	-1.35	+1.35	-0.00	+0.00	-2.40	+2.40	-0.00	+0.00	-0.00	+0.00	-0.00	+0.00	-0.00	+0.00	-0.00	+0.00	-0.00	+0.00	-8.98	+8.98
Quadrature	-6.40	+6.73	-5.02	+4.48	-9.51	+10.49	-12.55	+13.92	-4.98	+4.43	-14.79	+16.99	-26.89	+27.38	-59.32	+59.02	-68.35	+69.20	-8.98	+8.98

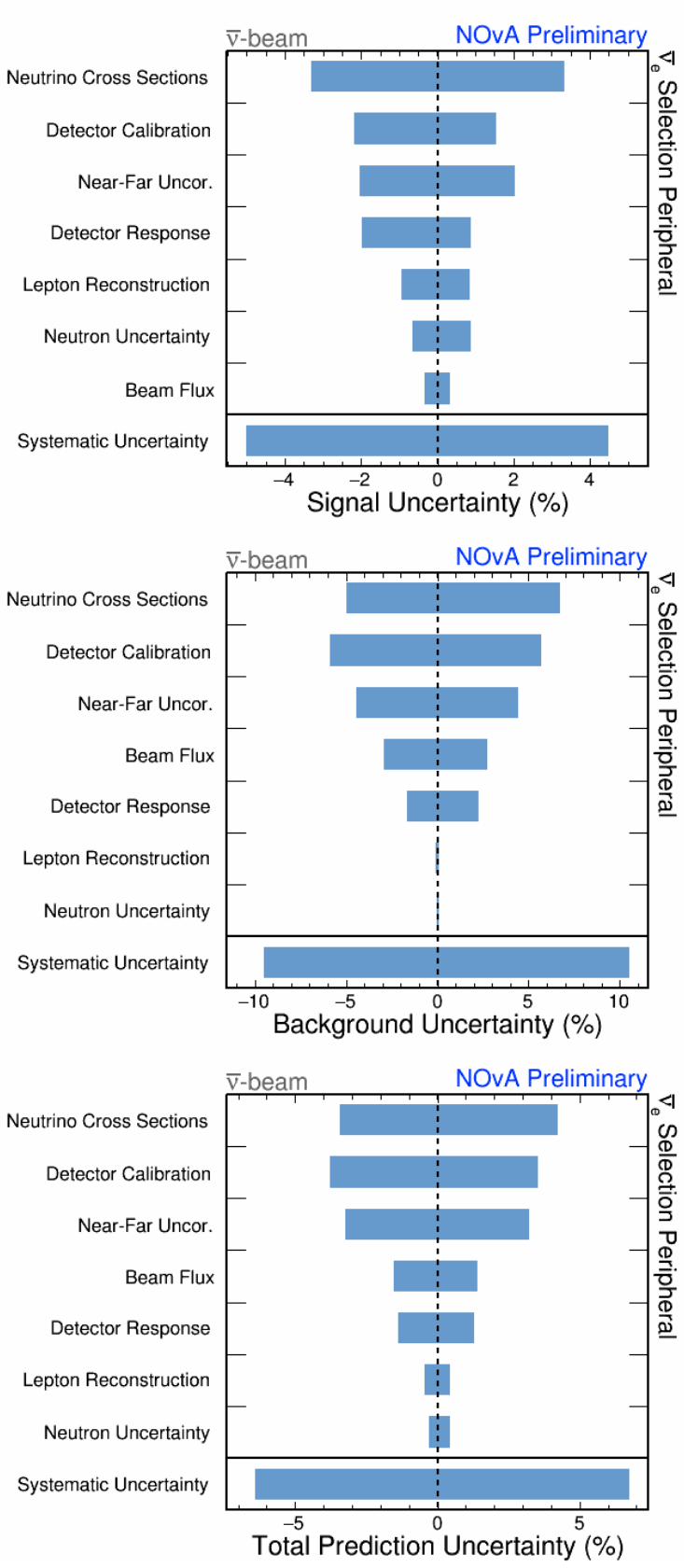

Figure C.28: Relative 1σ syst. uncertainties on the integral number of signal (top), background (middle), and total (bottom) predicted events in the $\bar{\nu}_e$ app. $\bar{\nu}$-beam peripheral bin.

All prediction

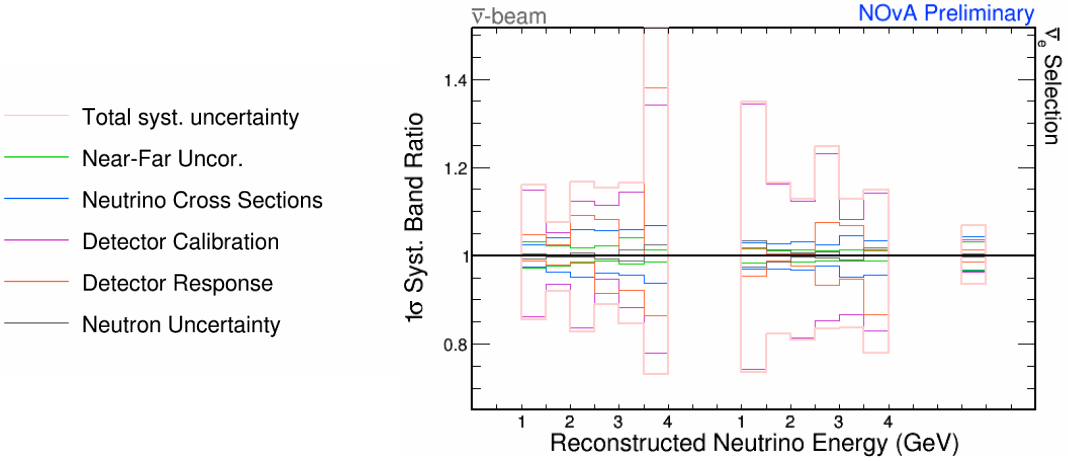

Figure C.29: 1σ systematic bands relative to the nominal prediction for the $\bar{\nu}$-beam $\bar{\nu}_e$ app. samples in the reconstructed neutrino energy. Bins correspond to low, high PID and peripheral sample from left to right, respectively.

Table C.18: Relative 1σ systematic uncertainties on the integral numbers of predicted events for the $\bar{\nu}_e$ app. $\bar{\nu}$-beam all samples.

Systematic summary for ν_e appearance $\bar{\nu}$-beam all samples (%)

Systematic	Total pred		$\bar{\nu}_e$ Signal		Total bkg		Beam bkg		ν_e WS		Beam ν_e CC		NC		ν_μ CC		ν_τ CC		Cosmics	
CCQE z-exp.ax.vec. 1	-0.13	+0.15	-0.14	+0.15	-0.13	+0.14	-0.14	+0.16	-0.10	+0.11	-0.33	+0.36	-0.74	+0.70	-0.47	+0.45	-2.56	+2.78	-0.00	+0.00
CCQE z-exp.ax.vec. 2	-0.13	+0.15	-0.14	+0.16	-0.12	+0.14	-0.14	+0.15	-0.11	+0.12	-0.28	+0.31	-0.56	+0.53	-0.35	+0.34	-2.16	+2.33	-0.00	+0.00
CCQE z-exp.ax.vec. 3	-0.26	+0.33	-0.28	+0.36	-0.22	+0.28	-0.25	+0.32	-0.28	+0.36	-0.35	+0.44	-0.52	+0.47	-0.21	+0.21	-3.04	+3.62	-0.00	+0.00
CCQE z-exp.ax.vec. 4	-0.06	+0.06	-0.06	+0.07	-0.05	+0.05	-0.06	+0.06	-0.07	+0.07	-0.07	+0.07	-0.07	+0.06	-0.01	+0.01	-0.61	+0.65	-0.00	+0.00
M_A^{CCRES}	-0.33	+0.68	-0.17	+0.29	-1.19	+1.84	-1.34	+2.07	-0.14	+0.52	-2.82	+3.88	-4.12	+2.74	-0.00	+6.86	-5.98	+9.10	-0.00	+0.00
M_V^{CCRES}	-0.17	+0.36	-0.30	+0.31	-0.83	+1.27	-0.94	+1.43	-0.00	+0.20	-2.09	+3.00	-3.21	+1.97	-0.00	+1.72	-4.13	+6.43	-0.00	+0.00
M_A^{NCRES}	-0.18	+0.28	-0.05	+0.02	-0.46	+0.72	-0.52	+0.81	-0.05	+0.03	-1.67	+0.96	-6.39	+10.62	-3.02	+1.66	-0.00	+0.00	-0.00	+0.00
M_V^{NCRES}	-0.00	+0.02	-0.00	+0.00	-0.00	+0.05	-0.00	+0.05	-0.00	+0.00	-0.06	+0.00	-0.00	+0.46	-0.13	+0.00	-0.00	+0.00	-0.00	+0.00
CCQE z-exp.norm.	-0.53	+0.67	-0.63	+0.76	-0.40	+0.55	-0.45	+0.62	-0.53	+0.64	-0.94	+1.24	-2.43	+1.98	-1.52	+1.25	-7.20	+9.60	-0.00	+0.00
RPA high Q^2 enh.	-0.25	+0.30	-0.32	+0.37	-0.16	+0.20	-0.18	+0.23	-0.30	+0.37	-0.37	+0.47	-0.61	+0.53	-0.26	+0.24	-0.00	+0.00	-0.00	+0.00
RPA low Q^2 supp.	-0.05	+0.05	-0.04	+0.04	-0.07	+0.08	-0.08	+0.09	-0.04	+0.04	-0.02	+0.02	-0.45	+0.46	-0.32	+0.33	-0.00	+0.00	-0.00	+0.00
RES low Q^2 supp.	-0.00	+0.00	-0.04	+0.00	-0.00	+0.05	-0.00	+0.05	-0.03	+0.00	-0.11	+0.00	-0.00	+0.64	-0.00	+0.46	-0.02	+0.00	-0.00	+0.00
DIS CC $\nu n \to 1\pi$	-0.08	+0.08	-0.01	+0.01	-0.21	+0.21	-0.23	+0.23	-0.08	+0.08	-0.37	+0.37	-0.59	+0.61	-3.48	+3.42	-0.47	+0.47	-0.00	+0.00
FSI π free path	-0.37	+0.29	-0.29	+0.26	-0.47	+0.34	-0.53	+0.38	-0.28	+0.26	-0.24	+0.08	-1.76	+1.45	-1.27	+1.08	-0.13	+0.34	-0.00	+0.00
FSI fate fraction	-0.04	+0.09	-0.07	+0.09	-0.00	+0.11	-0.00	+0.12	-0.05	+0.08	-0.00	+0.26	-0.22	+0.00	-0.35	+0.15	-0.05	+0.05	-0.00	+0.00
MEC E_ν shape	-0.04	+0.00	-0.02	+0.00	-0.07	+0.04	-0.07	+0.04	-0.08	+0.03	-0.16	+0.12	-0.18	+0.25	-0.11	+0.18	-0.55	+0.07	-0.00	+0.00
MEC $E_{\bar{\nu}}$ shape	-0.07	+0.00	-0.11	+0.00	-0.09	+0.00	-0.10	+0.00	-0.23	+0.16	-0.51	+0.23	-0.62	+0.95	-0.36	+0.65	-0.64	+0.08	-0.00	+0.00
MEC ν (q_0, q) response	-0.31	+0.00	-0.06	+0.00	-0.64	+0.00	-0.72	+0.00	-0.16	+0.02	-0.94	+0.00	-0.13	+0.13	-0.12	+1.10	-4.43	+0.00	-0.00	+0.00
MEC $\bar{\nu}$ (q_0, q) response	-0.56	+0.00	-0.84	+0.00	-0.65	+0.00	-0.73	+0.00	-0.89	+0.10	-1.15	+0.20	-0.74	+0.16	-0.94	+0.00	-3.13	+0.56	-0.00	+0.00
MEC ν init. np frac.	-0.00	+0.02	-0.00	+0.00	-0.02	+0.05	-0.02	+0.06	-0.00	+0.00	-0.03	+0.11	-0.06	+0.02	-0.00	+0.02	-0.08	+0.25	-0.00	+0.00
MEC $\bar{\nu}$ init. np frac.	-0.00	+0.02	-0.03	+0.10	-0.09	+0.03	-0.10	+0.03	-0.06	+0.18	-0.10	+0.03	-0.22	+0.08	-0.36	+0.12	-0.88	+0.29	-0.00	+0.00
ν_e/ν_μ radiative corr.	-0.16	+0.16	-0.20	+0.20	-0.10	+0.10	-0.11	+0.11	-0.32	+0.32	-0.17	+0.17	-0.24	+0.24	-0.21	+0.21	-0.00	+0.00	-0.00	+0.00
$\bar{\nu}_e/\bar{\nu}_\mu$ radiative corr.	-1.24	+1.24	-1.82	+1.82	-0.45	+0.45	-0.51	+0.51	-1.71	+1.71	-0.55	+0.55	-0.62	+0.64	-0.52	+0.53	-0.00	+0.00	-0.00	+0.00
Second class currents	-1.09	+1.09	-1.62	+1.62	-0.35	+0.35	-0.40	+0.40	-1.39	+1.39	-0.38	+0.38	-0.38	+0.39	-0.31	+0.32	-0.00	+0.00	-0.00	+0.00
XSecs PC00	-0.19	+0.20	-0.06	+0.06	-0.35	+0.38	-0.40	+0.43	-0.06	+0.06	-1.30	+1.39	-2.44	+2.31	-1.30	+1.48	-0.00	+0.00	-0.00	+0.00
XSecs PC01	-0.09	+0.10	-0.04	+0.04	-0.16	+0.16	-0.18	+0.19	-0.03	+0.03	-0.75	+0.78	-1.73	+1.67	-1.11	+1.18	-0.00	+0.00	-0.00	+0.00
XSecs PC02	-0.05	+0.06	-0.05	+0.06	-0.05	+0.05	-0.05	+0.06	-0.23	+0.27	-0.00	+0.00	-0.27	+0.27	-1.40	+1.37	-0.00	+0.00	-0.00	+0.00
XSecs PC03	-0.14	+0.14	-0.02	+0.02	-0.30	+0.31	-0.34	+0.35	-0.08	+0.08	-0.33	+0.34	-1.09	+1.12	-2.30	+2.26	-0.00	+0.00	-0.00	+0.00
XSecs PC04	-0.24	+0.25	-0.44	+0.45	-0.03	+0.03	-0.03	+0.04	-0.53	+0.54	-0.14	+0.14	-0.24	+0.24	-0.16	+0.16	-0.00	+0.00	-0.00	+0.00
XSecs PC05	-0.06	+0.06	-0.05	+0.05	-0.07	+0.08	-0.08	+0.08	-0.05	+0.05	-0.19	+0.19	-0.08	+0.09	-1.81	+1.79	-0.00	+0.00	-0.00	+0.00
XSecs PC06	-0.12	+0.12	-0.22	+0.22	-0.02	+0.02	-0.03	+0.03	-0.23	+0.23	-0.03	+0.03	-0.46	+0.45	-0.06	+0.06	-0.00	+0.00	-0.00	+0.00
XSecs PC07	-0.28	+0.28	-0.44	+0.45	-0.05	+0.05	-0.06	+0.06	-0.46	+0.47	-0.32	+0.32	-0.96	+0.95	-0.31	+0.33	-0.00	+0.00	-0.00	+0.00
XSecs PC08	-0.08	+0.08	-0.00	+0.00	-0.17	+0.18	-0.19	+0.20	-0.02	+0.02	-0.61	+0.64	-1.02	+1.00	-0.24	+0.26	-0.00	+0.00	-0.00	+0.00
XSecs PC09	-0.27	+0.28	-0.29	+0.30	-0.24	+0.25	-0.27	+0.28	-0.30	+0.31	-0.34	+0.35	-0.07	+0.08	-0.26	+0.27	-0.00	+0.00	-0.00	+0.00
XSecs PC10	-0.22	+0.22	-0.28	+0.28	-0.13	+0.14	-0.15	+0.15	-0.30	+0.31	-0.12	+0.12	-0.18	+0.19	-0.34	+0.34	-0.00	+0.00	-0.00	+0.00
XSecs PC11	-0.28	+0.28	-0.40	+0.41	-0.11	+0.11	-0.12	+0.12	-0.42	+0.43	-0.20	+0.20	-0.96	+0.96	-0.28	+0.28	-0.00	+0.00	-0.00	+0.00
ν_τ scale	-0.64	+0.64	-0.00	+0.00	-1.51	+1.51	-1.70	+1.70	-0.00	+0.00	-0.00	+0.00	-0.00	+0.00	-0.06	+0.06	-66.27	+66.27	-0.00	+0.00
Flux PC00	-0.00	+0.00	-0.08	+0.08	-0.13	+0.12	-0.15	+0.13	-0.05	+0.05	-0.23	+0.19	-0.24	+0.25	-0.07	+0.07	-2.58	+2.58	-0.00	+0.00
Flux PC01	-0.13	+0.09	-0.21	+0.21	-0.06	+0.00	-0.07	+0.00	-0.19	+0.18	-0.24	+0.08	-0.03	+0.02	-0.78	+0.72	-4.92	+4.88	-0.00	+0.00
Flux PC02	-0.20	+0.12	-0.09	+0.07	-0.58	+0.41	-0.65	+0.46	-0.08	+0.04	-0.89	+0.58	-0.14	+0.15	-0.07	+0.07	-3.28	+3.29	-0.00	+0.00
Flux PC03	-0.07	+0.05	-0.21	+0.20	-0.15	+0.13	-0.17	+0.15	-0.17	+0.14	-0.06	+0.06	-0.13	+0.06	-1.02	+0.90	-7.01	+6.94	-0.00	+0.00
Flux PC04	-0.02	+0.02	-0.00	+0.00	-0.05	+0.04	-0.05	+0.05	-0.10	+0.10	-0.12	+0.11	-0.18	+0.18	-0.19	+0.19	-0.09	+0.08	-0.00	+0.00
Absolute calib.	-0.83	+0.00	-0.39	+0.16	-1.43	+0.00	-1.61	+0.00	-0.04	+2.07	-3.78	+0.53	-3.66	+1.41	-1.82	+0.00	-0.01	+0.00	-0.00	+0.00
ND/FD relative calib.	-1.07	+0.88	-0.20	+0.01	-2.56	+2.36	-2.88	+2.65	-1.07	+1.80	-4.96	+4.53	-1.38	+0.82	-1.93	+1.45	-0.00	+0.00	-0.00	+0.00
Calibration shape	-1.54	+1.54	-0.49	+0.49	-2.98	+2.98	-3.35	+3.35	-0.15	+0.15	-4.76	+4.76	-2.68	+2.68	-1.82	+1.82	-0.01	+0.01	-0.00	+0.00
Calibration drift	-0.00	+0.20	-0.02	+0.00	-0.00	+0.51	-0.00	+0.57	-0.28	+0.00	-0.00	+0.55	-0.00	+1.87	-1.14	+0.00	-0.03	+0.00	-0.00	+0.00
Light level FD	-0.00	+0.05	-0.43	+0.37	-0.39	+0.63	-0.44	+0.70	-0.14	+0.30	-0.76	+1.30	-0.03	+0.21	-2.34	+0.00	-0.03	+0.00	-0.00	+0.00
Light level ND	-1.70	+0.17	-0.74	+0.00	-3.02	+0.69	-3.39	+0.77	-0.80	+0.00	-5.73	+0.00	-0.00	+5.78	-0.00	+3.52	-0.00	+0.00	-0.00	+0.00
Cherenkov	-0.00	+0.48	-0.18	+0.00	-0.00	+1.39	-0.00	+1.56	-0.14	+0.00	-0.00	+2.42	-0.00	+1.67	-4.69	+0.00	-0.02	+0.00	-0.00	+0.00
E_μ ND uncorr.	-0.07	+0.08	-0.11	+0.13	-0.02	+0.03	-0.03	+0.03	-0.14	+0.16	-0.00	+0.00	-0.00	+0.00	-0.00	+0.00	-0.00	+0.00	-0.00	+0.00
E_μ μ-catcher uncorr.	-0.02	+0.02	-0.02	+0.02	-0.02	+0.02	-0.02	+0.02	-0.11	+0.11	-0.00	+0.00	-0.00	+0.00	-0.00	+0.00	-0.00	+0.00	-0.00	+0.00
E_μ n pile-up	-0.19	+0.00	-0.27	+0.00	-0.07	+0.00	-0.08	+0.00	-0.42	+0.00	-0.00	+0.00	-0.00	+0.00	-0.00	+0.00	-0.00	+0.00	-0.00	+0.00
E_μ correlated	-0.43	+0.46	-0.64	+0.68	-0.14	+0.15	-0.16	+0.17	-0.86	+0.93	-0.00	+0.00	-0.00	+0.00	-0.00	+0.00	-0.00	+0.00	-0.00	+0.00
Lepton angle xz ND	-0.18	+0.09	-0.27	+0.13	-0.06	+0.03	-0.07	+0.04	-0.36	+0.20	-0.00	+0.00	-0.00	+0.00	-0.00	+0.00	-0.00	+0.00	-0.00	+0.00
Lepton angle yz ND	-0.12	+0.03	-0.19	+0.05	-0.03	+0.00	-0.03	+0.00	-0.17	+0.00	-0.00	+0.00	-0.00	+0.00	-0.00	+0.00	-0.00	+0.00	-0.00	+0.00
Lepton angle xz FD	-0.00	+0.00	-0.00	+0.00	-0.00	+0.00	-0.00	+0.00	-0.00	+0.00	-0.00	+0.00	-0.00	+0.00	-0.00	+0.00	-0.00	+0.00	-0.00	+0.00
Lepton angle yz FD	-0.00	+0.00	-0.00	+0.00	-0.00	+0.00	-0.00	+0.00	-0.00	+0.00	-0.00	+0.00	-0.00	+0.00	-0.00	+0.00	-0.00	+0.00	-0.00	+0.00
Neutron systematic	-0.44	+0.66	-0.60	+0.89	-0.22	+0.33	-0.25	+0.37	-0.98	+1.24	-0.14	+0.28	-0.13	+0.09	-0.06	+0.11	-0.14	+0.09	-0.00	+0.00
Normalization beam corr.	-0.79	+0.79	-0.83	+0.83	-0.73	+0.73	-0.83	+0.83	-0.83	+0.83	-0.86	+0.86	-0.72	+0.72	-0.58	+0.58	-0.91	+0.91	-0.00	+0.00
Normalization $\bar{\nu}$-beam	-0.71	+0.71	-0.74	+0.74	-0.68	+0.68	-0.76	+0.76	-0.74	+0.74	-0.80	+0.80	-0.67	+0.67	-0.54	+0.54	-0.84	+0.84	-0.00	+0.00
Acceptance $\bar{\nu}_\mu/\bar{\nu}_e$ ND/FD	-0.26	+0.26	-0.42	+0.42	-0.04	+0.04	-0.05	+0.05	-0.27	+0.27	-0.00	+0.00	-0.00	+0.00	-0.00	+0.00	-0.00	+0.00	-0.00	+0.00
Rock scale	-0.70	+0.70	-0.27	+0.27	-1.29	+1.29	-1.45	+1.45	-0.30	+0.30	-0.51	+0.51	-1.88	+1.88	-26.92	+26.92	-0.00	+0.00	-0.00	+0.00
Cosmic scale	-0.73	+0.88	-0.00	+0.00	-1.73	+2.09	-0.00	+0.00	-0.00	+0.00	-0.00	+0.00	-0.00	+0.00	-0.00	+0.00	-0.00	+0.00	-15.62	+18.84
Quadrature	-3.82	+3.41	-3.47	+3.35	-6.29	+5.83	-6.80	+6.13	-3.59	+4.33	-10.97	+9.21	-11.02	+14.18	-28.42	+28.79	-68.12	+68.75	-15.62	+18.84

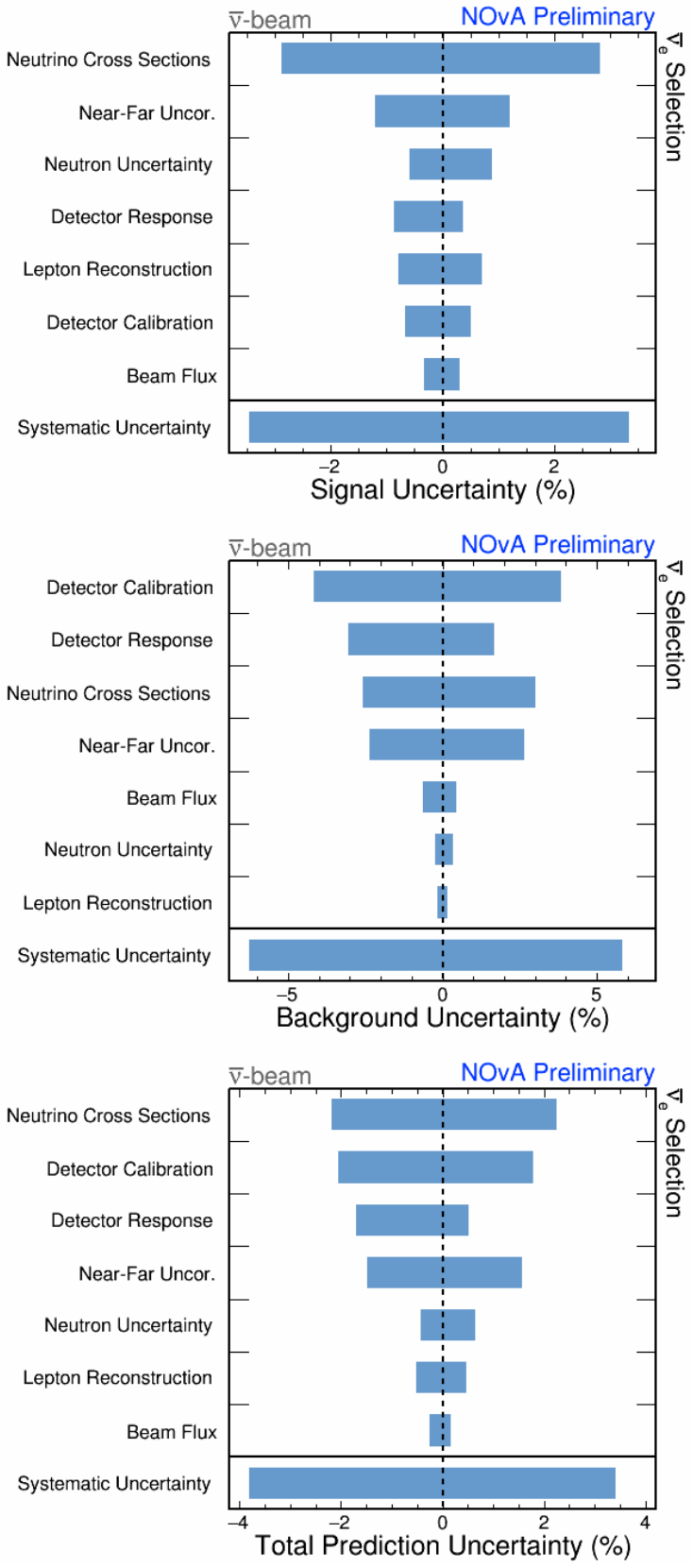

Figure C.30: Relative 1σ syst. uncertainties on the integral number of signal (top), background (middle), and total (bottom) predicted events in the $\bar{\nu}_e$ app. $\bar{\nu}$-beam all samples.

References

[1] M. A. Acero *et al.* [NOvA], Phys. Rev. D **98**, 032012 (2018), arXiv:1806.00096 [hep-ex]

[2] M. A. Acero *et al.* [NOvA], Phys. Rev. Lett. **123**, 151803 (2019), arXiv:1906.04907 [hep-ex]

[3] C. Giunti and C. W. Kim, *Fundamentals of Neutrino Physics and Astrophysics*, Oxford University Press (2007)

[4] S. Bilenky, *Introduction to the Physics of Massive and Mixed Neutrinos*, Lecture Notes in Physics, 2nd ed., Springer International Publishing (2018), ISBN 9783319748016

[5] K. Zuber, *Neutrino Physics*, 3rd ed., CRC Press (2020), ISBN 9781315195612, 10.1201/9781315195612

[6] J. W. F. Valle and J. Romao, *Neutrinos in High Energy and Astroparticle Physics*, Physics textbook, Wiley (2015), ISBN 9783527411979

[7] P. Zyla *et al.* [Particle Data Group], Prog. Theor. Exp. Phys. **2020**, 083C01 (2020), 10.1093/ptep/ptaa104

[8] C. Giunti and M. Laveder, 2003, arXiv:hep-ph/0310238

[9] B. Kayser, 2012, arXiv:1206.4325 [hep-ph]

[10] B. Kayser, 2008, arXiv:0804.1121 [hep-ph]

[11] R. N. Mohapatra *et al.*, Rept. Prog. Phys. **70**, 1757 (2007), arXiv:hep-ph/0510213

[12] M. C. Gonzalez-Garcia, AIP Conf. Proc. **917**, 3 (2007), 10.1063/1.2751934

[13] M. Blennow and A. Y. Smirnov, Adv. High Energy Phys. **2013**, 972485 (2013), arXiv:1306.2903 [hep-ph]

[14] C. Burgess and G. Moore, *The Standard Model: A Primer*, Cambridge books online, Cambridge University Press (2007), ISBN 9780521860369

[15] T. Frankel, *The Geometry of Physics: An Introduction*, Cambridge University Press (2011), ISBN 9781139505611

[16] A. Salam and J. C. Ward, Nuovo Cim. **11**, 568 (1959), 10.1007/BF02726525

[17] S. Weinberg, Phys. Rev. Lett. **19**, 1264 (1967), 10.1103/PhysRevLett.19.1264

[18] J. Hořejší, *Fundamentals of Electroweak Theory*, Karolinum Press (2002), ISBN 9788024606392

[19] F. Englert and R. Brout, Phys. Rev. Lett. **13**, 321 (1964), 10.1103/PhysRevLett.13.321

[20] P. Higgs, Phys. Rev. Lett. **13**, 508 (1964), 10.1103/PhysRevLett.13.508

[21] W. Greiner, D. A. Bromley, S. Schramm, and E. Stein, *Quantum Chromodynamics*, Springer Berlin Heidelberg (2013), ISBN 9783662047071

[22] T. Takagi, Japanese J. Math. **1**, 83 (1924), 10.4099/jjm1924.1.0_83

[23] S. Schael *et al.* [ALEPH, DELPHI, L3, OPAL, SLD, LEP], Phys. Rept. **427**, 257 (2006), arXiv:hep-ex/0509008

[24] E. K. Akhmedov and J. Kopp, JHEP **04**, 008 (2010), arXiv:1001.4815 [hep-ph], [Erratum: JHEP **10**, 052 (2013)]

[25] L. Wolfenstein, AIP Conf. Proc. **52**, 108 (1979), 10.1063/1.31797

[26] E. K. Akhmedov, JHEP **02**, 107 (2021), arXiv:2010.07847 [hep-ph]

[27] S. P. Mikheyev and A. Y. Smirnov, Yadernaya Fizika **42**, 1441 (1985)

[28] M. Freund, Phys. Rev. D **64**, 053003 (2001), arXiv:hep-ph/0103300

[29] E. K. Akhmedov, R. Johansson, M. Lindner, T. Ohlsson, and T. Schwetz, JHEP **2004**, 078–078 (2004), 10.1088/1126-6708/2004/04/078

[30] J. N. Bahcall, W. F. Huebner, S. H. Lubow, P. D. Parker, and R. K. Ulrich, Rev. Mod. Phys. **54**, 767 (1982), 10.1103/RevModPhys.54.767

[31] B. T. Cleveland *et al.* [Homestake], Astrophys. J. **496**, 505 (1998), 10.1086/305343

[32] W. Hampel *et al.* [GALLEX], Phys. Lett. B **447**, 127 (1999), 10.1016/S0370-2693(98)01579-2

[33] M. Altmann *et al.* [GNO], Phys. Lett. B **616**, 174–190 (2005), 10.1016/j.physletb.2005.04.068

[34] Y. Fukuda *et al.* [Kamiokande], Phys. Rev. Lett. **77**, 1683 (1996), 10.1103/PhysRevLett.77.1683

[35] B. Aharmim *et al.* [SNO], Phys. Rev. C **88** (2013), 10.1103/physrevc.88.025501

[36] S. Abe *et al.* [KamLAND], Phys. Rev. C **84** (2011), 10.1103/physrevc.84.035804

[37] K. Abe *et al.* [Super-Kamiokande], Phys. Rev. D **94**, 052010 (2016), 10.1103/PhysRevD.94.052010

[38] M. Agostini *et al.* [Borexino], Phys. Rev. D **101** (2020), 10.1103/physrevd.101.062001

[39] J. N. Abdurashitov *et al.* [SAGE], Phys. Rev. C **80** (2009), 10.1103/physrevc.80.015807

[40] K. S. Hirata *et al.*, Phys. Lett. B **205**, 416 (1988), 10.1016/0370-2693(88)91690-5

[41] M. Ambrosio *et al.* [MACRO], Phys. Lett. B **517**, 59 (2001), 10.1016/S0370-2693(01)00992-3

[42] M. Sanchez *et al.* [Soudan2], Phys. Rev. D **68**, 113004 (2003), 10.1103/PhysRevD.68.113004

[43] A. Albert *et al.* [ANTARES], JHEP **06**, 113 (2019), arXiv:1812.08650 [hep-ex]

[44] M. G. Aartsen *et al.* [IceCube], Phys. Rev. Lett. **120**, 071801 (2018), arXiv:1707.07081 [hep-ex]

[45] K. Abe *et al.* [Super-Kamiokande], Phys. Rev. D **97**, 072001 (2018), 10.1103/PhysRevD.97.072001

[46] S. Adrián-Martínez *et al.* [KM3NeT], J. Phys. G: Nucl. and Part. Phys. **43**, 084001 (2016), 10.1088/0954-3899/43/8/084001

[47] A. V. Avrorin *et al.* [Baikal-GVD], Phys. Atom. Nucl. **83**, 916 (2020), 10.1134/S1063778820060046

[48] M. G. Aartsen *et al.* [IceCube], J. Phys. G: Nucl. and Part. Phys. **44**, 054006 (2017), arXiv:1607.02671 [hep-ex]

[49] S. Ahmed *et al.* [ICAL], Pramana **88**, 79 (2017), arXiv:1505.07380 [physics.ins-det]

[50] B. Abi *et al.* [DUNE], 2018, arXiv:1807.10334 [physics.ins-det]

[51] Y. Kudenko [Hyper-Kamiokande Proto], JINST **15**, C07029 (2020), arXiv:2005.13641 [physics.ins-det]

[52] A. Aguilar *et al.* [LSND], Phys. Rev. D **64**, 112007 (2001), 10.1103/PhysRevD.64.112007

[53] A. A. Aguilar-Arevalo *et al.* [MiniBooNE], Phys. Rev. Lett. **121**, 221801 (2018), 10.1103/PhysRevLett.121.221801

[54] M. H. Ahn *et al.* [K2K], Phys. Rev. D **74**, 072003 (2006), 10.1103/PhysRevD.74.072003

[55] P. Adamson *et al.* [MINOS+], Phys. Rev. Lett. **125**, 131802 (2020), arXiv:2006.15208 [hep-ex]

[56] N. Agafonova *et al.* [OPERA], Phys. Rev. Lett. **120** (2018), 10.1103/physrevlett.120.211801

[57] M. Antonello *et al.* [ICARUS], Eur. Phys. J. C **73**, 2599 (2013), arXiv:1307.4699 [hep-ex]

[58] K. Abe *et al.* [T2K], Nature **580**, 339 (2020), arXiv:1910.03887 [hep-ex], [Erratum: Nature **583**, E16 (2020)]

[59] P. Dunne, Latest Neutrino Oscillation Results from T2K, 2020, 10.5281/zenodo.4154355

[60] A. Himmel, New Oscillation Results from the NOvA Experiment, 2020, 10.5281/zenodo.4142045

[61] B. Armbruster *et al.* [KARMEN], Phys. Rev. D **65**, 112001 (2002), 10.1103/PhysRevD.65.112001

[62] R. Acciarri *et al.* [SBN], 2015, arXiv:1503.01520 [physics.ins-det]

[63] S. Ajimura *et al.* [JSNS^2], 2017, arXiv:1705.08629 [physics.ins-det]

[64] T. Araki *et al.* [KamLAND], Phys. Rev. Lett. **94**, 081801 (2005), 10.1103/PhysRevLett.94.081801

[65] F. An *et al.* [JUNO], J. Phys. G: Nucl. and Part. Phys. **43**, 030401 (2016), 10.1088/0954-3899/43/3/030401

[66] D. Adey *et al.* [Daya Bay], Phys. Rev. Lett. **121**, 241805 (2018), 10.1103/PhysRevLett.121.241805

[67] G. Bak *et al.* [RENO], Phys. Rev. Lett. **121**, 201801 (2018), 10.1103/PhysRevLett.121.201801

[68] H. de Kerret *et al.* [Double Chooz], Nature Phys. **16**, 558 (2020), arXiv:1901.09445 [hep-ex]

[69] G. Mention *et al.*, Phys. Rev. D **83**, 073006 (2011), 10.1103/PhysRevD.83.073006

[70] C. Giunti and M. Laveder, Phys. Rev. C **83**, 065504 (2011), 10.1103/PhysRevC.83.065504

[71] Y. J. Ko *et al.* [NEOS], Phys. Rev. Lett. **118** (2017), 10.1103/physrevlett.118.121802

[72] I. Alekseev *et al.* [DANSS], Phys. Lett. B **787**, 56–63 (2018), 10.1016/j.physletb.2018.10.038

[73] H. Almazán *et al.* [STEREO], Phys. Rev. Lett. **121** (2018), 10.1103/physrevlett.121.161801

[74] J. Ashenfelter *et al.* [PROSPECT], Phys. Rev. Lett. **121** (2018), 10.1103/physrevlett.121.251802

[75] A. Serebrov *et al.* [Neutrino-4], JETP Lett. **109**, 213–221 (2019), 10.1134/s0021364019040040

[76] Y. Abreu *et al.* [Solid], JINST **12**, P04024–P04024 (2017), 10.1088/1748-0221/12/04/p04024

[77] I. Esteban, M. C. Gonzalez-Garcia, M. Maltoni, T. Schwetz, and A. Zhou, JHEP **09**, 178 (2020), arXiv:2007.14792 [hep-ph]

[78] [FNAL], 2002, https://www-numi.fnal.gov/numwork/tdh/tdh_index.html

[79] G. J. Feldman, J. Hartnell, and T. Kobayashi, Adv. High Energy Phys. **2013**, 475749 (2013), arXiv:1210.1778 [hep-ex]

[80] D. S. Ayres *et al.*, 2007, 10.2172/935497

[81] P. Adamson *et al.* [NOvA], Phys. Rev. D **93**, 051104 (2016), arXiv:1601.05037 [hep-ex]

[82] P. Adamson *et al.* [NOvA], Phys. Rev. Lett. **116**, 151806 (2016), arXiv:1601.05022 [hep-ex]

[83] P. Adamson *et al.* [NOvA], Phys. Rev. D **96**, 072006 (2017), arXiv:1706.04592 [hep-ex]

[84] S. P. Kasetti *et al.* [NOvA], J. Phys. Conf. Ser. **888**, 012144 (2017), 10.1088/1742-6596/888/1/012144

[85] M. A. Acero *et al.* [NOvA], Phys. Rev. D **102**, 012004 (2020), arXiv:1902.00558 [hep-ex]

[86] B. Behera [NOvA], Springer Proc. Phys. **234**, 329 (2019), 10.1007/978-3-030-29622-3_44

[87] M. A. Acero *et al.* [NOvA], Phys. Rev. D **99**, 122004 (2019), arXiv:1904.12975 [physics.ins-det]

[88] M. A. Acero *et al.* [NOvA], Phys. Rev. D **101**, 112006 (2020), arXiv:2001.07240 [hep-ex]

[89] F. Jediny, A. Hatzikoutelis, S. Kotelnikov, and B. Wang, PoS **FPCP2017**, 056 (2017), 10.22323/1.304.0056

[90] M. A. Acero *et al.* [NOvA], JCAP **10**, 014 (2020), arXiv:2005.07155 [physics.ins-det]

[91] M. A. Acero *et al.* [NOvA], Phys. Rev. D **103**, 012007 (2021), arXiv:2009.04867 [hep-ex]

[92] A. Back, 2020, NOVA-doc-46337-v3

[93] L. Aliaga and P. Snopok, 2019, NOVA-doc-41931-v1

[94] A. Himmel, 2017, NOVA-doc-20855-v2

[95] R. M. Zwaska, *Accelerator Systems and Instrumentation for the NuMI Neutrino Beam*, PhD thesis, Texas U., 2005, 10.2172/879065

[96] L. Aliaga *et al.* [MINERvA], Phys. Rev. D **94**, 092005 (2016), 10.1103/PhysRevD.94.092005

[97] L. Aliaga, 2017, NOVA-doc-20843-v12

[98] B. Baugh *et al.*, Nucl. Instrum. Meth. A **799**, 1 (2015), 10.1016/j.nima.2015.07.026

[99] A. Norman, E. Niner, and A. Habig, J. Phys. Conf. Ser. **664**, 082040 (2015), 10.1088/1742-6596/664/8/082040

[100] C. G. L. Bassin, G. Laske, and G. Masters, EOS Trans. AGU **81**, F897 (2000), https://igppweb.ucsd.edu/∼gabi/rem.html

[101] M. Baird, L. Suter, and J. Wolcott, 2020, NOVA-doc-44422-v3

[102] A. Back, R. S. Bowles, M. Elkins, B. Ramson, and S. Sanchez, 2020, NOVA-doc-44226-v1

[103] C. Andreopoulos *et al.* [GENIE], Nucl. Instrum. Meth. A **614**, 87 (2010), arXiv:0905.2517 [hep-ph]

[104] C. Andreopoulos *et al.* [GENIE], 2015, arXiv:1510.05494 [hep-ph]

[105] C. Hagmann, D. Lange, and D. Wright, Cosmic-ray shower generator (CRY) for Monte Carlo transport codes, in *2007 IEEE Nuclear Science Symposium Conference Record*, Vol. 2, pp. 1143–1146, 2007, 10.1109/NSSMIC.2007.4437209

[106] S. Agostinelli *et al.* [Geant4], Nucl. Instrum. Meth. A **506**, 250 (2003), 10.1016/S0168-9002(03)01368-8

[107] J. Allison *et al.* [Geant4], IEEE Trans. Nucl. Sci. **53**, 270 (2006), 10.1109/TNS.2006.869826

[108] J. Allison *et al.* [Geant4], Nucl. Instrum. Meth. A **835**, 186 (2016), 10.1016/j.nima.2016.06.125

[109] A. Aurisano *et al.* [NOvA], J. Phys. Conf. Ser. **664**, 072002 (2015), 10.1088/1742-6596/664/7/072002

[110] [FNAL], 2020, https://cdcvs.fnal.gov/redmine/projects/numi-beam-sim/wiki/G4numi

[111] L. Aliaga, *Neutrino Flux Prediction for the NuMI Beamline*, PhD thesis, William-Mary Coll., 2016, 10.2172/1250884

[112] A. Booth, 2020, NOVA-doc-42861-v2

[113] J. A. Formaggio and G. P. Zeller, Rev. Mod. Phys. **84**, 1307–1341 (2012), 10.1103/revmodphys.84.1307

[114] R. Gran, J. Nieves, F. Sanchez, and M. J. V. Vacas, Phys. Rev. D **88**, 113007 (2013), 10.1103/PhysRevD.88.113007

[115] M. A. Acero *et al.* [NOvA, R. Group], Eur. Phys. J. C **80**, 1119 (2020), arXiv:2006.08727 [hep-ex]

[116] K. Bays *et al.*, 2020, NOVA-doc-43962-v3

[117] P. A. Rodrigues *et al.* [MINERvA], Phys. Rev. Lett. **116**, 071802 (2016), 10.1103/PhysRevLett.116.071802

[118] P. A. Rodrigues *et al.* [MINERvA], Phys. Rev. Lett. **121**, 209902 (2018), 10.1103/PhysRevLett.121.209902

[119] E. S. P. Guerra *et al.* [T2K, DUET], Phys. Rev. D **99**, 052007 (2019), 10.1103/PhysRevD.99.052007

[120] M. Dolce, H. Gallagher, and J. Wolcott, 2020, NOVA-doc-43724-v4

[121] J. Nieves, J. E. Amaro, and M. Valverde, Phys. Rev. C **70**, 055503 (2004), 10.1103/PhysRevC.70.055503

[122] A. S. Meyer, M. Betancourt, R. Gran, and R. Hill, Phys. Rev. D **93**, 113015 (2016), 10.1103/PhysRevD.93.113015

[123] L. A. Ahrens *et al.*, Phys. Rev. D **35**, 785 (1987), 10.1103/PhysRevD.35.785

[124] A. Bodek and U. K. Yang, J. Phys. G: Nucl. and Part. Phys. **29**, 1899 (2003), arXiv:hep-ex/0210024

[125] A. Bodek and U. K. Yang, Modeling neutrino and electron scattering inelastic cross-sections in the few GeV region with effective LO PDFs TV Leading Order, in *2nd International Workshop on Neutrino-Nucleus Interactions in the Few GeV Region*, , 2003, arXiv:hep-ex/0308007

[126] C. Berger and L. M. Sehgal, Phys. Rev. D **76**, 113004 (2007), 10.1103/PhysRevD.76.113004

[127] D. Rein and L. M. Sehgal, Nucl. Phys. B **223**, 29 (1983), 10.1016/0550-3213(83)90090-1

[128] D. Rein and L. M. Sehgal, Phys. Lett. B **657**, 207 (2007), arXiv:hep-ph/0606185

[129] Z. Koba, H. B. Nielsen, and P. Olesen, Nucl. Phys. B **40**, 317 (1972), 10.1016/0550-3213(72)90551-2

[130] T. Sjöstrand, S. Mrenna, and P. Skands, JHEP **2006**, 026–026 (2006), 10.1088/1126-6708/2006/05/026

[131] S. Dytman, Acta Phys. Polon. B **40**, 2445 (2009), https://www.actaphys.uj.edu.pl/R/40/9/2445/pdf

[132] A. Bodek and J. L. Ritchie, Phys. Rev. D **24**, 1400 (1981), 10.1103/PhysRevD.24.1400

[133] M. Dolce and M. Martinez-Casales, 2020, NOVA-doc-45359-v7

[134] R. M. Sternheimer, Phys. Rev. **88**, 851 (1952), 10.1103/PhysRev.88.851

[135] M. Strait, 2020, NOVA-doc-20816-v23

[136] M. Strait, 2019, NOVA-doc-39106-v2

[137] J. Hewes and O. Samoylov, 2020, NOVA-doc-43935-v3

[138] J. B. Birks, Proc. Phys. Soc. A **64**, 874 (1951), 10.1088/0370-1298/64/10/303

[139] N. Anfimov, A. Antoshkin, O. Samoylov, and A. Sotnikov, 2019, NOVA-doc-31369-v3

[140] P. A. Cherenkov, Dokl. Akad. Nauk SSSR **2**, 451 (1934), 10.3367/UFNr.0093.196710n.0385

[141] I. Frank and I. Tamm, *Coherent Visible Radiation of Fast Electrons Passing Through Matter*, Springer Berlin Heidelberg (1991), ISBN 978-3-642-74626-0, pp. 29–35, 10.1007/978-3-642-74626-0_2

[142] S. Yu, 2019, NOVA-doc-39328-v1

[143] A. Aurisano, 2015, NOVA-doc-13577-v3

[144] J. Huang, M. Judah, and D. Pershey, 2019, NOVA-doc-27689-v5

[145] M. Baird *et al.*, J. Phys. Conf. Ser. **664**, 072035 (2015), 10.1088/1742-6596/664/7/072035

[146] A. Rodriguez and A. Laio, Science **344**, 1492 (2014), 10.1126/science.1242072

[147] R. C. Prim, Bell Labs Tech. J. **36**, 1389 (1957), 10.1002/j.1538-7305.1957.tb01515.x

[148] M. Baird, 2013, NOVA-doc-9195-v1

[149] M. Ester, H. Kriegel, J. Sander, and X. Xu, A density-based algorithm for discovering clusters in large spatial databases with noise, in *Proceedings of the Second International Conference on Knowledge Discovery and Data Mining*, KDD'96, p. 226–231, AAAI Press, 1996

[150] T. Nosek, 2017, NOVA-doc-23102-v7

[151] E. Smith, 2019, NOVA-doc-42539-v1

[152] T. Nosek, 2019, NOVA-doc-42437-v1

[153] L. Fernandes and M. Oliveira, Pattern Recognit. **41**, 299 (2008), 10.1016/j.patcog.2007.04.003

[154] M. Baird, 2012, NOVA-doc-8241-v1

[155] M. Ohlsson, C. Peterson, and A. L. Yuille, Comput. Phys. Commun. **71**, 77 (1992), 10.1016/0010-4655(92)90074-9

[156] M. Gyulassy and M. Harlander, Comput. Phys. Commun. **66**, 31 (1991), 10.1016/0010-4655(91)90005-6

[157] M. Ohlsson, Comput. Phys. Commun. **77**, 19 (1993), 10.1016/0010-4655(93)90033-9

[158] R. Frühwirth and A. Strandlie, Comput. Phys. Commun. **120**, 197 (1999), 10.1016/S0010-4655(99)00231-3

[159] M. Messier, 2012, NOVA-doc-7530-v4

[160] R. Krishnapuram and J. M. Keller, IEEE Trans. Fuzzy. Syst. **1**, 98 (1993), 10.1109/91.227387

[161] M. Yang and K. Wu, Pattern Recognit. **39**, 5 (2006), 10.1016/j.patcog.2005.07.005

[162] E. Niner, 2012, NOVA-doc-7648-v2

[163] R. E. Kalman, J. Basic Eng. **82**, 35 (1960), 10.1115/1.3662552

[164] N. Raddatz, 2015, NOVA-doc-13545-v1

[165] B. Rebel, 2016, NOVA-doc-15977-v1

[166] T. Alion and M. Campbell, 2017, NOVA-doc-13579-v35

[167] D. Pershey, 2016, NOVA-doc-14789-v1

[168] L. W. Koerner and R. Nichol, 2020, NOVA-doc-43820-v2

[169] P. Singh, 2016, NOVA-doc-15472-v7

[170] L. Vinton, 2017, NOVA-doc-13475-v3

[171] M. Baird *et al.*, 2020, NOVA-doc-43162-v3

[172] K. He, X. Zhang, S. Ren, and J. Sun, 2015, arXiv:1512.03385 [cs.CV]

[173] A. Himmel, A. Moren, and E. Niner, 2020, NOVA-doc-42766-v2

[174] B. Mayes and A. T. C. Sutton, 2019, NOVA-doc-42268-v1

[175] N. S. Altman, Am. Stat. **46**, 175 (1992), 10.1080/00031305.1992.10475879

[176] N. Raddatz, 2014, NOVA-doc-11206-v1

[177] J. H. Friedman, Ann. Stat. **29**, 1189 (2001), 10.1214/aos/1013203451

[178] L. Mason, J. Baxter, P. Bartlett, and M. Frean, Adv. Neural Inf. Process Syst. **12**, 512 (1999)

[179] A. Hocker *et al.*, 2007, arXiv:physics/0703039

[180] J. Porter, 2019, NOVA-doc-42277-v1

[181] Y. Freund and R. E. Schapire, J. Comput. Syst. Sci. **55**, 119 (1997), 10.1006/jcss.1997.1504

[182] R. Gandrajula and L. Kolupaeva, 2019, NOVA-doc-42473-v1

[183] T. Warburton, 2019, NOVA-doc-42358-v2

[184] K. Fukushima, Biol. Cybern. **36**, 193 (2004), 10.1007/BF00344251

[185] I. Goodfellow, Y. Bengio, and A. Courville, *Deep Learning*, MIT Press (2016), http://www.deeplearningbook.org

[186] M. Groh and T. Warburton, 2020, NOVA-doc-42897-v2

[187] A. Aurisano *et al.*, JINST **11**, P09001 (2016), arXiv:1604.01444 [hep-ex]

[188] F. Psihas *et al.*, Phys. Rev. D **100**, 073005 (2019), arXiv:1906.00713 [physics.ins-det]

[189] M. Sandler, A. Howard, M. Zhu, A. Zhmoginov, and L. Chen, 2019, arXiv:1801.04381 [cs.CV]

[190] M. Groh, 2020, NOVA-doc-43911-v5

[191] M. Elkins and D. Doyle, 2020, NOVA-doc-42229-v2

[192] M. Groh, 2020, NOVA-doc-46539-v1

[193] S. Lein, 2016, NOVA-doc-15211-v1

[194] M. Wei, 2020, NOVA-doc-43757-v1

[195] M. Wei, 2020, NOVA-doc-46283-v8

[196] S. Yu, 2020, NOVA-doc-43814-v3

[197] E. Catano-Mur, B. N. Nayak, A. T. C. Sutton, and T. Warburton, 2020, NOVA-doc-44040-v1

[198] J. Vasel, 2015, NOVA-doc-14222-v1

[199] M. Baird and L. Vinton, 2017, NOVA-doc-23390-v2

[200] T. Blackburn, 2018, NOVA-doc-27185-v1

[201] E. Smith, 2020, NOVA-doc-46355-v7

[202] E. Catano-Mur, 2017, NOVA-doc-23174-v2

[203] S. Yu, 2018, NOVA-doc-27833-v6

[204] M. Elkins, 2020, NOVA-doc-43712-v3

[205] M. Elkins, 2020, NOVA-doc-45865-v4

[206] S. Yu, 2018, NOVA-doc-29612-v10

[207] A. Mislivec, 2020, NOVA-doc-44401-v5

[208] A. Mislivec, 2020, NOVA-doc-45980-v3

[209] A. T. C. Sutton, 2020, NOVA-doc-44588-v1

[210] M. Elkins and L. Kolupaeva, 2020, NOVA-doc-44316-v2

[211] B. N. Nayak, 2020, NOVA-doc-45943-v2

[212] C. Backhouse, 2013, NOVA-doc-9222-v4

[213] A. Mislivec and T. Nosek, 2020, NOVA-doc-44298-v3

[214] T. Nosek, 2020, NOVA-doc-45668-v3

[215] A. Sutton [NOvA], PoS **NuFACT2018**, 058 (2018), 10.22323/1.341.0058

[216] R. B. Patterson and M. J. Wettstein, 2020, NOVA-doc-43811-v1

[217] R. B. Patterson, 2020, NOVA-doc-43811-v1

[218] J. Wolcott, 2018, NOVA-doc-29973-v4

[219] R. Gran, (2017), 10.2172/1414403

[220] P. Adamson *et al.* [MINOS], Phys. Rev. D **91**, 012005 (2015), arXiv:1410.8613 [hep-ex]

[221] J. E. Amaro, M. B. Barbaro, J. A. Caballero, and T. W. Donnelly, Phys. Rev. Lett. **108** (2012), 10.1103/physrevlett.108.152501

[222] M. Martini, M. Ericson, G. Chanfray, and J. Marteau, Phys. Rev. C **81**, 045502 (2010), 10.1103/PhysRevC.81.045502

[223] M. Tzanov *et al.* [NuTeV], Phys. Rev. D **74**, 012008 (2006), 10.1103/PhysRevD.74.012008

[224] Q. Wu *et al.* [NOMAD], Phys. Lett. B **660**, 19 (2008), https://doi.org/10.1016/j.physletb.2007.12.027

[225] M. Kordosky, Nucl. Phys. B (Proc. Suppl.) **159**, 223 (2006), 10.1016/j.nuclphysbps.2006.08.040

[226] A. Mislivec *et al.* [MINERvA], Phys. Rev. D **97**, 032014 (2018), arXiv:1711.01178 [hep-ex]

[227] K. Abe *et al.* [T2K], Phys. Rev. D **96** (2017), 10.1103/physrevd.96.092006

[228] M. Day and K. S. McFarland, Phys. Rev. D **86** (2012), 10.1103/physrevd.86.053003

[229] I. Jolliffe, *Principal Component Analysis*, Springer Series in Statistics, Springer (2002), ISBN 9780387954424

[230] J. Shlens, A Tutorial on Principal Component Analysis, 2014, arXiv:1404.1100 [cs.LG]

[231] B. N. Nayak, 2020, NOVA-doc-44049-v1

[232] B. N. Nayak, 2017, NOVA-doc-22532-v5

[233] T. Nosek, 2020, NOVA-doc-44274-v3

[234] M. Groh, 2018, NOVA-doc-27914-v3

[235] L. Aliaga, C. Beunneti, L. Cremonesi, K. Maan, and A. Radovic, 2017, NOVA-doc-17608-v5

[236] M. Strait, S. Bending, K. Kephart, and P. Lukens, NOvA muon energy scale systematic, 2019, arXiv:1902.02805 [physics.ins-det]

[237] D. E. Groom, N. V. Mokhov, and S. I. Striganov, At. Data Nucl. Data Tables **78**, 183 (2001), 10.1006/adnd.2001.0861

[238] B. Zamorano, 2015, NOVA-doc-13639-v2

[239] Z. Vallari, 2020, NOVA-doc-43917-v4

[240] T. Nosek, 2017, NOVA-doc-22478-v7

[241] M. Strait, 2017, NOVA-doc-16889-v2

[242] T. Nosek, 2020, NOVA-doc-44271-v7

[243] J. Hewes, 2020, NOVA-doc-44031-v1

[244] H. Duyang *et al.*, 2015, NOVA-doc-13584-v6

[245] A. Booth, 2020, NOVA-doc-43838-v6

[246] J. Neyman, Philos. Trans. R. Soc. A **236**, 333 (1937), 10.1098/rsta.1937.0005

[247] S. S. Wilks, Ann. Math. Stat. **9**, 60 (1938), 10.1214/aoms/1177732360

[248] M. Tanabashi *et al.* [Particle Data Group], Phys. Rev. D **98**, 030001 (2018), 10.1103/PhysRevD.98.030001

[249] F. James and M. Roos, Comput. Phys. Commun. **10**, 343 (1975), 10.1016/0010-4655(75)90039-9

[250] Y. Zhang, 2020, NOVA-doc-45826-v2

[251] A. T. C. Sutton, 2020, NOVA-doc-45809-v7

[252] A. M. Hall, 2020, NOVA-doc-45889-v7

[253] M. Groh, 2020, NOVA-doc-45740-v4

[254] G. J. Feldman and R. D. Cousins, Phys. Rev. D **57**, 3873 (1998), 10.1103/PhysRevD.57.3873

[255] Y. Nakajima, Recent results and future prospects from Super-Kamiokande, 2020, 10.5281/zenodo.4134680

[256] A. T. C. Sutton, 2020, NOVA-doc-48345-v4

[257] S. Y. Calvez, 2020, NOVA-doc-46331-v1

List of Figures

List of Tables

List of Abbreviations & Acronyms

1, 2, 3D	1, 2, 3 Dimensions
3ν-paradigm	three active neutrinos paradigm
4DSlicer	light-like interval clustering with DBSCAN
ADC	Analogue-to-Digital Converter
AGKY	Andreopoulos-Gallagher-Kehayias-Yang
APD	Avalanche PhotoDiode
BDT(G)	(Gradient) Boosted Decision Tree
BEN	Beam Electron Neutrino decomposition
CC	Charged Current
CCQE	Charged Current Quasi-Elastic scattering
CERN	Conseil Européen pour la Recherche Nucléaire (European Organization for Nuclear Research)
CL	Confidence Level
CMC	Comprehensive Model Configuration
CNGS	CERN Neutrinos to Gran Sasso
CNN	Convolutional Neural Network
COH	COHerent π production
CPT	Charge-Parity-Time
CPU	Central Processing Unit
CRY	Cosmic-RaY shower generator
CVN	Convolutional Visual Network (NOvA's CNN particle identification)
CosRej	Cosmic Rejection
DBSCAN	Density-Based Spatial Clustering of Applications with Noise
DCM	Data Concentrator Module
DDT	Data Driven Trigger
DIS	Deep Inelastic Scattering
DUNE	Deep Underground Neutrino Experiment
EW, EWT	ElectroWeak, ElectroWeak Theory
F/N	Far over Near (Near to Far) extrapolation ratio
FD	Far Detector
FEB	Front-End Board
FHC	Forward Horn Current, ν-beam
FOM	Figure Of Merit
FSI	Final State Interactions
Fermilab, FNAL	Fermi National Accelerator Laboratory
G4NuMI	Geant4 for NuMI simulation package
GALLEX	GALLium EXperiment
GENIE	Generates Events for Neutrino Interaction Experiments
GPS	Global Positioning System
GWS	Glashow-Weinberg-Salam model
Geant4	GEometry ANd Tracking 4
HO	Higher Octant ($\theta_{23} > 45°$)
ID	IDentification (number)
IO/IH	Inverted Ordering or Inverted Hierarchy
K2K	KEK To Kamioka experiment
KARMEN	KArlsruhe Rutherford Medium Energy Neutrino experiment
KEK	Kō Enerugī Kasokuki Kenkyū Kikō (High Energy Accelerator Research Organization)

KNO	Koba-Nielsen-Olesen
LO	Lower Octant ($\theta_{23} < 45°$)
LOWESS	LOcally WEighted Scatter plot Smoothing
LSND	Liquid Scintillator Neutrino Detector
MC	Monte-Carlo simulation
MEC	Meson Exchange Current interaction
MID	Michel e IDentification
MINERvA	Main Injector Experiment for $\nu - A$
MINOS	Main Injector Neutrino Oscillation Search
MIP	Minimum Ionizing Particle
MIPP	Main Injector Particle Production
MSB	Methyl-Styryl-Benzene
MSW	Mikheev-Smirnov-Wolfenstein effect
NA49	North Area 49/61
NA61/SHINE	SPS Heavy Ion and Neutrino Experiment
NC	Neutral Current
NCEL	Neutral Current ELastic scattering
ND	Near Detector
NDOS	Near Detector On the Surface
NO/NH	Normal Ordering or Normal Hierarchy
NOvA	NuMI Off-axis ν_e Appearance Experiment
NuMI	Neutrinos at the Main Injector ν_μ beam
OPERA	Oscillation Project with Emulsion-tRacking Apparatus
PCA	Principal Component Analysis
PCAC	Partially Conserved Axial Current
PDF	probability distribution function
PE	PhotoElectron
PID	Particle IDentification
POT	Protons On Target (a unit of exposure)
PPFX	Package to Predict FluX
PPO	2,5-Diphenyloxazole
PVC	PolyVinyl Chloride
QCD	Quantum ChromoDynamics
QED	Quantum ElectroDynamics
QFD	Quantum FlavorDynamics
RENO	Reactor Experiment for Neutrino Oscillations
RES	RESonant baryon production
RHC	Reverse Horn Current, $\bar{\nu}$-beam
RMS	Root Mean Square
RPA	Random Phase Approximation
RR	Reconstructed to Reconstructed
RTR	Reconstructed to True to Reconstructed
ReMId	Reconstructed Muon Identification
SAGE	Soviet–American Gallium Experiment
SM	Standard Model
SNO	Sudbury Neutrino Observatory
SPS	Super Proton Synchrotron
SSM	Standard Solar Model
T2K	Tokai To Kamioka experiment
TDSlicer	Time Density Slicer (clustering)
(M)TDU	(Master) Time Distributing Unit

TMVA	Toolkit for Multivariate Data Analysis
UO	Upper Octant ($\theta_{23} > 45°$)
USA	United States of America
UV	UltraViolet
WLS	WaveLength Shifting
WS	Wrong Sign ($\bar{\nu}$ in ν-beam and *vice versa*)
XSec	Cross Section
e.g.	*exempli gratia*, for example
et al.	*et alii*, and others
etc.	*et cetera*, and the others
i.e.	*id est*, that is
n.b.	*nota bene*, note well
vs.	*versus*, against
k-NN	k-Nearest Neighbor algorithm
pCVN	Prong (single particle) Convolutional Visual Network
w.r.t.	with respect to

Notation

The list contains notation applied in general, *i.e.* unless specified differently.

$SU(n), U(n)$	special unitary group of degree n, unitary group of degree n
$W^{\pm}, Z$	massive vector bosons mediating the weak interaction
γ	photon mediating the electromagnetic interaction
θ_{W}	Weinberg angle
$^{\top}$	transpose
*	complex conjugate
†	hermitian conjugate
P, P_L, P_R	parity, left- and right-handed chiral projectors
$^{C}, C$	charge conjugation, charge conjugation operator (matrix)
CP	charge-parity conjugation
ψ, ν, l	fermionic, neutrino, charged lepton fields
ν_L, ν_R	left- and right-handed chiral components of neutrino fields
ν^{M}	Majorana neutrino field
$\gamma^{\lambda}, \gamma_5 \equiv \mathrm{i}\gamma^0\gamma^1\gamma^2\gamma^3$	Dirac γ matrices
M, D, M_L, M_R	mass matrix, Dirac and Majorana mass matrices
$\nu, \bar{\nu}$	neutrino and antineutrino
N, p, n	observed nucleons, proton neutron
e, μ, τ	electron, muon and tau, observed charged leptons
ν_e, ν_μ, ν_τ	electron, muon and tau neutrino, observed neutral leptons
$i, j, k \ldots$	denotation of mass states, general sum indices
$\alpha, \beta, \gamma \ldots$	denotation of flavor states, auxiliary sum indices
V, U	neutrino mass and interaction mixing matrices
$V_{\alpha i}, U_{\alpha i}$	elements of mixing matrices
$\lvert\nu_\alpha\rangle$	flavor eigenstate of neutrino
$\lvert\nu_i\rangle$	mass eigenstate of neutrino
m_i	masses of neutrino mass eigenstate
$\Delta m^2_{ij} = m^2_i - m^2_j$	squared-mass splittings
θ_{ij}	neutrino mixing angles
δ_{CP}	the Dirac CP phase
δ_{ij}	Kronecker symbol
a, b	Majorana phases
$H, \mathcal{H}$	Hamiltonian, effective Hamiltonian in medium
$S, \mathcal{S}$	evolution matrix, effective evolution matrix in medium
E	energy
E_{true}	simulated true energy
$E_{\mathrm{had}}, E_{\mathrm{em}}$	reconstructed hadronic and electromagnetic calorimetric energy
p, p_t	momentum and transverse momentum
t	time
x	space coordinate, position
L	baseline or travelling distance
$\mathrm{Amp}(\cdot)$	amplitude of a particular process
$\nu_\alpha \to \nu_\beta$	neutrino flavor transition from a flavor α to β
$P(\nu_\alpha \to \nu_\beta)$	oscillation probability from a flavor α to β, appearance probability of ν_β for initial ν_α
$\langle\cdot\lvert\cdot\rangle$	inner product
V_e	electron interaction potential
G_F	Fermi coupling constant

N_e, N_n	electron and nucleon density
$\mathfrak{Re}, \mathfrak{Im}$	real and imaginary part of a complex number
q, q_0	transferred four-momentum and its first coordinate (energy)
$Q^2 = -q^2$	invariants of the transferred four-momentum
σ	standard deviation, standard error
$\mathcal{N}(\mu, \sigma^2)$	normal distribution with expectation μ and variance σ^2
$L(\cdot), \lambda(\cdot)$	likelihood function, likelihood ratio
$\chi^2_{(N)}$	chi-square distribution (with N degrees of freedom)
$\mathbf{N}, N_i$	vector of ND event rates in reconstructed energy bins
$\mathbf{F}, F_i$	vector of FD predicted event rates in reconstructed energy bins
$\mathbf{F_p}, \mathbf{F_p^r}, \mathbf{F_p^{MC}}$	FD event rates prediction with (or w/o) different ND constraints

List of publications

NOvA publications with direct contribution

M. A. Acero *et al.* [NOvA], Phys. Rev. Lett. **123**, 151803 (2019), arXiv:1906.04907 [hep-ex]

M. A. Acero *et al.* [NOvA], Phys. Rev. D **98**, 032012 (2018), arXiv:1806.00096 [hep-ex]

NOvA technical notes

T. Nosek, 3Flavor 2020 Systematic Uncertainties Summary, 2020, NOVA-doc-45962-v2

A. Mislivec, T. Nosek, 3Flavor Systematics 2020 with p_{T} Extrap, 2020, NOVA-doc-44298-v3

A. Mislivec, T. Nosek, 3Flavor Systematics 2020, 2020, NOVA-doc-43974-v6

T. Nosek, Genie Cross Section Systematics for the 2020 3Flavor Analysis Using PCA, 2020, NOVA-doc-44274-v3

T. Nosek, Michel Electron Tagging Systematic for 3Flavor Analysis 2020, 2020, NOVA-doc-44271-v7

T. Nosek, Comparisons of ND RHC Data of Epochs 7d+8b and Periods 4+6 and Data/MC Comparison of Epochs 7d+8b for 2019 $\nu_e + \bar{\nu}_e$ Analysis, 2019, NOvA-doc-36780-v3

T. Nosek, Michel Decomposition for FHC 2018 ν_e Analysis, 2018, NOvA-doc-27938-v5

T. Nosek, Acceptance Systematics for 2018 ν_e+$\bar{\nu}_e$ Analysis – ND Subcomponents and ND/FD Kinematics, 2018, NOvA-doc-27935-v5

T. Nosek, ND ν_e RHC Data and MC Stability for 2018 ν_e Appearance Analysis, 2018, NOvA-doc-26690-v2

T. Nosek, ND ν_e Data and MC Stability for 2017 ν_e Appearance Analysis, 2017, NOvA-doc-23102-v7

T. Nosek, ND Subcomponents / Kinematics Systematics for 2017 ν_e Appearance Analysis, 2017, NOvA-doc-22478-v7

Selected proceedings

T. Nosek (for NOvA), Systematic Uncertainties of the NOvA Neutrino Oscillation Analysis, in PoS ICHEP2020, 210 (2021), 10.22323/1.390.0210

T. Nosek (for NOvA), Results on Neutrino and Antineutrino Oscillations from the NOvA Experiment, in Ukr. J. Phys. **64**, 613 (2019), 10.15407/ujpe64.7.613

T. Nosek (for NOvA), NOvA Recent Results with Neutrino+Antineutrino Data, in New Trends in High-Energy Physics, Dubna, JINR, ISBN 978-5-9530-0509-8 (2019), arXiv:1905.09109 [hep-ex]

T. Nosek, Effects of Matter in Neutrino Oscillations and Determination of Neutrino Mass Hierarchy at Long-baseline Experiments, in WDS'16 Proceedings of Contributed Papers – Physics (eds. J. Šafránková and J. Pavlů), Prague, Matfyzpress (2016), arXiv:1612.09132 [hep-ph]